はじめに

平成16年度金沢医科大学共同研究・奨励研究の成果報告書を発刊しましたのでお手元にお届けいたします。

平成16年度は、国立大学の法人化にみられる大学改革が急速に進み、成果主義、評価主義の厳しい時代が幕を開けました。本学では平成15年度に大学院を改組し、医学部と総合医学研究所を含む全学的な教育・研究体制を構築しました。本学の研究助成はこの状況下で学術研究をさらに活性化させる目的で導入されていましたが、平成15年度からは装いを新たにし、本学の研究基盤を充実させるため将来を嘱望され特徴ある独創的な企画の研究に対して助成することとしています。

本書は、平成16年度に学内公募で申請があった共同研究13件、奨励研究25件のうち、それぞれ4件、18件が採択された研究の成果をまとめたものであります。今後、これらの共同研究と奨励研究を中心に本学の学術研究がさらに発展することを期待します。

最後に、本報告書の取りまとめの労をとられた研究推進評価委員会、研究助成センター事務課並びに関係各位に感謝します。

平成18年12月

金沢医科大学
学長　山本　達

目　　次

はじめに

平成16年度　共同研究成果報告書

C2004－1. 循環ショックの病態生理の解明と治療法の共同開発
研究代表者・芝　本　利　重 …… 1

C2004－2. 肺癌の新しい機能的および形態的診断法の確立と分子標的治療法を指向した標的遺伝子の特定に関する研究
研究代表者・東　　光太郎 …… 77

C2004－3. 悪性神経膠腫の分化誘導と遺伝子治療に関する研究
研究代表者・飯　塚　秀　明 …… 101

C2004－4. モデル動物を利用した肥満・高脂血症の発がんへの関与とその阻止に関する研究
研究代表者・杉　江　茂　幸 …… 105

平成16年度　奨励研究成果報告書

S2004－1. 各種脂肪酸・抗酸化ビタミン摂取量、血清高感度CRPと血圧との関連に関する大規模疫学研究
研究代表者・三　浦　克　之 …… 203

S2004－2. ウイルス感染症を伴う肥満者におけるアディポサイトカインの診断及び治療への応用
研究代表者・高　橋　　孝 …… 207

S2004－3. RNA interferenceにおける二本鎖RNA依存性プロテインキナーゼPKRの関与
研究代表者・松　井　　理 …… 253

S2004－4. 心筋梗塞の新しい治療法の開発―体性幹細胞を用いた再生医療
研究代表者・赤　澤　純　代 …… 265

S2004－5. レトロウイルス発現系を用いたタイラーウイルス増殖メカニズムにおけるL*蛋白の役割の解明
研究代表者・紺　谷　靖　英 …… 269

S2004－6. 日本人の白内障病型別有所見率・発症率と発症・進行予測および危険因子探索
研究代表者・佐々木　　洋 …… 279

S2004－7. 敗血症血管におけるαカテコラミン受容体刺激時の
平滑筋収縮および内皮機能変化の検討
研究代表者・関　純彦 …… 283
S2004－8. IL-2投与が肺胞上皮細胞の分子生物学的機能特性に及ぼす
影響に関する研究
研究代表者・杉田　真 …… 287
S2004－9. 異なる感覚情報の大脳新皮質における統合機序
及びその生後発達に関する研究
研究代表者・吉村　弘 …… 289
S2004－10. ヒト口唇小唾液腺由来の幹細胞の同定
研究代表者・河南崇典 …… 293
S2004－11. Chorea-acanthocytosisの発症機序に関する研究
研究代表者・斉木臣二 …… 297
S2004－12. ミトコンドリア障害に関与する活性酸素生成酵素の研究
研究代表者・島田ひろき …… 301
S2004－13. Gene33/mig-6による心肥大シグナルの制御
研究代表者・竹田健史 …… 305
S2004－14. プロテインキナーゼPKU-βの姉妹染色体の
正確な分配に対する関与
研究代表者・橋本光正 …… 309
S2004－15. 骨粗鬆症への応用を目的としたコラーゲントリペプチドの
生理活性作用の解析
研究代表者・鶴岡直樹 …… 313
S2004－16. ヒト型モノクローナル抗体によるEBウイルス関連蛋白を
標的とした特異的治療法の開発
研究代表者・正木康史 …… 317
S2004－17. 迷走神経によるグルカゴン様ペプチド1受容機構の
分子生物学的検討
研究代表者・中川　淳 …… 319
S2004－18. 傍腫瘍性神経症候群に関連する神経抗原の
in vivoにおける機能の解析
研究代表者・斉木三鈴 …… 323

平成１６年度

共同研究成果報告書

1．研究課題名：循環ショックの病態生理の解明と治療法の共同開発（研究番号 C2004-1）

2．キーワード：1）循環ショック（circulatory shock）
2）虚血再灌流（ischemia reperfusion）
3）肺水腫（pulmonary edema）
4）肝循環（hepatic circulation）
5）冠循環（coronary circulation）

3．研究代表者：芝本　利重・医学部・教　授・生理機能制御学（生理学）
研究分担者：土田　英昭・医学部・教　授・侵襲制御学（麻酔学）
佐久間　勉・医学部・教　授・呼吸機能治療学（呼吸器外科）
久保　恵嗣・信州大学・医学部・教　授・内科学第一講座
大久保信司・医学部・助教授・循環制御学（循環器内科学）
（現東京医科大学霞ヶ浦病院）
倉田　康孝・医学部・助教授・生理機能制御学（生理学）

4．研究目的

循環ショックの病態は単に血圧低下にとどまらず、組織の微小循環障害から機能障害に発展する複雑な全身反応である。血行力学的に心原性ショックと非心原性ショックに大別され、前者は心臓ポンプ機能の失調による。一方、非心原性ショックの血圧低下とその臓器循環・機能障害の機序については十分には解明されてない。しかしながら、これらのショックに共通した病態として微小循環障害と虚血再灌流障害、それに基づく炎症反応としてのサイトカインをはじめとしたmediatorが病態形成に関わり多臓器不全を惹起し、肝臓では肝不全、肺では透過性亢進型肺水種であるARDS、心臓では冠不全、心不全にいたるものと考えられる。本研究の目的は心原性、出血性、アナフィラキシィー、敗血症による循環ショックの血圧低下機序とそれによる臓器循環障害の病態生理を肝循環、肺循環、冠循環に注目してwhole animal、臓器、細胞、遺伝子レベルからの多面的アプローチにより明らかにすることである。

5．研究計画

① ラットにおいてin vivoでの肝循環のモニター可能なアナフィラキシィーモデルを作成し、肝病変の血圧低下における役割を肝切除動物と肝血管収縮が弱い肥満細胞欠損動物にて検討する（芝本担当）。
② ウサギとマウスの肝アナフィラキシーの血管収縮部位と肝血液動態を解明する（芝本・土田担当）。
③ ラット摘出灌流肺で、アナフィラキシー・エンドトキシン傷害モデルを作成し，その血行動態と肺血管透過性を炎症性サイトカインならびに傷害惹起の責任細胞に注目して検討する（芝本担当）。
④ 緬羊に肺循環・肺リンパ動態測定及び門脈血行動態測定の手術を施し、アナフィラキシィーショック時の肝循環・肺循環動態を観察し、その役割を明らかにする（久保担当）。
⑤ 分岐理論的アプローチ（心室筋細胞の分岐構造解析）により、心原性ショックの一因である致死的心室性不整脈（異常自動能・早期後脱分極）の非線形力学的発生機序を解明する。さらに、不整脈による心原性ショックの原因・病態解明とバイオペースメーカー・システム設計における心筋細胞分岐構造解析の有用性を検証し、致死的不整脈の合理的制御（予防・治

療）方法を開発・確立するための理論的基盤を構築する（倉田担当）。

⑥ 敗血症ラットから胸部下行大動脈を取り出して摘出血管標本を作成し、血管収縮性の変化とそれらに及ぼす内皮細胞の役割、血管平滑筋の組織学的変化について検討する。（土田担当）

⑧ 虚血再潅流肺傷害の回復期における肺胞水分再吸収機序を研究する．特に２型肺胞上皮細胞とβ交換刺激薬の関係を研究する．誤嚥性肺炎モデルの作成する．（佐久間担当）

⑨ ラット冠動脈狭窄心不全モデルを用いてテプレノン投与による heat shock protein 産生と各種サイトカインの変動ならびに心筋保護作用について検討する（大久保担当）。

６．研究成果　（各項目末尾の番号は研究発表論文の番号である）

１）ラットのアナフィラキシィーショックにおける肝血管収縮の役割を肝摘除かつ腹腔血流遮断処置を施したラットと正常ラットと比較検討して解明した(No. 4)。

２）アナフィラキシーショック時に肝臓の酸素消費量が減少する機序についてラット摘出灌流肝のアナフィラキシーモデルを作成して検討した。その結果、アナフィラキシー反応自体で酸素消費量が減少することを肝酸素消費量測定システムを新規に確立して明らかにした(No. 8)。

３）アナフィラキシー化学伝達物質である血小板活性化因子、トロンボキサン、ロイコトリエンのラット肝血管への作用を収縮部位、酸素消費量、胆汁産生量、肝内血液量について解明した(No. 9)。

４）ラット肝アナフィラキシーの一酸化窒素の役割を灌流血液との関係で明らかにした(No. 10, 11)。

５）モルモットのアナフィラキシィー肝血管収縮における化学伝達物質についてヒスタミン、プロスタグランジン、血小板活性化因子(PAF)とロイコトリエン(LT)の関与をそれぞれの受容体阻害剤を用いて検討し、PAF と LT がそれぞれ前類洞と後類洞収縮に関与していることを解明にした(No. 6)。

６）マウス肝血管アナフィラキシー解明の前段階としてその肝血管の特性とアナフィラキシーショックと心原性ショック時放出されるヒスタミンとノルエピネフリンの作用を明らかにした(No. 3)。

７）ラット肺を用いて UTP が肺胞水分クリアランスを亢進すること，β交感神経刺激薬の効果を促進すること，その作用はクロライドチャンネルを介することを明らかにした (No. 1)。

８）ラット肺を用いて選択的α_1-，β_1-，β_2-，β_3-交感神経刺激薬が肺胞水分クリアランスを亢進させることを報告した．ただし，α_1-，β_1-，β_2-交感神経刺激薬は選択的受容体を介するが，β_3-交感神経刺激薬はβ_2-受容体を介することを示唆する成績を得た(No. 2)。

９）選択的β_1-，β_2-交感神経刺激薬は肺胞水分クリアランスを亢進し，肺水腫の治療薬として有用な薬剤であることを明らかにした(No. 7)。

10）静水圧型肺水腫と透過性亢進型肺水腫では内因性カテコールアミンは上昇するが，肺胞水分クリアランスを亢進させる濃度には至らないこと，吸入により達成できる濃度でのエピネフリン気道内投与により肺胞水分クリアランスを亢進するが，ノルエピネフリン気道内投与では亢進しないこと，エピネフリンの効果は CFTR クロライドチャンネルを介していることを明らかにした。

11）ヒト心室筋細胞の分岐構造を解析して、内向き整流K^+チャネル電流の抑制によりヒト心室筋に自動能が生じ得ること、また、その発現機構は本質的に洞結節の生理的自動能と同じであることを明らかにした。さらに、自動能発現における各イオンチャネル電流の役割を解明することにより、分岐構造解析が不整脈発生機序の統一的理解と記述、合理的な不整脈制御方法の開発（バイオペースメーカーシステム設計など）において有用（必要不可欠）であることを証明した。(No. 5)。

7．研究の考察・反省

各研究課題において当初に計画された多くのものは達成されたと考える。研究課題が多すぎたために来年度へ持ち越したものもある。また、実験は終了しているにもかかわらず論文にまとめる作業が遅れているものもある。しかし、全体としては活発な研究活動が行われたものと考える。

8．研究発表

Sakuma T, Gu X, Sugita M, Sagawa M, Sakuda M, Toga H. Uridine 5'-triphosphate stimulates alveolar fluid clearance in the isolated rat lungs. J Pharmacol Sci 2004; 95: 420-425. (MLDB)

Gu X, Sugita M, Sagawa M, Sakuda M, Osanai K, Toga H, Sakuma T. Effects of α_1-, β_1-, β_2-, β_3-adrenergic agonists on alveolar fluid clearance in isolated rat lungs. J Kanazawa Med Univ 2004; 29(2): 91-96.

Shibamoto T, Cui S, Ruan Z, Kurata Y. Effects of norepinephrine and histamine on vascular resistance in isolated perfused mouse liver. Jpn J Physiol 2005; 55: 143-148. (MLDB)

Shibamoto T, Cui S, Ruan Z, Liu W, Takano H, Kurata Y. Hepatic venoconstriction is involved in anaphylactic hypotension in rats. Am J Physiol Heart Circ Physiol 2005; 289: H1436-H1441 (MLDB)

Kurata Y, Hisatome I, Matsuda H, Shibamoto T. Dynamical mechanisms of pacemaker generation in IK1-downregulated human ventricular myocytes: Insights from bifurcation analyses of a mathematical model. Biophys J 2005; 89: 2865-2887. (MLDB)

Shibamoto T, Ruan Z, Cui S, Liu W, Kurata Y. Involvement of platelet-activating factor and leukotrienes in anaphylactic segmental venoconstriction in ovalbumin sensitized guinea pig livers. Prostaglandins Other Lipid Mediator 2005; 78: 218-230. (MLDB)

Sakuma T, Wang Z, Xu J, Maeda S, Sugita M, Sagawa M. Beta-adrenergic agonist therapy for alveolar edema in postoperative pulmonary complications. J Kanazawa Med Univ 2005; 30: 6-11.

Cui S, Shibamoto T, Ruan Z, Takano H, Liu W, Kurata Y. Oxygen consumption, assessed with the oxygen absorption spectrophotometer, decreases during hepatic anaphylaxis in perfused rat liver. Shock 2006; 26: 62-68, 2006. (MLDB)

Cui S, Shibamoto T, Liu W, Takano H, Kurata Y. Effects of platelet-activating factor, thromboxane A_2 and leukotriene D_4 on isolated perfused rat liver. Prostaglandins Other Lipid Mediators 2006; 80: 35-45. (MLDB)

Shibamoto T, Ishibashi T, Shimo T, Cui S, Takano H, Tsuchida H, Nishio M, Kurata Y. N-nitro-l-arginine methylester potentiates anaphylactic venoconstriction in perfused rat livers. Clin Exp Pharmacol Physiol 2006; 33: 1073-1077. (MLDB)

Cui S, Shibamoto T, Liu W, Takano H, Zhao Z-S, Kurata Y. Effects of Hct on L-NAME-induced potentiation of anaphylactic presinusoidal constriction in perfused rat livers. J Cardiovasc Pharmacol 2006; 48: 827-833. (MLDB)

芝本利重, 崔　森、刘　威、高野博充、倉田康孝.　ノルエピネフリンは種差なく前類洞優位の血管収縮により肝内血液量を減少させる. 自律神経 2005; 42: 271-274.

Dynamical Mechanisms of Pacemaker Generation in I_{K1}-Downregulated Human Ventricular Myocytes: Insights from Bifurcation Analyses of a Mathematical Model

Yasutaka Kurata,* Ichiro Hisatome,† Hiroyuki Matsuda,* and Toshishige Shibamoto*
*Department of Physiology, Kanazawa Medical University, Ishikawa 920-0293, Japan; and †Division of Regenerative Medicine and Therapeutics, Tottori University Graduate School of Medical Science, Yonago 683-0826, Japan

ABSTRACT Dynamical mechanisms of the biological pacemaker (BP) generation in human ventricular myocytes were investigated by bifurcation analyses of a mathematical model. Equilibrium points (EPs), periodic orbits, stability of EPs, and bifurcation points were determined as functions of bifurcation parameters, such as the maximum conductance of inward-rectifier K^+ current (I_{K1}), for constructing bifurcation diagrams. Stable limit cycles (BP activity) abruptly appeared around an unstable EP via a saddle-node bifurcation when I_{K1} was suppressed by 84.6%. After the bifurcation at which a stable EP disappears, the I_{K1}-reduced system has an unstable EP only, which is essentially important for stable pacemaking. To elucidate how individual sarcolemmal currents contribute to EP instability and BP generation, we further explored the bifurcation structures of the system during changes in L-type Ca^{2+} channel current ($I_{Ca,L}$), delayed-rectifier K^+ currents (I_K), or Na^+/Ca^{2+} exchanger current (I_{NaCa}). Our results suggest that 1), $I_{Ca,L}$ is, but I_K or I_{NaCa} is not, responsible for EP instability as a requisite to stable BP generation; 2), I_K is indispensable for robust pacemaking with large amplitude, high upstroke velocity, and stable frequency; and 3), I_{NaCa} is the dominant pacemaker current but is not necessarily required for the generation of spontaneous oscillations.

INTRODUCTION

The cardiac biological pacemaker (BP) was recently created by genetic suppression of the inward-rectifier K^+ current (I_{K1}) in guinea pig ventricular myocytes (1), suggesting possible development of the functional BP as a therapeutic alternative to the electronic pacemaker. A first step for creation of the functional BP would be engineering of single BP cells, which requires deep understanding of the BP mechanisms. Using the Luo-Rudy guinea pig ventricle model (2), Silva and Rudy (3) simulated BP activity by reducing I_{K1} conductance (g_{K1}) and investigated the ionic mechanisms of BP generation in the I_{K1}-downregulated ventricular myocyte. They reported that BP activity was yielded by 81% suppression of I_{K1}, concluding that Na^+/Ca^{2+} exchanger current (I_{NaCa}) was the dominant pacemaker current. However, the mechanistic difference between ventricular pacemaking and natural sinoatrial (SA) node pacemaking, as well as whether I_{K1} downregulation also induces BP activity in human ventricular myocytes (HVMs), remains to be clarified.

The aim of this study was to elucidate the mechanisms of BP generation in I_{K1}-downregulated HVMs and the roles of individual sarcolemmal currents in HVM pacemaking in terms of the nonlinear dynamics and bifurcation theory. In previous studies (4–11), bifurcation structures of ventricular or SA node models, i.e., ways of changes in the number or stability of equilibrium and periodic states of the model systems, were investigated for elucidating the mechanisms of normal and abnormal pacemaker activities. These theoretical works indicate that the mathematical approach provides a convenient way of understanding how individual currents contribute to pacemaker activities. In this study, therefore, local stability and bifurcation analyses, as well as numerical simulations, were performed for a mathematical model of the HVM. We constructed bifurcation diagrams by calculating equilibrium points (EPs), periodic orbits, stability of the EP, and saddle-node or Hopf bifurcation points as functions of bifurcation parameters (for details, see Theory and Methods). During I_{K1} suppression, BP activity abruptly emerged around an unstable EP via a saddle-node bifurcation at which a stable EP corresponding to the resting state disappeared. Our results suggested that BP activity could be developed by reducing I_{K1} alone in HVMs as well and that the instability of an EP at depolarized potentials is essentially important for BP generation.

To elucidate the ionic mechanisms of EP destabilization and BP generation in the I_{K1}-downregulated HVM, we further explored bifurcation structures of the I_{K1}-reduced BP system during decreases or increases in an L-type Ca^{2+} channel current ($I_{Ca,L}$), delayed-rectifier K^+ currents (I_K), and I_{NaCa}, which appear to be essentially important for pacemaker generation (3,11). Moreover, we determined stability of the BP system at the steady-state potential (V_0) during applications of the constant bias current (I_{bias}) and how the unstable V_0 and I_{bias} regions, where BP oscillations occur, change with decreasing or increasing the sarcolemmal currents. This would reveal the contributions of each current to EP instability and robustness of BP activity to hyperpolarizing or depolarizing loads (11). Our study suggests that the dynamical mechanism of the ventricular pacemaking is

Submitted February 7, 2005, and accepted for publication July 15, 2005.

Address reprint requests to Yasutaka Kurata, Dept. of Physiology, Kanazawa Medical University, 1-1 Daigaku, Uchinada-machi, Kahoku-gun, Ishikawa 920-0293, Japan, E-mail: yasu@kanazawa-med.ac.jp.

© 2005 by the Biophysical Society

0006-3495/05/10/2865/23 $2.00

doi: 10.1529/biophysj.105.060830

essentially the same as that of the natural SA node pacemaking as reported by Kurata et al. (11).

This article clearly shows that bifurcation analyses of a mathematical model allow us to notice the essential importance of EP instability for pacemaker generation and to elucidate the roles of individual ionic currents in pacemaking. Thus, the nonlinear dynamical approach is useful for general understanding of the mechanisms of normal and abnormal pacemaker activities and may also be applicable to engineering of a functional BP as a therapeutic alternative to the electronic pacemaker. Definitions of the terms specific to the nonlinear dynamics and bifurcation theory are provided at the end of the Theory and Methods section to help understand the theory and methods for bifurcation analysis as well as our results and conclusions. Abbreviations and acronyms repeatedly used in this article are listed in Table 1.

THEORY AND METHODS

Development of a modified HVM model

A mathematical model of cardiac myocytes is described as an n-dimensional nonlinear dynamical system, i.e., a set of ordinary differential equations of the form

TABLE 1 Abbreviations and acronyms

AP	Action potential
APA	Action potential amplitude
$APD_{(90)}$	Action potential duration (at 90% repolarization)
βAS	β-adrenergic stimulation
BP	Biological pacemaker
CL	Cycle length
C-LTCC	High voltage-activated L-type Ca^{2+} channel
D-LTCC	Low voltage-activated L-type Ca^{2+} channel
EP	Equilibrium point
hESC	Human embryonic stem cell
HVM	Human ventricular myocyte
I_{bias}	Constant bias current
$I_{Ca,L}$	L-type Ca^{2+} channel current
I_K	Delayed-rectifier K^+ current
I_{Kr}	Rapidly activating component of I_K
I_{Ks}	Slowly activating component of I_K
I_{K1}	Inward-rectifier K^+ current
I_{Na}	Na^+ channel current
I_{NaCa}	Na^+/Ca^{2+} exchanger current
I_{to}	4-Aminopyridine-sensitive transient outward current
$I_{X,b}$	Background current carried by ion X
I_h	Hyperpolarization-activated current
MDP	Maximum diastolic potential
ODE	Ordinary differential equation
PB	Priebe-Beuckelmann
POP	Peak overshoot potential
SA	Sinoatrial
SR	Sarcoplasmic reticulum
V	Membrane potential
V_0	Steady-state potential at an EP
$[Ca^{2+}]_{rel}$	Free Ca^{2+} concentration in the junctional SR
$[Ca^{2+}]_{up}$	Free Ca^{2+} concentration in the network SR
$[X]_i$	Intracellular concentration of ion X
$[X]_o$	Extracellular concentration of ion X

$$dx_i/dt = f_i(x_1, x_2, \ldots, x_n), i = 1, 2, \ldots, n. \quad (1)$$

This is usually written in the vector form

$$d\boldsymbol{x}/dt = \boldsymbol{f}(\boldsymbol{x}), \quad (2)$$

where the state variable $\boldsymbol{x}$ is a vector-valued function of time t, and the vector field $\boldsymbol{f}$ is a function of the state variable $\boldsymbol{x}$ (12–14). For a model system to be suitable for bifurcation analysis, the vector field $\boldsymbol{f}$ should be continuous and smooth (i.e., sufficiently differentiable) and should not depend on time or initial conditions but depend only on the state variable $\boldsymbol{x}$. Such a system is called an "autonomous" system (see also Definitions of Terms at the end of this section).

On the basis of single-cell patch-clamp data from undiseased and failing HVMs, Priebe and Beuckelmann (15) have first developed a single HVM model (referred to as the Priebe-Beuckelmann (PB) model) as a modified version of the Luo-Rudy phase II model for the guinea pig ventricle (2). Recently, ten Tusscher et al. (16) and Iyer et al. (17) developed more elaborate HVM models based on detailed experimental data. Their models appear to be superior to the PB model in reproducing experimental data but less suitable for bifurcation analyses for the following reasons: 1), the ten Tusscher et al. model has the vector field containing many complex functions that are not continuous or smooth, thus they are not always differentiable or yield noncontinuous derivatives; and 2), the Iyer et al. model ($n = 67$) is much larger than the PB model ($n = 15$) or the ten Tusscher et al. model ($n = 17$), making bifurcation analyses practically much harder. We have therefore chosen to modify the PB model on the basis of recent experimental findings as well as other human or animal heart models. The original PB model explicitly contains time t in the formula for the sarcoplasmic reticulum (SR) Ca^{2+} release, making it nonautonomous. Thus, modifications of the PB model were required for converting it into an autonomous system, as well as for improving the capability of reproducing experimental data.

The standard model for the normal activity is described as a nonlinear dynamical system of 15 first-order ordinary differential equations. The membrane current system includes $I_{Ca,L}$, the rapid and slow components of I_K (denoted I_{Kr} and I_{Ks}, respectively), 4-aminopyridine-sensitive transient outward current (I_{to}), Na^+ channel current (I_{Na}), I_{K1}, background Na^+ ($I_{Na,b}$) and Ca^{2+} ($I_{Ca,b}$) currents, Na^+-K^+ pump current (I_{NaK}), I_{NaCa}, and Ca^{2+} pump current (I_{pCa}). The expressions for $I_{Ca,L}$ and I_{Ks} as well as SR Ca^{2+} release were reformulated, whereas the formulas for other ionic currents and intracellular Ca^{2+} handling are essentially the same as those in the original PB model or adopted from other existing models (16,18–20). Modifications of the model are summarized in Table 2; details on major modifications are described below. All expressions (Eqs. 3–64) and the standard parameter values used are provided in Appendix 1 and Table 5, respectively.

Formulation of $I_{Ca,L}$

The kinetics of $I_{Ca,L}$ was described by Eqs. 3–8 with the activation (d_L), voltage-dependent inactivation (f_L), and Ca^{2+}-dependent inactivation (f_{Ca}) gating variables. Voltage dependences of $I_{Ca,L}$ gating kinetics in the current (modified) and original human heart models are shown in Fig. 1 (*top*), together with temperature-corrected experimental values for comparison. As ten Tusscher et al. (16) pointed out, the steady-state activation and inactivation curves ($d_{L\infty}$, $f_{L\infty}$) yielded by the original PB formulas were somewhat unusual for unknown reasons (see Fig. 1, *left top*), resulting in a very large window current. We therefore renewed the expressions for $I_{Ca,L}$. For the steady-state activation and inactivation ($d_{L\infty}$, $f_{L\infty}$), we used the data of Bénitah et al. (21). The expression of the activation time constant (τ_{dL}) was adopted from the ten Tusscher et al. model (16). The formulas for the time constants of the voltage-dependent inactivation and recovery (τ_{fL}) employed by the original models appeared not to fit the experimental data for single HVMs from Bénitah et al. (21) or other articles (see Fig. 1, *right top*, and also Fig. 2 *E* of ten Tusscher et al. (16)). Therefore, we originally formulated τ_{fL} from the data of Bénitah et al. (21), which were corrected for

TABLE 2 Equations and parameter values adopted for individual components of the HVM model

Component	Expressions	Parameter values		PB*	TNNP*
	$d_{L,\infty}$, $f_{L,\infty}$: Bénitah et al. (21)				
$I_{Ca,L}$	τ_{dL}: Same as the TNNP model (16)	$g_{Ca,L}$ (nS/pF)	0.2496	*0.064*	
	τ_{fL}: Original formula based on Bénitah et al. (21)				
	$p_{a,\infty}$: Li et al. (24)				
I_{Kr}	$p_{i,\infty}$: Same as the CRN model (19)†	g_{Kr} (nS/pF)	0.012	*0.015*	*0.096*
	τ_{pa}: Same as the CRN model (19)†				
	n_∞: Li et al. (24)				
I_{Ks}	τ_n: Original formula based on Virág et al. (34)	g_{Ks} (nS/pF)	0.036	*0.02*	*0.245*
I_{to}	Same as the PB model (15)	g_{to} (nS/pF)‡	0.3/0.4	0.3	*0.294*
I_{Na}	Same as Bernus et al. (18)§	g_{Na} (nS/pF)	7.8	*16*	*14.838*
I_{K1}	Same as the PB model (15)	g_{K1} (nS/pF)	3.9	2.5	5.405
$I_{Na,b}$	Same as the PB model (15)	$g_{Na,b}$ (nS/pF)	0.001	0.001	0.00029
$I_{Ca,b}$	Same as the PB model (15)	$g_{Ca,b}$ (nS/pF)	0.00051	0.00085	0.000592
I_{NaK}	Same as the PB model (15)	$I_{NaK,max}$ (pA/pF)	0.884	1.3	*1.362*
I_{NaCa}	Same as the PB model (15)	k_{NaCa}	1000	1000	1000
I_{pCa}	Same as the CRN model (19)¶	$I_{pCa,max}$ (pA/pF)	0.11	0	0.025
J_{rel}	Modified formulas base on Faber and Rudy (20)	P_{rel}	50	*22*	*24.696*
J_{up}	Same as the TNNP model (16)¶	P_{up}	0.00221	*0.0045*	*0.000425*
J_{tr}	Same as the PB model (15)	τ_{tr}	180	180	
Ca^{2+} buffers	Same as the PB model (15)				

*Parameter values used for the PB model (15) and ten Tusscher et al. (TNNP) model (16) are given for comparison. Values are shown in italics or not shown, when the formula is different from that of the current model and thus direct comparison is impossible.

†Formulas of the Courtemanche et al. (CRN) model for human atrial myocytes (19) were used. For details, see text.

‡The g_{to} (nS/pF) was set equal to 0.4, the value for epicardial cells (18), for the simulation of paced APs, and to 0.3, the value of the original PB model, for the BP simulations and bifurcation analyses.

§Formulas for I_{Na} were adopted from Bernus et al. (18) to reduce the number of state variables as well as to avoid the use of noncontinuous functions.

¶To reduce the diastolic $[Ca^{2+}]_i$ during pacing at 0.25–2 Hz to <0.3 μM, 1), a small amount of I_{pCa} was added, and 2), the formula for SR Ca^{2+} uptake was adopted from the TNNP model (16).

a temperature of 37°C with a Q_{10} of 2.2 and $[Ca^{2+}]_o$-dependent factor (16). The τ_{fL} data were fitted to a function similar to that used by Courtemanche et al. (19) for their human atrial model, using a least square minimization procedure. The formula for the Ca^{2+}-dependent inactivation ($f_{Ca,\infty}$) is also the same as used by Courtemanche et al. (19). Maximum $I_{Ca,L}$ was formulated as a fully selective Ca^{2+} current, with its reversal potential ($E_{Ca,L}$) fixed at a constant value of +52.8 mV as reported by Bénitah et al. (21) and the maximum conductance ($g_{Ca,L}$) set equal to 249.6 pS/pF at 2 mM $[Ca^{2+}]_o$.

The model-generated $I_{Ca,L}$ during voltage-clamp pulses and peak $I_{Ca,L}$-V relationship are depicted in Fig. 1 (*bottom*). The simulated peak $I_{Ca,L}$-V relation is comparable to the experimental data from Bénitah et al. (21), Pelzmann et al. (22), and Li et al. (23).

Formulation of I_{Kr}

The kinetics of I_{Kr} was described by Eqs. 9–14 with the activation (p_a) and inactivation (p_i) gating variables. Voltage dependences of I_{Kr} activation and inactivation in the current and original human heart models are shown in Fig. 2 (*top*), together with experimental data for comparison; the model-generated I_{Kr} during voltage-clamp pulses are also depicted. There are limited experimental data available for the gating kinetics of native I_{Kr} channels in HVMs. Nevertheless, experimentally observed activation of native I_{Kr} in human cardiac myocytes (24,25) appeared to be faster than the I_{Kr} activation simulated by the original PB formulas. To formulate I_{Kr} kinetics, the recently developed HVM models (16,17) employed the experimental data from human ether-a-go-go-related gene (HERG) channels expressed in human embryonic kidney (HEK) cells (26,27), Chinese hamster ovary cells (28), or *Xenopus* oocytes (29). However, voltage- and time-dependent kinetics of expressed HERG channels appear to depend on cell lines or conditions for expression, as well as conditions for current recordings such as temperatures, and thus may be different from those of native I_{Kr} channels in human hearts (26–28,30–32). We therefore adopted the data from HVMs of Li et al. (24) for the steady-state activation curve ($p_{a,\infty}$) and the formula of Courtemanche et al. (19) based on the data from human atrial myocytes of Wang et al. (25) for the activation time constant (τ_{pa}). We also employed the expression of Courtemanche et al. (19) for the steady-state inactivation curve ($p_{i,\infty}$). No detailed experimental data are available on the time constant of I_{Kr} inactivation (τ_{pi}) in intact HVMs. Inactivation and recovery of native I_{Kr} in animal hearts or expressed HERG channels are very rapid (28,33); thus, we assumed that I_{Kr} inactivation is instantaneous. The maximum I_{Kr} conductance (g_{Kr}) was set equal to 12 pS/pF, according to the data of Li et al. (24). With this g_{Kr} value, the complete block of I_{Kr} prolonged the action potential duration (APD) of the model HVM paced at 1 Hz by 34.6–48.9%; the simulated APD prolongation by I_{Kr} block is comparable to the experimentally observed effects of the selective I_{Kr} blocker E-4031 as reported by Li et al. (24).

Formulation of I_{Ks}

On the basis of the recent data from Li et al. (24) and Virág et al. (34), the kinetics of I_{Ks} was reformulated as Eqs. 15–18. Voltage dependences of I_{Ks} kinetics in the current and original models are shown in Fig. 2 (*bottom*), together with experimental data for comparison; the model-generated I_{Ks} during voltage-clamp pulses are also depicted. Steady-state I_{Ks} activation curve (n_∞) is from Li et al. (24). Virág et al. (34) recently reported that I_{Ks} in HVMs slowly activates and rapidly deactivates. According to their report, therefore, we reformulated the time constant of I_{Ks} activation (τ_n) as Eq. 18. The expression of E_{Ks} is the same as for the PB model. The maximum conductance (g_{Ks}) was set equal to 36 pS/pF so as to yield the APD at 90% repolarization (APD_{90}) during 1 Hz pacing of 336 ± 16 ms, as reported by Li et al. (24).

Formulation of SR Ca^{2+} release

In the original PB model, SR Ca^{2+} release kinetics was represented by the formula that explicitly contains time t and also $\Delta[Ca^{2+}]_{i,2}$, which is not

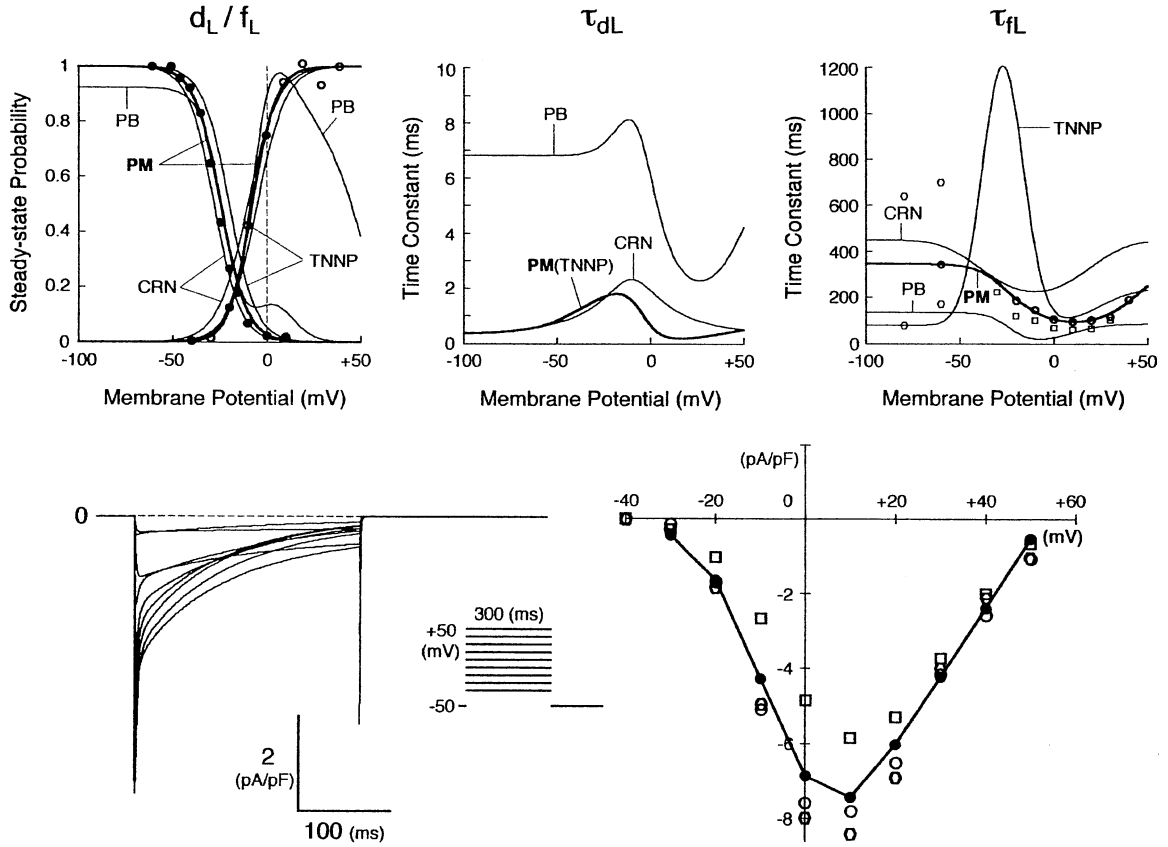


FIGURE 1 Kinetics of $I_{Ca,L}$. (*Top*) Voltage dependence of steady-state probabilities ($d_{L\infty}$, $f_{L\infty}$) and time constants for $I_{Ca,L}$ activation (τ_{dL}) and inactivation (τ_{fL}). Equations used for the current (modified) model are shown with the thick lines (labeled "PM"). For comparison, those for existing (original) models are also shown with the thin lines: PB, Priebe and Beuckelmann (15); TNNP, ten Tusscher et al. (16); CRN, Courtemanche et al. (19). The experimental data for $d_{L\infty}$, $f_{L\infty}$, and τ_{fL} are from Bénitah et al. (21) (*circles*), Pelzmann et al. (22) (*squares*), and Li et al. (23) (*hexagons*). (*Bottom*) Computed voltage-clamp records for $I_{Ca,L}$ (*left*) and peak $I_{Ca,L}$-V relationship (*right*). Currents were evoked by 300-ms step pulses from a holding potential of −50 mV to test potentials ranging from −30 to +50 mV in 10 mV increments. Simulating the whole-cell perforated-patch recording, $[Ca^{2+}]_i$ was not clamped, whereas $[Na^+]_i$ and $[K^+]_i$ were fixed at 5 and 140 mM, respectively. The experimental data for the peak $I_{Ca,L}$-V relation are from Bénitah et al. (21) (*open circles*), Pelzmann et al. (22) (*squares*), and Li et al. (23) (*hexagons*).

a state variable but the sum of net Ca^{2+} influx during the first 2 ms after initiation of the action potential (AP). Thus, the original PB model is a non-autonomous system, the vector field of which depends on time and initial conditions, not suitable for bifurcation analysis. We had therefore to renew the SR Ca^{2+} release formula to convert the model into an autonomous system. Owing to the lack of available data for updating the kinetic formulation of SR Ca^{2+} release in HVMs, we utilized simple expressions, Eqs. 47–51. The formula for conductance of the Ca^{2+} release channel (g_{rel}) was adopted from Faber and Rudy (20), with the P_{rel} value reduced to one-third of the original value to obtain the peak $[Ca^{2+}]_i$ transient of ~1 μM during APs elicited at 1 Hz. For gating behaviors of the Ca^{2+} release channel (d_R, f_R), we used the expressions similar to those for the $I_{Ca,L}$ gating variables to make the model an autonomous system suitable for bifurcation analyses.

Ion concentration homeostasis

The model also includes material balance expressions to define the temporal variation in $[Ca^{2+}]_i$, $[Na^+]_i$, and $[K^+]_i$, whereas $[Ca^{2+}]_o$, $[Na^+]_o$, and $[K^+]_o$ were fixed at 2, 140, and 5.4 mM, respectively. As pointed out by Hund et al. (35) and Krogh-Madsen et al. (36), the second-generation models incorporating ion concentration changes have two major problems: 1), drift, with very slow long-term trends in state variables; and 2), degeneracy, with nonuniqueness of steady-state solutions. The current model did not show a long-term drift in the intracellular ion concentrations but reached a steady state during pacing, as well as during BP oscillation, when the principle of charge conservation was taken into account (35).

An n-dimensional fully differential system formulated as a cardiac second-generation model can usually be converted into a differential-algebraic system composed of $n - 1$ differential equations and one algebraic equation, resulting in $n - 1$ equations for n unknowns (35,36). In such a system, the Jacobian matrix of which is singular, the EP or limit cycle is not unique but depends on initial conditions; e.g., our full system has a continuum of EPs, because Eq. 65 can be derived from Eqs. 66, 69, and 70 (see Appendix 2). Thus, second-generation models including our full system exhibit degeneracy not suitable for bifurcation analysis to be applicable to isolated equilibria. As suggested by Krogh-Madsen et al. (36), one of the ways to remove degeneracy and thus allow bifurcation analyses of isolated equilibria is to make some ionic concentrations fixed. Variations in $[K^+]_i$ during changes in parameters or stimulation rates (0.25–2 Hz) were relatively small (<5 mM), being too small to significantly alter the model cell behaviors. For stability and bifurcation analyses, therefore, $[K^+]_i$ was fixed at 140 mM. The degenerate system with the fixed $[K^+]_i$ has the finite number of EPs and limit cycles, being suitable for bifurcation analyses.

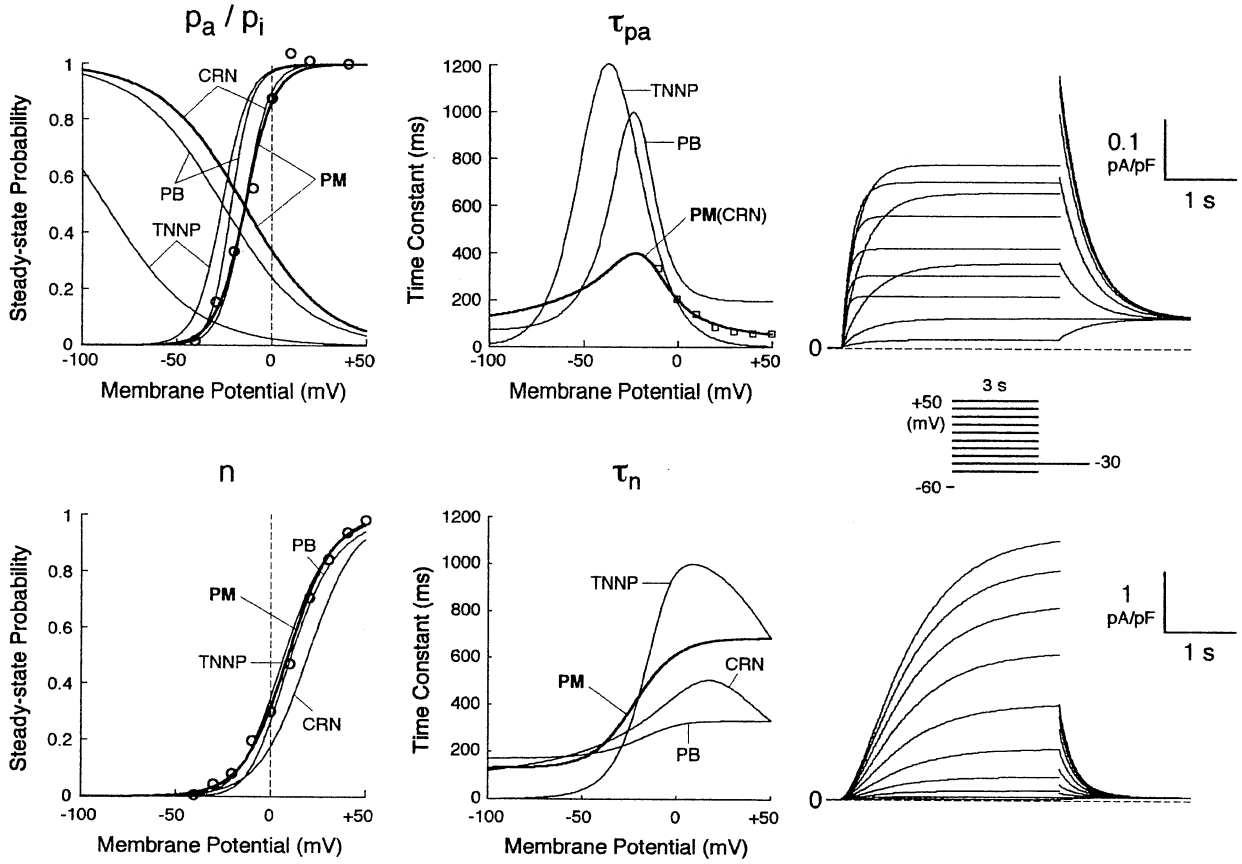


FIGURE 2 Kinetics of I_{Kr} (*top*) and I_{Ks} (*bottom*). (*Left, middle*) Voltage dependence of steady-state probabilities and time constants of I_{Kr} activation ($p_{a,\infty}$, τ_{pa}) and inactivation ($p_{i,\infty}$) as well as I_{Ks} activation (n_∞, τ_n). The thick lines are for this study (PM); the thin lines are from the existing models (PB, TNNP, CRN). The experimental data for $p_{a,\infty}$, τ_{pa}, and n_∞ are from Li et al. (24) (*circles*) and Wang et al. (25) (*squares*). (*Right*) Computed voltage-clamp records for I_{Kr} and I_{Ks}. Currents were elicited by 3-s step pulses from a holding potential of −60 mV to test potentials ranging from −50 to +50 mV in 10 mV increments.

Determination and validation of model HVM dynamics

Numerical methods for dynamic simulations of HVM behaviors

Dynamic behaviors of the model HVM were determined by solving a system of nonlinear ordinary differential equations numerically. Numerical integration, as well as bifurcation analyses, were performed on Power Macintosh G4 computers (Apple Computer, Cupertino, CA) with MATLAB 5.2 (The MathWorks, Natick, MA). We used the numerical algorithms available as MATLAB ODE solvers: 1), a fourth-order adaptive-step Runge-Kutta algorithm which includes an automatic step-size adjustment based on an error estimate (37), and 2), a variable time-step numerical differentiation approach selected for its suitability to stiff systems (38). The former (named *ode45*) is the best function for most problems. However, the latter (named *ode15s*) was much more efficient than *ode45* and both solvers usually yielded nearly identical results. Therefore, *ode15s* was usually used, and *ode45* was only sometimes used to confirm the accuracy of calculations. The maximum relative error tolerance for the integration methods was set to 1×10^{-6}.

Dynamic properties of the model HVM: simulated APs, ionic currents, and $[Ca^{2+}]_i$ dynamics

The steady-state AP, sarcolemmal currents, and $[Ca^{2+}]_i$ transient of the current model paced at 1 Hz with the standard parameter values are shown in Fig. 3 *A*. According to the report of Hund et al. (35), the stimulus current was assumed to carry K^+ ions into the cell for charge conservation. During pacing, the model cell dynamics reached a steady state, with no long-term drift in the state variables. Steady-state values of the resting potential, maximum upstroke velocity, and APD_{90} during 1 Hz pacing were −84.9 mV, 411 V/s, and 338 ms, respectively. The diastolic $[Ca^{2+}]_i$ and peak $[Ca^{2+}]_i$ transient in the model HVM paced at 1 Hz were 0.169 and 0.961 μM, respectively. The simulated AP parameters and $[Ca^{2+}]_i$ dynamics of the current and original HVM models are listed in Table 3, together with corresponding experimental data for comparison. The AP parameters and $[Ca^{2+}]_i$ dynamics of the current model appear to be in reasonable agreement with the mean experimental values recently determined for single HVMs, as well as those of the original PB and other HVM models. The values of $[Ca^{2+}]_{rel}$ and $[Ca^{2+}]_{up}$ were 0.41 mM (identical) for the resting state and 0.59–2.68 and 2.84–2.92 mM, respectively, in a steady state during 1 Hz pacing. These values are comparable to the experimental data from rat and rabbit ventricular myocytes (40,41), as well as those in the original PB model, although experimental values for HVMs are unknown.

Rate dependence of APD, $I_{Ca,L}$, $[Ca^{2+}]_i$ transients, and $[Na^+]_i$

We also tested the rate dependence of APD (dynamic restitution), as well as that of the $I_{Ca,L}$ waveform, $[Ca^{2+}]_i$ transients and $[Na^+]_i$ (Fig. 3 *B*). The steady-state values of APD_{90} at 0.5, 1, and 2 Hz were 369, 338, and 298 ms, respectively, compatible with the averaged experimental values (23,42).

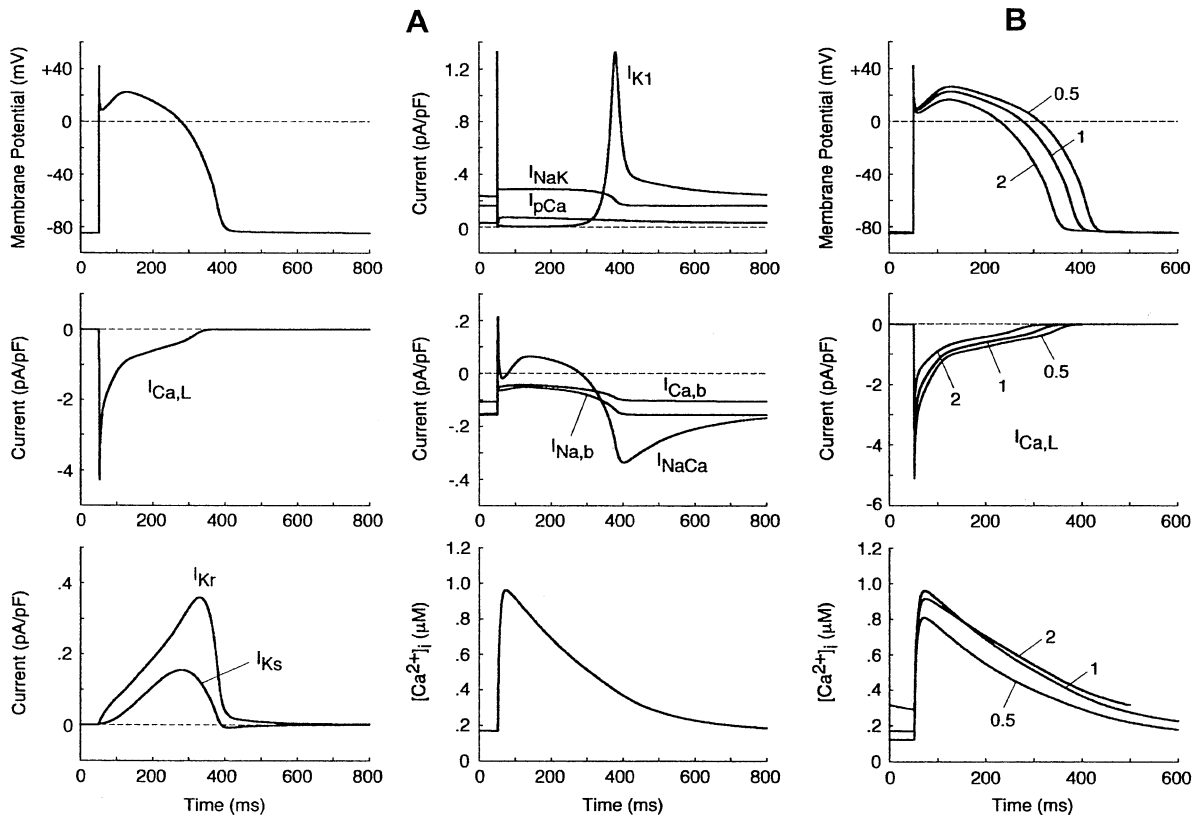


FIGURE 3 Simulated dynamics of the model HVM. (*A*) Steady-state behaviors of the AP, underlying sarcolemmal currents, and $[Ca^{2+}]_i$ transient. The model HVM was paced at 1 Hz with 1-ms stimuli of 80 pA/pF. Differential equations (Eqs. 55–64) were numerically solved for 20 min with the initial conditions appropriate to a resting state, which were determined by Eqs. 65–69 with $[K^+]_i$ fixed at 140 mM. Model cell behavior after the last stimulus (during the last AP) is depicted. (*B*) Rate dependence of APD, $I_{Ca,L}$, and $[Ca^{2+}]_i$ transients. The model HVM was paced at 0.5, 1, and 2 Hz with 1-ms stimuli of 80 pA/pF. The differential equations were numerically solved for 20 min at each pacing rate; model cell behaviors after the last stimulus are depicted.

$I_{Ca,L}$ attenuated with increasing the pacing rate as observed in the AP clamp experiment of Li et al. (23). The values of $[Na^+]_i$ during stimuli at 0 (resting state), 0.25, 0.5, 1, and 2 Hz averaged 6.14, 7.47, 8.26, 9.22, and 9.57 mM, respectively, comparable to experimental data (43,44).

The peak $[Ca^{2+}]_i$ transient predicted by the current model was a little smaller at 2 Hz than at 1 Hz. In most experiments, however, the peak $[Ca^{2+}]_i$ transient and/or developed tension increased as the pacing rate increased up to 2.5 Hz (45–47). This inconsistency may result from the lack of intracellular modulating factors such as those involved in the rate-dependent potentiation of $I_{Ca,L}$ (48,49). Alternatively, the kinetic formulation of $I_{Ca,L}$ and/or SR Ca^{2+} handling may be inappropriate. We found that the use of the τ_{fL} formula from the ten Tusscher et al. model (16) led to the successful reproduction of the rate-dependent increase in the peak $[Ca^{2+}]_i$ transient. Nevertheless, their τ_{fL} formula was not used, because it appeared not to fit the experimental data as shown in Fig. 1 and because a very large I_{Ks} (>8 times larger than the experimental values) was required to counteract the large $I_{Ca,L}$ during phase 2 (16). In the preliminary study, BP dynamics or bifurcation structures of the HVM model were not essentially altered by the use of different formulas for $I_{Ca,L}$ (τ_{fL}) or the change in the rate dependence of $[Ca^{2+}]_i$ transients.

Stability and bifurcation analyses

Constructing bifurcation diagrams

We examined how the stability and dynamics of the model cell alter with changes in bifurcation parameters and constructed bifurcation diagrams for one or two parameters. Bifurcation parameters chosen in this study were the maximum conductance of the ionic channels (g_{K1}, $g_{Ca,L}$, g_{Kr}, g_{Ks}) and amplitude of I_{NaCa} or I_{bias}; the maximum conductance and I_{NaCa} amplitude are expressed as normalized values, i.e., ratios to the control values.

In the HVM model with the fixed $[K^+]_i$, 14 state variables define a 14-dimensional state point in the 14-dimensional state space of the system. We calculated EPs and periodic orbits in the state space. An EP was determined as a point at which the vector field vanishes (i.e., $f(x) = 0$); steady-state values of the state variables were calculated by Eqs. 65–69 (see Appendix 2). Asymptotic stability of the EP was also determined by computing 14 eigenvalues of a 14 × 14 Jacobian matrix derived from the linearization of the nonlinear system around the EP (for more details, see Vinet and Roberge (7)). Periodic orbits were located with the MATLAB ODE solvers. When spontaneous oscillation (BP activity) appeared, the AP amplitude (APA) as a voltage difference between the maximum diastolic potential (MDP) and peak overshoot potential (POP), as well as the cycle length (CL), was determined for each calculation of a cycle. Numerical integration was continued until the differences in both APA and CL between the newly calculated cycle and the preceding one became $<1 \times 10^{-3}$ of the preceding APA and CL values. Potential extrema (MDP, POP) and CL of the steady-state oscillation were plotted against bifurcation parameters. When periodic behavior was irregular or unstable, model dynamics were computed for 60 s; all potential extrema and CL values were then plotted in bifurcation diagrams.

Codimension one and two bifurcations to occur in the model system were explored by constructing bifurcation diagrams with one and two parameters, respectively (10,11). For construction of one-parameter bifurcation diagrams in which values of a state variable at EPs or extrema of periodic orbits are shown as a function of one bifurcation parameter, a bifurcation parameter was systematically changed while keeping all other parameters at their

TABLE 3 AP parameters and $[Ca^{2+}]_i$ dynamics for single HVMs paced at 1 Hz: model-generated values and experimentally observed values

	$[Ca^{2+}]_o$ (mM)	$[K^+]_o$ (mM)	$[Na^+]_i$* (mM)	RP (mV)	V_{max} (V/s)	APD_{90} (ms)	$[Ca^{2+}]_{i,r}$† (nM)	$\Delta[Ca^{2+}]_i$ (nM)
Model values	2.0	4.0	10	−91.2	385	357	200	900
Priebe-Beuckelmann (15)‡	2.0	4.0	10	−90.2	386	357	400	0
Bernus et al. (18)	2.0	4.0	10	−90.4	369	333	119	784
Sachse et al. (39)	2.0	5.4	>11.5	−87.3	288	276	70	930
Ten Tusscher et al. (16)	2.0	4.0	9.80	−90.7	350	322	68	797
Iyer et al. (17)	2.0	5.4	9.18	−84.9	411	338	169	792
Current (modified) model								
Experimental values								
Peeters et al. (90)	1.2	4.0		−84 ± 6		381 ± 94		
Li et al. (24)	1.0	5.4	10	−83 ± 3		336 ± 16		
Li et al. (42)	2.0	5.4	10	−82 ± 2		298 ± 17		
Péréon et al. (91), epicardium	2.7	4.0		−86 ± 1	196 ± 20	324 ± 19		
Péréon et al. (91), midmyocardium	2.7	4.0		−86 ± 1	446 ± 46	432 ± 19		
Piacentino et al. (92)	1.0	5.4	12.5				153 ± 20	804 ± 197

*The steady-state mean $[Na^+]_i$ values during 1 Hz pacing are shown for the TNNP (16), Iyer et al. (17), and the current model; the resting state or fixed value is shown for others. The experimental values were for the perforated- or ruptured-patch recording. A $[Na^+]_i$ value was unknown (not shown) when the conventional microelectrode method was used.

†Minimum $[Ca^{2+}]_i$ values during the diastolic phase, i.e., $[Ca^{2+}]_i$ values at the end of phase 4.

‡Data for AP parameters are from Table 3 of Bernus et al. (18). The values of $[Ca^{2+}]_{i,r}$ (200) and $\Delta[Ca^{2+}]_i$ (900) are only approximations from the original figures.

Abbreviations: RP, resting potential; V_{max}, maximum upstroke velocity.

standard values. The membrane potential (V) at EPs (steady-state branches) and local potential extrema of periodic orbits (periodic branches) were determined and plotted for each value of the bifurcation parameter. The saddle-node bifurcation point at which two EPs coalesce and disappear was determined as a point at which the steady-state current-voltage (I/V) curve and zero-current axis come in touch with each other. The Hopf bifurcation point at which the stability of an EP reverses was also detected by the stability analysis as described above. For construction of two-parameter bifurcation diagrams in which codimension one bifurcation points are plotted in a parameter plane, the secondary parameter was systematically changed with the primary parameter fixed at various different values. The path of saddle-node and Hopf bifurcation points was traced in the parameter plane; i.e., bifurcation values for the secondary parameter were plotted as a function of the primary parameter.

Definition and evaluation of structural stability for the BP system

We also evaluated the structural stability of the BP system, which is defined as the robustness of pacemaker activity to various interventions or modifications that may cause a bifurcation to quiescence or irregular dynamics (11). Interventions or modifications leading to quiescence or irregular dynamics include injections of I_{bias}, electrotonic loads of normal HVMs, current leakage via myocardial injury, and intrinsic changes in channel conductance or gating kinetics. In this study, the structural stability of the BP system was tested for hyperpolarizing and depolarizing loads by exploring bifurcation structures during applications of I_{bias}.

The way of evaluating the structural stability to I_{bias} is essentially the same as in our previous study for the SA node pacemaker (11). Changes in V_0 and its stability with I_{bias} applications were depicted as the I_{bias}-V_0 curve (for more details, see Fig. 1 of Kurata et al. (11)). There are one or two Hopf bifurcation points and two saddle-node bifurcation points corresponding to the current exrema in the I_{bias}-V_0 curve. In the unstable I_{bias} region between two Hopf (or a Hopf and saddle-node) bifurcation points, the system has an unstable EP only, usually exhibiting stable limit cycles without annihilation (6,8). When the system removes to the stable I_{bias} region, it would come to rest at the stable EP via gradual decline of limit cycles, annihilation, or irregular dynamics, as reported by Guevara and Jongsma (8). Note that *system A* is considered structurally more stable than *system B* when the amplitude of I_{bias} required for stabilizing an EP or causing a bifurcation to quiescence is greater in *system A* than in *system B* (11). Thus, the larger the unstable I_{bias} range over which limit cycles continue is, the more structurally stable the system is.

The Hopf and saddle-node bifurcation points, as well as the control V_0 at $I_{bias} = 0$, in the I_{bias}-V_0 curve were determined as functions of bifurcation parameters and plotted on both the potential and current coordinates, as in previous studies (7,11). Exploring how the unstable V_0 and I_{bias} regions change with decreasing or increasing the sarcolemmal currents would enable us to determine the contribution of each current to the structural stability of the BP system to hyperpolarizing or depolarizing loads, as well as to EP instability itself, which is evaluated by positive real parts of eigenvalues of Jacobian matrices (see Fig. 4 of Kurata et al. (11)).

Definitions of terms specific to nonlinear dynamics and bifurcation theory

Autonomous system

An nth-order "autonomous" continuous-time dynamical system is defined by the state equation $d\boldsymbol{x}/dt = \boldsymbol{f}(\boldsymbol{x})$, where the vector field $\boldsymbol{f}$, a smooth function of the state variable $\boldsymbol{x} = \boldsymbol{x}(t)$, does not depend on time, but depends only on the state variable $\boldsymbol{x}$ (13).

Nonautonomous system

An nth-order "nonautonomous" continuous-time dynamical system is defined by the state equation $d\boldsymbol{x}/dt = \boldsymbol{f}(\boldsymbol{x}, t)$, where the vector field $\boldsymbol{f}$ depends on time, i.e., explicitly contains time t (13).

EP

A time-independent steady-state point at which the vector field vanishes (i.e., $d\boldsymbol{x}/dt = 0$) in the state space of an autonomous system, constructing the steady-state branch in one-parameter bifurcation diagrams. This state point corresponds to the zero-current crossing in the steady-state I/V curve, i.e., a quiescent state of a cell if it is stable.

Periodic orbit

A closed trajectory in the state space of a system, constructing the periodic branch in one-parameter bifurcation diagrams.

Limit cycle

A periodic limit set onto which a trajectory is asymptotically attracted in an autonomous system. A stable limit cycle corresponds to an oscillatory state, i.e., pacemaker activity, of a cell.

Bifurcation

A qualitative change in a solution of differential equations caused by altering parameters, e.g., a change in the number of EPs or periodic orbits, a change in the stability of an EP or periodic orbit, and a transition from a periodic to quiescent state. Bifurcation phenomena we can see in cardiac myocytes include a generation or cessation of pacemaker activity and occurrence of irregular dynamics such as skipped-beat runs and early afterdepolarizations.

Hopf bifurcation

This is a bifurcation at which the stability of an EP reverses with emergence or disappearance of a limit cycle, occurring when eigenvalues of a Jacobian matrix for the EP have a single complex conjugate pair and its real part reverses the sign through zero.

Saddle-node bifurcation

This is a bifurcation at which two EPs (steady-state branches) or two periodic solutions (periodic branches) emerge or disappear. The saddle-node bifurcation of EPs occurs when one of eigenvalues of a Jacobian matrix is zero.

Codimension

The codimension of a bifurcation is the minimum dimension of the parameter space in which the bifurcation may occur in a persistent way (12,50). In other words, the codimension is the number of independent conditions determining the bifurcation (14). A bifurcation with codimension one is a point in one-parameter bifurcation diagrams such as Fig. 6 or a line in two-parameter bifurcation diagrams such as Fig. 7, whereas a bifurcation with codimension two is a point in the two-parameter space.

RESULTS

BP generation in I_{K1}-downregulated HVM

BP activity appears in model HVM during I_{K1} suppression

We first examined whether I_{K1} downregulation leads to BP generation in the model HVM by decreasing g_{K1} at an interval of 0.01 (1%). Spontaneous oscillations (BP activity) abruptly appeared when g_{K1} was reduced to 0.15 (15%). Fig. 4 shows the simulated BP activity of the I_{K1}-downregulated HVM with g_{K1} of 0.15 or 0, depicting the membrane potential oscillations, underlying sarcolemmal currents, and $[Ca^{2+}]_i$ transients in steady state. The values of MDP, POP, APA, CL, and maximum upstroke velocity were determined for the BP oscillations at each g_{K1} value. The simulated AP parameters are listed in Table 4, together with the data from the guinea pig ventricle (3) and rabbit SA node (51) models, as well as from real BP systems (1,52), for comparison. The average $[Na^+]_i$ during the BP oscillations at g_{K1} of 0.15 and 0 were 6.55 and 6.42 mM, respectively. Decreasing g_{K1} caused the decrease of

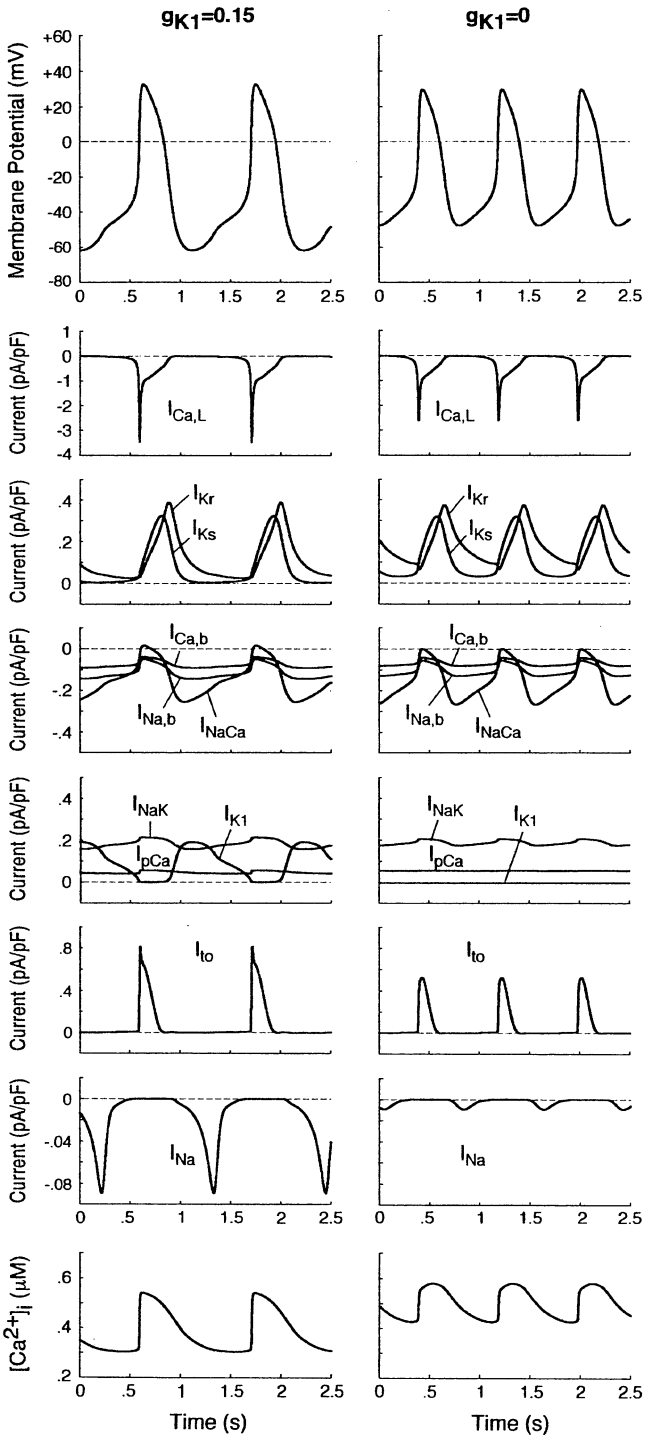


FIGURE 4 Simulated steady-state BP activities (spontaneous APs, ionic currents, and $[Ca^{2+}]_i$ dynamics) in the model HVM at $g_{K1} = 0.15$ (*left*) and 0 (*right*). Differential equations (Eqs. 55–63) were numerically solved for 20 min at each g_{K1} with initial conditions appropriate to an EP and a 1-ms stimulus of 1 pA/pF for triggering an AP; model cell behaviors during the last 2.5 s starting from MDP are depicted. Note the differences in the ordinate scales for individual currents.

TABLE 4 AP parameters for pacemaker systems: Model-generated values and experimental values

	Normalized g_{K1}	MDP (mV)	POP (mV)	APA (mV)	CL (ms)	V_{max} (V × s^{-1})
Model values						
Silva and Rudy (3)*	0.19	−67.3			594	15
	0				366	
This study	0.15	−61.9	+32.7	94.7	1117	3.2
	0.10	−54.3	+31.6	86.0	938	2.8
	0	−47.9	+29.8	77.7	795	2.3
Kurata et al. (51)†	0	−58.6	+16.6	75.2	308	6.4
Experimental values						
Miake et al. (1)*	0.20	−60.7			600	
Plotnikov et al. (52)‡					1091	

*Data from the model and real guinea pig ventricular myocytes.
†Primary pacemaker model for the rabbit SA node.
‡Data for Purkinje myocytes expressing I_h (HCN2) in the canine left ventricle.

APA with depolarization of MDP, decrease of CL, increase of $[Ca^{2+}]_i$, and decrease of $[Na^+]_i$. Consistent with the result from the guinea pig ventricular model (3), I_{NaCa} was the dominant inward current during phase 4 depolarization in the HVM pacemaking. In contrast, $I_{Ca,L}$ was very small during the early phase of the depolarization, although predominantly contributing to phase 0 upstroke. I_{Na} was also very small due to the voltage-dependent inactivation.

Ionic basis of phase 4 depolarization in simulated BP activity

Before investigating the dynamical mechanisms of BP generation via bifurcation analyses of the HVM model, we examined the ionic basis of phase 4 depolarization of the BP activity. The contributions of I_{Kr} and I_{Ks} deactivation, as well as individual inward currents ($I_{Ca,L}$, I_{Na}, I_{NaCa}, $I_{Na,b}$, $I_{Ca,b}$), to the pacemaker depolarization were assessed by the conventional freezing and blocking methods (53–55). Phase 4 depolarization of the I_{K1}-reduced BP system disappeared on clamping I_{Kr} deactivation (gating variable p_a) at the time of MDP, but not on clamping I_{Ks} deactivation (gating variable n). Thus, the g_{Kr}-decay theory for the natural SA node pacemaker (53–55) appears to be applicable to the HVM pacemaker as well. Removal of $I_{Ca,L}$ at the time of MDP little altered the initial phase of pacemaker depolarization, although reducing the rate of the later phase depolarization with cessation of BP activity. Eliminating I_{Na} did not significantly affect BP oscillations. Furthermore, in the I_{K1}-removed system, eliminating I_{NaCa} (the most dominant pacemaker current) at the MDP abolished phase 4 depolarization, leading to cessation of BP activity, whereas the removal of $I_{Na,b}$ (the second dominant pacemaker current) or $I_{Ca,b}$ only reduced the depolarization rate.

Bifurcation structure of HVM system during I_{K1} suppression

BP activity abruptly appears around unstable EP via saddle-node bifurcation

To elucidate the dynamical mechanisms of BP generation, we explored EP stability, dynamics, and bifurcation structures of the HVM system during I_{K1} suppression by constructing bifurcation diagrams for g_{K1}. As shown in Fig. 5, the zero-current potential in the steady-state I/V curve, as well as steady-state $[Ca^{2+}]_i$ and $[Na^+]_i$, was plotted as a function of g_{K1}; when BP activity appeared, AP parameters (MDP, POP, CL), extrema of $[Ca^{2+}]_i$, and average $[Na^+]_i$ were also plotted. There are three EPs corresponding to the zero-current crossings of the I/V curve in the state space of the system at $g_{K1} = 1$ (denoted as EP1, EP2, and EP3). The stability analysis revealed that EP1 with the most depolarized potential as well as EP2 is unstable, whereas EP3 with the most negative potential corresponding to the resting state is stable. The zero-current potential at EP3 positively shifted with decreasing g_{K1}; the stable EP3 (and EP2) disappeared via a saddle-node bifurcation when g_{K1} reduced to 0.154. After the bifurcation, the system has only one EP at depolarized potentials (EP1), which is always unstable, not stabilized during g_{K1} decreases. Limit cycles (BP oscillations) abruptly emerged around the unstable EP1 on occurrence of the saddle-node bifurcation, with APA and CL gradually decreasing during further reductions in g_{K1}.

Decrease in $[Na^+]_i$ accelerates BP generation

The steady-state $[Na^+]_i$, 6.14 mM in the control resting state (at $g_{K1} = 1$), reduced as g_{K1} decreased, reaching 4.64 mM just before the saddle-node bifurcation at $g_{K1} = 0.154$ (see Fig. 5, *right bottom*). This reduction in $[Na^+]_i$ during I_{K1} suppression was due to the enhancement of Na^+ efflux via the Na^+-K^+ pump, as well as decrease of Na^+ influx via the Na^+/Ca^{2+} exchanger and $I_{Na,b}$, with resting potential depolarization. To determine how the $[Na^+]_i$ decrease affects BP generation, we constructed bifurcation diagrams for g_{K1} using the reduced system with $[Na^+]_i$ fixed at the control value of 6.14 mM or critical value of 4.64 mM (data not shown). The critical g_{K1} at which BP activity emerges via a saddle-node bifurcation was larger in the system with the reduced $[Na^+]_i$ of 4.64 mM (0.153) than with the control $[Na^+]_i$ of 6.14 mM (0.117), suggesting that the $[Na^+]_i$ reduction facilitates BP generation during I_{K1} suppression.

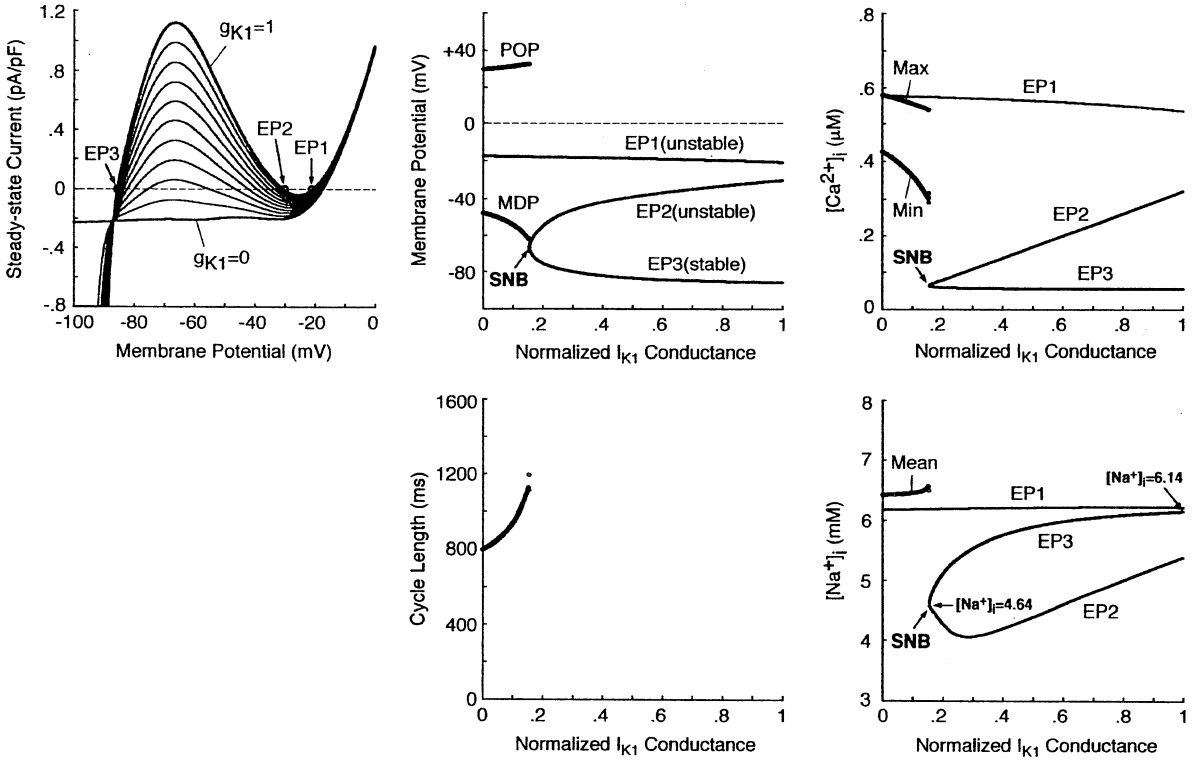


FIGURE 5 Bifurcation structure of the model HVM during g_{K1} decreases. (*Left*) Steady-state I/V relations for $g_{K1} = 0 - 1$, depicted at an interval of 0.1 with $[K^+]_i$ fixed at 140 mM. The zero-current crossings, corresponding to EPs, are designated by EP1, EP2, and EP3. (*Middle*) A bifurcation diagram for g_{K1} with the steady-state (*EP1–3*) and stable periodic (*MDP, POP*) branches (*top*), and CL plotted as a function of g_{K1} (*bottom*). EPs were determined by the algebraic equations (Eqs. 65–69). The model cell dynamics were computed by numerically solving the differential equations (Eqs. 55–63) for 10 min at each g_{K1}, which was reduced at an interval of 0.001, with the initial $[Na^+]_i$ at $g_{K1} = 1$ set equal to 6.14 mM. The saddle-node bifurcation point at which EP2 and EP3 merge together and disappear is located (labeled *SNB* at $g_{K1} = 0.154$). (*Right*) Steady-state $[Ca^{2+}]_i$ (*top*) and $[Na^+]_i$ (*bottom*) at EPs as functions of g_{K1}. The minimum (*Min*) and maximum (*Max*) of $[Ca^{2+}]_i$, as well as average $[Na^+]_i$, during the BP oscillations are also plotted. Note that the steady-state $[Na^+]_i$ at EP3 reduces with decreasing g_{K1}.

Ionic bases of EP instability and BP generation in I_{K1}-downregulated HVM

Instability of the EP at depolarized potentials (EP1) appears to be essentially important for BP generation. To elucidate the ionic mechanisms of EP instability and BP generation, therefore, we further explored how modulating individual sarcolemmal currents or $[Ca^{2+}]_i$ transients affects EP stability, oscillation dynamics, and bifurcation structures of the BP system. We focused on $I_{Ca,L}$, I_K, and I_{NaCa}, which appear to be essentially important for BP generation.

Influences of blocking $I_{Ca,L}$ or I_K on stability and dynamics of the BP system

Fig. 6 shows the effects of reducing the maximum conductance of $I_{Ca,L}$ ($g_{Ca,L}$), I_{Kr} (g_{Kr}), or I_{Ks} (g_{Ks}) on EP stability and BP dynamics of the I_{K1}-removed system. The zero-current potential (EP1) negatively shifted with decreasing $g_{Ca,L}$; the EP became stable via a Hopf bifurcation when $g_{Ca,L}$ was reduced by 86.6%. During the $g_{Ca,L}$ decreases, a limit cycle (BP oscillation) gradually contracted in size and finally disappeared at the Hopf bifurcation point. In contrast, a Hopf bifurcation to abolish BP activity did not occur during decreases in g_{Kr} or g_{Ks}, although APA significantly reduced with decreasing g_{Kr}. Spontaneous oscillation continued even when I_{Kr} or I_{Ks} was completely blocked, whereas it was abolished by eliminating both I_{Kr} and I_{Ks}.

As shown in Fig. 7, we also examined the effects of blocking $I_{Ca,L}$, I_{Kr}, or I_{Ks} on the unstable V_0 and I_{bias} regions in the I_{bias}-V_0 curve for further clarifying the contributions of the individual currents to EP instability and structural stability to depolarizing or hyperpolarizing loads of the BP system. Hopf and saddle-node bifurcation points in the I_{bias}-V_0 curve determined with decreasing conductance values were plotted on the potential and current coordinates to display how blocking each current shrinks the unstable ranges where BP oscillations occur (for more details, see Theory and Methods). The more prominent shrinkage in the unstable V_0 region is, the greater the contribution of the current to EP instability is; the more prominent shrinkage in the unstable I_{bias} region is, the greater the contribution to the robustness to depolarizing or hyperpolarizing loads is. The unstable regions, shrinking with decreases in $g_{Ca,L}$, disappeared via a codimension two saddle-node bifurcation at

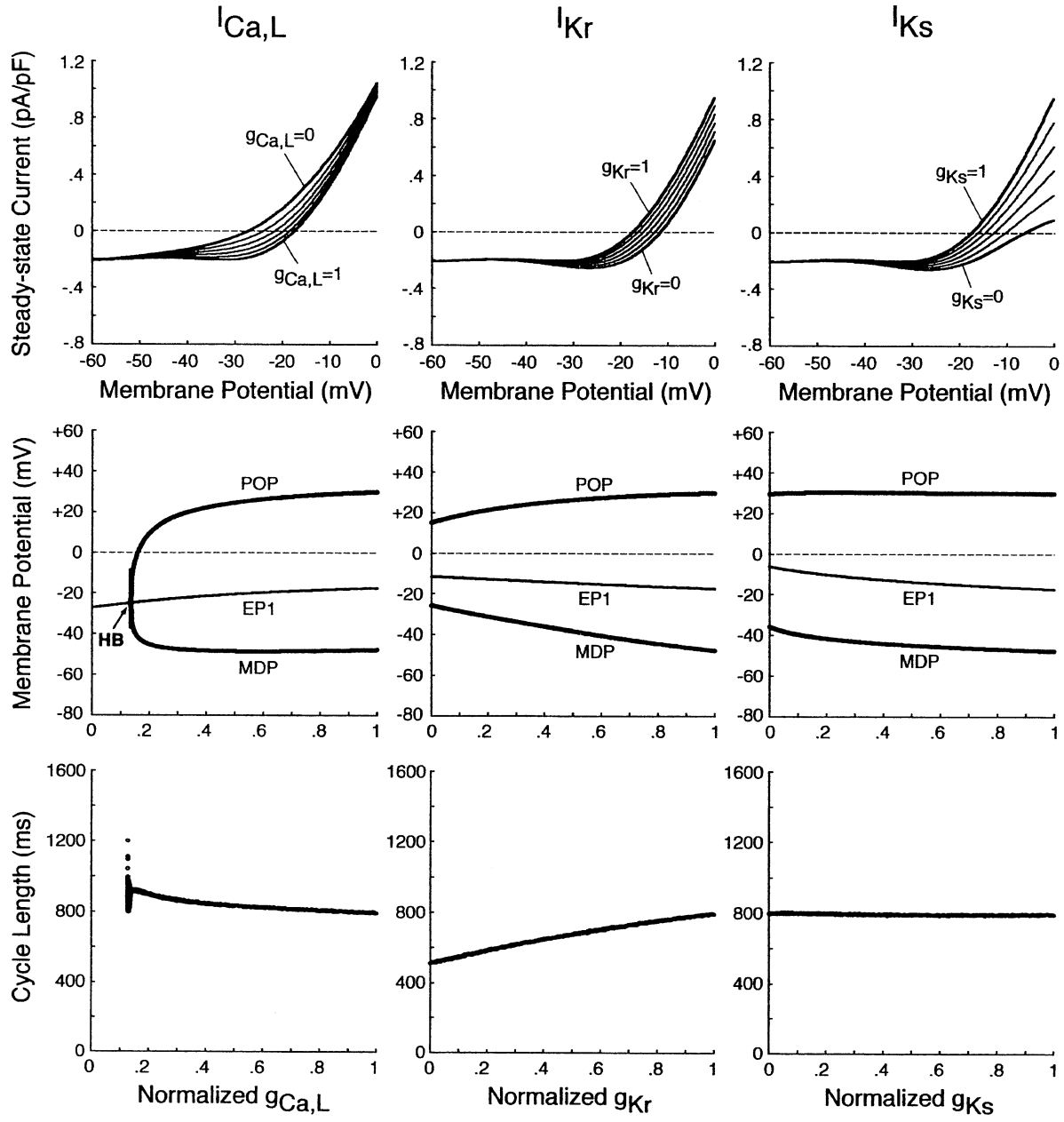


FIGURE 6 EP stability and BP dynamics of the I_{K1}-removed system during inhibition of $I_{Ca,L}$, I_{Kr}, or I_{Ks}. (*Top*) Steady-state I/V relations for $g_{Ca,L} = 0 - 1$ (*left*), $g_{Kr} = 0 - 1$ (*middle*), and $g_{Ks} = 0 - 1$ (*right*), depicted at an interval of 0.2. (*Middle, bottom*) Bifurcation diagrams with the steady-state (*EP1*) and stable periodic (*MDP, POP*) branches (*middle*), as well as CL (*bottom*), are shown as functions of $g_{Ca,L}$, g_{Kr}, or g_{Ks}, which was reduced at an interval of 0.001. The differential equations were numerically solved for 2–3 min at each conductance value. A Hopf bifurcation occurred at $g_{Ca,L} = 0.134$ (labeled *HB*), with the loci of MDP and POP converging at the bifurcation point.

a 87.4% reduction of $g_{Ca,L}$. Pacemaker activity never appeared in the system with $g_{Ca,L}$ reduced to less than the saddle-node bifurcation value. In contrast, reducing g_{Kr} or g_{Ks} little affected the unstable V_0 range, eigenvalues of Jacobian matrices at V_0 being not significantly altered. The unstable I_{bias} region shrunk with decreasing g_{Kr} or g_{Ks}, though it did not disappear even when I_{Kr} or I_{Ks} was completely blocked; the robustness to depolarizing I_{bias} was attenuated by decreasing g_{Kr} or g_{Ks}.

Effects of incorporating various K^+ currents on stability and automaticity of an I_K-removed system

The results shown in Figs. 6 and 7 suggest that I_{Kr} or I_{Ks} contributes little to the instability of the EP leading to the generation of spontaneous oscillations. To elucidate the roles of I_{Kr} and I_{Ks} in the HVM pacemaking, we tested how the stability and dynamics of the reduced BP system not including either I_{Kr} or I_{Ks} are affected by incorporating different K^+ currents. Both I_{Kr} and I_{Ks} were first removed from the

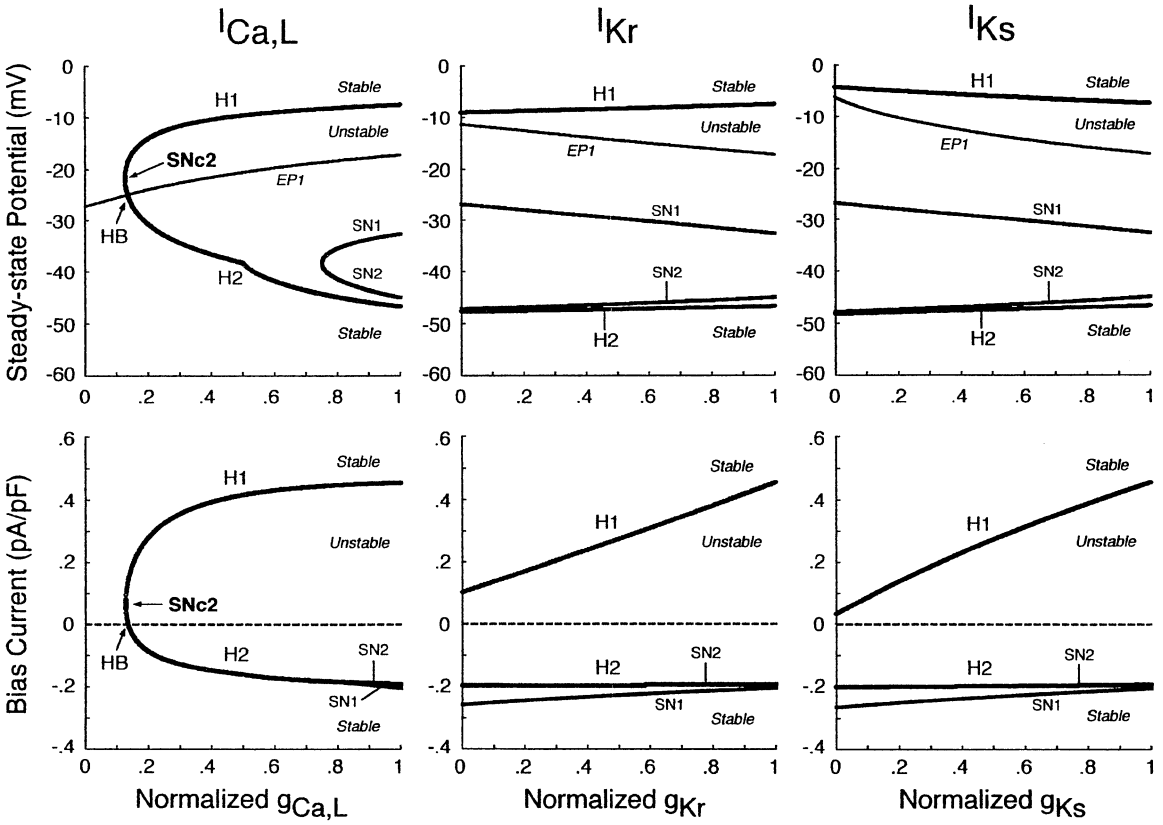


FIGURE 7 Changes in the unstable regions of the I_{bias}-V_0 curve during inhibition of $I_{Ca,L}$, I_{Kr}, or I_{Ks}. Displacements of Hopf (*H1*, *H2*) and saddle-node (*SN1*, *SN2*) bifurcation points in the I_{bias}-V_0 curve with decreasing $g_{Ca,L}$, g_{Kr}, or g_{Ks} at an interval of 0.001 are shown for the I_{K1}-removed BP system. Values of V_0 and I_{bias} at the bifurcation points were plotted on the potential (*top*) and current (*bottom*) coordinates, respectively, as functions of the conductance. The path of the control V_0 at $I_{bias} = 0$ (i.e., *EP1* in Fig. 6) is also shown on the potential coordinates, intersecting the locus of H2 at $g_{Ca,L} = 0.134$ (labeled *HB*). Note that the unstable region exists between H1 and H2 (or *H1* and *SN2*), where spontaneous oscillations occur. A codimension two saddle-node bifurcation at which the loci of H1 and H2 merge together, i.e., the unstable region disappears occurred at $g_{Ca,L} = 0.126$ (labeled *SNc2*).

standard I_{K1}-eliminated BP system, and the background K^+ current of linear I/V relation ($I_{K,b}$) or the original I_{Kr} or I_{Ks} (one of the three) was then incorporated. Eliminating both I_{Kr} and I_{Ks} abolished BP activity, with the model cell coming to a rest at a stable zero-current potential of +16.15 mV. Fig. 8 shows how EP stability and automaticity of the reduced system change with increasing the K^+ current conductance up to 10–50 pS/pF. As the K^+ conductance increased, the zero-current potential was negatively shifted and eventually destabilized via a Hopf bifurcation, with limit cycles emerging at the bifurcation. It should be noted that all the K^+ currents, including $I_{K,b}$, could individually create an unstable EP and induce spontaneous oscillations. However, $I_{K,b}$, the effect of which was very similar to the electrotonic influence of the adjacent normal HVM in a coupled-cell system (data not shown), produced the oscillation of relatively small amplitude and low upstroke velocity, as well as unstable CL and irregular dynamics. The $I_{K,b}$ conductance ($g_{K,b}$) range where an EP is unstable and spontaneous oscillations occur was very limited, with further increases in $g_{K,b}$ leading to quiescence via emergence of a stable EP. In contrast, I_{Kr} could yield the large amplitude oscillation with relatively high upstroke velocity and stable CL; however, I_{Kr} caused irregular dynamics at higher g_{Kr} values (>31.5 pS/pF), whereas I_{Ks} did not.

We further examined how incorporating the K^+ currents affects the structural stability of the reduced model to depolarizing or hyperpolarizing loads. The unstable regions in the I_{bias}-V_0 curve were determined for individual K^+ currents with the conductance increased up to 50 pS/pF (data not shown). Note that the structural stability to hyperpolarizing or depolarizing loads is considered as improved when the unstable I_{bias} region is enlarged, i.e., when larger I_{bias} is required to cause a bifurcation to quiescence. The results are summarized as follows: 1), Increasing I_{Kr} (g_{Kr}) continuously enlarged the unstable I_{bias} region, sufficiently improving the structural stability to depolarizing I_{bias}; 2), I_{Ks} could also enlarge the unstable I_{bias} region, but did not improve the structural stability as efficiently as I_{Kr}; and 3), $I_{K,b}$ could not enlarge the I_{bias} region of instability; with increasing $g_{K,b}$, the unstable regions shrunk and finally disappeared via a codimension two saddle-node bifurcation. These findings are essentially the same as those reported for the SA node pacemaker (see Fig. 9 of Kurata et al. (11)).

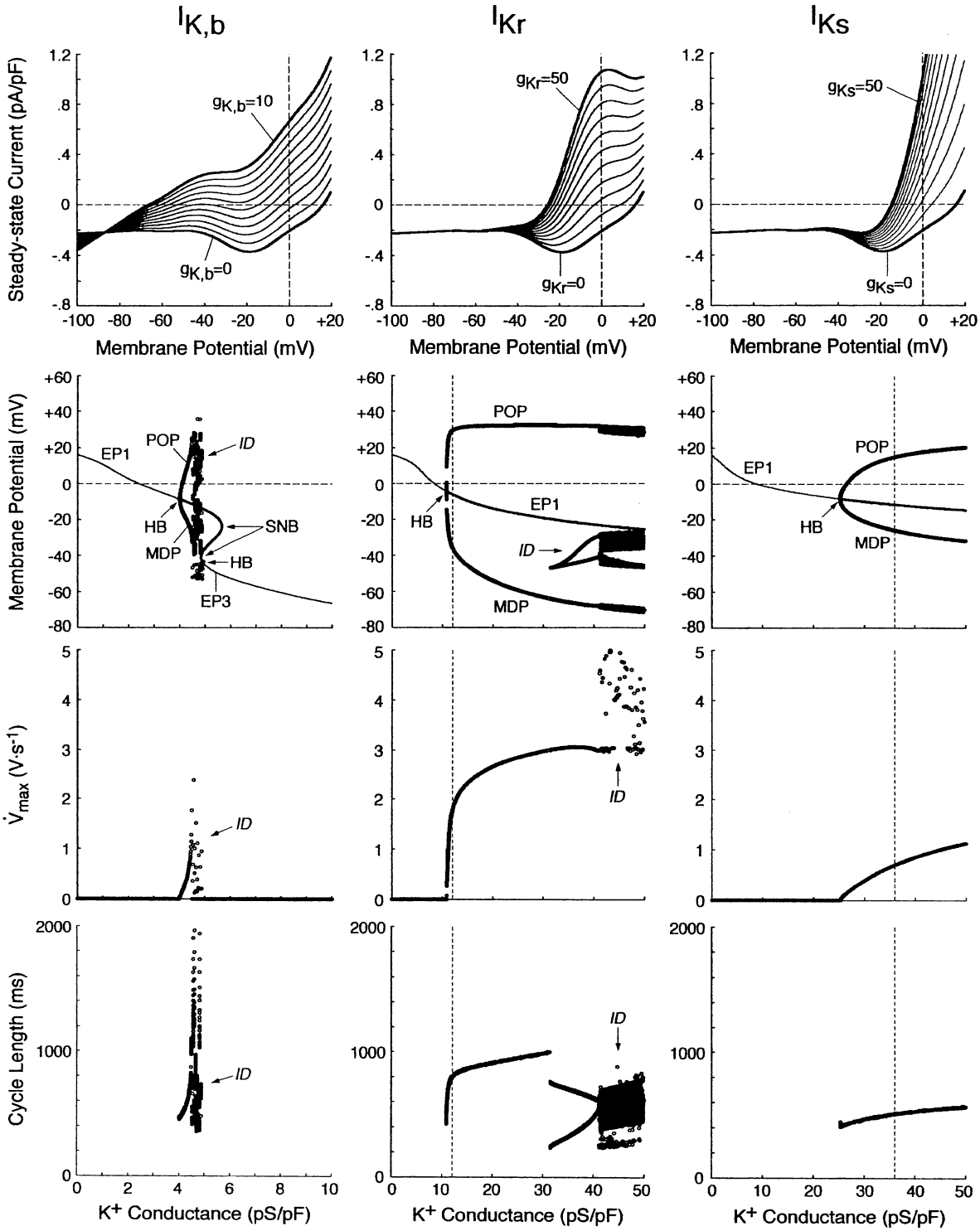


FIGURE 8 Effects of incorporating various K^+ currents with different kinetics ($I_{K,b}$, I_{Kr}, or I_{Ks}) on EP stability and dynamics of the I_K-removed model cell ($g_{K1} = 0$). (*Top*) Steady-state I/V relations for $g_{K,b} = 0$–10 pS/pF (*left*), $g_{Kr} = 0$–50 pS/pF (*middle*), and $g_{Ks} = 0$–50 pS/pF (*right*), depicted at an interval of 1 or 5 pS/pF. (*Middle, bottom*) Oscillatory behaviors, as well as zero-current potentials and their stability, of the model system, calculated during increases in $g_{K,b}$, g_{Kr}, or g_{Ks} at an interval of 0.01–0.1 pS/pF. Bifurcation diagrams with the steady-state (*EP1–3*) and periodic (*MDP*, *POP*) branches, as well as Hopf bifurcation (*HB*) and saddle-node bifurcation (*SNB*) points, were constructed for $g_{K,b}$, g_{Kr}, or g_{Ks} (*middle*). Maximum upstroke velocity (V_{max}) and CL of the potential oscillations were also plotted against $g_{K,b}$, g_{Kr}, or g_{Ks} (*bottom*). The vertical lines for I_{Kr} and I_{Ks} represent the standard values of g_{Kr} (12 pS/pF) and g_{Ks} (36 pS/pF). The symbol "*ID*" designates the irregular dynamics.

Influences of blocking I_{NaCa} or $[Ca^{2+}]_i$ transients on the stability and dynamics of the BP system

SR Ca^{2+} release, $[Ca^{2+}]_i$ transients, and activation of I_{NaCa} possibly play an important role in the generation and regulation of BP activity; as in the guinea pig ventricular pacemaking (3), I_{NaCa} was the dominant pacemaker current in the HVM pacemaking (Fig. 4). We therefore assessed the contributions of I_{NaCa} and $[Ca^{2+}]_i$ transients (SR Ca^{2+} release) to the EP instability and oscillation dynamics of the BP system by decreasing I_{NaCa} and/or clamping $[Ca^{2+}]_i$. As shown in Fig. 9 (*left*), BP oscillation ceased via a Hopf bifurcation when I_{NaCa} was reduced by 99.44% in the

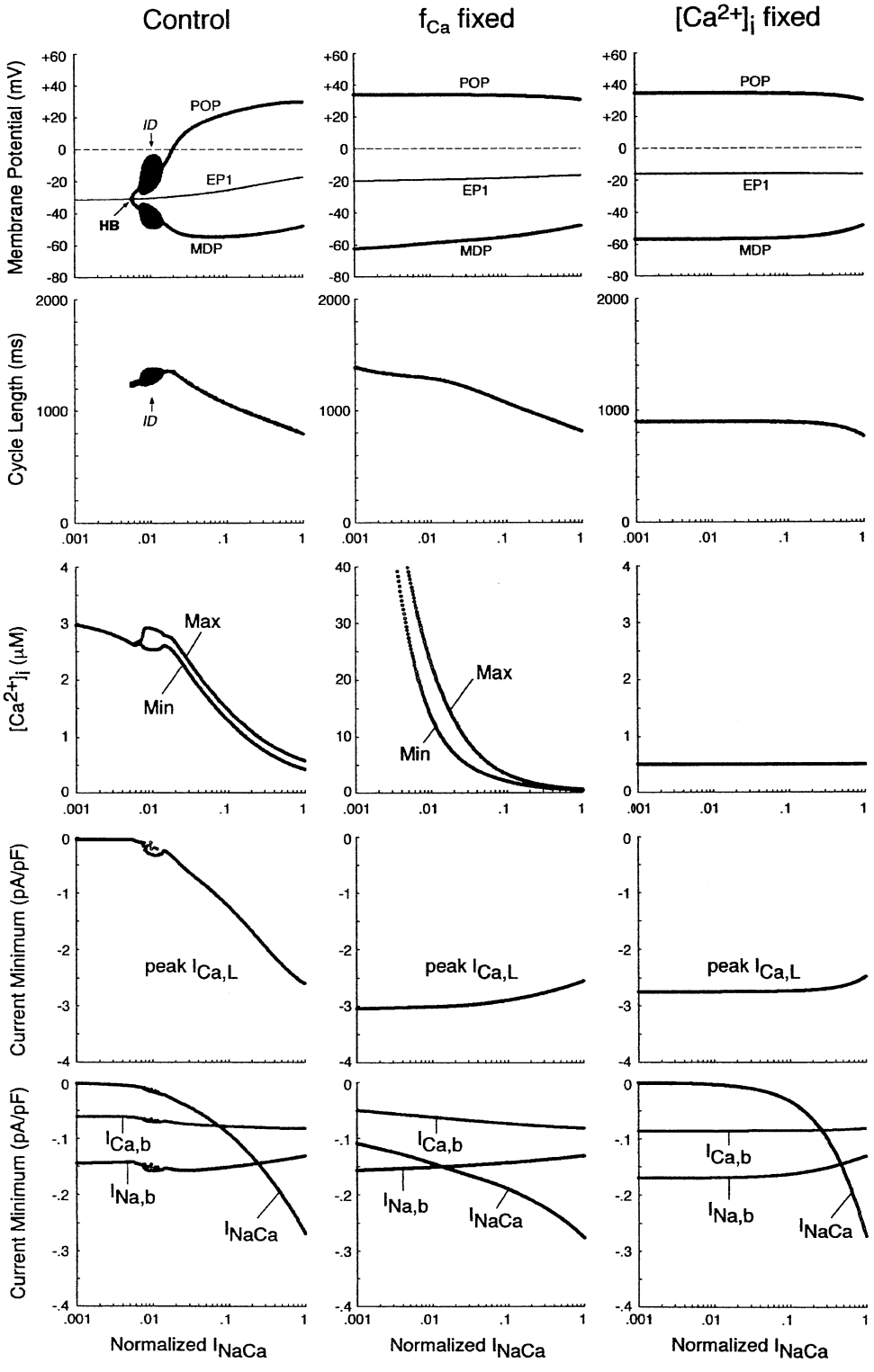


FIGURE 9 EP stability and BP dynamics of the I_{K1}-removed system during I_{NaCa} inhibition, determined for the unmodified system (*left*) and the modified system in which f_{Ca} was fixed at 0.412, the value for $[Ca^{2+}]_i$ = 0.5 μM (*middle*), or $[Ca^{2+}]_i$ itself was fixed at 0.5 μM (*right*). The amplitude of I_{NaCa} as a ratio to the control value was decreased from 1 (control) to 0.001 (0.1%); practically, the log(I_{NaCa}) value was reduced from 0 (I_{NaCa} = 1) to −3 (I_{NaCa} = 1 × 10^{-3}) at an interval of 0.01. The zero-current potential (*EP1*) and BP dynamics (*MDP*, *POP*, *CL*), as well as the minimum (*Min*) and maximum (*Max*) of $[Ca^{2+}]_i$ and minimum values of the inward currents ($I_{Ca,L}$, I_{NaCa}, $I_{Na,b}$, $I_{Ca,b}$), are plotted as functions of log(I_{NaCa}). Note that a Hopf bifurcation to abolish BP activity occurred only in the unmodified system (HB at I_{NaCa} = 0.0056).

I_{K1}-removed system. However, this may be due to the Ca^{2+}-dependent inactivation of $I_{Ca,L}$ after the induction of Ca^{2+}-overload conditions, rather than the decrease of I_{NaCa} itself. Therefore, we further tested the stability and dynamics during I_{NaCa} inhibition of the modified BP system for which $[Ca^{2+}]_i$ or Ca^{2+}-dependent $I_{Ca,L}$ inactivation (f_{Ca}) was fixed at a control value. In the modified systems, inhibition of I_{NaCa} caused neither EP stabilization nor BP cessation, with $I_{Ca,L}$ being not attenuated, although I_{NaCa} was still the dominant pacemaker current in control (Fig. 9, *middle, right*). Eliminating $[Ca^{2+}]_i$ transients or blocking SR Ca^{2+} release little altered BP dynamics.

We also examined the contributions of I_{NaCa} or $[Ca^{2+}]_i$ dynamics to the EP instability and structural stability to depolarizing or hyperpolarizing loads of the BP system by determining the unstable regions in the I_{bias}-V_0 curve during decreases in I_{NaCa} or $[Ca^{2+}]_i$ transients. As shown in Fig. 10 (*left*), inhibition of I_{NaCa} significantly shrunk the unstable regions, though a codimension two saddle-node bifurcation did not occur. When $[Ca^{2+}]_i$ or f_{Ca} was fixed at the control value, however, the unstable regions did not shrink during I_{NaCa} reduction (Fig. 10, *middle, right*). The influences of eliminating $[Ca^{2+}]_i$ transients or blocking SR Ca^{2+} release on the unstable regions were very small.

DISCUSSION

Mechanisms of BP generation in I_{K1}-downregulated HVM

Nonlinear dynamical aspects of BP generation

This study shows that pacemaker activity appears in the I_{K1}-downregulated HVM system via a saddle-node bifurcation (disappearance of a stable EP) or Hopf bifurcation (destabilization of an EP) and that the instability of an EP at depolarized potentials underlies the stable HVM pacemaking. The term "mechanisms of pacemaker generation" is usually interpreted as meaning how individual sarcolemmal currents drive or contribute to phase 4 depolarization. From the viewpoint of the nonlinear dynamics and bifurcation theory, however, "EP instability" seems to be most important for the generation of robust pacemaking: if the system has a stable EP, it will be quiescent at the stable EP or in a bistable zone where stable steady states and periodic states

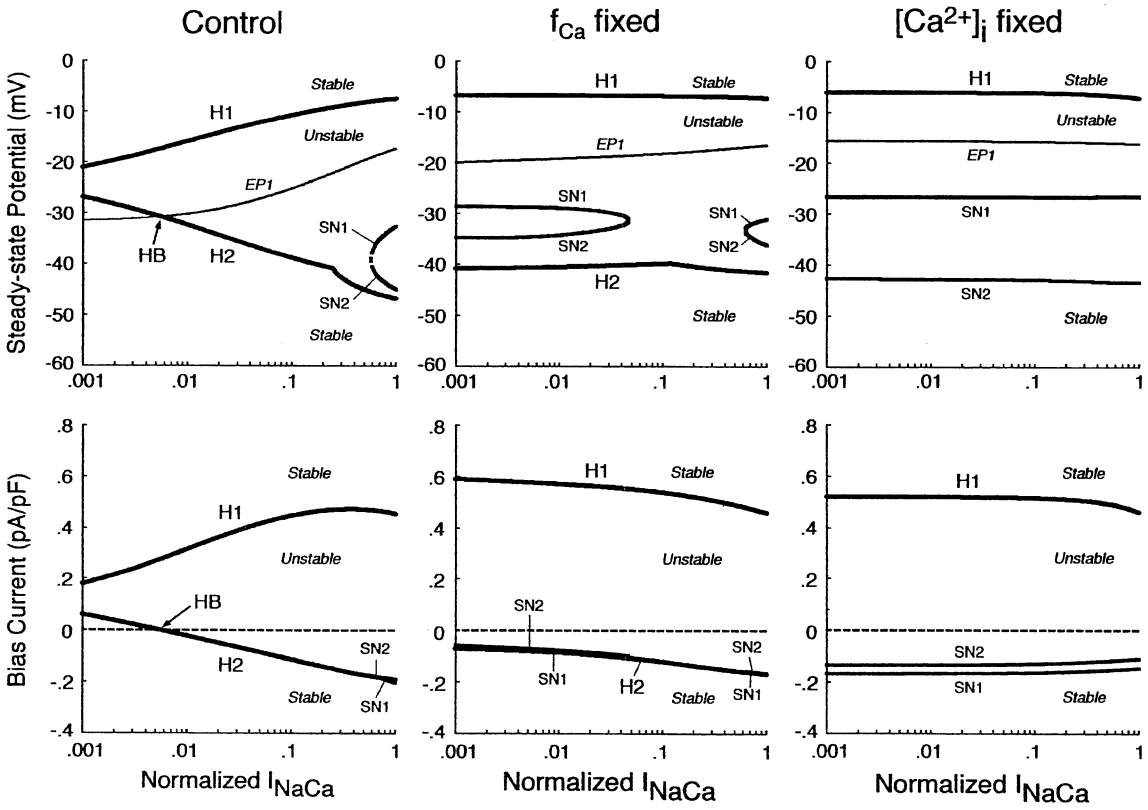


FIGURE 10 Changes in the unstable regions of the I_{bias}-V_0 curve during I_{NaCa} suppression in the I_{K1}-removed systems. Displacements of the bifurcation points (*H1–2, SN1–2*), as well as the control V_0 at $I_{bias} = 0$ (*EP1*), in the I_{bias}-V_0 curve with decreasing I_{NaCa} are shown for the unmodified system (*left*) and the modified system with f_{Ca} fixed at the value for $[Ca^{2+}]_i = 0.5$ μM (*middle*) or $[Ca^{2+}]_i$ itself fixed at 0.5 μM (*right*). The $\log(I_{NaCa})$ value was reduced from 0 to −3 at an interval of 0.01. As in Fig. 7, values of V_0 and I_{bias} at the bifurcation points are plotted on both the potential (*top*) and current (*bottom*) coordinates as functions of $\log(I_{NaCa})$. In the unmodified system, the path of EP1 intersected the locus of H2 at $I_{NaCa} = 0.0056$ (labeled *HB*).

coexist and thus annihilation occurs (for details on bistability and annihilation, see Landau et al. (6) and Guevara and Jongsma (8)). When considering the pacemaker mechanisms, therefore, one must elucidate the ionic mechanism of EP destabilization, which may be different from that of phase 4 depolarization. In the HVM pacemaker, $I_{Ca,L}$ is responsible for EP instability, whereas I_{NaCa} as well as I_{Kr} deactivation most contributes to phase 4 depolarization. Our study also suggests that the question "which current is dominant during phase 4" is relevant to the ionic mechanism not for EP instability as a requisite to stable pacemaking, but for the regulation of the destabilization rate (Figs. 4, 9, and 10). These viewpoints would be important particularly for engineering of functional BP cells to exhibit robust pacemaking.

It should be noted that the EP with the most depolarized potential (EP1) is always unstable, not stabilized during I_{K1} suppression (Fig. 5). The saddle-node bifurcation may also be yielded by increasing inward currents such as $I_{Na,b}$ or $I_{Ca,b}$. Nevertheless, increasing the inward currents would not lead to BP generation, because the positively shifted EP1 becomes stable via a Hopf bifurcation, resulting in an arrest at depolarized potentials. Another approach to create a BP cell may be overexpression of the hyperpolarization-activated current (I_h), which has been reported to induce BP activity in canine atrial or Purkinje myocytes (52,56). However, incorporating I_h did not cause a saddle-node bifurcation nor BP generation in the HVM model with normal I_{K1}, although accelerating BP generation during I_{K1} suppression via shifting the saddle-node bifurcation point toward higher g_{K1} values (data not shown). This discrepancy is at least in part due to the difference in I_{K1} density, which is much higher in ventricular cells than in atrial or Purkinje cells (56,57). These findings suggest that I_{K1} downregulation, ensuring both the occurrence of a saddle-node bifurcation and instability of EP1, is necessary and sufficient for constructing BP cells from HVMs.

Roles of individual sarcolemmal currents in HVM pacemaking

$I_{Ca,L}$

$I_{Ca,L}$ contributes little to the initial phase of pacemaker depolarization, although it contributes significantly to the terminal phase of the depolarization as well as to phase 0 upstroke (Fig. 4). Nevertheless, $I_{Ca,L}$ appears to be indispensable for the HVM pacemaking in that it is responsible for EP instability as a requisite to stable pacemaking (Figs. 7 and 8). The Ca^{2+} channel responsible for $I_{Ca,L}$ in the current model and original ventricular or SA node models corresponds to the high voltage-activated subtype (C-LTCC) formed by an α_{1C} subunit ($Ca_v1.2$), which is a major component in the heart of mouse or other species (58–60). However, the low voltage-activated subtype (D-LTCC), the α-subunit of which is α_{1D} ($Ca_v1.3$), activating at the pacemaker potential range, has recently been reported to contribute to phase 4 depolarization in the mouse SA node (61–63) and possibly in the rabbit SA node as well (64). Nevertheless, it is unlikely that D-LTCC plays an important role in the ventricular pacemaking, because $Ca_v1.3$ m-RNA is not present in the mouse or human ventricle (58,63).

I_K

In contrast to $I_{Ca,L}$, I_{Kr} or I_{Ks} was suggested to be inessential for EP destabilization leading to spontaneous activity, because 1), eliminating I_{Kr} and/or I_{Ks} did not significantly attenuate the EP instability as evaluated by positive real parts of eigenvalues of Jacobian matrices, little shrinking the unstable V_0 region in the I_{bias}-V_0 curve (Fig. 7); and 2), the I_K-removed BP system, quiescent in control (at $g_K = 0$), resumed automaticity when an EP was destabilized by incorporation of $I_{K,b}$ (Fig. 8) or electrotonic influences of adjacent normal HVMs (data not shown). Although I_{Kr} or I_{Ks} is not necessarily required for the generation of spontaneous oscillations, the K^+ currents appear to play pivotal roles in the modulation of BP dynamics. As suggested by Fig. 8, I_K would be necessary for the BP generation with large amplitude, high upstroke velocity, and stable frequency. Decreasing I_{Kr} or I_{Ks} shrunk the unstable I_{bias} region in the I_{bias}-V_0 curve, i.e., it attenuated the structural stability to depolarizing loads of the BP system (Fig. 7). The K^+ conductance region, as well as the I_{bias} region, where EPs are unstable and thus spontaneous oscillations occur, was much larger for the I_K-incorporated system than for the $I_{K,b}$-incorporated system (Fig. 8). Therefore, I_K may also contribute to the robust maintenance of BP activity, i.e., prevention of a bifurcation to quiescence.

I_{NaCa}

As in the guinea pig ventricular pacemaking (3), I_{NaCa} was suggested to be the dominant pacemaker current in the HVM pacemaking, with its removal leading to cessation of BP activity via a Hopf bifurcation (Figs. 4 and 9). However, the stabilization of an EP and cessation of BP activity during I_{NaCa} decreases appear to be a consequence of the Ca^{2+}-dependent inactivation of $I_{Ca,L}$, rather than the I_{NaCa} decrease itself: when f_{Ca} was fixed or when $[Ca^{2+}]_i$ was kept low by rapid Ca^{2+} buffering or tentative electroneutral Ca^{2+} transport, BP activity did not cease, being quite stable, during I_{NaCa} suppression (Fig. 9). It is also suggested that I_{NaCa} is not required for the destabilization of an EP or generation of spontaneous oscillations (Fig. 10). Thus, the major role of I_{NaCa} would be the maintenance of relatively low $[Ca^{2+}]_i$ to prevent Ca^{2+}-dependent inactivation of $I_{Ca,L}$ as well as cellular remodeling under Ca^{2+}-overload conditions, rather than the contribution to phase 4 depolarization as a pacemaker current. In all existing heart models, the Na^+/Ca^{2+} exchanger is assumed to mediate only the current I_{NaCa} via

the $3Na^+:1Ca^{2+}$ transport mode. However, it is also reported to carry a significant part of $I_{Na,b}$ via the Na^+-conducting mode (65,66). The background inward current $I_{Na,b}$ is the second dominant pacemaker current in the HVM model and the most dominant pacemaker current in most SA node models (51). Thus, the Na^+/Ca^{2+} exchanger may also contribute to pacemaker depolarization by generating $I_{Na,b}$.

Comparisons of HVM pacemaker with other pacemaker systems

Conditions for BP generation and BP dynamics

Real and model guinea pig ventricular myocytes exhibited spontaneous activities on 80–81% suppression of I_{K1} channels (1,3). In the HVM model, BP activity appeared when I_{K1} was suppressed by 84.6%, which is close to the critical values for BP generation in the guinea pig ventricle. The BP rates of the I_{K1}-reduced HVM (54–75 bpm), lower than those of the real or model guinea pig ventricular myocytes (100–164 bpm), appear to be in reasonable agreement with the mean human heart rate under normal conditions (refer to Table 4).

Pacemaker mechanisms

It has been reported for the rabbit SA node primary pacemaker that 1), $I_{Ca,L}$ is, but I_K is not, responsible for EP instability leading to spontaneous oscillations (11); 2), I_{Kr} contributes to the robust pacemaking with large amplitude and stable frequency (11); 3), I_{Kr} deactivation is crucial for phase 4 depolarization (53–55); and 4), $I_{Na,b}$ and I_{NaCa} are the predominant inward currents during phase 4 depolarization, with $I_{Ca,L}$ contributing only to the terminal phase of the depolarization as well as to phase 0 upstroke (51,55). These findings for the SA node pacemaker are in good agreement with our conclusions for the HVM pacemaker. As mentioned in the preceding section, the low voltage-activated $I_{Ca,L}$ mediated by D-LTCC may serve as a pacemaker current in the SA node pacemaking, but not in the ventricular pacemaking (61–63). However, the knockout of D-LTCC did not lead to sinus arrest, but led only to sinus bradycardia and arrhythmias (61–63), whereas the deletion of C-LTCC caused fetal death (60). These findings and our study suggest that the roles of C-LTCC and D-LTCC in pacemaking are different: C-LTCC would contribute mainly to EP destabilization as a requisite for basal pacemaking, whereas D-LTCC is not necessary for basal pacemaking, rather playing a pivotal role in pacemaker regulation by contributing mainly to phase 4 depolarization. Thus, the dynamical mechanism of the HVM pacemaking appears to be essentially the same as that of the basal SA node pacemaking. This consistency may reflect that cardiac myocytes, both pacemaker and nonpacemaker cells, in different regions or species share the common mechanism for the generation of basal pacemaking. Nevertheless, previous reports suggest the regional difference in pacemaker mechanisms. Blocking $I_{Ca,L}$ abolished spontaneous activity in central SA node tissues, but not in peripheral tissues (67,68); in the peripheral SA node, I_{Na} might contribute to EP destabilization and pacemaker generation. I_h is also suggested to play a predominant role in the subsidiary pacemaker mechanism (69,70). Bifurcation analyses of mathematical models for various regions or species are required for further investigations of the regional difference in pacemaker mechanisms.

Because there is transmural heterogeneity of electrophysiological properties of ventricular myocytes (16,18,71), one may also expect the transmural difference in BP mechanisms. Electrophysiological differences between epicardial, midmyocardial, and endocardial cells are attributable mainly to the differences in density and kinetics of I_{to} or I_{Ks}, and possibly I_{NaCa}, as summarized by ten Tusscher et al. (16). Reducing g_{to} only increased POP without affecting other AP parameters or EP stability (data not shown). Changing g_{Ks} or I_{NaCa} exerted only minor effects on stability and dynamics of the BP system (Figs. 6, 7, 9, and 10). These results suggest that bifurcation structures of epicardial, midmyocardial, and endocardial cells are essentially the same; thus we do not expect the transmural difference in BP mechanisms.

Responsiveness to β-adrenergic stimulation

As suggested by Silva and Rudy (3), a potential advantage of the BP over the electronic pacemaker is responsiveness to β-adrenergic stimulation (βAS). In the guinea pig ventricular model, BP responsiveness to βAS was very limited (3). We did not show the data on this issue, which is very important but out of the aim of this study. Nevertheless, we also found in the simulations according to the method of Silva and Rudy (3) that the HVM pacemaker did not exhibit a significant rate increase in response to βAS, suggesting that the ventricular pacemaker is less sensitive to βAS than the SA node pacemaker. The low sensitivity to βAS of the ventricular pacemaker may be at least in part due to the lack or low density of the regulatory inward currents, such as the low voltage-activated $I_{Ca,L}$, sustained-inward current (I_{st}) and I_h, which are known to be enhanced by βAS and abundant in SA node primary pacemaker cells (11,51,61–63,72–74).

Significance of applying bifurcation theory to BP system analysis and engineering

In this study, we used stability and bifurcation analyses to investigate the mechanisms of BP generation. As mentioned in the Introduction, the nonlinear dynamical approach is known to be useful for general understanding and systematic descriptions of the mechanisms of normal and abnormal pacemaker activities (4–11), as well as reentrant arrhythmias or conduction block (75–78). This study demonstrates that bifurcation theory also provides a reliable way of elucidating the roles of individual currents in pacemaker generation of I_{K1}-downregulated ventricular myocytes.

Our work suggests that exploring bifurcation structures of model cells can reveal the conditions and ways for oscillatory behavior to emerge or disappear in cardiac myocytes and possibly allow us to accurately predict and properly control the dynamics of real cells. Thus, the mathematical approach would also be applicable to engineering BP cells from native myocytes in vivo (1,52,56) or from human embryonic stem cells (hESCs) ex vivo (79–81) for the gene or cell therapy of bradyarrhythmias usually requiring implantation of an electronic pacemaker (for review, see Gepstein et al. (80)). Bifurcation analyses of model systems may lead to appropriate design of a functional BP, like the SA node, as a therapeutic alternative to the electronic pacemaker. Further investigations based on the bifurcation theory will possibly find out the most efficient ways to 1), create BP cells, 2), control BP dynamics, 3), improve the robustness of BP activity as well as BP sensitivity to βAS, and 4), improve BP ability to drive surrounding nonpacemaker tissues via modulating the existing currents or newly expressing the regulatory inward currents.

Limitations and perspectives of the study

Incompleteness of the HVM model

One limitation of this study is the incompleteness of the HVM model due to the lack of experimental data from HVMs. The formulas for $I_{Ca,L}$, I_{Kr}, SR Ca^{2+} release, and others were partly adopted from human atrial or animal heart models (see also Priebe and Beuckelmann (15)). In addition, for simplicity, the current model does not incorporate detailed descriptions of intracellular Ca^{2+} dynamics, SR Ca^{2+} handling, or the intracellular modulating factors such as cAMP and protein kinases, as in recently developed models (73, 82–84). More elaborate HVM models have recently been developed (16,17); however, these models with the larger number of equations and/or very complex formulas are less suitable for bifurcation analyses than the current model (for more details, see Theory and Methods). We believe that the current model is valuable and highly appropriate for exploring the essential mechanisms of BP generation. Nevertheless, further sophisticated but simplified HVM models with refinements of the formulas based on the data from HVMs, as well as incorporating more detailed descriptions of the intracellular Ca^{2+} handling and modulating factors, would have to be developed for future investigations.

The recently developed HVM models (16,17) are based mainly on the data from expressed channels whose electrophysiological properties may be different from those of native channels in HVMs. As suggested recently (79,81, 85), hESCs would provide an unlimited and renewable source of human cardiomyocytes for basic research as well as implantation therapies. Thus, cell system engineering to establish hESC-derived experimental models of HVMs may facilitate the development of more sophisticated HVM models.

Lack of experimental evidence

The conclusions in this study are of course the predictions from the model system; thus, they must be verified and supported by experimental works using real HVMs. However, there is no experimental study on BP activity in genetically modified HVMs. The hESC-derived experimental models of ventricular or nodal cells may also be useful for future investigations of BP mechanisms and thus verification of the model predictions. We hope that this study provides a stimulus to further experimentation on this issue.

Requirement of multicellular models involving electrotonic interactions

As suggested by Silva and Rudy (3), it should be recognized that the engineering of single BP cells is only a first step toward creation of the functional BP. Pacemaker mechanisms of the intact SA node are reported to involve electrotonic interactions with the atrium (86–88). BP cells in vivo would also suffer hyperpolarizing loads of adjacent nonpacemaker cells, which may abolish BP activity. Thus, BP ability to drive the heart would depend on its architecture to facilitate optimization of the electrical loading by the surrounding atrial or ventricular tissue (86,87). Recently, hESC-derived pacemaking cardiomyocytes implanted into the guinea pig ventricle in vivo have been found to integrate with the host tissue via forming gap junctions and drive the quiescent ventricle with nearly the same rate as in the isolated state (81). This suggested that the engrafted BP could efficiently interact with the surrounding nonpacemaker tissue to minimize the electrotonic load. However, the hESC-derived pacemaker may not be as robust to excessive hyperpolarizing loads as the native SA node pacemaker. Multicellular models such as for the SA node tissue (68,86,89) are required for further investigating the roles of electrotonic interactions in BP mechanisms in vivo and how to create a real functional BP with robust pacemaking.

APPENDIX 1: MODEL EQUATIONS

The mathematical expressions used in this study are given below. Units are mV, pA, nS, ms, nF, mM, and L. The temperature assumed for the model is 37°C. The symbols used and their definitions are the same as those in our rabbit SA node model (51) or the original PB model (15). The stimulus current I_{stim} in Eqs. 55 and 64 was assumed to carry K^+ ions into the cell for charge conservation during paced AP simulations, being set equal to zero for BP simulations. Standard parameter values and initial conditions for computations are given in Tables 5 and 6, respectively.

Sarcolemmal ionic currents

L-type Ca^{2+} channel current ($I_{Ca,L}$)

$$I_{Ca,L} = g_{Ca,L}(V - E_{Ca,L}) \times d_L \times f_L \times f_{Ca,\infty} \quad (3)$$

$$d_{L,\infty} = 1/\{1 + \exp[-(V + 7.64)/6.32]\} \quad (4)$$

$$f_{L,\infty} = 1/\{1 + \exp[(V + 24.6)/6.9]\} \quad (5)$$

TABLE 5 Standard parameter values

Parameters	Values	Parameters	Values
F	96485 (C/mol)	I_{pCamax}	0.11 (pA/pF)
R	8.3144 (J/mol/K)	K_{mCap}	0.0005 (mM)
T	310.15 (K)	P_{rel}	50 (ms^{-1})
C_m	153.4 (pF)	P_{up}	0.00221 (mM/ms)
V_{cell}	38 (pL)	P_{leak}	0.00026 (ms^{-1})
V_i	25.84 (pL)	K_{up}	0.00025 (mM)
V_{rel}	0.182 (pL)	τ_{tr}	180 (ms)
V_{up}	2.098 (pL)	$[CM]_{tot}$	0.05 (mM)
$[Na^+]_o$	140 (mM)	$[CQ]_{tot}$	10 (mM)
$[K^+]_o$	5.4 (mM)	$[TC]_{tot}$	0.07 (mM)
$[Ca^{2+}]_o$	2.0 (mM)	K_{dCM}	0.00238 (mM)
$g_{Ca,L}$	0.2496 (nS/pF)	K_{dCQ}	0.8 (mM)
g_{Kr}	0.012 (nS/pF)	K_{dTC}	0.0005 (mM)
g_{Ks}	0.036 (nS/pF)	k_{fTC}	400 ($mM^{-1} \times ms^{-1}$)
g_{to}	0.3 or 0.4 (nS/pF)	k_{bTC}	0.2 (ms^{-1})
g_{Na}	7.8 (nS/pF)		
g_{K1}	3.9 (nS/pF)		
$g_{Na,b}$	0.001 (nS/pF)		
$g_{Ca,b}$	0.00051 (nS/pF)		
$E_{Ca,L}$	+52.8 (mV)		
K_{mfCa}	0.00035 (mM)		
I_{NaKmax}	0.884 (pA/pF)		
K_{mNap}	10 (mM)		
K_{mKp}	1.5 (mM)		
k_{NaCa}	1000 (pA/pF)		
k_{sat}	0.1		
r_{NaCa}	0.35		
K_{mNaex}	87.5 (mM)		
K_{mCaex}	1.38 (mM)		

$$\tau_{dL} = (1.4/\{1 + \exp[-(V + 35)/13]\} + 0.25) \times 1.4/\{1 + \exp[(V + 5)/5]\} + 1/\{1 + \exp[-(V - 50)/20]\} \quad (6)$$

TABLE 6 State variable initial conditions for simulations of paced APs and BP oscillations

State variables	APs during 1 Hz pacing*	BP activity at $g_{K1} = 0.15^\dagger$	BP activity at $g_{K1} = 0^\dagger$
V	−84.86	−61.91	−47.88
d_L	4.941×10^{-6}	1.862×10^{-4}	1.714×10^{-3}
f_L	0.8873	0.5298	0.3868
p_a	9.095×10^{-3}	0.3382	0.5371
n	1.974×10^{-2}	0.1350	0.2321
q	0.9997	0.9890	0.8999
h	0.9925	0.2811	1.640×10^{-2}
$[Ca^{2+}]_i$	1.691×10^{-4}	3.502×10^{-4}	4.889×10^{-4}
$[Ca^{2+}]_{rel}$	2.683	5.207	6.378
$[Ca^{2+}]_{up}$	2.843	5.349	6.473
$[Na^+]_i$	9.224	6.548	6.418
$[K^+]_i$	136.4	140	140
d_R	4.941×10^{-6}	1.866×10^{-4}	1.718×10^{-3}
f_R	0.9998	0.9954	0.9645
f_{TC}	0.2529	0.4125	0.4949

*Initial conditions for simulations of paced APs in the standard system ($g_{K1} = 1$), obtained at 30 min during 1 Hz pacing, i.e., just before the 1801st stimulus, starting from a resting state.

†Initial conditions for simulations of BP activity in the I_{K1}-reduced systems, obtained at MDP after 15 min calculations starting from an EP.

$$\tau_{fL} = 17.925/\{0.1389 \times \exp[-(0.0358 \times (V - 10.9))^2] + 0.0519\} \quad (7)$$

$$f_{Ca,\infty} = 1/[1 + (K_{mfCa}/[Ca^{2+}]_i)] \quad (8)$$

Rapidly activating delayed-rectifier K^+ current (I_{Kr})

$$I_{Kr} = g_{Kr} \times (V - E_K) \times p_a \times p_{i,\infty} \quad (9)$$

$$p_{a,\infty} = 1/\{1 + \exp[-(V + 14)/7.7]\} \quad (10)$$

$$p_{i,\infty} = 1/\{1 + \exp[(V + 15)/22.4]\} \quad (11)$$

$$\tau_{pa} = 1/(\alpha_{pa} + \beta_{pa}) \quad (12)$$

$$\alpha_{pa} = 0.0003 \times (V + 14)/\{1 - \exp[-(V + 14)/5]\} \quad (13)$$

$$\beta_{pa} = 0.000073898 \times (V - 3.4328)/\{\exp[(V - 3.4328)/5.1237] - 1\} \quad (14)$$

Slowly activating delayed-rectifier K^+ current (I_{Ks})

$$I_{Ks} = g_{Ks} \times (V - E_{Ks}) \times n^2 \quad (15)$$

$$E_{Ks} = (RT/F) \times \ln[(0.01833 \times [Na^+]_o + [K^+]_o)/(0.01833 \times [Na^+]_i + [K^+]_i)] \quad (16)$$

$$n_\infty = 1/\{1 + \exp[-(V - 9.4)/11.8]\}^{0.5} \quad (17)$$

$$\tau_n = 555/\{1 + \exp[-(V + 22)/11.3]\} + 129 \quad (18)$$

Transient outward current (It_o)

$$I_{to} = g_{to} \times (V - E_{to}) \times q \times r_\infty \quad (19)$$

$$E_{to} = (RT/F) \times \ln[(0.043 \times [Na^+]_o + [K^+]_o)/(0.043 \times [Na^+]_i + [K^+]_i)] \quad (20)$$

$$r_\infty = \alpha_r/(\alpha_r + \beta_r) \quad (21)$$

$$\alpha_r = 0.5266 \times \exp[-0.0166 \times (V - 42.2912)]/\{1 + \exp[-0.0943 \times (V - 42.2912)]\} \quad (22)$$

$$\beta_r = \{0.5149 \times \exp[-0.1344 \times (V - 5.0027)] + 0.00005186 \times V\}/\{1 + \exp[-0.1348 \times (V - 0.00005186)]\} \quad (23)$$

$$q_\infty = \alpha_q/(\alpha_q + \beta_q) \quad (24)$$

$$\tau_q = 1/(\alpha_q + \beta_q) \quad (25)$$

$$\alpha_q = \{0.0721 \times \exp[-0.173 \times (V + 34.2531)] + 0.00005612 \times V\}/\{1 + \exp[-0.1732 \times (V + 34.2531)]\} \quad (26)$$

$$\beta_q = \{0.0767 \times \exp[-0.00000000166 \times (V + 34.0235)] + 0.0001215 \times V\}/\{1 + \exp[-0.1604 \times (V + 34.0235)]\} \quad (27)$$

Na^+ channel current (I_{Na})

$$I_{Na} = g_{Na} \times (V - E_{mh}) \times m_\infty^3 \times h^2 \quad (28)$$

$$E_{mh} = (RT/F) \times \ln[([Na^+]_o + 0.12 \times [K^+]_o)/([Na^+]_i + 0.12 \times [K^+]_i)] \quad (29)$$

$$m_\infty = \alpha_m/(\alpha_m + \beta_m) \quad (30)$$

$$\alpha_m = 0.32 \times (V + 47.13)/\{1 - \exp[-0.1 \times (V + 47.13)]\} \quad (31)$$

$$\beta_m = 0.08 \times \exp(-V/11) \quad (32)$$

$$h_\infty = 0.5 \times [1 - \tan h(7.74 + 0.12 \times V)] \quad (33)$$

$$\tau_h = 0.25 + 2.24 \times [1 - \tan h(7.74 + 0.12 \times V)]/\{1 - \tan h[0.07 \times (V + 92.4)]\} \quad (34)$$

Inward-rectifier K^+ channel current (I_{K1})

$$I_{K1} = g_{K1} \times (V - E_K) \times k_{1a}/(k_{1a} + k_{1b}) \quad (35)$$

$$k_{1a} = 0.1/\{1 + \exp[0.06 \times (V - E_K - 200)]\} \quad (36)$$

$$k_{1b} = \{3 \times \exp[0.0002 \times (V - E_K + 100)] + \exp[0.1 \times (V - E_K - 10)]\}/\{1 + \exp[-0.5 \times (V - E_K)]\} \quad (37)$$

Background Na^+/Ca^{2+} currents ($I_{Na,b}$, $I_{Ca,b}$)

$$I_{Na,b} = g_{Na,b} \times (V - E_{Na}) \quad (38)$$

$$I_{Ca,b} = g_{Ca,b} \times (V - E_{Ca}) \quad (39)$$

Na^+-K^+ pump current (I_{NaK})

$$I_{NaK} = I_{NaKmax} \times \{[K^+]_o/([K^+]_o + K_{mKp})\}/\{1 + (K_{mNap}/[Na^+]_i)^{1.5}\}/\{1 + 0.1245 \times \exp(-0.1 \times V \times F/RT) + 0.0365 \times [\exp([Na^+]_o/67.3) - 1]/7 \times \exp(-V \times F/RT)\} \quad (40)$$

Na^+/Ca^{2+} exchanger current (I_{NaCa})

$$I_{NaCa} = k_{NaCa}/(K_{mNacx}^3 + [Na^+]_o^3)/(K_{mCaex} + [Ca^{2+}]_o) \times \{[Ca^{2+}]_o \times [Na^+]_i^3 \times \exp(r_{NaCa} \times V \times F/RT) - [Na^+]_o^3 \times [Ca^{2+}]_i \times \exp[(r_{NaCa} - 1) \times V \times F/RT]\}/\{1 + k_{sat} \times \exp[(r_{NaCa} - 1) \times V \times F/RT]\} \quad (41)$$

Sarcolemmal Ca^{2+} pump current (I_{pCa})

$$I_{pCa} = I_{pCamax}/[1 + (K_{mCap}/[Ca^{2+}]_i)] \quad (42)$$

Total membrane current (I_{total})

$$I_{total} = I_{Ca,L} + I_{Kr} + I_{Ks} + I_{to} + I_{Na} + I_{K1} + I_{Na,b} + I_{Ca,b} + I_{NaK} + I_{NaCa} + I_{pCa} \quad (43)$$

Net ion fluxes

$$J_{Na,net} = (I_{Na} + I_{Na,b} + 3 \times I_{NaK} + 3 \times I_{NaCa}) \times C_m/F \quad (44)$$

$$J_{K,net} = (I_{Kr} + I_{Ks} + I_{to} + I_{K1} - 2 \times I_{NaK}) \times C_m/F \quad (45)$$

$$J_{Ca,net} = (I_{Ca,L} + I_{Ca,b} - 2 \times I_{NaCa} + I_{pCa}) \times C_m/(2 \times F) \quad (46)$$

Intracellular Ca^{2+} dynamics (SR Ca^{2+} handling)

SR Ca^{2+} release

$$J_{rel} = g_{rel} \times (d_R \times f_R)^3 \times ([Ca^{2+}]_{rel} - [Ca^{2+}]_i) \quad (47)$$

$$g_{rel} = P_{rel}/\{1 + \exp[(I_{Ca,L} + I_{Ca,b} - 2 \times I_{NaCa} + I_{pCa} + 5)/0.9]\} \quad (48)$$

$$d_{R\infty} = d_{L\infty} = 1/\{1 + \exp[-(V + 7.64)/6.32]\} \quad (49)$$

$$f_{R\infty} = f_{L\infty} = 1/\{1 + \exp[(V + 24.6)/6.9]\} \quad (50)$$

$$\tau_{dR} = \tau_{fR} = 4 \quad (51)$$

SR Ca^{2+} uptake via Ca^{2+} pump

$$J_{up} = P_{up} \times [Ca^{2+}]_i^2/([Ca^{2+}]_i^2 + K_{up}^2) \quad (52)$$

SR Ca^{2+} transfer and leak

$$J_{tr} = ([Ca^{2+}]_{up} - [Ca^{2+}]_{rel})/\tau_{tr} \quad (53)$$

$$J_{leak} = P_{leak} \times ([Ca^{2+}]_{up} - [Ca^{2+}]_i) \quad (54)$$

Differential equations for state variables

Membrane potential (V)

$$dV/dt = I_{stim} - I_{total} \quad (55)$$

Gating variables

$$dx/dt = (x_\infty - x)/\tau_x \; [x = d_L, f_L, p_a, n, q, h, d_R, f_R] \quad (56)$$

Ca^{2+} buffering flux

$$df_{TC}/dt = k_{fTC} \times [Ca^{2+}]_i \times (1 - f_{TC}) - k_{bTC} \times f_{TC} \quad (57)$$

$$B_{CM} = 1/\{1 + [CM]_{tot} \times K_{dCM}/(K_{dCM} + [Ca^{2+}]_i)^2\} \quad (58)$$

$$B_{CQ} = 1/\{1 + [CQ]_{tot} \times K_{dCQ}/(K_{dCQ} + [Ca^{2+}]_{rel})^2\} \quad (59)$$

Intracellular ion concentrations

$$d[Ca^{2+}]_i/dt = B_{CM} \times \{(-J_{Ca,net} + J_{rel} \times V_{rel} - J_{up} \times V_{up} + J_{leak} \times V_{up})/V_i - [TC]_{tot} \times df_{TC}/dt\} \quad (60)$$

$$d[Ca^{2+}]_{rel}/dt = B_{CQ} \times (J_{tr} - J_{rel}) \quad (61)$$

$$d[Ca^{2+}]_{up}/dt = J_{up} - J_{tr} \times V_{rel}/V_{up} - J_{leak} \quad (62)$$

$$d[Na^{+}]_i/dt = -J_{Na,net}/V_i \quad (63)$$

$$d[K^{+}]_i/dt = (I_{stim} \times C_m/F - J_{K,net})/V_i \quad (64)$$

APPENDIX 2: DETERMINATION OF EPS AS INITIAL CONDITIONS

To determine an EP (resting state) of the HVM system as initial conditions for AP simulations, steady-state values of the state variables V, $[Ca^{2+}]_i$, $[Na^{+}]_i$, $[K^{+}]_i$, $[Ca^{2+}]_{rel}$, and $[Ca^{2+}]_{up}$ were calculated numerically by the differential or algebraic method of Hund et al. (35). Differential equations given in Appendix 1 (Eqs. 55, 60–64) were used for the differential method with the MATLAB ODE solvers, whereas the following algebraic equations derived from the differential equations were used for the algebraic method with a nonlinear equation solver available in MATLAB.

$$I_{total} = 0\ (dV/dt = 0) \quad (65)$$

$$J_{Ca,net} = 0\ (d[Ca^{2+}]_i/dt = 0) \quad (66)$$

$$J_{rel} - J_{tr} = 0\ (d[Ca^{2+}]_{rel}/dt = 0) \quad (67)$$

$$J_{up} - J_{tr} \times V_{rel}/V_{up} - J_{leak} = 0\ (d[Ca^{2+}]_{up}/dt = 0) \quad (68)$$

$$J_{Na,net} = 0\ (d[Na^{+}]_i/dt = 0) \quad (69)$$

$$J_{K,net} = 0\ (d[K^{+}]_i/dt = 0) \quad (70)$$

$$V = (V_i \times F/C_m) \times ([K^{+}]_i + [Na^{+}]_i + 2[Ca^{2+}]_{i,tot} + 2 \times (V_{rel}/V_i) \times [Ca^{2+}]_{rel,tot} + 2 \times (V_{up}/V_i) \times [Ca^{2+}]_{up} - C_0) \quad (71)$$

$$[Ca^{2+}]_{i,tot} = [Ca^{2+}]_i + [CM]_{tot} \times [Ca^{2+}]_i/([Ca^{2+}]_i + K_{dCM}) + [TC]_{tot} \times [Ca^{2+}]_i/([Ca^{2+}]_i + K_{dTC}) \quad (72)$$

$$[Ca^{2+}]_{rel,tot} = [Ca^{2+}]_{rel} + [CQ]_{tot} \times [Ca^{2+}]_{rel}/([Ca^{2+}]_{rel} + K_{dCQ}) \quad (73)$$

The symbol C_0 in Eq. 71 is a constant of integration determined by initial conditions (35). Note that Eq. 65 can be derived from Eqs. 66, 69, and 70 (see Eqs. 43–46). The algebraic method for the full system with variable $[K^{+}]_i$ practically used Eqs. 66–70 and Eqs. 71–73 instead of Eq. 65, assuming that $[K^{+}]_i$ is equal to 140 mM under control conditions (e.g., at $g_{K1} = 1$). The differential and algebraic methods yielded nearly identical results. For BP simulations and bifurcation analyses using the $[K^{+}]_i$-fixed system, steady-state values of the state variables were calculated by Eqs. 65–69.

This work was supported in part by a Ministry for Education, Science, and Culture of Japan Grant-in-Aid for Scientific Research 15590195 and 17590192 (to Y. Kurata and T. Shibamoto) and a Kanazawa Medical University Grant for Collaborative Research C2003-1, C2004-1, and C2005-1 (to Y. Kurata and T. Shibamoto).

REFERENCES

1. Miake, J., E. Marbán, and H. B. Nuss. 2002. Gene therapy: biological pacemaker created by gene transfer. *Nature*. 419:132–133.
2. Luo, C. H., and Y. Rudy. 1994. A dynamic model of the cardiac ventricular action potential: I. Simulations of ionic currents and concentration changes. *Circ. Res.* 74:1071–1096.
3. Silva, J., and Y. Rudy. 2003. Mechanism of pacemaking in I_{K1}-downregulated myocytes. *Circ. Res.* 92:261–263.
4. Chay, T. R., and Y. S. Lee. 1985. Phase resetting and bifurcation in the ventricular myocardium. *Biophys. J.* 47:641–651.
5. Chay, T. R., and Y. S. Lee. 1990. Bursting, beating, and chaos by two functionally distinct inward current inactivations in excitable cells. *Ann. N. Y. Acad. Sci.* 591:328–350.
6. Landau, M., P. Lorente, D. Michaels, and J. Jalife. 1990. Bistabilities and annihilation phenomena in electrophysiological cardiac models. *Circ. Res.* 66:1658–1672.
7. Vinet, A., and F. A. Roberge. 1990. A model study of stability and oscillations in the myocardial cell membrane. *J. Theor. Biol.* 147:377–412.
8. Guevara, M. R., and H. J. Jongsma. 1992. Three ways of abolishing automaticity in sinoatrial node: ionic modeling and nonlinear dynamics. *Am. J. Physiol.* 262:H1268–H1286.
9. Gibb, W. J., M. B. Wagner, and M. D. Lesh. 1994. Effects of simulated potassium blockade on the dynamics of triggered cardiac activity. *J. Theor. Biol.* 168:245–257.
10. Varghese, A., and R. L. Winslow. 1994. Dynamics of abnormal pacemaking activity in cardiac Purkinje fibers. *J. Theor. Biol.* 168:407–420.
11. Kurata, Y., I. Hisatome, S. Imanishi, and T. Shibamoto. 2003. Roles of L-type Ca^{2+} and delayed-rectifier K^{+} currents in sinoatrial node pacemaking: insights from stability and bifurcation analyses of a mathematical model. *Am. J. Physiol. Heart Circ. Physiol.* 285:H2804–H2819.
12. Guckenheimer, J., and P. Holmes. 1983. Nonlinear Oscillations, Dynamical Systems, and Bifurcations of Vector Fields. Springer-Verlag, New York.
13. Parker, T. S., and L. O. Chua. 1989. Practical Numerical Algorithms for Chaotic Systems. Springer-Verlag, New York.
14. Kuznetsov, Y. A. 2003. Elements of Applied Bifurcation Theory, 3rd ed. Springer-Verlag, New York.
15. Priebe, L., and D. J. Beuckelmann. 1998. Simulation study of cellular electric properties in heart failure. *Circ. Res.* 82:1206–1223.
16. Ten Tusscher, K. H. W. J., D. Noble, P. J. Noble, and A. V. Panfilov. 2004. A model for human ventricular tissue. *Am. J. Physiol. Heart Circ. Physiol.* 286:H1573–H1589.
17. Iyer, V., R. Mazhari, and R. L. Winslow. 2004. A computational model of the human left-ventricular epicardial myocyte. *Biophys. J.* 87:1507–1525.
18. Bernus, O., R. Wilders, C. W. Zemlin, H. Verschelde, and A. V. Panfilov. 2002. A computationally efficient electrophysiological model of human ventricular cells. *Am. J. Physiol. Heart Circ. Physiol.* 282: H2296–H2308.
19. Courtemanche, M., R. J. Ramirez, and S. Nattel. 1998. Ionic mechanisms underlying human atrial action potential properties: insights from a mathematical model. *Am. J. Physiol.* 275:H301–H321.
20. Faber, G. M., and Y. Rudy. 2000. Action potential and contractility changes in $[Na^{+}]_i$ overloaded cardiac myocytes: a simulation study. *Biophys. J.* 78:2392–2404.
21. Bénitah, J. P., P. Bailly, M. C. D'Agrosa, J. P. Da Ponte, C. Delgado, and P. Lorente. 1992. Slow inward current in single cells isolated from adult human ventricles. *Pflugers Arch.* 421:176–187.
22. Pelzmann, B., P. Schaffer, E. Bernhart, P. Lang, H. Mächler, B. Rigler, and B. Koidl. 1998. L-type calcium current in human ventricular myocytes at a physiological temperature from children with tetralogy of Fallot. *Cardiovasc. Res.* 38:424–432.
23. Li, G. R., B. Yang, J. Feng, R. F. Bosch, M. Carrier, and S. Nattel. 1999. Transmembrane I_{Ca} contributes to rate-dependent changes of action potentials in human ventricular myocytes. *Am. J. Physiol.* 276: H98–H106.

24. Li, G. R., J. Feng, L. Yue, M. Carrier, and S. Nattel. 1996. Evidence for two components of delayed rectifier K^+ current in human ventricular myocytes. *Circ. Res.* 78:689–696.

25. Wang, Z., B. Fermini, and S. Nattel. 1994. Rapid and slow components of delayed rectifier current in human atrial myocytes. *Cardiovasc. Res.* 28:1540–1546.

26. Zhou, Z., Q. Gong, B. Ye, Z. Fan, J. C. Makielski, G. A. Robertson, and C. T. January. 1998. Properties of HERG channels stably expressed in HEK 293 cells studied at physiological temperature. *Biophys. J.* 74:230–241.

27. Mazhari, R., J. L. Greenstein, R. L. Winslow, E. Marbán, and H. B. Nuss. 2001. Molecular interactions between two long-QT syndrome gene products, HERG and KCNE2, rationalized by in vitro and in silico analysis. *Circ. Res.* 89:33–38.

28. Johnson, J. P., F. M. Mullins, and P. B. Bennett. 1999. Human *ether-à-go-go*-related gene K^+ channel gating probed with extracellular Ca^{2+}: evidence for two distinct voltage sensors. *J. Gen. Physiol.* 113:565–580.

29. Smith, P. L., and G. Yellen. 2002. Fast and slow voltage sensor movements in HERG potassium channels. *J. Gen. Physiol.* 119:275–293.

30. Sanguinetti, M. C., C. Jiang, M. E. Curran, and M. T. Keating. 1995. A mechanistic link between an inherited and an acquired cardiac arrhythmia: *HERG* encodes the I_{Kr} potassium channel. *Cell.* 81:299–307.

31. Weerapura, M., S. Nattel, D. Chartier, R. Caballero, and T. E. Hébert. 2002. A comparison of currents carried by HERG, with and without coexpression of MiRP1, and the native rapid delayed rectifier current. Is MiRP1 the missing link? *J. Physiol.* 540:15–27.

32. Berecki, G., J. G. Zegers, A. O. Verkerk, Z. A. Bhuiyan, B. de Jonge, M. W. Veldkamp, R. Wilders, and A. C. G. van Ginneken. 2005. HERG channel (dys)function revealed by dynamic action potential clamp technique. *Biophys. J.* 88:566–578.

33. Shibasaki, T. 1987. Conductance and kinetics of delayed rectifier potassium channels in nodal cells of the rabbit heart. *J. Physiol.* 387: 227–250.

34. Virág, L., N. Iost, M. Opincariu, J. Szolnoky, J. Szécsi, G. Bogáts, P. Szenohradsky, A. Varró, and J. G. Papp. 2001. The slow component of the delayed rectifier potassium current in undiseased human ventricular myocytes. *Cardiovasc. Res.* 49:790–797.

35. Hund, T. J., J. P. Kucera, N. F. Otani, and Y. Rudy. 2001. Ionic charge conservation and long-term steady state in the Luo-Rudy dynamic cell model. *Biophys. J.* 81:3324–3331.

36. Krogh-Madsen, T., P. Schaffer, A. D. Skriver, L. K. Taylor, B. Pelzmann, B. Koidl, and M. R. Guevara. 2005. An ionic model for rhythmic activity in small clusters of embryonic chick ventricular cells. *Am. J. Physiol. Heart Circ. Physiol.* 289:H398–H413.

37. Dormand, J. R., and P. J. Prince. 1980. A family of embedded Runge-Kutta formulae. *J. Comput. Appl. Math.* 6:19–26.

38. Shampine, L. F., and M. W. Reichelt. 1997. The MATLAB ODE Suite. *SIAM J. Sci. Comput.* 18:1–22.

39. Sachse, F. B., G. Seemann, K. Chaisaowong, and D. Weiß. 2003. Quantitative reconstruction of cardiac electromechanics in human myocardium: assembly of electrophysiologic and tension generation models. *J. Cardiovasc. Electrophysiol.* 14:S210–S218.

40. Shannon, T. R., and D. M. Bers. 1997. Assessment of intra-SR free [Ca] and buffering in rat heart. *Biophys. J.* 73:1524–1531.

41. Shannon, T. R., T. Guo, and D. M. Bers. 2003. Ca^{2+} scraps: local depletions of free $[Ca^{2+}]$ in cardiac sarcoplasmic reticulum during contractions leave substantial Ca^{2+} reserve. *Circ. Res.* 93:40–45.

42. Li, G. R., J. Feng, L. Yue, and M. Carrier. 1998. Transmural heterogeneity of action potentials and I_{to1} in myocytes isolated from the human right ventricle. *Am. J. Physiol.* 275:H369–H377.

43. Despa, S., M. A. Islam, C. R. Weber, S. M. Pogwizd, and D. M. Bers. 2002. Intracellular Na^+ concentration is elevated in heart failure but Na/K pump function is unchanged. *Circulation.* 105:2543–2548.

44. Pieske, B., L. S. Maier, V. Piacentino III, J. Weisser, G. Hasenfuss, and S. Houser. 2002. Rate dependence of $[Na^+]_i$ and contractility in nonfailing and failing human myocardium. *Circulation.* 106:447–453.

45. Schmidt, U., R. J. Hajjar, P. A. Helm, C. S. Kim, A. A. Doye, and J. K. Gwathmey. 1998. Contribution of abnormal sarcoplasmic reticulum ATPase activity to systolic and diastolic dysfunction in human heart failure. *J. Mol. Cell. Cardiol.* 30:1929–1937.

46. Pieske, B., L. S. Maier, D. M. Bers, and G. Hasenfuss. 1999. Ca^{2+} handling and sarcoplasmic reticulum Ca^{2+} content in isolated failing and nonfailing human myocardium. *Circ. Res.* 85:38–46.

47. Maier, L. S., P. Barckhausen, J. Weisser, I. Aleksic, M. Baryalei, and B. Pieske. 2000. Ca^{2+} handling in isolated human atrial myocardium. *Am. J. Physiol. Heart Circ. Physiol.* 279:H952–H958.

48. Tiaho, F., C. Piot, J. Nargeot, and S. Richard. 1994. Regulation of the frequency-dependent facilitation of L-type Ca^{2+} currents in rat ventricular myocytes. *J. Physiol.* 477:237–252.

49. Yuan, W., and D. M. Bers. 1994. Ca-dependent facilitation of cardiac Ca current is due to Ca-calmodulin-dependent protein kinase. *Am. J. Physiol.* 267:H982–H993.

50. Fukai, H., S. Doi, T. Nomura, and S. Sato. 2000. Hopf bifurcations in multiple-parameter space of the Hodgkin-Huxley equations I. Global organization of bistable periodic solutions. *Biol. Cybern.* 82:215–222.

51. Kurata, Y., I. Hisatome, S. Imanishi, and T. Shibamoto. 2002. Dynamical description of sinoatrial node pacemaking: improved mathematical model for primary pacemaker cell. *Am. J. Physiol. Heart Circ. Physiol.* 283:H2074–H2101.

52. Plotnikov, A. N., E. A. Sosunov, J. Qu, I. N. Shlapakova, E. P. Anyukhovsky, L. Liu, M. J. Janse, P. R. Brink, I. S. Cohen, R. B. Robinson, P. Danilo Jr., and M. R. Rosen. 2004. Biological pacemaker implanted in canine left bundle branch provides ventricular escape rhythms that have physiologically acceptable rates. *Circulation.* 109: 506–512.

53. Brown, H. F., J. Kimura, D. Noble, S. J. Noble, and A. Taupignon. 1984. The ionic currents underlying pacemaker activity in rabbit sinoatrial node: experimental results and computer simulations. *Proc. R. Soc. Lond. B Biol. Sci.* 222:329–347.

54. Noble, D. 1984. The surprising heart: a review of recent progress in cardiac electrophysiology. *J. Physiol.* 353:1–50.

55. Dokos, S., B. Celler, and N. Lovell. 1996. Ion currents underlying sinoatrial node pacemaker activity: a new single cell mathematical model. *J. Theor. Biol.* 181:245–272.

56. Qu, J., A. N. Plotnikov, P. Danilo Jr., I. Shlapakova, I. S. Cohen, R. B. Robinson, and M. R. Rosen. 2003. Expression and function of a biological pacemaker in canine heart. *Circulation.* 107:1106–1109.

57. Joyner, R. W., Y.-G. Wang, R. Wilders, D. A. Golod, M. B. Wagner, R. Kumar, and W. N. Goolsby. 2000. A spontaneously active focus drives a model atrial sheet more easily than a model ventricular sheet. *Am. J. Physiol. Heart Circ. Physiol.* 279:H752–H763.

58. Takimoto, K., D. Li, J. M. Nerbonne, and E. S. Levitan. 1997. Distribution, splicing and glucocorticoid-induced expression of cardiac alpha 1C and alpha 1D voltage-gated Ca^{2+} channel mRNAs. *J. Mol. Cell. Cardiol.* 29:3035–3042.

59. Bohn, G., S. Moosmang, H. Conrad, A. Ludwig, F. Hofmann, and N. Klugbauer. 2000. Expression of T- and L-type calcium channel mRNA in murine sinoatrial node. *FEBS Lett.* 481:73–76.

60. Seisenberger, C., V. Specht, A. Welling, J. Platzer, A. Pfeifer, S. Kühbandner, J. Striessnig, N. Klugbauer, R. Feil, and F. Hofmann. 2000. Functional embryonic cardiomyocytes after disruption of the L-type α_{1C} ($Ca_v1.2$) calcium channel gene in the mouse. *J. Biol. Chem.* 275:39193–39199.

61. Platzer, J., J. Engel, A. Schrott-Fischer, K. Stephan, S. Bova, H. Chen, H. Zheng, and J. Striessnig. 2000. Congenital deafness and sinoatrial node dysfunction in mice lacking class D L-type Ca^{2+} channels. *Cell.* 102:89–97.

62. Zhang, Z., Y. Xu, H. Song, J. Rodriguez, D. Tuteja, Y. Namkung, H.-S. Shin, and N. Chiamvimonvat. 2002. Functional roles of $Ca_v1.3$ (α_{1D}) calcium channel in sinoatrial nodes: insight gained using gene-targeted null mutant mice. *Circ. Res.* 90:981–987.

63. Mangoni, M. E., B. Couette, E. Bourinet, J. Platzer, D. Reimer, J. Striessnig, and J. Nargeot. 2003. Functional role of L-type $Ca_v1.3$ Ca^{2+}

channels in cardiac pacemaker activity. *Proc. Natl. Acad. Sci. USA.* 100:5543–5548.

64. Verheijck, E. E., A. C. G. van Ginneken, R. Wilders, and L. N. Bouman. 1999. Contribution of L-type Ca^{2+} current to electrical activity in sinoatrial nodal myocytes of rabbits. *Am. J. Physiol. Heart Circ. Physiol.* 276:H1064–H1077.
65. Hilgemann, D. W. 2004. New insights into the molecular and cellular workings of the cardiac Na^+/Ca^{2+} exchanger. *Am. J. Physiol. Cell Physiol.* 287:C1167–C1172.
66. Kang, M., and D. W. Hilgemann. 2004. Multiple transport modes of the cardiac Na^+/Ca^{2+} exchanger. *Nature.* 427:544–547.
67. Kodama, I., M. R. Nikmaram, M. R. Boyett, R. Suzuki, H. Honjo, and J. M. Owen. 1997. Regional differences in the role of the Ca^{2+} and Na^+ currents in pacemaker activity in the sinoatrial node. *Am. J. Physiol. Heart Circ. Physiol.* 272:H2793–H2806.
68. Zhang, H., A. V. Holden, I. Kodama, H. Honjo, M. Lei, T. Varghese, and M. R. Boyett. 2000. Mathematical models of action potentials in the periphery and center of the rabbit sinoatrial node. *Am. J. Physiol. Heart Circ. Physiol.* 279:H397–H421.
69. Zhang, H., and M. Vassalle. 2000. Role of dual pacemaker mechanisms in sinoatrial node discharge. *J. Biomed. Sci.* 7:100–113.
70. Zhang, H., and M. Vassalle. 2001. Role of I_K and I_f in the pacemaker mechanisms of sino-atrial node myocytes. *Can. J. Physiol. Pharmacol.* 79:963–976.
71. Seemann, G., F. B. Sachse, D. L. Weiß, and O. Dössel. 2003. Quantitative reconstruction of cardiac electromechanics in human myocardium: regional heterogeneity. *J. Cardiovasc. Electrophysiol.* 14:S219–S228.
72. Noma, A. 1996. Ionic mechanisms of the cardiac pacemaker potential. *Jpn. Heart J.* 37:673–682.
73. Demir, S. S., J. W. Clark, and W. R. Giles. 1999. Parasympathetic modulation of sinoatrial node pacemaker activity in rabbit heart: a unifying model. *Am. J. Physiol.* 276:H2221–H2244.
74. Mitsuiye, T., Y. Shinagawa, and A. Noma. 2000. Sustained inward current during pacemaker depolarization in mammalian sinoatrial node cells. *Circ. Res.* 87:88–91.
75. Chay, T. R., and Y. S. Lee. 1992. Studies on re-entrant arrhythmias and ectopic beats in excitable tissues by bifurcation analyses. *J. Theor. Biol.* 155:137–171.
76. Vinet, A., and F. A. Roberge. 1994. Analysis of an iterative difference equation model of the cardiac cell membrane. *J. Theor. Biol.* 170:201–214.
77. Chay, T. R. 1996. Proarrhythmic and antiarrhythmic actions of ion channel blockers on arrhythmias in the heart: model study. *Am. J. Physiol. Heart Circ. Physiol.* 271:H329–H356.
78. Landau, M., and P. Lorente. 1997. Conduction block and chaotic dynamics in an asymmetrical model of coupled cardiac cells. *J. Theor. Biol.* 186:93–105.
79. He, J.-Q., Y. Ma, Y. Lee, J. A. Thomson, and T. J. Kamp. 2003. Human embryonic stem cells develop into multiple types of cardiac myocytes: action potential characterization. *Circ. Res.* 93:32–39.
80. Gepstein, L., Y. Feld, and L. Yankelson. 2004. Somatic gene and cell therapy strategies for the treatment of cardiac arrhythmias. *Am. J. Physiol. Heart Circ. Physiol.* 286:815–822.
81. Xue, T., H. C. Cho, F. G. Akar, S.-Y. Tsang, S. P. Jones, E. Marbán, G. F. Tomaselli, and R. A. Li. 2005. Functional integration of electrically active cardiac derivatives from genetically engineered human embryonic stem cells with quiescent recipient ventricular cardiomyocytes: insights into the development of cell-based pacemakers. *Circulation.* 111:11–20.
82. Greenstein, J. L., and R. L. Winslow. 2002. An integrative model of the cardiac ventricular myocytes incorporating local control of Ca^{2+} release. *Biophys. J.* 83:2918–2945.
83. Shannon, T. R., F. Wang, J. Puglisi, C. Weber, and D. M. Bers. 2004. A mathematical treatment of integrated Ca dynamics within the ventricular myocyte. *Biophys. J.* 87:3351–3371.
84. Saucerman, J. J., L. L. Brunton, A. P. Michailova, and A. D. McCulloch. 2003. Modeling β-adrenergic control of cardiac myocyte contractility *in silico*. *J. Biol. Chem.* 278:47997–48003.
85. Mummery, C., D. Ward-van Oostwaard, P. Doevendans, R. Spijker, S. van den Brink, R. Hassink, M. van der Heyden, T. Opthof, M. Pera, A. B. de la Riviere, R. Passier, and L. Tertoolen. 2002. Differentiation of human embryonic stem cells to cardiomyocytes: role of coculture with visceral endoderm-like cells. *Circulation.* 107:2733–2740.
86. Boyett, M. R., H. Honjo, and I. Kodama. 2000. The sinoatrial node, a heterogeneous pacemaker structure. *Cardiovasc. Res.* 47:658–687.
87. Boyett, M. R., H. Dobrzynski, M. K. Lancaster, S. A. Jones, H. Honjo, and I. Kodama. 2003. Sophisticated architecture is required for the sinoatrial node to perform its normal pacemaker function. *J. Cardiovasc. Electrophysiol.* 14:104–106.
88. Verheijck, E. E., R. Wilders, and L. N. Bouman. 2002. Atrio-sinus interaction demonstrated by blockade of the rapid delayed rectifier current. *Circulation.* 105:880–885.
89. Garny, A., P. Kohl, P. J. Hunter, M. R. Boyett, and D. Noble. 2003. One-dimensional rabbit sinoatrial node models: benefits and limitations. *J. Cardiovasc. Electrophysiol.* 14:S121–S132.
90. Peeters, G. A., M. C. Sanguinetti, Y. Eki, H. Konarzewska, D. G. Renlund, S. V. Karwande, and W. H. Barry. 1995. Method for isolation of human ventricular myocytes from single endocardial and epicardial biopsies. *Am. J. Physiol.* 268:H1757–H1764.
91. Péréon, Y., S. Demolombe, I. Baró, E. Drouin, F. Charpentier, and D. Escande. 2000. Differential expression of KvLQT1 isoforms across the human ventricular wall. *Am. J. Physiol. Heart Circ. Physiol.* 278: H1908–H1915.
92. Piacentino III, V., C. R. Weber, X. Chen, J. Weisser-Thomas, K. B. Margulies, D. M. Bers, and S. R. Houser. 2003. Cellular basis of abnormal calcium transients of failing human ventricular myocytes. *Circ. Res.* 92:651–658.

ELSEVIER Prostaglandins & other Lipid Mediators 78 (2005) 218–230

PROSTAGLANDINS & other LIPID MEDIATORS

Involvement of platelet-activating factor and leukotrienes in anaphylactic segmental venoconstriction in ovalbumin sensitized guinea pig livers

Toshishige Shibamoto *, Zonghai Ruan, Sen Cui, Wei Liu, Yasutaka Kurata

Department of Physiology, Kanazawa Medical University, Uchinada, Ishikawa 920-0293, Japan

Received 5 July 2005; received in revised form 18 August 2005; accepted 19 August 2005
Available online 19 September 2005

Abstract

The hepatic anaphylactic venoconstriction is partly involved in anaphylactic hypotension, and is characterized by significant post-sinusoidal constriction and liver congestion in guinea pigs. We determined what chemical mediators are involved in anaphylaxis-induced segmental venoconstriction and liver congestion in perfused livers isolated from ovalbumin sensitized guinea pigs. Livers were perfused portally and recirculatingly at constant flow with diluted blood. The sinusoidal pressure was measured by the double occlusion pressure (Pdo), and was used to determine the pre-sinusoidal (Rpre) and post-sinusoidal (Rpost) resistances. An antigen injection increased both the portal vein pressure and Pdo, resulting in 4.1- and 2.3-fold increases in Rpre and Rpost, respectively. Hepatic congestion was observed as reflected by liver weight gain. Pretreatment with TCV-309 (10 μM, platelet-activating factor (PAF) receptor antagonist) or ONO-1078 (100 μM, human cysteinyl-leukotriene (Cys-LT) receptor 1 antagonist), but not indomethacin (10 μM, cyclooxygenase inhibitor), ketanserin (10 μM, serotonin receptor antagonist), or diphenhydramine (100 μM, histamine H_1 antagonist), significantly attenuated this anaphylactic hepatic venoconstriction. Anaphylaxis-induced increases in Rpre and

Abbreviations: PAF, platelet-activating factor; Cys-LTs, cysteinyl-leukotrienes; $CysLT_1$, cysteinyl-leukotriene receptor 1; $CysLT_2$, cysteinyl-leukotriene receptor 2; Tx, thromboxane; IVC; inferior vena cava; Ppv, portal venous pressure; Phv, hepatic venous pressure; Pdo, double occlusion pressure; Q, portal blood flow rate; Rt, total portal-hepatic venous resistance; Rpre, pre-sinusoidal resistance; Rpost, post-sinusoidal resistance

* Corresponding author. Tel.: +81 76 218 8104; fax: +81 76 286 8010.
E-mail address: shibamo@kanazawa-med.ac.jp (T. Shibamoto).

1098-8823/$ – see front matter © 2005 Elsevier Inc. All rights reserved.
doi:10.1016/j.prostaglandins.2005.08.003

Rpost were significantly inhibited by TCV-309 (by 48%) and ONO-1078 (by 36%), respectively. Combined TCV-309 and ONO-1078 pretreatment exerted additive inhibitory effects on anaphylactic hepatic venoconstriction. Anaphylactic hepatic weight gain was converted to weight loss when post-sinusoidal constriction was attenuated. It is concluded that anaphylaxis-induced pre-sinusoidal constriction is mainly caused by PAF and the post-sinusoidal constriction by Cys-LTs in guinea pig livers.
© 2005 Elsevier Inc. All rights reserved.

Keywords: Leukotriene; Platelet-activating factor; Histamine; Hepatic circulation; Antigen; Double occlusion pressure; Hepatic vascular resistance

1. Introduction

Anaphylactic hypotension is sometimes life-threatening, and is caused by a decrease in effective circulating blood volume [1]. It is reported that livers are partly involved in anaphylactic hypotension [2,3]. Anaphylaxis causes hepatic venoconstriction, as observed in rats [3,4], guinea pigs [5] and dogs [6,7], resulting in portal hypertension which then causes congestion of the upstream splanchnic organs, with resultant decrease in venous return and effective circulating blood volume, and finally augmentation of anaphylactic hypotension. Furthermore, if anaphylactic venoconstriction occurs substantially in the hepatic post-sinusoidal veins, hepatic congestion, pooling of blood in liver itself develops, which could contribute to anaphylactic hypotension, as observed in canine anaphylaxis [7,8]. We have recently reported that hepatic anaphylactic venoconstriction in guinea pigs is also accompanied by liver congestion [5]. Measurement of the sinusoidal pressure with the vascular occlusion method revealed that this hepatic congestion was caused by significant post-sinusoidal constriction, although the pre-sinusoidal constriction was predominant [5].

Anaphylaxis is the classic well-established immunoglobulin E dependent reaction [9]. Various inflammatory mediators, including histamine, serotonin, platelet-activating factor (PAF), and eicosanoids such as cysteinyl-leukotrienes (CysLTs), thromboxane (Tx) A_2, and prostaglandin D_2, are involved in the initiation and propagation of the anaphylactic responses [10–14]. However, the primary mediators responsible for the local anaphylactic response may differ among organs and tissues involved. The mediators responsible for hepatic anaphylaxis in any species including guinea pigs have not been determined. Indeed, histamine, which is stored in mast cells and released during degranulation, causes hepatic venoconstriction in guinea pigs [15]. PAF [16], TxA_2 [16] and LTD_4 [17,18], all of which are the products of the arachidonic acid cascade and are synthesized upon mast cell activation, induce hepatic venoconstriction. However, it is not known which mediator is mainly involved in the anaphylactic pre- or post-sinusoidal constriction, and hepatic congestion. Thus, the purpose of the present study was to determine the role of histamine, serotonin, eicosanoids, and PAF in the pre- and post-sinusoidal constriction and hepatic congestion during guinea pig hepatic anaphylaxis by using the corresponding receptor antagonists or enzyme-synthesis inhibitors.

2. Materials and methods

2.1. Animals

The experiments conducted in the present study were approved by the Animal Research Committee of Kanazawa Medical University.

Forty-two male Hartley guinea pigs weighing 356 ± 5 (S.E.) g were used in this study. The animals were housed in a temperature-controlled animal facility with alternating 12-h light/12-h dark cycles and fed standard lab chow ad libitum with free access to water.

2.2. Antigen sensitization

Guinea pigs were actively sensitized by the subcutaneous injection of an emulsion made by mixing complete Freund's adjuvant (0.5 ml) with 1 mg ovalbumin (grade V, Sigma) dissolved in physiological saline (0.5 ml).

2.3. Isolated liver preparation

Two weeks after sensitization, the animals were anesthetized with pentobarbital sodium (35 mg/kg, i.p.) and mechanically ventilated with room air. The methods of isolation and perfusion of guinea pig livers were previously described [5]. A polyethylene tube was placed in the right carotid artery. After laparotomy, the cystic duct and the hepatic artery were ligated and the bile duct was cannulated with the polyethylene tube (1.0 mm i.d., 1.3 mm o.d.). At 5 min after intraarterial heparinization (500 U/kg), 8–9 ml of blood was withdrawn with a plastic syringe through the carotid arterial catheter. The intra-abdominal inferior vena cava (IVC) above the renal veins was ligated, and the portal vein was cannulated with a stainless cannula (2.1 mm i.d., 3.0 mm o.d.) for portal perfusion. After thoracotomy, the supradiaphragmatic IVC was cannulated through a right atrium incision with the same size stainless cannula, then portal perfusion was begun with the heparinized autologous blood that was diluted with 5% bovine albumin (Sigma) in Krebs solution (118 mM NaCl, 5.9 mM KCl, 1.2 mM $MgSO_4$, 2.5 mM $CaCl_2$, 1.2 mM NaH_2PO_4, 25.5 mM $NaHCO_3$, and 5.6 mM glucose) at Hct of 8%. The liver was rapidly excised, suspended from an isometric transducer (TB-652T, Nihon-Kohden, Japan) and weighed continuously throughout the experimental period.

The sensitized livers were perfused at a constant flow rate in a recirculating manner via the portal vein with blood that was pumped using a Masterflex roller pump from the venous reservoir through a heat exchanger (37 °C). The recirculating blood volume was 40 ml. The height of the reservoir and the portal blood flow rate could be adjusted independently to maintain the portal and hepatic venous pressures at any desired level. The perfused blood was oxygenated in the venous reservoir by continuous bubbling with 95% O_2 and 5% CO_2. The portal venous (Ppv) and the hepatic venous (Phv) pressures were measured with pressure transducers (TP-400T, Nihon-Kohden, Japan) attached by sidearm to the appropriate cannulas with the reference points at the hepatic hilus. To occlude inflow and outflow perfusion lines simultaneously for measurement of the double occlusion pressure

(Pdo), two solenoid valves were placed in such a position that each sidearm cannula was between the corresponding solenoid valve and the liver. Portal blood flow rate (Q) was measured with an electromagnetic flow meter (MFV 1200, Nihon-Kohden, Japan), and the flow probe was positioned in the inflow line. Bile was collected drop by drop in a small tube suspended from the force transducer (SB-1T, Nihon-Kohden, Japan). One bile drop yielded 0.027 g and the time between drops was measured for determination of the bile flow rate [4]. The hepatic vascular pressures, blood flow rate, liver weight and bile weight were monitored continuously and displayed through a thermal physiograph (RMP-6008, Nihon-Kohden, Japan). Outputs were also digitized by the analog-digital converter at a sampling rate of 100 Hz. These digitized values were displayed and recorded using a personal computer for later determination of Pdo.

2.4. Experimental protocols

Hepatic hemodynamic parameters were observed for at least 20 min after the start of perfusion until an isogravimetric state (no weight gain or loss) was obtained by adjusting the flow rate and the height of the reservoir at a Phv of 0–1 cmH_2O, and at a Q of 44 ± 1 ml/min/10 g liver wt. After the baseline measurements, the perfused livers excised from the sensitized animals were randomly assigned to one of the following six groups.

In the Control group ($n=6$), ovalbumin 0.1 mg was injected into the reservoir. In all other groups, 10 min before an injection of antigen (0.1 mg), the following receptor antagonists or inhibitors were injected into the perfusate: (1) diphenhydramine HC1 (100 μM), a histamine H_1-receptor antagonist, for the Diphenhydramine group ($n=6$); (2) ketanserin (10 μM), a serotonin-receptor antagonist, for the Ketanserin group ($n=6$); (3) indomethacin (10 μM), a cyclooxygenase inhibitor, for the Indomethacin group ($n=6$); (4) TCV-309 (l0 μM; {3-bromo-5-[*N*-phenyl-*N*-(2-{[2-(1,2,3,4-tetrahydro-2-isoquinolyl-carbonyloxy)-ethyl]carbamoyl}ethyl)carbamyl]-l-propylpyridi nium nitrate}), a PAF-receptor antagonist [19], for the TCV-309 group ($n=6$); (5) ONO-1078 (100 μM; 4-oxo-8-[p-(4-phenylbutyloxy) benzoylamino]-2-(tetrazol-5-yl)-4H-1-benzopyran hemihydrate), a specific antagonist for human cysteinyl leukotriene receptor 1 ($CysLT_1$) [20], for the ONO-1078 group ($n=6$); and (6) both TCV-309 (10 μM) and ONO-1078 (100 μM) for the combined TCV-309 and ONO-1078 group ($n=6$).

The effects of each inhibitor or antagonist were evaluated by comparing the response of the agent-treated group with that of the Control group. The concentrations of TCV-309 (10 μM), diphenhydramine (100 μM), and ketanserin (10 μM) employed in this study were high enough to completely inhibit submaximal hepatic venoconstriction induced by 10 μM PAF, 100 μM histamine, and 10 μM serotonin, respectively, in the isolated guinea pig livers in our preliminary studies. The concentrations of indomethacin and ketanserin were chosen as previously described [21,22].

The hepatic sinusoidal pressure was measured by the double occlusion method [7]. Both the inflow and outflow lines were simultaneously and instantaneously occluded for 13 s using the solenoid valves, after which Ppv and Phv rapidly equilibrated to a similar or identical pressure, which was Pdo. Actually, Pdo values were obtained from the digitized data of Ppv and Phv using an original program (LIVER software, Biomedical

Science, Kanazawa, Japan). In each experimental group, Pdo was measured at baseline and 4, 6, and 10 min, and then at a 10-min intervals up to 120 min after an injection of ovalbumin.

The total portal-hepatic venous (Rt), pre-sinusoidal (Rpre) and post-sinusoidal (Rpost) resistances were calculated by the following equations.

$$\mathrm{Rt} = \frac{(\mathrm{Ppv} - \mathrm{Phv})}{Q} \tag{1}$$

$$\mathrm{Rpre} = \frac{(\mathrm{Ppv} - \mathrm{Pdo})}{Q} \tag{2}$$

$$\mathrm{Rpost} = \frac{(\mathrm{Pdo} - \mathrm{Phv})}{Q} \tag{3}$$

2.5. Drugs

TCV-309 and ONO-1078 were kindly provided by Takeda Chemical, (Osaka, Japan) and Ono Pharmaceutical (Osaka, Japan), respectively. Diphenhydramine-HCl, indomethacin and ketanserin were purchased from Sigma (St. Louis, MO, USA). TCV-309, ketanserin, and diphenhydramine-HC 1 were dissolved in saline. ONO-1078 was dissolved in 1N NaOH and ethanol. Indomethacin was dissolved in DMSO. Concentrations of drugs were expressed as a final concentration in the perfusate.

2.6. Statistics

All results are expressed as the means ± S.E. Data were analyzed by one- and two-way analysis of variance, using repeated-measures for two-way comparison within groups. Comparisons of individual points between groups and within groups were made by Bonferroni's test. Differences were considered as statistically significant at P-values less than 0.05.

3. Results

3.1. Antigen-induced hepatic segmental venoconstriction and hepatic weight gain

Fig. 1(left) shows a representative example of the response to 0.1 mg ovalbumin in the Control group. Within 1 min after an ovalbumin injection, venoconstriction occurred as evidenced by an increase in Ppv, which reached peak levels of 23.5 ± 1.2 cmH_2O from the baseline of 7.2 ± 0.2 cmH_2O. The Ppv-to-Phv gradient, the determinant of Rt, increased to 3.3 times the baseline, indicating that Rt increased by the same degree, as shown in Fig. 2. The double occlusion maneuver performed at 4 min after antigen revealed the sinusoidal pressure of Pdo (7.2 ± 0.4 cmH_2O) higher than that of the baseline (3.3 ± 0.1 cmH_2O). The Pdo-to-Phv gradient increased from the baseline of 2.9 ± 0.1 to 6.7 ± 0.4 cmH_2O, indicating an increase in Rpost (2.3-fold baseline). However, the increase in the Ppv-to-Pdo gradient (3.9 ± 0.2 cmH_2O versus 16.3 ± 1.1 cmH_2O, baseline versus peak) was greater than that

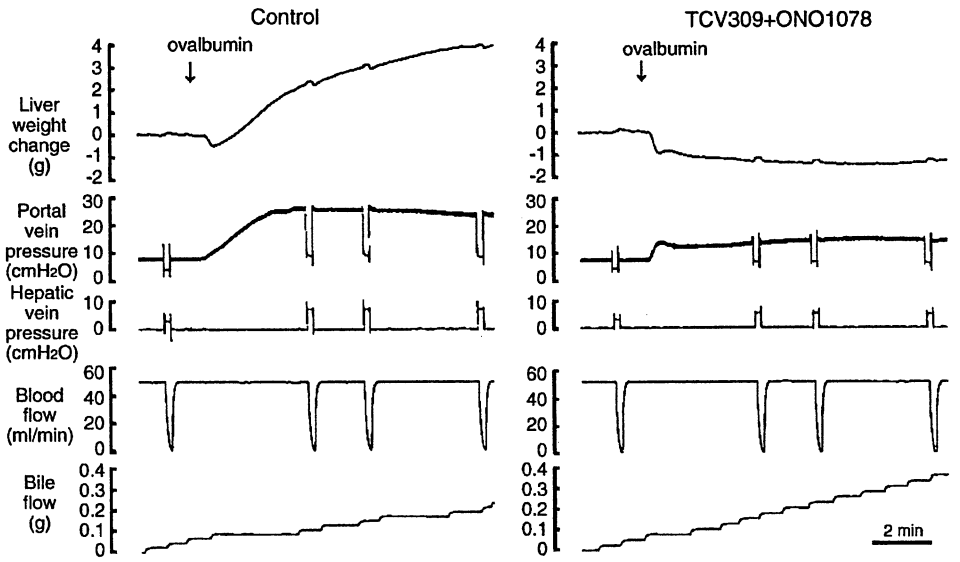


Fig. 1. Representative recordings of the response to the antigen, ovalbumin 0.1 mg in the Control (left) and the combined TCV-309 and ONO-1078 (right) groups.

in the Pdo-to-Phv gradient, indicating a greater increase in Rpre (4.2-fold baseline) than Rpost. At the same time the liver weight showed a gradual increase, reaching the peak of 2.1 ± 0.5 g/10 g liver weight at 10 min. Concomitant with venoconstriction, the bile flow rate decreased to 57% of the baseline of 0.03 ± 0.01 g/min/10 g liver wt.

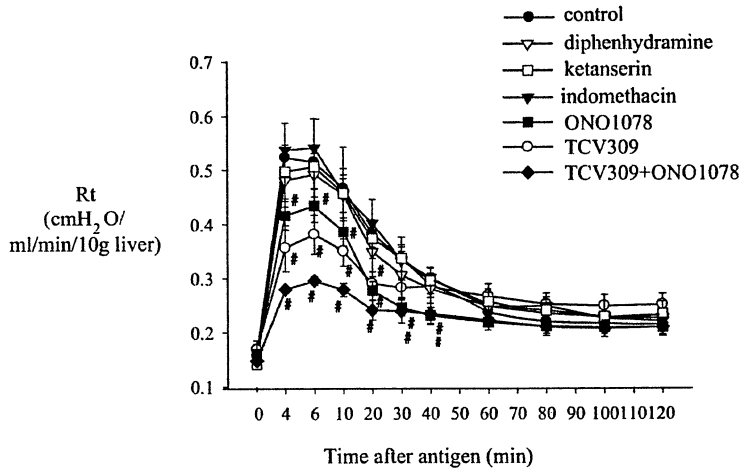


Fig. 2. Time course of total vascular resistance (Rt) in all seven groups. Values are means ± S.E.; $^{\#}P < 0.05$ vs. the Control group. All values of Rt after antigen in each group were significantly different from the corresponding baseline values.

3.2. *Effects of diphenhydramine, ketanserin, indomethacin, TCV-309, ONO-1078, and combined TCV-309 and ONO-1078 on antigen-induced hepatic segmental venoconstriction and hepatic weight gain*

Fig. 2 shows the time course of changes in Rt after antigen in all groups studied. In the control sensitized group, Rt increased from the baseline levels of 0.16 ± 0.01 to the peak levels of 0.52 ± 0.02 cmH_2O/ml/min/10 g liver wt. at 4 min after antigen, followed by a gradual return towards the baseline. Pretreatment with TCV-309, ONO-1078, or the combination of TCV-309 and ONO-1078 (TCV-309 + ONO-1078), but not indomethacin, ketanserin, or diphenhydramine, significantly attenuated this increase in Rt. The order of the degrees of the inhibition was the combined TCV-309 and ONO-1078 > TCV-309 > ONO-1078, as shown in Fig. 2. Actually the peak levels of Rt after antigen decreased to 54, 71, and 79% of that of the Control group in the TCV-309 + ONO-1078, TCV-309, and ONO-1078 group, respectively. Thus the inhibitory effect of the combination of TCV-309 and ONO-1078 seemed to be exerted in an additive, rather than synergistical, manner of an inhibitory effect of each drug. Fig. 3 shows the results for Rpre and Rpost. Anaphylaxis-

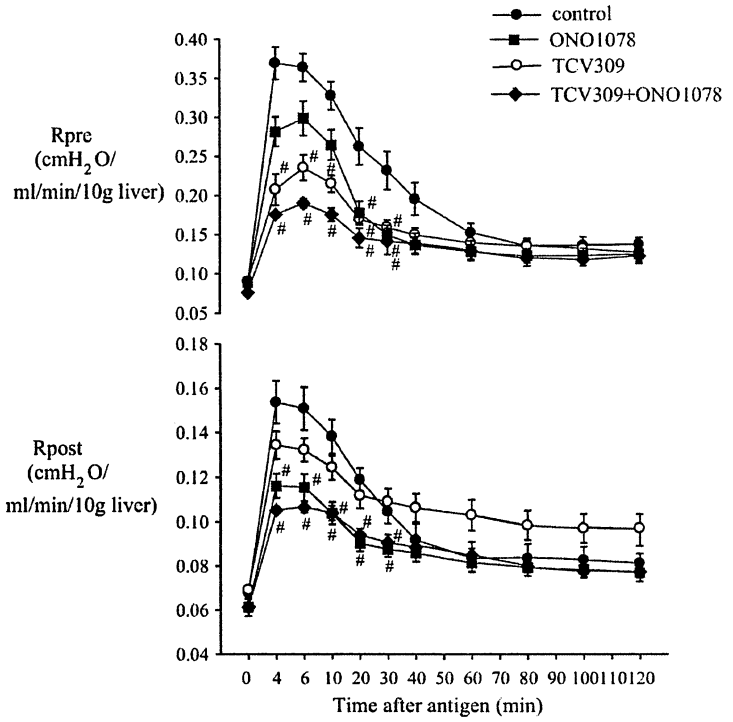


Fig. 3. Time course of the pre-sinusoidal resistance (Rpre) and post-sinusoidal resistance (Rpost) in the Control, the TCV-309, the ONO-1078, and the combined TCV-309 and ONO-1078 groups. Values are means ± S.E.; $^{\#}P < 0.05$ vs. the Control group. All values of Rpre and Rpost after antigen in each group were significantly different from the corresponding baseline values.

induced increases in Rpre and Rpost were significantly attenuated by TCV-309 (by 44%) and ONO-1078 (by 25%), respectively. Combined TCV-309 and ONO-1078 pretreatment exerted additive inhibitory effects on anaphylactic segmental venoconstriction, with pre- and post-sinusoidal vessel constriction decreased by 49 and 27%, respectively. Fig. 1 (right) shows a representative example of the response in the combined TCV-309 and ONO-1078 group.

Fig. 4 shows Pdo and liver weight changes in all groups studied. In the Control group the sinusoidal pressure of Pdo increased significantly from the baseline of 3.3 ± 0.1 cmH_2O to the peak of 7.2 ± 0.4 cmH_2O at 4 min after the antigen. Pretreatment with ONO-1078 and combined TCV-309 and ONO-1078 significantly attenuated the increase in Pdo after antigen, with the peak value of Pdo at 4 min in the ONO-1078 and the combined groups being 5.6 ± 0.2 and 5.2 ± 0.1 cmH_2O, respectively. Anaphylactic hepatic weight gain was observed in all groups but not in the ONO-1078, TCV-309, or the combined TCV-309 and ONO-1078 groups. In the ONO-1078 and the combined groups, the liver weight after antigen significantly decreased to the nadir of -1.0 ± 0.1 and -1.3 ± 0.1 g/10 g liver wt., respectively. In the TCV-309 group, the liver weight tended to decrease but not significantly after antigen.

4. Discussion

In the present study, we determined the chemical mediators responsible for anaphylactic hepatic segmental venoconstriction in isolated sensitized guinea pig livers perfused at a constant flow. The hepatic vascular resistances were assigned to the Rpre and Rpost by measuring the sinusoidal pressure with the vascular occlusion methods [7]. We found that hepatic anaphylactic venoconstriction was characterized by predominant pre-sinusoidal constriction and liver weight gain. This finding was consistent with our previous findings [5] although the method of sensitization of the guinea pigs with ovalbumin was different: the antigen was injected intraperitoneally in the previous study [5], while subcutaneously in the present study. The main finding of the present study was that anaphylaxis-induced pre-sinusoidal constriction was significantly inhibited by a PAF-receptor antagonist, TCV-309, and post-sinusoidal constriction by a $CysLT_1$ receptor antagonist, ONO-1078. The combined TCV-309 and ONO-1078 pretreatment exerted additive inhibitory effects on this segmental venoconstriction. On the other hand, inhibition of the receptor of histamine or serotonin, or inhibition of cyclooxygenase, alone did not affect the hepatic anaphylactic response. Another major finding was that anaphylactic hepatic weight gain was converted to weight loss when post-sinusoidal constriction was attenuated by ONO-1078 and combined TCV-309 and ONO-1078.

In the present study, pretreatment with TCV-309, a PAF antagonist, most intensely inhibited the increase in Rt after antigen (by 29%). This finding suggests that PAF is the primary mediator of the hepatic anaphylactic venoconstriction in guinea pigs. This hepatic venoconstriction was characterized by predominant pre-sinusoidal constriction rather than post-sinusoidal constriction. Actually, TCV-309 significantly attenuated this anaphylactic pre-sinusoidal constriction, but not the post-sinusoidal constriction, as shown in Fig. 3. With respect to the effects of PAF on the segmental hepatic vascular resistances of guinea pigs,

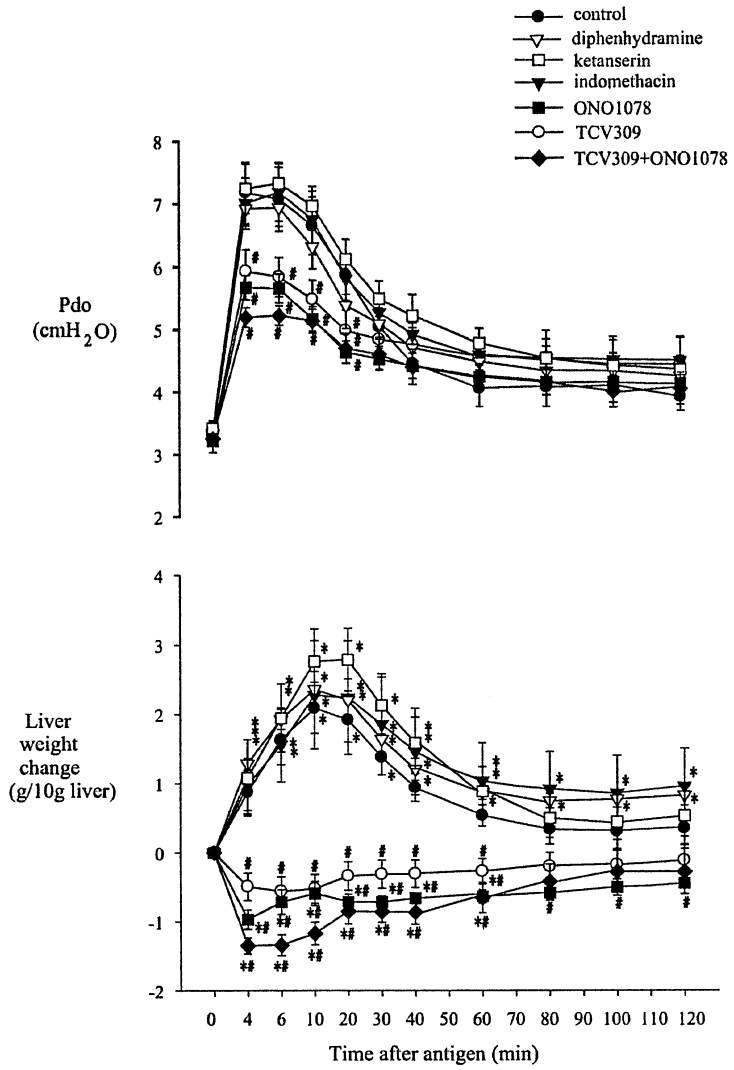


Fig. 4. Time course of the double occlusion pressure (Pdo) and the liver weight change in all seven groups. Values are means ± S.E.; $^{*}P<0.05$ vs. baseline. The asterisks were not given in Pdo after antigen, because all these values were significantly different from the corresponding baseline values. $^{\#}P<0.05$ vs. the Control group.

we have recently reported that PAF injected into the isolated guinea pig livers perfused in the same way as in the present study caused predominant pre-sinusoidal constriction with liver weight gain, the response similar to the anaphylactic response [16]. The crucial role of PAF was also reported in guinea pig anaphylaxis in vivo and in isolated lung parenchymal strips in vitro [23]. Darius et al. [23] demonstrated that the histamine- and leukotriene-independent component of anaphylactic hypotension and bronchoconstriction

in guinea pigs is mediated by PAF. These findings are consistent with the present results on the hepatic anaphylaxis in guinea pigs.

Cys-LTs are demonstrated to be as another main mediator in the guinea pig hepatic vascular anaphylaxis since pretreatment with ONO-1078 significantly attenuated the increase in Rt after antigen (by 21%). In contrast to TCV-309, which selectively inhibited the pre-sinusoidal constriction, ONO-1078, selective $CysLT_1$ antagonist, significantly inhibited anaphylactic post-sinusoidal constriction, but not the pre-sinusoidal constriction. Although Cys-LTs constrict hepatic vessels [17,18], it is not known which vascular segment of hepatic vessels is preferentially constricted by Cys-LTs. The present study suggests that Cys-LTs contract significantly the post-sinusoidal vessels of guinea pig livers via the $CysLT_1$ receptor, and substantially contribute to anaphylactic hepatic venoconstriction of this animal. It has been known that the vasoactive effects of Cys-LTs are mediated by at least 2 specific receptors, $CysLT_1$ and Cys-LT receptor 2 ($CysLT_2$) [24,25]. However there are only a limited number of studies that revealed the roles of these specific receptors in hepatic circulation [26]. Graupera et al. [26] reported using intact perfused rat livers that $CysLT_1$ receptor blockade mimics the effect on portal perfusion pressure caused by 5-lipoxygenase inhibition, suggesting that regulation of normal vascular tone by Cys-LTs is mediated by the activation of $CysLT_1$ receptors. We here show that anaphylactic post-sinusoidal constriction in guinea pigs is mediated by the activation of $CysLT_1$ receptors. However, the roles of $CysLT_2$ receptor and a third class of Cys-LT receptor could not be examined due to the lack of specific antagonists [24,25]. In future, further studies are required in this respect.

Combined TCV-309 and ONO-1078 pretreatment inhibited the anaphylaxis-induced increases in Rt, Rpre, and Rpost by 46, 49, and 27%, respectively. This suggests that PAF and Cys-LTs exert the hepatic venoconstrictive actions in not synegistical but additive manner.

In the present study, diphenhydramine, a histamine H_1-receptor antagonist, did not attenuate the venoconstriction induced by ovalbumin antigen. Histamine is known to be released during systemic anaphylaxis in humans [27] and in animals [12,28,29]. Actually, Selig et al. [13] showed, by using isolated perfused lungs of guinea pigs that were sensitized with ovalbumin, that the histamine H_1-receptor antagonist prevented the antigen-induced changes in pulmonary hemodynamics, intratracheal pressure, and edematogenic responses. Organ dependent difference in responsiveness to antigen may account for the difference in the effect of histamine antagonist between lungs and livers. Indeed, we have recently shown that in guinea pigs, the hepatic vascular response to histamine was relatively weak and short-lasting as observed in isolated perfused livers: even at high concentration of 100 μM, Rt increased only to 1.7-fold baseline, and this response lasted only 3 min [15]. Another explanation why a histamine antagonist did not prevent anaphylactic response is that histamine is released only early stage of anaphylaxis in guinea pigs [23,30]. Mest et al. [30] reported by examining the time course changes in chemical mediators during guinea pig anaphylaxis that histamine and serotonin were released immediately after antigen, reaching peak levels at 20–30 s, and then the release decreased rapidly within 60 s. Thus, when the maximum venoconstriction occurred in the present perfused guinea pig livers, histamine might have disappeared in perfusing blood. Failure of the histamine antagonist to prevent the physiological changes after the antigen administration in the present study suggests a minor role

of histamine in anaphylactic vasoconstriction in guinea pig livers. Finally, a more plausible explanation for the absence of the effect of diphenhydramine (histamine inhibitor), and also ketanserin (serotonin inhibitor) or indomethacin (cyclooxygenase inhibitor) on vasoconstriction is that more than one mediators are released at supramaximal concentrations, and thus inhibition of a single mediator has no effect on the magnitude of the constriction. For instance, even if the response to histamine, serotonin or TxA_2 is completely blocked, the response to PAF and Cys-LTs still remain intact, and no change in the constriction is observed.

In this study, liver weight gain was observed after antigen in the Control group but not in either TCV-309, ONO-1078, or the combined ONO-1078 and TCV-309 group. Moreover, the latter two groups showed the liver weight loss response. The weight gain in the Control group might be caused by post-sinusoidal venoconstriction as evidenced by a substantial increase in Rpost. This post-sinusoidal contraction could induce the upstream sinusoidal engorgement and increased extravascular fluid filtration caused by an increase in Pdo, the sinusoidal hydrostatic pressure. The absence of liver weight gain after antigen in the TCV-309, ONO-1078, or the combined groups may be due to the attenuation of post-sinusoidal constriction. Actually in these three groups, the sinusoidal pressure of Pdo, which is the indicator of post-sinusoidal resistance as well as the determinant of transvascular fluid movement and hepatic congestion, was not so much increased. We previously reported that the magnitude of an increase in Pdo in response to PAF and the TxA_2 analogue was strongly associated with the liver weight change in the same guinea pig liver preparation [16]. The perfused liver with pre-sinusoidal venoconstriction does not show liver weight gain until post-sinusoidal vessels contract enough to elevate Pdo to more than 6.5 cmH_2O. In the present study, the peak Pdo in the TCV-309, ONO-1078 and the combined ONO-1078 and TCV-309 groups was less than 6.5 cmH_2O (Fig. 4). On the other hand, the conversion from liver weight gain to liver weight loss after antigen in the ONO-1078 and the combined groups may be explained as follows: In these two groups, the anaphylaxis-induced post-sinusoidal constriction was substantially attenuated, but the pre-sinusoidal constriction was preserved. In the presence of pre-sinusoidal constriction, the blood volume of sinusoids, that was distal to the constricted pre-sinusoidal portal venules, could be passively reduced due to a decrease in distending pressure of the sinusoids. This reduction of blood volume may result in liver weight loss.

In summary, the chemical mediators responsible for the hepatic anaphylactic segmental venoconstriction induced by ovalbumin antigen were determined in isolated guinea pig livers. Anaphylaxis-induced pre- and post-sinusoidal constriction was inhibited markedly by the PAF inhibitor TCV-309 and the Cys-LT receptor 1 antagonist ONO-1078, respectively, whereas histamine, serotonin or cyclooxygenase inhibitors did not affect this response. We conclude that anaphylaxis-induced pre-sinusoidal constriction is mainly caused by PAF and the post-sinusoidal constriction by Cys-LTs in guinea pig livers.

Acknowledgements

The authors thank Takeda Chemical Industries (Osaka, Japan) and Ono Pharmaceutical Company (Osaka, Japan) for the gift of TCV-309 and ONO-1078, respectively.

This study was supported by a Grant for Collaborative Research from Kanazawa Medical University (C2004-1, C2005-1) and a Grant-in-Aid for Scientific Research from the Ministry of Education, Culture, Sports, Sciences and Technology of Japan (No. 15591665).

References

[1] Brown AFT. Anaphylactic shock: mechanism and treatment. J Accid Emerg Med 1995;12:89–100.
[2] Pavek K, Piper PJ, Smedegard G. Anaphylatoxin-induced shock and two patterns of anaphylactic shock: hemodynamics and mediators. Acta Physiol Scand 1979;105:393–403.
[3] Shibamoto T, Cui S, Ruan Z, Liu W, Takano H, Kurata Y. Hepatic venoconstriction is involved in anaphylactic hypotension in rats. Am J Physiol Heart Circ Physiol, May 27 [Epub], in press.
[4] Hines KL, Fisher RA. Regulation of hepatic glycogenolysis and vasoconstriction during antigen-induced anaphylaxis. Am J Physiol 1992;262:G868–77.
[5] Ruan Z, Shibamoto T, Shimo T, Tsuchida H, Koizumi T, Nishio M. NO, but not CO, attenuates anaphylaxis-induced postsinusoidal contraction and congestion in guinea pig liver. Am J Physiol Regul Integr Comp Physiol 2004;286:R94–100.
[6] Weil R. Studies in anaphylaxis. XXI Anaphylaxis in dogs: a study of the liver in shock and peptone poisoning. J Immunol 1917;2:525–56.
[7] Yamaguchi Y, Shibamoto T, Hayashi T, Saeki Y, Tanaka S. Hepatic vascular response to anaphylaxis in isolated canine liver. Am J Physiol Regul Integr Comp Physiol 1994;267:R268–74.
[8] Essex HE. Anaphylactic and anaphylactoid reactions with special emphasis on the circulation. In: Hamilton, W.F., editor. Handbook of physiology circulation, Section 2, vol. III, Chapter 66, Bethesda, MD: Am. Physiol. Soc.;1965, p. 2391–408.
[9] Patterson R, Roberts M, Pruzansky JJ. Comparisons of reaginic antibodies from three species. J Immunol 1969;102:466–75.
[10] Hagmann W, Hacker HJ, Buchholz U. Resident mast cells are the main initiators of anaphylactic leukotriene production in the liver. Hepatology 1992;16:1477–84.
[11] Lieberman PL. Specific and idiopathic anaphylaxis: pathophysiology and treatment. In: Bierman CW, Pearlman DL, Shapiro CG, et al., editors. Allergy, asthma, and immunology from infancy to adulthood. 3rd ed. Philadelphia: WB. Saunders; 1996. p. 297–319.
[12] Morel DR, Skoskiewicz M, Robinson DR, Bloch KJ, Hoaglin DC, Zapol WM. Leukotrienes, thromboxane A_2, and prostaglandins during systemic anaphylaxis in sheep. Am J Physiol Heart Circ Physiol 1991;261:H782–92.
[13] Selig WN, Tocker JE, Tannu SA, Cerasoli F, Durham SK. Pharmacologic modulation of antigen-induced pulmonary responses in the perfused guinea pig lung. Am Rev Respir Dis 1993;147:262–9.
[14] Terashita Z, Imura Y, Nishikawa K. Possible pathophysiological roles of platelet-activating factor in shock and the PAF antagonists, CV-3988 and CV-6209. In: Handley DA, Sauders RN, Houlihan WJ, Tomesch JC, editors. Platelet-activating factor in endotoxin and immune diseases. New York: Marcel Dekker; 1990. p. 547–75.
[15] Shibamoto T, Narushima M, Ling YQ, et al. Different hepatic vascular response to noradrenaline and histamine between guinea pig and rat. Acta Physiol Scand 2004;180:255–63.
[16] Ruan Z, Shibamoto T, Shimo T, et al. Effects of platelet-activating factor and thromboxane A_2 on isolated perfused-guinea pig liver. Prostaglandins Other Lipid Mediat 2004;73:73–85.
[17] Bilzer M, Lauterburg BH. Peptidoleukotrienes increase the efflux of glutathione from perfused rat liver. Prostaglandins Leukot Essent Fatty Acids 1993;49:715–21.
[18] Haussinger D, Stehle T, Gerok W. Effects of leukotrienes and the thromboxane A2 analogue U-46619 in isolated perfused rat liver. Metabolic, hemodynamic and ion-flux responses. Biol Chem Hoppe Seyler 1988;369:97–107.
[19] Terashita Z, Kawamura M, Takatani M, Tsuchima S, Imura Y, Nishikawa K. Beneficial effects of TCV-309, a novel potent and selective platelet activating factor antagonist in endotoxin and anaphylactic shock in rodents. J Pharmacol Exp Ther 1992;260:748–55.

[20] Lynch KR, O'Neill GP, Liu Q, et al. Characterization of the human cysteinyl leukotriene CysLT1 receptor. Nature 1999;399:789–93.
[21] Martin GR. Vascular receptors for 5-hydroxytryptamine: distribution, function and classification. Pharmacol Ther 1994;62:283–324.
[22] vom Dahl S, Wettstein M, Gerok W, Haussinger D. Stimulation of release of prostaglandin D2 and thromboxane B2 from perfused rat liver by extracellular adenosine. Biochem J 1990;270:39–44.
[23] Darius HD, Lefer DJ, Smith JB, Lefer AM. Role of platelet-activating factor-acether in mediating guinea pig anaphylaxis. Science 1986;232:58–60.
[24] Hui Y, Funk CD. Cysteinyl leukotrienes receptors. Biochem Pharmacol 2002;64:1549–57.
[25] Capra V. Molecular and functional aspects of human cysteinyl leukotriene receptors. Pharmacol Res 2004;50:1–11.
[26] Graupera M, Garcia-Pagan J-C, Titos E, et al. 5-Lipoxygenase inhibition reduces intrahepatic vascular resistance of cirrhotic rat livers: A possible role of cysteinyl-leukotrienes. Gastroenterology 2002;122:387–93.
[27] Smith PL, Sobotka AK, Bleecker ER, et al. Physiologic manifestations of human anaphylaxis. J Clin Invest 1980;66:1072–80.
[28] Krell RD. Investigation of the role of histamine in antigen-induced bronchoconstriction in the ascaris-hypersensitive dog. Br J Pharmacol 1978;62:519–28.
[29] Silverman HJ, Taylor WR, Smith PL, et al. Effects of antihistamines on the cardiopulmonary changes due to canine anaphylaxis. J Appl Physiol 1988;64:210–7.
[30] Mest HJ, Ponicke K, Heinroth-Hoffmann I, Meissner N, Giessler C. Relevance of mediators to cardiac parameters of isolated anaphylactic guinea-pig heart. Prostaglandins Leukot Essent Fatty Acids 1995;53:21–9.

金医大誌 (J. Kanazawa Med. Univ.) 30 : 6－11, 2005

Beta-Adrenergic Agonist Therapy for Alveolar Edema in Postoperative Pulmonary Complications

Tsutomu Sakuma, Zheng Wang, Jin Xu, Sumiko Maeda, Makoto Sugita, Motoyasu Sagawa

Abstract: Over the past one and a half decade, we have established and developed an *ex vivo* human lung model for the investigation of alveolar fluid reabsorption (alveolar fluid clearance) in the human lung. Alveolar fluid clearance primarily depends on active sodium transport via apical sodium channel and basolateral Na^+-K^+ ATPase on alveolar epithelial cells. Beta-adrenergic agonists stimulate β_1- and β_2-, but not β_3-adrenergic receptors followed by the increase of cAMP and alveolar fluid clearance. Cystic fibrosis transmembrane conductance regulator plays a role in β-adrenergic agonist stimulated alveolar fluid clearance. Hypothermia followed by rewarming preserves alveolar fluid clearance capacity and the function of β-receptors, the results are favorable in the preservation of donor lung for lung transplantation. Since there was a species difference between alveolar fluid clearance among animals, our date from human lungs have contributed to the research area of ion and fluid transport on the alveolar epithelial cells and to the clinical area of pulmonary edema and lung injury.

Key words: pulmonary edema, alveolar epithelium, ion transport, beta-adrenergic agonist

Introduction

There are a number of postoperative pulmonary complications in which fluid accumulates in the alveolar spaces (Table 1). In such diseases, excess alveolar fluid deteriorates alveolar gas exchange and exposes the patients to hypoxemia. If the therapy for the diseases was not successful, the patient will be exposed to high mortality because of respiratory failure followed by multiple organ failure.

Alveolar fluid clearance plays an important role in resolution of alveolar edema in a number of diseases that occur during intra- and post-operative period in patients who undergo pulmonary resection. Over the past two decades, the mechanism responsible for alveolar fluid clearance has been studied in normal and pathological lungs of sheep (1-3), goats (4) , dogs (5, 6) , rats (7-18), rabbits (19), and mice (20-24). Those studies indicated that apical sodium channel and basolateral Na^+-K^+ ATPase on alveolar type II epithelial cells drive excess alveolar fluid out of the alveolar spaces. In human, active ion and fluid transport was suggested by the

Department of Thoracic Surgery, Kanazawa Medical University, Ishikawa 920-0293, Japan
Corresponding to: Tsutomu Sakuma
Accepted: August 22, 2005

Table 1. Postoperative pulmonary complications in which fluid accumulates in the alveolar spaces

Hydrostatic pulmonary edema
Cardiogenic pulmonary edema
Hyperperfusion pulmonary edema
Post-pneumonectomy pulmonary edema
Increased permeability pulmonary edema
Acute respiratory distress syndrome
Re-expansion pulmonary edema
Ischemia-reperfusion lung injury
Ventilator-induced lung injury
Pulmonary reimplantation response
Interstitial inflammation
Idiopathic interstitial pneumonias
Drug-induced interstitial pneumonia
Alveolar inflammation
Aspiration pneumonia: gastric juice, pleural effusion
Bronchopneumonia
Atelectasis

observation that protein concentration increased greater in pulmonary edema fluid than in simultaneously obtained plasma (25-29), but it was not possible to examine the effect of known inhibitors or agonists of alveolar fluid clearance in the clinical setting. We have established and developed the method to measure alveolar fluid clearance in *ex vivo* human lung, and studied the mechanism responsible for alveolar fluid clearance in human lungs. In this article, human studies for alveolar ion and fluid clearance are summarized.

Methods for alveolar fluid clearance in ex vivo human lung

Since we had studied that alveolar fluid clearance occurred in the presence of pulmonary blood flow in sheep (2), we have advanced the method and tested if alveolar fluid clearance occurred in the isolated human lungs. The instillate consisted of a physiologic albumin solution that was adjusted to be isosmolar (290 mOsm/l) with human serum. The solution consisted of total protein 5.0 g/dl; albumin>99 %; Na^+ 155 mEq/l; K^+ 0.3 mEq/l; Cl^- 115 mEq/l; Ca^{2+} 1.8 mEq/l; HCO_3^- 11 mEq/l; glucose 10 mg/dl; and pH 6.8. Human lungs were obtained from patients who underwent pulmonary resection for bronchogenic carcinoma. The age of the patients was 65 ± 8 years. Preoperative pulmonary function test revealed to be normal. Within 10 minutes of surgical removal, a segmental bronchus was occluded by a balloon catheter. Through the catheter, 40 – 50 ml of isosmolar 5% human albumin solution warmed to 37°C was instilled into the occluded segmental lobe followed by 40 ml of air to advance the instilled solution into the alveolar spaces. The lungs were inflated with 100% oxygen at an airway pressure of 7 cmH_2O. The lung was placed in a plastic bag and a humidified incubator at 37°C in order to minimize dehydration (Figure 1). At the conclusion of the experiment over 1 – 4 h, the lung was removed and alveolar fluid was aspirated with a small catheter (0.75 mmID). Aspirated alveolar fluid (1 – 2 ml) was centrifuged at 3,000 rpm for 10 min. The supernatant of the fluid was obtained for measurement of the protein concentration. The total protein concentrations of the instilled albumin solution and the final alveolar fluid were measured by a biuret method. The albumin content was measured by electrophoresis using a cellulose acetate membrane.

Alveolar fluid clearance was estimated by measuring the increase in the protein concentration of the instilled albumin solution. Since protein leaves the air space very slowly (30), the change of the albumin concentration in the alveolar spaces over 1 – 4 h was used as an index of alveolar fluid clearance. Alveolar liquid clearance (AFC) (% of instilled) was calculated according to the following equation:

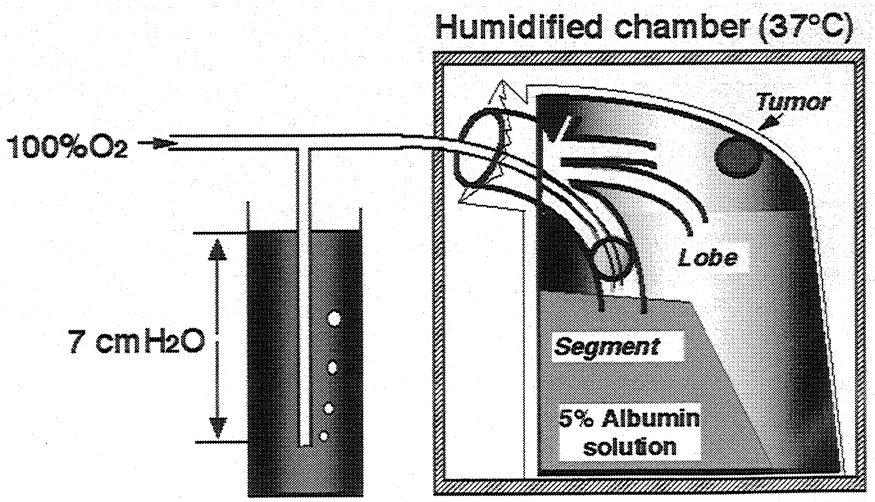


Fig 1. Schematic diagram of the experiment. An isosmolar albumin solution was instilled through the segmental bronchus that was located distant from the tumor.

AFC = (Vi X Fwi-Vf X Fwf) / (Vi X Fwi) X 100
in which V is the volume of the instilled albumin solution (i) and the final alveolar fluid (f), Fw is the water content of the instilled albumin solution (i) and the final alveolar fluid (f). Water content was measured by the albumin concentration. Vf (ml) is measured by the following equation:
Vf (ml) = (Vi X Pi) / Pf
in which P is the albumin concentration of the instilled albumin solution (i) and the final alveolar fluid (f).

Alveolar fluid clearance in ex vivo human lung

Basal alveolar fluid clearance in *ex vivo* human lung in the absence of pulmonary perfusion was 12 ± 2 % over 4 h (31). Amiloride (10^{-5} M), an inhibitor of apical sodium uptake, and ouabain (10^{-3} M), an inhibitor of Na^+-K^+ ATPase activity, reduced alveolar fluid clearance by 40% and 49%, respectively. Hypothermia (8°C) completely inhibited alveolar fluid clearance. These data provided the first direct evidence for active metabolic processes and sodium transport as the major mechanism driving alveolar fluid clearance in *ex vivo* human lung.

β-adrenergic agonists stimulate alveolar fluid clearance

There was a species difference in the effect of β-adrenergic agonists on alveolar fluid clearance. Although β-adrenergic agonists increased alveolar fluid clearance in sheep (1), dogs (5), rats (7), and mice (20), β-adrenergic agonists did not in rabbits (19) and hamsters (32). Therefore, it was an urgent and important issue to determine if β-adrenergic agonists increased alveolar fluid clearance in human lungs.

We determined if a β-adrenergic agonist, terbutaline, stimulated alveolar fluid clearance in *ex vivo* human lungs (31). Terbutaline (10^{-3} or 10^{-4} M) doubled alveolar liquid clearance to 28 ± 9 % over 4 h. Propranolol (10^{-4} M) and amiloride (10^{-5} M) inhibited the terbutaline-increased alveolar fluid clearance. In a subsequent study, salmeterol, a lipophilic β_2-adrenergic agonist, was more potent stimulator of alveolar fluid clearance than terbutaline in ex vivo human lungs (8).

In terms of the distribution of b-receptors in the human alveolar epithelium, 70% are β_2-adrenoceptors and 30% are β_1-adrenoceptors in the human alveolar walls (33). Similar to β_2-agonists, a β_1-adrenergic agonist can increase alveolar fluid clearance in rat lungs (12). Norepinephrine increased alveolar fluid reabsorption via the activation of both α_1- and β-adrenergic receptors in rats (10, 34). However, it is yet uncertain if a β_1-adrenergic agonist and norepinephrine increase alveolar alveolar fluid clearance in human lungs.

Recently we found that endogenous catecholamine concentrations in pulmonary edema fluid increased to the level of 10^{-9} – 10^{-8} M and that administration of exogenous epinephrine (10^{-7} M), but neither epinephrine (10^{-9} M) nor norepinephrine (10^{-7} M), into the distal airspaces could stimulate alveolar fluid clearance in the human lung (22). These results indicate that endogenous catecholamine concentrations in pulmonary edema fluid are probably not sufficient to stimulate alveolar fluid clearance and that administration of exogenous β-agonists into the distal airspaces can be a potent therapy for patients with pulmonary edema.

Glibenclamide(10^{-5}M) and $CFTR_{inh}$-172(10^{-5}M), cystic fibrosis transmembrane conductance regulator (CFTR) inhibitors, inhibited the epinephrine-induced stimulation of alveolar fluid clearance in ex vivo human lungs (18). Our results are consistent with the results that glibenclamide inhibited isoproterenol-stimulated alveolar fluid clearance in human lungs that were obtained from human lung donors whose lungs were rejected for transplantation (22).

Human lung versus rat lung

We determined if there was a difference in the rate of basal alveolar fluid clearance between *ex vivo* human and *ex vivo* rat lungs, and if there was a difference in the effect of β-adrenergic agonist therapy on alveolar epithelial fluid clearance between *ex vivo* human and *ex vivo* rat lungs (8). The results indicated that basal alveolar fluid clearance in rat lungs was significantly faster than in human lungs (24 ± 4% over 4 h in rat lungs compared to 11 ± 2% over 4 h in human lungs). Comparison of equivalent doses of salmeterol indicated that stimulated clearance rates were also faster in rat lungs than in human lungs. Very low doses of salmeterol were effective in *ex vivo* rat lungs (10^{-8} M). Relatively low doses were effective in the *ex vivo* human lungs (10^{-6} M) as a treatment for increasing alveolar fluid clearance. In summary, there are significant differences in the basal and stimulated rates of alveolar epithelial fluid clearance between rat and human lungs. The human lung responds well to relatively low doses of β-adrenergic agonist, a finding with potentially important clinical implications for hastening the resolution of alveolar edema.

Temperature dependent alveolar fluid clearance

Since hypothermia abolished alveolar fluid clearance in the excised human lungs (35), we advanced the study to determine whether alveolar fluid clearance resumed in the human lungs that were rewarmed after severe hypothermia (36). An isosmolar albumin solution was instilled into *ex vivo* human lungs that were rewarmed to 37°C after hypothermia (7 ± 3°C) over 5 h, and then alveolar fluid clearance was measured by the concentration of albumin in the alveolar fluid sample after 4 h. Although hypothermia completely abolished alveolar fluid clearance, alveolar fluid clearance resumed to a normal level of 12 ± 1% over 4 h in the lungs that were rewarmed after hypothermia. Amiloride decreased alveolar fluid clearance by 47% in the rewarmed lungs. Terbutaline increased alveolar fluid clearance by nearly 300% in the rewarmed lungs.

Alveolar fluid clearance was also measured in human lungs that were obtained from human lung donors whose lungs were rejected for transplantation (14, 17). The donor lungs were transported under hypothermic conditions and then warmed to 37°C over 3 – 4 h. Next, 60 – 120 ml of isosmolar 5% human albumin solution containing 5 mCi ^{131}I-albumin that was used for calculation of alveolar fluid clearance. Alveolar fluid clearance capacity in donor lungs was similar to that in *ex vivo* human lungs from patients with bronchogenic carcinoma (36).

These studies indicated that basal and stimulated alveolar fluid clearance is normal in the excised human lung that has been exposed to severe hypothermia followed by rewarming to human body temperature. Amiloride-sensitive sodium transport and β-adrenoceptors that mediate alveolar fluid clearance are preserved in the rewarmed human lungs after hypothermia. The results provide further evidence of the resistance of alveolar epithelial transport mechanisms to injury, a finding that has been documented under a variety of clinically relevant pathological conditions.

In addition, a study was conducted to determine whether hypothermia inhibited alveolar epithelial injury in the resected human lung during preservation (37). A hyposmolar albumin solution, 248 mOsm/kg, was instilled into the alveolar spaces of the resected human lungs which were inflated with an airway pressure of 7 cmH_2O and stored at either 37°C or 8°C for 4 h. Alveolar fluid was aspirated and the influx of lactate dehydrogenase (LDH) and globulin into the alveolar spaces, as markers of alveolar epithelial injury, was measured. Ion transport and fluid clearance across the alveolar epithelium were calculated by the changes in electrolyte and albumin concentrations in the alveolar fluid, respectively. While the LDH levels and globulin concentrations increased significantly in the hyposmolar experiments at 37°C, hypothermia inhibited these increases. Alveolar fluid clearance at 37°C increased to 20% in the hyposmolar experiments compared with 12% in the control isosmotic experiments, however, sodium and chloride transport in the hyposmolar experiments was not significantly different from that in the isosmolar experiments. This study indicates that hypothermia at 8°C inhibits alveolar epithelial injury caused by the hyposmolar solution in excised human lungs. Moreover, alveolar ion and fluid clearance mechanisms were preserved across the injured alveolar epithelial cells.

K_{ATP} channel opener stimulates alveolar fluid clearance

Since the effect of ATP-sensitive potassium channel (K_{ATP} channel) opener on the function of alveolar epithelial cells is unknown, the effect of YM-934, a newly synthesized K_{ATP} channel opener, on potassium influx into the alveolar spaces and alveolar fluid clearance was determined in the resected human lung (38). An isosmolar albumin solution with a low potassium concentration was instilled into the distal airway of the resected human lungs. Net potassium transport and alveolar fluid clearance were measured for 4 h using both the changes in the potassium concentration of the alveolar fluid as well as changing the alveolar fluid volume. YM934 (10^{-4} M) increased net influx of potassium by 76% into the alveolar spaces and also increased alveolar fluid clearance by 48 % in the experiments with a potassium concentration of 0.3 mEq/l. Glibenclamide (10^{-4} M), a K_{ATP} channel blocker, inhibited the YM934-increased influx of potassium transport and the increase in alveolar fluid clearance. Also amiloride (10^{-5} M) blocked the YM934-increase in alveolar fluid clearance. These results indicate that a K_{ATP} channel opener can affect potassium transport and net vectorial fluid movement across the human alveolar epithelium.

Recently, Kir channel (Kir6.1) and sulfonylurea receptor (SUR 2B) forming K_{ATP} channel were detected in freshly isolated and cultured rat alveolar type II cells (39). Glibenclamide reduced amiloride-sensitive sodium current and abolished chloride current stimulation by forskolin in

cultured monolayer of alveolar type II epithelial cells. In addition, K_{ATP} channel activation by pinacidil increased sodium and chloride transepithelial transport. Although further studies are necessary to elucidate the relationships among K_{ATP} channel, β-adrenoceptor and chloride channel in the alveolar epithelial cells, it is noted that K_{ATP} channels may be necessary for β-agonist mediated stimulation of chloride transport.

Alveolar fluid clearance in the remaining lung after thoractomy

We studied the effect of thoracotomy on alveolar fluid clearance in the remaining lungs in a patient who underwent exploratory thoracotomy (40). The first exploratory thoracotomy was carried out 9 days before the second thoracotomy. Since the tumor was malignant, the second thoracotomy was carried out and alveolar fluid clearance was measured in the excised lungs. We found that alveolar sodium and fluid clearance increased by nearly 200 %. Histological examination showed that the number of alveolar type II epithelial cells was markedly increased particularly in the alveoli near the visceral pleura (41). These results suggest that an increase in the number of alveolar type II cells may accelerate alveolar fluid clearance under certain clinical conditions.

Summary

We have established a method to study ion and fluid transport across the alveolar epithelium in *ex vivo* human lung and determined the mechanisms responsible for alveolar fluid clearance. The principle results were as follows. Alveolar fluid clearance occurred in the excised human lung. Active ion transports mediated by amiloride-sensitive sodium channels and Na^+-K^+ ATPase accounted for the mechanisms responsible for alveolar fluid clearance. β_2-adrenergic agonists (terbutaline, salmeterol, and epinephrine) were potent stimulators of alveolar liquid clearance via β-adrenergic receptors and sodium channels. A potassium channel opener (YM934) also increased alveolar fluid clearance. Hypothermia abolished alveolar fluid clearance and rewarm following hypothermia resumed normal alveolar fluid clearance. Proliferation of type II alveolar epithelial cells played a role in the increase in alveolar fluid clearance in a patient who had undergone partial pneumonectomy of the lung. CFTR may play a potential role in epinephrine stimulated alveolar fluid clearance. These observations have important clinical implications because stimulation of alveolar fluid clearance may accelerate the resolution of alveolar edema in many diseases (Table 2). However, further studies are needed because little data are available regarding alveolar fluid clearance in *in vivo* human lungs.

Table 2. Strategies to accelerate the resolution of pulmonary edema in the human lung

Increase alveolar fluid clearance capacity
Aerosolized b-adrenergic agonists
β_1-adrenergic agonist (Denopamine)
β_2-adrenergic agonist (Salmeterol, Terbutaline, Epinephrine)
Intravenous administration
Dobutamine
Dopamine
Potassium channel opener
Prevent collapse of the alveolar spaces
Proliferation of type II alveolar epithelial cells
Nutrition

These studies were supported by Grant for Project Research from High-Technology Center of Kanazawa Medical University (H2003-7, H2004-7, H2005-7), Grant for Collaborative Research from Kanazawa Medical University (C2003-1, C2004-1, C2005-1), Grant-In-Aid for Scientific Research from the MEXT, Japan (14571289, 17591492).

References

1. Berthiaume Y, Staub NC, Matthay MA: Beta-adrenergic agonists increase lung liquid clearance in anesthetized sheep. J Clin Invest 1987; **79:** 335-43.
2. Sakuma T, Pittet JF, Jayr C et al: Alveolar liquid and protein clearance in the absence of blood flow or ventilation in sheep. J Appl Physiol 1993; **74:** 176-85.
3. Campbell AR, Folkesson HG, Berthiaume Y et al: Alveolar epithelial fluid clearance persists in the presence of moderate left atrial hypertension in sheep. J Appl Physiol 1999; **86:** 139-51.
4. Serikov VB, Grady M, Matthay MA: Effect of temperature on alveolar liquid and protein clearance in an in situ perfused goat lung. J Appl Physiol 1993; **75:** 940-7.
5. Berthiaume Y, Broaddus VC, Gropper MA et al: Alveolar liquid and protein clearance from normal dog lungs. J Appl Physiol 1988; **65:** 585-93.
6. Sugita M, Ferraro P, Dagenais A et al: Alveolar liquid clearance and sodium channel expression are decreased in transplanted canine lungs. Am J Respir Crit Care Med 2003; **167:** 1440-50.
7. Crandall ED, Heming TA, Palombo RL et al: Effects of terbutaline on sodium transport in isolated perfused rat lung. J Appl Physiol 1986; **60:** 289-94.
8. Sakuma T, Folkesson HG, Suzuki S et al: Beta-adrenergic agonist stimulated alveolar fluid clearance in ex vivo human and rat lungs. Am J Respir Crit Care Med 1997; **155:** 506-12.
9. Sakuma T, Tsukano C, Ishigaki M et al: Lung deflation impairs alveolar epithelial fluid transport in ischemic rabbit and rat lungs. Transplantation 2000; **69:** 1785-93.

10. Sakuma T, Hida M, Nambu Y et al: Effects of hypoxia on alveolar fluid transport capacity in rat lungs. J Appl Physiol 2001; **91:** 1766-74.
11. Sakuma T, Hida M, Nambu Y et al: Beta1-adrenergic agonist is a potent stimulator of alveolar fluid clearance in hyperoxic rat lungs. Jpn J Pharmacol 2001; **85:** 161-6.
12. Sakuma T, Tuchihara C, Ishigaki M et al: Denopamine, a beta(1)-adrenergic agonist, increases alveolar fluid clearance in ex vivo rat and guinea pig lungs. J Appl Physiol 2001; **90:** 10-6.
13. Sakuma T, Sagawa M, Hida M et al: Time-dependent effect of pneumonectomy on alveolar epithelial fluid clearance in rat lungs. J Thorac Cardiovasc Surg 2002; **124:** 668-74.
14. Sakuma T, Zhao Y, Sugita M et al: Malnutrition impairs alveolar fluid clearance in rat lungs. Am J Physiol Lung Cell Mol Physiol 2004; **286:** L1268-74.
15. Sakuma T, Zhao Y, Sugita M et al: A prostacyclin analogue, OP-41483alpha-CD, restores the ability of a beta2-adrenergic agonist to stimulate alveolar fluid clearance in rats. Surg Today 2004; **34:** 429-36.
16. Sakuma T, Gu X, Sugita M et al: Uridine 5'-triphosphate stimulates alveolar fluid clearance in the isolated rat lungs. J Pharmacol Sci 2004; **95:** 420-5.
17. Sakuma T, Gu X, Sugita M et al: Catecholamine clearance from alveolar spaces of rat and human lungs. Respiration 2005; **72:** 189-96.
18. Sakuma T, Gu X, Maeda S et al: Epinephrine dependent stimulation of alveolar fluid clearance in the human lung is CFTR dependent. Am J Respir Crit Care Med 2005; **2:** A299.
19. Smedira N, Gates L, Hastings R et al: Alveolar and lung liquid clearance in anesthetized rabbits. J Appl Physiol 1991; **70:** 1827-35.
20. Garat C, Carter EP, Matthay MA: New in situ mouse model to quantify alveolar epithelial fluid clearance. J Appl Physiol 1998; **84:** 1763-7.
21. Fukuda N, Folkesson HG, Matthay MA: Relationship of interstitial fluid volume to alveolar fluid clearance in mice: ventilated vs. in situ studies. J Appl Physiol 2000; **89:** 672-9.
22. Fang X, Fukuda N, Barbry P et al: Novel role for CFTR in fluid absorption from the distal airspaces of the lung. J Gen Physiol 2002; **119:** 199-207.
23. Mutlu GM, Dumasius V, Burhop J et al: Upregulation of alveolar epithelial active Na+ transport is dependent on beta2-adrenergic receptor signaling. Circ Res 2004; **94:** 1091-100.
24. Mutlu GM, Koch WJ, Factor P: Alveolar epithelial beta 2-adrenergic receptors: their role in regulation of alveolar active sodium transport. Am J Respir Crit Care Med 2004; **170:** 1270-5.
25. Matthay MA, Wiener-Kronish JP: Intact epithelial barrier function is critical for the resolution of alveolar edema in humans. Am Rev Respir Dis 1990; **142:** 1250-7.
26. Matthay MA, Folkesson HG, Verkman AS: Salt and water transport across alveolar and distal airway epithelia in the adult lung. Am J Physiol 1996; **270:** L487-503.
27. Ware LB, Matthay MA: The acute respiratory distress syndrome. N Engl J Med 2000; **342:** 1334-49.
28. Ware LB, Matthay MA: Alveolar fluid clearance is impaired in the majority of patients with acute lung injury and the acute respiratory distress syndrome. Am J Respir Crit Care Med 2001; **163:** 1376-83.
29. Ware L, Wang Y, Fang X et al: Assessment of lungs rejected for transplantation and implications for donor selection. Lancet 2002; **360:** 619.
30. Hastings RH, Grady M, Sakuma T et al: Clearance of different-sized proteins from the alveolar space in humans and rabbits. J Appl Physiol 1992; **73:** 1310-6.
31. Sakuma T, Okaniwa G, Nakada T et al: Alveolar fluid clearance in the resected human lung. Am J Respir Crit Care Med 1994; **150:** 305-10.
32. Goodman BE: Lung fluid clearance. In R. C. Effros, HK, editor (Eds). Fluid and solute transport in the air spaces of the lungs. New York. Marcel Dekker, 1993; 139-83.
33. Carstairs JR, Nimmo AJ, Barnes PJ: Autoradiographic visualization of beta-adrenoceptor subtypes in human lung. Am Rev Respir Dis 1985; **132:** 541-7.
34. Azzam ZS, Adir Y, Crespo A et al: Norepinephrine increases alveolar fluid reabsorption and Na, K-ATPase activity. Am J Respir Crit Care Med 2004; **170:** 730-6.
35. Sakuma T, Okaniwa G, Nakada T et al: Effects of hypothermia and hyperpotassium on alveolar fluid clearance in the resected human lung. Surg Today 1995; **25:** 694-700.
36. Sakuma T, Suzuki S, Usuda K et al: Preservation of alveolar epithelial fluid transport mechanisms in rewarmed human lung after severe hypothermia. J Appl Physiol 1996; **80:** 1681-6.
37. Sakuma T, Nishimura T, Usude K et al: Hypothermia inhibits the alveolar epithelial injury caused by hyposmotic albumin solution during preservation of the resected human lung. Surg Today 1997; **27:** 527-33.
38. Sakuma T, Takahashi K, Ohya N et al: Effects of ATP-sensitive potassium channel opener on potassium transport and alveolar fluid clearance in the resected human lung. Pharmacol Toxicol 1998; **83:** 16-22.
39. Leroy C, Dagenais A, Berthiaume Y et al: Molecular identity and function in transepithelial transport of K(ATP) channels in alveolar epithelial cells. Am J Physiol Lung Cell Mol Physiol 2004; **286:** L1027-37.
40. Sakuma T, Usuda K, Handa M et al: Increased alveolar fluid clearance following thoracotomy: report of a case and results of an analysis. Surg Today 1997; **27:** 762-5.
41. Sakuma T: Proliferation of alveolar type II epithelial cells in residual lungs following thoracotomy. Jpn J Thorac Cardiovasc Surg 1999; **47:** 43-6.

SHOCK, Vol. 26, No. 1, pp. 62–68, 2006

OXYGEN CONSUMPTION, ASSESSED WITH THE OXYGEN ABSORPTION SPECTROPHOTOMETER, DECREASES INDEPENDENTLY OF VENOCONSTRICTION DURING HEPATIC ANAPHYLAXIS IN PERFUSED RAT LIVER

Sen Cui, Toshishige Shibamoto, Zonghai Ruan, Hiromichi Takano, Wei Liu, and Yasutaka Kurata

Department of Physiology, Kanazawa Medical University, Uchinada, Ishikawa, Japan

Received 15 Jul 2005; first review completed 22 Sep 2005; accepted in final form 23 Jan 2006

ABSTRACT—Anaphylactic shock is accompanied by a decrease in oxygen consumption. However, it is not well known whether oxygen consumption decreases during local anaphylactic reaction in liver. We determined the effects of anaphylaxis and norepinephrine on oxygen consumption in isolated rat livers perfused portally and recirculatingly at constant flow with blood (hematocrit, 12%). Oxygen consumption was continuously measured by monitoring the portal–hepatic venous oxygen saturation differences using the absorption spectrophotometer, the probes of which were built in perfusion lines. Hepatic anaphylaxis was induced by an injection of ovalbumin (0.01 or 0.1 mg) into the perfusate of the isolated liver of the rat sensitized with subcutaneous ovalbumin (1 mg). Hepatic venoconstriction and liver weight loss were similarly observed in response to norepinephrine (0.01–10 μmol L^{-1}) and anaphylaxis. However, hepatic anaphylaxis reduced oxygen consumption, whereas norepinephrine increased it. There was a possibility that anaphylactic venoconstriction could reduce the perfused surface area, resulting in decreased oxygen consumption. However, pretreatment with a vasodilator of sodium nitroprusside substantially attenuated venoconstriction but not the decrease in oxygen consumption during anaphylaxis. Thus, we conclude that local hepatic anaphylaxis decreases oxygen consumption independently of venoconstriction in isolated blood-perfused rat livers.

KEYWORDS—Anaphylactic shock, hepatic circulation, norepinephrine, hepatic venoconstriction, portal venous pressure

INTRODUCTION

Circulatory shock is characterized by generalized cellular hypoxia and a decrease in oxygen consumption of organs and tissues (1–3). The severity and the mortality after shock is strongly associated with decreased oxygen consumption (2, 4). Indeed, anaphylactic shock is accompanied by decreased oxygen consumption (5, 6). There is a possibility that anaphylactic reaction itself reduces oxygen consumption. However, there are only a limited number of studies (7) to determine the effect of local anaphylaxis on oxygen consumption of organs such as the liver.

Therefore, for determination of the effect of local anaphylaxis on oxygen consumption of the liver, we used the isolated perfused liver, which was free from the influences of the other organs or many humoral mediators released from other organs during the time course of anaphylactic shock. We continuously measured the oxygen consumption of isolated blood-perfused livers during hepatic anaphylaxis by monitoring the oxygen (O_2) saturation differences between the inflow and outflow blood using a custom-made absorption spectrophotometer. To check the validity of this absorption spectrophotometer, we also measured the oxygen consumption during administration of norepinephrine because norepinephrine is known to increase oxygen consumption in the perfused rat liver (8–10). Another reason for investigating the effect of norepinephrine is that it induces hepatic venoconstriction. Oxygen consumption depends not only on metabolic factors but also on hemodynamic factors. From the hemodynamic point of view, isolated perfused rat livers showed similar predominant presinusoidal constrictive responses to anaphylaxis (11) and norepinephrine (12). In addition, to determine the effect of hepatic anaphylaxis on oxygen consumption without its hemodynamic influence, anaphylaxis-induced venoconstriction was suppressed by pretreatment with sodium nitroprusside (SNP) and then changes in oxygen consumption were determined during hepatic anaphylaxis.

MATERIALS AND METHODS

Animals

Seventy-four male Sprague-Dawley rats (Japan SLC, Shizuoka, Japan) weighing 270 to 370 g (mean ± SD, 325 ± 4 g) were used in this study. Rats were maintained at 23°C and under pathogen-free conditions on a 12-h dark/light cycle and received food and water *ad libitum*. The study protocol was approved by the Animal Research Committee of Kanazawa Medical University.

Sensitization

Twenty-one rats were sensitized by subcutaneous injection of an emulsion made by mixing complete Freund's adjuvant (0.5 mL) with 1 mg ovalbumin (grade V, Sigma, Saint Louis, MO) dissolved in physiological saline (0.5 mL) as previously described (11). Two weeks after injection, rats were used for the isolated perfused liver experiments.

Isolated liver preparation

The animals were anesthetized with pentobarbital sodium (50 mg kg^{-1} i.p.) and were mechanically ventilated with room air. The method for perfusion of isolated rat livers was previously described (11). In brief, after the right carotid artery

Address reprint requests to Toshishige Shibamoto, Department of Physiology, Kanazawa Medical University, Uchinada Ishikawa 920-0293, Japan. E-mail: shibamo@kanazawa-med.ac.jp.

This work was supported by a grant for collaborative research from Kanazawa Medical University (C2004-1, C2005-1).
DOI: 10.1097/01.shk.0000215315.76370.8a
Copyright © 2006 by the Shock Society

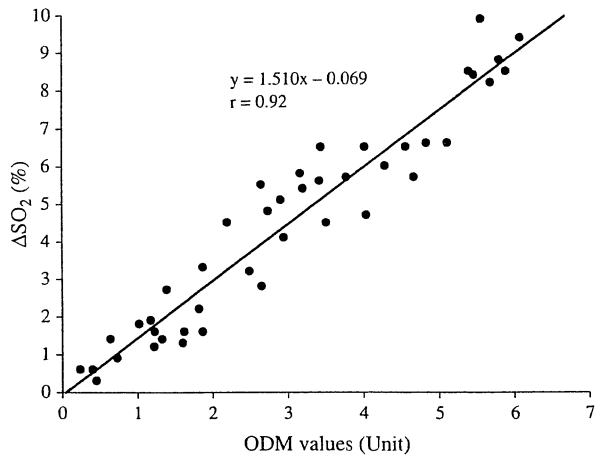


FIG. 1. **The relationship between the ODM values and the measured ΔSo_2 that were obtained in 10 intact livers.** The regression line equation is $\Delta So_2 = 1.5103 \times ODM - 0.0685$ ($r = 0.92$, $P < 0.05$).

cannulation and laparotomy, the hepatic artery was ligated, and the bile duct was cannulated with polyethylene tube (inner diameter [ID], 0.5 mm; outer diameter [OD], 0.8 mm). After intra-arterial heparinization (500 U kg^{-1}), 8 to 9 mL of blood was withdrawn through the carotid arterial catheter. The intra-abdominal inferior vena cava above the renal veins was ligated, and the portal vein was cannulated with a stainless cannula (ID, 1.3 mm; OD, 2.1 mm) for portal perfusion. After thoracotomy, the supradiaphragmatic inferior vena cava was cannulated through a right atrium incision with a larger stainless cannula (ID, 2.1 mm; OD, 3.0 mm), then portal perfusion was begun with the heparinized autologous blood diluted with 5% bovine albumin (Sigma-Aldrich, St. Louis, Mo) in Krebs solution (118 mmol L^{-1} NaCl, 5.9 mmol L^{-1} KCl, 1.2 mmol L^{-1} $MgSO_4$, 2.5 mmol L^{-1} $CaCl_2$, 1.2 mmol L^{-1} NaH_2PO_4, 25.5 mmol L^{-1} $NaHCO_3$, and 5.6 mmol L^{-1} glucose) at hematocrit of 12%. The liver was rapidly excised, suspended from an isometric transducer (TB-652T, Nihon-Kohden, Tokyo, Japan), and weighed continuously throughout the experimental period.

The livers were perfused at a constant flow rate in a recirculating manner *via* the portal vein with blood that was pumped using a Masterflex roller pump from the venous reservoir through a heat exchanger (37°C). The recirculating blood volume was 40 mL. The perfused blood was oxygenated in the venous reservoir by continuous bubbling with 95% O_2 and 5% carbon dioxide (perfusate Po_2 = 300 mmHg). The portal and hepatic venous pressures (Ppv and Phv, respectively) were measured using pressure transducers (TP-400T, Nihon-Kohden) attached by sidearm to the appropriate cannulas with the reference points at the hepatic hilus. Portal blood flow rate was measured with an electromagnetic flow meter (MFV 1200, Nihon-Kohden), and the flow probe was positioned in the inflow line. Bile was collected drop by drop in a small tube suspended from the force transducer (SB-1T, Nihon-Kohden). One bile drop yielded 0.018 g, and the time between drops was measured for determination of the bile flow rate. To determine the oxygen consumption, the blood oxygen saturation difference between the portal and hepatic venous blood was monitored continuously with a custom-made absorption spectrophotometer (ODM-1, Biomedical Science, Kanazawa, Japan), the probe of which consisted of a 660-nm wavelength light-emitting diode, a cuvette, and a photodiode detector. These 2 probes were built in the inflow and outflow perfusion lines. The blood oxygen saturation differences measured with this absorption spectrophotometer were expressed as the oxygen difference meter (ODM) values. The hepatic vascular pressures, ODM values, blood flow rate, liver weight, and bile weight were monitored continuously and displayed through a thermal physiograph (RMP-6008, Nihon-Kohden). All output were also digitized by the analog–digital converter at a sampling rate of 100 Hz. These digitized values were also displayed and recorded using a personal computer.

Measurement of oxygen consumption

Oxygen consumption was calculated according to the Fick principle by the following equation

$$\text{Portalbloodflow/liverweight(g)} \times 1.39\text{(mL/g)} \times \text{hemoglobin(g/mL)} \times \Delta S_{O_2} \quad (1)$$

where ΔSo_2 is the oxygen saturation difference between the inflow (portal) and outflow (hepatic vein) blood. To estimate ΔSo_2 by the ODM value of the absorption spectrophotometer, the validity of the ODM values was examined by comparing the ODM values with the ΔSo_2, which was determined by measuring the oxygen saturation of the inflow and outflow blood with the use of automatic blood gas analyzer. To determine the correlation of ODM value and ΔSo_2, the intact isolated rat livers (n = 10) were perfused at various blood flow rates (12 – 60 mL/min) to obtain various inflow-to-outflow oxygen saturation differences. Blood samples were collected simultaneously from the inflow (portal) and outflow (hepatic venous) lines at a given flow rate and the oxygen saturation of the inflow (So_2in) and outflow (So_2out) blood were measured by the blood gas analyzer (AVL OMNI Modular System, AVL Scientific Corp., Roswell, GA). The calculated oxygen saturation differences ($\Delta So_2 = So_2in - So_2out$) were compared with the corresponding ODM values. We obtained the regression line equation for So_2 measured and ODM values.

Experimental protocol

Hepatic hemodynamic parameters were observed for at least 20 min after the start of perfusion until an isogravimetric state (no weight gain or loss) was obtained by adjusting the portal blood flow rate and the height of the reservoir at a Phv of 0 to 1 cmH_2O and at a portal blood flow of 37 ± 1 mL min^{-1} per 10 g of liver. After the baseline measurements, the perfused livers excised from nonsensitized animals were randomly assigned to the control group or norepinephrine group and those from sensitized animals to the anaphylaxis group. In the norepinephrine group (n = 35), norepinephrine was administered into the perfusate to get the final concentration of 0.001, 0.01, 0.1, 1, and 10 μmol L^{-1}. The concentrations of norepinephrine were randomly assigned for individual preparations. In the anaphylaxis group, ovalbumin 0.01 (n = 7) or 0.1 mg (n = 7) was administered into the perfusate. In addition, to eliminate a possible effect of anaphylaxis-induced venoconstriction on oxygen consumption, a vasodilator of SNP at 100 μmol L^{-1} was administered 10 min before injection of 0.01 mg of ovalbumin (SNP group, n = 7). In the control group (n = 8), ovalbumin 0.1 mg was administered into the perfusate of the livers from nonsensitized rats.

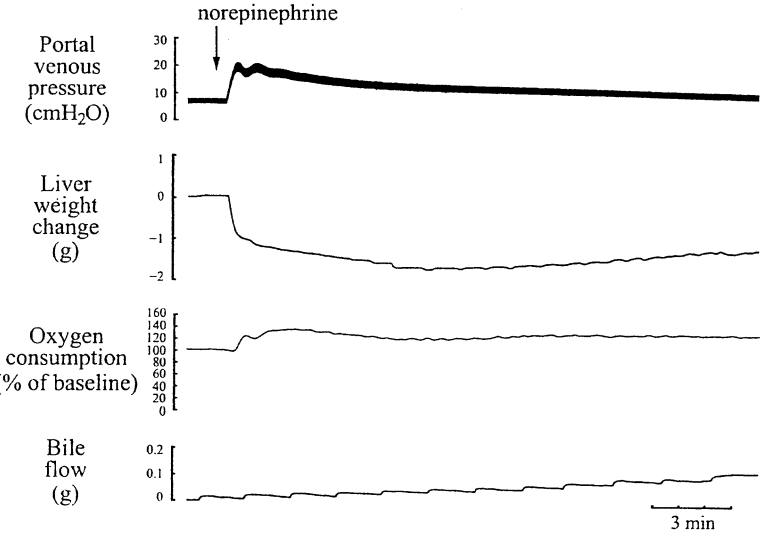


FIG. 2. **A representative recording of the response to norepinephrine at 1 μmol L^{-1}.**

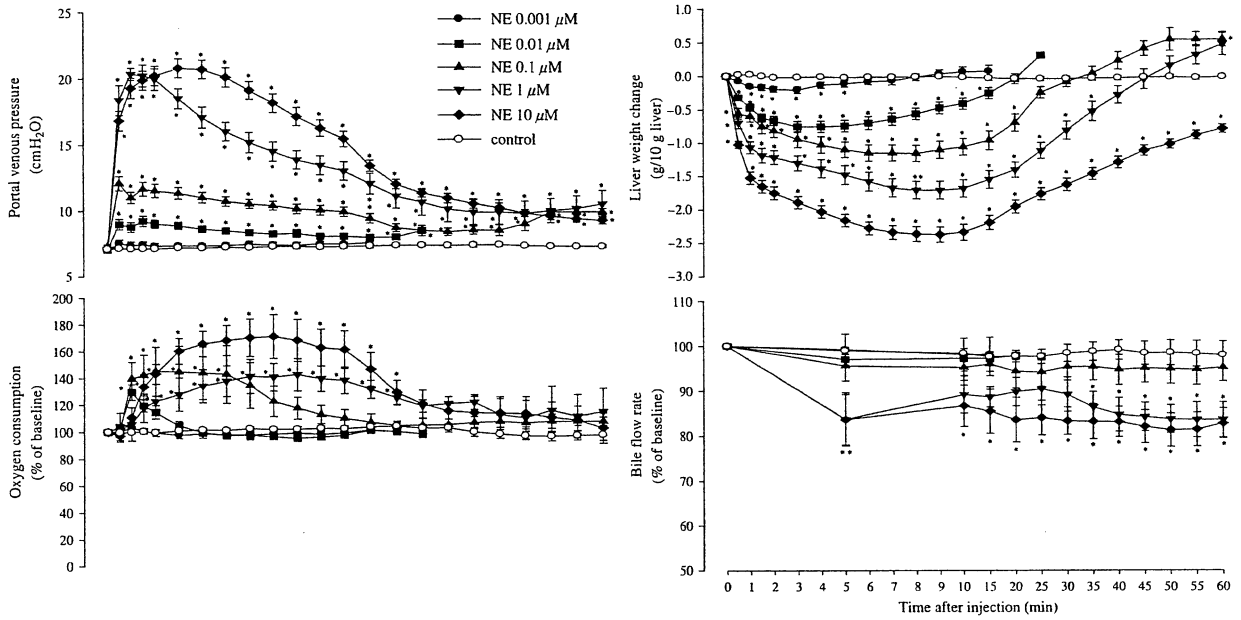


FIG. 3. **The time course changes in the Ppv, liver weight changes, oxygen consumption, and bile flow rate in the norepinephrine (n = 35) and control (n = 8) groups.** Values are given as means ± SE. *$P < 0.05$ versus the baseline. NE indicates norepinephrine.

Statistics

All results are expressed as means ± SE. Data were analyzed by one- and two-way analysis of variance, using repeated measures for 2-way comparison within groups. Comparisons of individual points between groups and within groups were made by Bonferroni test. The correlation between the ODM values and the measured oxygen saturation differences was analyzed by linear regression. Differences were considered as statistically significant at P values of <0.05.

RESULTS

Relationship between the ODM values and the measured oxygen saturations

Figure 1 shows the relationship between the ODM values and the measured ΔSo_2 that were obtained in 10 intact livers. The regression line equation is

$$\Delta S_{O_2} = 1.510 \times ODM - 0.069 \ (r = 0.92, \ P < 0.05). \quad (2)$$

This indicates that the ΔSo_2 can be estimated by ODM values in isolated perfused rat liver. The basal oxygen consumption calculated using the ODM values in the control, 0.1-mg ovalbumin, 0.01-mg ovalbumin, SNP, and 0.001-, 0.01-, 0.1-, 1-, and 10-μmol L^{-1} norepinephrine groups were 0.0072 ± 0.0005, 0.0078 ± 0.0002, 0.0054 ± 0.0005, 0.0055 ± 0.0003, 0.0065 ± 0.0008, 0.0069 ± 0.0009, 0.0066 ± 0.0008, 0.0070 ± 0.0008, and 0.0064 ± 0.0005 mL min^{-1} per gram of liver, respectively. In the present study, the changes in oxygen consumption in a given perfused liver were directly proportional to the ODM values because the other determinants of oxygen consumption such as perfusate hemoglobin and portal blood flow rate were not changed during the experimental period. Thus, oxygen consumption was expressed as the percentage of the baseline ODM value.

Effects of norepinephrine on hepatic oxygen consumption, Ppv, liver weight, and bile flow

Figure 2 shows a representative example of the hepatic response to administration of norepinephrine at 1 μmol L^{-1}. Figure 3 shows the summary data of the time-dependent changes in Ppv, liver weight, hepatic oxygen consumption, and bile flow rate of the norepinephrine groups. Significant changes in the variables were observed in response to norepinephrine at concentrations higher than 0.01 μmol L^{-1}. Hepatic oxygen consumption increased dose-dependently after norepinephrine, with the peak values being 129% ± 13% of the baseline at 0.01 μmol L^{-1}, 145% ± 42% at 0.1 μmol L^{-1}, 142% ± 27% at 1 μmol L^{-1}, and 171% ± 43% at 10 μmol L^{-1}. Norepinephrine at 0.01, 0.1, and 1 μmol L^{-1} dose-dependently increased Ppv to the peak, 9.2 ± 0.3, 12.1 ± 0.5, and 20.4 ± 0.8 cmH_2O, respectively, within 3 min. Maximal venoconstriction was observed at 1 μmol L^{-1}; the peak of Ppv after norepinephrine at 10 μmol L^{-1} (20.8 ± 0.7 cmH_2O) was comparable to that at 1 μmol L^{-1}. After administration of norepinephrine at 0.01, 0.1, 1, and 10 μmol L^{-1}, the liver weight decreased by 0.8 ± 0.1, 1.2 ± 0.2, 1.7 ± 0.2, and 2.4 ± 0.2 g per 10 g of liver, respectively. The bile flow rates decreased after norepinephrine administration at 1 and 10 μmol L^{-1} to 84% ± 6% and 84% ± 8% of the baseline of 8.6 ± 0.4 and 9.8 ± 0.5 mg min^{-1} per 10 g of liver, respectively.

Effects of anaphylaxis on hepatic oxygen consumption, Ppv, liver weight, and bile flow

Figure 4 shows a representative example of the response of the sensitized liver to the antigen (0.01 mg of ovalbumin). Figure 5 shows the summary data of the time course changes in Ppv, liver weight, hepatic oxygen consumption, and bile flow rate of the 0.01-mg ovalbumin group along with the data

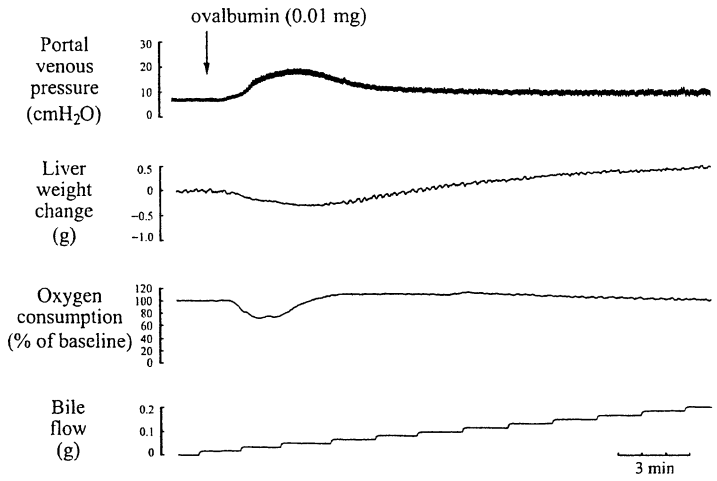


FIG. 4. **A representative recording of the responses to the antigen of ovalbumin (0.01 mg).**

of the 0.1-mg ovalbumin, 1- and 10-μmol L^{-1} norepinephrine, and control groups. After injection of 0.01 mg of ovalbumin, Ppv increased from the baseline of 6.9 ± 0.13 cmH_2O to the peak of 20.0 ± 1.4 cmH_2O at 4 min. Hepatic oxygen consumption decreased to the nadir of 75% ± 6% of the baseline at 2 min and then recovered to the baseline level at 4 min after administration of 0.01 mg of ovalbumin. The decrease in oxygen consumption after antigen administration contrasts with its increase after norepinephrine administration in that hepatic venoconstriction was similar in magnitude between the 0.01-mg ovalbumin group and the high dose of norepinephrine (1 or 10 μmol L^{-1}) group. The liver weight showed a rapid decrease, reaching the bottom of −0.4 ± 0.1 g per 10 g of liver at 4 min after 0.01 mg ovalbumin administration. The bile flow rate significantly decreased to 86% ± 1% of the baseline of 8.7 ± 0.5 mg min^{-1} per 10 g of liver at 5 min after antigen (0.01 mg of ovalbumin) administration and then gradually recovered. The responses of the variables to the high-dose ovalbumin (0.1 mg) were qualitatively similar to that of the low-dose ovalbumin (0.01 mg), but greater in magnitude, as shown in Figure 5.

Effects of SNP on Hepatic Anaphylactic Response

Figure 6 shows a representative example of the response of the sensitized liver to the antigen (0.01 mg of ovalbumin) after pretreatment with SNP at 100 μmol L^{-1}. Figure 7 shows the summary data of the time course changes of the 0.01-mg ovalbumin and SNP groups. The increase in Ppv in response to the 0.01-mg ovalbumin antigen was much smaller with SNP than without SNP. However, the decrease in hepatic oxygen consumption was similarly observed with or without pretreatment with SNP. At 2 min after antigen administration, hepatic oxygen consumption decreased to the nadir of 79% ± 3% of the baseline, which was not significantly different from that of the 0.01-mg ovalbumin group without administration of SNP. In contrast, Ppv increased only slightly to the peak of 9.9 ± 1.2 cmH_2O at 4 min from the baseline of 6.6 ± 0.15 cmH_2O. The liver weight showed a mild, but significant, decrease, reaching the nadir of −0.2 ± 0.1 g per 10 g of liver at 3 min after ovalbumin administration. The bile flow rate significantly decreased to 89% ± 1% of the baseline of 8.6 ± 0.5 mg min^{-1} per 10 g of liver at 5 min after antigen administration and did not return to the baseline.

DISCUSSION

In the present study, oxygen consumption was for the first time measured continuously by a custom-made absorption spectrophotometer, the probes of which were built in the perfusing circuit to monitor the portal–hepatic venous oxygen saturation difference of isolated perfused rat livers. We have shown that anaphylaxis decreased hepatic oxygen consumption, whereas norepinephrine increased it, although both caused similar hepatic venoconstriction and liver weight loss. Pretreatment with a vasodilator of SNP did not prevent the anaphylaxis-induced decrease in hepatic oxygen consumption, whereas it substantially attenuated the anaphylaxis-induced hepatic venoconstriction. These findings suggest that the decrease in hepatic oxygen consumption during anaphylactic shock could be caused by local hepatic anaphylaxis itself, and that it is independent of hepatic venoconstriction.

We demonstrated that there was a significant and good correlation between the ODM values of the absorption spectrophotometer and ΔS_{O_2} measured with the blood gas analyzer. This indicates that the ΔS_{O_2} and oxygen consumption can be indirectly measured by the absorption spectrophotometer in isolated perfused liver. Oxygen consumption of the perfused liver is usually measured with a Clark-type oxygen electrode (7, 13–15). However, this oxygen electrode monitors only the effluent, but not the influent, oxygen concentration and, thus, it alone cannot directly assess the portal– hepatic venous oxygen difference, which is the determinant of oxygen consumption. The application of the custom-made oxygen absorption spectrophotometer permits the continuous measurement of the portal–hepatic venous oxygen difference of the perfused livers.

An increase in oxygen consumption has been observed after norepinephrine administration in perfused rat livers (8, 16). In these studies, oxygen consumption was determined by measuring the effluent oxygen concentration with a Clark-type oxygen electrode. In the present study, we confirmed by using the oxygen absorption spectrophotometer that norepinephrine at concentrations higher than 0.01 μmol L^{-1}

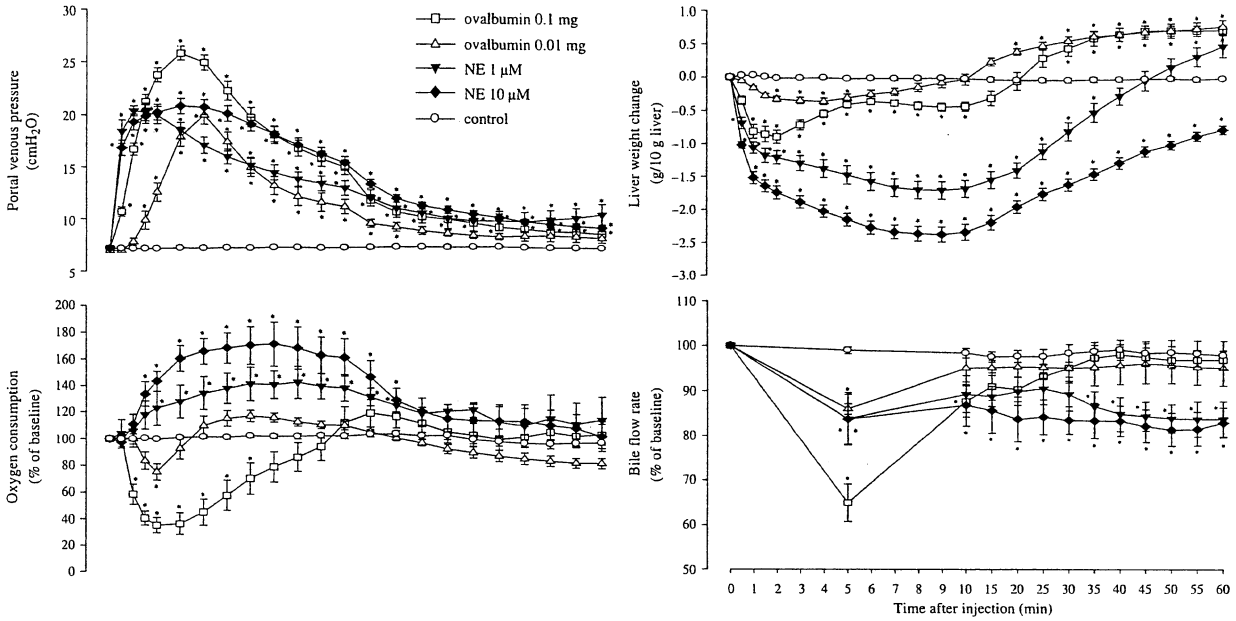


FIG. 5. **The time course changes in the Ppv, liver weight changes, oxygen consumption, and bile flow rate in the 0.1-mg ovalbumin (n = 7), 0.01-mg ovalbumin (n = 7), 1-μmol L^{-1} norepinephrine (n = 7), 10-μmol L^{-1} norepinephrine (n = 8), and control (n = 8) groups.** Values are given as means ± SE. *$P < 0.05$ versus the baseline. NE indicates norepinephrine.

increased hepatic oxygen consumption in isolated blood-perfused livers. This effect is ascribed to the metabolic effect of norepinephrine; norepinephrine is known to increase glycogenolysis using energy, which is reflected by an increase in oxygen consumption. Indeed, norepinephrine increases oxygen consumption of isolated cultured hepatocytes (17).

In the present study, in contrast to norepinephrine administration increasing hepatic oxygen consumption, anaphylaxis obviously reduced hepatic oxygen consumption (35% and 75% of baseline with ovalbumin at 0.1 and 0.01 mg, respectively). This finding is consistent with the investigation of Hines and Fisher (7), in which hepatic oxygen consumption initially increased and then largely decreased to about 24% during the antigen infusion. However, their experimental method was different from that of this study: In their study, the isolated rat livers were perfused with blood-free solutions in a nonrecirculating manner, whereas the livers in the present study were perfused more physiologically with blood. Another difference is that oxygen consumption was determined by measuring only the effluent oxygen concentration with an oxygen electrode in the previous study, whereas it was measured by directly determining the portal–hepatic venous oxygen saturation difference with the oxygen absorption spectrophotometer in the present study.

Hepatic oxygen consumption is regulated by the factors that affect metabolic and hemodynamic components of the liver. Thus, metabolic and hemodynamic factors may be involved in the anaphylaxis-induced decrease in oxygen consumption observed in the present study. With respect to the metabolic factors, pharmacologically active mediators, such as leukotrienes, thromboxane A_2 (TXA_2), platelet-activating factor, histamine, and serotonin are released during anaphylactic reaction. These mediators could directly inhibit oxygen consumption. Indeed, leukotriene C_4 and D_4 reduced oxygen consumption by 29% ± 3% and 30% ± 3% of baseline, respectively, and these inhibitory effects were independent of

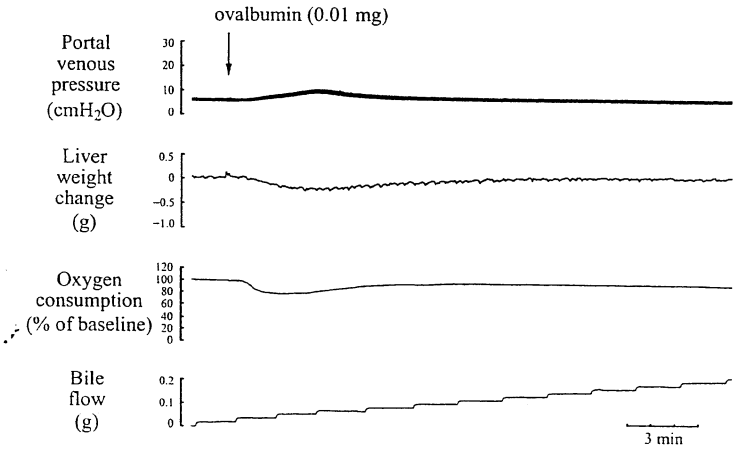


FIG. 6. **A representative recording of the responses to the antigen of ovalbumin (0.01 mg) after pretreatment with SNP at 100 μmol L^{-1}.**

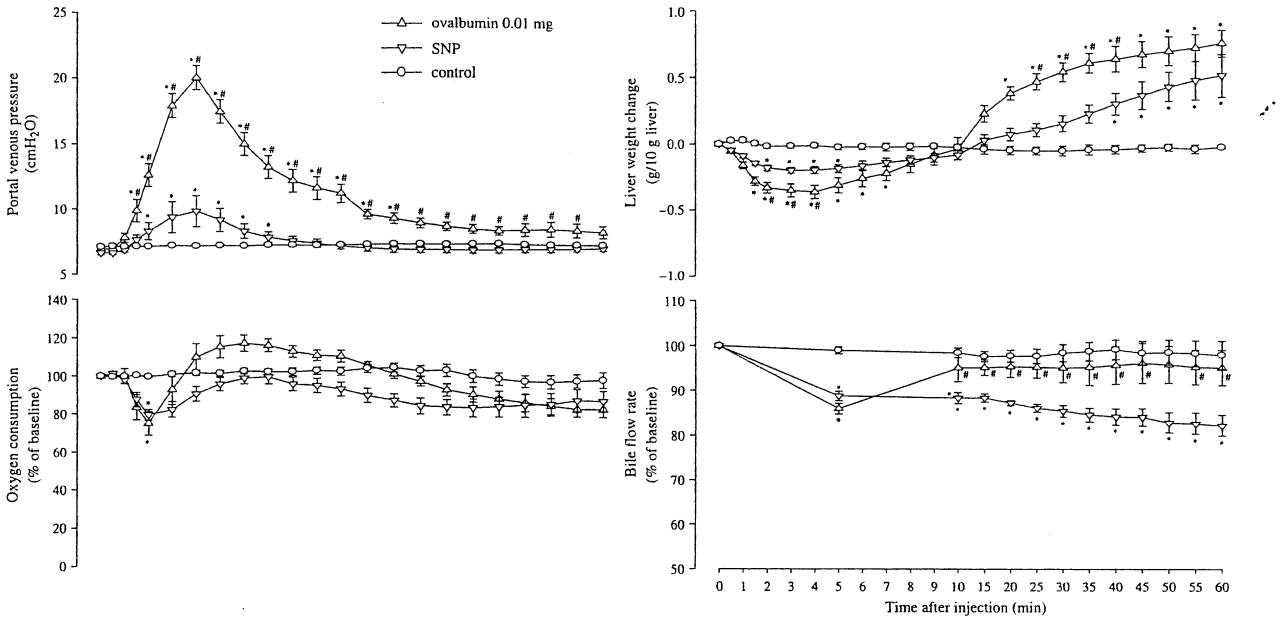


FIG. 7. **The time course changes in the Ppv, liver weight changes, oxygen consumption, and bile flow rate in the 0.01-mg ovalbumin (n = 7), SNP (n = 7), and control (n = 8) groups.** Values are given as means ± SE. $^{*}P < 0.05$ versus the baseline, $^{\#}P < 0.05$ versus SNP group.

changes in hemodynamic factors (13). U-46619, a TXA_2 analogue, also decreased oxygen consumption by 27% in perfused rat livers (13). Altin and Bygrave (14) also found that ONO-11113, another TXA_2 analogue, induced an initial small transient stimulation followed by a marked and sustained inhibition of oxygen uptake in perfused rat livers. Finally, platelet-activating factor increased glucose production concomitant with suppression of oxygen consumption in perfused rat livers (15). On the other hand, from the hemodynamic point of view, presinusoidal constriction observed during anaphylactic venoconstriction of the perfused sensitized rat livers (11) may account for decreased oxygen consumption—presinusoidal constriction caused a decrease in hepatic vascular surface area, which might result in a decrease in the number of active hepatocytes. However, even when anaphylactic hepatic venoconstriction to be induced by 0.01 mg of ovalbumin was substantially suppressed by pretreatment with SNP, a potent vasodilator, the anaphylaxis-induced decrease in oxygen consumption was still preserved (Fig. 7). Thus, although hemodynamic changes might partially contribute to the anaphylaxis-induced decrease in oxygen consumption, the contribution of the hemodynamic effect seems to be small.

To the best of our knowledge, this is the first study to measure oxygen consumption of perfused rat liver using absorption spectrophotometer, although this method has been well adopted for isolated perfused heart experiments (18, 19). Kameyama et al. (18) reported that the basal oxygen consumption of isolated perfused rat hearts measured with an absorption spectrophotometer (AVOX system) was 0.65 to 0.70 $\mu L\ g^{-1}\ beat^{-1}$ (about 0.16 mL min^{-1} per gram of heart weight). Oxygen consumption of isolated perfused rat hearts measured with an oxygen content difference analyzer (model PWA-200S, Shoe Technica, Chiba, Japan) was about 0.5 $\mu L\ g^{-1}\ beat^{-1}$ (0.15 mL min^{-1} per gram of heart weight) (19). The basal oxygen consumption of the present perfused rat livers calculated from the ODM values was 0.0054 to 0.0078 mL min^{-1} per gram of liver. Thus, these values are approximately one twentieth of those of perfused hearts (18, 19). This difference in oxygen consumption between heart and liver was also observed when a Clark-type oxygen electrode was used for the perfused rat heart (20–23) and perfused rat liver (8, 24–27): 28 to 49 $\mu mol\ L^{-1}\ min^{-1}$ per gram of heart (20–23) and 1.78 to 3.0 $\mu mol\ L^{-1}\ min^{-1}$ per gram of liver (8, 23–26), respectively. This indicates that the absorption spectrophotometer used in the present study can be used to measure oxygen consumption continuously in isolated perfused liver experiments.

In the present study, the bile flow rate decreased after norepinephrine at concentrations of 1 and 10 $\mu mol\ L^{-1}$. The reason for this decrease is not known, but it seems to be secondary to the hemodynamic effects (28). In hepatic anaphylaxis, the bile flow rate also reduced significantly at 5 min after antigen administration, even when the hemodynamic effect was eliminated by SNP. We therefore speculate that it is related to the reduction of hepatocyte activity, as reflected by a decrease in oxygen consumption during anaphylaxis.

In summary, we measured the changes in oxygen consumption during hepatic anaphylaxis and norepinephrine administration using a custom-made absorption spectrophotometer in isolated perfused rat livers. Hepatic venoconstriction and liver weight loss were similarly observed in response to norepinephrine and anaphylaxis. However, hepatic anaphylaxis caused a decrease in oxygen consumption, whereas norepinephrine increased oxygen consumption, as reported previously. Pretreatment with a vasodilator of SNP substantially attenuated anaphylaxis-induced venoconstriction, but not anaphylaxis-induced decrease in oxygen consumption. We conclude that local hepatic anaphylaxis decreases oxygen consumption independently of venoconstriction in isolated perfused rat livers.

REFERENCES

1. Ba ZF, Wang P, Koo DJ, Cioffi WG, Bland KI, Chaudry IH: Alterations in tissue oxygen consumption and extraction after trauma and hemorrhagic shock. *Crit Care Med* 28:2837–2842, 2000.
2. Roy JW, Graham MC, Griffin AM, Gainer JL: A novel fluid resuscitation therapy for hemorrhage shock. *Shock* 10:213–217, 1998.
3. Ottosson J, Persson T, Dawidson I: Oxygen consumption and central hemodynamics in septic shock treated with antibiotics, fluid infusions, and corticosteroids. *Crit Care Med* 17:772–779, 1989.
4. Dawidson I, Eriksson B, Gelin LE, Soderberg R: Oxygen consumption and recovery from surgical shock in rats: a comparison of the efficacy of different plasma substitutes. *Crit Care Med* 7:460–465, 1979.
5. Brown SG: Clinical features and severity grading of anaphylaxis. *J Allergy Clin Immunol* 114:371–376, 2004.
6. Catala JC, Llagunes J, Marin JP, Aguar F, Grau F: Oxygen consumption during anaphylactic shock. *Rev Esp Anestesiol Reanim* 44:154–156, 1997.
7. Hines KL, Fisher RA: Regulation of hepatic glycogenolysis and vasoconstriction during antigen-induced anaphylaxis. *Am J Physiol* 262: G868–G877, 1992.
8. Beckh K, Otto R, Ji S, Jungermann K: Control of oxygen uptake, microcirculation and glucose release by circulating noradrenaline in perfused rat liver. *Biol Chem Hoppe Seyler* 366:671–678, 1985.
9. Becker G, Beuers U, Jungermann K: Modulation by oxygen of the actions of noradrenaline, sympathetic nerve stimulation and prostaglandin F_2 α on carbohydrate metabolism and hemodynamics in perfused rat liver. *Biol Chem Hoppe Seyler* 371:983–990, 1990.
10. Binet A, Claret M: α-Adrenergic stimulation of respiration in isolated rat hepatocytes. *Biochem J* 210:867–873, 1983.
11. Shibamoto T, Cui S, Ruan Z, Liu W, Takano H, Kurata Y: Hepatic venoconstriction is involved in anaphylactic hypotension in rats. *Am J Physiol Heart Circ Physiol* 289:H1436–H1441, 2005.
12. Shibamoto T, Narushima M, Ling YQ, Shimo T, Tsuchida H, Kurata Y, Ogura T: Different hepatic vascular response to noradrenaline and histamine between guinea pig and rat. *Acta Physiol Scand* 18:255–263, 2004.
13. Haussinger D, Stehle T, Gerok W: Effects of leukotrienes and the thromboxane A_2 analogue U-46619 in isolated perfused rat liver. *Biol Chem Hoppe Seyler* 369:97–107, 1988.
14. Altin JG, Bygrave FL: Prostaglandin F_2 α and the thromboxane A_2 analogue ONO-11113 stimulate Ca^{2+} fluxes and other physiological responses in rat liver. Further evidence that prostanoids may be involved in the action of arachidonic acid and platelet-activating factor. *Biochem J* 249:677–685, 1988.
15. Kimura K, Moriyama M, Nishisako M, Kannan Y, Shiota M, Sakurada K, Musashi M, Sugano T: Modulation of platelet activating factor–induced glycogenolysis in the perfused rat liver after administration of endotoxin *in vivo*. *J Biochem (Tokyo)* 123:142–149, 1998.
16. Taylor WM, Reinhardt PH, Bygrave FL: Stimulation by α-adrenergic agonists of Ca^{2+} fluxes, mitochondrial oxidation and gluconeogenesis in perfused rat liver. *Biochem J* 212:555–565, 1983.
17. Dehaye JP, Hughes BP, Blanckmore PF, Exton JH: Insulin inhibition of α-adrenergic actions in liver. *Biochem J* 194:949–956, 1981.
18. Kameyama T, Chen Z, Bell SP, VanBuren P, Maughan D, LeWinter MM: Mechanoenergetic alterations during the transition from cardiac hypertrophy to failure in Dahl salt–sensitive rats. *Circulation* 98:2919–2929, 1998.
19. Hata Y, Sakamoto T, Hosogi S, Ohe T, Suga H, Takaki M: Linear O_2 use-pressure-volume area relation from curved end-systolic pressure-volume relation of the blood-perfused rat left ventricle. *Jpn J Physiol* 48:197–204, 1998.
20. Kurzelewski M, Duda M, Stanley WC, Boemke W, Beresewicz A: Nitric oxide synthase inhibition and elevated endothelin increase oxygen consumption but do not affect glucose and palmitate oxidation in the isolated rat heart. *J Physiol Pharmacol* 55:27–38, 2004.
21. Kreutzer U, Jue T: Role of myoglobin as a scavenger of cellular NO in myocardium. *Am J Physiol* 286:H985–H991, 2004.
22. Lopaschuk GD, Barr R, Thomas PD, Dyck JR: Beneficial effects of trimetazidine in *ex vivo* working ischemic hearts are due to a stimulation of glucose oxidation secondary to inhibition of long-chain 3–ketoacyl coenzyme a thiolase. *Circ Res* 93:e33–e37, 2003.
23. Schlenker EH, Tamura T, Gerdes AM: Gender-specific effects of thyroid hormones on cardiopulmonary function in SHHF rats. *J Appl Physiol* 95: 2292–2298, 2003.
24. Nakagawa Y, Matsumura T, Goto M, Qu W, Kauffman FC, Thurman RG: Increase in oxygen uptake due to arachidonic acid is oxygen dependent in the perfused liver. *Am J Physiol* 266:G953–G959, 1994.
25. Qu W, Zhong Z, Arteel GE, Thurman RG: Stimulation of oxygen uptake by prostaglandin E_2 is oxygen dependent in perfused rat liver. *Am J Physiol* 275:G542–G549, 1998.
26. Ji S, Beckh K, Jungermann K: Regulation of oxygen consumption and microcirculation by α-sympathetic nerves in isolated perfused rat liver. *FEBS Lett* 167:117–122, 1984.
27. Matsumura T, Yoshihara H, Jeffs R, Takei Y, Nukina S, Hijioka T, Evans RK, Kauffman FC, Thurman RG: Hormones increase oxygen uptake in periportal and pericentral regions of the liver lobule. *Am J Physiol* 262:G645–G650, 1992.
28. Lenzen R, Funk A, Kolb-Bachofen V, Strohmeyer G: Norepinephrine-induced cholestasis in the isolated perfused rat liver is secondary to its hemodynamic effects. *Hepatology* 12:314–321, 1990.

ELSEVIER

Prostaglandins & other Lipid Mediators 80 (2006) 35–45

PROSTAGLANDINS & other LIPID MEDIATORS

Effects of platelet-activating factor, thromboxane A_2 and leukotriene D_4 on isolated perfused rat liver

Sen Cui, Toshishige Shibamoto*, Wei Liu, Hiromichi Takano, Yasutaka Kurata

Department of Physiology, Kanazawa Medical University, Uchinada 920-0293, Japan

Received 21 January 2006; received in revised form 17 March 2006; accepted 30 March 2006
Available online 11 May 2006

Abstract

Vasoconstrictive lipid mediators, thromboxane A_2 (TxA_2), platelet-activating factor (PAF) and leukotriene D_4 (LTD_4) have been implicated as mediators of liver diseases. There are species differences in the primary site of hepatic vasoconstriction in response to these mediators. We determined the effects of a TxA_2 analogue (U-46619), PAF and LTD_4 on the vascular resistance distribution, weight and oxygen consumption of isolated rat livers portally perfused with blood. The sinusoidal pressure was measured by the double occlusion pressure (P_{do}), and was used to determine the pre- (R_{pre}) and post-sinusoidal (R_{post}) resistances. All these three mediators increased the hepatic total vascular resistance (R_t). The responsiveness to PAF was 100 times greater than that to U-46619 or LTD_4. Both of PAF and U-46619 predominantly increased R_{pre} over R_{post}. At the comparable increased R_t levels, U-46619 more preferentially increased R_{pre} than PAF. In contrast, LTD_4 increased both the R_{pre} and R_{post} to similar extent. U-46619 caused liver weight loss, while high concentrations of either LTD_4 or PAF produced liver weight gain, which was caused by substantial post-sinusoidal constriction and increased P_{do}. PAF and U-46619 decreased hepatic oxygen consumption while LTD_4 induced biphasic change of an initial transient decrease followed by an increase. In conclusion, PAF is the most potent vasoconstrictor of rat hepatic vessels among these three mediators. Both TxA_2 and PAF constrict the pre-sinusoidal veins predominantly. TxA_2 more preferentially constricts the pre-sinusoids than PAF, resulting in liver weight loss. However LTD_4 constricts both the pre- and post-sinusoidal veins similarly. High concentrations of LTD_4 and PAF cause liver weight gain by substantial post-sinusoidal constriction. PAF and TxA_2 decrease hepatic oxygen consumption, whereas LTD_4 causes a biphasic change of it.
© 2006 Elsevier Inc. All rights reserved.

Keywords: PAF; The double occlusion pressure; Hepatic circulation; U-46619; Sinusoidal pressure; Microcirculation; LTD_4; Oxygen consumption

1. Introduction

Lipid mediators such as platelet-activating factor (PAF), thromboxane A_2 (TxA_2) and leukotriene D_4 (LTD_4) are potent vasoconstrictors, and are released from a variety of cells including platelets, neutrophils, macrophages (e.g., Kupffer cells), monocytes, lymphocytes, endothelial and smooth muscle cells in response to various stimuli [1–3]. Each substance is implicated as a mediator of various types of liver diseases such as hepatic anaphylaxis [3,4], endotoxin

Abbreviations: IVC, inferior vena cava; PAF, platelet-activating factor; R_{pre}, pre-sinusoidal resistance; R_{post}, post-sinusoidal resistance; R_t, total portal-hepatic venous resistance; P_{pv}, portal venous pressure; P_{hv}, hepatic venous pressure; P_{do}, double occlusion pressure; Q, portal blood flow rate; Wt, liver weight; LT, leukotriene; TxA_2, thromboxane A_2

* Corresponding author. Tel.: +81 76 218 8104; fax: +81 76 286 8010.
E-mail address: shibamo@kanazawa-med.ac.jp (T. Shibamoto).

1098-8823/$ – see front matter © 2006 Elsevier Inc. All rights reserved.
doi:10.1016/j.prostaglandins.2006.03.004

liver injury [5–7], ischemia-reperfusion liver injury [8–10] and hepatic resection [9–11]. The microcirculation of the hepatic sinusoid plays a crucial role in the integrity of liver function [12]. PAF, TxA_2 and LTD_4 may influence the sinusoidal circulation, as a result of their vasoconstrictive action. Indeed, an infusion of a TxA_2 analogue or LTD_4 into the isolated perfused rat liver increases portal vein pressure, indicative of constriction of the hepatic vasculature [13,14]. PAF also causes an increase in the portal vein pressure in in vivo animals [15] and isolated perfused livers [16]. We have reported by measuring the sinusoidal pressure with the hepatic vascular occlusion methods in isolated blood-perfused canine livers that a TxA_2 analogue predominantly constricts the post-sinusoidal veins [17], while PAF constricts both the pre- and post-sinusoidal veins similarly [18]. On the other hand, both agents predominantly constrict the pre-sinusoidal veins over the post-sinusoidal veins in the isolated blood-perfused guinea pig livers [19]. These investigations indicated that there are species differences in the primary site of hepatic vasoconstriction for these mediators. However, the dominant vascular segments that these lipid mediators constrict in rat livers are not well known. Using the hepatic vascular occlusion method for measurement of the sinusoidal pressure [20], therefore, we determined the effects of PAF, a TxA_2 mimetic of U-46619 and LTD_4 on hepatic vascular resistance distribution and liver weight in isolated blood-perfused rat livers. Simultaneously, their effects on hepatic oxygen consumption were also determined with a custom-made oxygen absorption spectrophotometer [21].

2. Materials and methods

Sixty-seven male Sprague-Dawley rats (Japan SLC, Shizuoka, Japan) weighing 327 ± 3 g were used in this study. Rats were maintained at 23 °C and under pathogen-free conditions on a 12/12-h dark/light cycle, and received food and water ad libitum. The experiments conducted in the present study were approved by the Animal Research Committee of Kanazawa Medical University.

2.1. Isolated liver preparation

The animals were anesthetized with pentobarbital sodium (50 mg kg^{-1}, i.p.) and were mechanically ventilated with room air. The methods for the isolated perfused rat liver preparation were previously described [22]. In brief, a polyethylene tube was placed in the right carotid artery. After laparotomy, the hepatic artery was ligated and the bile duct was cannulated with the polyethylene tube (0.5 mm i.d., 0.8 mm o.d.). At 5 min after intraarterial heparinization (500 U kg^{-1}), 8–9 ml of blood was withdrawn through the carotid arterial catheter. The intra-abdominal inferior vena cava (IVC) above the renal veins was ligated, and the portal vein was cannulated with a stainless cannula (1.3 mm i.d., 2.1 mm o.d.). After thoracotomy, the supradiaphragmatic IVC was cannulated through a right atrium incision with a larger stainless cannula (2.1 mm i.d., 3.0 mm o.d.), then portal perfusion was begun with the heparinized autologous blood diluted with 5% bovine albumin (Sigma–Aldrich Co., St. Louis, MO) in Krebs solution (118 mM NaCl, 5.9 mM KCl, 1.2 mM $MgSO_4$, 2.5 mM $CaCl_2$, 1.2 mM NaH_2PO_4, 25.5 mM $NaHCO_3$, and 5.6 mM glucose) at Hct of 12%. The liver was rapidly excised, suspended from an isometric transducer (TB-652T, Nihon-Kohden, Japan) and weighed continuously throughout the experimental period.

The liver was perfused at a constant flow rate in a recirculating manner via the portal vein with blood that was pumped using a Masterflex roller pump from the venous reservoir through a heat exchanger (37 °C). The recirculating blood volume was 40 ml. The perfused blood was oxygenated in the venous reservoir by continuous bubbling with 95% O_2 and 5% CO_2 (perfused $PO_2 = 300$ mmHg).

2.2. Measurement of hepatic vascular pressures and vascular resistances

The portal venous (P_{pv}) and the hepatic venous (P_{hv}) pressures were measured using pressure transducers (TP-400T, Nihon-Kohden, Japan) attached by sidearm to the appropriate cannulas with the reference points at the hepatic hilus. Portal blood flow rate (Q) was measured with an electromagnetic flow meter (MFV 1200, Nihon-Kohden, Japan), and the flow probe was positioned in the inflow line. The hepatic sinusoidal pressure was measured by the double occlusion pressure (P_{do}) [20,23]. Both the inflow and outflow lines were simultaneously and instantaneously occluded for 13 s using the solenoid valves, after which P_{pv} and P_{hv} rapidly equilibrated to a similar or identical pressure, which was P_{do}. The principle of the double occlusion method to estimate the sinusoidal pressure [20] is derived from the concept of the mean circulating filling pressure (P_{mcf}) of the systemic circulation [24]. The P_{mcf} in the systemic circulation

represents the pressure of the most compliant vascular segments, and therefore the P_{do}, the P_{mcf} in the isolated perfused livers, represents the pressure of the most compliant vessels in the liver, that is the sinusoids. Actually, P_{do} values were obtained from the digitized data of P_{pv} and P_{hv} using an original program (LIVER software, Biomedical Science, Kanazawa, Japan). The total portal-hepatic venous (R_t), pre-sinusoidal (R_{pre}) and post-sinusoidal (R_{post}) resistances were calculated by the following equations:

$$R_t = (P_{pv} - P_{hv})/Q \quad (1)$$

$$R_{pre} = (P_{pv} - P_{do})/Q \quad (2)$$

$$R_{post} = (P_{do} - P_{hv})/Q \quad (3)$$

2.3. Bile flow rate measurement

Bile was collected drop-by-drop in a small tube suspended from the force transducer (SB-1T, Nihon-Kohden, Japan). One bile drop yielded 0.018 g and the time between drops was measured for determination of the bile flow rate [22].

2.4. Hepatic oxygen consumption measurement

To determine the oxygen consumption, the blood oxygen saturation difference between the inflow and outflow blood (ΔSO_2) was monitored continuously with a custom-made oxygen absorption spectrophotometer (ODM-1, Biomedical Science, Kanazawa, Japan), the cuvettes and sensors of which were built in the inflow and outflow perfusion lines [21]. The measured ΔSO_2 was expressed as the ODM values [21]. ΔSO_2 was calculated using the following regression line equation as determined in our previous study [21]:

$$\Delta SO_2 = 1.5103 \times \text{ODM} - 0.0685 \quad (4)$$

Using ΔSO_2, oxygen consumption (ml min^{-1} 10 g liver $weight^{-1}$) was calculated according to the Fick principle by the following equation:

$$\text{Portal blood flow/liver weight (g)} \times 10 \times 1.39\ \text{(ml/g)} \times \text{Hb (g/ml)} \times \Delta SO_2 \quad (5)$$

where Hb is the perfusing blood hemoglobin measured using spectrophotometer (UV-1200, SHIMADZU, Japan).

2.5. Data recording

The hepatic vascular pressures, blood flow rate, liver weight, bile weight and ODM values were monitored continuously and displayed through a thermal physiograph (RMP-6008, Nihon-Kohden, Japan). All outputs were also digitized by the analog-digital converter at a sampling rate of 100 Hz. These digitized values were also displayed and recorded using a personal computer for later determination of P_{do}.

2.6. Experimental protocol

Hepatic hemodynamic parameters were observed for at least 20 min after the start of perfusion until an isogravimetric state (no weight gain or loss) was obtained by adjusting the portal blood flow rate and the height of the reservoir at a P_{hv} of 0–1 cmH_2O, and at a Q of 36 ± 0.5 ml min^{-1} 10 g liver wt^{-1}. After the baseline measurements, the perfused livers were randomly divided into the three groups of the PAF, U-46619 and LTD_4 groups. To determine the concentration dependence, the drug was administered as a bolus into the reservoir to gain the final concentration of 0.0001–1 μM for PAF, 0.001–3 μM for U-46619 and 0.001–1 μM for LTD_4. The concentrations were randomly assigned for individual preparations.

In each experimental group, P_{do} was measured at baseline and maximal venoconstriction (when P_{pv} reached the peak), 6, 10, 20 and 30 min after injection of PAF, U-46619 or LTD_4.

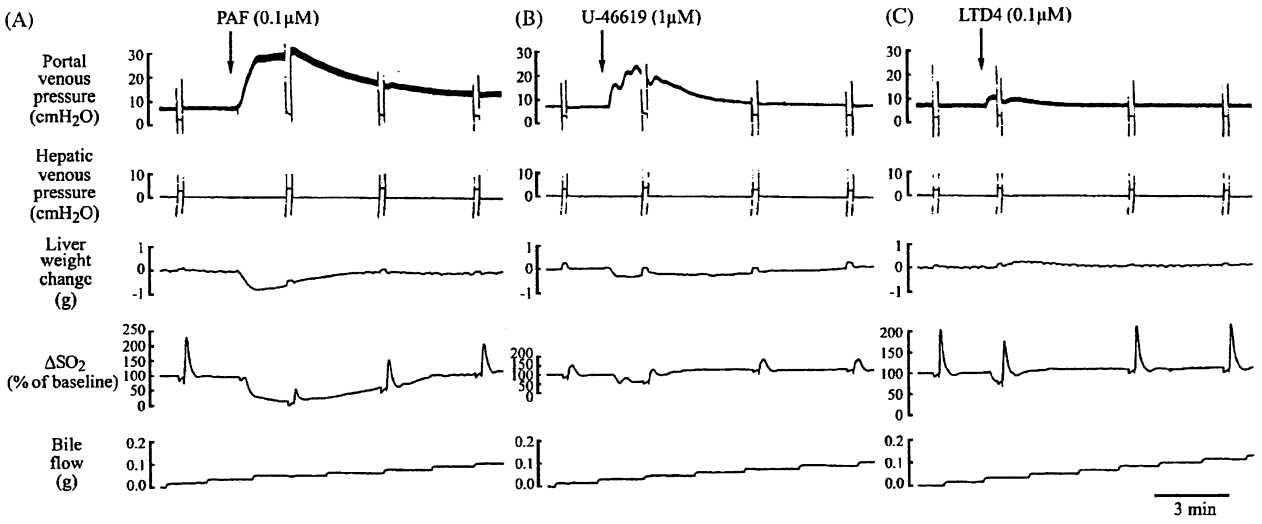


Fig. 1. Representative recordings of the responses of rat livers to PAF at 0.1 μM (A), to U-46619 at 1 μM (B) and to LTD_4 at 0.1 μM (C). ΔSO_2, the blood oxygen saturation difference between the inflow and outflow blood.

2.7. Statistics

All results are expressed as the means ± S.E. Data were analyzed by one- and two-way analysis of variance, using repeated-measures for two-way comparison within groups. Comparisons of individual points between groups and within groups were made by Bonferroni's test. Differences were considered as statistically significant at P-values less than 0.05.

3. Results

3.1. Effects of PAF, U-46619 and LTD_4 on hepatic hemodynamic variables

Fig. 1 shows the representative examples of variables after injections of PAF at 0.1 μM (A), U-46619 at 1 μM (B) and LTD_4 at 0.1 μM (C). Fig. 2 shows the summary data of the time-dependent changes in P_{pv}, P_{do}, liver weight, hepatic oxygen consumption and bile flow rate of all groups.

Soon after administrations of PAF (0.0001–1 μM), vasoconstriction occurred, as evidenced by the increase in P_{pv} (Figs. 1A and 2A). At 0.1 μM, P_{pv} increased to the peak of 25.5 ± 1.9 cmH_2O from the baseline of 7.1 ± 0.1 cmH_2O within 1.5–2.5 min after injection. The double occlusion maneuver revealed that P_{do} increased from the baseline of 2.5 ± 0.1 to 4.4 ± 0.3 cmH_2O. The pressure gradient of P_{do}-to-P_{hv} was significantly increased from the baseline of 2.2 ± 0.1 to 4.1 ± 0.1 cmH_2O, indicating the increase in R_{post}. However, the increase in the P_{pv}-to-P_{do} gradient, from 4.7 ± 0.1 to 21.2 ± 0.9 cmH_2O, was much greater than that in the P_{do}-to-P_{hv} gradient, indicating that the increase in R_{pre} was greater than that in R_{post}. Fig. 3 shows the peak levels of segmental vascular resistance, liver weight change and bile flow after PAF (closed column). R_t and R_{pre} showed concentration-dependent increases with peak levels of 3.7-fold and 4.6-fold the baseline at 0.1 μM PAF. In contrast, R_{post} at 0.1 μM PAF reached only 1.9-fold the baseline. Thus, the R_{post}/R_t ratio decreased with increasing concentrations of PAF, as shown in Fig. 3. The peaks of R_t, R_{pre} and R_{post} at 1 μM PAF were not significantly different from those at 0.1 μM PAF.

U-46619 caused venoconstriction at concentrations higher than 0.01 μM (Figs. 1B and 2B). Similar to PAF, the U-46619-induced venoconstriction was also characterized by dominant pre-sinusoidal constriction: the increase in Pdo was relatively smaller than that in P_{pv}, as shown in Fig. 2B. Actually, at the maximal vasoconstriction with 3 μM U-46619, the increase in P_{pv}-to-P_{do} gradient (from 4.8 ± 0.1 to 23.1 ± 0.5 cmH_2O) was much greater than that in the P_{do}-to-P_{hv} gradient (from 2.3 ± 0.1 to 3.3 ± 0.1 cmH_2O). Indeed, in response to 3 μM U-46619, R_{pre} increased to 4.8 times the baseline, while R_{post} increased to only 1.3 times the baseline (Fig. 3). This predominant pre-sinusoidal constriction over post-sinusoidal constriction was reflected by a progressive decrease in R_{post}/R_t ratio (Fig. 3). The U-

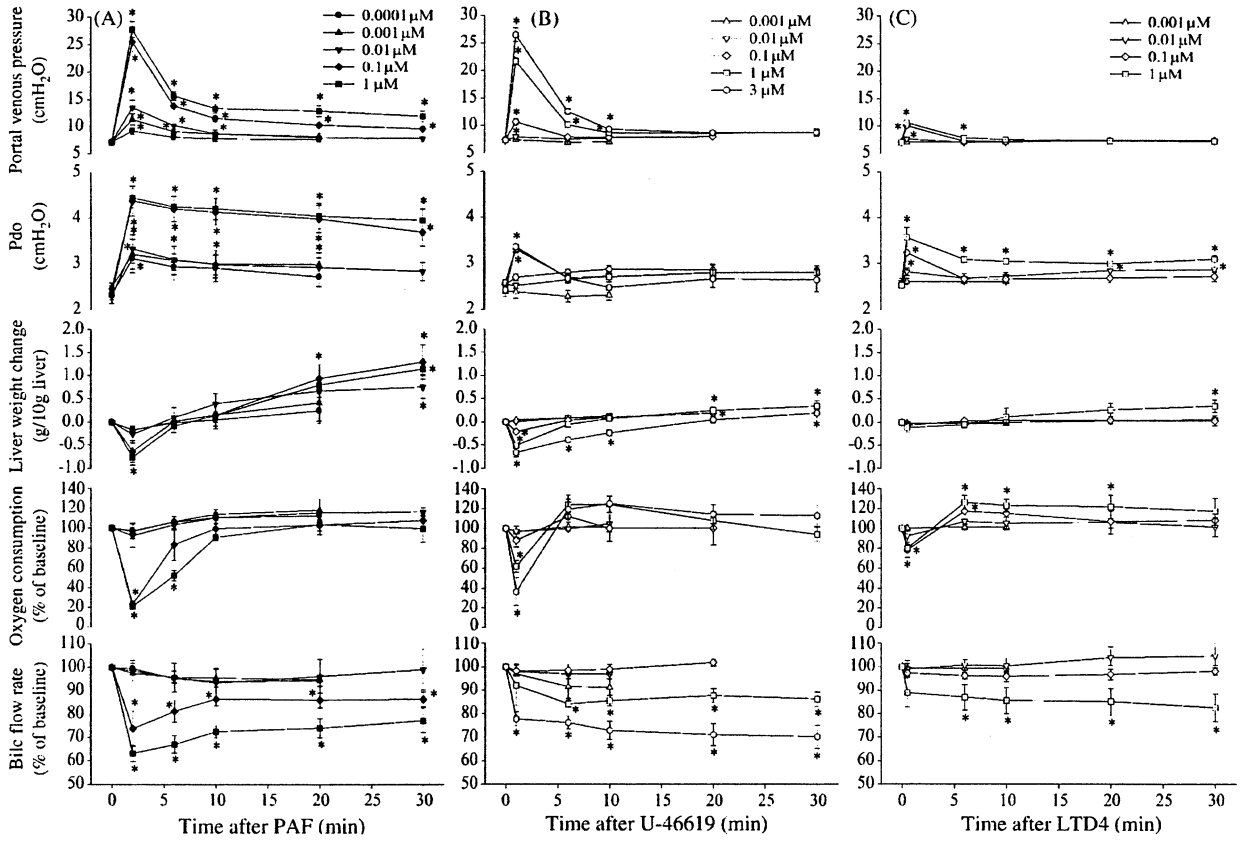


Fig. 2. The summary data of time course changes in portal venous pressure, double occlusion pressure (P_{do}), liver weight change, hepatic oxygen consumption and bile flow rate in the PAF (A), U-46619 (B) and LTD_4 (C) groups. Values are given as mean ± S.E. $n = 4$–6. $^*P < 0.05$ vs. the baseline.

46619-induced increase in R_t was smaller in magnitude than that at the corresponding concentration of PAF. However, at the comparable increased R_t levels, the R_{post}/R_t ratio in U-46619 groups was smaller than that in PAF groups, indicating that U-46619 more preferentially constricts the pre-sinusoids than PAF. R_t, R_{pre} and R_{post} recovered almost to the baseline levels within 20 min after U-46619.

LTD_4 caused a dose-dependent increase in P_{pv} at concentrations higher than 0.01 μM, as shown in Figs. 1C and 2C. The vasoconstrictive effect of LTD_4 is much weaker than that of PAF or U-46619. However, the venoconstrictive responsiveness of either pre- or post-sinusoids to LTD_4 was almost the same: the increase in R_{pre} (1.6 times the baseline) was nearly the same as that of R_{post} (1.3 times the baseline) with 0.1 μM LTD_4. This was also reflected by no significant change in R_{post}/R_t ratio (Fig. 3). R_t, R_{pre} and R_{post} recovered almost to the baseline levels within 10 min after LTD_4.

Table 1 shows the basal hemodynamic variables in all groups.

3.2. Effects of PAF, U-46619 and LTD_4 on liver weight

Concomitant with hepatic vasoconstriction at high concentrations of PAF (0.01–1 μM), the liver weight showed a biphasic change characterized by an initial decrease followed by an increase, as shown in Fig. 2A. There are no significant differences in peak liver weight levels between the 0.1 and 1 μM PAF groups.

U-46619 caused a progressive and dose-dependent decrease in the liver weight, resulting in the nadirs of -0.22 ± 0.02, -0.51 ± 0.05, and -0.67 ± 0.09 g 10 g liver wt^{-1}, at 0.1, 1 and 3 μM, respectively, at 1 min (Fig. 2B).

In contrast to PAF and U-46619, LTD_4, did not significantly change liver weight for 20 min, but slightly increased it at 30 min after 1 μM LTD_4 (Fig. 2C).

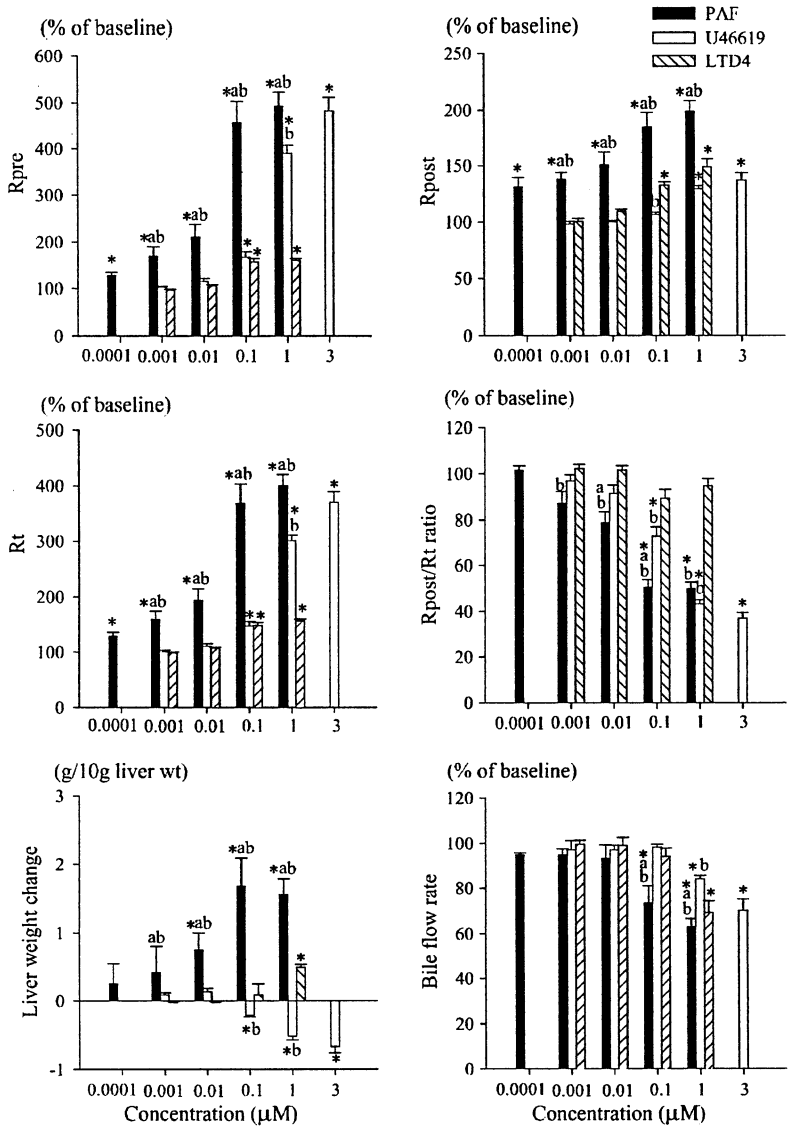


Fig. 3. The peak changes in the total (R_t), pre- (R_{pre}) and post-sinusoidal (R_{post}) resistances, the R_{post}/R_t ratio, bile flow rate and liver weight change at 0.0001–3 μM of PAF, U-46619 and LTD_4. Percent changes are expressed by those of the baseline. Values are given as mean ± S.E. $n = 4$–6. $^{*}P < 0.05$ vs. the baseline, $^{a}P < 0.05$ vs. U-46619, $^{b}P < 0.05$ vs. LTD_4.

Table 1
Basal hemodynamic variables of isolated perfused rat livers in the PAF, U-46619 and LTD_4 groups

	PAF	U-46619	LTD_4
Number of preparations	22	27	18
Portal venous pressure (cmH_2O)	7.1 ± 0.1	7.2 ± 0.1	7.0 ± 0.1
Hepatic venous pressure (cmH_2O)	0.20 ± 0.02	0.18 ± 0.02	0.21 ± 0.03
Double occlusion pressure (cmH_2O)	2.4 ± 0.1	2.5 ± 0.1	2.6 ± 0.1
Blood flow rate ($ml^{-1}\ min^{-1}\ 10\,g^{-1}$)	35 ± 1	38 ± 1	34 ± 1
Total vascular resistance ($cmH_2O\ ml^{-1}\ min^{-1}\ 10\,g^{-1}$)	0.20 ± 0.01	0.19 ± 0.01	0.20 ± 0.01
Pre-sinusoidal resistance ($cmH_2O\ ml^{-1}\ min^{-1}\ 10\,g^{-1}$)	0.14 ± 0.01	0.13 ± 0.01	0.13 ± 0.01
Post-sinusoidal resistance ($cmH_2O\ ml^{-1}\ min^{-1}\ 10\,g^{-1}$)	0.06 ± 0.01	0.06 ± 0.01	0.07 ± 0.01
R_{post}/R_t ratio	0.32 ± 0.01	0.33 ± 0.01	0.34 ± 0.01

Values are given as mean ± S.E.

3.3. Effects of PAF, U-46619 and LTD_4 on bile flow rate

Basal bile flow rate in livers studied was 8.7 ± 0.1 mg min^{-1} 10 g liver wt^{-1}. After PAF at 0.1 and 1 μM, bile flow rate significantly decreased to nadirs of 74 ± 8 and $63 \pm 4\%$ of the baseline, respectively, at 2 min and then gradually recovered. In response to U-46619 at 1 and 3 μM, it also significantly decreased to 84 ± 5 and $70 \pm 5\%$ of the baseline. In contrast, a significant decrease in the bile flow rate was observed after LTD_4 only at 1 μM, and it decreased to $69 \pm 5\%$ of the baseline at 30 min.

3.4. Effects of PAF, U-46619 and LTD_4 on hepatic oxygen consumption

The hepatic oxygen consumption was not significantly changed by PAF at 0.0001–0.01 μM, but significantly decreased at 0.1 and 1 μM (Figs. 1A and 2A). It recovered to the baseline at 10 min. There was no significant difference between the nadirs of hepatic oxygen consumption, $23 \pm 3\%$ of the baseline of 0.049 ± 0.006 ml min^{-1} 10 g liver wt^{-1} at 0.1 μM and $21 \pm 2\%$ of the baseline of 0.053 ± 0.010 ml min^{-1} 10 g liver wt^{-1} at 1 μM.

In response to U-46619, the hepatic oxygen consumption was also not significantly changed at lower concentrations (0.001–0.1 μM), but was significantly decreased at higher concentrations (1 and 3 μM). It reached the nadirs, 62 ± 6 and $36 \pm 14\%$ of the baseline of 0.041 ± 0.005 and 0.044 ± 0.008 ml min^{-1} 10 g liver wt^{-1}, respectively, at 1 min, and then recovered quickly, as shown in Fig. 2B. The magnitude of decrease in the hepatic oxygen consumption was smaller with U-46619 than with PAF at corresponding concentrations.

In contrast, LTD_4 induced biphasic changes at high concentrations of 0.1 and 1 μM. It initially decreased to $78 \pm 8\%$ and $80 \pm 4\%$ of the baseline at 0.5 min, and then quickly and significantly increased to the peak of $118 \pm 4\%$ and $126 \pm 7\%$, at 0.1 and 1 μM, respectively (Fig. 2C).

4. Discussion

In the present study, we determined the effects of a TxA_2 analogue (U-46619), PAF and LTD_4 on the vascular resistance distribution, liver weight and oxygen consumption in isolated rat livers portally perfused with blood. The main findings are that both PAF and U-46619 predominantly constricted the pre-sinusoidal veins over the post-sinusoidal veins, with U-46619 more preferentially constricting the pre-sinusoids than PAF. In contrast, LTD_4 constricted both the pre- and post-sinusoidal veins similarly in isolated blood-perfused rat livers. U-46619 caused liver weight loss, while PAF and LTD_4 at the high concentrations increased liver weight via substantial post-sinusoidal constriction. PAF and U-46619 decreased hepatic oxygen consumption, but LTD_4 induced a biphasic change of an initial transient decrease followed by an increase.

Hepatic vascular responsiveness to various vasoactive substances differs depending on the vascular segments and the animal species. Histamine causes marked constriction of the hepatic vein in dogs [25] and guinea pigs [26], while it does not constrict hepatic vessels of cats [27] and rats [26]. In contrast, norepinephrine preferentially constricts the pre-sinusoidal vessels similarly in dog [28,29], rat [28,29], rabbit [23,28], guinea pig [26] and mouse [30]. With respect to the venoconstrictive site of PAF and TxA_2, we previously reported using canine isolated blood-perfused livers that TxA_2 predominantly constricts the hepatic vein [17], while PAF constricts both portal veins and hepatic veins similarly [18]. We have recently shown that both PAF and TxA_2 predominantly constrict pre-sinusoidal veins over post-sinusoidal veins in guinea pigs, although the post-sinusoidal action of TxA_2 was weaker than that of PAF [19]. In rat livers, we herein demonstrated that both PAF and TxA_2 predominantly constricted pre-sinusoidal veins over post-sinusoidal veins, and TxA_2 more preferentially constricted the pre-sinusoids than PAF in rat livers. In contrast, LTD_4 constricted both the pre- and post-sinusoidal veins similarly in rat livers. Thus the hepatic vascular responsiveness to PAF and TxA_2 of rats appears to be similar to that of guinea pigs rather than dogs. Furthermore, we have shown that the order of vasoconstrictive effects was PAF > TxA_2 > LTD_4.

We have recently reported using the same isolated rat liver preparation that hepatic anaphylaxis induced by antigen of ovalbumin causes marked pre-sinusoidal venoconstriction and liver weight change of initial loss followed by a gradually increase, which could account for the portal hypertension and hepatic congestion associated with anaphylactic shock [21,22]. Anaphylactic reaction is accompanied by an increased release of vasoactive substances such as PAF [31], TxA_2 [31] and LTD_4 [32]. In the present study, PAF induced substantial pre-sinusoidal constriction, and an initial slight liver weight loss followed by liver weight gain. The response to PAF may be compatible with the hepatic anaphylactic

response in rats [21,22]. In contrast, TxA_2or LTD_4 seems not to be a main mediator responsible for the rat hepatic anaphylaxis, because the vasoconstriction induced by these mediators was very weak, as shown in the present study. However, in this respect, further pharmacological studies are required using the antagonists of these lipid mediators.

The mechanism whereby PAF or U-46619 predominantly constricts the pre-sinusoids over the post-sinusoids in rat is not known. One possibility is related to platelet and neutrophil aggregation, because both PAF and TxA_2 can activate these cells, resulting in intravascular aggregation [1,2]. The aggregation of neutrophils and platelets may obstruct the sinusoids, which could represent an increase in the pre-sinusoidal resistance. However, this assumption seems unlikely because heparin that was used in the present study has been shown not only to inhibit adhesion of leukocyte in the endothelium [33] but also to cause platelet dysfunction [34]. Thus, even if platelet or leukocyte aggregation occurs, they might play a minor role in the vascular resistance change. The second, contraction of the hepatic pericytes, hepatic stellate cells, may account for either PAF or U-46619-induced pre-sinusoidal venoconstriction. Hepatic stellate cells are located around the endothelial cells and their multiple cellular appendages reach out to wrap around the sinusoid [35]. Hepatic stellate cells are highly contractile in response to PAF and TxA_2 [36]. PAF and TxA_2 could constrict sinusoidal hepatic stellate cells directly, resulting in increased sinusoidal resistance, which might represent increased pre-sinusoidal resistance. However, other investigators could not confirm the physiological contractility of the stellate cells [37,38]. Finally, a more plausible explanation is that functional PAF and TxA_2 receptors are distributed more abundantly in the smooth muscle cells of the rat pre-sinusoidal vein than in those of the post-sinusoidal vein. However, there is no direct evidence of the presence of nonhomogenous distribution of PAF or TxA_2 receptors in rat hepatic vessels.

We believe that the hepatic vasoconstrictive response to PAF, U-46619 or LTD_4 in the present study was due to the direct effects of these substances, because the vasoconstriction occurred immediately after injection without a latent period that might have been required for activation, release or synthesis of other vasoconstrictors. However, we cannot rule out a possibility of modulation of an endogenous hepatic vasoconstrictor that could be released in response to U-46619, PAF or LTD_4. In organs other than livers, some of the vasoconstrictive effects of TxA_2 seem to be mediated by the induction of LTC_4 and LTD_4 [39], and endothelins [40]. PAF is also able to activate the hepatic intravascular macrophages of Kupffer cells, with resultant release of the cyclooxygenase metabolites [41]. LTD_4 could stimulate the synthesis of TxA_2 [42,43]. Further studies are required to examine the interactions among these mediators.

We measured liver weight changes to know the intrahepatic blood volume alterations. U-46619 induced obvious liver weight loss. In contrast, PAF mainly induced liver weight gain although it initially and transiently caused liver weight loss. Liver weight also increased in response to LTD_4 at the highest concentration of 1 μM. The decrease in liver weight may be produced by pre-sinusoidal constriction, which may prevent the entrance of blood into the liver capillaries, resulting in weight loss. The liver weight gain after PAF and LTD_4 may be caused by substantial post-sinusoidal constriction and an increase in P_{do}, both of which would lead to hepatic congestion, enhanced extravascular fluid filtration and interstitial water accumulation. The magnitude of increased P_{do} may represent the liver weight change. Fig. 4 shows the relationship between the peak P_{do} and liver weight change in all groups studied. There was a significant correlation between the peak P_{do} and liver weight change ($r=0.746$, $p<0.0001$) after administrations of PAF, U-46619 and LTD_4. This finding indicated that the liver weight change was strongly associated with the P_{do} increase, as described previously in our study [19].

In the present study, we have demonstrated that PAF and U-46616 decreased hepatic oxygen consumption, while LTD_4 caused a biphasic change of it. These results are in agreement with the previous studies [44–46]. Haussinger et al. reported that U-46619 decreased oxygen consumption by 27% in perfused rat livers [44]. ONO-11113, another TXA_2 analogue, induced an initial small stimulation followed by a marked inhibition of oxygen uptake in perfused rat livers [45]. PAF also suppressed oxygen consumption in perfused rat livers [46]. However, Haussinger et al. reported that LTC_4 and LTD_4 of 20 nM reduced oxygen consumption by $29 \pm 3\%$ and $30 \pm 3\%$ of baseline, respectively, in isolated rat livers [44]. The difference may be related to the different perfusion methods. In the study of Haussinger et al., the livers were perfused without recirculation with blood-free Krebs solution [44]. In addition, in the present study, a biphasic change in oxygen consumption was observed only at high concentrations (0.1 and 1 μM) of LTD_4. In contrast, Haussinger et al. examined only one small dose (20 nM) of LTD_4, but not the high dose of LTD_4.

There is a criticism that the relevance of the present findings to the in vivo situation seems to be limited by the fact that the experiments were done in an isolated organ, and perfusion was done using diluted blood. However, one of the main purposes of the present study is to determine the venoconstrictive site of the lipid mediators in rat hepatic circulation. Currently, this could not be accomplished in in vivo intact animals, if the measurement of the hepatic

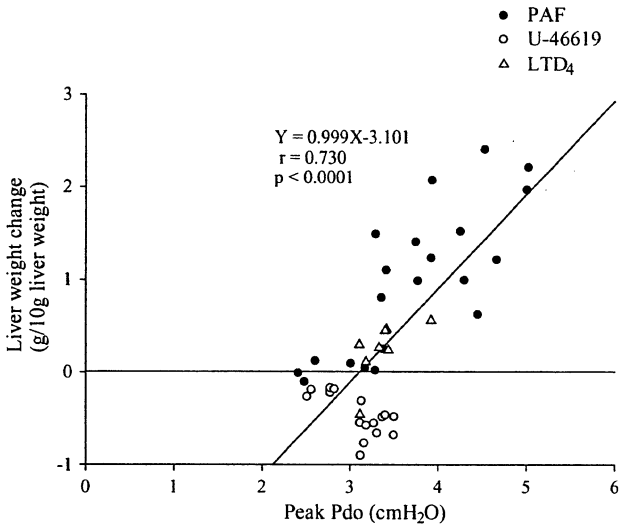


Fig. 4. Relationship between peak P_{do} values and liver weight changes after injections of PAF (closed circle), U-46619 (open circle) and LTD_4 (triangle). Equations of linear lines are given in the text.

microvascular pressures using the micropipette method were not performed [47]. However, no measurement of the hepatic microvessels with micropipettes in in vivo animals has been performed so far to determine the effects of lipid mediators such as PAF, TxA_2, and LTD_4 on the hepatic vascular resistance distribution. Although limitations inherent to isolated perfused livers exist, we think that P_{do} [20] in the present perfused livers has provided estimation of the sinusoidal pressure and therefore the pre- and post-sinusoidal resistances in the livers exposed to the lipid mediators studied.

In conclusion, both TxA_2 and PAF predominantly constrict pre-sinusoidal veins, and TxA_2 more preferentially constricts the pre-sinusoids than PAF. However LTD_4 constricts both pre- and post-sinusoidal veins similarly. The order of the extent of hepatic venoconstrictive effects was PAF > TxA_2 > LTD_4. TxA_2 causes liver weight loss at high concentrations, while LTD_4 and PAF increase liver weight via substantial post-sinusoidal constriction in isolated rat livers. PAF and TxA_2 decrease hepatic oxygen consumption, whereas LTD_4 induces a biphasic change of it in isolated blood-perfused rat livers.

Acknowledgement

This work was supported by a Grant for Collaborative Research from Kanazawa Medical University (C2004-1, C2005-1).

References

[1] Braquet P, Touqui L, Shen TY, Vargaftig BB. Perspective in platelet-activating factor research. Pharmacol Rev 1987;39:97–145.
[2] Samuelsson B, Goldyne M, Granstrom E, Hamberg M, Hammarstrom S, Malmsten C. Prostaglandins and thromboxanes. Ann Rev Biochem 1978;47:997–1029.
[3] Hagmann W, Hacher HJ, Buchholz U. Resident mast cells are the main initiators of anaphylactic leukotriene production in the liver. Hepatology 1992;16:1477–84.
[4] Shibamoto T, Ruan Z, Cui S, Liu W, Kurata Y. Involvement of platelet-activating factor and leukotrienes in anaphylactic segmental venoconstriction in ovalbumin sensitized guinea pig livers. Prostaglandins Other Lipid Mediat 2005;78:218–30.
[5] Guarner F, Wallace JL, MacNaughton WK, Ibbotson GC, Arroyo V, Rodes J. Endotoxin-induced ascites formation in the rat: partial mediation by platelet-activating factor. Hepatology 1989;10:788–94.
[6] Ishiguro S, Arii S, Monden K, et al. Identification of the thromboxane A_2 receptor in hepatic sinusoidal endothelial cells and its role in endotoxin-induced liver injury in rats. Hepatology 1994;20:1281–6.
[7] Tiegs G, Wendel A. Leukotriene-mediated liver injury. Biochem Pharmacol 1988;37:2569–73.
[8] Ishiguro S, Arii S, Monden K, et al. Involvement of thromboxane A2–thromboxane A2 receptor system of the hepatic sinusoid in pathogenesis of cold preservation/reperfusion injury in the rat liver graft. Transplantation 1995;59:957–61.

[9] Iwazaki S, Takeyoshi I, Ohawada S, et al. FR128998 ameliorates liver injury in extended liver resection with ischemia in dogs. Hepatogastroenterology 2001;48:197–202.
[10] Takeyoshi I, Sunose Y, Iwazaki S, et al. The effect of a selective cycloxygenase-2 inhibitor in extended liver resection with ischemia in dogs. J Surg Res 2001;100:25–31.
[11] Shimada M, Matsumata T, Taketomi A, Shirabe K, Yamamoto K, Sugimachi K. The role of prostaglandins in hepatic resection. Prostaglandins Leukot Essent Fatty Acids 1994;50:65–8.
[12] Chun K, Zhang J, Biewer J, Ferguson D, Clemens MG. Microcirculatory failure determines lethal hepatocyte injury in ischemic/reperfusion rat livers. Shock 1994;1:3–9.
[13] Fisher RA, Robertson SM, Olson MS. Stimulation of glycogenolysis and vasoconstriction in the perfused rat liver by the thromboxane A2 analogue U-46619. J Biol Chem 1987;262:4631–8.
[14] Haussinger D, Stehle T, Gerok W. Effects of leukotrienes and the thromboxane A2 analogue U-46619 in isolated perfused rat liver. Metabolic, hemodynamic and ion-flux responses. Biol Chem 1988;369:97–107.
[15] Hines KL, Braillon A, Fisher RA. PAF increases hepatic vascular resistance and glycogenolysis in vivo. Am J Physiol 1991;260:G471–80.
[16] Buxton DB, Fisher RA, Hanahan DJ, Olson MS. Platelet-activating factor mediated vasoconstriction and glycogenolysis in the perfused rat liver. J Biol Chem 1986;261:644–9.
[17] Urayama H, Shibamoto T, Wang HG, Koyama S. Thromoboxane A_2 analogue contracts predominantly the hepatic veins in isolated canine livers. Prostaglandins 1996;52:483–95.
[18] Wang HG, Shibamoto T, Koyama S. Effect of platelet-activating factor on hepatic capillary pressure in isolated dog liver. Prostaglandins Leukot Essent Fatty Acids 1997;57:293–8.
[19] Ruan Z, Shibamoto T, Shimo T, et al. Effects of platelet-activating factor and thromboxane A_2 on isolated perfused guinea pig liver. Prostaglandins Other Lipid Mediat 2004;73:73–85.
[20] Yamaguchi Y, Shibamoto T, Hayashi T, Saeki Y, Tanaka S. Hepatic vascular response to anaphylaxis in isolated canine liver. Am J Physiol 1994;267:R268–74.
[21] Cui S, Shibamoto T, Ruan Z, Takano H, Liu W, Kurata Y. Oxygen consumption, assessed with the oxygen absorption spectrophotometer, decreases independently of venoconstriction during hepatic anaphylaxis in perfused rat liver. Shock; in press.
[22] Shibamoto T, Cui S, Ruan Z, Liu W, Takano H, Kurata Y. Hepatic venoconstriction is involved in anaphylactic hypotension in rats. Am J Physiol Heart Circ Physiol 2005;289:H1436–41.
[23] Shibamoto T, Wang HG, Miyahara T, Tanaka S, Haniu H, Koyama S. Presinusoidal vessels predominantly contract in response to norepinephrine, histamine, and KCl in rabbit liver. J Appl Physiol 1999;87:1404–12.
[24] Rothe CF. Mean circulatory filling pressure: its meaning and measurement. J Appl Physiol 1993;74:499–509.
[25] Lautt WW, Legare DJ. Effect of histamine, norepinephrine, and nerves on vascular pressures in dog liver. Am J Physiol 1987;252:G472–8.
[26] Shibamoto T, Narushima M, Ling YQ, et al. Different hepatic vascular response to norepinephrine and histamine between guinea pig and rat. Acta Physiol Scand 2004;180:255–63.
[27] Greenway CV, Lautt WW. Effects of infusions of catecholamines, angiotensin, vasopressin and histamine on hepatic blood volume in the anaesthetized cat. Br J Pharmacol 1972;44:177–84.
[28] Bohlen HG, Maass-Moreno R, Rothe CF. Hepatic venular pressures of rats, dogs, and rabbits. Am J Physiol 1991;261:G539–47.
[29] Shibamoto T, Wang HG, Tanaka S, Koyama S. Hepatic capillary pressure is estimated using triple vascular occlusion method in isolated canine liver. Am J Physiol 1996;271:R1130–41.
[30] Shibamoto T, Cui S, Ruan Z, Kurata Y. Effects of norepinephrine and histamine on vascular resistance in isolated perfused mouse liver. Jpn J Physiol 2005;55:143–8.
[31] Kemp SF, Lockey RF. Anaphylaxis: a review of causes and mechanisms. J Allergy Clin Immunol 2002;110:341–8.
[32] Foster A, Letts G, Charleson S, Fitzsimmons B, Blacklock B, Rokach J. The in vivo production of peptide leukotrienes after pulmonary anaphylaxis in the rat. J Immunol 1988;141:3544–50.
[33] Bazzoni G, Beltran NA, Mascellani G, Bianchini P, Dejana E, Del Maschio A. Effect of heparin, dermatan sulfate, and related oligo-derivatives on human polymorphonuclear leukocyte functions. J Lab Clin Med 1993;121:268–75.
[34] Khuri SF, Valeri CR, Loscalzo J, et al. Heparin causes platelet dysfunction and induces fibrinolysis before cardiopulmonary bypass. Ann Thorac Surg 1995;60:1008–14.
[35] Wake K. Perisinusoidal stellate cells (fat-storing cells, interstitial cells, lipocytes), their related structure in and around the liver sinusoids, and vitamin A-storing cells in extrahepatic organs. Int Rev Cytol 1980;66:303–53.
[36] Rockey DC. Hepatic blood flow regulation by stellate cells in normal and injured liver. Semin Liver Dis 2001;21:337–49.
[37] McCuskey R, Ito Y, McCuskey M, et al. Morphological mechanism for regulating blood flow through hepatic sinusoids: 1998 update and overview. In: Wisse E, Knock D, De Zanger R, editors. Cell of the hepatic sinusoid. Rijswijk: Kupffer Cell Foundation; 1999. p. 129–34.
[38] Ekataksin W, Kaneda K. Liver microvascular architecture: an insight into the pathophysiology of portal hypertension. Semin Liver Dis 1999;19:359–82.
[39] Soifer SJ, Schreiber MD, Heymann MA. Leukotriene antagonists attenuate thromboxane-inducible pulmonary hypertension. Pediatr Res 1989;26:83–7.
[40] Yamamoto T, Hosoki K, Karasawa T. Possible involvement of endothelin in thromboxane A_2 receptor agonist (U-46619)-induced angina in the rat. Eur J Pharmacol 1993;250:189–91.
[41] Altin JG, Dieter P, Bygrave FL. Evidence that Ca^{2+} fluxes and respiratory, glycogenolytic and vasoconstrictive effects induced by the action of platelet-activating factor and L-α-lysophosphatidylcholine in the perfused rat liver are mediated by products of the cyclo-oxygenase pathway. Biochem J 1987;245:145–50.

[42] Smith LJ, Shamsuddin M, Houston M. Effect of leukotriene D_4 and platelet-activating factor on human alveolar macrophage eicosanoid and PAF synthesis. Am Rev Respir Dis 1993;148:682–8.
[43] Bochnwicz S, Underwood DC. Dose-dependent mediation of leukotriene D4-induced airway microvascular leakage and bronchoconstriction in the guinea pig. Prostaglandins Leukot Essent Fatty Acids 1995;52:403–11.
[44] Haussinger D, Stehle T, Gerok W. Effects of leukotrienes and the thromboxane A_2 analogue U-46619 in isolated perfused rat liver. Biol Chem 1988;369:97–107.
[45] Altin JG, Bygrave FL. Prostaglandin F_2 alpha and the thromboxane A_2 analogue ONO-11113 stimulate Ca^{2+} fluxes and other physiological responses in rat liver. Further evidence that prostanoids may be involved in the action of arachidonic acid and platelet-activating factor. Biochem J 1988;249:677–85.
[46] Kimura K, Moriyama M, Nishisako M, et al. Modulation of platelet activating factor-induced glycogenolysis in the perfused rat liver after administration of endotoxin in vivo. J Biochem (Tokyo) 1998;123:142–9.
[47] Rothe CF, Maass-Moreno R. Active and passive liver microvascular responses from angiotensin, endothelin, norepinephrine, and vasopressin. Am J Physiol Heart Circ Physiol 2000;279:H1147–56.

Clinical and Experimental Pharmacology and Physiology (2006) **33**, 1073–1077 doi: 10.1111/j.1440-1681.2006.04489.x

N^G-NITRO-L-ARGININE METHYL ESTER POTENTIATES ANAPHYLACTIC VENOCONSTRICTION IN RAT PERFUSED LIVERS

Toshishige Shibamoto,* Takaharu Ishibashi,† Tomohiro Shimo,‡ Sen Cui,* Hiromichi Takano,* Hideaki Tsuchida,‡ Matomo Nishio† and Yasutaka Kurata*

*Departments of *Physiology, †Pharmacology and ‡Anaesthesiology, Kanazawa Medical University, Uchinada, Japan*

SUMMARY

1. The effects of the nitric oxide (NO) synthase inhibitor N^G-nitro-L-arginine methyl ester (L-NAME) on anaphylaxis-induced venoconstriction were examined in rat isolated livers perfused with blood-free solutions in order to clarify the role of NO in anaphylactic venoconstriction.

2. Rats were sensitized with ovalbumin (1 mg) and, 2 weeks later, livers were excised and perfused portally in a recirculating manner at a constant flow with Krebs'–Henseleit solution. The antigen (ovalbumin; 0.1 mg) was injected into the reservoir 10 min after pretreatment with L-NAME (100 μmol/L) or D-NAME (100 μmol/L) and changes in portal vein pressure (Ppv), hepatic vein pressure (Phv) and perfusate flow were monitored. In addition, concentrations of the stable metabolites of NO (NO_2^- and NO_3^-) were determined in the perfusate using an HPLC–Griess system.

3. The antigen caused hepatic venoconstriction, as evidenced by an increase in Ppv from a mean (±SEM) baseline value of 7.7 ± 0.1 cmH_2O to a peak of 21.4 ± 1.1 cmH_2O at 3 min in D-NAME-pretreated livers. Pretreatment with L-NAME augmented anaphylactic venoconstriction, as reflected by a higher Ppv (27.4 ± 0.8 cmH_2O) after antigen than observed following D-NAME pretreatment. The addition of L-arginine, a precursor for the synthesis of NO, reversed the augmentation of anaphylactic venoconstricion by L-NAME. This suggests that hepatic anaphylaxis increased the production of NO, which consequently attenuated anaphylactic venoconstriction. However, perfusate NO_x levels did not increase significantly after antigen in livers pretreated with either L-NAME or D-NAME.

4. In conclusion, L-NAME potentiates rat anaphylactic hepatic venoconstriction, suggesting that NO contributes to the attenuation of the venoconstriction. However, this functional evidence was not accompanied by corresponding changes in perfusate NO_x concentrations.

Key words: anaphylactic shock, HPLC–Griess system, isolated perfused rat liver, nitric oxide, NO_x.

INTRODUCTION

Anaphylactic hypotension is sometimes life threatening and is caused by a decrease in effective circulating blood volume.[1] Nitric oxide (NO), which is produced in endothelial cells in response to either hormonal or physical stimuli, such as shear stress, regulates the vascular system.[2,3] Nitric oxide seems to play an important pathophysiological role in modulating the systemic changes associated with anaphylaxis. An NO synthase (NOS) inhibitor was shown to attenuate hypotension and haemoconcentration and decrease venous return in this condition, although it did not improve cardiac depression.[4] Conversely, NO functionally antagonizes the effects of vasoconstrictors released during anaphylaxis and there is experimental evidence that NO may reduce some pathophysiological changes associated with anaphylaxis, except for vasodilatation.[4]

It is well known that vasoconstriction of the liver contributes to the control of systemic circulation: passive blood mobilization to and from the liver, which is caused by hepatic vasoconstriction, influences venous return to the heart and, hence, systemic circulation.[5] Indeed, it has been reported that hepatic venoconstriction is involved, in part, in anaphylactic hypotension.[6,7] Anaphylaxis causes hepatic venoconstriction, as observed in rats,[7,8] guinea-pigs[9] and dogs,[10,11] resulting in portal hypertension that then causes congestion of the upstream splanchnic organs, with a resultant decrease in venous return and effective circulating blood volume and finally augmentation of anaphylactic hypotension. We have shown recently that hepatic venoconstriction is observed in response to antigen in sensitized guinea-pig livers and that NO attenuates constriction of these vessels.[9] Anaphylactic hepatic venoconstriction, based on an increase in portal venous pressure, was also observed in rats.[7,8] However, it is not known whether NO can be released in rat liver vasculature exposed to anaphylaxis and can modulate anaphylactic hepatic venoconstriction.

Thus, to investigate these issues, anaphylactic venoconstriction was examined with rat isolated livers that were perfused with a blood-free solution under constant flow in the presence of the NOS inhibitor N^G-nitro-L-arginine methyl ester (L-NAME) or D-NAME, an inactive enantiomer of L-NAME. The effect of L-NAME was further examined with simultaneous pretreatment with L-arginine. In addition to this functional study, we attempted to provide physical evidence by measuring perfusate NO_2^- and NO_3^- (stable metabolites of NO) with the sophisticated HPLC–Griess system (ENO-10) to elucidate the contribution of NO to functional effects observed.

Correspondence: Dr Toshishige Shibamoto, Department of Physiology, Kanazawa Medical University, Daigaku 1-1, Uchinada, Ishikawa 920-0293, Japan. Email: shibamo@kanazawa-med.ac.jp

Received 8 October 2005; revision 2 April 2006; accepted 18 April 2006.

© 2006 Blackwell Publishing Asia Pty Ltd

METHODS

Animals

Twenty-three male Sprague-Dawley rats (Japan SLC, Shizuoka, Japan) weighing 333 ± 4 g were used in the present study. Rats were maintained under pathogen-free conditions on a 12 h dark–light cycle and allowed food and water *ad libitum*. The experiments conducted in the present study were approved by the Animal Research Committee of Kanazawa Medical University. Rats were actively sensitized by the subcutaneous injection of an emulsion made by mixing equal volumes of complete Freund's adjuvant (0.5 mL) with 1 mg ovalbumin (grade V; Sigma, St Louis, MO, USA) dissolved in physiological saline (0.5 mL).

Isolated perfused liver

Two weeks after sensitization, animals were anaesthetized with pentobarbital sodium (70 mg/kg, i.p.) and ventilated mechanically with room air. The basic methods for rat isolated perfused livers have been described elsewhere.[7] Briefly, a catheter was placed in the right carotid artery for the injection of heparin. After laparotomy, the hepatic artery was ligated. After intra-arterial heparinization (500 U/kg), the intra-abdominal inferior vena cava (IVC) above the renal veins was ligated and the portal vein was cannulated with a stainless-steel cannula (1.3 mm ID, 2.1 mm OD) for portal perfusion. After thoracotomy, the supradiaphragmatic IVC was cannulated through an incision in the right atrium with a large stainless-steel cannula (2.1 mm ID, 3.0 mm OD). Then, portal perfusion was started at a constant flow rate (43 mL/min) with Krebs'–Henseleit solution (composition (in mmol/L): NaCl 118; KCl 5.9; $MgSO_4$ 1.2; $CaCl_2$ 2.5; NaH_2PO_4 1.2; $NaHCO_3$ 25.5; glucose 5.6). Initially, livers were perfused in a non-recirculating manner with perfusate that was pumped using a Masterflex pump (Cole-Parmer, Chicago, IL, USA) from the venous reservoir through a heat exchanger (37°C). When the colour of the effluent became translucent, the perfusion mode was changed to re-circulating. The recirculating perfusate volume was 40 mL. The perfusate was oxygenated in the venous reservoir by continuous bubbling with 95% O_2 and 5% CO_2. The portal venous (Ppv) and hepatic venous (Phv) pressures were measured with pressure transducers (TP-400T; Nihon-Kohden, Tokyo, Japan) attached by a sidearm to the appropriate cannulas with the reference points at the hepatic hilus. Portal perfusate flow rate (Qpv) was measured with an electromagnetic flow meter (MFV 1200; Nihon-Kohden) and the flow probe was positioned in the inflow line. The Ppv, Phv and Qpv were monitored continuously and displayed through a thermal physiograph (RMP-6008; Nihon-Kohden). Outputs were also digitized by the analogue–digital converter at a sampling rate of 100 Hz using a personal computer.[7]

Hepatic haemodynamic parameters were observed for at least 20 min after the start of perfusion. Then, the livers were divided into three groups: (i) D-NAME ($n = 9$), in which 100 μmol/L D-NAME (Sigma) was administered into the reservior; (ii) L-NAME ($n = 9$), in which 100 μmol/L L-NAME (Sigma) was administered into the reservior; and (iii) L-arginine + L-NAME ($n = 5$), in which L-arginine (1 mmol/L; Sigma) plus L-NAME (100 μmol/L) were administered into the reservoir. Thus, any livers studied were pretreated with either L-NAME or D-NAME. Ovalbumin (0.1 mg) was injected into the reservoir 10 min after the injection of L-NAME or D-NAME. In each experimental group, measurements were performed up to 30 min after the administration of antigen. The total portal–hepatic venous (Rt) resistance was calculated using the formula:

$$Rt = (Ppv - Phv)/Qpv$$

Measurement of NO_x

Portal (inflow) and hepatic venous (outflow) perfusate samples (0.5 mL) were simultaneously and instantaneously obtained from the inflow and outflow lines, respectively, before injection of L- or D-NAME just before antigen injection (baseline) and 0.5, 1, 3 and 6 min after antigen injection. NO_2^- and NO_3^- were separated and measured using the HPLC–Griess system (ENO-10; Eicom, Kyoto, Japan). The detection limit and the sensitivity for NO_3^- were 10 nmol/L under routine setup, whereas under the highly sensitive mode for NO_2^- (the reduction column was omitted and 100 μL sample was loaded without deproteinization), the detection limit was 2 nmol/L and the sensitivity was 1–2 nmol/L. The inter- and intra-assay coefficients of variation were below 0.5% for NO_3^- and approximately 5% for NO_2^- for highly sensitive quantification.[12,13] Special attention was paid to avoid any contamination with NO_x throughout the entire procedure.[14]

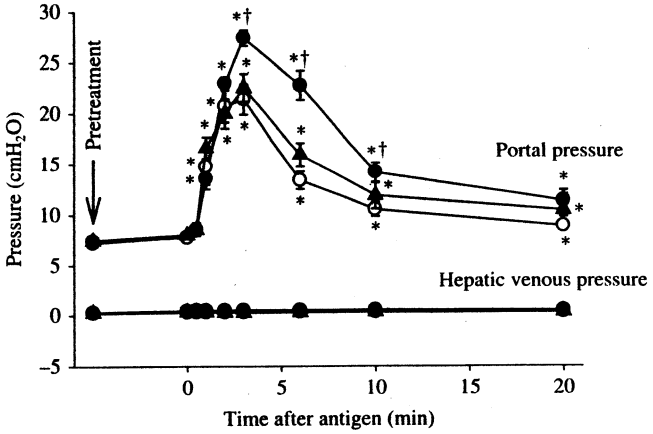


Fig. 1 Summary of changes in portal venous pressure and hepatic venous pressure after antigen injection in N^G-nitro-D-arginine methyl ester (D-NAME; $n = 9$; ○), N^G-nitro-L-arginine methyl ester (L-NAME; $n = 9$; ●) and L-arginine + L-NAME ($n = 5$; ▲) groups. Data are the mean±SEM. $^*P < 0.05$ compared with baseline; $^\dagger P < 0.05$ compared with the D-NAME and L-arginine + L-NAME groups.

Statistics

All results are expressed as the mean±SEM. Analysis of variance followed by Bonferroni's test was used to test the significance of differences. Differences were considered statistically significant at $P < 0.05$.

RESULTS

Response of Ppv to antigen

After injection of L-NAME or D-NAME into the blood-free constant-flow perfused liver, Ppv did not change significantly. As shown in Fig. 1, after injection of 0.1 mg ovalbumin into a D-NAME-pretreated liver, venoconstriction occurred, as evidenced by an increase in Ppv. The Ppv reached peak levels of 21.4 ± 1.1 cmH_2O 3 min after the injection of antigen from a baseline value of 7.7 ± 0.1 cmH_2O. The Ppv-to-Phv gradient, the determinant of Rt, increased 2.9-fold baseline, indicating that Rt increased by the same degree, as indicated in Table 1. In fact, Rt increased from a baseline value of 0.17 ± 0.01 to 0.47 ± 0.04 cmH_2O/mL per min per 10 g. Thereafter, Ppv and Rt decreased gradually towards baseline values.

In the L-NAME group, Ppv also increased after the injection of antigen, but the peak Ppv levels of 27.4 ± 0.8 cmH_2O 3 min after antigen injection were significantly greater than those seen in the D-NAME group (21.4 ± 1.1 cmH_2O). Thus, the peak Rt level in the L-NAME group was 1.7-fold greater than that in the D-NAME group. This significant difference was observed until 10 min after antigen injection (Fig. 1). However, as shown in Fig. 1, the augmentation of antigen-induced venoconstriction induced by L-NAME was

© 2006 Blackwell Publishing Asia Pty Ltd

Table 1 Effects of N^G-nitro-L-arginine methyl ester (L-NAME) and N^G-nitro-D-arginine methyl ester (D-NAME) on haemodynamic variables and NO_x after antigen injection in rat isolated perfused livers

	L-NAME			D-NAME			L-Arginine + L-NAME		
Groups	Pretreatment	Baseline	3 min	Pretreatment	Baseline	3 min	Pretreatment	Baseline	3 min
Ppv (cmH_2O)	7.2 ± 0.2	7.8 ± 0.4	27.4 ± 0.8*	7.4 ± 0.1	7.7 ± 0.1	21.4 ± 1.1*	7.4 ± 0.2	8.0 ± 0.4	22.6 ± 1.4*
Phv (cmH_2O)	0.3 ± 0.1	0.4 ± 0.2	0.5 ± 0.2	0.2 ± 0.1	0.3 ± 0.1	0.3 ± 0.1	0.3 ± 0.1	0.3 ± 0.1	0.3 ± 0.1
Qpv (mL/min per 10 g)	41 ± 3	41 ± 3	41 ± 3	42 ± 2	42 ± 2	42 ± 2	38 ± 1	38 ± 1	38 ± 1
Rt	0.19 ± 0.03	0.20 ± 0.04	0.74 ± 0.10*	0.17 ± 0.01	0.17 ± 0.01	0.47 ± 0.04*	0.19 ± 0.01	0.20 ± 0.01	0.59 ± 0.04*
NO_x concentration (μmol/L)									
Inflow	0.45 ± 0.05	0.51 ± 0.05	0.54 ± 0.05	0.45 ± 0.02	0.52 ± 0.02	0.55 ± 0.02	0.40 ± 0.05	0.50 ± 0.05	0.52 ± 0.05
Outflow	0.45 ± 0.06	0.50 ± 0.06	0.54 ± 0.06	0.53 ± 0.03	0.45 ± 0.06	0.54 ± 0.02	0.41 ± 0.05	0.48 ± 0.05	0.51 ± 0.06

Values are the mean±SEM. *$P < 0.05$ compared with baseline.
Ppv, portal vein pressure; Phv, hepatic venous pressure; Qpv, perfusate flow; Rt, vascular resistance (in cmH_2O/mL per min per 10 g).

reversed by additional perfusion with L-arginine (1 mmol/L). The pressure response in the L-arginine + L-NAME group was similar in magnitude to that in the D-NAME group. These results suggest that the anaphylactic reaction in rat livers produced NO, which then attenuated the anaphylactic hepatic venoconstriction.

Perfusate concentrations of NO_x

Perfusate levels of either NO_2^- or NO_3^- did not change significantly after antigen injection in any group studied (Table 1). Moreover, differences in NO_2^- and NO_3^- between the outflow and inflow did not change significantly in any group and the differences between the two groups were not significant throughout the experimental period, as shown in Fig. 2.

DISCUSSION

The present study showed that the NOS inhibitor L-NAME augmented anaphylactic venoconstriction in rat isolated livers perfused with blood-free solution under constant flow. L-Arginine completely reversed enhancement of the anaphylactic venoconstriction by L-NAME. This finding suggests that, similar to guinea-pig livers,[5] rat livers produce NO during the anaphylactic reaction and that the NO released then attenuates anaphylactic hepatic venoconstriction. We also measured perfusate concentrations of NO metabolites before and after antigen in order to confirm the production of NO. However, unexpectedly, we could not detect significant differences in perfusate NO_x concentrations between the outflow and inflow perfusate, even though we used the highly sensitive HPLC–Griess system (ENO-10) for measurement of NO_x.

We have reported previously that anaphylactic venocostriction occurs in rat isolated blood-perfused livers.[7] In the present study, a similar response was observed in rat livers perfused with blood-free solution. This indicates that the intrahepatic mast cells rather than circulating blood cells, such as basophils and platelets, were involved in the hepatic regional anaphylaxis in the present study.

N^G-Nitro-L-arginine methyl ester is widely used to inhibit endothelial synthesis of NO. However, multiple non-specific actions of L-NAME other than simple inhibition of NO synthesis have also been reported.[15–18] These include generation of superoxide anions and prostaglandin endoperoxides, both of which cause vasoconstriction. Thus, NO-independent mechanism may have been involved in the effect of L-NAME in the present study. However, we found that the addition of L-arginine completely reversed the augmentation by L-NAME. This finding suggests that the effect of L-NAME is due to inhibition of NO synthesis rather than due to the production of vasoconstrictors, such as superoxide anions and prostaglandin endoperoxide.

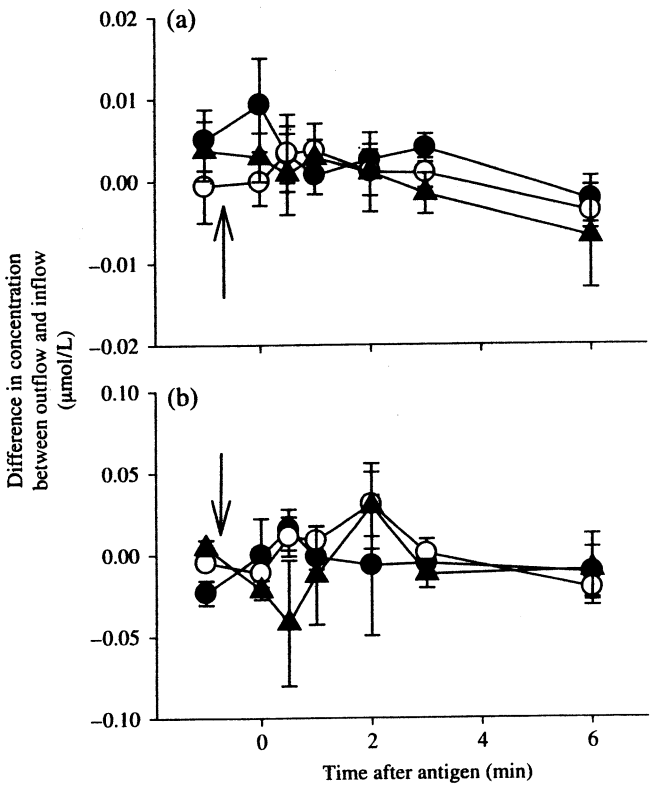


Fig. 2 Summary of changes in differences in (a) NO_2^- and (b) NO_3^- concentrations between inflow and outflow perfusate after antigen injection in the N^G-nitro-D-arginine methyl ester (D-NAME; ○), N^G-nitro-L-arginine methyl ester (L-NAME; ●) and L-arginine + L-NAME (▲) groups. The arrows indicate the time of pretreatment. Data are the mean±SEM ($n = 5$). *$P < 0.05$ compared with baseline.

© 2006 Blackwell Publishing Asia Pty Ltd

The mechanism responsible for NO release during hepatic anaphylaxis may be ascribed to shear stress-dependent and -independent mechanisms.[19] In rat livers perfused at constant flow, anaphylaxis contracted hepatic vessels, where shear stress could be increased, resulting in NO release from the constricted endothelium. Conversely, the shear stress-independent mechanism may be related to humoral substances released by the anaphylactic reaction *per se*. We assume that chemical mediators, such as platelet-activating factor (PAF), thromboxane (TX) A_2, histamine, cysteinyl leukotrienes and serotonin, may act on their corresponding receptors on the endothelium, resulting in the subsequent activation of endothelial (e) NOS and production of NO. In fact, it has been reported that most mediators of anaphylaxis, such as histamine,[20,21] leukotrienes,[22] TXA_2[21] and PAF,[23] all stimulate NO release from the vascular endothelium.

The percentage proportion of NO counter-regulation in anaphylactic venoconstriction of the portal vein in rats was approximately 28% (6.0 cmH_2O). This seems to be smaller than that of similarly examined guinea-pig livers, in which NO inhibition augmented the anaphylaxis-induced increase in Ppv by 80% (18.1 cmH_2O).[9] The relatively lesser augmentation induced by L-NAME in the present study may be ascribed to differences in the perfusate, as well as species differences. The Krebs' solution used in the present study had a very low viscosity and, thus, produced a low vascular resistance, resulting in low shear stress and small NO production compared with the diluted blood used in the previous guinea-pig liver study.[6] The reason why we used blood-free Krebs' solution as the perfusate in the present study was that a solution including free haemoglobin could prevent accurate measurement of perfusate NO_2^- and NO_3^- concentrations.[24] Haemolysis and, thus, the presence of free haemoglobin in the perfusate could not be avoided in the present experimental set up including a roller pump. Because NO_2^- has been suggested to be a more sensitive and specific marker of NO than NO_3^-[25] and it has been suggested that NO_2^- is the main metabolite of NO in haemoglobin-free medium,[26] we endeavoured to quantify the substance at nmol/L levels. The possible reasons why the highly sensitive HPLC–Griess system could not detect the expected increase in NO_2^- as a reflection of enhanced NO release during anaphylaxis in rat isolated perfused livers reamin obscure. However, some possible causes may be derived from the following. The device we used may still be insufficient to detect smaller changes in NO_2^- from the vascular bed in an excised organ with a large volume of perfusate compared with changes in a whole body and the substance may be easily influenced by the surrounding atmosphere. In addition, we have experienced disappearance of NO_2^- or NO_3^- after perfusion of certain organs.[12,13]

In conclusion, we are able to present functional evidence that NO production may be increased during rat hepatic anaphylaxis. This hepatic anaphylactic response was independent of circulating blood cells. However, perfusate NO_x measurements using the highly sensitive HPLC–Griess system could not detect physical evidence of increased intrahepatic NO production in rat isolated perfused anaphylactic livers; thus, this issue requires further examination.

ACKNOWLEDGEMENTS

This work was supported by a Grant for Collaborative Research (C2004-1, C2005-1) and a Grant for Promoted Research (S2005-10) from Kanazawa Medical University.

REFERENCES

1. Brown AFT. Anaphylactic shock: Mechanism and treatment. *J. Accid. Emerg. Med.* 1995; **12**: 89–100.
2. Moncada S, Higgs A. The L-arginine–nitric oxide pathway. *N. Engl. J. Med.* 1993; **329**: 2002–12.
3. Rees DD, Palmer RMJ, Moncada S. Role of endothelium-derived nitric oxide in regulation of blood pressure. *Proc. Natl Acad. Sci. USA* 1989; **86**: 3375–8.
4. Mitsuhata H, Shimizu R, Yokoyama MM. Role of nitric oxide in anaphylactic shock. *J. Clin. Immunol.* 1995; **15**: 277–83.
5. Maass-Moreno R, Rothe CF. Nonlinear resistances in hepatic microcirculation. *Am. J. Physiol.* 1995; **269**: H1922–30.
6. Pavek K, Piper PJ, Smedegard G. Anaphylatoxin-induced shock and two patterns of anaphylactic shock: Hemodynamics and mediators. *Acta Physiol. Scand.* 1979; **105**: 393–403.
7. Shibamoto T, Cui S, Ruan Z, Liu W, Takano H, Kurata Y. Hepatic venoconstriction is involved in anaphylactic hypotension in rats. *Am. J. Physiol. Heart Circ. Physiol.* 2005; **289**: H1436–41.
8. Hines KL, Fisher RA. Regulation of hepatic glycogenolysis and vasoconstriction during antigen-induced anaphylaxis. *Am. J. Physiol.* 1992; **262**: G868–77.
9. Ruan Z, Shibamoto T, Shimo T, Tsuchida H, Koizumi T, Nishio M. NO, but not CO, attenuates anaphylaxis-induced postsinusoidal contraction and congestion in guinea pig liver. *Am. J. Physiol. Regul. Integr. Comp. Physiol.* 2004; **286**: R94–100.
10. Weil R. Studies in anaphylaxis. XXI. Anaphylaxis in dogs: A study of the liver in shock and peptone poisoning. *J. Immunol.* 1917; **2**: 525–56.
11. Yamaguchi Y, Shibamoto T, Hayashi T, Saeki Y, Tanaka S. Hepatic vascular response to anaphylaxis in isolated canine liver. *Am. J. Physiol.* 1994; **267**: R268–74.
12. Ishibashi T, Matsubara T, Ida T *et al.* Negative NO_3^- balance in human coronary circulation with severe atherosclerotic stenosis. *Life Sci.* 2000; **66**: 173–84.
13. Ishibashi T, Himeno M, Kubota K *et al.* Decrease in plasma NO_x concentration by isosorbide dinitrate, an organic nitrate ester. *J. Cardiovasc. Pharmacol.* 2003; **41**: 40–8.
14. Ishibashi T, Himeno M, Imaizumi N *et al.* NO_x contamination in laboratory ware and effect of countermeasures. *Nitric Oxide Biol. Chem.* 2000; **4**: 516–25.
15. Buxton IL, Cheek DJ, Eckman D, Westfall DP, Sanders KM, Keef KD. N^G-Nitro-L-arginine methyl ester and other alkyl esters of arginine are muscarinic receptor antagonists. *Circ. Res.* 1993; **72**: 387–95.
16. Peterson DA, Peterson DC, Archer S, Weir EK. The non specificity of specific nitric oxide synthase inhibitors. *Biochem. Biophys. Res. Commun.* 1992; **187**: 797–801.
17. Nakaike R, Shimokawa H, Yasutake H *et al.* Effects of L-arginine analogues on vasomotion of isolated porcine coronary arteries. *Am. J. Physiol.* 1995; **268**: H1966–72.
18. Heim KF, Thomas G, Ramwell PW. Effect of substituted arginine compounds on superoxide production in the rabbit aorta. *J. Pharmacol. Exp. Ther.* 1991; **257**: 1130–5.
19. Shibamoto T, Ruan Z, Cui S, Kurata Y, Koizumi T, Kubo K. Anaphylactic hepatic venoconstriction is attenuated by nitric oxide released via shear stress-dependent and -independent mechanisms in guinea-pig. *Clin. Exp. Pharmacol. Physiol.* 2005; **32**: 288–93.
20. Lantoine F, Iouzalen L, Devynck MA *et al.* Nitric oxide production in human endothelial cells stimulated by histamine requires Ca^{2+} influx. *Biochem. J.* 1998; **330**: 695–9.
21. Levi R, Gross SS, Lamparter B *et al.* Evidence that L-arginine is the biosynthetic precursor of vascular and cardiac nitric oxide. In: Moncada S, Higgs EA (eds). *Nitric Oxide From l-Arginine: A Bioregulatory System.* Elsevier, Amsterdam. 1990; 35–45.
22. Sakuma I, Gross S, Levi R. Peptidoleukotrienes induce an endothelium-dependent relaxation of guinea pig main pulmonary artery and thoracic aorta. *Prostaglandins* 1987; **34**: 685–96.

© 2006 Blackwell Publishing Asia Pty Ltd

23. Kamata K, Mori T, Shigenobu K, Kasuya Y. Endothelium-dependent vasodilator effects of platelet activating factor on rat resistance vessels. *Br. J. Pharmacol.* 1989; **98**: 1360–4.
24. Ishibashi T, Kubota K, Himeno M *et al.* Respiratory alkalosis does not alter NO_x concentrations in human plasma and erythrocytes. *Am. J. Physiol. Heart Circ. Physiol.* 2001; **281**: H2757–61.
25. Kleinbongard P, Dejam A, Lauer T *et al.* Plasma nitrite reflects constitutive nitric oxide synthase activity in mammals. *Free Radic. Biol. Med.* 2003; **35**: 790–6.
26. Williams DLH. A chemist's view of the nitric oxide story. *Org. Biomol. Chem.* 2003; **1**: 441–9.

© 2006 Blackwell Publishing Asia Pty Ltd

Effects of Hct on L-NAME–induced Potentiation of Anaphylactic Presinusoidal Constriction in Perfused Rat Livers

Sen Cui, MD, Toshishige Shibamoto, MD, PhD, Wei Liu, MD, Hiromichi Takano, PhD, Zhan-Sheng Zhao, MD, PhD, and Yasutaka Kurata, MD, PhD

Abstract: Effects of hematocrit (Hct) on N^G-nitro-L-arginine methyl ester (L-NAME)–induced modulation of anaphylactic venoconstriction were determined in isolated perfused rat livers. The rats were sensitized with ovalbumin (1 mg), and the livers were excised 2 weeks later and perfused portally and recirculat-ingly under constant flow at Hct of 0%, 5%, 16%, and 22%. The hepatic sinusoidal pressure was estimated via the double occlusion pressure (Pdo), and the presinusoidal resistance (Rpre) and the postsinusoidal resistance (Rhv) were calculated. The antigen of ovalbumin 0.1 mg was injected into the reservoir at 10 minutes after pretreatment with L-NAME (100 μM) or D-NAME (100 μM). Perfusate viscosity, a determinant of vascular resistance and shear stress, was increased in parallel with Hct. In the D-NAME groups, antigen caused predominant presinusoidal constriction. The magnitude of venoconstriction was significantly smaller at Hct 0% than at Hct 5% to 22%, whereas no significant differences were found among Hct 5% to 22%. L-NAME potentiated the antigen-induced increase in Rpre, but not in Rpost at Hct 5% to 22% as compared with D-NAME. But the augmentative effects of L-NAME were similar in magnitude among Hct 5% to 22%. These findings suggest that hepatic anaphylaxis increases production of nitric oxide, which consequently attenuates anaphylactic presinusoidal constriction in rat livers, and that these effects are independent of perfusate Hct or viscosity in blood-perfused rat livers.

Key Words: anaphylactic shock, nitric oxide, viscosity, shear stress, hepatic circulation

(*J Cardiovasc Pharmacol*™ 2006;48:827–833)

Anaphylactic hypotension is sometimes life-threatening, and is caused by a decrease in effective circulating blood volume.[1] It is reported that the liver is partly involved in animal models of anaphylactic hypo-tension.[2,3] Anaphylactic hepatic venoconstriction, as observed in rats,[3,4] guinea pigs,[5] and dogs,[6,7] causes portal hypertension which then induces congestion of the upstream splanchnic organs, with resultant decrease in venous return and effective circulating blood volume, and finally augmentation of anaphylactic hypotension.

Nitric oxide (NO), a potent vasodilator, regulates the vascular system,[8,9] and seems to play an important pathophysiologic role in modulating the systemic changes associated with anaphylaxis.[10] We have recently reported that N^G-nitro-L-arginine methyl ester (L-NAME), a NO synthase inhibitor, augmented anaphylactic hepatic venoconstriction in guinea pig.[5] And further, we demonstrated, using the vascular occlusion method for measurement of the hepatic sinusoidal pressure, that the anaphylactic venoconstriction of the presinusoids, but not the postsinusoids, was enhanced by L-NAME.[5] However, it is not known whether L-NAME also induces augmentation of anaphylactic hepatic venoconstriction in other animals such as rats.

NO is produced by the activation of the NO synthase 3 present in endothelial cells either by hormonal or physical stimuli such as shear stress.[8,9] The viscosity, an important determinant of shear stress and vascular resistance, highly depends on hematocrit (Hct). Indeed, the vascular resistance increased as Hct elevates at a given blood flow in rat liver, as we previously reported.[11] However, it is not well known how the changes in blood viscosity modulate anaphylactic hepatic segmental venoconstriction.

Thus, we herein determined the effect of Hct on the L-NAME–induced modulation of anaphylactic hepatic segmental venoconstriction in rats. To accomplish this purpose, we measured the sinusoidal pressure with the vascular occlusion method, and determined the pre and postsinusoidal resistances during hepatic anaphylaxis in isolated rat livers perfused portally and recirculatingly under constant flow at different Hct of 0%, 5%, 16%, or 22% in the presence of L-NAME or D-NAME (an inactive enantiomer of L-NAME). In addition, we determined the anaphylaxis-induced changes in hepatic oxygen consumption and bile production.

METHODS

Animals and Sensitization

Forty male Sprague-Dawley rats (Japan SLC, Shizuoka, Japan) weighing 341 ± 3 g were maintained at 23°C and under

Received for publication January 24, 2006; accepted May 23, 2006.
From the Department of Physiology, Kanazawa Medical University, Uchinada 920-0293, Japan.
Supported by a Grant for Collaborative Research from Kanazawa Medical University (C2004-1, C2005-1) and a Grant-in-Aid for Scientific Research (18591730) from the Ministry for Education, Culture, Science and Technology of Japan.
Reprints: Toshishige Shibamoto, MD, PhD, Department of Physiology, Kanazawa Medical University, Daigaku 1-1, Uchinada, Ishikawa 920-0293, Japan (e-mail: shibamo@kanazawa-med.ac.jp).
Copyright © 2006 by Lippincott Williams & Wilkins

pathogen-free conditions on a 12/12-hours dark/light cycle, and received food and water ad libitum. The experiments conducted in the present study were approved by the Animal Research Committee of Kanazawa Medical University. Rats were actively sensitized by the subcutaneous injection of an emulsion made by mixing equal volumes of complete Freund's adjuvant (0.5 mL) with 1 mg ovalbumin (grade V, Sigma) dissolved in physiologic saline (0.5 mL).[3]

Isolated Liver Preparation

Two weeks after sensitization, the animals were anesthetized with pentobarbital sodium (50 mg kg^{-1}, IP) and were mechanically ventilated with room air. The methods for the isolated perfused rat liver preparation were previously described.[3] In brief, a polyethylene tube was placed in the right carotid artery. After laparotomy, the hepatic artery was ligated and the bile duct was cannulated with the polyethylene tube (0.5 mm ID, 0.8 mm OD). At 5 minutes after intra-arterial heparinization (500 U kg^{-1}), 8 to 9 mL of blood was withdrawn through the carotid arterial catheter. The intra-abdominal inferior vena cava above the renal veins was ligated, and the portal vein was cannulated with a stainless cannula (1.3 mm ID, 2.1 mm OD). After thoracotomy, the supra-diaphragmatic inferior vena cava was cannulated through a right atrium incision with a larger stainless cannula (2.1 mm ID, 3.0 mm OD), then portal perfusion was begun with the heparinized blood diluted with 5% bovine albumin (Sigma-Aldrich Co, St Louis, MO) in Krebs solution (118 mM NaCl, 5.9 mM KCl, 1.2 mM $MgSO_4$, 2.5 mM CaCl2, 1.2 mM NaH_2PO_4, 25.5 mM $NaHCO_3$, and 5.6 mM glucose) at the following Hct levels: 0% (n = 10), 5% (n = 10), 16% (n = 10), and 22% (n = 10). At Hct 5%, only the autologous blood was used, while at Hct 16% and 22%, additional blood was obtained by exsanguination of an anesthetized and heparinized intact donor rat. At Hct 0%, the liver was perfused with only 5% albumin-Krebs solution without blood. The liver was rapidly excised, suspended from an isometric transducer (TB-652T, Nihon-Kohden, Japan), and weighed continuously throughout the experimental period.

The liver was perfused at a constant flow rate in a recirculating manner via the portal vein using perfusate with or without blood that was pumped using a Masterflex roller pump from the venous reservoir through a heat exchanger (37°C). The recirculating perfusate volume was 40 mL. The perfusate was oxygenated in the venous reservoir by continuous bubbling with 95% O_2 and 5% CO_2 (perfusate PO_2 = 300 mm Hg).

The viscosity of the perfusate was measured using cone plate type of viscometer (Biorheolizer, Tokyo Keiki, Japan).

Measurement of Hepatic Vascular Pressures and Vascular Resistances

The portal venous (Ppv) and the hepatic venous (Phv) pressures were measured using pressure transducers (TP-400T, Nihon-Kohden, Japan) attached by sidearm to the appropriate cannulas with the reference points at the hepatic hilus. Portal blood flow rate (Q) was measured with an electromagnetic flow meter (MFV 1200, Nihon-Kohden, Japan), and the flow probe was positioned in the inflow line. The hepatic sinusoidal pressure was measured by the double occlusion pressure (Pdo).[7] Both the inflow and outflow lines were simultaneously and instantaneously occluded for 17 seconds using the solenoid valves, after which Ppv and Phv rapidly equilibrated to a similar or identical pressure, which was Pdo. Actually, Pdo values were obtained from the digitized data of Ppv and Phv using an original program (LIVER software, Biomedical Science, Kanazawa, Japan). The total portal-hepatic venous (Rt), presinusoidal (Rpre), and postsinu-soidal (Rpost) resistances were calculated as follows:

$$Rt = (Ppv - Phv)/Q \quad (1)$$

$$Rpre = (Ppv - Pdo)/Q \quad (2)$$

$$Rpost = (Pdo - Phv)/Q \quad (3)$$

Bile Flow Rate Measurement

Bile was collected drop by drop in a small tube suspended from the force transducer (SB-1T, Nihon-Kohden, Japan). One bile drop yielded 0.018 g and the time between drops was measured for determination of the bile flow rate.[3]

Hepatic Oxygen Consumption Measurement

To determine the oxygen consumption, the blood oxygen saturation difference between the inflow and outflow blood (ΔSO_2) was monitored continuously with a custom-made oxygen absorption spectrophotometer (ODM-1, Biomedical Science, Kanazawa, Japan), the cuvettes and sensors of which were built in the inflow and outflow perfusion lines.[12] The measured ΔSO_2 was expressed as the oxygen consumption difference meter (ODM) values.[12] ΔSO_2 was calculated using the following regression line equation as determined in our previous study[12]:

$$\Delta SO_2 = 1.5103 \times ODM - 0.0685 \quad (4)$$

Using ΔSO_2, oxygen consumption (mL min^{-1} 10 g liver wt^{-1}) was calculated according to the Fick principle by the following equation:

$$\text{Portal blood flow/liver weight } (g) \times 10 \times 1.39 \text{ (ml/g)} \times \text{Hb (g/ml)} \times \Delta SO_2 \quad (5)$$

where Hb is the perfusing blood hemoglobin measured by cyanmethohemoglobin method (Hb-B test Wako, Wako, Japan) with a spectrophotometer (UV-1200, Shimadzu, Japan).

Data Recording

The hepatic vascular pressures, blood flow rate, liver weight, bile weight, and ODM values, were monitored continuously and displayed through a thermal physiograph (RMP-6008, Nihon-Kohden, Japan). All outputs were also digitized through the analog-digital converter at a sampling rate of 100 Hz. These digitized values were also displayed and recorded using a personal computer for later determination of Pdo.

© 2006 Lippincott Williams & Wilkins

Experimental Protocol

Hepatic hemodynamic parameters were observed for at least 20 minutes after the start of perfusion until an isogravimetric state (no weight gain or loss) was obtained by adjusting the portal blood flow rate and the height of the reservoir at a Phv of 0 to 1 cm H_2O, and at a Q of 36 ± 0.5 mL min^{-1} 10 g liver wt^{-1}. Then, the livers perfused at various Hct were further divided into the following 2 groups of the D-NAME and L-NAME groups, in which D-NAME (100 μM: Sigma) and L-NAME (100 μM: Sigma), respectively, were administered into the reservoir. Thus, any liver studied was pretreated with either D-NAME or L-NAME. Ovalbumin 0.1 mg was injected into the reservoir at 10 minutes after injection of D-NAME or L-NAME. In each experimental, measurement was performed up to 30 minutes after antigen.

In each experimental group, the double occlusion was performed at baseline, just before antigen injection, and at the maximal venoconstriction (when Ppv reached the peak), 6, 10, 20, and 30 minutes after injection of antigen.

Statistics

All results are expressed as the means ± SE. Data were analyzed by 1 and 2-way analysis of variance, using repeated-measures for 2-way comparison within groups. Comparisons of individual points between groups and within groups were made by Bonferroni test. Differences were considered as statistically significant at P values less than 0.05.

RESULTS

Perfusate Hct and Viscosity

The perfusate viscosity increased in parallel with Hct from 0% to 22% in both D-NAME and L-NAME groups. The viscosity was 0.879 ± 0.007 mPa s^{-1} at Hct 0%, 1.232 ± 0.014 mPa s^{-1} at Hct 5%, 1.706 ± 0.019 mPa s^{-1} at Hct 16%, and 2.222 ± 0.039 mPa s^{-1} at Hct 22%.

The Basal Hepatic Vascular Resistances

Figure 1 shows basal Ppv, Rpre, and Rpost. Basal Rpre was higher than basal Rpost in livers of any Hct (0% to 22%), resulting in basal Rpost/Rt ratio of 0.3 to 0.35. The basal Ppv and vascular resistances of Hct 22% groups were significantly greater than those of other Hct groups. D-NAME pretreatment did not change basal Ppv or resistances at any Hct level. However, basal Ppv and Rpre were significantly increased by L-NAME pretreatment at Hct 16% and 22%.

Effects of Hct on the Responses of D-NAME Pretreated Livers to Antigen

Figure 2 shows the summary data of the time-dependent changes in Ppv, Pdo, liver weight, oxygen consumption, and bile flow rate of D-NAME groups. Antigen induced venoconstriction, as reflected by an increase in Ppv. Ppv peaked at 3 minutes after antigen and gradually decreased towards baseline at 30 minutes. The magnitude of venoconstriction at Hct 0% was significantly smaller than that at Hct 5% to 22%: The Ppv peak at Hct 0% was 20.9 ± 1.4 cm H_2O, and that at Hct 5% was 27.8 ± 0.8 cm H_2O. However, no significant differences were found in the peak values of Ppv

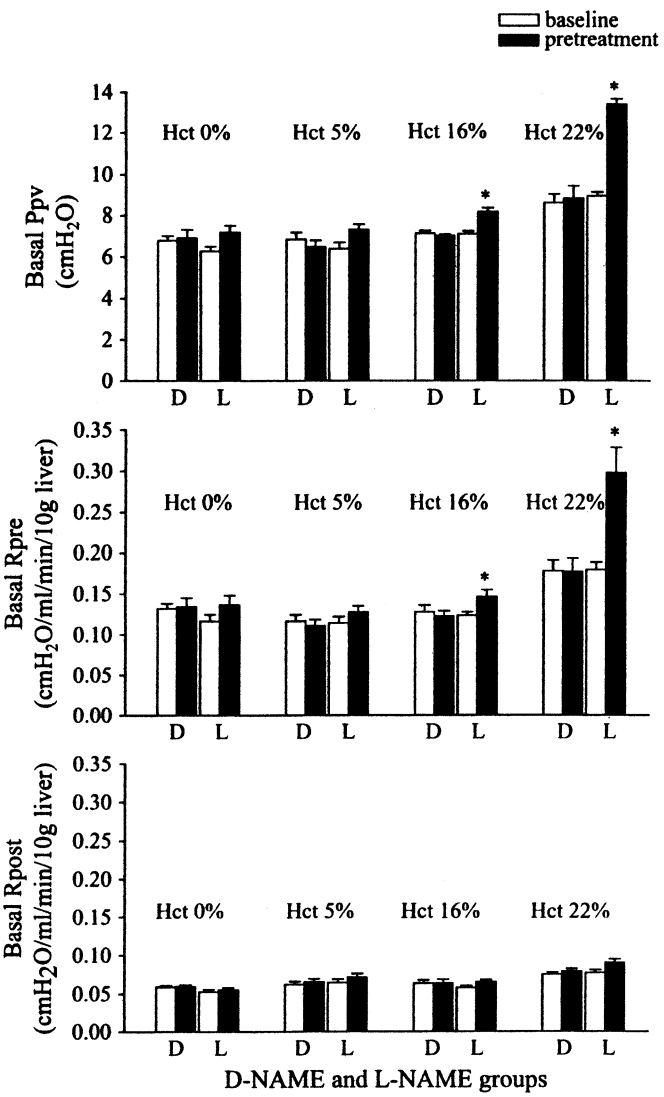


FIGURE 1. The basal portal venous pressure (Ppv), presinusoidal resistance (Rpre), and postsinusoidal resistance (Rpost) of the baseline and after pretreatment with D-NAME (D) and L-NAME (L) at Hct of 0%, 5%, 16%, and 22%. *$P < 0.05$ versus the baseline.

after antigen among Hct 5%, 16%, and 22%. Pdo increased slightly but significantly after antigen, and the increase at Hct 0% was smaller than that at Hct 5% to 22%.

Figure 3 shows changes in Rpre and Rpost after antigen. In the D-NAME groups, both Rpre and Rpost significantly increased after antigen. However, the magnitudes of the increases in Rpre were much larger than that in Rpost: At Hct 16%, Rpre increased 0.612 ± 0.067 cmH_2O mL^{-1} min^{-1} 10 g^{-1} liver, whereas Rpost increased only 0.050 ± 0.003 cm H_2O mL^{-1} min^{-1} 10 g^{-1} liver $weight^{-1}$. The antigen-induced increases in Rpre and Rpost in blood-perfused livers (Hct 5% to 22%) were significantly greater than those in livers perfused without blood (Hct 0%). However, there were no significant differences in increases of Rpre or Rpost among Hct 5%, 16%, and 22%. These results indicate that the antigen induces

© 2006 Lippincott Williams & Wilkins

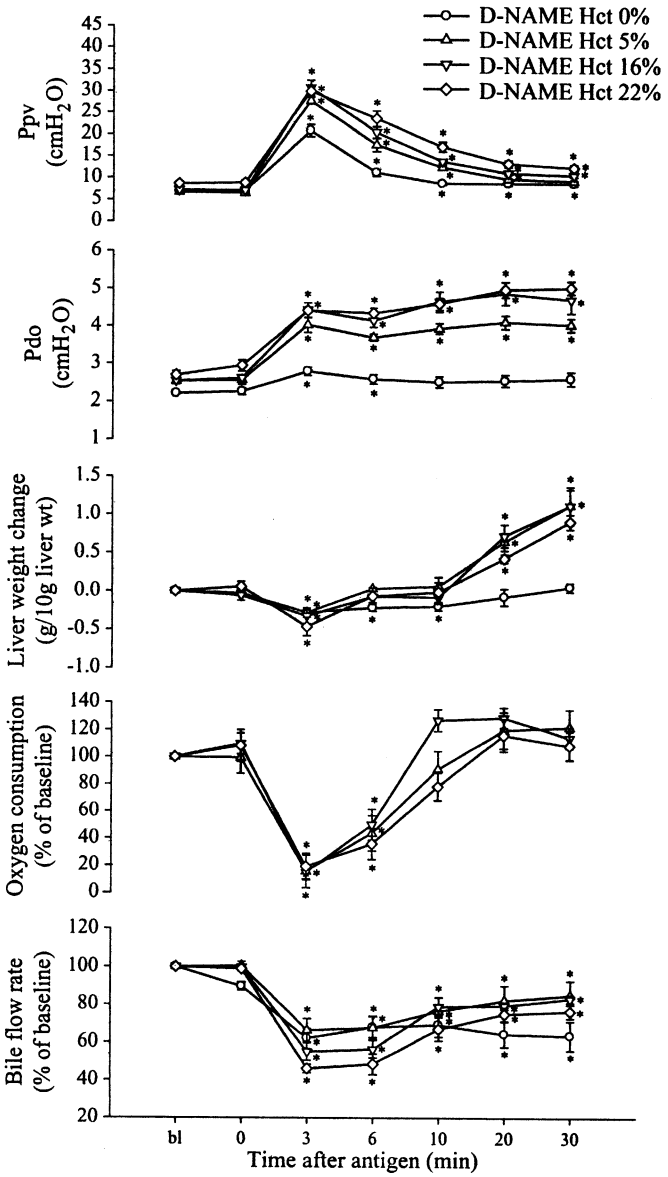


FIGURE 2. The summary data of time course changes in the portal venous pressure (Ppv), double occlusion pressure (Pdo), liver weight change, hepatic oxygen consumption, and bile flow rate after antigen injection at Hct of 0%, 5%, 16%, and 22% in the D-NAME groups. Values are given as mean ± SE, n = 5. *$P < 0.05$ versus the baseline.

predominant presinusoidal constriction independently of blood Hct (5% to 22%) in blood-perfused rat livers.

The liver weight showed a biphasic change of an initial decrease followed by an increase in response to antigen, as shown in Figure 2. The lowest nadir was −0.521 ± 0.054 g 10 g^{-1} liver at Hct 22%. There were no significant differences in the nadirs among all D-NAME groups.

Bile flow rate decreased Hct dependently, reaching 47 ± 3% of the baseline of 8.7 ± 0.6 mg min^{-1} 10 g^{-1} liver at Hct 22% group, as shown in Figure 2. It did not recover to the baseline at the end of experiment.

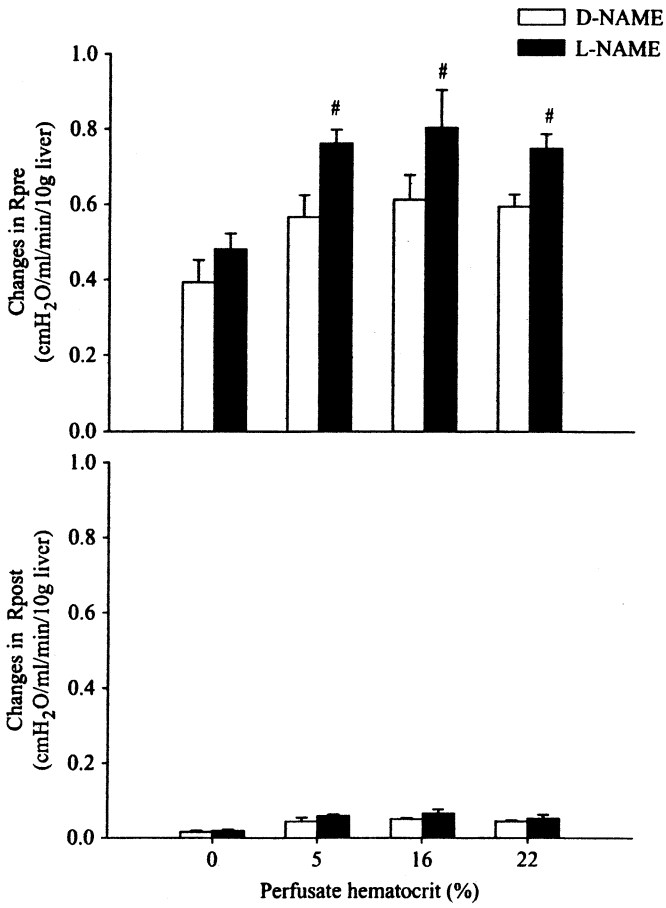


FIGURE 3. The changes in Rpre and Rpost after antigen injection at Hct of 0%, 5%, 16%, and 22% in D-NAME and L-NAME groups. Values are given as mean ± SE. All values in both D-NAME and L-NAME groups were significantly different from the corresponding baseline, and therefore asterisks were omitted. #$P < 0.05$ versus the D-NAME group.

The basal hepatic oxygen consumption increased as Hct increased: The basal levels were 0.015 ± 0.002 for Hct 5%, 0.070 ± 0.005 for Hct 16%, and 0.096 ± 0.034 mL min^{-1} 10 g^{-1} liver for Hct 22%. The oxygen consumption in livers of Hct 0% could not be determined in the present system because of absence of red blood cells in the perfusate. The hepatic oxygen consumption was significantly decreased after antigen injection. It reached the lowest value, 13.5 ± 4.1% of the baseline of 0.072 ± 0.006 mL min^{-1} 10 g^{-1} liver at Hct 16%. Actually, the decreases of hepatic oxygen consumption were similar in magnitudes among Hct 5% to 22%. Oxygen consumption almost recovered to the baseline at 20 minutes after antigen.

Effects of L-NAME on Hepatic Responses to Antigen Under Different Hct

Figure 4 shows the summary data of the time course changes in Ppv, Pdo, liver weight, oxygen consumption, and bile flow rate of the L-NAME groups. As compared with D-NAME groups, the antigen-induced increases in Ppv in the L-NAME groups were qualitatively similar but greater in

© 2006 Lippincott Williams & Wilkins

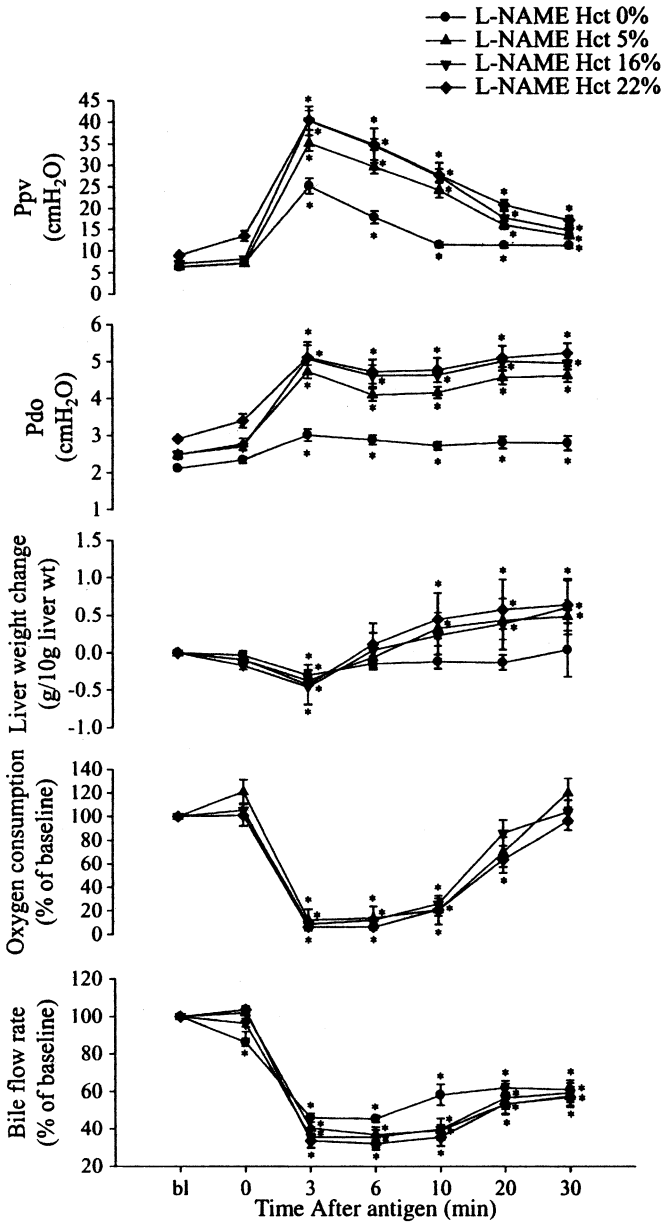


FIGURE 4. The summary data of time course changes in the portal venous pressure (Ppv), double occlusion pressure (Pdo), liver weight change, hepatic oxygen consumption, and bile flow rate after antigen injection at Hct of 0%, 5%, 16%, and 22% in the L-NAME groups. Values are given as mean ± SE. n = 5. *$P < 0.05$ versus the baseline.

magnitude, although the increases in Pdo were comparable. Thus, as shown in Figure 3, the amplitudes of the increase in Rpre, but not in Rpost, were significantly larger in the L-NAME groups than in the D-NAME groups at any Hct level. However, the increases in Rpre were not significantly different among Hct levels of 5% to 22%, although they were significantly higher than those at Hct 0%.

The antigen-induced changes in liver weight, bile flow rate, and oxygen consumption in L-NAME groups were similar to those in D-NAME groups. However, bile flow rates more profoundly decreased than in D-NAME groups at corresponding Hct level: the nadir, 31.2 ± 3.6% of the baseline of 8.9 ± 1.1 mg min^{-1} 10 g^{-1} liver at Hct 22% was much lower than in D-NAME groups. Although there were no significant differences in the nadir of hepatic oxygen consumption in all groups studied, it was much lower at 6, 10, and 20 minutes after antigen in the L-NAME groups than in the D-NAME group, as shown in Figure 4.

DISCUSSION

In the present study, we examined anaphylactic venoconstriction in isolated perfused rat livers pretreated with either L-NAME or D-NAME under various Hct. The first of the main findings is that L-NAME augmented the antigen-induced increase in Rpre, but not Rpost. This suggested that hepatic anaphylaxis increases production of NO, which consequently attenuates presinusoidal constriction in rats. The second is that the magnitudes of the L-NAME–induced augmentation of the anaphylactic presinusoidal constriction were similar at various Hct (5% to 22%), although the perfusate viscosity increased depending on Hct.

In the present study, we first confirmed the previous finding that anaphylaxis induced predominant presinusoidal constriction in rat livers perfused with blood at Hct 12%,[3] and further extended it by showing the same result at various Hct ranging 0% to 22%.

The basal levels of Ppv and Rpre of Hct 22% groups were significantly greater than those of other Hct groups (Fig. 1). According to Poiseuille's law, this increase in basal hepatic vascular resistance could be attributed to the perfusate Hct-dependent increase in perfusate viscosity. We have here shown that L-NAME pretreatment increased the basal hepatic resistances, especially Rpre, only at Hct 16% and 22% (Fig. 1). This indicated that NO is not involved in the regulation of basal hepatic vascular tone of isolated rat livers perfused with blood at Hct of 5% or less. This finding is consistent with that on rat livers perfused with a blood-free solution, in which inhibition of NO did not increase basal vascular tone.[13] It is suggested that the low perfusate viscosity results only in small shear stress and thus low amount of NO production in livers perfused with low Hct. This might account for a negligible role of NO in maintenance of basal vascular tone in livers perfused at Hct of 5% or less.

The present study showed that L-NAME significantly potentiated the antigen-induced increase in Rpre, but not in Rpost, in rat livers, a finding similar to that observed in guinea pig livers.[5] This suggests that NO might be released selectively from presinusoidal vessels during anaphylaxis, and then attenuated the anaphylactic presinusoidal constriction. The mechanism for this selective vulnerability of presinusoids to NO may be considered as follows: anaphylaxis predominantly constricted presinusoidal vessels as shown in D-NAME groups, where elevated shear stress increased NO release from the same presinusoidal endothelium, leading to relaxation of the adjacent presinusoidal vascular smooth muscle cells in a paracrine manner. Indeed, the wall shear stress in isolated perfused vessels is inversely proportional to the third

© 2006 Lippincott Williams & Wilkins

power of internal radius theoretically.[14] The decrease in vascular internal radius caused by anaphylactic venoconstriction should result in an increase in shear stress. It would further be increased if turbulence did increase at the constricted site.[14] Thus, the NO release from vascular endothelium of the contracted presinusoids would be increased via the shear stress mechanism during anaphylactic venoconstriction.

In the present study, the magnitudes of the L-NAME–induced potentiation of anaphylactic venoconstriction were similar among livers perfused with blood at Hct 5% to 22% (Fig. 3), although perfusate viscosity increased depending on Hct. However, these results were unexpected, because the Hct-dependent increase in perfusate viscosity could produce more shear-stress,[14] and then increase production of NO, resulting in more dilation of the constricted vessels. Thus, we initially expected that L-NAME–induced potentiation of anaphylactic venoconstriction might increase when the perfusate Hct increased. With respect to the mechanisms for the absence of exaggerated venoconstriction by L-NAME at high Hct, it might be attributed to the concomitant increase in perfusate Hb concentration. It is reported that oxygenated Hb, even in extremely small amounts, inactivates NO, resulting in inhibition of its vasodilatory action.[15,16] Thus, augmented vasodilatory effect due to the over-produced NO at high perfusate Hct might be attenuated by elevated perfusate Hb, which could inactivate NO. Another possible explanation could be related to the isolated rat liver preparation perfused at a constant flow. It is possible that the hepatic vessels perfused at a low Hct of 5% in the presence of L-NAME contracted mechanically to the maximal levels and could not constrict further even when the perfusate Hct increased. In the present isolated perfused rat liver preparation, Ppv might not be able to increase to the levels higher than 45 cm H_2O. Actually, Ppv did not increase higher than 45 cm H_2O even when supraphysiologically high concentrations (>3 μM) of PAF, a potent vasoconstrictor, were administered into the similar perfused rat liver preparations.[17]

Hepatic oxygen consumption was significantly and markedly decreased to the level less than 20% of baseline, regardless of different perfusate Hct or pretreatment with L-NAME or D-NAME. This finding of anaphylaxis-induced reduction of hepatic oxygen consumption was consistent with previous studies.[4,12] The mechanisms for this decrease in oxygen consumption may be due to hemodynamic or nonhemodynamic factors. Nonhemodynamic factors may be anaphylaxis-related chemical mediators, such as PAF,[18,19] TXA_2,[20,21] and LTD_4,[19,21] all of which can decrease hepatic oxygen consumption. On the other hand, from the hemodynamic point of view, presinusoidal constriction observed during anaphylactic venoconstriction may account for the decreased oxygen consumption: presinusoidal constriction reduced hepatic vascular surface area, resulting in a decrease in the number of active hepatocytes. Actually, the difference in the recovery of decreased oxygen consumption between the L-NAME (slow recovery) and D-NAME (quick recovery) groups seems to be correlated to the difference in the time course changes in Ppv, hence hepatic venoconstriction, as shown in Figures 2 and 4. Thus, the hemodynamic factors might substantially contribute to the late phase of the anaphylaxis-induced decrease in oxygen consumption in the L-NAME group.

In summary, ovalbumin-induced anaphylactic hepatic venoconstriction is characterized by predominant presinusoidal constriction in all rat livers with Hct 0% to 22%, and L-NAME pretreatment augmented the antigen-induced venoconstriction, by increasing Rpre, but not Rpost. This suggests that hepatic anaphylaxis increases production of NO, which consequently attenuates anaphylactic presinusoidal constriction in isolated perfused rat livers. However, the magnitude of L-NAME–induced augmentation of anaphylactic venoconstriction was not variable and independent of perfusate Hct and viscosity in blood perfused rat livers. Anaphylaxis reduced hepatic oxygen consumption independently of perfusate Hct 5% to 22%.

REFERENCES

1. Brown AFT. Anaphylactic shock: mechanism and treatment. *J Accid Emerg Med.* 1995;12:89–100.
2. Pavek K, Piper PJ, Smedegard G. Anaphylatoxin-induced shock and two patterns of anaphylactic shock: hemodynamics and mediators. *Acta Physiol Scand.* 1979;105:393–403.
3. Shibamoto T, Cui S, Ruan Z, et al. Hepatic venoconstriction is involved in anaphylactic hypotension in rats. *Am J Physiol Heart Circ Physiol.* 2005; 289:H1436–H1441.
4. Hines KL, Fisher RA. Regulation of hepatic glycogenolysis and vasoconstriction during antigen-induced anaphylaxis. *Am J Physiol Gastrointest Liver Physiol.* 1992;262:G868–G877.
5. Ruan Z, Shibamoto T, Shimo T, et al. NO, but not CO, attenuates anaphylaxis-induced postsinusoidal contraction and congestion in guinea pig liver. *Am J Physiol Regul Integr Comp Physiol.* 2004;286:R94–R100.
6. Weil R. Studies in anaphylaxis. XXI Anaphylaxis in dogs: a study of the liver in shock and peptone poisoning. *J Immunol.* 1917;2:525–556.
7. Yamaguchi Y, Shibamoto T, Hayashi T, et al. Hepatic vascular response to anaphylaxis in isolated canine liver. *Am J Physiol Regul Integr Comp Physiol.* 1994;267:R268–R274.
8. Moncada S, Higgs A. The L-arginine-nitric oxide pathway. *N Engl J Med.* 1993;329:2002–2012.
9. Rees DD, Palmer RMJ, Moncada S. Role of endothelium-derived nitric oxide in regulation of blood pressure. *Proc Natl Acad Sci USA.* 1989;86: 3375–3378.
10. Osada S, Ichiki H, Oku H, et al. Participation of nitric oxide in mouse anaphylactic hypotension. *Eur J Pharmacol.* 1994;252:347–350.
11. Kamikado C, Shibamoto T, Hongo M, et al. Effects of Hct and norepinephrine on segmental vascular resistance distribution in isolated perfused rat livers. *Am J Physiol Heart Circ Physiol.* 2004;286:H121–H130.
12. Cui S, Shibamoto T, Ruan Z, et al. Oxygen consumption, assessed with the oxygen absorption spectrophotometer, decreases independently of venoconstriction during hepatic anaphylaxis in perfused rat liver. *Shock.* 2006. In press.
13. Suematsu M, Goda N, Sano T, et al. Carbon monoxide: an endogenous modulator of sinusoidal tone in the perfused rat liver. *J Clin Invest.* 1995; 96:2431–2437.
14. Kamiya A, Togawa T. Adaptive regulation of wall shear stress to flow change in the canine carotid artery. *Am J Physiol.* 1980;239:H14–H21.
15. Casadevall M, Pique JM, Cirera I, et al. Increased blood hemoglobin attenuates splanchnic vasodilation in portal-hypertensive rats by nitric oxide inactivation. *Gastroenterology.* 1996;110:1156–1165.
16. Rimar S, Gillis CN. Selective pulmonary vasodilation by inhaled nitric oxide is due to hemoglobin inactivation. *Circulation.* 1993;88:2884–2887.
17. Cui S, Shibamoto T, Liu W, et al. Effects of platelet-activating factor, thromboxane A_2 and leukotriene D_4 on isolated perfused rat liver. *Prostaglandins Other Lipid Mediat.* In press.
18. Kimura K, Moriyama M, Nishisako M, et al. Modulation of platelet activating factor-induced glycogenolysis in the perfused rat liver after administration of endotoxin in vivo. *J Biochem (Tokyo).* 1998;123:142–149.

© 2006 Lippincott Williams & Wilkins

19. Shibamoto T, Ruan Z, Cui S, et al. Involvement of platelet-activating factor and leukotrienes in anaphylactic segmental venoconstriction in ovalbumin sensitized guinea pig livers. *Prostaglandins Other Lipid Mediat.* 2005;78:218–230.
20. Altin JG, Bygrave FL. Prostaglandin F_2 alpha and the thromboxane A_2 analogue ONO-11113 stimulate Ca^{2+} fluxes and other physiological responses in rat liver. Further evidence that prostanoids may be involved in the action of arachidonic acid and platelet-activating factor. *Biochem J.* 1988;249:677–685.
21. Haussinger D, Stehle T, Gerok W. Effects of leukotrienes and the thromboxane A_2 analogue U-46619 in isolated perfused rat liver. *Biol Chem Hoppe Seyler.* 1988;369:97–107.

© 2006 Lippincott Williams & Wilkins

1．研究課題名：肺癌の新しい機能的および形態的診断法の確立と分子標的治療法を指向した標的遺伝子の特定に関する研究（研究番号 C2004-2）

2．キーワード：1）肺癌（lung cancer）
2）分子標的治療（molecular targeting therapy）
3）仮想気管支鏡（virtual bronchoscopy）
4）FDG PET（FDG PET）
5）furanonaphthoquinone 誘導体（conductor of furanonaphthoquinone）

3．研究代表者：東　光太郎・医学部・教授・放射線診断治療学（放射線医学）
研究分担者：竹上　勉・総合医学研究・教授・分子腫瘍学研究部門
上田　善道・医学部・教授・病理病態学（病理学）
栂　博久・医学部・教授・呼吸機能治療学（呼吸器内科学）
佐川　元保・医学部・教授・呼吸機能治療学（呼吸器外科）
小林　健・金沢大学・医学部・講師・放射線科（現　石川県立中央病院・放射線科）
松成　一朗・先端医学薬学研究センター・臨床研究開発部長
郭　建飛（JianFei Guo）・中国医科大学・医学部・講師・放射線科

4．研究目的

平成１５年度の肺癌による死亡者は５６０００人と癌死の一位を占め、さらに増加傾向にある。肺癌の治療成績は不良で、再発をきたしやすい。肺癌の予後を改善するためには、新たな診断法および治療法の開発が不可欠である。本研究の目的は、以下の1）、2）、3）、4）により新たな診断法および治療法を開発し肺癌の予後改善に寄与することである。

1）非小細胞性肺癌の進展に関わる癌関連遺伝子群を明らかにし、新規の分子標的治療法を指向し標的分子・遺伝子を特定する。（担当：竹上、上田）

2）極細経の気管支鏡と multi detector CT を用いた仮想気管支鏡内視像を組み合わせることにより，末梢型微小肺癌の確実な組織採取法を確立する。（担当：佐川）

3）肺癌の生物学的特性を捉え、肺癌の新たな機能的画像診断法を開発・確立する。（担当：東、小林、松成、郭）

4）新しい肺癌治療薬として furanonaphthoquinone 誘導体(J103)に注目し、furanonaphthoquinone 誘導体(J103)の肺がん細胞に対する抗腫瘍効果を明らかにし、その機構を解明する。（担当：栂）

5．研究計画

1）主としてp53関連の遺伝子について遺伝子異常、発現変動を調べる。他方で肺腺癌細胞株A549や肝癌由来株における遺伝子発現の制御機構の解析を行なう。（担当：竹上）
これまでの非小細胞性肺癌における検討から、肺扁平上皮癌組織での MMP-3 の産生・分泌が重要な予後因子であることを見出していたが、その制御機構の詳細は不明であった。今回、重要な腫瘍血管増生因子の一つであり、かつ in vitro の解析から MMP-3 遺伝子の発現亢進作用が示されている basic fibroblast growth factor（b-FGF；FGF-2)の肺扁平上皮癌組織

における MMP-3 遺伝子発現誘導への関与を、腫瘍浸潤部の癌細胞・間質細胞相互応答に着目し検討する。(担当：上田)

2）Virtual Bronchoscopy の末梢微小陰影に関する画像再構成の至適条件を確立し，実際の症例で観察および組織採取を行なう。また，より採取効率の良い組織・細胞採取の device の開発を行なう (担当：佐川)

3）非小細胞性肺癌の血管新生因子の一種である angiopoietin-2 の mRNA 発現を測定する。さらに、hypoxia-inducible factor-2α の発現を測定し、これらと FDG PET により測定した糖代謝活性との関連を明らかにする。これにより、血管新生因子を標的とした分子標的治療法の適応を明らかにする。(担当：東、小林、松成、郭)

4）肺腺癌由来細胞(A549)を用いて in vitro で furanonaphthoquinone 誘導体の抗腫瘍効果を測定し、Fas/FasL システムを介したアポトーシスとの関連を調べる。マウスを用いた in vivo の実験では、Lewis lung carcinoma 2 (LL/2)を移植し furanonaphthoquinone 誘導体の抗腫瘍効果を測定し、副作用の有無を調べる。(担当：栂)

6．研究成果

1）シフェラーゼ活性測定を行なうレポーターアッセイ法の活用で、p21 発現関連の遺伝子発現制御機構の解析が可能になった。遺伝子発現への RNAi の影響の有無の検討も可能になった。(担当：竹上)

高病期肺扁平上皮癌症例の腫瘍及び間質細胞では MMP-3 遺伝子の発現が，同間質細胞では bFGF 遺伝子発現が亢進していた。進行扁平上皮癌症例の一部では腫瘍細胞での bFGF 遺伝子発現が亢進していた。間質における bFGF 遺伝子発現と間質細胞および腫瘍細胞における MMP-3 遺伝子発現間に有意な関連が示された。肺扁平上皮癌間質細胞は bFGF 発現を介し肺癌組織における MMP-3 遺伝子発現を亢進させ，腫瘍進展に関与することが明らかになった。(担当：上田)

2）multi detector CT を用いた仮想気管支鏡内視像については、おおむね５次から７次気管支までの Virtual Bronchoscopy 画像再構成に関しては，安定して可能となるような条件を設定しえた。(担当：佐川)。

3）肺癌の血管新生因子である angiopoietin-2 の mRNA 発現および hypoxia-inducible factor-2α の発現の程度は肺癌の悪性度により異なり、angiopoietin-2 の mRNA 発現あるいは hypoxia-inducible factor-2α の発現が強い肺癌は悪性度が高く予後が悪いこと明らかにした。また、FDG PET で測定した肺癌の糖代謝活性は angiopoietin-2 の mRNA 発現および hypoxia-inducible factor-2α の発現と相関していた。このことから、FDG PET により angiopoietin-2 および hypoxia-inducible factor-2α を標的とした分子標的治療法の適応を決定できることが判明した。(担当：東、小林、松成、郭)

4）furanonaphthoquinone 誘導体 (J103) は 0.5-2.5 g/ml の濃度範囲で量依存性に A549 細胞の増殖を抑制した。同濃度の furanonaphthoquinone 誘導体は A549 の Fas mRNA の発現を増強し、細胞表面の Fas 発現を増強した。その効果は 1-7 日まで持続していた。furanonaphthoquinone 誘導体は 1.0-2.5 g/ml の範囲で A549 のアポトーシスを増加させ、同時に caspase 3 の発現も増強した。furanonaphthoquinone 誘導体は 2 週間後にマウスに移植された LL/2 腫瘍の増殖を抑制した。furanonaphthoquinone 誘導体は脾臓由来の T リンパ球

数を減少させず、細胞表面にFasLを発現させた。(担当：栂)

7．研究の考察・反省

平成１６年度の成果として、p21発現関連の遺伝子発現制御機構の解析が可能になった。今後、細胞癌化のプロセスにp21遺伝子発現がどの程度関わるのか、またそのシグナル伝達へのHCV-NS3の影響を調べ、癌化に関わる細胞内遺伝子発現について解析を進める予定である。併行して遺伝子発現制御のためのRNAiの活用をさらに検討する。

平成１６年度の成果として、肺扁平上皮癌間質細胞はbFGF発現を介し肺癌組織におけるMMP-3遺伝子発現を亢進させ，腫瘍進展に関与することが明らかになった。今後、腫瘍浸潤部の癌細胞・間質細胞相互応答におけるbFGFのMMP-1遺伝子発現亢進への関与をlaser-captured microdissection / real time RT-PCR法による定量解析により明らかにする。

multi detector CTを用いた仮想気管支鏡内視像については、おおむね５次から７次気管支までのVirtual Bronchoscopy画像再構成に関しては安定した適切な条件を設定しえた。しかし８次ないし９次気管支に関しては症例の条件の違いもあり不安定なため，今後若干の検討が必要である。

肺癌の血管新生因子については、FDG PETによりangiopoietin-2およびhypoxia-inducible factor-2αを標的とした分子標的治療法の適応を決定できることが判明した。今後、肺癌の血管新生因子の一種であるvascular endothelial growth factorのmRNAの発現を測定しFDG PETにより測定した糖代謝活性との関連を明らかにする。

furanonaphthoquinone誘導体(J103)については、平成１６年度の成果としてfuranonaphthoquinone誘導体の肺癌に対する効果を初めて明らかにするとともに、その作用機序がFas/FasLシステムを介したアポトーシスの増強であることを証明した。今後、furanonaphthoquinone誘導体の有効性とFas/FasLシステムの発現、およびアポトーシスについて臨床的に測定することや画像上に表現することについてさらに研究を進める予定である。

8．研究発表

Sagawa M, Higashi K, Sugita M, Ueda Y, Maeda S, Toga H, Sakuma T. Fluorodeoxyglucose uptake correlates with the growth pattern of small peripheral pulmonary adenocarcinoma. Surg Today 2006; 36: 230-234. (MLDB)

Takegami T. Japanese encephalitis virus RNA synthesis in vivo and in vitro. J Kanazawa Med Univ 2005; 305: 560-566.

上田善道, 島崎　都, Jiang D, Yang G, 佐藤勝明, Guo J, 東　光太郎, 岡田保典, Chada KK, 勝田省吾. 肺扁平上皮癌の浸潤・転移の分子機構 - Matrix metalloproteinase (MMP)の関与とその発現誘導機構 - . 金沢医科大学雑誌　2005; 30: 357-364.

Surg Today (2006) 36:230–234
DOI 10.1007/s00595-005-3123-3

SURGERY TODAY
© Springer-Verlag 2006

Fluorodeoxyglucose Uptake Correlates with the Growth Pattern of Small Peripheral Pulmonary Adenocarcinoma

MOTOYASU SAGAWA[1], KOTARO HIGASHI[2], MAKOTO SUGITA[1], YOSHIMICHI UEDA[3], SUMIKO MAEDA[1], HIROHISA TOGA[4], and TSUTOMU SAKUMA[1]

Departments of [1]Thoracic Surgery, [2]Radiology, [3]Pathology II, and [4]Respiratory Medicine, Kanazawa Medical University, 1-1 Daigaku, Uchinada, Ishikawa 920-0293, Japan

Abstract

Purpose. Noguchi and colleagues reported that the growth pattern of small-sized adenocarcinoma was related to the vascular involvement and the prognosis of the patient. Noguchi's type A/B tumors had no lymph node metastasis, rare vascular involvement, and an excellent prognosis, which meant that Noguchi's type A/B tumors were preinvasive tumors of the peripheral type. Although Noguchi's classification was usually determined based on resected specimens, it would be useful to make a decision about the therapeutic strategy if the classification could be determined preoperatively based on the fluorodeoxyglucose (FDG) uptake.

Methods. The FDG uptake in 61 pulmonary adenocarcinomas measuring 3 cm or smaller in diameter was compared with the mediastinal uptake and was classified into five grades. The relationship between the FDG uptake and Noguchi's classification (A to F) was analyzed.

Results. The FDG uptake was significantly lower in Noguchi's type A/B tumors than in type C or in type D/E/F. Eleven of 12 tumors (92%) with no increased or a weak FDG uptake were classified as type A/B, whereas 32 of 33 tumors (97%) with a strong or very strong FDG uptake were classified as type C–F.

Conclusions. The FDG uptake is helpful for making an accurate diagnosis of Noguchi's classification preoperatively in patients with pulmonary adenocarcinoma.

Key words ^{18}F-Fluorodeoxyglucose positron emission tomography · Noguchi's classification · Adenocarcinoma · Lung cancer · Limited resection

Reprint requests to: M. Sagawa
Received: April 1, 2005 / Accepted: July 12, 2005

Introduction

Lung cancer is the leading cause of cancer death in Japan as well as in the United States. Recently, thoracic computed tomography (CT) screening for the detection of early lung cancer has been suggested as a possible tool to decrease lung cancer mortality.[1–3] Using CT screening, a number of small-sized pulmonary adenocarcinomas have thus been detected and treated, and several characteristics of small-sized adenocarcinomas have also been elucidated. Noguchi and colleagues introduced a novel classification where small-sized pulmonary adenocarcinomas were classified according to their growth pattern. Noguchi's classification was strongly related with vascular involvement and the prognosis of the patient.[4] In particular, Noguchi's type A/B tumors had characteristics with no lymph node metastasis, rare vascular involvement, and an excellent prognosis (5-year survival rate: 100%).[4] Although Noguchi's classification was usually determined with resected specimens, it would be useful to decide the therapeutic strategy if the classification could be determined preoperatively.

Positron emission tomography imaging with ^{18}F-fluorodeoxyglucose (FDG PET) provides physiologic and metabolic information of pulmonary nodules, which cannot be provided by morphological examinations such as CT.[5–7] To date, little is known concerning the relationship between the FDG uptake and Noguchi's classification in small-sized primary pulmonary adenocarcinomas, which we retrospectively analyzed in this study.

Patients and Methods

Positron emission tomography scanning was performed with a PET camera, Headtome IV (Shimazu, Kyoto, Japan) or Advance (GE Medical System, Milwaukee,

WI, USA). Until March 2003, FDG PET was performed in 110 patients with 118 primary lung cancers, which were surgically resected at our university. Of them, 61 lesions of adenocarcinoma which pathologically measured 3 cm or smaller in diameter were analyzed.

All of the patients studied fasted for 6 h before undergoing scanning. Blood (1 ml) was drawn for baseline blood glucose estimation, and the data were recorded. Fluorodeoxyglucose was administered intravenously. The average injection dose of FDG was 370 MBq. After a 40–50-min uptake period, an emission scan was acquired. Transmission scans were obtained in all subjects for attenuation correction. Fluorodeoxyglucose accumulation within the primary lung cancer on the attenuation- and decay-corrected images was graded independently. A 5-point visual grading system (a modified method of Vansteenkiste et al.[8]) was used to interpret the FDG uptake within the primary lesions without any pathological information: no increased uptake (similar to background), weak uptake (lower than mediastinum), medium uptake (similar to mediastinum), strong uptake (higher than mediastinum), very strong uptake (remarkably higher than mediastinum).

Histological typing was classified according to the World Health Organization classification[9] without any radiological information. The growth pattern of the tumors was classified according to Noguchi's classification[4]: A, localized bronchiolo-alveolar carcinoma (LBAC); B, LBAC with foci of collapse of alveolar structure; C, LBAC with foci of active fibroblastic proliferation; D, poorly differentiated adenocarcinoma; E, tubular adenocarcinoma; and F, papillary adenocarcinoma with compressive and destructive growth. Type A/B/C tumors show a growth pattern involving replacement of alveolar lining cells, whereas type D/E/F tumors are nonreplacement-type adenocarcinomas. A statistical analysis was performed using the Mann–Whitney *U*-test.

Table 1. Characteristics of the patients in this study

Factor	*n*
Sex	
Male	21
Female	35
Age	
59 and below	19
60–69	16
70–79	18
80 and above	3
Histology	
Bronchiolo-alveolar carcinoma	9
Well-differentiated adenocarcinoma	28
Moderately differentiated adenocarcinoma	21
Poorly differentiated adenocarcinoma	3
Noguchi's classification	
A	2
B	14
C	16
D	4
E	7
F	18
Maximum diameter	
10 mm or less	4
11–15 mm	10
16–20 mm	17
21–25 mm	14
26–30 mm	16
FDG uptake	
0	6
1	6
2	16
3	17
4	16

FDG, fluorodeoxyglucose

Results

Table 1 shows the characteristics of the 61 lesions of the 56 patients. Figure 1 shows FDG PET findings of representative cases. The FDG uptake of each tumor according to Noguchi's classification and the tumor size are shown in Fig. 2.

Fifty-five of all the 61 adenocarcinomas (90%) had a positive FDG uptake. According to the tumor size, all 16 adenocarcinomas measuring from 26 to 30 mm in diameter (100%), 12 of 14 tumors measuring from 21 to 25 mm in diameter (86%), all 17 tumors measuring from 16 to 20 mm in diameter (100%), and 10 of 14 tumors measuring from 1 to 15 min in diameter (71%) had a positive FDG uptake. In the adenocarcinomas measuring from 1 to 15 mm in diameter, 9 of 10 Noguchi's type C–F tumors had a positive FDG uptake (90%), whereas only 1 of 4 Noguchi's type A/B tumors had (25%).

Although 11 of 16 type A/B tumors (69%) had a positive FDG uptake, 10 of the 11 FDG-positive type A/B tumors had a medium FDG uptake or weaker. On the other hand, 15 of 16 type C tumors (94%) and 29 of 29 type D/E/F tumors (100%) had a positive FDG uptake, and all of the FDG-positive type C–F tumors had a medium FDG uptake or stronger. The FDG uptake was lower in Noguchi's type A/B tumors than in type C tumors ($P = 0.0002$) or in type D/E/F tumors ($P < 0.0001$). The FDG uptake in type C tumors was not statistically different from that in type D/E/F tumors ($P = 0.104$).

Table 2 shows the number of tumors according to Noguchi's classification and the FDG uptake. Eleven of 12 tumors with no FDG uptake or a weak one (92%) were classified as Noguchi's type A/B. On the other hand, 32 of 33 tumors with strong or very strong FDG uptake (97%) were classified as Noguchi's type C, D, E, or F.

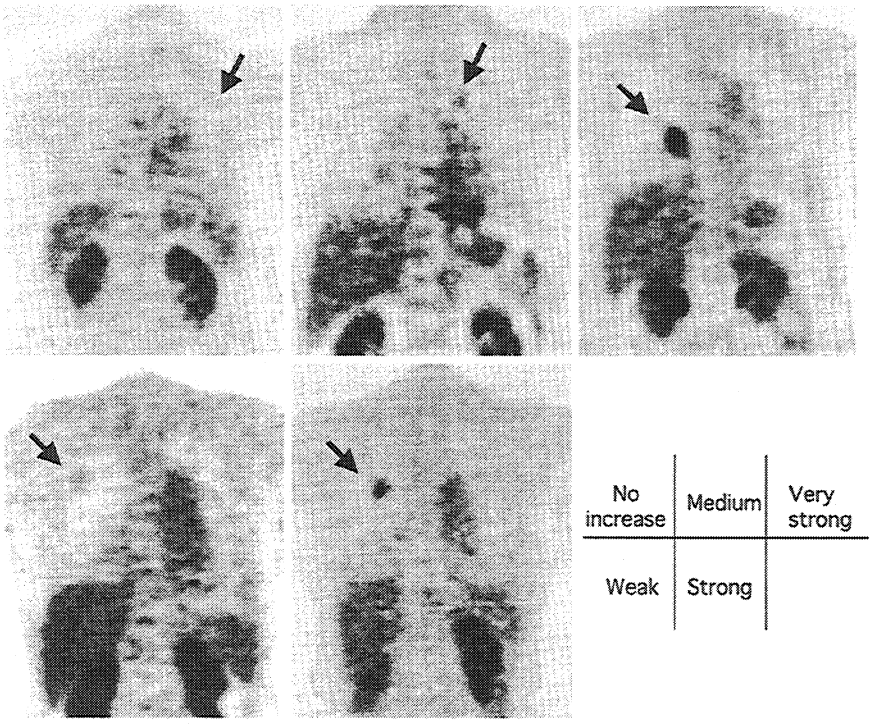


Fig. 1. ^{18}F-Fluorodeoxyglucose positron emission tomography findings in representative cases

Noguchi's classification	Tumor Size			
	0-15mm	16-20mm	21-25mm	26-30mm
Type A	○			◎
Type B	○ ○ □	○ ◎ □	◎ ◎ □	◎ □ ●
Type C	◎ □ ■	□ ●	□ ● ●	□ ● ■
Type D	□ ●	■		■
Type E	□ ● ●	□ ■	■	■
Type F	●	□ □ ■ ■	□ ■	● ■ ■

Uptake of FDG: ○ No increased ◎ Weak □ Medium ● Strong ■ Very strong

Fig. 2. Relationships among the fluorodeoxyglucose (*FDG*) uptake, Noguchi's classification, and the tumor size. Most of Noguchi's type A/B tumors had a medium FDG uptake or weaker, whereas most of Noguchi's type C–F had a medium FDG uptake or stronger, regardless of the size of the tumor

Table 2. Number of tumors according to Noguchi's classification and FDG uptake

FDG uptake	Noguchi's classification					
	A	B	C	D	E	F
No increased uptake	1	4	1	0	0	0
Weak uptake	1	5	0	0	0	0
Medium uptake	0	4	4	1	2	5
Strong uptake	0	1	9	1	2	4
Very strong uptake	0	0	2	2	3	9

Discussion

Recently a number of small pulmonary adenocarcinomas have been found due to advances in diagnostic radiology.[1–3] Noguchi et al. published a classification with which the aggressiveness of small adenocarcinomas was evaluated.[4] In this study, we examined the relationship between FDG uptake and Noguchi's classification with resected small-sized adenocarcinomas.

Our results showed that 90% of adenocarcinomas were FDG-positive even though the tumors measured

3 cm in size or smaller. According to the tumor size, 96% of the tumors measuring from 16 to 30 mm in diameter had a positive FDG uptake, whereas the sensitivity decreased to 71% in the tumors measuring 15 mm or smaller. However, 90% of type C–F tumors measuring 15 mm or smaller in diameter still had a positive FDG uptake. These results indicate that FDG PET is useful for detecting type C–F small adenocarcinomas. On the other hand, only 25% of type A/B tumors 15 mm or smaller in diameter were FDG-positive, thus indicating that FDG PET could not detect type A/B small adenocarcinoma.

A number of early adenocarcinomas detected by thoracic CT screening have raised a question as to whether a lobectomy would be indispensable for such kinds of tumor. A randomized trial concerning a limited resection for clinical T1N0M0 lung cancers revealed that a limited resection is not recommended for patients with clinical T1N0M0 diseases.[10] However, Noguchi's type A/B tumor is not the same as usual T1N0M0 lung cancer because it has rare nodal and vascular involvement,[4] and a limited resection might thus be sufficient for such a tumor.[11] Actually a clinical trial, where a wedge resection of the lung without nodal dissection would be performed instead of a lobectomy with systematic nodal dissection when the lung cancer was Noguchi's type A/B, is now being planned in Japan. Nevertheless, it is sometimes difficult to accurately differentiate type A/B from type C–F by transbronchial lung biopsy specimens or intraoperative frozen sections, which thus remains a great obstacle for conducting such a clinical trial.

Our results revealed that 92% of the pulmonary adenocarcinomas 3 cm or smaller in diameter with no increased or weak FDG uptake were Noguchi's type A/B tumors, and 97% of the pulmonary adenocarcinomas 3 cm or smaller in diagmeter with a strong or very strong FDG uptake were Noguchi's type C–F. Although the negative predictive values were not so high, the positive predictive values were considerably high. This means that FDG PET may therefore help us to make an accurate diagnosis of Noguchi's classification pre- and intraoperatively, and would also be useful for conducting a clinical trial where a wedge resection of the lung would be performed instead of a lobectomy for Noguchi's type A/B lung cancer.

In the present study there are some issues that remain to be discussed. First, a five-point visual grading system was used to interpret FDG uptake within the primary lesions, and the standard uptake value (SUV)threshold was not used. Vansteenkiste et al. reported that a visual scale was as accurate as the use of an SUV threshold for lymph nodes in the distinction between benign and malignant nodes.[8] The SUV is affected by many factors, including the partial volume effect, the method of drawing regions of interest, the period between FDG administration and the start of an emission scan, and whether the image is attenuation-corrected or nonattenuation-corrected.[12] Iterative reconstruction with segmented attenuation correction resulted in a significantly lower mean SUV and maximum SUV values compared to a filtered back-projection with measured attenuation correction.[13] Therefore, a visual scale was found to be more adequate than the SUV threshold in this study.

Second, the results of this study did not describe the sensitivity or positive predictive value of FDG PET to differentiate malignant tumors from benign tumors, which has already been reported by many investigators.[14–17] This study focused on the positive predictive value (probability) to differentiate Noguchi's type A/B from type C–F, which would be important for selecting appropriate candidates for a limited resection. Therefore, all of the patients in this study were lung cancer patients.

Third, this study did not focus on the negative predictive value or false-negative cases, such as type A/B tumors with a medium FDG uptake. The standard surgical procedure for lung cancer is a pulmonary lobectomy with a systematic nodal dissection, because a randomized trial revealed that the patients with clinical T1N0M0 lung cancer who underwent a limited resection had a significantly worse prognosis than those who underwent a pulmonary lobectomy.[10] At present, the important strategy in selecting candidates for a limited resection should be not to reduce the number of false-negative cases, but to reduce the number of false-positive cases. Therefore, this study focused on the positive predictive value to differentiate type A/B from type C–E.

Although the number of cases in this study was limited, the results were informative. FDG PET is useful for detecting Noguchi's type C–F small adenocarcinomas, but not type A/B small adenocarcinomas. FDG PET may be helpful for achieving an accurate diagnosis of Noguchi's classification, thus enabling us to conduct a clinical trail where a wedge resection would be performed instead of a lobectomy for selected lung cancer patients. Further studies will be required to clarify whether a limited resection is actually beneficial for such patients.

Acknowledgments. This study was supported in part by Grants for Collaborative Research from Kanazawa Medical University (C2003-2, C2004-2, C2005-2), Grant-in-Aid from Kurokawa Research Foundation (2005), and Grant-in-Aid for Scientific Research No. 16591419.

References

1. Henschke CI. Early lung cancer action project: overall design and findings from baseline screening. Cancer 2000;89:2474–82.

2. Sone S, Li F, Yang ZG, Honda T, Maruyama Y, Takashima S, et al. Results of three-year mass screening programme for lung cancer using mobile low-dose spiral computed tomography scanner. Br J Cancer 2001;84:25–32.
3. Kaneko M, Kusumoto M, Kobayashi T, Moriyama N, Naruke T, Ohmatsu H, et al. Computed tomography screening for lung carcinoma in Japan. Cancer 2000;89:2485–8.
4. Noguchi M, Morikawa A, Kawasaki M, Matsuno Y, Yamada T, Hirohashi S, et al. Small adenocarcinoma of the lung: histologic characteristics and prognosis. Cancer 1995;75:2844–52.
5. Coleman RE. PET in lung cancer. J Nucl Med 1999;40:814–20.
6. Vesselle H, Schmidt RA, Pugsley JM, Li M, Kohlmyer SG, Vallieres E, et al. Lung cancer proliferation correlates with [F-18]fluorodeoxyglucose uptake by positron emission tomography. Clin Cancer Res 2000;6:3837–44.
7. Higashi K, Ueda Y, Yagishita M, Arisaka Y, Sakurai A, Oguchi M, et al. FDG PET measurement of the proliferative potential on non-small cell lung cancer. J Nucl Med 2000;41:85–92.
8. Vansteenkiste JF, Stroobants SG, De Leyn PR, Dupont PJ, Bogaert J, Maes A, et al. Lymph node staging in non-small-cell lung cancer with FDG-PET scan: a prospective study on 690 lymph node stations from 68 patients. J Clin Oncol 1998;16:2142–9.
9. WHO. Histological typing of lung and pleural tumours. 3rd ed. Berlin: Springer; 1999. p. 31–47.
10. Lung cancer study group. Randomized trial of lobectomy versus limited resection for T1N0 non-small cell lung cancer. Ann Thorac Surg 1995;60:615–23.
11. Nakata M, Sawada S, Saeki H, Takashima S, Mogami H, Teramoto N, et al. Prospective study of thoracoscoic limited resection for ground-glass opacity selected by computed tomography. Ann Thorac Surg 2003;75:1601–6.
12. Keyes J. SUV: standard uptake or silly useless value? J Nucl Med 1995;36:1836–9.
13. Chin BB, Lyengar S, Sabundayo BP, Schwartz D. Standardized uptake values in 2-deoxy-2-[18F]Fluoro-d-glucose with positron emission tomography. Clinical significance of iterative reconstruction and segmented attenuation compared with conventional filtered back projection and measured attenuation correction. Mol Imaging Biol 2002;4:294–300.
14. Kubota K, Matsuzawa T, Fujiwara T, Ito M, Hatazawa J, Ishiwata K, et al. Differential diagnosis of lung tumor with positron emission tomography: a prospective study. J Nucl Med 1990;31:1927–32.
15. Gupta NC, Maloof J, Gunel E. Probability of malignancy in solitary pulmonary nodules using fluorine-18-FDG and PET. J Nucl Med 1996;37:943–8.
16. Lowe VJ, Fletcher JW, Gobar L, Lawson M, Kirchner P, Valk P, et al. Prospective investigation of positron emission tomography in lung nodules. J Clin Oncol 1998;16:1075–84.
17. Gould MK, Maclean CC, Kuschner WG, Rydzak CE, Owens DK. Accuracy of positron emission tomography for diagnosis of pulmonary nodules and mass lesions: a meta-analysis. JAMA 2001;285:914–25.

J Kanazawa Med Univ 30 : 560−566, 2005

Japanese encephalitis virus RNA synthesis *in vivo* and *in vitro*

Tsutomu Takegami

Abstract: In order to investigate the mechanism of Japanese encephalitis virus (JEV) RNA replication, viral RNA syntheses *in vivo* and *in vitro* were analyzed. First, an appearance of viral specific RNA in JEV-infected cells was examined by northern blot analysis. Minus RNA-probe recognized a negative strand of JEV-specific RNA synthesized in JEV-infected cells as early as 6 hrs post infection (p.i.). Full length genomic 42S positive RNAs were detected in the cells at 12 hrs p.i. Relative amounts of the 42 S positive RNA was much larger in the membrane fraction than the supernatant fraction of JEV-infected cells. To investigate the mechanism of RNA synthesis, it is important to establish the *in vitro* system of RNA synthesis. It was found that JEV specific positive RNAs were efficiently synthesized *in vitro* in the crude membrane and nuclear fractions prepared from the JEV-infected cells. The analyses by SDS-PAGE and immunofluorescence assay indicated that nonstructural proteins NS3 and NS5, considered to be RNA helicase, protease and RNA polymerase, respectively, were membrane associated proteins, even though they were hydrophilic proteins. Maybe other NS proteins, including NS4a and 4b, are responsible to the membrane association, because of the hydrophobicity. The data that monospecific antisera against NS3 and NS5 inhibited *in vitro* RNA synthesis indicate that those proteins strongly contributed for viral RNA synthesis in the JEV-infected cells.

Key Words : Japanese encephalitis virus, RNA replication, *in vitro* system

Introduction

Japanese encephalitis (JE) is an acute viral infection of the central nervous system in humans, with an estimation of 50,000 cases of encephalitis and 10,000 death annually in the world (1-3). Japanese encephalitis virus (JEV) is the leading cause of viral encephalitis in Asia. Even though recently JE cases in Japan are less than 10 in each year, still JE viruses circulate in wide area including Ishikawa (4). The genome of JEV, a member of the Flaviviridae, is a single-stranded, positive sense RNA ca 11kb in length which has no poly A at the 3'untranslated region (UTR) (5). Several process of JEV-RNA synthesis in the infected cells is unknown, although some studies related to this problem have been reported (6-8). Generally, it is thought that a negative stranded RNA must be synthesized in the early stage of JEV reproduction in cells, similarly to the early events of other positive RNA virus infections. The negative strand copied from positive genomic RNA leads to the formation of double-stranded replicative form (RF), which may have recycling role as a template (6). In order to examine the early events during JEV-RNA replication, it is essential to detect and distinguish the negative and positive strand.

The entire nucleotide sequence of JEV genomic RNA has been determined (9-11). It is suggested that JEV genomic RNA has a specific secondary structure at the 3' end, and this structure plays a significant role in the RNA replication of JEV and other flaviviruses (5-6,11-12). Sequencing data indicate that the genome organization of several flaviviruses is very similar to each other, though not identical (6), and suggest that these viruses have common features in their mechanism of RNA replication. The functions of nonstructural proteins including NS3 and NS5 in the replication complex (RC) is gradually clarified but not enough. Here we report the feature of JEV-RNA synthesis in JEV-infected cells and *in vitro* system using membrane fraction derived from JEV-infected cells.

Division of Molecular Oncology and Virology,
Medical Research Institute, Kanazawa Medical University
Uchinada, Ishikawa, 920-0293, Japan
Accepted: March 11, 2006

Materials and Methods

Cells, Viruses and RNA:

Mosquito cells C6/36 and Vero cells were cultured in the medium MEM containing 5-10% fetal bovine serum. Those cells were infected with JEV, JaGAr01 or Nakayama strains. Culture fluids were taken at proper time post-infection (p.i.) and subjected to the virus titration. Virus titer was estimated by plaque forming using confluent monolayer of BHK cells, as previously described (13). JEV virion were prepared from culture fluids by ultra-centrifugation method using discontinuous density gradient containing 10-40% sucrose. Viral RNA was extracted from virions with SDS-phenol/chroloform and precipitated with ethanol. To prepare RNA from JEV-infected cells, cells were washed with phosphate buffered saline (PBS) and harvested by the addition of 50 mM Tris buffer (pH7.5) containing 0.5% SDS and 1 mM EDTA.

Preparation of cell extracts

To obtain subcellular fractions, infected cells were dissolved in Tris buffer (pH7.5) containing 1.5 mM $MgCl_2$ and 10 mM KCl, and disrupted by 20 strokes in a Dounce homogenizer. Cellular homogenates were subjected to successive centrifugations, i.e. 500 x g for 10 min and then 10,000 x g for 30 min (7). The resulting pellets, nuclear and membrane fractions, were resuspended in 50 mM Tris buffer (pH8.0) containing 1.5 mM $MgCl_2$ and 50 mM KCl, and used for *in vitro* assay reactions.

Procedure of hybridization including Northern blot

Plasmid pJB11 has JEV cDNA sequences corresponding to the 3' end of JEV genomic RNA (9). DNA fragment at nucleotides 9183 to 10883 was prepared from pJB11, and inserted into pSPT18 and pSPT19, and then constructed new plasmids pJT18V and pJT19V (8). Each plasmid was then digested with restriction enzymes to prepare fragments. RNA probes were prepared through the RNA synthesis reaction carried out in the presence of T7 RNA polymerase (Toyobo, Tokyo) and α-^{32}P-UTP. The JT18V and JT19V probes could detect intracellular viral specific negative-sense RNA and positive-sense JEV-RNA including virion RNA, respectively.

For northern blot analysis, sample RNAs were denatured at 50℃ for 60 min in the presence of 1 M glyoxal and 50% DMSO and then were electrophoresed on 1% agarose gel in 10 mM phosphate buffer (pH7.0) which was recirculated continuously. Molecular weight standards were 23S (3.3 kb) and 16S (1.7 kb) *E. coli* rRNAs. RNAs were transferred to a nylon membrane (Pall, USA) with 20 x SSC (1xSSC:0.15M NaCl and 0.015M sodium citrate) and baked. The baked nylon membrane was treated with prehybridization buffer and then hybridized with ^{32}P labeled RNA probe at 42℃ for 16 hr. After hybridization, the nylon membrane was washed repeatedly with 2 x SSC containing 0.1% SDS. Slot hybridization was performed as similar protocol as described above. The dried filters were exposed to Fuji RX films.

In vitro assay of RNA synthesis.

In vitro RNA synthesis was carried out in 30 μl reaction mixture containing 50 mM HEPES (pH8.0), 3.5 mM MgCl2, 50 mM KCl, 5 mM DTT, 10 μg/ml actinomycin-D (Act-D), 0.7% NP40, 0.5 mM each of ATP, CTP and GTP, 10 μCi α-^{32}P-UTP and subcellular fractions (ca 5 μg protein). After an incubation at 30℃ for 60 min, 120 μl of 0.5% SDS solution was added, followed quickly by 150 μl of phenol. The RNAs in aqueous phase were precipitated with ethanol. To detect *in vitro* RNA product, 1% native agarose gels were used. Electrophoresis was carried out in TBE buffer (90 mM Tris-borate (pH 8.0) and 2 mM EDTA). To identify ds- and ss-RNA, RNAs were treated with 2M LiCl and fractionated by a centrifugation after the overnight-incubation. In ultra-centrifugation using 15-30% sucrose density gradient, ultra-centrifuge (Beckman) was used. The dried gels were exposed to Fuji RX films.

Labeling of protein with ^{35}S methionine

In a long labeling experiment, cells were pretreated with 1 μg/ml Act-D. After 4-hr pretreatment, cells were infected with JEV and added with 5 μCi/ml of ^{35}S-methionine (Met), and then cultured for further 24 hr and harvested. Subcellular fractions were prepared by centrifugation and subjected to SDS-10% polyacrylamide gel electrophoresis (SDS-PAGE) (7). The gels were exposed to X ray films.

Indirect immunofluorescence antibody assay (IFA)

For the IFA, JEV-infected Vero cells were fixed with acetone and incubated with specific antisera, as previously described (14). The specific antisera including anti-E, anti-NS3 and anti-NS5 were prepared from rabbits which were immunized with JEV proteins purified by the method using SDS-PAGE (14-15). After incubation with FITC conjugated goat anti-rabbit IgG, the cells were observed by a fluorescence microscope.

Results

Viral RNA in JEV-infected cells

JEV specific RNA in the infected cells was detected by hybridization using RNA probes. In order to examine the size of JEV-specific in the infected cells, RNA samples were subjected to glyoxal gel electrophoresis. The JT19V probe could detect positive-sense JEV-RNA including virion RNA, while the proves JT18V recognized only intracellular viral

specific negative-sense RNA. Since 2 kinds of genome sized RNA (42S) were detected in the hybridization with ^{32}P-plus (JT19V) and ^{32}P-minus probes (JT18V), we used both probes to examine viral RNAs in the infected cells (Fig.1). By using the minus probes, it was elucidated that the negative stranded viral RNA (42S) was synthesized in the early stage of infection. As shown in Fig. 1B, the amounts of

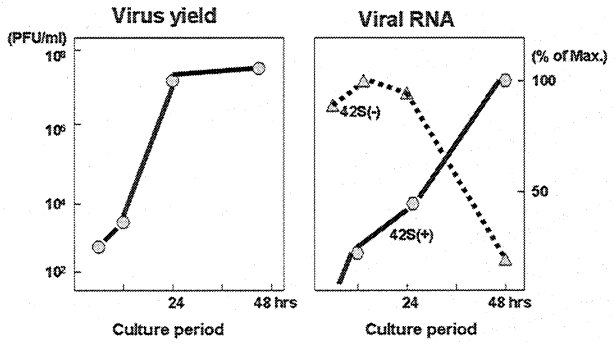


Fig. 1. Virus reproduction and appearance of JEV-specific RNAs in the infected cells.
(Left) JEV growth in C6/36 cells. Cells were infected with 10 m.o.i. of JEV and virus titers were assayed by plaque forming method.
(Right) RNAs were prepared from JEV-infected C6/36 cells at different times after virus infection. After glyoxal gel electrophoresis, RNA samples were transferred to nylon membrane and hybridized first with plus, ^{32}P-JT19V and second with minus probes, ^{32}P-JT18V. The amount of 42S vRNA were estimated and relative amounts are shown.

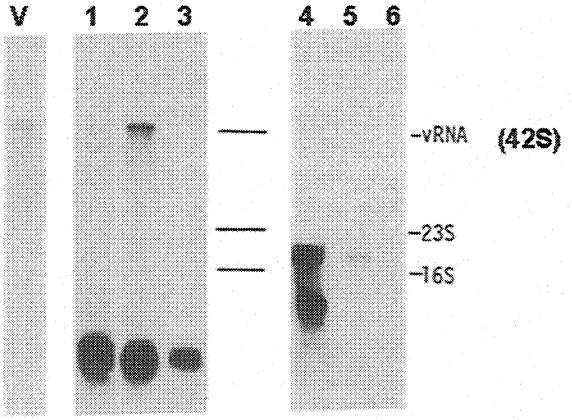


Fig. 2. Northern blot analysis of JEV-specific RNAs from the infected cells.
RNAs were extracted from virions or from the subcellular fractions of JEV-infected cells (48 hr p.i.) and electrophoresed using glyoxal gel, as described in the text. Lane V, JEV-vRNA. Lanes show RNAs from supernatant (lanes 1,4), crude membrane (lanes 2,5) and nuclear fractions (lanes 3, 6), respectively. After the transfer, hybridization was carried out by using RNA probes as described in the legend to Fig.1. Lanes V, 1-3 hybridized with JT19V. Lanes 4-6, JT18V.

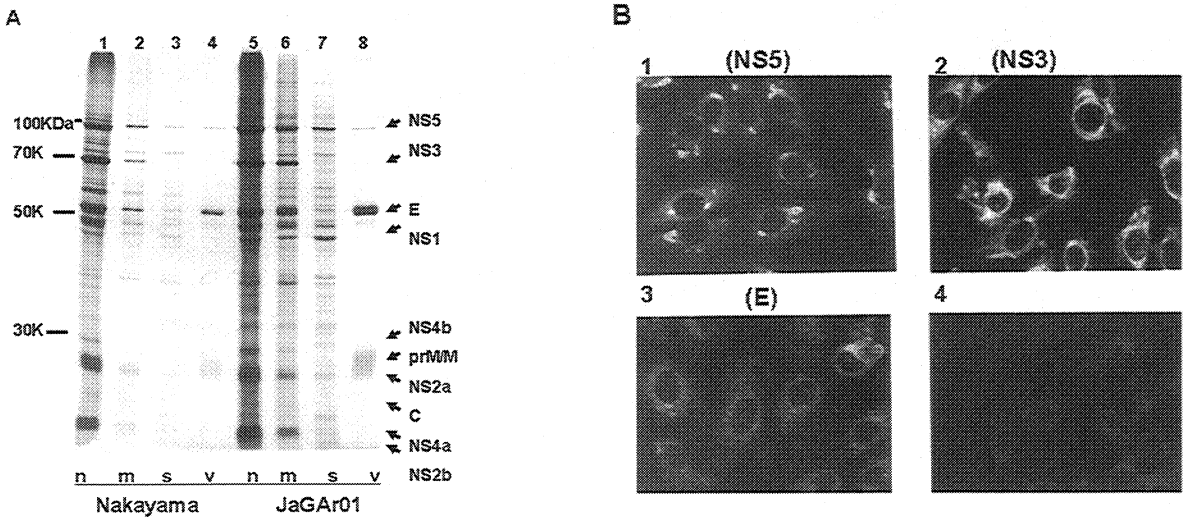


Fig. 3. Localization of viral proteins in JEV-infected cells.
A: JEV-infected cells labeled with ^{35}S-Met for 2hr were disrupted and fractionated into subcellular fractions including nuclear (lanes 1, 5), crude membrane (lanes 2, 6) and supernatant fractions (lanes 3, 7) by the centrifugation. Here we used 2 kinds of JEV strains for analysis. Lanes 4 and 8 indicate the partially purified JEV virion.
B: Indirect immunofluorescence assay (IFA) of JEV-infected cells.
Feature of JEV-proteins NS5, NS3 and E were shown in panels 1, 2 and 3. Panel 4 indicates IFA using preimmune rabbit sera.

negative stranded viral RNA reached a maximum level around 12 hr p.i. and then decreased. Appearance of the positive RNA (42S), however, was delayed, and it was obviously detected as 12 hr p.i. and then increased in amounts gradually. The accumulation of 42 S (+) RNA was similar to that of the virus growth curve assayed by plaque forming methods, as shown in Fig1.

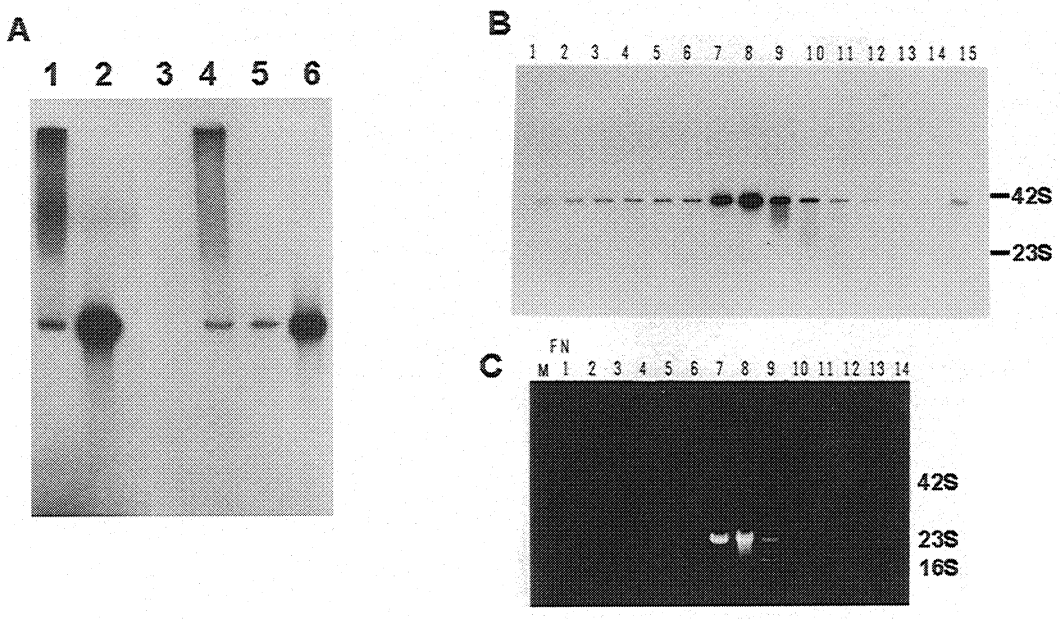


Fig. 4. Electrophoretic analysis of RNA products synthesized *in vitro*.
A: RNA synthesis *in vitro* using the crude membrane fraction were carried out in the absence (lane 1) or presence (lane 2) of NP40, and then ^{32}P RNA products were analyzed on the solubility in 2M LiCl. Lanes 3 and 5 were insoluble, and lanes 4 and 6 were soluble fractions.
B: ^{32}P RNA products were fractionated by the centrifugation using 15-30% sucrose density gradient.
C: *E.coli* ribosomal RNA was used as size marker in the fractionation by the ultra-centrifugation. 42S genomic RNAs were fractionated in the same fraction as *E. coli* rRNA by the ultra-centrifugation, since they formed duplex.

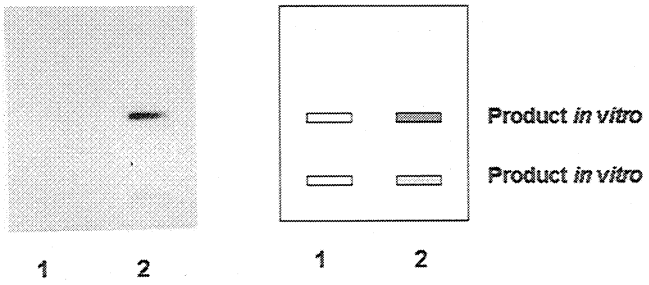


Fig. 5. Northern blot analysis of ^{32}P RNA *in vitro* products.
To determine polarity of ^{32}P RNA *in vitro* products, slot hybridization method was carried out. In the hybridization, both RNA fragments, JT18V (lane 1) and JT19V (lane 2) unlabeled were reacted with ^{32}P-RNA *in vitro* products used as probe. RNA fragment in upper side of figure contains 2 times higher than that of bottom.

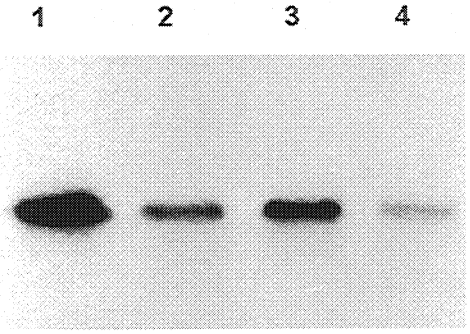


Fig. 6. Effect of antisera, anti- NS3 and -NS5 on *in vitro* RNA synthesis.
Preincubation of the crude membrane fraction and antisera was carried out prior to the addition of α-^{32}P-UTP. The procedure for *in vitro* reaction was the same as described in the text. Lane 1 (control); Products *in vitro* by treatment with preimmune sera at dilution 1:5. Lanes 2-3; treatment with anti-NS5 at dilution of 1:5 and 1:10, respectively. Lane 4; treatment with anti-NS3 at dilution of 1:5.

Localization of JEV-specific RNA in the infected cells.

To examine the localization of JEV-specific RNA in the cells, RNAs prepared from each of the subcellular fractions were subjected to Northern blot analysis. Fig. 2 shows the data of the hybridization using JT18V (right) and 19V (left) probes, respectively. In this experiment, the same sample filter was used and hybridized with both plus and minus probes. The 42S (+) RNA was abundantly in the crude membrane fraction (Fig. 2, lane 2). On the other hand, the amounts of the 42 S (-) RNA in the membrane fraction was almost same as those in the supernatant fraction (Fig.2, lanes 4 and 5). A large amount of small RNAs was observed in plus and minus hybridization shown in Fig. 2. Positive small 10S RNA was now clarified to contain the fragment at 3' end of genomic RNA (16) (data not shown).

Distribution of JEV-specific proteins in infected cells

To clarify the function of viral proteins, it is important to know the distribution of proteins in the cells. Fig.3A indicates the localization of viral proteins of 2 kinds of JEV strains (Nakayama and JaGAr01) labeled with ^{35}S-Met. Most of viral proteins were detected in nuclear and membrane fractions (Fig.3A, lanes 1, 2, 5 and 6). This nuclear fraction means not only nucleus but also nuclear membrane associated fraction. RNA dependent RNA polymerase (replicase) (NS5, 100KDa) and RNA helicase (NS3, 70KDa) were detected in the nuclear and membrane fractions. IFA indicated that both NS5 and NS3 were localized perinuclear fraction (Fig.3). NS5 appears to form some kinds of aggregates at the perinuclear site of the infected cells, as shown in Fig.3B, panel 1. NS3 also indicated the similar aggregates (Fig.3B, panel 2), which was different from the case of the distribution of E protein (Fig.3B, panel 3). E proteins were dispersed in the cytoplasm.

Viral RNA synthesis in vitro

In order to investigate viral RNA synthesis, it is useful to develop *in vitro* reaction system. By using crude membrane fractions from JEV-infected cells, we developed viral RNA synthesis system *in vitro*. As shown in Fig. 4, RNA products were clearly detected in cell-free fraction from JEV-infected cells at 48 hr p.i. In the presence of 0.7% NP-40 (Fig.4A, lane 2), larger quantities of RNA were synthesized. Next, RNA products were analyzed on solubility in LiCl, to identify ds- or ss-RNA. In the presence of 2M LiCl, most of RNA products were in the LiCl-soluble fraction (lanes 4 and 6), meaning dsRNA. By the ultra-centrifugation using sucrose density gradient 15-30%, products were fractionated at the position about 20S (Fig.4B and 4C). These indicate that *in vitro* RNA products are mainly of ds-RNA, may be replication form (RF). Next, in order to identify whether RNA product is positive RNA or negative, hybridization method using same probes JT18V (Fig.5, lane 1) and 19V (lane 2) was performed. Only JT19V probe could hybridized with ^{32}P-products *in vitro*, meaning that the products are positive strand (Fig.5).

Viral proteins influencing in vitro reaction of RNA synthesis

Viral proteins NS3 and NS5 are thought as helicase and RNA-dependent RNA polymerase, respectively and the important members of replication complex. In order to know the functions of NS3 and NS5 in viral RNA synthesis, we examined the effect of antisera, anti-NS3 and anti-NS5 on RNA synthesis *in vitro*. In the presence of antisera, anti-NS3 and anti-NS5, RNA synthesis level *in vitro* was decreased (Fig.6). The inhibitory effect of anti-NS3 on RNA syntheis was much more remarkable (Fig.6, lane 4). This was confirmed by repeated experiments.

Discussion

As described in the result, JEV-RNAs in the infected cells were clearly detected by the hybridization using the specific probes. The data indicated that the negative stranded JEV-RNA was synthesized before 6hr p.i. It is reasonable that the negative stranded RNA appears earlier than the positive stranded RNA during JEV infection. The facts that the positive JEV-RNAs (42S) were accumulated in the membrane fraction in the infected cells and it differed from the distribution of the negative RNAs suggest that the positive RNAs are continuously synthesized at the membrane, maybe endoplasmic reticulum (ER) and outer nuclear membrane during viral replication, as reported else about flavivirus replication (6). This fact seems to be related with the data of JEV-RNA synthesis *in vitro* that the membrane fractions have a high activity of RNA (mainly positive-stranded) synthesis (Fig.4).

Although several reports have been published describing flavivirus RNA synthesis, the mechanism of RNA synthesis is not yet fully understood (6-7,8,14). Here we described the *in vitro* RNA synthesis using the crude membrane fraction. The data indicated that RNAs produced *in vitro* were JEV specific, ds-RNA including positive strand labeled with ^{32}P. This *in vitro* RNA synthesis system, however, includes endogenous RNA template, so that most of the RNA polymerase reaction is probably a chain elongation. It is not obvious that the initiation occurs during the *in vitro* reaction (17).

The amounts of *in vitro* RNA products in the presence of non-ionic detergents such as NP40 and

Triton X 100 increased, and clear bands were detected in the agarose gel. It is thought that RNA synthesized *in vitro* formed duplex structure like replication intermediate (RI) or replication form (RF) under the native condition (6-7,18-19). Actually *in vitro* synthesized poliovirus RF (19) migrated slower than did genomic ssRNA in the native agarose gel. Most of products synthesized here, in the presence of NP40 seem to be RF, which migrates to the similar site with ssRNA (42S) in 1% native gel. The data that *in vitro* synthesized RNAs were in the LiCl-soluble fraction and fractionated at the similar site to rRNA of *E. coli* in the centrifugation also indicate that most of products are of dsRNA. The result that the clear band was observed in the agarose gel (Fig.4) is explainable as follows; It is likely that during the incubation in the presence of NP40, RI was degraded by some endogenous RNase and only RF was accumulated, since in the absence of NP40 some larger bands including RI were detected (Fig.4A).

It should be noted that the *in vitro* JEV-RNA synthetic activity was high in the crude membrane fraction including outer nuclear membrane. The study on West Nile virus RNA synthesis also showed that outer nuclear membrane contained RNA dependent RNA polymerase (20). Here, ^{35}S-labeling and immunofluorescence experiments indicated so much NS3 and NS5 proteins were accumulated in the crude nuclear and membrane fraction (Fig.3). It is obvious that NS3 is strongly associated with the nuclear and membrane fractions, although sequence data suggest that NS3 is hydrophilic and not a transmembrane protein (21). This phenomenon seems to be due to the function of hydrophobic and transmembrane protein NS4a/b (22). NS4 may work as an anchor for NS3. Actually we could see the NS4 band in the crude nuclear and membrane fractions as shown in the result (Fig.3A). Now it is well known that NS3 has protease activity at amino terminal region, and ATPase and RNA helicase in other region (21,23). Recently it has been reported that flavivirus (HCV) NS3 influences IFN pathway (24). Putative viral replication proteins NS3 and also NS5 actually work together in RNA replication (25), because anti-NS3 and anti-NS5 could inhibit RNA synthesis *in vitro* (Fig.6).

As previously described, even though recently JE cases in Japan are less than 10 in each year, still JE viruses circulate in wide area of Japan (4). In addition, it was found that recently isolated viruses including Ishikawa strains belonged to genotype I which differs from previous JEV strains (genotype III) (4,26). Now we need to be careful about the change in the pathogenesity of new genotype JEV. It is also necessary to develop new drug against JEV infection (27). To develop new drugs, it is important to elucidate the mechanism of virus reproduction including RNA replication.

Taken together the results here indicate that the membrane fractions have high activity for viral RNA synthesis, and contain a large amount of NS3, NS5 and other NS proteins which make the replication complex in the infected cells. In addition, we reported the sensitive probes for the detection of JEV specific RNAs. To know the mechanism of JEV-RNA synthesis, further study will be essential.

Acknowledgements

This study was supported in part by a Project Research from High-Technology Center (2005-8) and Grant for Collaborative Research (C2004-2 and C2005-2) of Kanazawa Medical University. The author is grateful to K. Hori and staffs in the Division of Molecular Oncology and Virology, Medical Research Institute for their assistance.

References

1. Williams DT, Wang L, Daniels PW et al: Molecular characterization of the first Australian isolate of Japanese encephalitis virus, the FU strain. J Gen Virol 2000; **81:** 2471-80.
2. Weissenbock H, Kolodziejek J, Url A et al: Emergence of Usutu virus, an African mosquito-borne flavivirus of the Japanese encephalitis virus group, central Europe. Emerg Infect Dis 2002; **8:** 652-6.
3. Solomon T, Dung NM, Wills B et al: Interferon alpha-2a in Japanese encephalitis: a randominised double-blind placebo-controlled trial. Lancet 2003; **361:** 821-6.
4. Takegami T, Ishak H, Miyamoto C et al: Isolation and molecular comparison of Japanese encephalitis virus in Ishikawa, Japan. Jpn J Infect Dis 2000; **53:** 178-9.
5. Takegami T, Washizu M, Yasui K: Nucleotide sequence at the 3' end of Japanese encephalitis virus genomic RNA. Virology 1986; **152:** 483-6.
6. Lindenbach BD, Rice CM: Flaviviridae: The viruses and their replication. Knipe DM (Eds), Virology (Fields) (4th ed), Philadelphia, Lippincott Williams & Wikins 2001; 991-1041.
7. Takegami T, Hotta S: In vitro synthesis of Japanese encephalitis virus (JEV) RNA: membrane and nuclear fractions of JEV-infected cells possess high levels of virus-specific RNA polymerase activity. Virus Res 1989; **13:** 337-50.
8. Takegami T, Hotta S: Synthesis and localization of Japanese encephalitis virus RNAs in the infected cells. Microbiol Immunol 1990; **34:** 849-57.
9. Hashimoto H, Nomoto A, Watanabe K et al: Molecular cloning and complete nucleotide sequence of the genome of Japanese encephalitis virus Beijin strain. Virus Genes 1988; **1:** 305-17.
10. Sumiyoshi H, Mori C, Fuke I et al: Complete nucleotide sequence of the Japanese encephalitis virus genome RNA. Virology 1987; **161:** 497-510.
11. Mangada MNM, Takegami T: Molecular characterization of the Japanese encephalitis virus representative immunotype strain JaGAr01. Virus Res 1999; **59:** 101-12.
12. Rice CM, Lenches EM, Eddy SR et al: Nucleotide sequence of yellow fever virus: Implication for flavivirus gene expression and evolution. Science 1985; **229:** 726-35.
13. Takegami T, Sahara M, Hotta S: A sensitive method for detection of flavivirus envelope protein and virus titration using a monospecific antiserum against Japanese encephalitis virus envelope protein. J Kanazawa Med Univ 1990; **15:** 73-9.
14. Takegami T, Miyamoto H, Nakamura H et al: Difference in the biological activity of the V3 envelope protein of two Japanese encephalitis virus. Acta Virol 1982; **26:** 321-27.
15. Zulkarnain E, Takegami T: Localization and functions of Japanese encephalitis virus nonstructural proteins NS3 and NS5 for viral RNA

synthesis in the infected cells. Microbiol Immunol 1993; **37:** 239-43.
16. Lin K, Chang H, Chang R: Accumulation of a 3'-terminal genome fragment in Japanese encephalitis virus-infected mammalian and mosquito cells. J Gen Virol 2004; **78:** 5133-38.
17. Chu PEG, Westaway EG: Characterization of Kunjin virus RNA-dependent RNA polymerase: Reinitiation of synthesis *in vitro* Virology 1987; **157:** 330-7.
18. Takegami T, Semler BL, Anderson CW et al: Membrane fractions active in poliovirus RNA replication contain VPg precursor polypeptides. Virology 1983; **128:** 33-47.
19. Takegami T, Kuhn RJ, Anderson CW et al: Membrane dependent uridylylation of the genome linked protein VPg of poliovirus. Proc Natl Acad Sci USA 1983; **80:** 7447-451.
20. Grun JB, Brinton NA: Dissociation of NS5 from cell fraction containing West Nile virus-specific polymerase activity. J Virol 1987; **61:** 3641-44.
21. Takegami T, Sakamuro R, Furukawa T: Japanese encephalitis virus nonstructural protein NS3 has RNA binding and ATPase activities. Virus Genes 1994; **9:** 105-12.
22. Tautz N, Kaiser A, Thiel H: NS3 serine protease of bovine viral diarrhea virus: Characterization of active site residues NS4A cofactor domain, and protease-cofactor interactions. Virology 2000; **273:** 351-63.
23. Utama A, Shimizu H, Hasebe F et al: Role of the DExH motif of the Japanese encephalitis virus and hepatitis C virus NS3 protein in the ATPase and RNA helicase activities. Virology 2000; **273:** 316-24.
24. Foy E, Li K, Wang C et al: Regulation of interferon regulatory factor-3 by the hepatitis C virus serine protease. Science 2003; **300:** 1145-8.
25. Uchil PD, Satchidanandam V: Characterization of RNA synthesis, replication mechanism, and in vitro RNA-dependent RNA polymerase activity of Japanese encephalitis virus. Virology 2003; **15:** 358-71.
26. Solomon T, Haolin N, Beasley DWC et al: Origin and evolution of Japanese encephalitis virus in southeast Asia. J Virol 2003; **77:** 3091-98.
27. Murakami M, Ota T, Nukuzuma S et al: Inhibitory effect of RNAi on Japanese encephalitis virus replication *in vitro* and *in vivo*. Microbiol Immunol 2005; **49:** 1047-56.

金医大誌（J Kanazawa Med Univ）30：357－364, 2005

肺扁平上皮癌の浸潤・転移の分子機構
－ Matrix metalloproteinase (MMP) の関与とその発現誘導機構 －

上田善道[1)]，島崎　都[1)]，Du Jiang[1)]，Guan Yang[1)]，佐藤勝明[1)]，
JianFei Guo[2)]，東光太郎[2)]，岡田保典[3)]，Kiran K. Chada[4)]，勝田省吾[1)]

要　約：肺癌の浸潤・転移機構の解明は臨床腫瘍学における最重要課題である。浸潤・転移は複数の異なる過程からなるが，蛋白分解酵素による基底膜をはじめとする細胞外基質成分の分解が各過程で必須である。本稿では，肺癌の主要亜型である肺扁平上皮癌の浸潤・転移機構における蛋白分解酵素，特にメタロプロテアーゼの関与に関し総説した。肺扁平上皮癌組織では，複数の matrix metalloproteinase (MMP) とその特異的インヒビターである tissue inhibitor of metalloproteinase (TIMP) の発現が亢進している。MMPs/TIMPs比の増加が腫瘍進展と予後に相関する。MMP-1, MMP-3など間葉系細胞特異的酵素が浸潤部腫瘍細胞で発現亢進し，特にMMP-3の分泌量は予後と関連する。その発現誘導には反応性間質細胞のみならず，浸潤腫瘍細胞が産生する basic fibroblast growth factor (bFGF/FGF2) が関与しており，更に上流では architectural factorであるhigh mobility group A2 (HMGA2/HMGIC) の発現による腫瘍細胞の epithelial-mesenchymal transition (mesenchymalization) が生じている。また肺扁平上皮癌では潜在型 MMP-2の活性化が亢進している。ここでも間葉系細胞特異的酵素であるmembrane type 1-MMP (MT1-MMP) とTIMP-2の浸潤性癌細胞における発現が生じている。これらに MMP-11, -12や ADAM-9, -12も加わり，腫瘍進展に適した微小環境が形成されている。メタロプロテアーゼとその誘導に関わる遺伝子群，特に浸潤・転移機構の最上流で働く癌細胞のmesenchymalizationにおいて重要な役割を演ずる HMGA2/HMGICが，肺扁平上皮癌の局所での制御，すなわち，悪性腫瘍の良性腫瘍化のための臨床腫瘍学上極めて重要な標的分子と考えられる。

キーワード：　肺扁平上皮癌，浸潤・転移，メタロプロテアーゼ，癌細胞間葉細胞化

緒　　言

人口の高齢化に伴い悪性腫瘍による死亡者数の増加はとどまるところを知らない。中でも肺癌は1998年以降男女とも悪性腫瘍による死因の首座を占め，年間5万人以上が肺癌により死亡している(1)。肺癌の特徴は，その強い浸潤・転移能にある。多くの肺癌症例は発見時に既に周囲組織への広範な浸潤，リンパ節や遠隔臓器への転移が存在し，外科的切除可能な症例は全体の30％に満たない。手術不可能な症例に対しては放射線照射あるいは抗癌剤による治療が行われるが，その予後は小細胞癌，非小細胞癌とも悲惨な状況である。手術可能な症例でも，術後の局所再発や転移発生率は高く，5年生存率も全体で約15～20％と決して満足できる数字は得られていない(2)。

転移は，細胞増殖，集塊からの離脱，移動，脈管内侵襲，免疫監視機構からの回避，標的臓器における微小塞栓形成，脈管外遊走，血管新生など複数の異なるステップからなる。がんの浸潤・転移に関する分子機構の研究が，新たな研究手段の開発・導入により，近年，急速な速度で展開されており，各ステップにおいて働く遺伝子群が明らかにされて来ている。さらに，これらの遺伝子群を標的とした分子標的治療が，ポストゲノム時代における創薬に関する方法論の進歩も重なり次々に開発され，腫瘍臨床に応用されてきている(3)。

蛋白分解酵素による基底膜をはじめとする細胞外基質の分解は，転移を構成する過程のいずれにおいても重要な要素である。近年，浸潤性増殖する癌細胞の膜表面における蛋白分解酵素の活性化機構の一端がin vitroの研究から明らかにされてきた。更に，蛋白分解酵素による細胞外基質分解による基質内に沈着し

[1)]金沢医科大学病理病態学
[2)]金沢医科大学放射線診断治療学
石川県河北郡内灘町大学1-1
[3)]慶応大学医学部病理学教室
[4)]Department of Biochemistry, University of Medicine and Dentistry of New Jersey-Robert Wood Johnson Medical School, USA
平成18年２月28日受理

ていた増殖因子の遊離 (マトリクライン)，生物活性を有する細胞外基質由来の分解産物の形成 (マトリカイン)，細胞膜表面に存在する種々のリガンドや受容体の分解などが協働して，浸潤部局所におけるがん細胞の増殖，アポトーシスからの回避，移動・遊走に有利な微小環境の形成に重要な働きを演ずる可能性が提唱されている(4,5)。

本稿では，肺癌の主要亜型の一つである肺扁平上皮癌の浸潤・転移における蛋白分解酵素，その中でも細胞外基質の限定分解において中心的役割を演ずることが知られているマトリックスメタロプロテアーゼ matrix metalloproteinase (MMP) に関して，1）肺扁平上皮癌の進展において働くMMP，2）発現誘導と活性化の分子機構，に注目し我々の最近の知見を中心に，文献的考察も加え論じたい。

1．マトリックスメタロプロテアーゼ (MMP)

1）メタロプロテアーゼ：MMPとADAMファミリー

生体中の蛋白分解酵素は，システインプロテアーゼ，セリンプロテアーゼ，メタロプロテアーゼの3種類に分類される。生体という中性域での最大活性とその広い基質特異性から，生理的および病的な細胞外基質の分解においてはメタロプロテアーゼが主要な役割を担うと考えられている。メタロプロテアーゼにはMMPとADAM (a disintegrin and matrix metalloprotease) の2種類が存在する(6)。

MMPの特徴として，1）活性中心に亜鉛イオンを有し，酵素活性にカルシウムイオンを必要とする，2）複数の細胞外基質成分を主要基質とするほか，増殖因子，ケモカイン，サイトカイン，細胞膜受容体などを分解する，3）多くはプロペプチドを有する潜在型で分泌され細胞外での活性化が必要である，4）組織特異的阻害分子 tissue inhibitor of metalloproteinase (TIMP) の存在が挙げられる。MMP分子はN-末端からプロペプチドドメイン，基質分解ドメイン，ヘモペキシンドメインの3つの基本ドメインにより構成されている。

MMPは異なる遺伝子からなる複数の分子種からなり，現在までに23種類がクローニングされている。MMPは分泌型と膜結合型に大きく分けられる。前者は，分子構造と基質特異性から，1）間質コラゲナーゼ群 (MMP-1, -8, -10：I，III型コラーゲンなど間質コラーゲンを主要基質とする)，2）ストロムライシン群 (MMP-3, -10：礎質成分であるプロテオグリカンを主要基質とする)，3）IV型コラゲナーゼ / ゼラチナーゼ群 (MMP-2, -9：ゼラチンと基底膜の主要構成成分である IV型コラーゲ

表1．ヒトMMP遺伝子ファミリー

名称	基質
分泌型MMP	
コラゲナーゼ群	
組織コラゲナーゼ(MMP-1)	I，II，III，VII，X型コラゲン，ゼラチン，プロテオグリカン，リンクプロテイン，エンタクチン，テネイシン，
好中球コラゲナーゼ(MMP-8)	I，II，III型コラゲン，ゼラチン，プロテオグリカン，リンクプロテイン
コラゲナーゼ-3 (MMP-13)	I，II，III，IV，IV，X，XIV型コラゲン，プロテオグリカン，フィブロネクチン，テネイシン
ゼラチナーゼ群	
ゼラチナーゼA(MMP-2)	ゼラチン，IV，V，VII，XI型コラゲン，ラミニン，フィブロネクチン，エラスチン，プロテオグリカン，リンクプロテイン
ゼラチナーゼB(MMP-9)	ゼラチン，III，IV，V型コラゲン，α2(I)コラゲン鎖、エラスチン，エンタクチン，リンクプロテイン
ストロムライシン群	
ストロムライシン-1(MMP-3)	プロテオグリカン，III，IV，IX，X型コラゲン，ラミニン，フィブロネクチン，ゼラチン，テネイシン，リンクプロテイン
ストロムライシン-2(MMP-10)	III，IV，V型コラゲン，フィブロネクチン，ラミニン，プロテオグリカン，リンクプロテイン
マトリライシン群	
マトリライシン(MMP-7)	プロテオグリカン，ゼラチン，フィブロネクチン，テネイシン，エラスチン，IV型コラーゲン，ラミニン，リンクプロテイン
マトリライシン-2(MMP-26)	IV型コラーゲン，フィブロネクチン，ゼラチン
Furin活性型群	
ストロムライシン-3(MMP-11)	フィブロネクチン，ラミニン，プロテオグリカン，ゼラチン
エピライシン(MMP-28)	カゼイン
その他の群	
メタロエラスターゼ(MMP-12)	エラスチン
RASI-1(MMP-19)	テネイシン，ゼラチン，ラミニン，フィブロネクチン，アグリカン
エナメライシン(MMP-20)	エナメル，ゼラチン
MMP-21	不明
MMP-27	不明
膜型MMP	
I型膜型群	
MT1-MMP(MMP-14)	I，II，III，型コラゲン，ゼラチン，プロテオグリカン，フィブロネクチン，ラミニン，
MT2-MMP(MMP-15)	フィブロネクチン，テネイシン，ナイドジェン，アグリカン，パールカン，ラミニン
MT3-MMP(MMP-16)	III型コラゲン，ゼラチン，フィブロネクチン
MT5-MMP(MMP-24)	プロテオグリカン
Glycosylphosphatidyl inositol(GPI)型群	
MT4-MMP(MMP-17)	ゼラチン，フィブロネクチン
MT6-MMP(MMP-25)	ゼラチン，IV型コラゲン，フィブリン，フィブロネクチン，ラミニン
II型膜型群	
MMP-23	ゼラチン

ンを基質とする)，4）マトリライシン群 (MMP-7, -26：ヘモペキシドメインを欠く最小単位分子)，5）furin活性型群 (MMP-11, -28: ストロムライシン－3などfurinにより細胞内で活性化され分泌される，6）その他の群 (MMP-12, -19, -20, 21-, -27: メタロエラスターゼやエナメライシンなど) に分類される。膜結合型 MMPは，プロペプチドドメインに furin認識配列をもち，C末端に細胞膜貫通ドメインを有することを特徴とする。更に，結合様式から，1）I型膜貫通型群 (MT1-MMP, MT2-MMP, MT3-MMP, MT5-MMP)，2）glycosylphosphatidyl inositol (GPI)型群 (MT4-MMP, MT6-MMP)，3）II型膜貫通型群 (MMP-23) に亜分類されている(表1)(6)。

ADAMは，ディスインテグリンドメインとメタロプロテアーゼドメインを合わせ持つ分子で，これまで40種類以上の分子種が同定されている。ADAMは，膜結合型とthrombospondinドメインを有し細胞外分泌される ADAMTSの2種類に大きく分けられる。生理的および病的状態における ADAMの関与に関する知見も近年徐々に集積されだしている。我々は，最近，ヒト椎間板ヘルニアの吸収にマクロファージから分泌される ADAMTS-4 (aggrecanase-1) が関わっていることを明らかにした(7)。

2）MMPの活性調節機構

MMPは病的状態だけでなく発生過程などの生理的状態でも重要な働きをする酵素であり，生体内では，1）遺伝子の転写，2）潜在型酵素の細胞外での活性化，3）TIMPによる活性阻害の3過程で，その酵素活性が厳重に調節されている。In vitroの実験結果から各 MMPの転写を upregulateする因子と down regulateする因子が報告されている(6)。しかし，癌浸潤部組織の局所で実際に遺伝子発現調節に関わる分子に関する証明は未だなされていない。分子内にfurin認識配列を有する stromelysin-3やmembrane type 1 MMP (MT1-MMP / MMP-14)などは例外的に細胞内で活性化されるが，ほとんどのMMPは潜在型で分泌され，細胞外で活性化されなければ働くことはできない。最近，細胞膜表面における潜在型MMPの活性化機構が注目されている(6,8)。

TIMPはMMP分子に対して1：1の関係で阻害する。活性化されたMMPが組織中で働くためにはモル比でTIMP分子数より多く存在する必要がある。TIMPに関しては，現在まで4種類の異なる分子種が同定されている。TIMPは活性型MMPの阻害のみならず，TIMP-1は潜在型MMP-9の，TIMP-2は潜在型MMP-2の活性化過程をも各々特異的に阻害することが知られている。興味深いことに，TIMP-2はC末端でMT1-MMPと，N末端で潜在型MMP-2と結合することが明らかになり，MT1-MMPによる細胞表面での潜在型 MMP-2の活性化にTIMP-2が重要な役割を果たしていることも近年明らかになった(8)。また，TIMP分子はMMPの阻害物質としての機能に加え，細胞増殖作用など多機能な分子であることが明らかになってきた(6)。

以上から，癌の浸潤・転移におけるMMPの関与を研究するには，単なる遺伝子・蛋白の発現解析だけでは十分ではなく，癌細胞浸潤部局所における各MMPの活性を示すと共に，遺伝子発現調節機構，潜在型MMPの活性化機構，TIMPとの不均衡に関する詳細な解析が必要となる(9)。

2．肺癌の進展における MMP/TIMPに関して

肺癌は治療対応性の違いから小細胞癌と非小細胞性肺癌に分けられる。小細胞癌は極めて高度の侵襲性を有し，発見時既に広範なリンパ節・遠隔転移を来していることがほとんどである。そのため手術適応になることが少なく，解析のための十分な組織採取が困難である。そのため，極めて重要な研究課題であるにもかかわらず人体材料を用いた詳細な検討はこれまでほとんどできていない。本稿では非小細胞性肺癌，特に肺扁平上皮癌の進展におけるメタロプロテアーゼの役割に関しこれまで明らかになっていることを自験データと文献的考察をまじえ総括する。なお，腺癌に関しては別の機会に論じる予定である。

1）肺扁平上皮癌の浸潤・転移におけるMMPの関与

我々は外科的に切除された肺扁平上皮癌49例に関し，新鮮腫瘍組織のexplantから無血清培養液中に24時間で分泌されるMMP-1, -2, -3, -9, TIMP-1, -2をELISAによる sandwich immunoassay法で解析した。肺扁平上皮癌では，1）MMP-1とMMP-3の分泌が病期進行と共に有意に増加する，2）MMP-3分泌が 0.2 nmol/ mg (乾燥重量) 以上の症例では，0.2 未満の症例と比べ有意に予後不良である，3）MMPs/TIMPs比が1.0以上の症例は，1.0未満の症例と比較し明らかに予後不良であった (表2)。進行肺扁平上皮癌ではMMPとTIMPの不均衡が生じMMP優位になっており，かつ，MMPs/TIMPs比が重要な予後因子となることが Kaplan Meyer解析で明らかになった。MMPの中でも，特に，間葉系細胞酵素である MMP-1，MMP-3の産生・分泌亢進が腫瘍進展と患者の予後に深く関わっていることもKaplan Meyer解析で示された。

非小細胞性肺癌のMMPに関するこれまでの研究では，gelatinase (IV型コラゲナーゼ)，特にMMP-9が組織中や血清で増加することが報告されている(10,11)。Sienelらは免疫染色でのMMP-9発現亢進が腫瘍進展や予後に関連すると報告している(11)。しかし，我々の検討では gelatinase/IV型コラゲナーゼ (MMP-2, -9) の分泌量は，非腫瘍部肺組織に比べ明らかに亢進していたが，臨床病理学的因子との関連は認められなかった。5）で後述するが gelatin zymography法を用いた解析でも潜在型 MMP-9の活性化程度と臨床病理学的因子間には関連はみられなかった。

MMPの特異的インヒビターである TIMP-1に関し，免疫染色での腫瘍組織での発現程度や血清中での値が，病期進行に伴ない亢進するという報告(12,13)と低下するという相反する報告(14)があり争点となっている。我々のデータは進行度とTIMP-1は逆相関し，かつ，MMPs/TIMPs比の増加が予後不良を示す

重要なパラメーターであることを示した。TIMP-2に比べTIMP-1分子が数十倍多いことを考慮すると，TIMP-1の発現低下が腫瘍進展に深く関わっていると考えられる。

今回検討しなかったが，その他のMMPでは，MMP-11 (stromelysin-3)，MMP-12 (metalloelastase) の発現亢進が扁平上皮癌を含めた非小細胞性肺癌の進展，術後再発や生命予後に関係することが最近報告された(15,16)。

2）進行性肺扁平上皮癌では反応性間質細胞と癌細胞の両者でMMP-1，-3遺伝子発現が亢進する

MMP-1やMMP-3は，元来，間葉系細胞が分泌する蛋白分解酵素である。「MMP-1，MMP-3を産生するのは癌細胞か反応性間質細胞か？」という疑問を解決するため，肺扁平上皮癌20例の浸潤部組織凍結切片を用いlaser captured microdissection (LCM)/real time reverse transcription-polymerase chain reaction (RT-PCR) 法にて癌細胞と反応性間質細胞におけるMMP-1，MMP-3の遺伝子発現を，各々別々に定量解析した。その結果，進行性肺扁平上皮癌では病期の進行と共に間質細胞のみならず浸潤性癌細胞においてもMMP-1，MMP-3両遺伝子が発現亢進することが示された。

肺扁平上皮癌の進展におけるMMP-3に関する詳細な検討はこれまでほとんど行われていない。しかし，皮膚，口腔底，食道発生の扁平上皮癌での検討では，MMP-3の発現は初期病変では間質細胞に限局するのに対して，進行に伴ない扁平上皮癌細胞でも発現することが報告されている(18－21)。Wrightらはマウス皮膚扁平上皮癌を用い分化型扁平上皮癌から高悪性の未分化紡錘形扁平上皮癌に転化するとMMP-3が発現誘導されることを観察している(22)。また，間質細胞におけるMMP-3の発現が乳癌の腫瘍発生を亢進させることも動物実験で明らかにされている(23)。MMP-3は線維性コラーゲン以外の多くのコラーゲン，プロテオグリカン，糖蛋白など多種類の細胞外基質成分を基質とするばかりでなく，最近，MMPを含めた潜在型プロテアーゼ (pro-MMPs，plasminogen etc)，増殖因子 (heparin binding EGF，insulin-like growth factor binding protein-3 etc)，細胞接着物質 (E-cadherin etc) などの非細胞外基質蛋白もその基質にすることが明らかにされてきた(5)。MMP-3は多様な基質を分解することで浸潤・転移に最適な微小環境を提供する扁平上皮癌の進展において極めて重要な分子の一つと考えられる(4)。さらに興味深いことに，MMP-3遺伝子のhaplotypeと肺癌発生の関係も最近明らかなりつつある(24)。

3）肺扁平上皮癌浸潤部におけるMMP-1，MMP-3遺伝子の発現亢進にはbFGFが関わっている

これまでのin vitroの実験から血管新生においても重要な因子であるbasic fibroblast growth factor (bFGF/FGF-2) がMMP-1，MMP-3遺伝子発現をupregulateすることが報告されている(25)。我々は「ヒト肺扁平上皮癌組織におけるMMP-1，MMP-3遺伝子発現亢進にもbFGFが関与しているのではないか？」という仮説のもと研究を進めた。免疫染色ではbFGFは血管基底膜に加え，肺扁平上皮癌細胞の細胞膜に一致した局在を認めた。この癌細胞細胞膜におけるbFGFは，強塩基やheparitinase前処理で消失し，細胞表面のsyndecan-1やperlecanなどheparansulfate

表2．肺扁平上皮癌組織からのMMP、TIMPsの分泌と臨床病理学的因子との関係

		n	MMP-1	MMP-2	MMP-3	MMP-9	TIMP-1	TIMP-2
Stage	I	(19)	0.71*	0.35	0.12*	0.68	2.18	0.07
	II	(6)	1.41	0.45	0.19	0.43	1.21	0.09
	III	(15)	1.45	0.44	0.28	0.67	1.69	0.06
	IV	(1)	2.04	0.43	0.43	0.29	1.55	0.04
LN metastasis								
	(-)	(21)	0.71*	0.36	0.13	0.67	1.87	0.07
	(+)	(20)	1.46	0.44	0.28	0.54	1.62	0.07
Prognosis								
	alive	(17)	0.86	0.36	0.13**	0.58	2.36	0.07
	dead	(14)	1.49	0.35	0.33	0.67	1.45	0.06

		n	MMPs/TIMPs
Stage	I	(19)	1.25*
	II	(6)	1.36
	III	(15)	1.72
	IV	(1)	1.14
Prognosis			
	alive	(17)	1.18*
	dead	(14)	1.74

* P<0.05, ** P<0.01

proteoglycanと非共有結合していることが示唆された。肺扁平上皮癌細胞はbFGF受容体 (FGFR-1, -2) を有することもRT-PCRと免疫染色で示された。bFGFも主に間葉系細胞により産生・分泌される増殖因子である。LCM / real time RT-PCRによる肺扁平上皮癌浸潤部局所におけるbFGFの産生細胞の同定と定量化，さらにMMP-1及び-3遺伝子発現との発現との相関を解析した。bFGFは進行性肺扁平上皮癌組織の反応性間質細胞に加え，浸潤部癌細胞においても遺伝子発現の亢進を認めた。さらに，間質細胞及び癌細胞におけるbFGF遺伝子発現と扁平上皮癌細胞におけるMMP-1, -3遺伝子発現には有意な相関を認めた。以上の結果から，ヒト肺扁平上皮癌浸潤部では，間質・癌細胞両者から産生されたbFGFがheparansulfate proteoglycanとの結合を介し細胞膜表面に捕獲され，受容体と結合し，その効果の一つとして扁平上皮癌細胞におけるMMP-1, MMP-3遺伝子の発現亢進に連なっていることが強く示唆された。

非小細胞性肺癌組織おけるangiogenesisが予後因子になるかどうかに関しては，測定法により異なる結果が報告され，未だ議論のあるところである(26)。最近我々は抗CD105抗体陽性の活動性血管数が非小細胞性肺癌の予後と相関することを明らかにしangiogenesisが非小細胞性肺癌の進展において必要なことを報告した(27)。一方，血管増生因子であるbFGFとVEGFの発現と予後に関してはその関連は明らかである。Shouら(28)，Iwasakiら(29)はbFGFの発現亢進は非小細胞性肺癌の予後因子の一つと報告している。また，血清中の可溶性syndecan-1とbFGF量が予後と関連することも示された(30)。癌細胞の浸潤前戦では，1）で述べたように複数のプロテアーゼが働いており，基底膜の限定分解や細胞膜表面分子のsheddingが亢進しており，その結果として侵襲性の高い肺癌では血清中のsyndecan-1やbFGFが上昇していると考えられる。さらに，非小細胞性肺癌ではbFGF及びFGF receptor発現と細胞増殖活性との関連も示されている(31)。以上の情報を総合すると，bFGFは複数の異なる経路を活性化し肺扁平上皮癌の進展をup regulationする重要な分子と考えられ，soluble FGFRsを用いた分子標的治療の基礎検討も既に始まっている(32)。

4）浸潤部における癌細胞のepithelial mesenchymal transition (mesenchymalization)にはHMGA2/HMGIC遺伝子発現誘導が関与する

扁平上皮癌は上皮系腫瘍である。「進行性肺扁平上皮癌の浸潤癌細胞においてなぜ間葉系細胞の機能分子であるbFGFやMMP-1, -3遺伝子が発現亢進するか？」が疑問となる。間質に浸潤すること自体が，上皮細胞でなく間葉系細胞特有の性質である。最近我々は，発生段階の間葉系細胞の増殖と分化の調節に重要な役割を有し，その遺伝子のknockoutはpigmy形質を来すことが知られているHMGA2 (HMGIC) 遺伝子(33)が肺扁平上皮癌細胞のepithelial mesenchymal transition (mesenchymalization) (34)に重要な役割を演じていること，さらに，HMGA2/HMGIC遺伝子発現が病期の進行と共に亢進することを示すデータを得て，さらに詳細に解析中である。HMGA2/HMGICはAT hook構造を介しDNAに結ることでDNAのconformationを変化させ転写因子の結合を促し，結合部周辺遺伝子の転写活性を亢進させる(35)。Miyazawaらはヒト口腔底扁平上皮癌浸潤部におけるHMGA2/HMGICの発現が予後と相関すると最近報告している(36)。肺癌でのHMGA2/HMGICの発現は1998年にRogallaら(37)により報告されたが，機能的な解析は未だなされていない。HMGA2/HMGICの発現に引き続き，mesenchymalizationのための重要な遺伝子群の発現が順次誘導されると推測される。今後どのような機構で肺癌細胞がepithelial-mesenchymal transitionしていくかに関し明らかになれば，この過程で働く遺伝子群の制御が浸潤・転移を押さ込み癌を局所にとどめる，すなわち悪性腫瘍を良性腫瘍化させる臨床腫瘍学上極めて重要な標的分子になると考え現在精力的に研究を行っている。

5）扁平上皮癌における活性化ゼラチナーゼ

腫瘍組織から分泌されるMMP-2, -9のsandwich immunoassayではリンパ節転移，病期の進行や生命予後との関連は見いだされなかった。しかし，ゼラチンザイモグラフィーならびにfilm in situ gelatin zymography (FIZ) 法により，肺扁平上皮癌組織では非腫瘍部肺組織と比較し潜在型MMP-2の活性化が有意に亢進していることが明らかになった。この潜在型MMP-2の活性化亢進は肺扁平上皮癌の早期から既に認められた。一方，潜在型MMP-9の活性化亢進と臨床病理学的因子間には明らかな関連は認められなかった。この結果はHrabecら(38)の報告と一致する。FIZ法により浸潤部腫瘍細胞に一致したゼラチン分解活性が示され，特異抗体を用いた免疫染色による蛋白とin situ hybridizationによるMMP-2, MT1-MMP, TIMP-2遺伝子の浸潤部癌細胞と反応性間質細胞での局在に加え，LCM / real time RT-PCRによる両者でのMMP-2, MT1-MMP, TIMP-2遺伝子発現の定量解析により，浸潤部扁平上皮癌細胞におけるMT1-MMP, TIMP-2遺伝子の発現亢進が潜在型MMP-2の活性化と有意に相関することが示された。この結果はTokurakuら(39)のデータを支持する。免疫染色におけるMMP-2の過剰発現が非小細胞性肺癌の予後と逆相関するという報告もあるが(40)，最近，Yamamuraら(41)は，MMP-2, MT1-MMPとも正常組織と比べ非小細胞性肺癌組織で発現は亢進しているが独立した予後因子ではなかったと報告している。MMP-2は発現量自体ではなく，活性化が肺扁平上皮癌の進展に重要と考えられ，そこでは浸潤部腫瘍細胞に発現されるMT1-MMP / TIMP-2が重要な役割を演ずると考えられる。MT1-MMPは，潜在型MMP-2の活性化だけでなく，細胞表面のCD44やsyndecan-1などのsheddingを介し細胞の遊走に有利な微小環境形成にも関わっている重要な分子であることが最近明らかにされ，分子標的治療のターゲットとして有望視されている(8)。

3．肺扁平上皮癌の浸潤・転移における ADAM: ADAM9, ADAM15が扁平上皮癌の進展に関与する

ADAMは，癌の浸潤・転移にとって重要なステップである蛋白分解と接着のための両ドメインを分子内に有するユニークな分子であり，癌の浸潤・転移機構で重要な役割を演ずる可能性が推測される。癌の浸潤・転移におけるADAMに関する研究が，近年，展開され始めた。肺癌では，ADAM9の過剰発現と脳転移の関係を示唆する in vitroでのデータが報告されている(42)。大腸癌の肝転移が，肝臓の伊東細胞が産生する分泌型ADAM9により up regulationされることも示されており，ADAM9は癌転移における主要分子の一つと考えられる(43)。肺癌臨床検体での検討では，ADAM15の非小細胞性肺癌，特に，肺腺癌での発現亢進がSchutzらにより免疫染色で示されたが，臨床病期や予後などとの関連は認められていない(44)。ADAM9とADAM15の発現亢進は胃癌でも報告されている(45)。ADAM分子が肺癌細胞表面に過剰発現されることにより，インテグリンを介した細胞・細胞間，細胞・細胞外基質間の接着，メタロプロテアーゼ作用による細胞外基質成分の分解や細胞表面シグナル分子の sheddingに引き続き，細胞内シグナルの増強と複数遺伝子の発現変化が生じ，癌細胞の増殖，浸潤に有利な微小環境の形成に関与することが推測される(4)。癌の局所での制御を考える場合の重要な標的分子の候補と考えられる。

最　後　に

以上，肺扁平上皮癌の浸潤・転移機構におけるプロテアーゼの役割とその発現誘導機序に関し総括した。プロテアーゼは基底膜など細胞外基質成分の分解だけでなく，浸潤部局所に存在する多くの細胞外および細胞表面の機能蛋白を分解あるいは遊離することで癌細胞の進展に有利な微小環境形成にかかわっている。さらに，癌細胞のepithelial-mesenchymal transition (mesenchymalization) が浸潤・転移に重要であり，そこに関わる遺伝子群の一端をようやく捕らえた所である。局所での癌制御，すなわち，癌の良性腫瘍化という新たな分子標的治療の確立を目指し，精力的に研究を進めていきたい。

研究のための資料提供をいただいた金沢医科大学肺癌研究グループ，特に栂　博久呼吸器機能治療学教授と佐久間　勉　呼吸機能治療学教授，四方裕夫　心血管外科学助教授，bFGF抗体を供与いただいたゲノム医科学講座の吉竹佳の助教授，西川克巳元教授，Film in situ zymographyを提供いただいた富士フィルム株式会社足柄研究所の根守良一博士に感謝いたします。なお，この研究は文部科学省科学研究費 (13670192, 17590320, 16591232, 国11694311)，金沢医科大学共同研究　C2004-2から助成を受けた。

文　献

1. 横瀬智之: 肺癌の疫学と発癌因子. 末舛恵一 (監修) 肺癌の最新医療, 東京, 先端医療技術研究所, 2003; 6-9.
2. 福岡正博: 肺癌化学療法の課題と展望. 末舛恵一 (監修) 肺癌の最新医療, 東京, 先端医療技術研究所, 2003; 219-27.
3. Hanahan D, Weinberg RA: The hallmarks of cancer. Cell 2000; **100**: 57-70.
4. Liotta LA, Kohn EC: The microenvironment of the tumour-host interface. Nature 2001; **441**: 375-9.
5. Egeblad M, Werb Z: New functions for the matrix metalloproteinases in cancer progression. Nat Rev Cancer 2002; **2**: 161-74.
6. Okada Y: Proteinases and matrix degradation. In Harris ED, Budd RC, Genovese MC, Firestein GS, Sargent JS (Eds), Kelley's Textbook of Rheumatology (7th ed), Pholadelphia, Elsevier Saunders, 2005; 63-81.
7. Hatano E, Fujita T, Ueda Y et al: Expression of ADAMTS-4 (Aggrecanase-1) and involvement in regression of human lumbar disc hernia. Spine (2006, in press).
8. Itoh Y, Seiki M: MT1-MMP: A potent modifier of pericellular microenvironment. J Cell Physiol 2006; **206**: 1-8.
9. Ueda Y, Imai K, Tsuchiya H et al: Matrix metalloproteinase 9 (gelatinase B) is expressed in multinucleated giant cells of human giant cell tumor of bone and is associated with vascular invasion. Am J Pathol 1996; **148**: 611-22.
10. Yang SF, Hsieh YS, Lin CL et al: Increased plasma levels of urokinase plasminogen activator and matrix metalloproteinase-9 in nonsmall cell lung cancer patients. Clin Chem Acta 2005; **354**: 91-9.
11. Sienel W, Hellers J, Morresi-Hauf A et al: Prognostic impact of matrix metalloproteinase-9 in operable non-small cell lung cancer. Int J Cancer 2003; **20**: 647-51.
12. Aljada IS, Ramnath N, Donohue K et al: Upregulation of the tissue inhibitor of metalloproteinase-1 protein is associated with progression of human non-small-cell lung cancer. J Clin Oncol 2004; **22**: 3218-9.
13. Ylisirnio S, Hoyhtya M, Turpeenniemi-Hujanen T: Serum matrix metalloproteinase-2, -9 and tissue inhibitors of metalloproteinases-1, -2 in lung cancer - TIMP-1 as a prognostic marker. Anticancer Res 2000; **20**: 1311-6.
14. Hoikkala S, Paakko P, Soini Y et al: Tissue MMP-2/TIMP-2-complex are better prognostic facters than serum MMP-2, MMP-9 or TIMP-1 in stage I to III lung carcinoma. Cancer Lett (2006, in press).
15. Hofmann HS, Hansen G, Richter G et al: Matrix metalloproteinase-12 expression correlates with local recurrence and metastatic disease in non-small cell lung cancer patients. Clin Cancer Res 2005; **11**: 1086-92.
16. Delebecq TJ, Porte H, Zerimech F et al: Overexpression level of stromelysis 3 is related to the lymph node involvement in non-small cell lung cancer. Clin Cancer Res 2000; **6**: 1086-92.
17. Kerkela E, Saarialho-Kere U: Matrix metalloproteinases in tumor progression: focus on basal and squamous cell skin cancer. Exp Dermatol 2003; **12**: 106-25.
18. Shima I, Sasaguri Y, Kusukawa J et al: Production of matrix metalloproteinase-2 and metalloproteinase-3 related to malignant behavior of esophageal carcinoma: a clinicopathologic study. Cancer 1992; **70**: 2747-53.
19. Kusukawa J, Sasaguri Y, Morimatsu M et al: Expression of matrix metalloproteinase-3 in stage I and II squamous cell carcinoma of the oral cavity. J Oral Maxillofac Surg 1995; **53**: 530-4.
20. Ariola K, Johansson N, Kariniemi AL et al : Human collagenase-3 is expressed in malignant squamous epithelium of the skin. J Investig Dermatol 1997; **109**: 225-31.
21. Kerkela E, Ala-aho R, Lohi J et al: Patterns of stromelysin-2 (MMP-10) and MT1-MMP (MMP-14) expression in epithelial skin cancers. Br J Cancer 2001; **84**: 659-69.
22. Wright Jh, McDonnell S, Portella G et al: A switch from stromal to tumor cell expression of stromelysin-1 mRNA associated with the conversion of squamous to spindle carcinomas during mouse skin tumor progression. Mol Carcinog 1994; **10**: 207-15.
23. Sternlicht MD, Lochter A, Sympson CJ et al: The stromal proteinase MMP-3/stromelysin-1 promotes mammary carcinogenesis. Cell 1999; **98**: 137-46.
24. Su L, Zhou W, Asomaning K et al: Genotypes and haplotypes of matrix metalloproteinase-1, 3 and 12 genes and the risk of lung cancer. Carcinogenesis (2006, in press).
25. Pintucci G, Yu PJ, Sharony R et al: Induction of stromelysin-1 (MMP-3) by fibroblast growth factor-2 (FGF-2) in FGF-2 -/- microvascular endothelial cells requires prolonged activation of extracellular signal-regulated kinases-1 and -2 (ERK-1/2). J Cell Biochem 2003; **90**: 1012-25.
26. Giatromanolaki A: Prognostic role of angiogenesis in non-small cell lung cancer. Anticancer Res 2001; **21**: 4373-82.
27. Guo J, Higashi K, Ueda Y et al: Microvessle density: the orrelation with FDG uptake and the prognostic impact in lung adenocarcinomas. J Nucl

Med 2006; **47:** 419-25.
28. Shou Y, Hirano T, Gong Y et al: Influence of angiogenetic factors and matrix metalloproteinases upon tumour progression in non-small-cell lung cancer. Br J Cancer 2001; **85**: 1706-12.
29. Iwasaki A, Kuwahara M, Yoshinaga Y et al: Basic fibroblastic growth factor (bFGF) and vascular endothelial growth factor (VEGF) levels, as prognostic indicators in NSCLC. Eur J Cardiothorac Surg 2004; **25**: 443-8.
30. Makitaro R, Alfthan H, Kinnula V et al: Soluble syndecan-1 and serum basic fibroblast growth factor are new prognostic factors in lung cancer. Cancer Res 2002; **62**: 5210-7.
31. Berger W, Setinek U, Mohr T et al: Evidence for a role of FGF-2 and FGF receptors in the proliferation of non-small cell lung cancer cells. Int J Cancer 1999; **83**: 415-23.
32. Ogawa T, Takayama K, Takakuwa N et al: Anti-tumor angiogenesis therapy using soluble receptors: enhanced inhibition of tumor growth when soluble fibroblast growth factor receptor-1 is used with soluble vascular endothelial growth factor receptor. Cancer Gene Ther 2002; **9**: 633-40.
33. Xiang X, Benson KF, Chada K: Mini-mouse: disruption of the pygmy locus in a transgenic insertinal mutant. Science 1990; **247**: 967-9.
34. Thiery JP: Epithelial-mesenchymal transitions in tumour progression. Nat Rev Cancer 2002; **2**: 442-54.
35. Wolffe A: Architectural factors. Science (Wash.DC) 2001; **204**: 1100-1.
36. Miyazawa J, Mitoro A, Kawashiri S et al: Expression of mesenchyme-specific gene HMGA2 in squamous cell carcinomas of the oral cavity. Cancer Res 2004; **64**: 2024-9.
37. Rogalla P, Drechsler K, Schoeder-Babo W et al: HMGIC expression patterns in non-small lung cancer and surrounding tissue. Anticancer Res 1998; **18**: 3327-30.
38. Hrabec E, Strek M, Novwak D et al: Activity of type IV collagenases (MMP-2 and MMP-9) in primary pulmonary carcinomas: a quantative analysis. J Cancer Res Clin Oncol 2002; **128**: 197-204.
39. Tokuraku,M, Sato,H, Murakami S et al:Activation of the precursor of gelatinase A/72 kDa type IV collagenase/MMP-2 in lung carcinomas correlates with the expression of membrane-type matrix metalloproteinase (MT-MMP) and with lymph node metastasis. Int J Cancer 1995; **64**: 355-9.
40. Passlick B, Sienel W, Seen-Hibler R et al: Overexpression of matrix metalloproteinase 2 predicts unfavorable outcome in early-stage non-small cell lung cancer. Clin Cancer Res 2000; **6**: 3944-8.
41. Yamamura T, Nakanishi K, Hoiroi S et al: Expression of membrane-type 1 matrix metalloproteinase and metalloproteinase-2 in nonsmall cell lung carcinomas. Lung Cancer 2002; **35**: 249-55.
42. Sintani Y, Higashiyama S, Ohta M et al: Overexpression of ADAM9 in non-small cell lung cancer correlates with brain metastasis. Cancer Res. 2004; **64**: 4190-6.
43. Mazzocca A, Coppari R, De Franco R et al: A secreted form of ADAM9 promotes carcinoma invasion through tumor-stromal interactions. Cancer Res 2005; **65**: 4728-38.
44. Scutz A, Hartig W, Wobus M et al: Expression of ADAM15 in lung carcinomas. Virchows Archiv 2005; **446**: 421-9.
45. Carl-McGrath S, Lendeckel U, Ebertt M et al: The disintegrin - metalloproteinases ADAM9, ADAM12, and ADAM15 are upregulated in gastric cancer. Int J Oncol 2005; **26**: 17-24.

Involvement of Metalloproteases in Progression of Squamous Cell Carcinoma of the Lung

Yoshimichi Ueda[1], Miyako Shimazaki[1], Du Jiang[1], Guan Yang[1], Katsuaki Sato[1], JianFei Guo[2], Kotaro Higashi[2], Yasunori Okada[3], Kiran K. Chada[4], Shogo Katsuda[1]

[1]*Department of Pathophysiological and Experimental Pathology, Kanazawa Medical University, Uchinada, Ishikawa 920-0293, Japan*

[2]*Department of Radiology, Kanazawa Medical University, Uchinada, Ishikawa 920-0293, Japan*

[3]*Keio University, Department of Pathology,*

[4]*Department of Biochemistry, University of Medicine and Dentistry of New Jersey-Robert Wood Johnson Medical School, USA*

This article reviewed roles of proteases and mechanism of their upregulation in progression of squamous cell carcinoma of the lung (SCC). In various kinds of proteases, metalloproteases, matrix metalloproteinase (MMP) and ADAM (a disintegrin and metalloprotease), play a central role in the proteolysis of extracellular matrix (ECM) components during invasion of SCC. ELISA sandwich immunoassays of secretary MMP-1, -2, -3, -9 and tissue inhibitor of MMP (TIMP)-1 and -2 from tumor tissues to serum-free culture media showed increased MMPs/TIMPs ratios in advanced SCCs. Production of mesenchymal MMPs, such as MMP-1 and -3, was dominantly elevated in the advanced SCCs. MMPs/TIMPs ratio and value of MMP-3 were reversely correlated with survival of patients. Laser-captured microdissection (LCM)/real time reverse transcription-polymerase chain reaction (RT-PCR) revealed a relation between mRNA expressions of basic fibroblast growth factor (bFGF)/FGF2 gene, not only in stromal cells but also tumor cells of advanced stages, and those of MMP-3 gene in invading tumor cells. While secretion of gelatinases, either MMP-2 or -9, was not related to progression of SCC, activation of proMMP-2 was enhanced even in the early stage. Combined analyses of gelatinolytic activities by FIZ, immunostaining, ISH and LCM/real time RT-PCR clearly showed that overexpressions of MT1-MMP and TIMP-2, which are also mesenchymal features, in the invasing tumor cells are involved in the activation of proMMP-2. In the epithelial mesenchymal transition (mesenchymalization) of invading SCC cells, HMGA2/HMGIC gene was expressed, and the mRNA expression was correlated with the tumor progression. In summary, epithelial mesenchymal transition induces upregulations of mesenchymal MMPs (MMP-1, -3, -11, -12, MT1-MMP) and TIMP-2, partly through bFGF/FGF2 stimulation, forming an adequate microenvironment for invasion of SCC cells at front of tumor invasion. HMGA2/HMGIC, involved in the mesenchymalization of SCC cells, may be one of the target molecules for local regulation of SCC of the lung.

Key Words: squamous cell carcinoma of lung, matrix metalloproteinase (MMP), basic fibroblast growth factor (bFGF/FGF2), high mobility group A2 (HMGA2/HMGIC), epithelial-mesenchymal transition (mesenchymalization)

1．研究課題名：悪性神経膠腫の分化誘導と遺伝子治療に関する研究（研究番号 C2004-3）

2．キーワード：1）悪性神経膠腫（glioblastoma）
2）HMGI-C
3）分化誘導（induction of differentiation）
4）遺伝子治療（gene therapy）

3．研究代表者：飯塚秀明・医学部・教授・脳脊髄神経治療学（脳神経外科学）
研究分担者：伊達孝保・医学部・教授・ゲノム医科学（生化学）
野島孝之・医学部・教授・病態診断医学（臨床病理学）
栗原孝行・総合医学研究所・講師・共同利用部門

4．研 究 目 的

中枢神経に原発する腫瘍のなかで、悪性神経膠腫の治療成績は未だ不良である。現在、摘出手術・放射線・化学療法が治療の主体であるが、5 生率は 20%以下であり新たな治療法の開発が望まれる。なかでも膠芽腫は、他の分化型神経膠腫と比べ最も予後が悪く、また分化型神経膠腫が膠芽腫へ悪性転化することも稀ならず経験される。腫瘍発生に関わる遺伝子発現の機構には、①特定の配列に結合する転写因子によるものと、②転写活性化ドメインを持たず、DNA に結合してその framework を変化させることにより転写複合体を形成させ、その結果転写の亢進を促す architectural factor によるものとがある。このような Architectural factor のひとつとして、High mobility Group I-C （HMGI-C）蛋白が知られている。間葉系腫瘍ではすでに *HMGI-C* 遺伝子の転位が確認されており、この因子が細胞の分化および腫瘍発生やその分化度に深く関与している可能性が示唆されている。

膠芽腫は、星細胞が起源とされているが、いわゆる脱分化が著しく、細胞起源を特定できる形態学的特徴は失われ、著しい多型性を呈し、細胞の分化に破綻をきたした状態であることは知られている。申請者らは、原発性脳腫瘍の摘出生検組織で、分化型星細胞腫では HMGI－C 遺伝子、蛋白質が過剰発現しているのに対し、膠芽腫ではその発現がほとんどみられないことを見出した。即ち、HMGI-C 蛋白・遺伝子などの細胞分化に関与する architectural factor の異常が生じていることが予想され、逆に、膠芽腫細胞に HMGI-C 蛋白を発現させ分化した星細胞へと誘導することによる治療の可能性が期待できる。本研究は、星細胞腫などの分化型神経膠腫と膠芽腫における HMGI-C 蛋白・遺伝子の発現の差異を検討し、膠芽腫の遺伝子治療への臨床応用の可能性について検討することを目的とする。

5．研 究 計 画

本研究では以下のような計画をたてた。

①臨床生検および剖検摘出組織を用いて、さらに多数例で、分化型神経膠腫（星細胞腫・上衣腫・乏突起膠腫）と、膠芽腫（分化型神経膠腫から悪性転化した膠芽腫例を含む）における HMGI-C 蛋白質・遺伝子発現の差異を検討する。

②培養膠芽腫細胞株へ *HMGI-C* 遺伝子を導入し、*HMGI-C* 遺伝子を導入した膠芽腫細胞の細胞生物学的特徴を *in vitro* で検討する。

③膠芽腫親細胞株と *HMGI-C* 遺伝子導入膠芽腫細胞株をヌードマウスの脳に移植し、造腫瘍能、増殖能、浸潤能などを比較する。

④臨床での遺伝子治療のための準備を行う。

6．研 究 成 果

HMGI-C に対する抗体を作成するために、HMGI-C とグルタチオン-S-トランスフェラーゼ（GST）の融合蛋白質を大腸菌で発現させ、GST とグルタチオンとの結合を利用して GST-HMGI-C 融合蛋白質を精製した。GST-HMGI-C 融合蛋白質をウサギに免疫し、GST-HMGI-C 融合蛋白質に対する抗体を作成した。この抗体を用いて、免疫組織化学法および Western blot 法で、摘出生検および剖検組織での HMGI-C 蛋白質の発現を調べた。その結果、ほとんどの膠芽腫では HMGI-C 蛋白質の発現がみられないのに対し、分化型神経膠腫の大部分では HMGI-C 蛋白質が発現していることが確認できた。RT-PCR による解析から、HMGI-C 蛋白質発現消失例では、*HMGI-C* 遺伝子の転写が起こっていないことが確認された。さらに、経過中に分化型神経膠腫から膠芽腫へ悪性転化した 2 症例では、初回摘出組織では *HMGI-C* mRNA の発現がみられたにも拘らず、悪性転化後はその発現がみられなくなっていた。

HMGI-C の発現を欠いた膠芽腫細胞株 T98G に、HMGI-C 発現プラスミドを導入し、テトラサイクリン濃度依存性に HMGI-C を発現する細胞株、T98GHMGI-C、を樹立した。光学顕微鏡による観察では、T98GHMGI-C 細胞と親細胞 T98G の間で明らかな形態の差は認められなかった。また細胞の増殖速度、さらには FACS による細胞周期 profile についても大きな差がみられなかった。

7．研究の考察・反省

本研究における多数例の解析から、分化型神経膠腫の多くは HMGI-C 蛋白質の発現を認めるが、膠芽腫の多くではその発現が消失している事がわかった。この蛋白質発現の消失は、*HMGI-C* mRNA 転写の消失によることが、RT-PCR による解析から確認されている。このことは、HMGI-C 抗体を用いた免疫組織染色法が、分化型神経膠腫と膠芽腫との鑑別に利用できることを示している。さらに、分化型神経膠腫から膠芽腫へ悪性転化した2症例で、悪性転化後 *HMGI-C* 発現が消失したことから、悪性化の過程で *HMGI-C* 遺伝子に何らかの変異が発生した可能性が示唆される。本研究では、*HMGI-C* 遺伝子の

転位まで解析できなかったが、もし間葉系腫瘍に報告されているような転位が確認されれば、神経系腫瘍と間葉系腫瘍に共通する機序として、癌細胞の脱分化の原因を考えるうえで重要な所見となると考える。

HMGI-C を発現する膠芽腫細胞株 T98GHMGI-C を樹立した。T98GHMGI-C 細胞と親細胞 T98G の間で明らかな増殖速度の差が認められなかったことより、HMCI-C は細胞増殖抑制効果をもたないことが分かった。また、光学顕微鏡レベルでは、両細胞株の間で明らかな形態の差は認められず、HMCI-C 発現による膠芽腫細胞株の分化誘導を示す所見は得られなかった。しかし、HMCI-C と細胞分化の関係については、電子顕微鏡による形態観察や膠芽腫細胞の分化抗原の発現検討などを待たないと、はっきりした結論は出せないと考える。

本研究期間には到達できなかったが、今後も計画に従って、両細胞株をそれぞれヌードマウスの脳内に移植し、造腫瘍能、増殖能、浸潤能などを比較検討していきたい。

1．研究課題名：モデル動物を利用した肥満・高脂血症の発がんへの関与とその阻止に関する研究
（研究番号 C2004-4）

2．キーワード：1）大腸がん（colon cancer）
2）肥満（obesity）
3）高脂血症（hyperlipidemia）
4）動物モデル（animal model）
5）脂肪肝（fatty liver）

3．研究代表者：杉江茂幸・医学部・教　授・腫瘍病理学（病理学Ⅰ）
分担研究者：甲野裕之・医学部・助教授・腫瘍病理学（病理学Ⅰ）
：堤　幹宏・奈良医科大学・医学部・教　授・医療情報学
：吉谷新一郎・医学部・助手・消化器外科治療学（消化器外科学）
：久野　壽也・岐阜大学・医学部・助手・腫瘍病理学

4．研究目的

高脂肪食に代表される食事の欧米化や運動不足などが大腸などでの発がんに対して促進的に働くことが疫学や動物実験から示唆されている。同時に、これらライフスタイルの変化は昨今の肥満者の急増をもたらしており、さらに肥満はいわゆる生活習慣病の根底をなす病態とされている。肥満の発症に関与する遺伝子群(以下肥満関連遺伝子と称する)にはレプチンやperoxisome proliferator-activated receptor γ(PPARγ)などがあり、エネルギー倹約遺伝子とも称される。　一般に大腸がんには生活習慣病に属するべき側面が多々あると思われるが、大腸発がんの危険因子としての肥満の重要性あるいは大腸発がんと肥満関連遺伝子との関係についての解析には乏しいのが現状である。一方、肝臓においては、肥満に伴う脂肪肝はよく知られるが、肥満、高脂血症からの非アルコール性脂肪性肝炎nonalcoholic steatohepatitis (NASH)の増加が近年報告され、肝硬変、肝癌へ進行することやその発症は高率であるとの報告も見られる。従って、肥満者・高脂血症患者における肝がんの発生を阻止することは重要と考えられる。　そこで、本研究では、柑橘類化合物（auraptene、nobiletin）についてレプチン受容体欠損のため高レプチン血症を伴うdbマウスや高脂血症を伴うMinマウスを用いて、azoxymethane（AOM）誘発大腸発がん及びdiethylnitrosamine(DEN) ないし 2-amino-3,8-dimethylimidazo[4,5-f]quinoxaline(MeIQx)誘発肝発がんに対する修飾効果を検討する。これにより、肥満阻止、大腸・肝発がん阻止のための基礎的資料を得、柑橘類化合物（auraptene、nobiletin）の肥満に係る発がん阻止物質としての可能性を探る。

5．研究計画

（実験１）遺伝子改変マウス、遺伝子改変動物や疾患モデルマウスを用いて自然発症肝癌発症の有無を問うと共に、発がん剤による肝癌発症状況の検討と本研究のモデルとして利用可能かを検討する。その結果から、本研究モデルの作成を検討する。（杉江）

（実験２）①db/db マウスにおける azoxymethane（AOM）誘発大腸発がんモデルの作製：レプチン受容体欠損の db/db マウスを用いて、AOM 誘発による大腸がん発生を検討した。②Min マウスにおける大腸発がんモデルの作製：Apc 遺伝子に異常をもつ Min マウスは加齢とともに小腸ポリープが発生するが、大腸腫瘍の発生は稀である。そこで、大腸炎誘発物質である dextran sodium sulfate（DSS）を投与することにより、短期間にかつ高率に大腸がんを発生させる新たなモデルの作製を試みた。（甲野、吉谷）

（実験３）OLETF ラットおよびその lean control ラットである LETO ラットを 56 週間飼育した。各群を２週間隔で屠殺し、肝組織については、HE 染色と Azan 染色およびαSMA、Ⅳ型コラーゲンとアディポネクチンの発現を免疫組織化学的に染色し、内臓脂肪については脂肪細胞のサイズ、アディポネクチンの発現の程度について検討を行った。また、血液学的には、AST、ALT、アディポネクチン、TNF-α、HOMA-IR、総コレステロール、中性脂肪、遊離脂肪酸、Fe、フェリチン、Ⅳ型コラーゲン、ヒアルロン酸を測定した。（堤）

（実験４）151 匹の F344 雄ラットを７群に分け、1 群から５群に対し N-nitrosomethylbenzylamine（NMBA）を 0.5mg ずつ週３回５週間皮下投与した。１群には基礎食、2，３群に対して 5%発酵玄米食を、4、5 群に対して 10%発酵玄米食をそれぞれ initiation 期と post-initiation 期に混餌投与した。6 群は 10%発酵玄米食、7 群は基礎食を通期で与え、コントロールとした。実権開始後 27 週で全匹犠牲死とし、腫瘍発生率、腫瘍多発性、増殖活性を病理組織学的に検討した。加えて、肝臓の cytochrome P450 および b5 を測定した。（久野）

6．研究成果

（実験１）６週齢雄 H2-ras mice に MeIQx、DEN を 200mg/Kg 体重の胃内強制投与を行い、系時的に安楽死、肝および全身諸臓器の検討を行った。

①MeIQx 投与群、投与１週間後（５匹）：肝を含め全身諸臓器に著変を認めなかった。　16 週後（５匹）：MeIQx の腫瘍標的臓器である肝には著変を認めなかった。他の標的臓器の大腸にも著変を認めなかったが、前立腺に過形成を認めた。MeIQx 投与によって、前立腺過形成が認められたことから、前立腺発がんモデルへの展望があると考えられた。②DEN 投与群、投与１週間後（５匹）：び漫性ではないが、門脈域を中心に肝細胞の空胞変性が著明に認められた。　16 週後（５匹）：DEN のメインターゲットである肝には核の異型性を強く認めたが、NASH に類似する空胞変性所見や腫瘍発生はなかった。全例、前胃に扁平上皮癌を認め、１例は、著明な腹空内転移を認めた。

（実験２）①db/db マウスは実験開始 20 週以降から死亡例が認められ、観察期間中に大腸

発がんの発生を認めなかった。そこで、大腸がんの前駆病変である aberrant crypt foci (ACF)およびb-catenin accumulated crypt (BCAC)を指標とした動物実験モデルを検討した。個体あたりの ACF および BCAC 発生個数は野生型に比べ有意に増加することが確認された。②Min マウスは DSS を投与による大腸炎誘発により、実験開始後３ー４週という短期間に大腸がんが高率に発生することを見いだした。

（実験３）OLETF および LETO のいずれのラットにおいても飼育 56 週目まで順調に体重は増加した。OLETF ラットの体重は、LETO ラットに比べ重い傾向にはあったが、推計学的に両郡間で差は認めらなかった。また、肝重量も OLETF ラットでは、LETO ラットに比べ重い傾向にはあったが、推計学的に両郡間で差は認められず、体重 100g 当たりの肝重量においても同様であった。しかし、OLETF ラットでは、飼育 12 週目から脂肪肝が認められた。肝の脂肪沈着の程度は、飼育 12 週目には 10%程度であったが、飼育 20 週目には 50%にまで増加した。しかし、その後は増加せず、飼育 40 目からは、脂肪沈着の程度はむしろ減少する傾向にあった。一方、コントロールラットである LETO では、脂肪肝は認められなかった。血液学的には、AST、ALT、総コレステロール、アディポネクチン、Fe、フェリチン、Ⅳ型コラーゲン、およびヒアルロン酸値は両群間で明らかな差は認められなかった。また、HOMA-IR と中性脂肪は、飼育開始前より OLETF ラットでは LETO ラットよりも有意に高値であった。しかし、OLEFT ラットについて、飼育開始時期の 6 週齢と脂肪肝発生時期の 12 週齢についてみると、インスリン、HOMA-IR および中性脂肪は、12 週齢で有意に高値を示した。

（実験４）食道腫瘍の発生率は基礎食群に対してpost-initiation期に5%、10%の玄米発酵食を投与した群ではそれぞれ有意な減少を認めた。同時に腫瘍多発性においても同様の結果を得た。前腫瘍性病変と考えられる異型性編膜の発生率、多発性において発酵玄米食投与により有意に抑制された。非腫瘍部粘膜の細胞増殖活性は、発酵玄米食投与群で有意に減少していた。発癌物質を活性化する肝臓中のCytochrome P450とb2の量は群間に差を認めなかった。

７．研究の考察・反省

（実験１）H2-ras mice を用い、肝におけるモデル系確立のための検索を行った。その結果、DEN 投与急性期には、肝に脂肪変性を認めたが、持続性ではなく、また、肝が標的臓器である MeIQx 投与においては、明らかな変化が認められなかったことから、この動物を用いる場合、投与法の変更や、これに加えて他の物質の持続的投与などの実験系の改良が必要と考えられた。H2-ras mice は、比較的早期に前胃に扁平上皮癌ができてしまうため、肝における長期的変化を追いにくいと考えられた。さらに他の遺伝子改変動物や疾患モデルマウスを用いた実験系で検討する予定である。

（実験 2）①レプチン受容体欠損により肥満を示す db/db マウスでは、大腸がんの前駆病

変の ACF および BCAC の発生個数が+/+マウスに比べ有意に増加しており、大腸発がん過程において、肥満が促進的に作用する可能性が示唆された。しかし、今回試みた実験では AOM のみの投与では大腸がんの誘発が出来なかったことから、今後は実験プロトコルの変更あるいは異なる系統の肥満マウスを用いて大腸発がんの誘発を試みる必要がある。また、db/db マウスにおける前がん病変発生個数と血中レプチン量、インスリン量、グルコース量との関連性に関しては明確な結果を得ていないので、さらなる検討を行う必要がある。② Min マウスでは DSS のみの大腸炎の誘発により、きわめて短時間に高率の腫瘍が発生することから、すでに Apc 遺伝子などのがん抑制遺伝子に以上が存在する場合には、炎症反応によるプロモーション作用のみにより大腸腫瘍が発生する可能性が示唆された。今後、腫瘍発生の経時的な変化に伴う炎症関連物質の発現および血中脂質成分濃度の変化との関連性について検討を行う必要がある。

（実験３）今回、OLETF ラットがどのような経過で内臓肥満、2 型糖尿病、高脂血症および脂肪肝を発生するかについて検討したが、血糖値に変化がなくてもインシュリン抵抗性を示すか、血中の中性脂肪の値が高値を示す頃に肝に脂肪沈着が始まることが明らかになった。今後、このモデルを用い、抗高脂血症薬を投与することにより脂肪肝を予防しうるかの検討を行うことにする。

（実験４）発酵玄米食のラット食道腫瘍に対するの効果を検討した。post-initiation 期投与発酵玄米食が NMBA 誘発ラット食道腫瘍の発生を抑制し、そのメカニズムは NMBA によって修飾を受けた粘膜の増殖活性を抑制し、腫瘍抑制効果を来すと推察された。実験前の予測とほぼ一致した結果を得た。さらに、多臓器での修飾効果を検討したい。

８．研究発表

Sugie S., Vinh P.Q., Rahman K.M. W., Ushida J.[3], Kohno H., Suzuki R., Hara A., Quang L.B., Tanaka T. and Mori H.:Suppressive effect of 1,4-phenylene diisothiocyanate on *N*-butyl-*N*-(4-hydroxybutyl)nitrosamine-induced urinary bladder carcinogenesis in male ICR mice. Int J Cancer, 2005; 117: 524-530. (MLDB)

Sugie S, Ohnishi M, Ushida J, Yamamoto T, Hara A, Koide A, Mori Y, Kohno H, Suzuki R, Tanaka T, Wakabayashi K, Mori H.:Effect of alpha-naphthyl isothiocyanate on 2-amino-3-methylimidazo[4,5-b]pyridine (PhIP)-induced mammary carcinogenesis in rats. Int J Cancer, 2005; 115: 346-350. (MLDB)

Kohno H, Suzuki R, Sugie S, Tanaka T.: β-Catenin mutations in a mouse model of inflammation-related colon carcinogenesis induced by 1,2-dimethylhydrazine and dextran sodium sulfate. Cancer Sci, 2005; 96: 69-76. (MLDB)

Suzuki R, Kohno H, Sugie S, Tanaka T.: Dose-dependent promoting effect of dextran sodium sulfate on mouse colon carcinogenesis initiated with azoxymethane. Histol Histopathol , 2005; 20: 483-492. (MLDB)

Tanaka T, Suzuki R, Kohno H, Sugie S, Takahashi M, Wakabayashi K.: Colonic adenocarcinomas rapidly induced by the combined treatment with 2-amino-1-methyl-6-phenylimidazo[4,5-b] pyridine and dextran sodium sulfate in male ICR mice possess b-catenin gene mutations and increases immunoreactivity for b-catenin, cyclooxygenase-2 and inducible nitric oxide synthase. Carcinogenesis, 2005; 26: 229-238. (MLDB)

Suzuki R, Kohno H, Sugie S, Tanaka T.: Sequential observations on the occurrence of preneoplastic and neoplastic lesions in mouse colon treated with azoxymethane and dextran sodium sulfate. Cancer Sci, 2004; 95: 721-727. (MLDB)

Sugie S., Kuno T., Kawabata K., Shimada S., Mori H.:Suppressing effects of yeast, magnesium(Mg), zink(Zn), Mg-enriched yeast and Zn-enriched yeast on azoxymethane-induced aberrant crypt foci in rats. Carcinogenesis and Modification of Carcinogenesis, 2005; 177-185.

Suzuki R, Kohno H, Sugie S, Yamaguchi F., Kataoka, S., Ariga T., Tanaka T.:A polyisoprenylated benzophenone garcinol inhibits azoxymethane-induce rat colon carcinogenesis. Carcinogenesis and Modification of Carcinogenesis, 2005; 187-198.

Tanaka T, Suzuki R, Kohno H, Sugie S, Kominami T.: The modifying effects of hesperidin glycoside on chemically-induced tongue and colon carcinogenesis in F344 rats. Carcinogenesis and Modification of Carcinogenesis, 2005; 213-227.

Tanaka T, Kohno H, Suzuki R, Hata K, Sugie S, Niho N, Sakano K, Takahashi M, Wakabayashi K.: Dextran sodium sulfate strongly promotes colorectal carcinogenesis in $Apc^{Min/+}$ mice: Inflammatory stimuli by dextran sodium sulfate results in development of multiple colonic neoplasms. Int J Cancer, 2006; 118: 25-34. (MLDB)

Int. J. Cancer: **117**, 524–530 (2005)
© 2005 Wiley-Liss, Inc.

Suppressive effect of 1,4-phenylene diisothiocyanate on *N*-butyl-*N*-(4-hydroxybutyl)nitrosamine-induced urinary bladder carcinogenesis in male ICR mice

Shigeyuki Sugie[1]*, Pham Quang Vinh[2], K.M. Wahidur Rahman[3], Jun Ushida[3], Hiroyuki Kohno[1], Rikako Suzuki[1], Akira Hara[3], Le Bach Quang[2], Takuji Tanaka[1] and Hideki Mori[3]

[1]*Department of Pathology, Kanazawa Medical University, Uchinada, Ishikawa, Japan*
[2]*Department of Urology, 103 University Hospital, Military Academy of Medicine, Thanh tri, Hanoi, Vietnam*
[3]*Department of Tumor Pathology, Gifu University School of Medicine, Gifu, Japan*
[4]*Department of Parasitology, 103 University Hospital, Military Academy of Medicine, Tranhtri, Hanoi, Vietnam*

The modifying effects of dietary administration of 1,4-phenylene diisothiocyanate (DITC) on *N*-butyl-*N*-(4-hydroxybutyl) nitrosamine (BBN)-induced urinary bladder carcinogenesis during the initiation and post-initiation phases were examined in male ICR mice. Five-week-old animals were divided into 5 groups. Groups 1–3 were given BBN (500 ppm) in drinking water for 6 weeks starting at age 6 week. Mice in Group 2 were given the diet containing 100 ppm DITC for 8 weeks during the initiation phase, starting 1 week before BBN exposure. Animals in Group 3 were fed the experimental diet for 24 weeks during the post-initiation phase starting 1 week after the cessation of BBN exposure. Mice in Group 4 were given only the diet containing the test compound, and those in Group 5 were given the basal diet alone throughout the experiment (32 weeks). The frequency of bladder lesions, neoplasms, dysplasia and hyperplasia, was analyzed histopathologically. The cell-proliferation activity estimated by the 5-bromodeoxyuridine labeling index (BrdU-LI), and cell cycle progression by counting cyclin D1-positive cell ratios were compared among the groups using immunohistochemistry. Administration of DITC in the initiation phase reduced significantly the incidence of urinary bladder carcinoma and dysplasia. The frequencies of any lesions of urinary bladder were not reduced by DITC in post-initiation phase. Dietary exposure of this agent in initiation phase reduced significantly both BrdU-LI and cyclin D1-positive cell ratios in any bladder lesions. Administration of DITC in post-initiation phase also significantly reduced BrdU-LI in bladder neoplasms and hyperplasia and cyclin D1-positive cell ratios in urinary bladder carcinoma as well as dysplasia. These results suggest that dietary DITC could be a preventive agent against BBN-induced bladder carcinogenesis in mice when fed during the initiation phase.
© *2005 Wiley-Liss, Inc.*

Key words: chemoprevention; DITC; BBN; cyclin D1; BrdU labeling index; urinary bladder carcinogenesis

Epidemiologic studies suggest that the consumption of green and yellow vegetables has an inverse relationship with cancer risk.[1–7] Organosulfur compounds that are present abundantly in a group of cruciferous vegetables or allium species have been shown to possess cancer chemopreventive properties.[8–10] Especially, isothiocyanates (ITC) are versatile chemopreventive agents in many animal systems.

Cancer prevention studies of our group have demonstrated that benzyl isothiocyanate (BITC) inhibit methylazoxymethanol (MAM)-acetate induced intestinal carcinogenesis and diethylnitrosamine (DEN) induced hepatocarcinogenesis in rats, and sinigrin reduced 4-nitroquinoline 1-oxide-induced rat tongue carcinogenesis and DEN-induced hepatocarcinogenesis.[11–14] We also found that BITC reduced not only unscheduled DNA synthesis (UDS) but also replicative DNA synthesis (RDS), induced by some genotoxic carcinogens, *e.g.*, 2-acetylaminofluorene (AAF), MAM acetate, 9,10-dimethyl-1,2-benzanthracene (DMBA), and DEN.[15] Other ITC, including β-naphthyl isothiocyanate, α-naphthyl isothiocyanate, phenethyl isothiocyanate (PEITC), 6-phenylhexyl isothiocyanate (PHITC), phenyl isothiocyanate (PITC) and phenylpropyl isothiocyanate (PPITC) have been reported to possess strong anticarcinogenic effects in animal models of cancer.[8–10]

1,4-Phenylene diisothiocyanate (DITC, Fig. 1) is one of ITC and chemically derived from mustard powder. DITC has been known as "Bitoscanate" or "Jonit," and widely used clinically for the treatment of parasitic diseases in Africa and the southeast Asia.[16–22] We have found the chemopreventive effect in hepatocarcinogenesis (unpublished data), however, it is not clear the effects in carcinogenesis.

In epidemiological study of urinary bladder cancer, it has been reported that high consumption of vegetables and fruit are protective against bladder cancer.[23–26] Michaud *et al.*[23] indicated that high cruciferous vegetable consumption might reduce bladder cancer risk.

In rodents, however, carcinogenicity of allyl isothiocyanate has been reported in urinary bladder.[27] National Toxicology Program has reported that allyl isothiocyanate was carcinogenic for male F344/N rats, causing transitional-cell papillomas in the urinary bladder. Evidence for associating allyl isothiocyanate with subcutaneous fibrosarcomas in female F344/N rats was equivocal. Allyl isothiocyanate was not carcinogenic for B6C3F1 mice of either gender.[27,28]

Recently, promotion effects of PEITC and BITC in urinary cancer induced by multiorgan carcinogenesis including *N*-butyl-*N*-(4-hydroxybutyl) nitrosamine (BBN), and initiation effect of PEITC on urinary bladder carcinogenesis have been reported.[29,30] Nishikawa *et al.*[31] investigated the effects of phenethyl and 6-phenylhexyl isothiocyanates (PEITC and PHITC) on urinary bladder tumorigenesis initiated with BBN in Wister rats. In their study, PEITC treatment did not affect the BBN-induced bladder tumorigenesis and PHITC suppressed bladder tumor development. Okazaki *et al.*[32] found that simultaneous treatment of BITC and BBN inhibits BBN-induced urinary bladder carcinogenesis in F344 rat. Those findings suggest that modifying effects of ITC on the urinary bladder carcinogenesis are depended to the difference of rodent species and strains, chemicals and treatment schedule.

We wondered how other ITC, particularly DITC, exert their modulating effect on chemically induced urinary bladder carcinogenesis in rodents. Inhibitory effects of ITC on cell cycle progression of human cancer cells have been observed.[33] Some investigators have reported the overexpression of cyclin D in neoplasia on urinary bladder carcinogenesis of rats.[34–36] In our previous experiment, its overexpression could be found in BBN-induced hyperplasia,

Grant sponsor: Ministry of Education, Culture, Sports, Science and Technology of Japan; Grant sponsor: Kanazawa Medical University; Grant number: C2004-4.
***Correspondence to:** Department of Pathology, Kanazawa Medical University, 1-1 Daigaku, Uchinada, Ishikawa, 920-0293 Japan.
Fax: +81-76-286-6926. E-mail: sugie@kanazawa-med.ac.jp
Received 2 November 2004; Accepted after revision 21 March 2005
DOI 10.1002/ijc.21233
Published online 31 May 2005 in Wiley InterScience (www.interscience.wiley.com).

UICC
global cancer control
Publication of the International Union Against Cancer

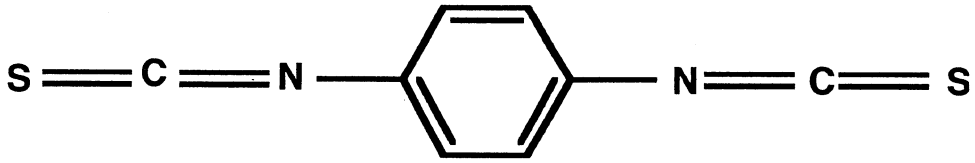


FIGURE 1 – Molecular structure of 1,4-phenylene diisothiocyanate (DITC).

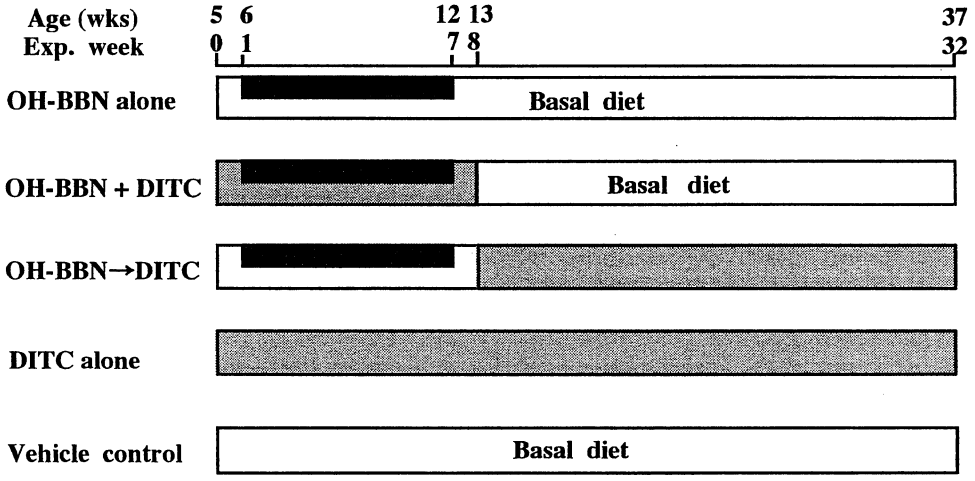


FIGURE 2 – Experimental design.

dysplasia, papilloma and carcinoma in mice and silymarin reduced the expression of cyclin D1.[37]

In our study, modifying effects of DITC was examined in BBN-induced mouse urinary bladder carcinogenesis and analyzed the cell positive ratio for cyclin D1 and 5-bromodeoxyuridine labeling index (BrdU-LI) in normal, preneoplastic and neoplastic lesions of urinary bladder in BBN-treated mice using immunohistochemistry.

Material and methods

Animals, diets and chemicals

A total 150 5-week-old male ICR mice were purchased from Japan SLC Inc. (Hamamatsu, Japan). All animals were housed in plastic cages with wood chips in an air-conditioned room at 23 ± 2°C (SD), 50 ± 10% relative humidity, under a 12-hr light/dark cycle. BBN was obtained from Tokyo Chemical Industry Co. Ltd, Tokyo, Japan. Powdered CE-2 (Clea Japan, Inc., Tokyo, Japan) was used as a basal diet throughout the experiment. BBN was purchased from Tokyo Chemical Industry Co. Ltd, Tokyo, Japan. DITC was purchased from Sigma (St. Louis, MO). Experimental diet was prepared twice a week. The drinking water containing carcinogen was prepared every other day. All the animals were allowed free access to food and water. We attempted to define the maximum tolerated dose (MTD) of DITC, and determined the level with 100 ppm (unpublished data).

Experimental procedure

The mice were randomly divided into 5 groups (Fig. 2). After 1 week quarantine, animals in Groups 1–3 (44 mice, 35 mice and 29 mice, respectively) were given BBN (500 ppm) in the drinking water for 6 weeks. Mice in Group 2 were given the diets containing 100 ppm DITC, starting 1 week before BBN exposure until the end of Week 8, then they were maintained on the basal diet for subsequent 24 weeks. Group 3 was fed food mixed with DITC, starting 1 week after cessation of the BBN treatment and kept until the termination. Group 4 (18 mice) was not exposed to the carcinogen and fed the diet with the test compounds throughout the experiment. Group 5 (24 mice) was given the basal diet and tap water without BBN throughout the experiment, serving as an untreated control. All mice were weighed once a week for the first 8 weeks, and once a month for the subsequent period until the end. The experiment was terminated at 32 weeks, and all animals were killed under ether anesthesia. For measurement of the BrdU-incorporating nuclei, BrdU solution (Sigma-Aldrich Co., Ltd., Tokyo) was injected i.p. at a dose of 50 mg/kg body weight 1 hr before each death. At autopsy, urinary bladders were fully inflated with 10% buffered formalin, fixed for 5 hr and embedded in paraffin for histopathological evaluation on hematoxylin and eosin-stained sections according to the criteria described by Fukushima *et al.*[38] Other organs including liver, kidney, lungs, stomach and intestine were fixed in 10% buffered formalin, embedded in paraffin blocks, and processed by conventional histological methods using H&E staining.

Immunohistochemical staining

For the evaluation of the cell proliferation and cell cycle activity of the epithelium cells, BrdU and cyclin D1 immunohistochemistry was carried out according to the methods described previously with some modifications.[17] Briefly, 3 μm paraffin-imbedded sections were deparaffinized with 3 changes of xylene and hydrated using a graded series of alcohol. Before staining, slides for cyclin D1 immunohistochemistry were incubated in 1 mM EDTA (pH 8.0) at 121°C twice in an autoclave, 5 min each to effect antigen retrieval, then exposed overnight to 1:100 diluted cyclin D1 mouse monoclonal antibody (Novocastra Laboratories, Newcastle upon Tyne, UK), thereafter slides were developed by the avidin-biotin-peroxidase complex method. Slides for BrdU immunohistochemistry were incubated in 3% hydrogen peroxide at room temperature for 30 min to block endogenous peroxidase and then tissue sections were treated with 2N HCl at room temperature for 20 min and neutralized with Tris-buffered saline. Subsequently, they were incubated with 0.02% actinase E (Kaken, Tokyo, Japan) at 37°C for 20 min. After incubation with normal horse serum at room temperature for 30 min, they were exposed overnight at 4°C with mouse monoclonal antibody to BrdU

TABLE I – BODY, LIVER AND RELATIVE LIVER WEIGHTS IN EACH GROUP

Group	Treatment	No. of mice	Body weight (g)	Liver weight (g)	Relative liver wt (%)
1	BBN	44	50.2 ± 3.6[1,2]	2.9 ± 0.52	5.75 ± 0.5[3]
2	BBN + DITC	35	50.7 ± 5.0	3.0 ± 0.50	5.69 ± 0.5
3	BBN → DITC	29	52.4 ± 5.8	3.1 ± 0.64	6.05 ± 0.9
4	DITC	18	51.9 ± 7.4	3.0 ± 0.50	5.61 ± 0.6
5	Vehicle control	24	53.4 ± 3.8	3.1 ± 0.58	6.12 ± 0.2

[1]Mean ± SD.–[2]Significantly different from Group 5 by Welch's *t*-test ($p < 0.002$).–[3]Significantly different from Group 5 by Student's *t*-test ($p < 0.001$).

TABLE II – INCIDENCE OF TUMORS IN THE BLADDER OF MICE

Group	Treatment	No. of mice examined	No. of mice (%) with papilloma	TCC[1]
1	BBN	44	2 (5)	17 (39)
2	BBN + DITC	35	4 (11)	5 (14)[2]
3	BBN → DITC	29	2 (7)	9 (31)
4	DITC	18	0 (0)	0 (0)
5	Vehicle control	24	0 (0)	0 (0)

[1]TCC, transitional cell carcinoma.–[2]Significantly different from Group 1 by Fisher's exact probability test ($p < 0.02$).

TABLE III – INCIDENCE OF HYPERPLASIA AND DYSPLASIA IN THE BLADDER OF MICE

Group	Treatment	No. of mice examined	No. of mice (%) with hyperplasia			No. of mice (%) with dysplasia
			Total	SH[1]	PN[1]	
1	BBN	44	43 (98)	39 (88)	30 (70)	30 (68)
2	BBN + DITC	35	32 (91)	29 (83)	13 (37)[2]	15 (43)[3]
3	BBN → DITC	29	23 (79)	21 (72)	20 (69)	22 (75)
4	DITC	18	0 (0)	0 (0)	0 (0)	0 (0)
5	Vehicle control	24	0 (0)	0 (0)	0 (0)	0 (0)

[1]SH, simple hyperplasia; PN, papillary or nodular hyperplasia.–[2]Significantly different from Group 1 by χ^2 test ($p < 0.01$).–[3]Significantly different from Group 1 by Fisher's exact probability test ($p < 0.05$).

(Amersham Bioscience Corp., Piscataway, NJ) diluted 1:100. The subsequent steps were the same as those for cyclin D1 staining. Cells were considered positive for cyclin D1 or BrdU when definite nuclear staining was identified. To score each parameter, the positive cell ratio for cyclin D1 (or BrdU-LI) was determined by randomly observing 500 epithelial cells under 400× magnification (over 50 fields). Positive cell ratios (or LI) were calculated as numbers per 100 cells. Overexpression of cyclin D1 in preneoplastic lesions and tumors was defined as positive when nuclear staining of >5% of nuclei was evident.[39]

Statistical analysis

Body, liver and relative liver weights, the incidence of lesions, BrdU-LI or cyclin D1 positive cell ratios between groups were evaluated with Fisher's exact probability test, χ_2 test, Welch's *t*-test or Student's *t*-test.

Results

General observations

No mice died during the experiment period. Mean intakes of food were constant and similar among the groups during the whole treatment period (4.65–5.12 g/day/mouse). Mean body, liver and relative liver weights (g/100 g body wt) in all groups are shown in Table I. Mean body and relative liver weights of Group 1 were significantly less than those of Group 5 ($p < 0.002$ and $p < 0.001$ respectively). During our study, administration of DITC provoked neither clinical signs of toxicity nor poor condition of animals.

Incidence of tumors and preneoplastic lesions of urinary bladder

Tumors were developed only in the urinary bladder of mice in BBN-treated groups (Groups 1–3). Macroscopically, no abnormal lesions were found in other organs. The incidences of urinary bladder tumors are summarized in Table II. In Group 1, bladder papillomas and carcinomas were recognized in 2/44 mice (5%) and 17/44 mice (39%), respectively. The incidence of urinary bladder carcinoma of Group 2 was significantly smaller than that of Group 1 ($p < 0.02$). The incidence of carcinoma of Group 3 was smaller than that of Group 1, but statistical significance was not found. The incidences of preneoplastic lesions in all groups are described in Table III. The incidences of papillary or nodular hyperplasia of Group 2 were lower than of Group 1 ($p < 0.01$), and those of dysplasia of the Group 2 were also significantly lower than of group 1 ($p < 0.02$). Incidence of dysplasia of Group 3 was higher than that of Group 1, but statistical significance was not found. No abnormalities were found microscopically as well as macroscopically in urinary bladder of mice without BBN treatment (Groups 4 and 5).

Cyclin D1 positive cell ratios

The intensity of cyclin D1 staining was generally strong among the various lesions of the urinary bladder, and weak in simple hyperplasias and papillary or nodular (PN) hyperplasias. As summarized in Table IV, cyclin D1 overexpression was observed in various types of lesions. Cyclin D1 positive ratios of hyperplasia and papilloma of Group 2 were significantly smaller than that of Group 1 ($p < 0.001$ and $p < 0.005$ respectively). Cyclin D1 positive ratios of Groups 2 and 3 were significantly smaller than those of Group 1 for both of dysplasia ($p < 0.001$) and transitional cell carcinoma, ($p < 0.001$).

BrdU-LI

Data for BrdU-LI are summarized in Table V. BrdU-LI of hyperplasia of both Groups 2 and 3 were significantly lower than those of Group 1 ($p < 0.001$). Similarly, BrdU-LI of dysplasia of Group 2 and that of papilloma of both Groups 2 and 3 were respectively lower than of Group 1 ($p < 0.05$, $p < 0.001$ and $p < 0.05$). BrdU-LI of carcinoma of Groups 2 and 3 were significantly lower than those in Group 1 ($p < 0.001$ and $p < 0.005$ respectively).

TABLE IV – CYCLIN D1-POSITIVE RATIO (%) IN THE NORMAL TRANSITIONAL EPITHELIUM AND VARIOUS LESIONS OF THE BLADDER

Group	Treatment	Normal epithelium	Non-lesional areas	HP[1]	DYS[1]	PAP[1]	TCC[1]
1	BBN	ND	3.22 ± 0.54[2]	20.5 ± 2.2	30.6 ± 3.5	39.9 ± 7.5	53.1 ± 5.3
2	BBN + DITC	ND	3.01 ± 0.45	16.7 ± 2.6[3]	26.0 ± 5.8[4]	34.8 ± 6.6[5]	42.6 ± 4.4[3]
3	BBN → DITC	ND	3.28 ± 0.33	19.9 ± 3.3	27.1 ± 4.1[4]	39.6 ± 8.1	48.4 ± 1.8[3]
4	DITC	0.87 ± 0.53	ND	ND	ND	ND	ND
5	Vehicle control	0.35 ± 0.82	ND	ND	ND	ND	ND

[1]HP, hyperplasia; DYS, dysplasia; PAP, papilloma; TCC, transitional cell carcinoma; ND, not determined.–[2]Mean ± SD.–[3]Significantly different from Group 1 by Welch's test ($p < 0.001$).–[4]Significantly different from Group 1 by Student's t-test ($p < 0.001$).–[5]Significantly different from Group 1 by Student's t-test ($p < 0.005$).

TABLE V – BrdU-LABELING INDEX (%) IN THE NORMAL TRANSITIONAL EPITHELIUM AND VARIOUS LESIONS OF THE BLADDER

Group	Treatment	Normal epithelium	Non-lesional areas	HP[1]	DYS[1]	PAP[1]	TCC[1]
1	BBN	ND	1.35 ± 0.28[2]	3.08 ± 0.06	4.26 ± 1.62	4.04 ± 1.99	31.46 ± 7.29
2	BBN + DITC	ND	1.40 ± 0.45	2.33 ± 0.15[3]	3.16 ± 2.71[4]	2.06 ± 1.54[3]	16.62 ± 8.53[3]
3	BBN → DITC	ND	1.29 ± 0.34	2.85 ± 0.10[3]	3.98 ± 3.83	2.92 ± 1.44[4]	25.20 ± 8.63[5]
4	DITC	0.35 ± 0.66	ND	ND	ND	ND	ND
5	Vehicle control	0.49 ± 0.77	ND	ND	ND	ND	ND

[1]HP, hyperplasia; DYS, dysplasia; PAP, papilloma; TCC, transitional cell carcinoma; ND, not determined.–[2]Mean ± SD.–[3]Significantly different from Group 1 by Student's t-test ($p < 0.05$).–[4]Significantly different from Group 1 by Welch's test ($p < 0.001$).–[5]Significantly different from Group 1 by Welch's test ($p < 0.005$).

Discussion

The results of our present study demonstrated that DITC is a promising agent for bladder cancer chemoprevention. Dietary DITC effectively inhibited urinary bladder carcinogenesis in mice initiated by BBN, as shown by reducing the incidences of neoplastic and preneoplastic urinary bladder lesions in mice given DITC during initiation phase of carcinogenesis. This is the first report on chemopreventive effect of DITC in BBN-induced urinary bladder carcinogenesis. Feeding diet mixed with this compound also suppressed the expression of cell cycle and cell proliferation biomarkers.

A number of ITC have been shown to be capable of inhibiting chemically-induced tumorigenesis.[9–15] Particularly impressive results have been obtained in animal carcinogenesis models of digestive organs.[11–14] Mechanisms of their chemopreventive effects have been proposed. One of them has been suggested the inhibition of cell growth and modulation of the cell cycle.

The effects of ITC on cell growth and cell cycle progression were studied in HeLa cells and reported that AITC, BITC and PEITC inhibited cell growth. These results suggest that ITC delayed the cell cycle progression of HeLa cells, leading to inhibition of cell growth.[33] Similar effects on cell growth and the cell cycle were reported.[39]

PEITC and AITC and their conjugates also inhibited cellular growth and induced apoptosis of human leukemia HL60 (p53−) and human myeloblastic leukemia-1 cells (p53+) *in vitro*.[40] The cell cycle inhibitor p21 (p21WAF1/CIP1) was upregulated in DU-145 cells treated with PEITC.[41]

We have reported that BrdU-LI were reduced by BITC exposure in both rat small intestine and colon treated with methylazoxymethanol acetate.[12] Nishikawa *et al.*[42] also reported that proliferating cell nuclear antigen (PCNA) labeling indices demonstrated significant reduction by PEITC in the pancreatic acini and ducts, bronchioles, and renal tubules of the *N*-nitrosobis(2-oxopropyl)-amine (BOP)-treated animals in a dose-dependent manner in BOP-treated hamsters. BrdU-LI were increased by PEITC administration even in normal-looking rat urinary epithelium.[43] In our present study, DITC reduced BrdU-LI of neoplasia and pre-neoplasia in initiation phase and of pre-neoplasia in post initiation phase. In mice urinary bladder carcinogenesis, other chemopreventive agents were proved to reduce the cell proliferation of BBN-induced various bladder lesions.[37,44]

We also analyzed cyclin D1, cell cycle regulatory proteins control proliferation and cell cycle progression. Expression of cyclin D1 is believed to lead to progression through the G1-S cell cycle checkpoint, and both experimental and pathological evidence suggest that overexpression of this protein may increase the risk of several cancers, including transition cell carcinoma of the bladder. Overexpression of cyclin D1 is implicated in the etiology of urinary bladder carcinoma.[45–47] It has also been reported that cyclin D1 overexpression might play a critical role in urinary tumor progression in rodent.[34–37,48,49] Some reports indicated that its overexpression could be a useful marker for estimating malignancy in the early stage of urinary carcinogenesis.[36,50,51] Our results of immunohistochemical study indicated that the intensity of cyclin D1 overexpression was in the order of hyperplasia, dysplasia, papilloma and carcinoma. This is consistent with the data reported previously.[37,48–52] In this study, DITC effectively suppressed cyclin D1-positive cell ratios of urinary bladder, implying that reduction in the incidence of tumors and preneoplastic lesions of urinary bladder is related to effectively suppressed cell cycle progression by the treatment with DITC. In our recent study, another selective cyclin D1 inhibitor, silymarin have also been demonstrated to possess chemopreventive potential on BBN-induced urinary bladder carcinogenesis in male ICR mice.[37]

Administration of DITC in the initiation phase significantly reduced BrdU-LI and cyclin D1 positive cell ratios in bladder lesions, and decreased the incidence of urinary bladder carcinomas as well as dysplasia. Control of cell proliferation is important for cancer prevention because cell proliferation has essential roles in carcinogenesis including the process of initiation and promotion. In rodent models for carcinogenesis, chemopreventive agents suppress carcinogen-induced hyperproliferation of cells in the target organs during the initiation as well as the post initiation phases. Cell proliferation takes important role for an opportunity of DNA damage in the initiation of carcinogenesis.[15,53]

Dietary exposure of DITC in the post-initiation phase decreased BrdU-LI and cyclin D1 positive cell ratios in urinary bladder tumors, but did not significantly reduce the development of urinary bladder tumors. Recently, Tang and Zhang[54] found that ITC blocked cell-cycle progression and downregulated several cell-cycle regulators in human bladder carcinoma cells in certain concentration. The cytostatic activity of DITC in promotion phase was lower than that in initiation phase. This dose of DITC is enough to reduce the cell proliferation, but it may not have been adequate dose to suppress carcinogenesis. As other likelihood, these results may suggest that the other mechanisms are necessary to suppress the promotion in carcinogenesis.

Some other mechanisms, including induction of apoptosis, reduction of Phase I enzymes, induction of Phase II enzymes, modification of signal transduction pathways were reported.[10] ITC inhibited and inactivated cytochrome P450 isoforms and induced increased expression of Phase II enzymes, GST, NADPH: quinone oxidoreductase, aldo-keto reductase and γ-glutamylcysteine synthetase. ITC also induced apoptosis of pre-cancerous cells and tumor cells activated by caspase-8 and potentiated by JNK1.[10]

One more mechanism suggested is protection against oxidative damage by glucosinolates breakdown products and ITC.[55–57] ITC have been reported to have antioxidant properties, and some studies have demonstrated favorable effects on tumorigenesis and promotion.[57] It is well established that glucosinolate breakdown products induce endogenous antioxidant defenses such as UDP glucuronosyl transferase in cells and in vivo.[55] The free radical scavenging properties of representative extracts and of purified glucosinolate from cruciferous vegetables were studied and reported that glucosinolate are unlikely to account for the direct antioxidant effects.[55] Antioxidants may be helpful for cancer chemoprevention.[58] Some antioxidants has been reported to exert initiation, promotion, additive and synergistic effects on carcinogenesis.[59,60]

PEITC, a naturally occurring compound found in certain cruciferous vegetables, which inhibits carcinogenesis at the initiation stage in several organs, also exhibits cancer promoting potential in liver and urinary bladder in the post-initiation stage.[30] Strong promoting activities of PEITC and BITC were also reported using a rat urinary bladder carcinogenesis model.[29] In our experiment, dietary DITC did not show any promoting effect when fed to mice during the promotion phase of urinary bladder carcinogenesis, and moreover, it effectively reduced the tumor incidences when fed during the initiation phase. Structure-activity relationship studies showed that the modifying effects to Phase I and Phase II enzymes and apoptosis by ITC might depend on chemical structure of ITC.[9,10] Studies conducted by Hudson *et al.*,[61] for instance, have shown that PHITC enhances N-nitrosomethylbenzylamine (NMBA)-induced esophageal tumorigenesis in F344 rats, whereas the shorter chain analogs, PEITC and PPITC, inhibit NMBA-induced esophageal tumorigenesis.[62] These structure-related activities have been suggested to depend on alkyl chain length, phenyl substitution and secondary ITC.[9,10,52] The differences between our results and others that treatments with PEITC and BITC during the promotion phase do or do not possess strong promoting activity on urinary bladder carcinogenesis might be explained by shorter length of the alkyl chain or secondary ITC of DITC. In addition, the species differences in response to ITC could be considered. Because the inhibitory action of ITC has been attributed to their ability to modulate xenobiotic-metabolizing enzymes (*e.g.*, cytochrome P-450) that are required for the activation of many carcinogens or to induce Phase II detoxifying enzymes.[44,63–65]. One possibility is that cytochrome P-450 are critical targets in inhibition of the chemical-induced tumorigenesis by ITC, the distinct patterns of P-450 isozymes for carcinogen activation in rats and mice may be partially responsible for the differences observed.[66,67]

DITC suppressed BBN-induced mice bladder carcinogenesis. However, some other ITC have been reported to be carcinogenic in rats.[27–32] Especially, allyl isothiocyanate was reported to be carcinogenic for male F344 rats in the urinary bladder, but was not carcinogenic for B6C3F1 mice of either gender.[27] High cruciferous vegetable consumption is suggested to reduce bladder cancer risk from epidemiological study.[23] ITC blocked cell-cycle progression and downregulated several cell-cycle regulators in human bladder carcinoma cell lines.[54] Those findings may suggest that modifying effects of ITC on the urinary bladder carcinogenesis are depended to the difference of rodent species and strains. Further studies should be carried out to investigate the mechanisms and species difference.

Conclusion

In conclusion, our study has shown that DITC is efficacious chemopreventive agent against BBN-induced urinary bladder tumorigenesis in male ICR mice.

Acknowledgements

We appreciate the technical assistance of Miss K. Takahashi and C. Usui, the secretarial assistance of Miss A. Nagata and T. Kajita and the animal care given by Mr. K. Kinjo. This study was supported in part by a Grant-in-Aid from the Ministry of Education, Culture, Sports, Science and Technology of Japan, and a Grant (C2004-4) for Promoted Research from Kanazawa Medical University.

References

1. Mori H, Tanaka T, Sugie S, Yoshimi N. Chemopreventive effects of plant derived phenolic, organosulfur and other compounds on carcinogenesis in digestive organs. Environ Mutat Res Commun 1995;17: 127–33.
2. Weisburger JH. Worldwide prevention of cancer and other chronic diseases based on knowledge of mechanisms. Mutat Res 1998;402: 331–7.
3. Riboli E, Norat T. Epidemiologic evidence of the protective effect of fruit and vegetables on cancer risk. Am J Clin Nutr 2003;78:559S–69S.
4. Smith-Warner SA, Spiegelman D, Yaun SS, Albanes D, Beeson WL, van den Brandt PA, Feskanich D, Folsom AR, Fraser GE, Freudenheim JL, Giovannucci E, Goldbohm RA, et al. Fruits, vegetables and lung cancer: a pooled analysis of cohort studies. Int J Cancer 2003;107:1001–11.
5. Miller AB, Altenburg HP, Bueno-de-Mesquita B, Boshuizen HC, Agudo A, Berrino F, Gram IT, Janson L, Linseisen J, Overvad K, Rasmuson T, Vineis P, et al. Fruits and vegetables and lung cancer: findings from the European prospective investigation into cancer and nutrition. Int J Cancer 2004;108:269–76.
6. Mathew A, Peters U, Chatterjee N, Kulldorff M, Sinha R. Fat, fiber, fruits, vegetables, and risk of colorectal adenomas. Int J Cancer 2004; 108:287–92.
7. Malin AS, Qi D, Shu XO, Gao YT, Friedmann JM, Jin F, Zheng W. Intake of fruits, vegetables and selected micronutrients in relation to the risk of breast cancer. Int J Cancer 2003;105:413–8.
8. Talalay P, Fahey JW. Phytochemicals from cruciferous plants protect against cancer by modulating carcinogen metabolism. J Nutr 2001; 131:3027S–33S.
9. Hecht SS. Inhibition of carcinogenesis by isothiocyanates. Drug Metab Rev 2000;32:395–411.
10. Conaway CC, Yang YM, Chung FL. Isothiocyanates as cancer chemopreventive agents: their biological activities and metabolism in rodents and humans. Curr Drug Metab 2002;3:233–55.
11. Sugie S, Okumura A, Tanaka T, Mori ,H. Inhibitory effects of benzyl isothiocyanate and benzyl thiocyanate on diethylnitrosamine-induced hepatocarcinogenesis in rats. Jpn J Cancer Res 1993;84:865–70.
12. Sugie S, Okamoto K, Okumura A, Tanaka T, Mori H. Inhibitory effects of benzyl thiocyanate and benzyl isothiocyanate on methylazoxymethanol acetate-induced intestinal carcinogenesis in rats. Carcinogenesis 1994;15:1555–60.
13. Tanaka T, Kojima T, Morishita Y, Mori H. Inhibitory effects of the natural products indole-3-carbinol and sinigrin during initiation and promotion phases of 4-nitroquinoline 1-oxide-induced rat tongue carcinogenesis. Jpn J Cancer Res 1992;83:835–42.
14. Tanaka T, Mori Y, Morishita Y, Hara A, Ohno T, Kojima T, Mori H. Inhibitory effect of sinigrin and indole-3-carbinol on diethylnitrosamine-induced hepatocarcinogenesis in male ACI/N rats. Carcinogenesis 1990;11:1403–6.
15. Sugie S, Yoshimi N, Okumara A, Tanaka T, Mori H. Modifying effects of benzyl isothiocyanate and benzyl thiocyanate on DNA synthesis in primary cultures of rat hepatocytes. Carcinogenesis 1993;14: 281–83.
16. Ahmed SH, Vaishnava S. Trial of a new anthelmintic (bitoscanate) in ancylostomiasis in children. Prog Drug Res 1975;19:2–5.
17. Bhandari B, Upadhyay R, Shrimali L, Agarwal SS. Jonit in the treatment of hymenolepiasis: a new drug by cyclic regimen. Indian Pediatr 1973;10:675–7.

18. Chitrathorn S, Acalabol M, Thongkong M, Kamolsin C. A single dose of phenylene-di-iso-thiocyanate (1, 4), Jonit in the treatment of adult patients with hookworm infection in Sawan-Pracharak Hospital, Thailand. Southeast Asian J Trop Med Public Health 1972;3: 103–5.
19. Goldsmid JM, MacCabe RJ. Preliminary studies on the use of phenylene-diisothiocyanate-(1, 4) in the treatment of hookworm and Ternidens derminutus infections in Rhodesia. S Afr Med J 1972;18: 227–9.
20. Holz J, Adhman D, Gunardi AT, Murad S, Sadeli OR, Wuisan JO. A single dose of Jonit in the treatment of human ancylostomiasis. Southeast Asian J Trop Med Public Health 1972;3:99–102.
21. O'Holohan DR, Hugoe-Matthews J. Single dose regimens of phenylene di-iso-thiocyanate (1, 4) Jonit, in the treatment of hookworm infestation in Malaysia. Southeast Asian J Trop Med Public Health 1972;3:403–10.
22. Raghavan P, Nagendra AS. A preliminary report on treatment of ancylostomiasis with phenylene-di-iso-thiocyanate (1, 4,). J Postgrad Med 1965;XI:176–81.
23. Michaud DS, Spiegelman D, Clinton SK, Rimm EB, Willett WC, Giovannucci EL. Fruit and vegetable intake and incidence of bladder cancer in a male prospective cohort. J Natl Cancer Inst 1999;91:605–13.
24. Wakai K, Takashi M, Okamura K, Yuba H, Suzuki K, Murase T, Obata K, Itoh H, Kato T, Kobayashi M, Sakata T, Otani T, et al. Foods and nutrients in relation to bladder cancer risk: a case-control study in Aichi Prefecture, Central Japan. Nutr Cancer 2000;38:13–22.
25. Nagano J, Kono S, Preston DL, Moriwaki H, Sharp GB, Koyama K, Mabuchi K. Bladder-cancer incidence in relation to vegetable and fruit consumption: a prospective study of atomic-bomb survivors. Int J Cancer 2000;86:132–8.
26. Steinmaus CM, Nunez S, Smith AH. Diet and bladder cancer: a meta-analysis of six dietary variables. Am J Epidemiol 2000;151:693–702.
27. National Toxicology Program. Carcinogenesis bioassay of allyl isothiocyanate (CAS No. 57-06-7) in F344/N rats and B6C3F1 mice (Gavage Study). Natl Toxicol Program Tech Rep Ser 1982;234:1–142.
28. Bollard M, Stribbling S, Mitchell S, Caldwell J. The disposition of allyl isothiocyanate in the rat and mouse. Food Chem Toxicol 1997; 35:933–3.
29. Hirose M, Yamaguchi T, Kimoto N, Ogawa K, Futakuchi M, Sano M, Shirai T. Strong promoting activity of phenylethyl isothiocyanate and benzyl isothiocyanate on urinary bladder carcinogenesis in F344 male rats. Int J Cancer 1998;77:773–7.
30. Ogawa K, Hirose M, Sugiura S, Cui L, Imaida K, Ogiso T, Shirai T. Dose-dependent promotion by phenylethyl isothiocyanate, a known chemopreventer, of two-stage rat urinary bladder and liver carcinogenesis. Nutr Cancer 2001;40:134–9.
31. Nishikawa A, Morse MA, Chung FL. Inhibitory effects of 2-mercaptoethane sulfonate and 6-phenylhexyl isothiocyanate on urinary bladder tumorigenesis in rats induced by N-butyl-N-(4-hydroxybutyl)nitrosamine. Cancer Lett 2003;193:11–6.
32. Okazaki K, Yamagishi M, Son HY, Imazawa T, Furukawa F, Nakamura H, Nishikawa A, Masegi T, Hirose M. Simultaneous treatment with benzyl isothiocyanate, a strong bladder promoter, inhibits rat urinary bladder carcinogenesis by N-butyl-N-(4-hydroxybutyl)nitrosamine. Nutr Cancer 2002;42:211–6.
33. Hasegawa T, Nishino H, Iwashima A. Isothiocyanates inhibit cell cycle progression of HeLa cells at G2/M phase. Anticancer Drugs 1993;4:273–9.
34. Lee CC, Yamamoto S, Wanibuchi H, Wada S, Sugimura K, Kishimoto T, Fukushima S. Cyclin D1 overexpression in rat two-stage bladder carcinogenesis and its relationship with oncogenes, tumor suppressor genes, and cell proliferation. Cancer Res 1997;57:4765–76.
35. Ogawa K, Kimoto N, Asamoto M, Nakanishi M, Takahashi S, Shirai T. Aberrant expression of p27(Kip1) is associated with malignant transformation of the rat urinary bladder epithelium. Carcinogenesis 2000;21:117–21.
36. Wei M, Wanibuchi H, Morimura K, Iwai S, Yoshida K, Endo G, Nakae D, Fukushima S. Carcinogenicity of dimethylarsinic acid in male F344 rats and genetic alterations in induced urinary bladder tumors. Carcinogenesis 2002;23:1387–97.
37. Vinh PQ, Sugie S, Tanaka T, Hara A, Yamada Y, Katayama M, Deguchi T, Mori H. Chemopreventive effects of a flavonoid antioxidant silymarin on N-butyl-N-(4-hydroxybutyl)nitrosamine-induced urinary bladder carcinogenesis in male ICR mice. Jpn J Cancer Res 2002;93:42–9.
38. Fukushima S, Murasaki G, Hirose M, Nakanishi K, Hasegawa R, Ito N. Histopathological analysis of preneoplastic changes during N-butyl-N-(4-hydroxybutyl)-nitrosamine-induced urinary bladder carcinogenesis in rats. Acta Pathol Jpn 1982;32:243–50.
39. Gamet-Payrastre L, Li P, Lumeau S, Cassar G, Dupont M-A, Chevolleau S, Gasc N, Tulliez J, Tercé F. Sulforaphane, a naturally occurring isothiocyanate, induces cell cycle arrest and apoptosis in HT29 human colon cancer cells. Cancer Res 2000;60: 1426–33.
40. Xu K, Thornalley P.J. Studies on the mechanism of the inhibition of human leukaemia cell growth by dietary isothiocyanates and their cysteine adducts in vitro. Biochem Pharmacol 2000;60:221–31.
41. Chiao JW, Chung F-L, Krzeminski J, Amin S, Arshad R, Ahmed T, Conaway CC. Modulation of growth of human prostate cancer cells by the N-acetylcysteine conjugate of phenethyl isothiocyanate. Int J Oncol 2000;16:1215–9.
42. Nishikawa A, Lee IS, Uneyama C, Furukawa F, Kim HC, Kasahara K, Huh N, Takahashi M. Mechanistic insights into chemopreventive effects of phenethyl isothiocyanate in N-nitrosobis(2-oxopropyl)amine-treated hamsters. Jpn J Cancer Res 1997;88: 1137–42.
43. Sugiura S, Ogawa K, Hirose M, Takeshita F, Asamoto M, Shirai T. Reversibility of proliferative lesions and induction of non-papillary tumors in rat urinary bladder treated with phenylethyl isothiocyanate. Carcinogenesis 2003;24:547–53.
44. Yang M, Tanaka T, Hirose Y, Deguchi T, Mori H, Kawada Y. Chemopreventive effects of diosmin and hesperidin on N-butyl-N-(4-hydroxybutyl)nitrosamine-induced urinary-bladder carcinogenesis in male ICR mice. Int J Cancer 1997;73:719–24.
45. Lipponen PK, Eskelinen MJ. Cell proliferation of transitional cell bladder tumours determined by PCNA/cyclin immunostaining and its prognostic value. Br J Cancer 1992;66:171–6.
46. Lee CC, Yamamoto S, Morimura K, Wanibuchi H, Nishisaka N, Ikemoto S, Nakatani T, Wada S, Kishimoto T, Fukushima S. Significance of cyclin D1 overexpression in transitional cell carcinomas of the urinary bladder and its correlation with histopathologic features. Cancer 1997;79:780–9.
47. Romanenko A, Lee CC, Yamamoto S, Hori T, Wanibuchi H, Zaparin W, Vinnichenko W, Vozianov A, Fukushima S. Urinary bladder lesions after the Chernobyl accident: immunohistochemical assessment of p53, proliferating cell nuclear antigen, cyclin D1 and p21WAF1/Cip1. Jpn J Cancer Res. 1999;90:144–53.
48. Wanibuchi H, Yamamoto S, Chen H, Yoshida K, Endo G, Hori T, Fukushima S. Promoting effects of dimethylarsinic acid on N-butyl-N-(4-hydroxybutyl)nitrosamine-induced urinary bladder carcinogenesis in rats. Carcinogenesis 1996;17:2435–9.
49. Takaba K, Saeki K, Suzuki K, Wanibuchi H, Fukushima S. Significant overexpression of metallothionein and cyclin D1 and apoptosis in the early process of rat urinary bladder carcinogenesis induced by treatment with N-butyl-N-(4-hydroxybutyl)nitrosamine or sodium L-ascorbate. Carcinogenesis 2000;21:691–700.
50. Shin KY, Kong G, Kim WS, Lee TY, Woo YN, Lee JD. Overexpression of cyclin D1 correlates with early recurrence in superficial bladder cancers. Br J Cancer 1997;75:1788–92.
51. Suwa Y, Takano Y, Iki M, Takeda M, Asakura T, Noguchi S, Masuda M. Cyclin D1 protein overexpression is related to tumor differentiation, but not to tumor progression or proliferative activity, in transitional cell carcinoma of the bladder. J Urol 1998;160:897–900.
52. Jiao D, Eklind KI, Choi CI, Desai DH, Amin SG, Chung FL. Structure-activity relationships of isothiocyanates as mechanism-based inhibitors of 4-(methylnitrosamino)-1-(3-pyridyl)-1-butanone-induced lung tumorigenesis in A/J mice. Cancer Res 1994;54:4327–33.
53. Mori H, Sugie S, Yoshimi N, Hara A, Tanaka T. Control of cell proliferation in cancer prevention. Mutat Res 1999;428:291–8.
54. Tang L, Zhang Y. Dietary isothiocyanates inhibit the growth of human bladder carcinoma cells. J Nutr 2004;134:2004–10.
55. Williamson G, Faulkner K, Plumb GW. Glucosinolates and phenolics as antioxidants from plant foods. Eur J Cancer Prev 1998;7:17–21.
56. Talalay P, Fahey JW. Phytochemicals from cruciferous plants protect against cancer by modulating carcinogen metabolism. J Nutr 2001; 131:3027S–33S.
57. Thornalley PJ. Isothiocyanates: mechanism of cancer chemopreventive action. Anticancer Drugs 2002;13:331–8.
58. Ray G, Husain SA. Oxidants, antioxidants and carcinogenesis. Indian J Exp Biol 2002;40:1213–32.
59. Ito N, Hirose M. Antioxidants—carcinogenic and chemopreventive properties. Adv Cancer Res 1989;53:247–302.
60. Hirose M, Takesada Y, Tanaka H, Tamano S, Kato T, Shirai T. Carcinogenicity of antioxidants BHA, caffeic acid, sesamol, 4-methoxyphenol and catechol at low doses, either alone or in combination, and modulation of their effects in a rat medium-term multi-organ carcinogenesis model. Carcinogenesis 1998;19:207–12.
61. Hudson TS, Carlton PS, Gupta A, Stoner GD, Morse MA. Investigation of the enhancement of N-nitrosomethylbenzylamine-induced esophageal tumorigenesis by 6-phenylhexyl isothiocyanate. Cancer Lett 2001;162:19–26.

62. Wilkinson JT, Morse MA, Kresty LA, Stoner GD. Effect of alkyl chain length on inhibition of N-nitrosomethylbenzylamine-induced esophageal tumorigenesis and DNA methylation by isothiocyanates. Carcinogenesis 1995;16:1011–5.
63. Goosen TC, Kent UM, Brand L, Hollenberg PF. Inactivation of cytochrome P450 2B1 by benzyl isothiocyanate, a chemopreventative agent from cruciferous vegetables. Chem Res Toxicol 2000;13:1349–59.
64. Kent UM, Roberts ES, Chun J, Hodge K, Juncaj J, Hollenberg PF. Inactivation of cytochrome P450 2E1 by tert-butylisothiocyanate. Chem Res Toxicol 1998;11:1154–61.
65. Zhang Y, Talalay P. Mechanism of differential potencies of isothiocyanates as inducers of anticarcinogenic Phase 2 enzymes. Cancer Res 1998;58:4632–9.
66. Guo Z, Smith TJ, Thomas PE, Yang CS. Metabolism of 4-(methylnitrosamino)-1-(3-pyridyl)-1-butanone by inducible and constitutive cytochrome P450 enzymes in rats. Arch Biochem Biophys 1992;298:279–86.
67. Smith TJ, Guo ZY, Thomas PE, Chung FL, Morse MA, Elkind K, Yang CS. Metabolism of 4-(methylnitrosamino)-1-(3-pyridyl)-1-butanone in mouse lung microsomes and its inhibition by isothiocyanates. Cancer Res 1990;50:6817–22.

Int. J. Cancer: **115**, 346–350 (2005)
© 2005 Wiley-Liss, Inc.

Effect of α-naphthyl isothiocyanate on 2-amino-3-methylimidazo[4,5-*b*]pyridine (PhIP)-induced mammary carcinogenesis in rats

Shigeyuki Sugie[1]*, Masami Ohnishi[2], Jun Ushida[2], Tomohiro Yamamoto[3], Akira Hara[3], Akihiro Koide[4], Yukio Mori[4], Hiroyuki Kohno[1], Rikako Suzuki[1], Takuji Tanaka[1], Keiji Wakabayashi[5] and Hideki Mori[2]

[1]*Department of Pathology, Kanazawa Medical University, Uchinada, Ishikawa, Japan*
[2]*Department of Tumor Pathology, Gifu University School of Medicine, Gifu, Japan*
[3]*Laboratory of Biochemistry, Gifu Pharmaceutical University, Gifu, Japan*
[4]*Laboratory of Radiochemistry, Gifu Pharmaceutical University, Gifu, Japan*
[5]*Cancer Prevention Basic Research Project, National Cancer Center Research Institute, Chuo-ku, Tokyo, Japan*

The modifying effects of α-naphthyl isothiocyanate (ANIT) on 2-amino-3-methylimidazo[4,5-*b*]pyridine (PhIP)-induced mammary carcinogenesis were investigated in female Sprague-Dawley (SD) rats, and the hepatic activities of the phase II detoxifying enzymes glutathione *S*-transferase (GST) and quinone reductase (QR) were also assayed. Ninety-eight rats were divided into 4 groups. Starting at 6 weeks of age, rats were fed the high-fat diet without ANIT (Groups 1 and 4) or the experimental diet (high-fat diet mixed with 400 ppm ANIT, Groups 2 and 3). At 7 weeks of age, Groups 1 and 2 were given PhIP in corn oil (85 mg/kg body weight, 8 times for 11 days) by intragastric intubation. One week after the last PhIP injection, 5 rats in each group were sacrificed to assay GST and QR activities, and the experimental diets for Groups 2 and 3 were switched to the high-fat diet without ANIT until termination of the experiment. Group 4 served as the vehicle control. All rats were sacrificed at 24 weeks after the start of the experiment. At termination of the experiment, mammary tumours were detected in Groups 1 (PhIP alone) and 2 (PhIP + ANIT) and were shown histologically to be adenocarcinomas; their incidences (multiplicities) were 56.3% (1.66 ± 2.31/rat) in Group 1 and 6.7% (0.07 ± 0.25/rat) in Group 2 ($p < 0.001$). Mean sizes of the tumours were 10.6 ± 5.3 mm in Group 1 and 6.5 mm in Group 2. No mammary tumours were observed in rats of Groups 3 and 4. In addition, ANIT treatment significantly increased the activities of GST and QR in the livers of rats in Groups 2 and 3 as compared to Groups 1 and 4. These results imply that the isothiocyanate compound ANIT shows potent inhibitory effects on mammary carcinogenesis induced by PhIP in female SD rats when administered during the initiation stage.
© *2005 Wiley-Liss, Inc.*

Key words: PhIP; α-naphthyl isothiocyanate; mammary carcinogenesis; chemoprevention; rat

Among a number of environmental factors, dietary habits have been regarded as the most important determinant for cancer development in humans.[1–3] Epidemiological data suggest that individuals eating fried or broiled meat have a significantly elevated risk of intestinal cancer.[4,5] A number of carcinogenic heterocyclic amines (HCAs) have been detected in cooked foods. These HCAs show potent mutagenicity in the Ames test and their carcinogenic potential has been demonstrated in various organs, including the forestomach, liver, small intestine, large intestine, mammary gland, Zymbal's gland, clitoral glands, haematopoietic systems, blood vessels and skin of rodents.[6,7] For example, 2-amino-3-methylimidazo[4,5-*b*]pyridine (PhIP) has attracted considerable attention for potent mutagenicity and carcinogenic potential in the mammary gland and colon of rats.[8,9] In most previous studies of their carcinogenesis, the long-term administration of HCAs in the diet has been needed for the development of tumours.[10] In rat mammary carcinogenesis induced by PhIP, mammary cancers are induced at a rate of 47% by administration of 0.04% PhIP in the diet for 52 weeks.[8] Ghoshal *et al.*[11] found mammary tumours in 53% of Sprague-Dawley (SD) rats fed a high-fat diet 25 weeks after treatment with PhIP in 10 doses of 75 mg/kg body weight for 12 days. It was also reported that mammary tumours developed in 77% of CD rats 41 weeks after treatment with PhIP at 50 μmol/rat/week for 8 weeks on a high-fat diet.[12] In these studies, a high-fat diet was given throughout the experiment. These results indicate that the development of PhIP-induced mammary tumours is enhanced and induced earlier by feeding with a high-fat diet. On the other hand, a high-fat diet did not affect PhIP-induced mammary carcinogenesis in SD × F344 F_1 hybrid rats.[13]

α-Naphthyl isothiocyanate (ANIT), present as the glucosinolate precursor, is a constituent of cruciferous vegetables.[14] ANIT has been reported to induce cholestasis, bile duct proliferation and focal necrosis of hepatocytes, without the development of liver cancer, and to inhibit hepatocarcinogenesis in rats.[15–17] The mechanisms of its chemopreventive effect have been discussed;[18] one possible mechanism is the regulation of phase I and phase II enzymes. ANIT has been shown to decrease hepatic cytochrome P-450 content,[19,20] and hepatic mixed-function oxidase activities,[21] and increase microsomal epoxide hydrolase and cytosolic DT-diaphorase activities.[19] The promutagenic PhIP found in cooked foods is converted to the active form mainly by cytochromes P450 1A1, 1A2 and 1B1 in the liver and partially in the target organs.[21–27] Glutathione *S*-transferase (GST) has been reported to inhibit DNA binding of *N*-acetyl-PhIP *in vitro*.[28]

These findings suggested that the administration of P450 inhibitor in the initiation phase may reduce the carcinogenicity of PhIP. ANIT was used in early studies of cancer chemoprevention, although it is toxic to the liver and is a cholestatic agent.[15–17] Possibly as a result of this, it is now used rarely in chemoprevention studies and has not been scheduled for trials in humans. Toxicity is a serious problem for trials of cancer chemopreventive agents. However, if lower doses of such compounds do not exert clear toxicity in any organs, including the liver, these compounds should not be omitted from basic research on cancer chemoprevention.

In our study, we examined the effects of a low dose (400 ppm in diet) of ANIT on PhIP-induced mammary carcinogenesis in SD rats. In addition, the activities of phase II detoxifying GST and quinone reductase (QR) in the liver were measured to clarify whether these enzymes are involved in its modification of PhIP-induced mammary carcinogenesis.

Material and methods

Animals, diet, water and carcinogen

Weanling female SD rats were purchased from Japan SLC, Co. (Hamamatsu, Japan). PhIP was supplied by Dr. Wakabayashi

Grant support: Ministry of Health, Labour and Welfare of Japan; Grant support: Kanazawa Medical University; Grant number: C2004-4.
***Correspondence to:** Department of Pathology, Kanazawa Medical University, 1-1 Daigaku, Uchinada, Ishikawa 920-0293, Japan.
Fax: +81-76-286-6926. E-mail: sugie@kanazawa-med.ac.jp
Received 14 April 2004; Accepted after revision 12 October 2004
DOI 10.1002/ijc.20841
Published online 1 February 2005 in Wiley InterScience (www.interscience.wiley.com).

Publication of the International Union Against Cancer
global cancer control

TABLE I – PERCENT COMPOSITION OF EXPERIMENTAL SEMIPURIFIED HIGH FAT DIETS CONTAINING CORN OIL

Diet ingredients	Percents of ingredients by weight
Casein, vitamin-free	23.50
DL-Methionine	0.35
Corn starch	32.90
Dextrose	8.30
Alphacel	5.90
Corn oil	**23.52**
Mineral, AIN	4.11
Vitamin, AIN (revised)	1.18
Choline bitartrate	0.24

AIN: American Institute of Nutrition.

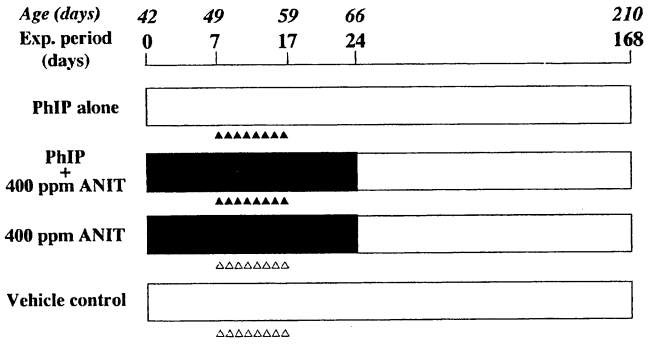


FIGURE 1 – Experimental protocol. Unshaded, high-fat diet; shaded, high-fat diet with 400 ppm α-naphthyl isothiocyanate (ANIT). Closed triangle, PhIP 85 mg/kg B.W. in corn oil by gavage Open triangle, Corn oil by gavage.

(National Cancer Center Research Institute, Tokyo, Japan). ANIT was purchased from Tokyo Kasei Kogyo Co., Ltd. (Tokyo, Japan). All diet ingredients were obtained from CLEA Japan Inc. (Tokyo, Japan) and experimental and high-fat diets were prepared weekly in our laboratory and stored in a cold room (<4°C). The composition of the high-fat diet is shown in Table I. All animals were housed in wire cages (3 rats/cage). Animals had free access to water and diets under controlled environmental conditions of humidity (50 ± 10%), lighting (12 hr light/dark cycle) and temperature (23 ± 2°C).

Animal treatment and pathological examination

A total of 98 rats, 5 weeks of age, were divided into 4 groups: Group 1, 37 rats given PhIP alone; Group 2, 35 rats given PhIP and 400 ppm ANIT in the initiation phase; Group 3, 13 rats given ANIT alone and Group 4, 13 rats as vehicle controls. All animals were given the high-fat diet throughout the experiment as the basal diet (Fig. 1).

Rats in Groups 2 and 3 were given diet containing 400 ppm ANIT from the start of the experiment and animals in the other groups were kept on the basal diet. Animals in Groups 1 and 2 were given 8 doses of PhIP (85 mg/kg body weight, gastric intubation) in 0.1 ml of corn oil for 11 days, starting 7 days after the commencement of the experiment. Vehicle control rats received an equal volume of corn oil. For rats in Groups 2 and 3, the experimental diet was changed to the basal diet 1 week after final treatment with the carcinogen. Five rats in each group were sacrificed to assay GST and QR activities at 1 week after the last PhIP injection. All other animals were sacrificed 24 weeks after the start of the experiment to assess the modifying effect of ANIT on mammary carcinogenesis induced by PhIP. At the end of the experiment, complete autopsies on these animals were performed after sacrifice by ether anaesthesia. At autopsy, the location, number

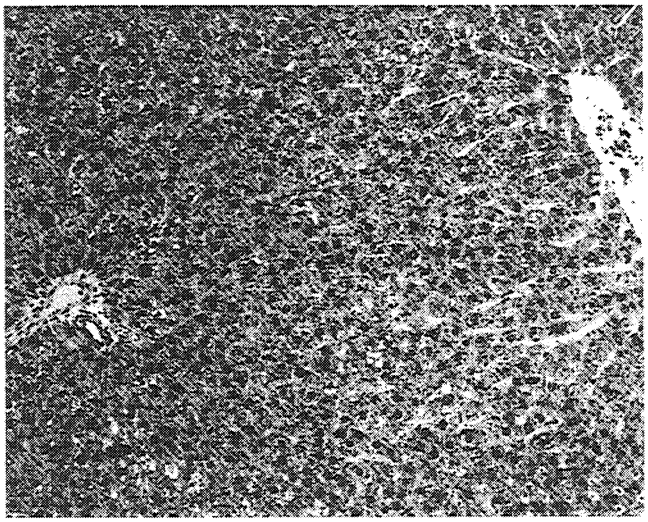


FIGURE 2 – Histology of liver of a rat from Group 3 (ANIT alone) reveals no abnormalities. Hematoxylin and eosin stain, ×10 (original magnification).

and size of mammary tumours were recorded. Tissues were fixed in 10% buffered formalin, embedded in paraffin blocks and processed for routine histological observation with haematoxylin and eosin staining. Pathological diagnosis of mammary tumours was performed according to the criteria outlined by Young and Hallowes.[29]

GST and QR assays

Aliquots of minced liver were processed to obtain the cytosolic fraction. The activities of GST and QR were determined using 1-chloro-2,4-dinitrobenzene (CDNB) or 1,2-dichloro-4-nitrobenzene (DCNB) for GST and NADH/menadione for QR as substrates, respectively, as described previously.[30–32] All spectrographic assays were based on absorption at 340 nm and all samples were examined in triplicate. One unit of enzyme activity was defined as the amount of enzyme catalysing the conversion of 1 μmol of substrate to product per min at 25°C. Cytosolic protein concentrations were determined by the Bradford method[33] using bovine serum albumin as the standard.

Statistical analysis

Differences in the incidence or multiplicity of mammary tumours between groups were analysed by Fisher's exact probability test, χ^2-test, Student's *t*-test or alternate Welch *t*-test.

Results

Table I shows body, liver and relative liver weights of rats in each group at the termination of the experiment. No significant differences were found in body or liver weights between Groups 1 (PhIP alone) and 2 (PhIP + ANIT). Body weight of Group 3 (ANIT alone) was significantly lower than that of Group 4 (vehicle control) ($p < 0.005$). Relative liver weight of rats in Group 3 (ANIT alone) was significantly greater than that in Group 4 (vehicle control) ($p < 0.005$). However, no clinical signs of toxicity of ANIT were noted during the study. Histological examination did not provide evidence of histological alterations, including cholestasis, bile duct proliferation or cell necrosis, in the livers of rats given ANIT alone (Fig. 2).

At the end of the experiment, mammary tumours were found in rats in Groups 1 and 2 but no tumours were found in animals of Groups 3 or 4 rats, as summarised in Table II. All of the mammary tumours were diagnosed as invasive or intraductal adenocarcino-

TABLE II – FINAL BODY AND LIVER WEIGHTS

Group	Treatment	Number of rats	Body weight (g)	Liver weight (g)	Relative liver weight (%)
1	PhIP alone	32	278 ± 20[1,2]	11.0 ± 2.4	3.94 ± 0.76
2	PhIP + ANIT	30	277 ± 19	10.3 ± 1.5	3.72 ± 0.52
3	ANIT alone	8	266 ± 19[2]	10.5 ± 1.1	3.94 ± 0.25[2]
4	No treatment	8	304 ± 20	10.4 ± 1.2	3.41 ± 0.30

[1]Mean ± SD.–[2]Significantly different from Group 4 by Student's *t*-test (b: $p < 0.005$).

TABLE III – INCIDENCE AND MULTIPLICITY OF MAMMARY CARCINOMA

Group	Treatment	Number of rats	Incidence (%)			Multiplicity (number/rat)		
			Total	Inv.d.Ca.[1]	Int.d.Ca.[2]	Total	Inv.d.Ca.	Int.d.Ca.
1	PhIP	32	18 (56.3)	17 (53.1)	8 (25.0)	1.66 ± 2.31[3]	1.19 ± 1.64	0.47 ± 1.29
2	PhIP + ANIT	30	2 (6.7)[4]	2 (6.7)[4]	0[5]	0.07 ± 0.25[6]	0.07 ± 0.25[6]	0
3	ANIT alone	8	0	0	0	0	0	0
4	Vehicle control	8	0	0	0	0	0	0

[1]Invasive ductal carcinoma.–[2]Intraductal carcinoma.–[3]a: Mean ± SD.–[4,5]Significantly different from Group 1 (PhIP alone) by Fisher's exact probability test (b: $p < 0.001$, c: $p < 0.005$).–[6]d: Significantly different from Group 1 (PhIP alone) by Student's *t*-test or alternate Welch *t*-test ($p < 0.001$).

TABLE IV – RESULTS OF LIVER GST AND QR ACTIVITIES

Group	Treatment	Number of rats	GST		QR
			CDNB (mU/mg)	DCNB (mU/mg)	NADH (mU/mg)
1	PhIP alone	5	415.6 ± 76.1[1,2]	8.41 ± 0.17[3]	126.7 ± 28.6[4]
2	PhIP + ANIT	5	491.0 ± 145.0	21.29 ± 0.44[5]	222.6 ± 2.2[6]
3	ANIT alone	5	322.4 ± 72.6	17.63 ± 0.39[3]	234.4 ± 94.5[7]
4	No treatment	5	269.0 ± 87.0	4.82 ± 0.87	61.4 ± 7.7

[1]Mean ± SD.–[2,3,4,7]Significantly different from Group 4 (No treatment) by Student's *t*-test or alternate Welch *t*-test (b: $p < 0.05$, c:$p < 0.001$, d: $p < 0.005$, g: $p < 0.02$).–[5,6]Significantly different from Group 1 (PhIP alone) by Student's *t*-test or alternate Welch *t*-test (e: $p < 0.001$, f: $p < 0.002$).

mas. The incidence of mammary adenocarcinoma in Group 2 (6.7%, $p < 0.001$) was significantly lower than that in Group 1 (56.3%). The average number of neoplasms in Group 2 (0.07 ± 0.25, $p < 0.001$) was also significantly lower than that in Group 1 (1.66 ± 2.31). Mean size of mammary tumours in Group 2 (6.5 mm) was smaller than that in Group 1 (10.6 ± 5.3 mm). No neoplastic lesions other than mammary tumours were observed in rats in any group.

Data regarding liver GST and QR activities as determined by short-term bioassay are summarised in Table III. GST activities toward CDNB in Group 1 was slightly but significantly ($p < 0.05$) higher than that in Group 4, whereas that in Group 2 was not significantly different from that in Group 1. GST activities toward DCNB in Groups 1 and 3 were significantly higher than that in Group 4 ($p < 0.001$). Combined treatment with PhIP and ANIT (Group 2) significantly increased GST-PCNB as compared to Group 1 treated with PhIP alone ($p < 0.001$) and showed a summation effect on induction of this activity. Liver QR activities in Groups 1 and 3 were significantly greater than that in Group 4 ($p < 0.005$). Combined treatment with PhIP and ANIT significantly increased QR activity ($p < 0.002$) but did not show a summation effect.

Discussion

In our study, a high incidence of mammary tumours was observed in rats given PhIP and a high-fat diet. It has been reported that long-term administration of HCAs is needed for the development of tumours in rodents.[8,11,12] We observed a higher incidence of mammary tumours as compared to the results reported previously by Ghoshal *et al.*[11] and El-Bayoumy *et al.*[12] Ghoshal *et al.*[11] reported that daily doses of 100 mg/kg of PhIP were toxic to the animals after the 7th dose and that weight loss was seen in surviving animals. In this experiment, 8 doses of 85 mg/kg PhIP were administered to rats for 11 days and did not cause body weight loss.

Treatment with ANIT alone in our study reduced the body weight as compared to that in vehicle-only controls. ANIT is known to induce hepatotoxicity and cholestasis in rats.[15–17] The dose (400 ppm in diet) of ANIT in our study was too low to induce liver toxicity or cholestasis and was about half the dose required to induce hepatotoxicity in rats. In fact, histological examination revealed neither hepatotoxicity nor cholestasis in rats given AINT. The experimental schedule (initiation feeding with ANIT) may be related to the lack of liver toxicity seen in our study.

Several chemopreventive agents for PhIP-induced mammary carcinogenesis, including synthetic or natural compounds with antioxidative properties, have been reported.[34–41] Their cancer chemopreventive effects were mostly observed when given during the entire experimental period or in the post-initiation phase of PhIP-induced mammary tumorigenesis, although diallyl disulfide and aspirin inhibited PhIP-induced mammary carcinogenesis when administered during the initiation phase.[34]

A number of mechanisms underlying chemoprevention by xenobiotics in PhIP-induced mammary tumorigenesis have been proposed. PhIP is oxidised to an *N*-hydroxy derivative [PhIP (NHOH)] in the liver by cytochrome P450 enzymes, and esterified by acetyltransferases or sulfotransferases to the ultimate carcinogen.[42–45] Adduct formation is thought to be crucial for PhIP-induced carcinogenesis and PhIP-DNA adducts have been detected in human tissues.[46] Certain isothiocyanates (*e.g.*, sulphoraphene, phenyl isothiocyanate and benzyl isothiocyanate (BITC)) have been reported to prevent chemically induced cancer development in laboratory animals.[47–55] Isothiocyanates exert their cancer chemopreventive action by modulating the activities of phase I and phase II drug metabolism enzymes.[47–53,55] ANIT can decrease hepatic cytochrome P-450 content.[16–18] PhIP is known to exert its carcinogenic

activity after metabolic activation by CYP1A2 or CYP1B1 mainly in the liver.[21–27] ANIT has been reported to inhibit carcinogenesis in the lung, liver, forestomach, intestine and mammary gland when given before or during carcinogen treatment.[15–18] In our study, ANIT elevated the activities of phase II enzymes, GST and QR in the liver. ANIT has been reported to increase the activity of GST,[20] which can inhibit DNA binding of *N*-acetyl-PhIP *in vitro*.[28] Thus, increased activities of GST and QR, particularly GST, in the liver may be one of the major causes of its cancer-suppressing effect observed in the present study. In our previous experiment, BITC failed to inhibit PhIP-induced mammary carcinogenesis in rats given 100 ppm of PhIP,[56] a higher dose than that used in the present study. The difference between the results of our previous and present studies may be due to the differences in enzyme induction capability of both compounds, BITC and ANIT; BITC shows weaker induction of enzymes involving oxidative metabolism and metabolic conversion than ANIT.[57]

In conclusion, ANIT significantly inhibited breast cancer development induced by PhIP, presumably through the induction of both GST and QR in the liver. Accordingly, ANIT may be a candidate chemopreventive agent for breast cancer. In relation to fat and PhIP, further studies of the effects on levels of CYP proteins, metabolic activation of PhIP by CYP isoforms and another typical phase II enzyme, UDP-glucuronyltrasferase, are necessary to confirm the suppression by ANIT in PhIP-induced mammary carcinogenesis, as UDP-glucuronyltransferase has also been reported to detoxify another heterocyclic amine, 2-amino-3-methylimidazo[4,5-*f*]quinoline (IQ).[58]

Acknowledgements

We thank Ms. K. Takahashi, Mrs. T. Hirose and Mr. K. Sato for technical support.

References

1. Doll R. Epidemiology and the prevention of cancer: some recent developments. J Cancer Res Clin Oncol 1988;114:447–8.
2. Sugimura T. Nutrition and dietary carcinogens. Carcinogenesis 2000;21:387–95.
3. Weisburger JH, Wynder EL. Dietary fat intake and cancer. Hematol Oncol Clin North Am 1991;5:7–23.
4. Adamson RH, Thorgeirsson UP, Sugimura T. Extrapolation of heterocyclic amine carcinogenesis data from rodents and nonhuman primates to humans. Arch Toxicol 1996;18:303–18.
5. Sinha R. An epidemiologic approach to studying heterocyclic amines. Mutat Res 2002;506–7:197–204.
6. Felton JS, Knize MG. Occurrence, identification, and potential mutagenicity of heterocyclic amines in cooked food. Mutat Res 1991; 259:205–17.
7. Wakabayashi K, Nagao M, Esumi H, Sugimura T. Food-derived mutagens and carcinogens. Cancer Res. 1992;52:2092s–8s.
8. Hasegawa R, Sano M, Tamano S, Imaida K, Shirai T, Nagao M, Sugimura T, Ito N. Dose-dependence of 2-amino-3-methylimidazo[4, 5-*b*]pyridine (PhIP) carcinogenicity in rats. Carcinogenesis 1993; 14:2553–7.
9. Ito N, Hasegawa R, Sano M, Tamano S, Esumi H, Takayama S, Sugimura T. A new colon and mammary carcinogen in cooked food, 2-amino-3-methylimidazo[4,5-*b*]pyridine (PhIP). Carcinogenesis 1991; 12:1503–6.
10. Sugimura T, Wakabayashi K, Ohgaki H, Takayama S, Nagao M, Esumi H. Heterocyclic amines produced in cooked food: unavailable xenobiotics. In: Ernster L, ed. Xenbiotics and cancer. Tokyo: Scientific Societies Press, 1991.279–88.
11. Ghoshal A, Preisegger K-H, Takayama S, Thorgeirsson SS, Snyderwine EG. Induction of mammary tumors in female Sprague-Dawley rats by the food-derived carcinogen 2-amino-3-methylimidazo[4, 5-*b*]pyridine and effect of dietary fat. Carcinogenesis 1994;15:2429–33.
12. El-Bayoumy K, Chae Y-H, Upadhyaya P, Rivenson A, Kurtzke C, Reddy BS, Hecht SS. Comparative tumorigenicity of benzo[*a*] pyrene, 1-nitropyrene and 2-amino-3-methylimidazo[4,5-*b*]pyridine administered by gavage to female CD rats. Carcinogenesis 1995; 16:431–4.
13. Weisburger JH, Rivenson A, Marcus LA, Lang J, Zang E, Pittman B, Nagao M, Sugimura T. Modification by dietary fat of mammary gland carcinogenesis induced by 2-amino-1-methyl-6-phenylimidazo[4,5-*b*] pyridine in female SD × F344 F1 hybrid rats. J Environ Pathol Toxicol Oncol 1997;16:329–34.
14. Murillo G, Mehta RG. Cruciferous vegetables and cancer prevention. Nutr Cancer 2001;41:17–28.
15. Sasaki S. Inhibitory effects by α-naphtyl-isothiocyanate on development of hepatoma in rats treated with 3′-methyl-4-dimethyl-aminoazobenzene. J Nara Med Assoc 1963;14:101–15.
16. Sidransky H, Ito N, Verney E. Influence of α-naphtyl-isothiocyanate on liver tumorigenesis in rats ingesting ethionine and N-2-fluorenylacetamide. J Natl Cancer Inst 1966;37:677–86.
17. Shinohara Y, Ogiso T, Hananouchi M, Nakanishi K, Yoshimura T, Ito N. Effect of various factors on the induction of liver tumors in animals by quinoline. Gann 1977;68:785–96.
18. Zhang Y, Talalay P. Anticarcinogenic activities of organic isothiocyanates: chemistry and mechanisms. Cancer Res 1994;54:1975s–81s.
19. Leonard TB, Popp JA, Graichen ME, Dent JG. α-Naphthylisothiocyanate induced alterations in hepatic drug metabolizing enzymes and liver morphology: implications concerning anticarcinogenesis. Carcinogenesis 1981;2:473–82.
20. Nikolaev V, Kerimova M, Naydenova E, Ivanov E, Dontchev N, Adjarov D. Biochemical changes in α-naphthyl isothiocyanate-induced chronic cholangitis in the rat. Exp Pathol 1988;33:261–3.
21. Kleman M, Overvik E, Mason G, Gustafsson JA. Effects of the food mutagens MeIQx and PhIP on the expression of cytochrome P450IA proteins in various tissues of male and female rats. Carcinogenesis 1990;11:2185–9.
22. Crofts FG, Strickland PT, Hayes CL, Sutter TR. Metabolism of 2-amino-1-methyl-6-phenylimidazo[4,5-*b*]pyridine (PhIP) by human cytochrome P4501B1. Carcinogenesis 1997;18:1793–98.
23. Wallin H, Mikalsen A, Guengerich FP, Ingelman-Sundberg M, Solberg KE, Rossland OJ, Alexander J. Differential rates of metabolic activation and detoxication of the food mutagen 2-amino-1-methyl-6-phenylimidazo[4,5-*b*]pyridine by different cytochrome P450 enzymes. Carcinogenesis 1990;11:489–92.
24. Watkins BE, Suzuki M, Wallin H, Wakabayashi K, Alexander J, Vanderlaan M, et al. The effect of dose and enzyme inducers on the metabolism of 2-amino-1-methyl-6-phenylimidazo[4,5-*b*]pyridine (PhIP) in rats. Carcinogenesis 1991;12:2291–5.
25. Zhao K, Murray S, Davies DS, Boobis AR, Gooderham NJ. Metabolism of the food derived mutagen and carcinogen 2-amino-1-methyl-6-phenylimidazo(4,5-*b*)pyridine (PhIP) by human liver microsomes. Carcinogenesis 1994;15:1285–8.
26. Davis CD, Ghoshal A, Schut HA, Snyderwine EG. Metabolic activation of heterocyclic amine food mutagens in the mammary gland of lactating Fischer 344 rats. Cancer Lett 1994;84:67–73.
27. Turesky RJ, Lang NP, Butler MA, Teitel CH, Kadlubar FF. Metabolic activation of carcinogenic heterocyclic aromatic amines by human liver and colon. Carcinogenesis 1991;12:1839–45.
28. Lin D, Meyer DJ, Ketterer B, Lang NP, Kadlubar FF. Effects of human and rat glutathione S-transferases on the covalent DNA binding of the N-acetoxy derivatives of heterocyclic amine carcinogens in vitro: a possible mechanism of organ specificity in their carcinogenesis. Cancer Res 1994;54:4920–6.
29. Young S, Hallowes RC. Tumours of the mammary gland. In: Turusov V, Mohr U, eds. Pathology of tumors in laboratory animals, vol. 1 Lyon: International Agency for Research on Cancer, 1973:31–74.
30. Benson AM, Hunkeler MJ, Talalay P. Increase of NAD (P)H: quinone reductase by dietary antioxidants: possible role in protection against carcinogenesis and toxicity. Proc Natl Acad Sci U S A 1980;77:5216–20.
31. Habig WH, Pabst MJ, Jakoby WB. Glutathione S-transferase: the first enzymatic step in mercapturic acid formation. J Biol Chem 1974;249:7130–9.
32. Prochaska H, Fernandes CL. Elevation of serum phase II enzymes by anticarcinogenic enzyme inducers: markers for a chemoprotected state? Carcinogenesis 1993;14:2441–5.
33. Bradford MM. A rapid and sensitive method for the quantitation of microgram quantities of protein utilizing the principle of protein-dye binding. Anal Biochem 1976;72:248–54.
34. Suzui N, Sugie S, Rahman KM, Ohnishi M, Yoshimi N, Wakabayashi K, Mori H. Inhibitory effects of diallyl disulfide or aspirin on 2-amino-1-methyl-6-phenylimidazo[4,5-*b*]pyridine-induced mammary carcinogenesis in rats. Jpn J Cancer Res 1997;88: 705–11.
35. Ohta T, Nakatsugi S, Watanabe K, Kawamori T, Ishikawa F, Morotomi M, Sugie S, Toda T, Sugimura T, Wakabayashi K. Inhibitory effects of Bifidobacterium-fermented soy milk on 2-amino-1-methyl-6-phenylimidazo[4,5-*b*]pyridine-induced rat mammary carcinogenesis, with a partial contribution of its component isoflavones. Carcinogenesis 2000;21:937–41.

36. Nakatsugi S, Ohta T, Kawamori T, Mutoh M, Tanigawa T, Watanabe K, Sugie S, Sugimura T, Wakabayashi K. Chemoprevention by nimesulide, a selective cyclooxygenase-2 inhibitor, of 2-amino-1-methyl-6-phenylimidazo[4,5-*b*]pyridine (PhIP)-induced mammary gland carcinogenesis in rats. Jpn J Cancer Res 2000;91:886–92.
37. Kawamori T, Uchiya N, Nakatsugi S, Watanabe K, Ohuchida S, Yamamoto H, Maruyama T, Kondo K, Sugimura T, Wakabayashi K. Chemopreventive effects of ONO-8711, a selective prostaglandin E receptor EP(1) antagonist, on breast cancer development. Carcinogenesis 2001;22:2001–4.
38. Hirose M, Akagi K, Hasegawa R, Yaono M, Satoh T, Hara Y, Wakabayashi K, Ito N. Chemoprevention of 2-amino-3-methylimidazo[4,5-*b*]pyridine-induced mammary gland carcinogenesis by antioxidants in female F344 rats. Carcinogenesis 1995;16:217–21.
39. Hasegawa R, Hirose M, Kato T, Hagiwara A, Boonyaphiphat P, Nagao M, Ito N, Shirai T. Inhibitory effect of chlorophyllin on PhIP-induced mammary carcinogenesis in female F344 rats. Carcinogenesis 1995;16:2243–6.
40. Hagiwara A, Boonyaphiphat P, Tanaka H, Kawabe M, Tamano S, Kaneko H, Matsui M, Hirose M, Ito N, Shirai T. Organ-dependent modifying effects of caffeine, and two naturally occurring antioxidants alpha-tocopherol and n-tritriacontane-16,18-dione, on 2-amino-1-methyl-6-phenylimidazo[4,5-*b*]pyridine (PhIP)-induced mammary and colonic carcinogenesis in female F344 rats. Jpn J Cancer Res 1999;90:399–405.
41. Hirose M, Nishikawa A, Shibutani M, Imai T, Shirai T. Chemoprevention of heterocyclic amine-induced mammary carcinogenesis in rats. Environ Mol Mutagen 2002;39:271–8.
42. Thorgeirsson SS, Davis CD, Schut HA, Adamson RH, Snyderwine EG. Possible relationship between tissue distribution of DNA adducts and genotoxicity of food-derived heterocyclic amines. Princess Takamatsu Symp 1995;23:85–92.
43. Snyderwine EG, Venugopal M, Yu M. Mammary gland carcinogenesis by food-derived heterocyclic amines and studies on the mechanisms of carcinogenesis of 2-amino-1-methyl-6-phenylimidazo[4,5-*b*] pyridine (PhIP). Mutat. Res. 2002;506–7:145–52.
44. Crofts FG, Sutter TR, Strickland PT. Metabolism of 2-amino-1-methyl-6-phenylimidazo[4,5-*b*]pyridine by human cytochrome P4501A1, P4501A2 and P4501B1. Carcinogenesis 1998;19:1969–73.
45. Lewis AJ, Walle UK, King RS, Kadlubar FF, Falany CN, Walle T. Bioactivation of the cooked food mutagen N-hydroxy-2-amino-1-methyl-6-phenylimidazo[4,5-*b*]pyridine by estrogen sulfotransferase in cultured human mammary epithelial cells. Carcinogenesis 1998;19:2049–53.
46. Nagao M. A new approach to risk estimation of food-borne carcinogens — heterocyclic amines – based on molecular information. Mutat Res 1999;431:3–12.
47. Wattenberg LW. Inhibition of carcinogenic effects of polycyclic hydrocarbons by benzyl isothiocyanate and related compounds. J Natl Cancer Inst 1977;58:395–8.
48. Lubet RA, Steele VE, Eto I, Juliana MM, Kelloff GJ, Grubbs CJ. Chemopreventive efficacy of anethole trithione, N-acetyl-L-cysteine, miconazole and phenethylisothiocyanate in the DMBA-induced rat mammary cancer model. Int J Cancer 1997;72:95–101.
49. Futakuchi M, Hirose M, Miki T, Tanaka H, Ozaki M, Shirai T. Inhibition of DMBA-initiated rat mammary tumour development by 1-O-hexyl-2,3,5-trimethylhydroquinone, phenylethyl isothiocyanate, and novel synthetic ascorbic acid derivatives. Eur J Cancer Prev 1998;7:153–9.
50. Zhang Y, Talalay P, Cho CG, Posner GH. A major inducer of anticarcinogenic protective enzymes from broccoli: isolation and elucidation of structure. Proc Natl Acad Sci U S A 1992;89:2399–403.
51. Zhang Y, Kensler TW, Cho CG, Posner GH, Talalay P. Anticarcinogenic activities of sulforaphane and structurally related synthetic norbornyl isothiocyanates. Proc Natl Acad Sci U S A 1994;91:3147–50.
52. Conaway CC, Yang YM, Chung FL. Isothiocyanates as cancer chemopreventive agents: their biological activities and metabolism in rodents and humans. Curr Drug Metab 2002;3:233–55.
53. Nishikawa A, Furukawa F, Lee IS, Tanaka T, Hirose M. Potent chemopreventive agents against pancreatic cancer. Curr Cancer Drug Targets 2004;4:373–84.
54. Jackson SJ, Singletary KW. Sulforaphane: a naturally occurring mammary carcinoma mitotic inhibitor, which disrupts tubulin polymerization. Carcinogenesis 2004;25:219–27.
55. Wattenberg LW. Inhibition of carcinogen-induced neoplasia by sodium cyanate, tert-butyl isocyanate, and benzyl isothiocyanate administered subsequent to carcinogen exposure. Cancer Res. 1981;41:2991–4.
56. Ino N, Sugie S, Ohnishi M, Mori H. Lack of inhibitory effect of benzyl isothiocyanate on 2-amino-1-methyl-6-phenylimidazo[4,5-*b*]pyridine (PhIP)-induced mammary carcinogenesis in rats. J Toxicol Sci 1996;21:189–94.
57. Lee MS. Enzyme induction and comparative oxidative desulfuration of isothiocyanates to isocyanates. Chem Res Toxicol 1996;9:1072–8.
58. Embola CW, Sohn OS, Fiala ES, Weisburger JH. Induction of UDP-glucuronosyltransferase 1 (UDP-GT1) gene complex by green tea in male F344 rats. Food Chem Toxicol 2002;40:841–4.

β-*Catenin* mutations in a mouse model of inflammation-related colon carcinogenesis induced by 1,2-dimethylhydrazine and dextran sodium sulfate

Hiroyuki Kohno,[1,3] Rikako Suzuki,[1,2] Shigeyuki Sugie[1] and Takuji Tanaka[1]

[1]Department of Oncologic Pathology, Kanazawa Medical University, 1–1 Daigaku, Uchinada, Ishikawa 920–0293, and [2]Research Fellow of the Japan Society for the Promotion of Science, 6 Ichiban-cho, Chiyoda-ku, Tokyo 102–8471, Japan

(Received October 29, 2004/Revised Novermber 24, 2004/Accepted November 26, 2004/Online publication 17 February, 2005)

In a previous study, we developed a novel mouse model for colitis-related carcinogenesis, utilizing a single dose of azoxymethane (AOM) followed by dextran sodium sulfate (DSS) in drinking water. In the present study, we investigated whether colonic neoplasms can be developed in mice initiated with a single injection of another genotoxic colonic carcinogen 1,2-dimethylhydrazine (DMH), instead of AOM and followed by exposure of DSS in drinking water. Male crj: CD-1 (ICR) mice were given a single intraperitoneal administration (10, 20 or 40 mg/kg body weight) of DMH and 1-week oral exposure (2% in drinking water) of a non-genotoxic carcinogen, DSS. All animals were killed at week 20, histological alterations and immunohistochemical expression of β-catenin, cyclooxygenase (COX-2) and inducible nitric oxide synthase (iNOS) were examined in induced colonic epithelial lesions (colonic dysplasias and neoplasms). Also, the β-*catenin* gene mutations in paraffin-embedded colonic adenocarcinomas were analyzed by the single strand conformation polymorphism method, restriction enzyme fragment length polymorphism and direct sequencing. The incidences of colonic neoplasms with dysplastic lesions developed were 100% with 2.29 ± 0.95 multiplicity, and 100% with 10.38 ± 4.00 multiplicity in mice given DMH at doses of 10 mg/kg or 20 mg/kg and 2%DSS, respectively. Although approximately half of the mice given DMH at a dose of 40 mg/kg bodyweight were dead after 2–3 days after the injection, mice who received DMH 40 mg/kg and 2%DSS had 100% incidence of colonic neoplasms with 9.75 ± 6.29 multiplicity. Immunohistochemical investigation revealed that adnocarcinomas, induced by DMH at all doses and 2%DSS, showed positive reactivities against β-catenin, COX-2 and iNOS. In DMH/DSS-induced adenocarcinomas, 10 of 11 (90.9%) adenocacrcinomas had β-*catenin* gene mutations. Half of the mutations were detected at codon 37 or 41, encoding serine and threonine that are direct targets for phosphorylation by glycogen synthase kinase-3β. The present results suggests that, as in the previously reported model (AOM/DSS) our experimental protocol, DMH initiation followed by DSS, may provide a novel and useful mouse model for investigating inflammation-related colon carcinogenesis and for identifying xenobiotics with modifying effects. (*Cancer Sci* 2005; 96: 69–76)

Colorectal cancer (CRC) is one of the most common non-smoking related cancers. The risk for CRC is associated with extent and duration of inflammatory bowel disease (IBD), including ulcerative colitis (UC) and Crohn's disease.[1,2] The etiopathogenesis of IBD remains uncertain, although it is generally assumed that chronic inflammation is the primary driving force.[3] To understand the pathogenesis of IBD and IBD-related CRC, several animal models were reported. The chemically induced and genetic models of colonic inflammation do not completely mimic the disease situation found in UC patients,[4] although they are more readily available, reproducible and conductive to therapeutic and mechanistic studies. Most used is an animal model with dextran sodium sulfate (DSS) administration through the diet, or drinking fluid. A non-genotoxic carcinogen, DSS[5] induces colonic inflammation in rodents with clinical and histopathological similarity to human UC.[6] However, the colitis model using DSS needs a long period or cycle administration of DSS to induce colitis and colitis-related CRC, and the incidence and/or multiplicity of induced tumors are relatively low.[7] Recently, we developed a novel mouse model for inflammation-related colon carcinogenesis utilizing a single and low dose of azoxymethane (AOM), a metabolite of 1,2-dimethylhydrazine (DMH), followed by a strong tumor-promoter DSS in drinking water.[8] This combined treatment with AOM and DSS resulted in a high incidence and greater multiplicity of colonic neoplasms within 20 weeks. Moreover, the first colonic malignancy was observed as early as 12 weeks of the experimental schedule. This model can be used for detecting the chemicals with weak colonic carcinogenicity in mice within a short-term period and for analyzing gene mutations in induced colonic neoplasms. The colon carcinogen DMH has been widely used to study chemically-induced colon cancer in rodents. Regardless of the mode of administration, DMH specifically induces colorectal tumors.[9] DMH-induced colon tumors in rodents are very close to human colon cancer with regard to morphology, pattern of growth and clinical manifestations.[10] Colorectal adenocarcinomas, induced by DMH in mice, often invade into the submucosa and muscular layer, but those induced by AOM and methylazoxymethanol did not show such biological and histological natures.[10,11] However, the major weakness of the model, using DMH, is that multiple injections of DMH and long-term experimental period are required to induce colon tumors in laboratory animals. β-Catenin, acting as a structural protein at cell–cell adherens junctions and as a transcriptional activator mediating Wnt signal transduction,[12] participates in a large cytoplasmic protein complex, which contains the tumor suppressor gene product of adenomatous polyposis coli (APC), glycogen synthase kinase-3β (GSK-3β) and axin/conductin.[13] Frequent mutation of the β-*catenin* gene was found in chemically induced colonic neoplasms in rodents.[14,15] For example, β-*catenin* mutations were frequently observed in AOM-induced colon tumors in rats and mice.[15,16] In rats, 32% of colonic adenocarcinomas, induced by DMH, possessed β-*catenin* gene mutations.[17] Mutation of the *APC* gene is known to repress the degradation and result in accumulation of β-catenin.[18] About 80% of colorectal neoplasms harbor mutations in the *APC* gene and half of the reminder have β-*catenin* mutation.[19–21] In the colonic neoplasms (adenomas and adenocarcinomas), β-catenin was universally localized to the cytoplasm and/or nucleus.[22] In addition, altered expression of

[3]To whom correspondence should be addressed. E-mail: h-kohno@kanazawa-med.ac.jp

© Japanese Cancer Association doi: 10.1111/j.1349-7006.2005.00020.x

β-catenin was reported in inflammation-related colonic cancer in rodents[8,23] and humans.[24] These findings suggest that the mutation of β-*catenin* gene plays an important role in the development of colon carcinogenesis in rodents as well as in humans. In the current study, we tried to induce colonic neoplasms in mice with a single administration of DMH at three dose levels followed by a 1-week exposure of DSS in drinking water. In addition, we analyzed mutations of the β-*catenin* gene in induced colonic adenocarcinomas and compared with those found in colonic malignancies induced by AOM and DSS.[8]

Materials and Methods

Animals, chemicals and diets. Male Crj: CD-1 (ICR) mice (Charles River Japan Inc., Tokyo, Japan) aged 5 weeks were used. They were maintained at the Animal Facility of Kanazawa Medical University according to the Institutional Animal Care Guidelines. All animals were housed in plastic cages (four or five mice/cage) with free access to drinking water and a pelleted basal diet (CRF-1; Oriental Yeast Co., Ltd, Tokyo, Japan), under controlled conditions of humidity (50 ± 10%), light (12:12 h light : dark cycle) and temperature (23 ± 2°C). After 7-days of quarantine, they were randomized by body weight into experimental and control groups. DMH was purchased from Wako Pure Chemical Ind. Ltd. (Osaka, Japan). DSS with a molecular weight of 36 000–50 000 was obtained from ICN Biochemicals, Inc. (Aurora, OH, USA [Cat no. 160110]).

Experimental procedure. A total of 43 male ICR mice were divided into seven experimental and control groups. DMH was dissolved in 0.9% saline and the pH adjusted to 6.5 using 0.25 M NaOH. Groups 1 (seven mice), 2 (eight mice) and 3 (eight mice) were given a single intraperitoneal (i.p.) injection of DMH at a dose of 10, 20 or 40 mg/kg body weight, respectively. Starting 1 week after the injection, animals in groups 1–3 were given 2% (w/v) DSS in drinking water for 7 days, and then followed without any further treatment for 18 weeks. Groups 4 (five mice) and 5 (five mice) were given DMH 20 and 40 mg/kg body weight alone, respectively. Group 6 (five mice) was given 2% DSS alone. Group 7 (five mice) was an untreated control. All animals were killed at week 20 by ether overdose. At the termination of the study, all organs, including small and large intestines, in the mice were carefully inspected for macroscopic pathological lesions. The large bowels were flushed with saline, excised, their length measured (from ileocecal junction to the anal verge), cut open longitudinally along the main axis, and then washed with saline. Macroscopic inspection on the large bowels was carefully carried out and they were cut and fixed in 10% buffered formalin for at least 24 h. Formalin-fixed colonic tissues were routinely processed for histological examination. Histological diagnosis was performed on hematoxylin–eosin (HE) stained section. Eleven colonic tumors, histologically diagnosed as adenocarcinoma, were stored in a deep-freezer at −80°C for analyzing β-*catenin* mutation. On HE-stained sections, histological alterations, such as mucosal ulceration, dysplasia and colonic neoplasms, were examined. Colitis with or without ulceration was scored on HE-stained sections, according to the following morphological criteria described by Cooper *et al.*:[25] grade 0, normal colonic mucosa; grade 1, shortening and loss of the basal one-third of the actual crypts with mild inflammation in the mucosa: grade 2, loss of the basal two-thirds of the crypts with moderate inflammation in the mucosa; grade 3, loss of the entire crypts with severe inflammation in the mucosa and submucosa, but with retainment of the surface epithelium; and grade 4, presence of mucosal ulcer with severe inflammation (neutrophil, lymphocyte, and plasma cell infiltration) in the mucosa, submucosa, musculaaris propria and/or subserosa. High- or low-grade of dysplasia of colonic mucosa was diagnosed according to the criteria described by Riddell *et al.*[26] and Pascal.[27] Colonic neoplasms were diagnosed according to the description by Ward.[28] Histopathological examination was also carried out in other organs.

Immunohistochemistry. As in our previous study,[8] immunohistochemistry for β-catenin, cyclooxygenase (COX)-2 and nitric oxide synthase (iNOS), was performed on 3-μm-thick paraffin-embedded sections from colons of mice in all groups, utilizing the labeled streptavidin–biotin method using a LSAB Kit (DAKO, Glostrup, Denmark) with microwave accentuation. The paraffin-embedded sections were heated for 30 min at 65°C, deparaffinized in xylene, and rehydrated through graded ethanols at room temperature. A 0.05 M Tris HCl buffer (pH 7.6) was used to prepare solutions and for washes between various steps. Incubations were performed in a humidified chamber. Sections were treated for 40 min at room temperature with 2% bovine serum albumin, and incubated overnight at 4°C with primary antibodies, such as anti-β-catenin mouse monoclonal antibody (diluted 1:1000; Transduction Laboratories, Lexington, KY, USA), anti-COX-2 mouse monoclonal antibody (diluted 1:200; Transduction Laboratories), and anti-iNOS mouse monoclonal antibody (cat. no. N32020-150; diluted 1:250, Transduction Laboratories). To reduce the non-specific staining of mouse tissue by the mouse antibodies, a mouse on mouse immunoglobulin G blocking reagent (Vector Laboratories Inc., Burlingame, CA, USA) was applied for 1 h. Horseradish peroxidase activity was visualized by treatment with H_2O_2 and 3,3′-diaminobenzidine for 5 min. At the last step, the sections were weakly counterstained with Mayer's hematoxylin (Merck Ltd, Tokyo, Japan). For each case, negative controls were performed on serial sections. On the control sections, incubation with the primary antibodies was omitted. Intensity and localization of immunoreactivities against all primary antibodies used were examined on all sections using a microscope (Olympus BX41, Olympus Optical Co., Ltd, Tokyo, Japan) and recorded.

DNA extraction. For analysis of β-*catenin* mutations, 11 colonic adenocarcinomas developed in DMH (10 or 20 mg/kg body weight)/DSS-treated mice were used. DNA was extracted from frozen tissue using Wizard® Genomic DNA Purification Kit (Promega, Madison, WI, USA).

Polymerase chain reaction-single strand conformation polymorphism analysis. DNA from colonic adenocarcinomas was polymerase chain reaction (PCR)-amplified with primers (5′-primer, GCTGACCTGATGGAGTTGGA; 3′-primer, GCTACTTGCTCTTGCGTGAA), which were designed to amplify exon 3 of the β-*catenin* gene containing the consensus sequence for GSK-3β phosphorylation.[15] The length of the PCR product with these primers is 227 bp. The primers were purchased from Sigma-Aldrich Japan K.K. (Tokyo, Japan). PCR for non-radioisotopic single strand conformation polymorphism (SSCP) was performed in 50 μL of reaction mixture consisting of 0.5 μM of each primer, 1 × PCR buffer (Takara Bio, Otsu, Japan), 250 μM each dNTP, 2.5 U TaKaRa Ex Taq (Takara Bio) and 1 μL of template DNA. The mixture was heated at 94°C for 1 min and subjected to 30 cycles of denaturation (94°C, 0.5 min), annealing (55°C, 0.5 min) and extension (72°C, 1 min) using a using a TaKaRa PCR Thermal Cycler Dice (Takara Bio). The amplified PCR product was analyzed for its mobility-shifted bands using a GenePhor (Amersham Biosciences Corp., NJ, USA) with a GeneGel Clean (Amersham Biosciences Corp.) according to the manufacturer's protocol. Electrophoresis was carried out at 90 V for 25 min and then 500 V for 50 min at 20°C, and the gels were soaked in 10% trichloroacetic acid and in 50% methanol for 10 min each. DNA bands were detected by silver staining using 2D Silver Staining Solution II (Daiichi Chemical DNA Co., Tokyo, Japan).

Restriction fragment length polymorphism assay for PCR products of β-*catenin*. To detect β-catenin mutations at codons 32, 33 and 34, PCR products were treated with a restriction enzyme HinfI

© Japanese Cancer Association doi: 10.1111/j.1349-7006.2005.00020.x

(Wako Pure Chemical Industries, Tokyo, Japan) and electrophoresed on 5% agarose gels. Recognition sequences of *Hin*fI are GANTC. The PCR product of 227 bp is digested by *Hin*fI to 82, 7 and 138 bp in the case of the wild-type, to 89 and 138 bp with mutations at the first or second bases of codons 32 or 33, and to 82 and 145 bp with mutations at the second or third bases of codons 34 or 35.

Direct DNA sequencing. The PCR products were purified and concentrated to 20 μL using Microcon 100 (Amicon Inc., Beverley, MA, USA). With 2 μL of the purified PCR products and 5′ or 3′ PCR primers, cycle sequencing reactions were carried out using a BigDye Terminator v1.1 Cycle Sequencing Kit (Applied Biosystems, Foster City, CA, USA) and purified by isopropanol precipitation. The sequences were determined with an ABI PRISM 310 Genetic Analyzer (PerkinElmer, Wellesley, MA, USA).

Statistical analysis. All measurements were compared by Student's *t*-test, Welch's *t*-test, chi-squared test or Fisher's exact probability test for multiple group comparisons.

Results

General observations. Approximately half of the mice injected 40 mg/kg body weight of DMH (four mice of group 3, and two mice of group 5) died of hepatotoxicity of DMH 2–3 days after the injection. This was confirmed by histological examination of liver. Also bloody stool was found during and soon after of DSS exposure (days 12–21) in a few mice who received 2% DSS in drinking water, and their body weight gains were slightly decreased (data not shown). Thereafter, however, no such clinical symptoms were observed. The body and liver weights, and lengths of large bowel of mice in all groups at the end of the study (week 20) are listed in Table 1. There were no significant differences among the groups in these measurements.

Pathological findings. Macroscopically, nodular, polypoid or flat-type colonic tumors were observed in the middle and distal colon of all mice in groups 1–3 (Fig. 1), but not in the small intestine. Their histopathology was well- or moderately-differentiated tubular adenocarcinoma (Fig. 2a) or tubular adenoma (Fig. 2b). Histologically, there were no tumors in any organs other than the large bowel in these groups. The incidences and multiplicities of large bowel adenoma, adenocarcinoma and total tumors (adenoma + adenocarcinoma) are summarized in Table 2. The incidences of total tumors and adenocarcinoma in mice of given DMH/DSS (groups 1–3) were 100%. The multiplicities of total tumors, adenoma and adenocarcinoma in groups 2 and 3 were significantly higher than those of group 1 ($P \leq 0.001$, $P \leq 0.01$ or $P \leq 0.05$, respectively). In mice of groups 4–7, no neoplasms developed in any organs including large bowel. Besides colonic neoplasms, all mice in groups 1–3 had colonic dysplasia (Fig. 2c). Their multiplicities were 4.71 ± 2.29, 7.13 ± 1.27 and 8.25 ± 3.10 in groups 1, 2 and 3, respecively (Table 3). The multiplicities of total dysplasia and high-grade dysplasia in groups 2 and 3 were significantly greater than those of group 1 ($P \leq 0.02$, $P \leq 0.01$ or $P \leq 0.05$, respectively). There were no such dysplatic lesions in mice of groups 4–7. In addition, colonic mucosal ulceration (grade 1) was found in the distal colon of mice in groups 1, 2, 3 and 5 (Table 3).

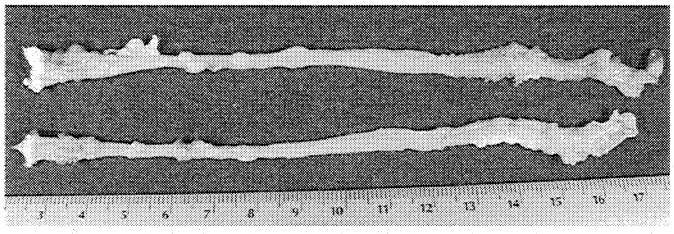


Fig. 1. Representative macroscopic view of the colonc from group 2 (1,2-dimethylhydrazine [DMH] 20 mg/kg body weight →2% dextran sodium sulfate [2%DSS]). Note the numerous polypoid tumors in the colon.

Table 1. Body weights, liver weights, and lengths of large bowel in each group

Group no.	Treatment (no. mice examined)	Body weight (g)	Liver weight (g)	Length of large bowel (cm)
1	DMH 10 mg/kg→2%DSS (7)	42.6 ± 2.7†	2.47 ± 0.29	13.8 ± 1.3
2	DMH 20 mg/kg→2%DSS (8)	43.3 ± 3.0	2.63 ± 0.35	13.5 ± 1.5
3	DMH 40 mg/kg→2%DSS (4)	44.3 ± 3.9	2.64 ± 0.21	13.9 ± 1.2
4	DMH 20 mg/kg (5)	45.9 ± 3.6	2.81 ± 0.41	14.5 ± 1.1
5	DMH 40 mg/kg (3)	43.2 ± 1.9	2.86 ± 0.46	14.9 ± 0.1
6	2%DSS (5)	42.1 ± 5.5	2.82 ± 0.31	13.9 ± 1.0
7	None (5)	44.6 ± 3.2	2.32 ± 0.45	15.0 ± 0.9

†Mean ± standard deviation. DMH, 1,2-Dimethylhydrazine; DSS, dextran sodium sulfate.

Table 2. Incidence of large bowel neoplasms in mice treated with 1,2-dimethylhydrazine and dextran sodium sulfate

Group no.	Treatment (no. mice examined)	No. mice with large bowel neoplasms		
		Total (%) (multiplicity)	Adenoma (%) (multiplicity)	Adenocarcinoma (%) (multiplicity)
1	DMH 10 mg/kg→2%DSS (7)	100 (2.29 ± 0.95)	57.1 (1.00 ± 1.15)	100 (1.29 ± 0.50)
2	DMH 20 mg/kg→2%DSS (8)	100 (10.38 ± 4.00)*	87.5 (4.63 ± 3.29)**	100 (5.75 ± 1.83)*
3	DMH 40 mg/kg→2%DSS (4)	100 (9.75 ± 6.29)**	100 (5.25 ± 4.65)***	100 (4.50 ± 1.73)*
4	DMH 20 mg/kg (5)	0	0	0
5	DMH 40 mg/kg (3)	0	0	0
6	2%DSS (5)	0	0	0
7	None (5)	0	0	0

Significantly different from group 1 by Student's *t*-test (*$P < 0.001$, **$P < 0.01$, and ***$P < 0.05$). DMH, 1,2-Dimethylhydrazine; DSS, dextran sodium sulfate. Numbers in parentheses are multiplicity (mean ± standard deviation) of large bowel tumors.

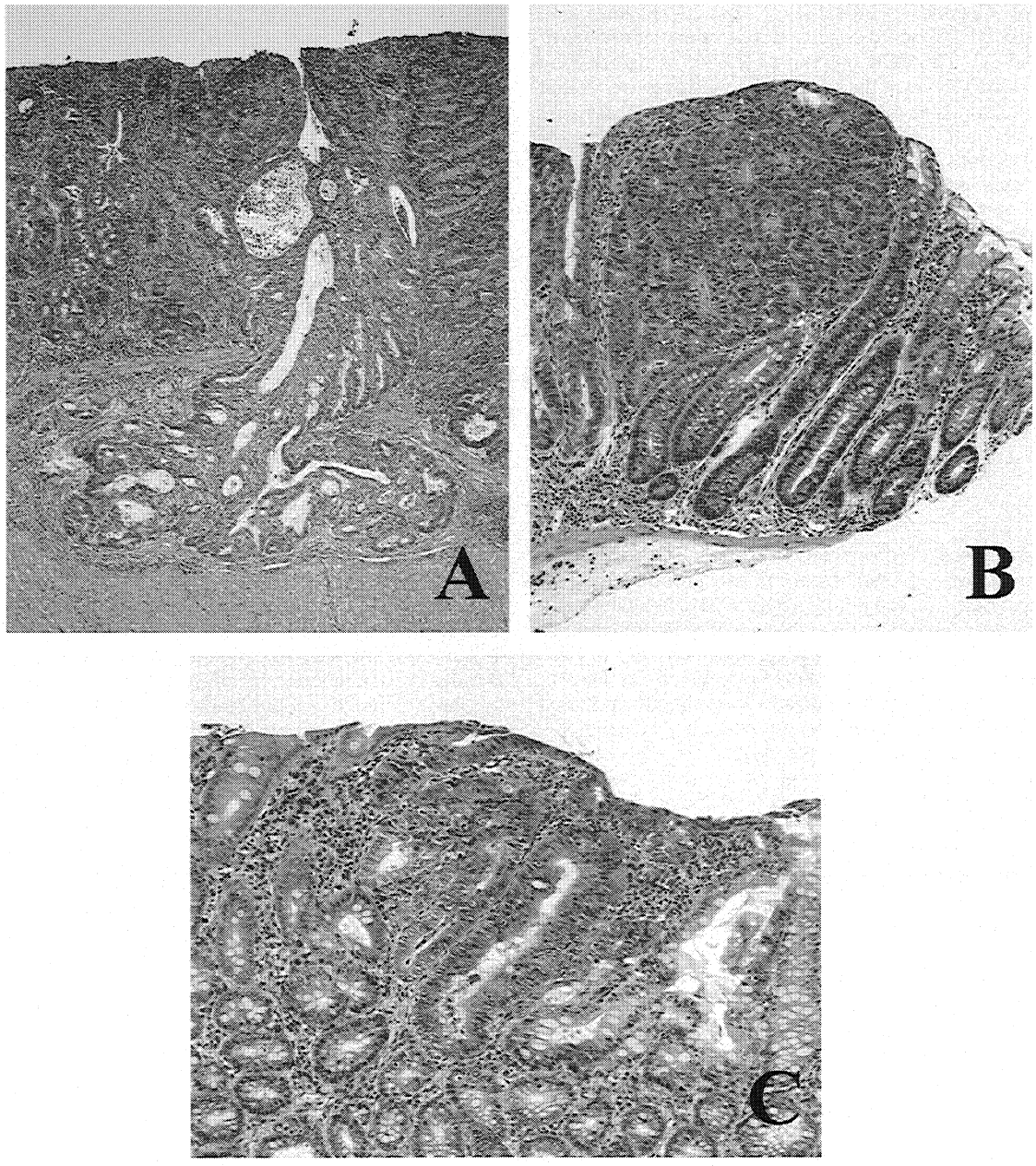


Fig. 2. Histopathology of colonic neoplasms developed in mice. (a) adenocarcinoma (b) adenoma, and (c) dysplasia. Hematoxylin–eosion stain. Original magnification (a) ×4, (b) ×10, and (c) ×20.

Immunohistochemical findings. The immunoreactivities against β-catenin, COX-2 and iNOS were noted in all colonic lesions, including neoplasms and dysplastic lesions. The immunoreactivity showed dark brown reaction products with slight variation in the intensity and distribution. Strong β-catenin expression was seen in the nucleus and cytoplasm of adenocarcinoma cells (Fig. 3a). Although the intensity was relatively weaker than carcinoma cells, adenoma cells showed positivity for β-catenin in their cytoplasm and cell membrane. β-Catenin immunoreactivity was also found in the cell membrane and cytoplasm of dysplastic cells, but intensity was weaker than adenoma cells. Non-lesional cryptal cells showed weak positivity of β-catenin in their cell membrane. In addition, positive reaction against β-catenin antibody was found in the cytoplasm of vascular endothelium, infiltrated inflammatory cells, and ganglion cells in myenteric (Auerbach's) plexus. Strong COX-2 immunoreactivity was found in adenocarcinoma cytoplasm (Fig. 3b). Adenoma cells also were found in their cytoplasm, and the intensity was weaker than adenocarcinoma cells. Dysplastic cells showed weak positivity for COX-2 when compared to neoplastic cells. Non-lesional cryptal cells at lower part of crypts were weakly positive for COX-2, and the stainability was lower than dysplastic crypts. Strongly positive reaction of COX-2 was also seen in the endothelium of small blood vessels, and inflammatory cells infiltrated in the lamina propria. Smooth muscle cells and fibroblasts in the wall of the large bowel showed weak reaction of COX-2. iNOS-immunohistochemistry showed strong immunoreactivity in the cytoplasm of adenocarcinoma (Fig. 3c) and adenoma cells; the intensity was greater in carcinoma cells when compared to adenoma cells. Also, dysplastic cells were positive for iNOS in their cytoplasm, but the intensity was weaker than adenoma cells. The faint positive

© Japanese Cancer Association doi: 10.1111/j.1349-7006.2005.00020.x

Table 3. Incidence of large bowel ulceration and dysplasia in mice treated with 1,2-dimethylhydrazine and dextran sodium sulfate

Group no.	Treatment (no. mice examined)	Incidence of mucosal ulcer (%) (multiplicity)	Incidence of colonic dysplasia (multiplicity)		
			Total	Low-grade	High-grade
1	DMH 10 mg/kg→2%DSS (7)	100 (2.43 ± 1.40)	100 (4.71 ± 2.29)	100 (3.00 ± 1.29)	100% (1.71 ± 1.11)
2	DMH 20 mg/kg→2%DSS (8)	100 (1.86 ± 0.4)	100 (7.13 ± 1.25)*	100 (2.88 ± 1.25)	100% (4.25 ± 1.58)**
3	DMH 40 mg/kg→2%DSS (4)	100 (2.50 ± 1.29)	100 (8.25 ± 3.10)	100 (4.00 ± 1.41)	100% (4.25 ± 2.22)***
4	DMH 20 mg/kg (5)	0 (0)	0 (0)	0 (0)	0 (0)
5	DMH 40 mg/kg (3)	0 (0)	0 (0)	0 (0)	0 (0)
6	2%DSS (5)	40 (0.51 ± 0.32)	0 (0)	0 (0)	0 (0)
7	None (5)	0 (0)	0 (0)	0 (0)	0 (0)

Significantly different from group 1 by Student's *t*-test (*$P < 0.02$, **$P < 0.01$, and ***$P < 0.05$). DMH, 1,2-Dimethylhydrazine; DSS, dextran sodium sulfate. Numbers in parentheses are multiplicity (mean ± standard deviation) of large bowel tumors.

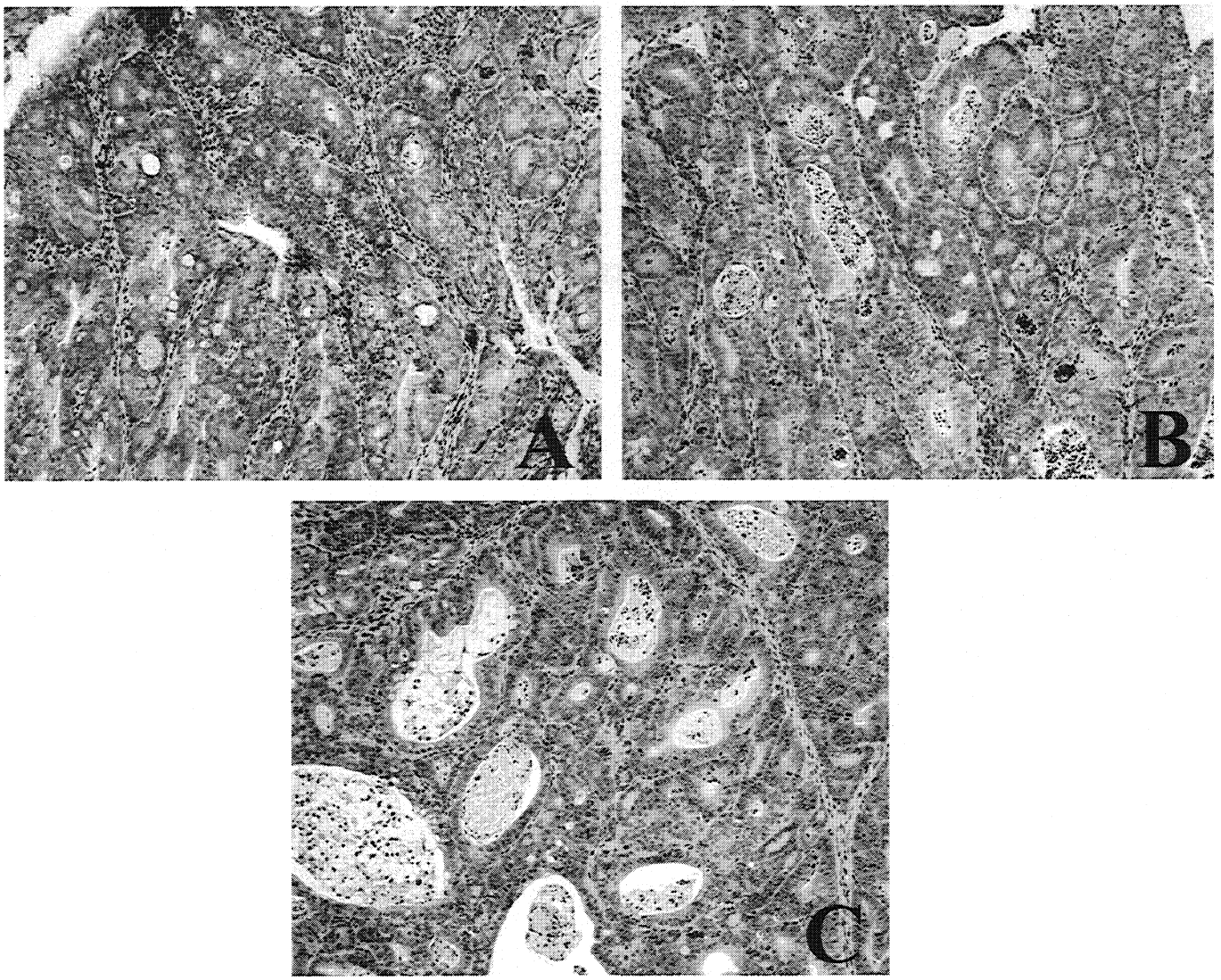


Fig. 3. Immunohistochemistry of (a) β-catenin, (b) cyclooxygenase (COX-2), and (c) nitric oxide synthase (iNOS), and immunofluorescent staining of β-catenin in colonic adenocarcinoma in mice. Original magnification (a–c) ×10.

Table 4. Expression of β-catenin, nitric oxide synthase and cyclooxygenase in 1,2-dimethylhydrazine/dextran sodium sulfate-induced mouse colon lesions

Protein	Normal mucosa	Dysplasia	Adenoma	Adenocarcinoma
β-Catenin	±~+	+~++	++	+++
	(M†)	(M, C‡)	(M, C)	(C, N§)
COX-2	−~±	+	++	+++
	(C)	(C)	(C)	(C)
iNOS	−~±	+	++	+++
	(C)	(C)	(C)	(C)

†Cell membrane; ‡cytoplasm, §nucleus. −, No staining; ±, faint and partial staining; +, weak staing; ++, moderate staining, +++, strong staining. COX-2, cyclooxygenase; iNOS, nitric oxide synthase.

Table 5. Mutations in exon 3 of the β-*catenin* gene in 1,2-dimethylhydrazine/dextran sodium sulfate-induced mouse colonic adenocarcinomas

Sample	β-catenin status		Amino acid substitution
DMH 10/DSS-1	Codon 37	TCT→CCT	Ser→Pro
DMH 10/DSS-2	Codon 32	GAT→AAT	Asp→Asn
DMH 10/DSS-3	Codon 37	TCT→CCT	Ser→Pro
DMH 20/DSS-4	Wild type		–
DMH 20/DSS-5	Codon 34	GGA→GAA	Gly→Glu
DMH 20/DSS-6	Codon 34	GGA→GAA	Gly→Glu
DMH 20/DSS-7	Codon 41	ACC→ATC	Thr→Ile
DMH 20/DSS-8	Codon 34	GGA→GAA	Gly→Glu
	Codon 41	ACC→ATC	Thr→Ile
DMH 20/DSS-9	Codon 34	GGA→GAA	Gly→Glu
DMH 20/DSS-10	Codon 41	ACC→ATC	Thr→Ile
DMH 20/DSS-11	Codon 34	GGA→GAA	Gly→Glu

DMH, 1,2-Dimethylhydrazine; DSS, dextran sodium sulfate.

reaction was found in the cytoplasm of non-lesional cryptal cells. Immunohistochemical iNOS expression was strong in the endothelial cells of small blood vessels and inflammatory cells in the lamina propria. COX-2- and iNOS-stained inflammatory cells were also frequently observed in areas of mucosal ulceration in groups 1, 2, 3 and 6. The results of immunoreactivities against β-catenin, COX-2, and iNOS are summarized in Table 4.

Mutation in β-*catenin* gene. In this study, we analyzed the status of the β-*catenin* gene in the histological sections of DMH/DSS-induced colon adenocarcinomas. We detected β-*catenin* gene mutations in 10 out of 11 colonic adenocarcinomas induced by DMH (10 or 20 mg/kg bodyweight) and 2% DSS (Figs 4,5). All mutations detected in colon adenocarcinomas converged at codons 32, 34, 37 and 41, all being functionally important codons for β-catenin degradation: five were located at the second base of codon 34, three at the second base of codon 41, two at the first base of codon 37 and one at the first base of codon 32. Except for mutation (A : T to G : C) at the first base of codon 37, all were G : C to A : T transitions (Table 5).

Discussion

In the current study, a single i.p. injection of DMH (10, 20 or 40 mg/kg body weight) followed by a 1-week exposure of 2% DSS in drinking water, could produced colonic adenocarcinomas with 100% incidence in male ICR mice within 20 weeks. All of the DMH/DSS-induced colonic adenocarcinomas were immunohistochemically positive for β-catenin, COX-2 and iNOS. Moreover, 10 (91%) out of 11 colonic adenocarcinomas had β-catenin mutations. However, no colonic neoplasms were found in mice treated with DMH alone or DSS alone. These findings indicated a powerful tumor-promoting ability of DSS on DMH-initiated colon carcinogenesis in male ICR mice, as found in our previous experiment using AOM as a carcinogen.[8] In the current study, dosing of 40 mg/kg body weight of DMH was lethal in almost half of the mice. This was caused by hepatotoxicity (necrosis and bleeding in the liver) of DMH at the dose. Therefore, appropriate dose of DMH was considered to be 10 or 20 mg/kg body weight in this model. β-Catenin is a multifunctional molecule involved in the cadherin-mediated cell–cell adhesion and Wnt-APC signal transduction.[29] Regulation of membrane, cytoplasmic and nuclear pools of β-catenin is crucial for modulating its adhesion and signaling functions.[30] Normally, β-catenin is localized in cell–cell junctions with very low levels of β-catenin in the cytoplasm and nucleus. Accumulation of β-catenin in the cytoplasm or nucleus as a consequence of mutant *APC*, β-*catenin* or *Axin*, is associated with colon carcinogenesis.[31] β-Catenin accumulation moves

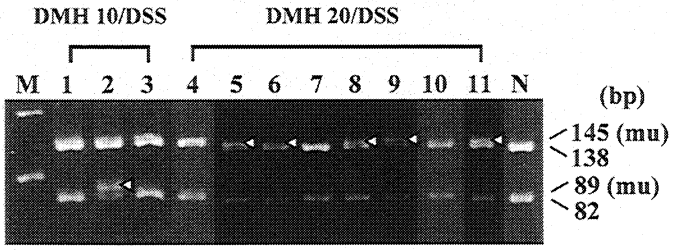


Fig. 5 Restriction fragment length polymorphism (RFLP) analysis of the β-*catenin* gene in mouse colon adenocarcinomas. Lanes 1–11: 1,2-dimethylhydrazine/dextran sodium sulfate (DMH/DSS)-induced mouse colon adenocarcinomas samples. Lanes 1–3: DMH (10 mg/kg bodyweight)/DSS-induced mouse colon adenocarcinoma samples. Lanes 4–11: DMH (20 mg/kg body weight)/DSS-induced mouse colon adenocarcinoma samples. Lane M: DNA size markers. Lane N: Negative control mouse colon mucosa sample. Arrowheads indicate tumor-specific bands.

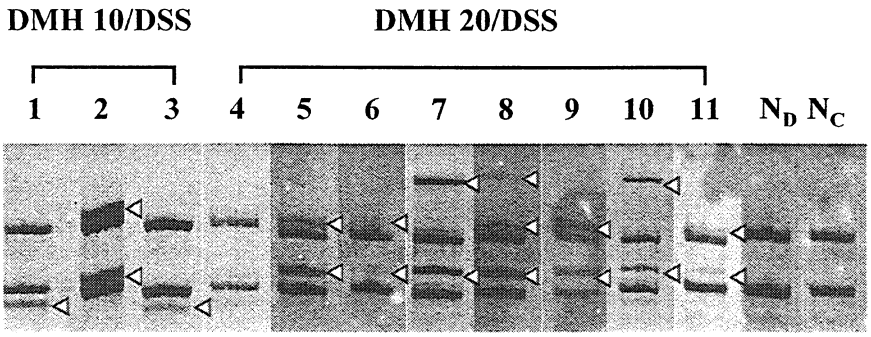


Fig. 4. Polymerase chain reaction–single strand conformation polymorphism (PCR-SSCP) analysis of the β-*catenin* gene in mouse colon adenocarcinomas. 1,2-Dimethylhydrazine/dextran sodium sulfate (DMH/DSS)-induced mouse colon adenocarcinomas (lanes 1–11). Lanes 1–3: DMH (10 mg/kg body weight)/DSS-induced mouse colon adenocarcinoma samples. Lanes 4–11: DMH (20 mg/kg body weight)/DSS-induced mouse colon adenocarcinoma samples. Lane N_D: DMH (20 mg/kg body weight)-induced mouse colon mucosa sample. Lane N_C: negative control mouse colon mucosa sample. Arrowheads indicate tumor-specific bands.

© Japanese Cancer Association doi: 10.1111/j.1349-7006.2005.00020.x

from the cytoplasm to the nucleus when the β-*catenin* or *APC* genes are mutated or the Wnt signaling pathway is activated.[32] Immunohistochemically aberrant expression of β-catenin was reported in colonic neoplasms and dysplasia in a DSS-induced mouse colitis model,[23] and human colitis-related dysplasia and neoplasms.[33,34] The observed frequent mutations in the GSK-3β phosphorylation consensus motif of the β-*catenin* gene appear to be associated with alteration of the cellular localization and functional site of the protein, as shown by immnohistochemical staining in the present study. Our results are comparable to those in a recent report describing altered distribution of β-catenin in UC-related CRC.[35] Although, the β-*catenin* gene is frequently mutated at codons 33, 41 and 45 of the GSK-3β phosphorylation motif in human colon cancers without APC mutations,[36] the mutations of the gene in chemically induced rat colon tumors is found at codons 32, 33 and 34.[15,17] In the present study, we detected β-*catenin* gene mutation of mouse colon adenocarcinomas, induced by DMH/DSS, at codon 32, 34, 37 and 41. The location was slightly different from a report documenting that β-*catenin* gene mutations of mouse colon tumors, induced by AOM, were present at codons 33, 34, 37 and 41, but not at codon 32.[16] Recently, we detected β-*catenin* gene mutations of mouse colon adenocarcinomas, induced by AOM/DSS, at codons 32, 33 and 34.[37] However, in the current protocol, half of the mutations caused by DMH/DSS treatment were at codon 37 and 41, which are important serine and threonine sites for GSK-3β phosphorylation. Koesters *et al.*[17] reported that the different mutational spectra, observed in *Ctnnb1*, directly relates to the particular carcinogenic treatment. They demonstrated that the β-*catenin* mutations at codons 37 and 41 possess higher oncogenic potential.[17] Therefore, it may be speculated that DSS exposure caused a shift in the mutation sites induced by DMH alone treatment. Since mutation of β-*catenin* is reported to be an early event of colorectal carcinogenesis,[38] molecular analysis at early stage of colon carcinogenesis should be carried out in this model. Although the mutations of the *APC* and β-*catenin* are rare in UC-related CRC, as compared with sporadic CRC, nuclear β-catenin expression is related to UC-related CRC development.[39] Since the data on β-*catenin* mutation in UC-related CRC are limited, more studies are required to determine the role of the β-*catenin* mutation in UC-related CRC. Also, expression of *c-myc, cyclinD1* and c-*jun*, which are targets of the β-catenin/APC pathway,[17,40,41] may also influence colon carcinogenesis in the present model. Such analysis is underway in our laboratory. Nitric oxide (NO) and prostaglandin, as the main inflammatory mediators, take part in the pathogenesis of IBD, with enhanced expression of iNOS and COX-2 in the morbid colonic mucosa.[42,43] Moreover, expression of the iNOS and COX-2 is increased in human colorectal tumors with inflammation,[44] and in carcinogen-induced colon tumors in rodents.[45] There exist various proposed pathways for NO-induced regulation of COX-2 expression and for modulation of cancer development.[46] They include cross–talk or interactions between endogenous NO and COX-2, and between β-catenin/APC pathway and COX-2.[47] β-Catenin/APC is reported to play a critical role in NO induction of COX-2 in colon epithelial cells.[48] Furthermore, Howe *et al.*[49] demonstrated that β-catenin/Tcf-4 complex transactivates the expression of PEA3, a transcription factor of Ets family, and stimulates COX-2 expression. More recently, it has been reported that NO increases PEA3 expression through β-catenin/APC pathway and directly augments the COX-2 promoter activity of the PEA3/p300 in YAMC cells.[50] In the present study, all colonic neoplasms were immunohistochemically positive for iNOS and COX-2, which was in accordance with the previous reports.[8] Furthermore, strong β-catenin expression was found in the nucleus and cytoplasm of adenocarcinoma cells. It may be possible that the increased expression of iNOS may be related to the altered localization of β-catenin, and/or increased expression of COX-2 in the colonic tumor formation and/or progression. Our recent work suggest involvement of oxidative/nitrosative stress in tumor-promoting effect of DSS on AOM-induced colon carcinogenesis in mice.[51]

In conclusion, the results in the current study indicate that a single dose of DMH followed by DSS resulted in a high incidence of colonic epithelial malignancies with β-*catenin* mutations within 20 weeks. Furthermore, half of the β-*catenin* mutations, detected in adenocarcinomas, were at codon 37 and 41, and strong β-catenin expression was seen in their nucleus and cytoplasm. Also, our findings suggest the importance of inflammation caused by DSS exposure in mouse colon carcinogenesis. The experimental protocol described here could be applied to investigate detailed molecular mechanism of inflammation-related CRC, as is the AOM/DSS model.[8]

Acknowledgments

This research was supported in part by the Grant-in-Aid (13–15) for Cancer Research from the Ministry of Health, Labour and Welfare of Japan; the Grant-in-Aid for the 3rd Term for a Comprehensive 10-year Strategy for Cancer Control from the Ministry of Health, Labour and Welfare of Japan; the Grants-in-Aid for Scientific Research from the Ministry of Education, Culture, Sports, Science and Technology of Japan; the grant (C2004-4) for the Collaborative Research from Kanazawa Medical University; and the grant (H2004-6) for the Project Research from the High-Technology Center of Kanazawa Medical University.

References

1 Eaden JA, Abrams KR, Mayberry JF. The risk of colorectal cancer in ulcerative colitis: a meta-analysis. *Gut* 2001; **48**: 526–35.
2 van Hogezand RA, Eichhorn RF, Choudry A, Veenendaal RA, Lamers BHW. Malignancies in inflammatory bowel disease: Fact or fiction? *Scand J Gastroenterol* 2002; **235**: (Suppl.) 48–53.
3 Weitzman SA, Gordon LI. Inflammation and cancer: role of phagocyte-generated oxidants in carcinogenesis. *Blood* 1990; **76**: 655–63.
4 Warren BF, Watkins PE. Animal models of inflammatory bowel disease. *J Pathol* 1994; **172**: 313–6.
5 Mori H, Ohbayashi F, Hirono I, Shimada T, Williams GM. Absence of genotoxicity of the carcinogenic sulfated polysaccharides carrageenan and dextran sulfate in mammalian DNA repair and bacterial mutagenicity assays. *Nutr Cancer* 1984; **6**: 92–7.
6 Okayasu I, Hatakeyama S, Yamada M, Ohkusa T, Inagaki Y, Nakaya R. Novel method in the induction of reliable experimental acute and chronic ulcerative colitis in mice. *Gastroenterology* 1990; **98**: 694–702.
7 Okayasu I, Yamada M, Mikami T, Yoshida T, Kanno J, Ohkusa T. Dysplasia and carcinoma development in a repeated dextran sulfate sodium-induced colitis model. *J Gastroenterol Hepatol* 2002; **17**: 1078–83.
8 Tanaka T, Kohno H, Suzuki R, Yamada Y, Sugie S, Mori H. A novel inflammation-related mouse colon carcinogenesis model induced by azoxymethane and dextran sodium sulfate. *Cancer Sci* 2003; **94**: 965–73.
9 Rogers AE, Nauss KM. Rodent models for carcinoma of the colon. *Dig Dis Sci* 1985; **30**: 87S–102S.
10 Pozharisski KM, Likhachev AJ, Klimashevski VF, Shaposhnikov JD. Experimental intestinal cancer research with special reference to human pathology. *Adv Cancer Res* 1979; **30**: 165–237.
11 Ross JS. Experimental large intestinal adenocarcinoma induced by hydrazines and human colorectal cancer: a comparative study. In: Malt RA, Williamson RCN, eds. *Colonic Carcinogenesis*. MTP Press, Hingham, 1982; 187–207.
12 Miller JR, Moon RT. Signal transduction through β-catenin and specification of cell fate during embryogenesis. *Genes Dev* 1996; **10**: 2527–39.
13 Kishida S, Yamamoto H, Ikeda S, Kishida M, Sakamoto I, Koyama S, Kikuchi A. Axin, a negative regulator of the wnt signaling pathway, directly interacts with adenomatous polyposis coli and regulates the stabilization of β-catenin. *J Biol Chem* 1998; **273**: 10823–6.
14 Dashwood RH, Suzui M, Nakagama H, Sugimura T, Nagao M. High frequency of β-catenin (*Ctnnb1*) mutations in the colon tumors induced by two heterocyclic amines in the F344 rat. *Cancer Res* 1998; **58**: 1127–9.

15 Takahashi M, Fukuda K, Sugimura T, Wakabayashi K. β-Catenin is frequently mutated and demonstrates altered cellular location in azoxymethane-induced rat colon tumors. *Cancer Res* 1998; **58**: 42–6.
16 Takahashi M, Nakatsugi S, Sugimura T, Wakabayashi K. Frequent mutations of the β-catenin gene in mouse colon tumors induced by azoxymethane. *Carcinogenesis* 2000; **21**: 1117–20.
17 Koesters R, Hans MA, Benner A, Prosst R, Boehm J, Gahlen J, Doeberitz MK. Predominant mutation of codon 41 of the β-catenin proto-oncogene in rat colon tumors induced by 1,2-dimethylhydrazine using a complete carcinogenic protocol. *Carcinogenesis* 2001; **22**: 1885–90.
18 Morin PJ, Sparks AB, Korinek V, Barker N, Clevers H, Vogelstein B, Kinzler KW. Activation of β-catenin-Tcf signaling in colon cancer by mutations in β-catenin or APC. *Science* 1997; **275**: 1787–90.
19 Miyoshi Y, Nagase H, Ando H, Horii A, Ichii S, Nakatsuru S, Aoki T, Miki Y, Mori T, Nakamura Y. Somatic mutations of the APC gene in colorectal tumors: mutation cluster region in the APC gene. *Hum Mol Genet* 1992; **1**: 229–33.
20 Powell SM, Zilz N, Beazer-Barclay Y, Bryan TM, Hamilton SR, Thibodeau SN, Vogelstein B, Kinzler KW. APC mutations occur early during colorectal tumorigenesis. *Nature* 1992; **359**: 235–7.
21 Sparks AB, Morin PJ, Vogelstein B, Kinzler KW. Mutational analysis of the APC/β-catenin/Tcf pathway in colorectal cancer. *Cancer Res* 1998; **58**: 1130–4.
22 Iwamoto M, Ahnen DJ, Franklin WA, Maltzman TH. Expression of β-catenin and full-length APC protein in normal and neoplastic colonic tissues. *Carcinogenesis* 2000; **21**: 1935–40.
23 Cooper HS, Murthy S, Kido K, Yoshitake H, Flanigan A. Dysplasia and cancer in the dextran sulfate sodium mouse colitis model. Relevance to colitis-associated neoplasia in the human. a study of histopathology, β-catenin and p53 expression and the role of inflammation. *Carcinogenesis* 2000; **21**: 757–68.
24 Hill KA, Wang KL, Stryker SJ, Gupta R, Weinrach DM, Rao MS. Comparative analysis of cell adhesion molecules, cell cycle regulatory proteins, mismatch repair genes, cyclooxygenase-2, and DPC4 in carcinomas arising in inflammatory bowel disease and sporadic colon cancer. *Oncol Report* 2004; **11**: 951–6.
25 Cooper HS, Murthy SN, Shah RS, Sedergran DJ. Clinicopathologic study of dextran sulfate sodium experimental murine colitis. *Laboratory Invest* 1993; **69**: 238–49.
26 Riddell RH, Goldman H, Ransohof DF, Appleman HD, Fenoglio CM, Haggitt RC, Ahren C, Correa P, Hamilton SR, Morson BC, Sommers SC, Yardley JH. Dysplasia in inflammatory bowel disease: standardized classification with provisional clinical application. *Human Pathol* 1983; **14**: 931–68.
27 Pascal RR. Dysplasia and early carcinoma in inflammatory bowel disease and colorectal carcinomas. *Human Pathol* 1994; **25**: 1160–71.
28 Ward JM. Morphogenesis of chemically induced neoplasms of the colon and small intestine in rats. *Laboratory Invest* 1974; **30**: 505–13.
29 Bullions LC, Levine AJ. The role of β-catenin in cell adhesion, signal transduction, and cancer. *Curr Opin Oncol* 1998; **10**: 81–7.
30 Morin PJ. β-Catenin signaling and cancer. *Bioessays* 1999; **21**: 1021–30.
31 Brabletz T, Jung A, Kirchner T. β-Catenin and the morphogenesis of colorectal cancer. *Virchows Arch* 2002; **441**: 1–11.
32 Hao XP, Pretlow TG, Rao JS, Pretlow TP. β-Catenin expression is altered in human colonic aberrant crypt foci. *Cancer Res* 2001; **61**: 8085–8.
33 Walsh SV, Loda M, Torres CM, Antonioli D, Odze R. P53 and β-catenin expression in chronic ulcerative colitis – associated polypoid dysplasia and sporadic adenomas: an immunohistochemical study. *Am J Surg Pathol* 1999; **23**: 963–9.
34 Mikami T, Mitomi H, Hara A, Yanagisawa N, Yoshida T, Tsuruta O, Okayasu I. Decreased expression of CD44, α-catenin, and deleted colon carcinoma and altered expression of β-catenin in ulcerative colitis-associated dysplasia and carcinoma, as compared with sporadic colon neoplasms. *Cancer* 2000; **89**: 733–40.
35 Aust DE, Terdiman JP, Willenbucher RF, Chew K, Ferrell L, Florendo C, Molinaro-Clark A, Baretton GB, Lohrs U, Waldman FM. Altered distribution of β-catenin, and its binding proteins E-cadherin and APC, in ulcerative colitis-related colorectal cancers. *Mod Pathol* 2001; **14**: 29–39.
36 Erdman SH, Wu HD, Hixson LJ, Ahnen DJ, Gerner EW. Assessment of mutations in Ki-ras and p53 in colon cancers from azoxymethane- and dimethylhydrazine-treated rats. *Mol Carcinog* 1997; **19**: 137–44.
37 Tanaka T, Suzuki R, Kohno H, Sugie S, Takahashi M, Wakabayashi K. Colonic adenocarcinomas rapidly induced by the combined treatment with 2-amino-1-methyl-6-phenylimidazo[4,5-*b*]pyridine and dextran sodium sulfate in male ICR mice possess β-catenin gene mutations and increase immunoreactivity for β-catenin, cyclooxygenase-2, and inducible nitric oxide synthase. *Carcinogenesis* 2005; **26**: 229–38.
38 Takahashi M, Mutoh M, Kawamori T, Sugimura T, Wakabayashi K. Altered expression of β-catenin, inducible nitric oxide synthase and cyclooxygenase-2 in azoxymethane-induced rat colon carcinogenesis. *Carcinogenesis* 2000; **21**: 1319–27.
39 Chiang JM, Chou YH, Chen TC, Ng KF, Lin JL. Nuclear β-catenin expression is closely related to ulcerative growth of colorectal carcinoma. *Br J Cancer* 2002; **86**: 1124–9.
40 Tetsu O, McCormick F. β-Catenin regulates expression of cyclin D1 in colon carcinoma cells. *Nature* 1999; **398**: 422–6.
41 He TC, Sparks AB, Rago C, Hermeking H, Zawel L, da Costa LT, Morin PJ, Vogelstein B, Kinzler KW. Identification of c-MYC as a target of the APC pathway. *Science* 1998; **281**: 1509–12.
42 Sakamoto C. Roles of COX-1 and COX-2 in gastrointestinal pathophysiology. *J Gastroenterol* 1998; **33**: 618–24.
43 Kankuri E, Asmawi MZ, Korpela R, Vapaatalo H, Moilanen E. Induction of iNOS in a rat model of acute colitis. *Inflammation* 1999; **23**: 141–52.
44 Ambs S, Merriam WG, Bennett WP, Felley-Bosco E, Ogunfusika MO, Oser SM, Klein S, Shields PG, Billiar TR, Harris CC. Frequent nitric oxide synthase-2 expression in human colon adenomas: implication for tumor angiogenesis and colon cancer progression. *Cancer Res* 1998; **58**: 334–41.
45 Takahashi M, Fukuda K, Ohata T, Sugimura T, Wakabayashi K. Increased expression of inducible and endothelial constitutive nitric oxide synthases in rat colon tumors induced by azoxymethane. *Cancer Res* 1997; **57**: 1233–7.
46 Takahashi M, Wakabayashi K. Gene mutations and altered gene expression in azoxymethane-induced colon carcinogenesis in rodents. *Cancer Sci* 2004; **95**: 475–80.
47 Araki Y, Okamura S, Hussain SP, Nagashima M, He P, Shiseki M, Miura K, Harris CC. Regulation of cyclooxygenase-2 expression by the Wnt and ras pathways. *Cancer Res* 2003; **63**: 728–34.
48 Mei JM, Hord NG, Winterstein DF, Donald SP, Phang JM. Expression of prostaglandin endoperoxide H synthase-2 induced by nitric oxide in conditionally immortalized murine colonic epithelial cells. *FASEB J* 2000; **14**: 1188–201.
49 Howe LR, Crawford HC, Subbaramaiah K, Hassell JA, Dannenberg AJ, Brown AM. PEA3 is up-regulated in response to Wnt1 and activates the expression of cyclooxygenase-2. *J Biol Chem* 2001; **276**: 20108–15.
50 Liu Y, Borchert GL, Phang JM. Polyoma enhancer activator 3, an Ets transcription factor, mediates the induction of cyclooxygenase-2 by nitric oxide in colorectal cancer cells. *J Biol Chem* 2004; **279**: 18694–700.
51 Suzuki R, Kohno H, Sugie S, Tanaka T. Sequential observations on the occurrence of preneoplastic and neoplastic lesions in the mouse colon treated with azoxymethane and dextrane sodium sulfate. *Cancer Sci* 2004; **95**: 721–7.

© Japanese Cancer Association doi: 10.1111/j.1349-7006.2005.00020.x

Histol Histopathol (2005) 20: 483-492

http://www.hh.um.es

Histology and Histopathology
Cellular and Molecular Biology

Dose-dependent promoting effect of dextran sodium sulfate on mouse colon carcinogenesis initiated with azoxymethane

R. Suzuki[1,2], H. Kohno[1], S. Sugie[1] and T. Tanaka[1]

[1]Department of Oncologic Pathology, Kanazawa Medical University, Uchinada, Ishikawa, Japan and

[2]Research Fellow of the Japan Society for the Promotion of Science, Chiyoda-ku, Tokyo, Japan

Summary. We previously reported a powerful tumor-promoting ability of dextran sodium sulfate (DSS) in a novel mouse model for colitis-related colon carcinogenesis initiated with azoxymethane (AOM). To determine the dose-dependent influence of DSS in our animal model, male ICR mice were given a single intraperitoneal injection of AOM (10 mg/kg body weight), followed by DSS at dose levels of 2, 1, 0.5, 0.25, and 0.1% (w/v) in drinking water for 1 week. All animals were sacrificed at week 14 and histological alterations in their colon and nitrotyrosine immunohistochemistry were examined to evaluate the nitrosative stress. In the mice which received AOM and 2% DSS, the incidences (multiplicity) of colonic tubular adenoma and adenocarcinoma were 75% (1.25±1.26/mouse) and 100% (2.75±2.22/mouse), respectively. Mice given AOM and 1% DSS had 80% incidence of adenoma (1.00±0.71/mouse) and 60% incidence of adenocarcinoma (1.40±2.07/mouse) in the colon. In a mouse treated with AOM and 0.5% DSS, only one colonic adenoma (20% incidence with 0.20±0.45 multiplicity) developed. Higher frequency of high-grade colonic dysplasia was noted in mice given AOM and 2% or 1% DSS when compared with mice treated with AOM and lower doses of DSS. Also, scoring of inflammation and nitrotyrosine immunoreactivity suggested that severe inflammation and nitrosation stress caused by high-doses (2% and 1%) of DSS contribute its tumor-promoting effects in mouse colon carcinogenesis initiated with a low dose of AOM. Thus, our findings indicate that a tumor-promoting effect of DSS was dose-dependent (1% or more) and the effect might occur under the condition of inflammation and nitrosation stress.

Key words: Dose-dependency, Promotion, DSS, AOM, Mouse colon carcinogenesis

Offprint requests to: Dr. Rikako Suzuki, Department of Oncologic Pathology, Kanazawa Medical University, 1-1 Daigaku, Uchinada, Ishikawa 920-0293, Japan. e-mail: rikako@kanazawa-med.ac.jp

Introduction

Inflammatory bowel diseases (IBD), including ulcerative colitis (UC) and Crohn's disease (Eaden et al., 2001; van Hogezand et al., 2002) are relatively common in North America, Europe, and Australia. It is well-known that UC patients have a high risk of colorectal cancer (CRC) (Devroede et al., 1971; Kewenter et al., 1978; Greenstein et al., 1979): patients with UC have a 2.0-8.2 relative risk of CRC compared with the normal population, accounting for about 2% of CRC (Hardy et al., 2000).

We recently developed a novel mouse model for colitis-related colon carcinogenesis (Tanaka et al., 2003). In this model, male ICR mice were initiated with a single dose (10 mg/kg body weight) of azoxymethane (AOM) by intraperitoneal (i.p.) injection, and then followed by one-week exposure to 2% dextran sodium sulfate (DSS) in drinking water, starting one week after the injection of AOM. This combined treatment with AOM and DSS resulted in a high incidence and greater multiplicity of colonic neoplasms within 20 weeks. Moreover, the first colonic malignancy was observed as early as 12 weeks into the experimental schedule. These findings suggest a powerful tumor-promoting effect of DSS in our model.

The effects of various tumor-promoters on carcinogenesis are known to be dose-dependent (Pereira et al., 1986) and a lower dose appeared to exhibit a threshold (Maekawa et al., 1992). In colon carcinogenesis, tumor-promoting effect of dietary fat depends on the amount of dietary fat (Reddy and Maeura, 1984). A non-genotoxic carcinogen DSS is widely used for induction of colitis (Okayasu et al., 1990; Cooper et al., 1993), since administration of DSS through diet or drinking water to rodents could induce colonic inflammation which resembled the symptomatic and histopathological findings in humans UC (Okayasu et al., 1990; Cooper et al., 1993). Also, colonic malignancies develop in chronic inflammation induced by long-term administration of DSS, which is similar to

human cases where colorectal adenocarcinoma occurs via the dysplasia-carcinoma sequence (Yamada et al., 1992; Tamaru et al., 1993; Cooper et al., 2000). Severity of mucosal injury caused by DSS relates to the administration dose and duration of DSS (Kitajima et al., 1999; Egger et al., 2000; Shimizu et al., 2003). These findings suggest that the tumor-promoting effect of DSS in our model (Tanaka et al., 2003) is dose-dependent and may be related to mucosal damage by DSS (Tanaka et al., 2001).

In the current study, we investigated the influence of various doses of DSS on our AOM/DSS-induced mouse colon carcinogenesis model to determine the lowest dose of DSS, which can exert its tumor-promoting ability, for utilizing the model for detecting the modifying effects of xenobiotics on colon carcinogenesis. Also, the immunohistochemistry of nitrotyrosine, which is a marker of the formation of peroxynitrite and its interaction with protein tyrosines (Singer et al., 1996), in the colon was performed to determine the possible involvement of inflammation damage by inducible nitric oxide synthase (iNOS), which is induced in inflamed colonic mucosa and is associated with the production of peroxynitrite and nitration of cellular protein in the colon of both human IBD (Singer et al., 1996; Kimura et al., 1998) and chemically-induced colitis of rodents (Zingarelli et al., 1999), in our model.

Materials and methods

Animals, chemicals and diets

Male Crj: CD-1 (ICR) mice (Charles River Japan, Inc., Tokyo), 5 weeks old, were used in this study. They were maintained at Kanazawa Medical University Animal Facility according to the Institutional Animal Care Guidelines. Mice were housed in plastic cages (4 or 5 mice/cage) under controlled conditions of humidity (50±10%), light (12/12 h light/dark cycle), and temperature (23±2 °C). Drinking water and a pelleted basal diet (CRF-1, Oriental Yeast Co., Ltd., Tokyo) were available *ad libitum*. They were quarantined for the first 7 days after arriving, and then randomized by body weight into experimental and control groups. A colonic carcinogen AOM was purchased from Sigma Chemical Co. (St. Louis, MO, USA). DSS with a molecular weight of 40,000 was purchased from ICN Biochemicals, Inc. (Aurora, OH, USA). DSS for induction of colitis was prepared every day by dissolving in distilled water at a concentration of 2, 1, 0.5, 0.25, and 0.1% (w/v).

Experimental procedure

Male ICR mice were divided into 8 groups, as shown in Fig. 1. Mice of groups 1 through 5 were given a single i.p. injection of AOM at a dose of 10 mg/kg body weight. Starting 1 week after the injection, animals of groups 1 through 5 received 2, 1, 0.5, 0.25, and 0.1% DSS in the drinking water for 7 days, respectively, and then were given no further treatment for 12 weeks. Group 6 was given a single i.p. injection of AOM (10 mg/kg body weight) alone. Mice of group 7 received 2% DSS the same as groups 1 through 5. Group 8 was an untreated control. All animals were sacrificed at the end of the study (week 14) by ether overdose. Their large bowel was flushed with saline and excised. Their length (from the ileocecal junction to the anal verge) was measured, cut open longitudinally along the main axis, and then washed with saline. The entire colon was macroscopically inspected, cut, fixed in 10% buffered formalin for at least 24 h, and embedded paraffin for histopathological and immunohistochemical examinations.

Histopathological analysis

Histopathology (mucosal inflammation with or without ulceration, dysplasia, and neoplasms) in the entire colon was analyzed on hematoxylin and eosin-stained sections. Colitis was graded according to the following morphological criteria (Cooper et al., 1993): showing normal appearance (grade 0); shortening and loss of the basal one-third of the actual crypts with mild inflammation in the mucosa (grade 1); loss of the basal two-thirds of the crypts with moderate inflammation in the mucosa (grade 2); loss of the entire crypts with severe inflammation in the mucosa and submucosa, but with retainment of the surface epithelium (grade 3); and presence of mucosal ulcer with severe inflammation (neutrophils, lymphocytes, macrophages, and plasma cells infiltration) in the mucosa, submucosa, muscularis propria, and/or subserosa (grade 4). The scoring was made on the entire colon with or without proliferative lesions and expressed as mean average score / mouse. Colonic mucosa dysplasia (low- and high-grade) and colonic neoplasms were diagnosed according to the earlier reports (Ward, 1974; Riddell et al., 1983; Pascal,

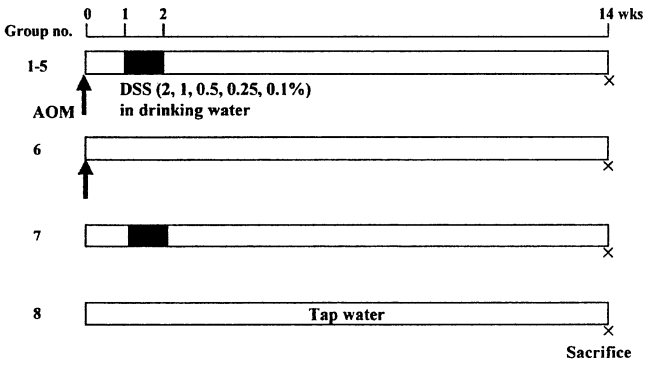


Fig. 1. Experimental protocol. Treatments are as follows: Group 1, AOM (10 mg/kg body weight)→2%DSS; Group 2, AOM→1%DSS; Group 3, AOM→0.5%DSS; Group 4, AOM→0.25%DSS; Group 5, AOM→0.1%DSS; Group 6, AOM alone; Group 7, 2%DSS alone; and Group 8, untreated.

1994). To determine the multiplicity of the colonic mucosal ulcer and dysplasia, the colon was cut into three equal parts from the anus, and then each part was cut in half longitudinally. Each tissue fixed in 10% buffered formation was totally submitted as multiple transverse sections for histological processing. This averaged two pieces/tissue and 12 pieces / total colon. The colon lesions were counted on all slides stained with hematoxylin and eosin, the sum was divided by the number of slides, and expressed as mean ± SD.

Nitrotyrosine immunohistochemistry

Immunohistochemistry was used to evaluate tyrosine nitration, a marker of nitrosative damage in the colon. Paraffin-embedded sections (4 μm) of the colon were deparaffinized, treated with 0.3% hydrogen peroxide for 15 minutes to block endogenous peroxidase activity, and then rinsed briefly in PBS. Non-specific binding was blocked by incubating the slides with a blocking solution (0.1M PBS containing 0.1% triton X-100 and 2% normal goat serum) for 2 hours. Sections were incubated overnight with a primary rabbit polyclonal anti-nitrotyrosine (diluted 1:500, Upstate Biotechnology, Lake Placid, New York, USA) or with control solution. Control sections included buffer alone or non-specific purified rabbit secondary antibody and the avidin-biotin-peroxidase complex (Vectastain Elite ABC kit, Vector Laboratories, Burlingame, CA, USA). Color was developed using 3-3'-diaminobenzidine-4HCl as the chromogen. To quantitate the degree of nitrotyrosine stainability, the grading system (grade 0-4) was used according to the following criteria (Zingarelli et al., 1999): grade 0, no immunoreactivity; grades 1-3, increasing degrees of intermediate immunoreactivity; and grade 4, extensive immunoreactivity. The nitrotyrosine immunohistochemistry was scored on the serial immunostained sections that were made for counting colonic mucosal ulcer and dysplasia.

Statistical analysis

All measurements were compared by the use of Fisher's exact probability test, Student's *t*-test or Welch's *t*-test for paired samples.

Results

General observation

The intake of DSS or tap water did not significantly differ among the groups (data not shown). A few mice receiving AOM and 2% or 1% DSS in the drinking water had bloody stools after the DSS administration. However, no such symptoms were observed in the groups which received AOM and other doses of DSS. Mean body, liver, and relative liver weights (g/100 g body weight) are listed in Table 1. The mean body weight of group 1 (AOM→2% DSS), group 2 (AOM→1% DSS), and group 3 (AOM→0.5% DSS) were significantly lower than that of groups 6 (AOM alone, $P<0.001$ vs. group 1, and $P<0.05$ vs. groups 2 and 3) and 8 (no treatment, $P<0.05$ vs. groups 1 and 2, and $P<0.01$ vs. groups 3). Also, the mean body weight of group 1 was lower ($P<0.05$) than that of group 7 (2% DSS alone). Although the mean liver weight of group 1 was significantly smaller than that of group 6 ($P<0.005$) and group 8 ($P<0.05$), relative liver weights had no statistical differences among the groups. Mean lengths of large bowel of all groups at the end of the study are also given in Table 1. Significant differences were observed between group 1 and group 6 ($P<0.05$) or group 8 ($P<0.01$).

Effects of various doses of DSS on the development of large bowel neoplasms

Macroscopically, flat, nodular, polypoid or caterpillar-like tumors were present in the middle and

Table 1. Body, liver, relative liver weights, and lengths of large bowel in each group.

GROUP no.	TREATMENT (No of mice examined)	BODY WEIGHT (g)	LIVER WEIGHT (g)	RELATIVE LIVER WEIGHT (g/100g body weight)	LENGTH OF LARGE BOWEL (cm)
1	AOM→2%DSS (4)	37.4±5.1[a,b,c,d]	2.27±0.43[d,e]	6.02±0.40	11.8±1.1[f,g]
2	AOM→1%DSS (5)	42.9±2.7[d,f]	2.95±0.16	6.91±0.68	13.7±1.1
3	AOM→0.5%DSS (5)	42.5±2.5[f,g]	2.90±0.23	6.83±0.70	13.7±0.7
4	AOM→0.25%DSS (5)	45.4±3.6	3.02±0.25	6.67±0.64	13.2±1.0
5	AOM→0.1%DSS (4)	48.9±7.0	3.14±0.79	6.37±0.93	13.2±1.3
6	AOM (5)	49.6±4.6	3.14±0.17	6.38±0.55	14.1±1.3
7	2%DSS (5)	45.1±3.4	2.99±0.63	6.60±1.07	13.2±0.8
8	None (5)	47.3±1.5	2.96±0.15	6.27±0.36	13.8±0.5

[a]: mean±SD; [b]: significantly different from group 6 by Student's t-test ($P<0.001$); [c]: significantly different from group 7 by Student's t-test ($P<0.05$): [d]: significantly different from group 8 by Welch's t-test ($P<0.05$); [e]: significantly different from group 6 by Welch's t-test ($P<0.005$). [f]: significantly different from group 6 by Student's t-test ($P<0.05$); [g]: significantly different from group 8 by Student's t-test ($P<0.01$).

Table 2. Incidence of large bowel neoplasms in mice treated with AOM and various doses of DSS.

GROUP	TREATMENT	INCIDENCE (MULTIPLICITY) OF LARGE BOWEL NEOPLASMS		
no.	(no. of mice examined)	Total	Adenoma	Adenocarcinoma
1	AOM→2%DSS (4)	100%* (4.00±3.37)	75%** (1.25±1.26)	100%* (2.75±2.22)
2	AOM→1%DSS (5)	100%*** (2.40±2.19)	80%** (1.00±0.71)	60% (1.40±2.07)
3	AOM→0.5%DSS (5)	20% (0.20±0.45)	20% (0.20±0.45)	0%
4	AOM→0.25%DSS (5)	0%	0%	0%
5	AOM→0.1%DSS (4)	0%	0%	0%
6	AOM (5)	0%	0%	0%
7	2%DSS (5)	0%	0%	0%
8	None (5)	0%	0%	0%

Numbers in parentheses are multiplicity (mean±SD) of large bowel tumors. *, **, ***: Significantly different from group 6 by Fisher's exact probability test (*P<0.01, **P<0.05, and ***P<0.005).

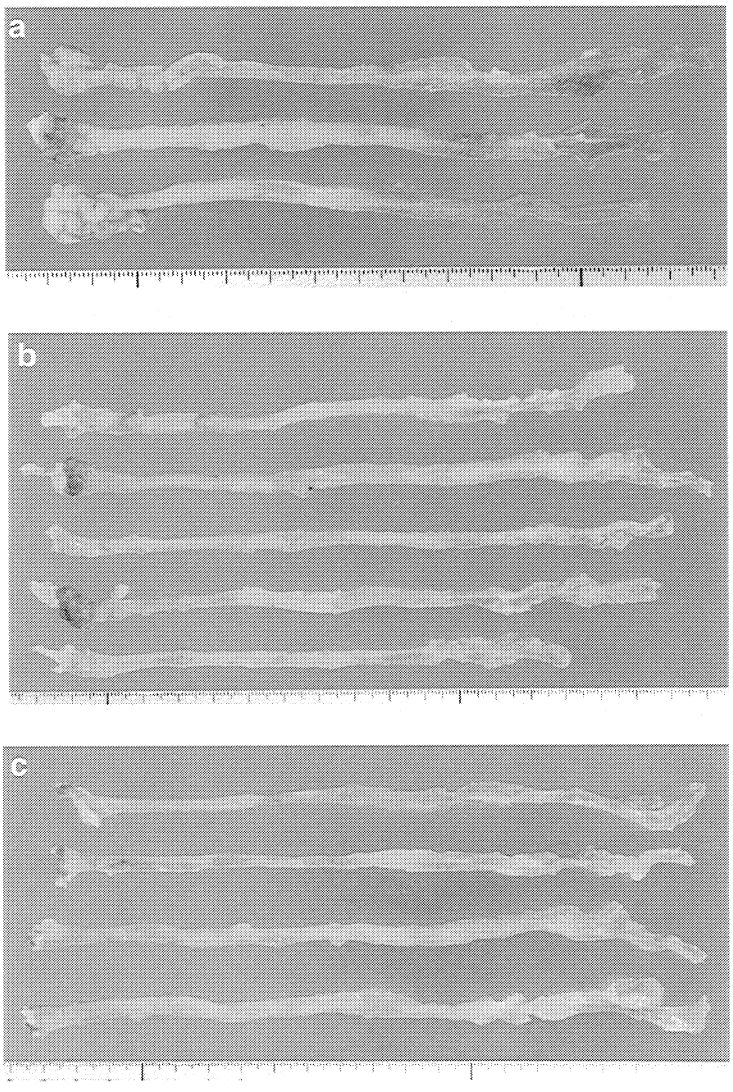


Fig. 2. Macroscopic view of the large bowel. **a.** A number of colonic tumors are seen in mice given AOM→2% DSS. **b.** A number of colonic tumors are seen in mice treated with AOM→1% DSS. **c.** One colonic tumor is present in a mouse received AOM→0.05% DSS. Arrow heads indicate colonic tumors.

distal colon of mice in groups 1 (AOM→2% DSS), 2 (AOM→1% DSS), and 3 (AOM→0.5% DSS) (Fig. 2). They were histologically tubular adenoma (Fig. 3a) or adenocarcinoma (Fig. 3b). As summarized in Table 2, the incidences of total large bowel neoplasms in groups 1 (100%, $P<0.01$) and 2 (100%, $P<0.005$) were significantly greater than group 3 (20%). As for colonic adenoma, the incidences in groups 1 (75%, $P<0.05$) and 2 (80%, $P<0.05$) were statistically higher than group 3 (20%). There was a significant difference ($P<0.01$) in the incidence of colonic adenocarcinoma between group 1 (100%) and group 2 (60%). In mice of group 3, no colonic adenocarcinomas were noted. No colonic neoplasms were found in mice of groups 4 (AOM→0.25% DSS), 5 (AOM→0.1% DSS), 6 (AOM alone), 7 (2% DSS alone), and 8 (untreated control). The multiplicity of colonic neoplasms was increased in proportion to the dose level of DSS, but the difference was not significant among the groups. To determine the dose-response effect of various levels of DSS on the multiplicity of colonic neoplasm, we used simple linear regression. The squared correlation coefficients for the multiplicities of total tumor, adenoma, and adenocarcinoma obtained by the regression were 0.98 ($P<0.01$), 0.94 ($P<0.05$), and 0.98 ($P<0.01$), respectively. These values suggested a dose-response promotion effect of DSS on development of colon tumors.

Effects of various doses of DSS on the occurrence of colonic mucosal inflammation, ulcer, and dysplasia

Colonic mucosal inflammation, ulcer or dysplasia

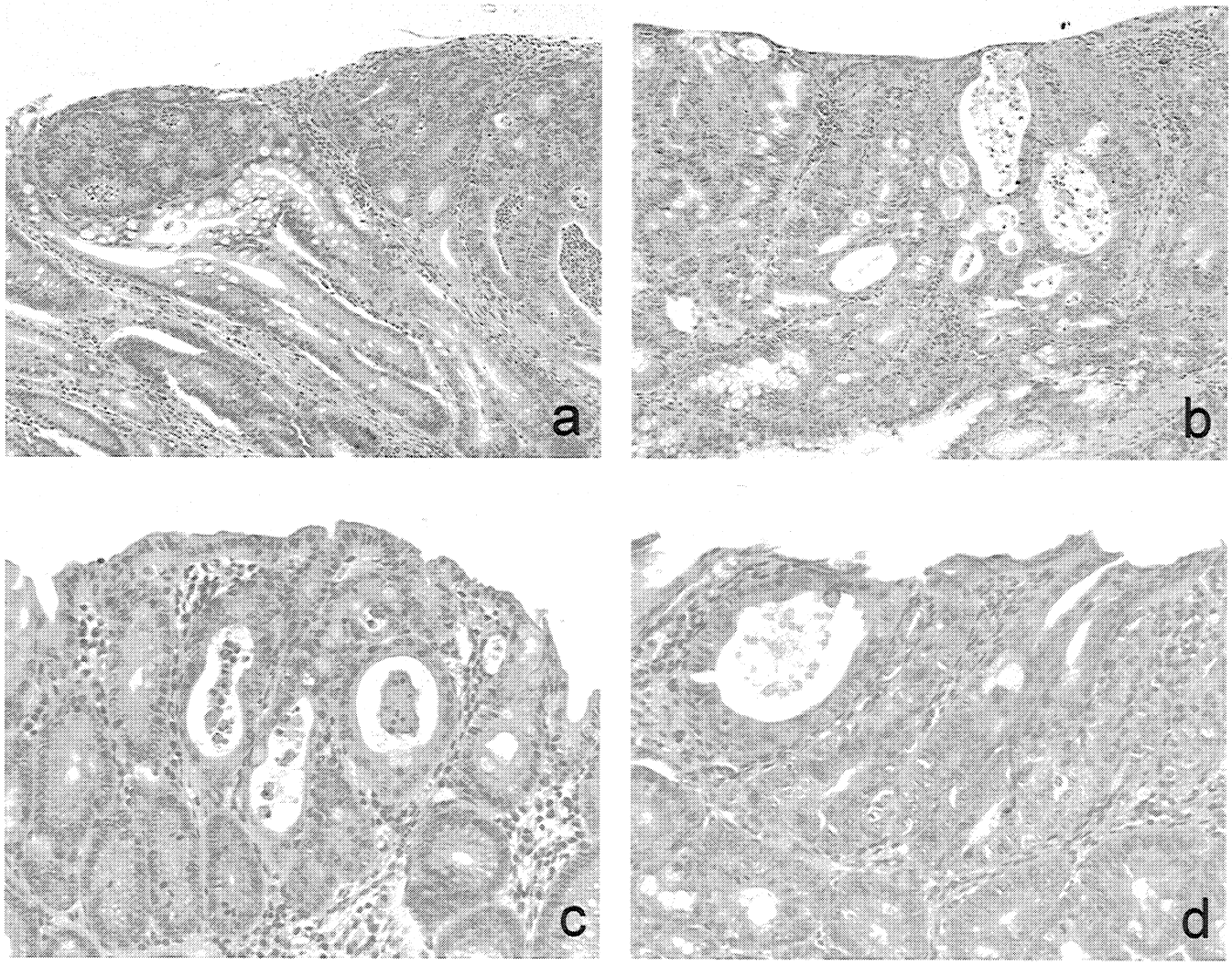


Fig. 3. Histopathology of colonic lesions in mice treated with AOM→2% DSS. **a.** Two tubular adenomas are seen. **b.** A tumor is histologically well differentiated tubular adenocarcinoma. **c.** Low-grade dysplasia with slight nuclear atypia. **d.** High-grade dysplasia with marked nuclear atypia. Hematoxylin and eosin stain, original magnification, a, b, x 10; c, d, x 20

were mainly found in the middle and distal parts of the colon. The severity of inflammation was greater in the distal region than other regions of the colon. Inflammation score of colonic mucosa is illustrated in Fig. 4. The score of group 1 (AOM→2% DSS, 2.25±0.50) was significantly higher than that of group 3 (AOM→0.5% DSS, 1.40±0.55, P<0.05), group 5 (AOM→0.1% DSS, 1.00±0.82, P<0.05), group 6 (AOM alone, 0.40±0.89, P<0.01), group 7 (2% DSS alone, 0.80±0.84, P<0.05), and group 8 (no treatment, 0.20±0.45, P<0.001). Group 2 (AOM→1% DSS, 2.00±0.71, P<0.005), group 3 (P<0.01), and group 4 (AOM→0.25% DSS, 1.20±0.84, P<0.05) were statistically higher than that of group 8. The value of group 2 was also significantly greater than group 6 (P<0.05). The correlation coefficient for the correlation between the inflammation score and dose of DSS was 0.95 (P<0.05).

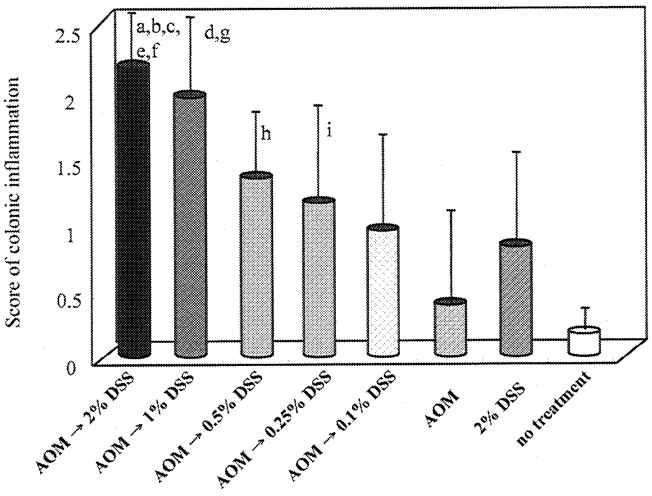


Fig. 4. Inflammation score. Statistical analysis using Student's t-test or Welch's t-test indicates significant difference: a (P<0.05), vs. the AOM→0.5% DSS group; b (P<0.05), vs. the AOM→0.1% DSS group; c (P<0.01) and d (P<0.05), vs. the AOM alone group; e (P<0.05), vs. the 2% DSS alone group; and f (P<0.001), g (P<0.005), h (P<0.01), and i (P<0.05), vs. the "no treatment group".

The frequencies of colonic mucosal ulceration and dysplasia are shown in Table 3. DSS administration increased dose-dependently the incidence and frequency of mucosal ulceration of the colon. However, the correlation coefficient was 0.59 (P>0.1). This might be caused by the high value of group 2 (6.80±1.92). All mice belonging to groups 1 through 5, which were initiated with AOM and followed by various doses of DSS exposure, developed mucosal dysplasia with low- (Fig. 3c) and/or high-grade (Fig. 3d), and one mouse in group 6 had low-grade dysplasia (Table 3). The multiplicities of total and high-grade dysplasia in groups 1 and 2 were much greater than those of groups 3 through 5. The incidences of the total dysplasia and low-grade dysplasia were 100% in groups 1-5 (P<0.05 vs. group 6). Their multiplicities significantly increased when the dose of DSS increased (P<0.05, P<0.01, P<0.005 or P<0.001). The incidences of high-grade

Table 3. Incidence of large bowel ulceration and dysplasia in mice treated with AOM and various doses of DSS.

GROUP	TREATMENT	INCIDENCE OF MUCOSAL ULCER	INCIDENCE (MULTIPLICITY) OF COLONIC MUCOSA		
no.	(no of mice examined)	(multiplicity)	Total	Low-grade	High-grade
1	AOM→2%DSS (4)	100%* (4.00±0.82^{a,b,c})	100%** (12.50±4.65^{d,e,f,g})	100%** (4.00±1.83^{g})	100%* (8.50±2.89^{e,h,i})
2	AOM→1%DSS (5)	100%* (6.80±1.92^{c,d,j})	100%** (9.00±3.94^{d,e,f,k})	100%** (3.80±2.17^{g})	100%* (5.20±2.86^{e,f})
3	AOM→0.5%DSS (5)	100%* (3.60±1.95^{f})	100%** (3.80±3.11)	100%** (2.00±1.22^{g})	80%** (1.80±1.92)
4	AOM→0.25%DSS (5)	80%** (1.40±1.14)	100%** (2.80±1.30^{k})	100%** (2.00±0.71^{l})	60% (0.80±0.84)
5	AOM→0.1%DSS (4)	50% (0.50±0.58)	100%** (2.50±0.58^{m})	100%** (1.75±0.50^{m})	50% (0.75±0.96)
6	AOM (5)	0%	20% (0.20±0.45)	20% (0.20±0.45)	0%
7	2%DSS (5)	0%	0%	0%	0%
8	None (5)	0%	0%	0%	0%

Numbers in parentheses are multiplicity (mean±SD) of large bowel tumors. *,**: significantly different from group 6 by Fisher's exact probability test (*P<0.01 and **P<0.05); [a]: significantly different from group 2 by Student's t-test (P<0.05); [b]: significantly different from group 4 by Student's t-test (P<0.01); [c]: significantly different from group 5 by Student's t-test (P<0.001); [d]: significantly different from group 3 by Student's t-test (P<0.05); [e]: significantly different from group 4 by Welch's t-test (P<0.05); [f]: significantly different from group 5 by Welch's t-test (P<0.05); [g]: significantly different from group 6 by Welch's t-test (P<0.05); [h]: significantly different from group 3 by Student's t-test (P<0.005); [i]: significantly different from group 5 by Student's t-test (P<0.005); [j]: significantly different from group 4 by Student's t-test (P<0.001); [k]: significantly different from group 6 by Welch's t-test (P<0.01); [l]: significantly different from group 6 by Student's t-test (P<0.005); [m]: significantly different from group 6 by Student's t-test (P<0.001).

dysplasia in groups 1 (P<0.01), 2 (P<0.01), and 3 (P<0.05) were significantly higher than group 6. The multiplicities of the lesion increased with increasing the concentration of DSS. The correlation coefficients for the multiplicities of total dysplasia, low-grade dysplasia, and high-grade dysplasia were 0.98 (P<0.01), 0.91 (P<0.05), and 0.99 (P<0.01), respectively. These values indicated that DSS exposure has a dose-dependent promoting effect on the development of colonic dysplasia.

Immunohistochemistry nitrotyrosine

Nitrotyrosine immunoreactivity was mainly observed in mononuclear cells infiltrated in the colonic mucosa with the lesions (Fig. 5). The stainability was very weak in the cryptal cells and neoplastic cells if present (Fig. 5). The score of nitrotyrosine immunohistochemistry is shown in Fig. 6. The scores of groups 1 (AOM→2% DSS, 3.08±0.31) and 2 (AOM→1% DSS, 2.54±0.40) were significantly higher than that of group 3 (AOM→0.5% DSS, 0.96±0.15, P<0.001), group 4 (AOM→0.25% DSS, 0.60±0.22, P<0.001), group 5 (AOM→0.1% DSS, 0.53±0.22, P<0.001), group 6 (AOM alone, 0.2±0.45, P<0.001) and group 8 (no treatment, 0.28±0.15, P<0.001). Also a significant difference (P<0.005) was found between groups 1 and 7 (2% DSS alone, 0.60±0.89). Immunohistochemical nitrotyrosine score of group 3 was significantly greater than that of groups 4 (P<0.05), 5 (P<0.01), 6 (P<0.05), and 8 (P<0.001). A significant difference was also noted between groups 4 and 8 (P<0.05). The dose dependent effect of DSS on the scores of nitrotyrosine immunohistochemistry was demonstrated by the calculated correlation coefficient (0.95, P<0.05).

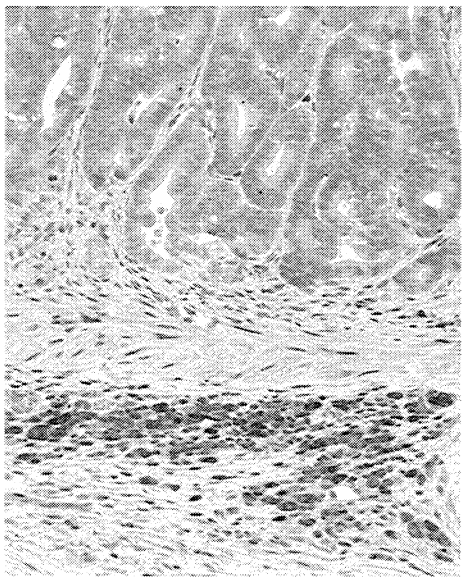


Fig. 5. Nitrotyrosine immunohistochemistry of the colon of a mouse from group 1 (AOM→2% DSS). The positive reaction is noted inflammatory cells under the dysplastic lesion. Original magnification, x 20

Discussion

We recently reported that exposure to DSS in the drinking water at a dose of 2% for a week after a single i.p. injection of AOM (10 mg/kg body weight) could produce a number of colonic neoplasms with ß-catenin gene mutation in male ICR mice within a short-term period (20 weeks) (Tanaka et al., 2003), suggesting a powerful tumor-promoting activity of DSS. Subsequent time-course observation confirmed the tumor-promoting effect of DSS on AOM-initiated mouse colon carcinogenesis and suggested involvement of inflammation and nitrosative stress (Suzuki et al., 2004). The current study conducted to determine the lowest dose of DSS with tumor-promoting ability in our model revealed that a number of colonic neoplasms (adenoma and adenocarcinoma) developed in mice treated with 1% or 2% DSS after AOM administration and the incidence and multiplicity of the groups given these dose levels of DSS were almost similar. In addition, only a few colonic neoplasms developed in mice give 0.5% DSS after AOM exposure. These results clearly indicate that treatment with 1% or more of DSS could exert its tumor-promoting ability after the initiation with a low dose of AOM in male ICR mice. Our recent work using female ICR mice also indicates that 1% is the lowest dose of DSS, which can promote AOM-induced colon carcinogenesis (manuscript in preparation).

Since colonic adenocarcinoma developed as early as 12 weeks in our previous work with an experimental period of 20 weeks (Tanaka et al., 2003), we shortened the experimental period (14 weeks) in the present study

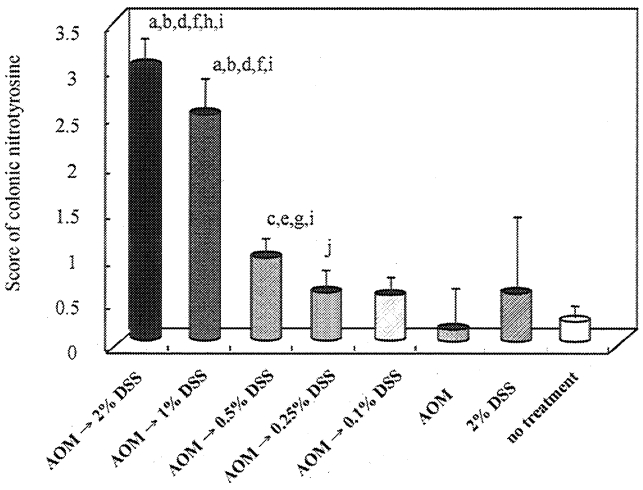


Fig. 6. Score for nitrotyrosine immunohistochemistry. Statistical analysis using Student's t-test or Welch's t-test indicates significant difference: a (P<0.001), vs. the AOM→0.5% DSS group; b (P<0.001) and c (P<0.05), vs. the AOM→0.25% DSS group; d (P<0.001) and e (P<0.01), vs. the AOM→0.1% DSS group; f (P<0.001) and g (P<0.05), vs. the AOM alone group; h (P<0.005), vs. the 2% DSS alone group; and i (P<0.001) and j (P<0.05), vs. the "no treatment group".

to investigate the dose-dependent effects of DSS on the occurrence of cryptal dysplasia, which is considered precursor lesions in colitis-related colon carcinogenesis in both humans (Riddell et al., 1983) and rodents (Cooper et al., 2000). As a result, the incidence of mucosal dysplasia was 100% in all groups treated with 2%, 1%, 0.5%, 0.25% or 0.1% DSS after AOM exposure (groups 1 through 5). However, the multiplicities of the lesion gradually increased with the dose of DSS. The values of high-grade dysplasia in groups 1 (AOM→2% DSS) and 2 (AOM→1% DSS) were over 2-fold of groups through 3-5. These findings suggest a dose-dependent tumor-promoting effect of DSS in AOM-initiated mouse colon carcinogenesis and the presence of the threshold. Although there are many studies showing that DSS exposure could induce colonic dysplasia and neoplasms, a long experimental period, high concentration of DSS and/or cycle treatment with DSS require induction of the lesions (Cooper et al., 2000; Kullmann et al., 2001; Takesue et al., 2001; Okayasu et al., 2002). Recently, Cooper et al. reported an interesting mouse model of colitis with dysplasia (Cooper et al., 2000), where mice were exposed to four cycles of 5% DSS in the drinking water (one cycle: 7 days DSS followed by 14 days of H_2O) and the incidence of dysplasia was 13.9% at week 12. On the other hand, in our mouse model cryptal dysplasia occurred in all mice given even 0.1% DSS. The results may be different by the use of a different strain of mice and the presence of initiation treatment.

In the current study, multiplicity of mucosal ulcer in mice given AOM and DSS was increased with increasing the dose of DSS except for those treated with AOM→1% DSS (Table 3). Treatment with 2% DSS alone did not cause mucosal ulcer, but colonic inflammation was noted even at week 14 and the severity was greater than AOM alone treatment (Fig. 4), as found in nitrotyrosine-immunohistochemistry (Fig. 6). In other groups, the score for nitrotyrosine immunoreactivity, a good biomarker for "nitrating species" (Halliwell, 1997), also paralleled with inflammation score. Both the scores in the groups exposed to more than 0.25% DSS were significantly higher than that of an untreated group. Thus, to induce a number of large bowel neoplasms, more than 1% DSS after AOM exposure was needed. These results also suggest that administration of 0.25% DSS can induce inflammation in the colon of mice, but this dose did not exert tumor-promoting effect in this experiment. Mice that received 2% or 1% DSS after AOM initiation produced a number of colonic adenocarcinoma. Scores of inflammation and nitrotyrosine immunoreactivity in mice treated with AOM→2% or 1% DSS were much greater than those that received AOM and other doses of DSS. In patients with UC, reactive oxygen and nitrogen species are over-produced (Rachmilewitz et al., 1993; Grisham, 1994; Lundberg et al., 1994; Buffinton and Doe, 1995; Oudkerk Pool et al., 1995; Lih-Brody et al., 1996; Singer et al., 1996; Kimura et al., 1997) and oxidative and nitrosative stress also may contribute to the increased CRC risk in these individuals (Babbs, 1992). Interestingly, mice with a number of colonic tumors had high scores of inflammation and nitrotyrosine in the current study. These findings indicate that inflammatory damage by production of nitric oxide (NO) is important to form the colonic adenocarcinoma in this model. Although we did not examine the expression of iNOS in the current study, our previous study demonstrated over-expression of iNOS in adenocarcinoma in this animal model (Tanaka et al., 2003). Thus, colonic damage from NO was partly caused through the iNOS pathway in our model.

An experimental model using pretreatment of AOM and administration of DSS was reported using CBA/J mice (Mitamura et al., 2002). In their study, male and female CBA/J mice aged 14 weeks were given i.p. injection with AOM (8 mg/kg body weight), and followed by 3% DSS (MW 61,600) exposure in drinking water for 7 days followed by tap water for the subsequent 14 days, and sacrificed at 19 weeks of age. Thirty-three colonic dysplastic lesions were found in mice, but there was no information about the colonic tumors. We need further experiments to know that combined treatment with AOM and DSS is able to induce a high incidence of colonic dysplasia as well as epithelial malignancy in other mouse strains with different susceptibilities for AOM and/or DSS. Such studies are underway in our laboratory.

In conclusion, our results demonstrate that 1% or more of DSS is sufficient to exert its powerful tumor-promoting effects in the colon of male ICR mice initiated with a low-dose of AOM within a short-term period (14 weeks).

Acknowledgements. We are indebted to Ms. S. Yamamoto for her excellent technical assistance and staff of the Research Animal facility of Kanazawa Medical University for taking good care of the animals. This study was supported in part by a Grant-in-Aid for the Third-Term Comprehensive 10-year Strategy for Cancer Control from the Ministry of Health, labour and welfare, Japan; by a Grant-in-Aid (nos. 15592007 and 15•2052) from the Ministry of Education, Culture, Sports, Science and Technology, Japan: and by grants (H2004-6 and C2004-4) from Kanazawa Medical University.

References

Babbs C.F. (1992). Oxygen radicals in ulcerative colitis. Free Rad. Biol. Med. 13, 169-181.

Buffinton G.D. and Doe W.F. (1995). Depleted mucosal antioxidant defenses in inflammatory bowel disease. Free Rad. Biol. Med. 19, 911-918.

Cooper H.S., Murthy S., Kido K., Yoshitake H. and Flanigan A. (2000). Dysplasia and cancer in the dextran sulfate sodium mouse colitis model. Relevance to colitis-associated neoplasia in the human: a study of histopathology, ß-catenin and p53 expression and the role of inflammation. Carcinogenesis 21, 757-768.

Cooper H.S., Murthy S.N., Shah R.S. and Sedergran D.J. (1993).

Clinicopathologic study of dextran sulfate sodium experimental murine colitis. Lab. Invest 69, 238-249.

Devroede G.J., Taylor W.F., Sauer W.G., Jackman R.J. and Stickler G.B. (1971). Cancer risk and life expectancy of children with ulcerative colitis. N. Engl. J. Med. 285, 17-21.

Eaden J.A., Abrams K.R. and Mayberry J.F. (2001). The risk of colorectal cancer in ulcerative colitis: a meta-analysis. Gut 48, 526-535.

Egger B., Bajaj-Elliott M., MacDonald T.T., Inglin R., Eysselein V.E. and Buchler M.W. (2000). Characterisation of acute murine dextran sodium sulphate colitis: cytokine profile and dose dependency. Digestion 62, 240-248.

Greenstein A.J., Sachar D.B., Smith H., Pucillo A., Papatestas A.E., Kreel I., Geller S.A., Janowitz H.D. and Aufses A.H.J. (1979). Cancer in universal and left-sided ulcerative colitis: factors determining risk. Gastroenterology 77, 290-294.

Grisham M.B. (1994). Oxidants and free radicals in inflammatory bowel disease. Lancet 344, 859-861.

Halliwell B. (1997). What nitrates tyrosine? Is nitrotyrosine specific as a biomarker of peroxynitrite formation in vivo? FEBS Lett. 411, 157-160.

Hardy R.G., Meltzer S.J. and Jankowski J.A. (2000). ABC of colorectal cancer. Molecular basis for risk factors. Br. Med. J. 321, 886-889.

Kewenter J., Ahlman H. and Hulten L. (1978). Cancer risk in extensive ulcerative colitis. Ann. Surg. 188, 824-848.

Kimura H., Hokari R., Miura S., Shigematsu T., Hirokawa M., Akiba Y., Kurose I., Higuchi H., Fujimori H., Tsuzuki Y., Serizawa H. and Ishii H. (1998). Increased expression of an inducible isoform of nitric oxide synthase and the formation of peroxynitrite in colonic mucosa of patients with active ulcerative colitis. Gut 42, 180-187.

Kimura H., Miura S., Shigematsu T., Ohkubo N., Tsuzuki Y., Kurose I., Higuchi H., Akiba Y., Hokari R., Hirokawa M., Serizawa H. and Ishii H. (1997). Increased nitric oxide production and inducible nitric oxide synthase activity in colonic mucosa of patients with active ulcerative colitis and Crohn's disease. Dig. Dis. Sci. 42, 1047-1054.

Kitajima S., Takuma S. and Morimoto M. (1999). Changes in colonic mucosal permeability in mouse colitis induced with dextran sulfate sodium. Exp. Anim. 48, 137-143.

Kullmann F., Messmann H., Alt M., Gross V., Bocker T., Scholmerich J. and Ruschoff J. (2001). Clinical and histopathological features of dextran sulfate sodium induced acute and chronic colitis associated with dysplasia in rats. Int. J. Colorectal Dis. 16, 238-246.

Lih-Brody L., Powell S.R., Collier K.P., Reddy G., Cerchia R., Kahn E., Weissman G.S., Katz S., Floyd R.A., McKinley M.J., Fisher S.E. and Mullin G.E. (1996). Increased oxidative stress and decreased antioxidant defenses in mucosa of inflammatory bowel disease. Dig. Dis. Sci. 41, 2078-2086.

Lundberg J.O., Hellstrom P.M., Lundberg J.M. and Alving K. (1994). Greatly increased luminal nitric oxide in ulcerative colitis. Lancet 344, 1673-1674.

Maekawa A., Onodera H., Ogasawara H., Matsushima Y., Mitsumori K. and Hayashi Y. (1992). Threshold dose dependence in phenobarbital promotion of rat hepatocarcinogenesis initiated by diethylnitrosamine. Carcinogenesis 13, 501-503.

Mitamura T., Sakamoto S., Sassa S., Suzuiki S., Kudo H. and Okayasu I. (2002). The more an ulcerative colitis is repeated, the more the risk of colorectal carcinogenesis is increased in mice. Anticancer Res. 22, 3955-3961.

Okayasu I., Hatakeyama S., Yamada M., Ohkusa T., Inagaki Y. and Nakaya R. (1990). A novel method in the induction of reliable experimental acute and chronic ulcerative colitis in mice. Gastroenterology 98, 694-702.

Okayasu I., Yamada M., Mikami T., Yoshida T., Kanno J. and Ohkusa T. (2002). Dysplasia and carcinoma development in a repeated dextran sulfate sodium-induced colitis model. J. Gastroenterol. Hepatol. 17, 1078-1083.

Oudkerk Pool M., Bouma G., Visser J.J., Kolkman J.J., Tran D.D., Meuwissen S.G.M. and Pena A.S. (1995). Serum nitrate levels in ulcerative colitis and Crohn's disease. Scand. J. Gastroenterol. 30, 784-788.

Pascal R.R. (1994). Dysplasia and early carcinoma in inflammatory bowel disease and colorectal adenomas. Hum. Pathol. 25, 1160-1171.

Pereira M.A., Herren-Freund S.L. and Long R.E. (1986). Dose-response relationship of phenobarbital promotion of diethylnitrosamine initiated tumors in rat liver. Cancer Lett. 32, 305-311.

Rachmilewitz D., Stamler J.S., Karmeli F., Mullins M.E., Singel D.J., Loscalzo J., Xavier R.J. and Podolsky D.K. (1993). Peroxynitrite-induced rat colitis--a new model of colonic inflammation. Gastroenterology 105, 1681-1688.

Reddy B.S. and Maeura Y. (1984). Tumor promotion by dietary fat in azoxymethane-induced colon carcinogenesis in female F344 rats: influence of amount and source of dietary fat. J. Natl. Cancer Inst. 72, 745-750.

Riddell R.H., Goldman H., Ransohoff D.F., Appelman H.D., Fenoglio C.M., Haggitt R.C., Ahren C., Correa P., Hamilton S.R. and Morson B.C. (1983). Dysplasia in inflammatory bowel disease: standardized classification with provisional clinical applications. Hum. Pathol. 14, 931-968.

Shimizu T., Suzuki M., Fujimura J., Hisada K., Yoshikazu O., Obinata K. and Yamashiro Y. (2003). The relationship between the concentration of dextran sodium sulfate and the degree of induced experimental colitis in weanling rats. J. Pediatr. Gastroenterol. Nutr. 37, 481-486.

Singer I.I., Kawka D.W., Scott S., Weidner J.R., Mumford R.A., Riehl T.E. and Stenson W.F. (1996). Expression of inducible nitric oxide synthase and nitrotyrosine in colonic epithelium in inflammatory bowel disease. Gastroenterology 111, 871-885.

Suzuki R., Kohno H., Sugie S. and Tanaka T. (2004). Sequential observations on the occurrence of preneoplastic and neoplastic lesions in mouse colon treated with azoxymethane and dextran sodium sulfate. Cancer Sci. 95, 721-727.

Takesue F., Korenaga D., Yao T., Kabashima A. and Sugimachi K. (2001). Development of colonic neoplasms and expressions of p53 and p21 proteins in experimental colitis of mice induced by dextran sulfate sodium. J. Exp. Clin. Cancer Res. 20, 413-418.

Tamaru T., Kobayashi H., Kishimoto S., Kajiyama G., Shimamoto F. and Brown W.R. (1993). Histochemical study of colonic cancer in experimental colitis of rats. Dig. Dis. Sci. 38, 529-537.

Tanaka T., Kohno H., Suzuki R., Yamada Y., Sugie S. and Mori H. (2003). A novel inflammation-related mouse colon carcinogenesis model induced by azoxymethane and dextran sodium sulfate. Cancer Sci. 94, 965-973.

Tanaka T., Kohno H., Yoshitani S., Takashima S., Okumura A., Murakami A. and Hosokawa M. (2001). Ligands for peroxisome proliferator-activated receptors a and g inhibit chemically induced colitis and formation of aberrant crypt foci in rats. Cancer Res. 61.

van Hogezand R.A., Eichhorn R.F., Choudry A., Veenendaal R.A. and

Lamers C.B. (2002). Malignancies in inflammatory bowel disease: fact or fiction? Scand. J. Gastroenterol. Suppl 236, 48-53.
Ward J.M. (1974). Morphogenesis of chemically induced neoplasms of the colon and small intestine in rats. Lab. Invest. 30, 505-513.
Yamada M., Ohkusa T. and Okayasu I. (1992). Occurrence of dysplasia and adenocarcinoma after experimental chronic ulcerative colitis in hamsters induced by dextran sulphate sodium. Gut 33, 1521-1527.
Zingarelli B., Szabo C. and Salzman A.L. (1999). Reduced oxidative and nitrosative damage in murine experimental colitis in the absence of inducible nitric oxide synthase. Gut 45, 199-209.

Accepted December 17, 2004

Carcinogenesis vol.26 no.1 pp.229–238, 2005
doi:10.1093/carcin/bgh292

Colonic adenocarcinomas rapidly induced by the combined treatment with 2-amino-1-methyl-6-phenylimidazo[4,5-*b*]pyridine and dextran sodium sulfate in male ICR mice possess β-*catenin* gene mutations and increases immunoreactivity for β-catenin, cyclooxygenase-2 and inducible nitric oxide synthase

Takuji Tanaka[1,4], Rikako Suzuki[1,2], Hiroyuki Kohno[1], Shigeyuki Sugie[1], Mami Takahashi[3] and Keiji Wakabayashi[3]

[1]The Oncologic Pathology, Kanazawa Medical University, 1-1 Daigaku, Uchinada, Ishikawa 920-0293, Japan, [2]Research Fellow of the Japan Science for the Promotion of Science, FS Building, 8 Ichibancho, Chiyoda-, Tokyo 102-8472, Japan and [3]Cancer Prevention Basic Research Project, National Cancer Research Institute, 5-1-1 Tsukiji, Chuo-ku, Tokyo 104-0045, Japan

[4]To whom correspondence should be addressed
Email: takutt@kanazawa-med.ac.jp

Heterocyclic amines are known to be important environmental carcinogens in several organs including the colon. The aim of this study was to induce colonic epithelial malignancies within a short-term period and analyze the expression of cycooxygenase (COX)-2, inducible nitric oxide synthase (iNOS) and β-catenin, and mutations of β-*catenin* gene in induced tumors. Male Crj: CD-1 mice were given a single i.g. administration (200 mg/kg body wt) of 2-amino-1-methyl-6-phenylimidazo[4,5-*b*]pyridine (PhIP) or 2-amino-3,8-dimethylimidazo[4,5-*f*]quinoxaline (MeIQx) followed by 2% dextran sodium sulfate (DSS) in the drinking water for a week. The expression of β-catenin, COX-2 and iNOS was immunohistochemically assessed in colonic epithelial lesions and the β-*catenin* gene mutations in colonic adenocarcinomas induced were analyzed by the single strand conformation polymorphism method, restriction enzyme fragment length polymorphism and direct sequencing. At week 16, a high incidence of colonic neoplasms with dysplastic lesions developed in mice that received PhIP and DSS, but only a few developed in those given MeIQx and DSS. Immunohistochemically, the adenocarcinomas induced were all positive for three proteins. All seven adenocarcinomas induced by PhIP and DSS have mutations. The findings suggest that DSS exerts powerful tumor-promoting effects on PhIP-initiated colon carcinogenesis in mice and this mouse model is useful for investigating environment-related colon carcinogenesis within a short-term period.

Introduction

Dietary factors intensively influence the occurrence of certain types of epithelial malignancies, such as colorectal and breast cancers (1). In Japan, the incidence of colorectal malignancy has been increasing with westernization of the dietary habits of Japanese people (2,3). Therefore, dietary factors involving the occurrence of this malignancy should be investigated extensively in order to control the disease.

In 1976, Sugimura's scientific group found new mutagenic chemicals, classified as heterocyclic amines (HCAs), from cooked meat and fish and heating amino acids and proteins (1,4,5). Thereafter, extensive work with rodents revealed the carcinogenicity of 10 HCAs, including 2-amino-1-methyl-6-phenylimidazo[4,5-*b*]pyridine (PhIP) and 2-amino-3,8-dimethylimidazo[4,5-*f*]quinoxaline (MeIQx) (6). The target organs for their tumorigenicity are liver, urinary bladder, intestine, blood vessels, skin, mammary gland, oral cavity, prostate, hematopoietic system, etc. (1,4–8). In 1991, Gerhardsson de Verdier *et al.* (9) reported that regular consumers of well-done fried meat led to colorectal and pancreatic malignancies. This was supported by the findings of the involvement of well-done cooked meat consumption and exposure of HCAs, specifically PhIP and MeIQx, in the occurrence of human colorectal and breast cancers (10,11). Thus, the intake of well-done meats containing HCAs is suspected to be associated with an increased risk of certain types of cancer in humans (5,7,12). Among various types of HCAs, PhIP and MeIQx are most abundant in cooked food. Thus, in view of environmental (especially dietary) factors and carcinogenesis, investigations (using genetic analysis and animal models) of the involvement of HCAs, particularly PhIP and MeIQx, in human colon carcinogenesis and genetic analysis are important (4).

In animal experiments, dietary feeding with PhIP induces aberrant crypt foci (ACF), which are putative precursor lesions for large bowel adenocarcinomas (13), in both rats (14) and mice (15). Dietary exposure to PhIP for 52 weeks, as other HCAs, such as 2-amino-6-methyldipyrido[1,2-*a*:3′, 2′-*d*]imidazole (Glu-P-1), 2-aminodipyrido[1,2-a:3′,2′-*d*] imidazole (Glu-P-2), 2-amino-3-methylimidazo[4,5-*f*] quinoline (IQ) and 2-amino-3,4-dimethylimidazo[4,5-f]quinoline (MeIQ), produces large intestinal carcinomas in rats (16), but not in mice (6). Ochiai *et al.* (17) reported recently that administration of 300 p.p.m. PhIP in a high-fat diet after 40 weeks followed by continuous feeding with a high-fat diet, mice developed small intestinal neoplasms. Although colonic adenocarcinomas developed in C57BL/6N and BBN female mice fed the diet containing 300 p.p.m. MeIQ for 92 weeks (18), there were no reports on the colonic carcinogenicity of MeIQx in rats and mice (6). However, MeIQx in a diet could induce ACF in both rats (19) and mice (20). These findings suggest a weak cancer initiating capability of both food-borne carcinogens in the large bowel of rats and mice, and therefore a long-term administration of PhIP and MeIQx is required for the induction of intestinal adenocarcinomas in rodents. In addition, the incidence and multiplicity of ACF and colonic malignancies except malignant lymphoma (17) induced by these two HCAs was relatively low. Therefore, we needed a novel and efficient animal model for

Abbreviations: ACF, aberrant crypt foci; AOM, azoxymethane; APC, adenomatous polyposis coli; COX, cyclooxygenase; DSS, dextran sodium sulfate; H&E, hematoxylin and eosin; HCA, heterocyclic amine; iNOS, inducible nitric oxide synthase; MeIQx, 2-amino-3,8-dimethylimidazo[4,5-*f*] quinoxaline; MeIQ, 2-amino-3,4-dimethylimidazo[4,5-*f*]quinoline; PhIP, 2-amino-1-methyl-6-phenylimidazo[4,5-*b*]pyridine.

Carcinogenesis vol.26 no.1 © Oxford University Press 2005; all rights reserved.

determining the possible involvement and mode of action of these two HCAs in human colon carcinogenesis.

β-Catenin, acting as a structural protein at cell–cell adherent junctions and as a transcriptional activator mediating Wnt signal transduction (21), participates in a large cytoplasmic protein complex, which contains the serine/threonine protein kinase glycogen synthase kinase-3β (GSK-3β), the tumor suppressor gene product of adenomatous polyposis coli (APC), and axin/conductin (22). Frequent mutation of the β-*catenin* gene was found in chemically induced colonic neoplasms in rodents (23–25). For example, β-catenin mutations were observed frequently in azoxymethane (AOM)-induced colon tumors in rats and mice (25,26). Also, colon adenocarcinomas induced by IQ or PhIP in rats have mutations in the β-*catenin* gene (23). Mutation of the *APC* gene is known to repress the degradation and result in the accumulation of the β-catenin (27). About 80% of colorectal neoplasms harbor mutations in the *APC* gene and half of the reminder have β-*catenin* gene mutations (28–30). In the colonic adenomas and adenocarcinomas, β-catenin was universally localized to the cytoplasm and/or nucleus (31). These findings suggest that the mutation of the β-*catenin* gene plays an important role in the development of colon carcinogenesis in rodents as well as in humans.

We recently have developed a novel mouse model for inflammation-related colon carcinogenesis utilizing a single and low dose of AOM, a specific colonic carcinogen in rodents, followed by a strong tumor-promoter dextran sodium sulfate (DSS) in drinking water (32). This model can be used for detecting the chemicals with weak colonic carcinogenicity in mice within a short-term period and for analyzing gene mutations in induced colonic neoplasms. Using this model with a slight modification, in the current study, we tried to induce colonic neoplasms in mice gavaged with a single dose of PhIP or MeIQx followed by a 1-week exposure of DSS in the drinking water. In addition, we analyzed mutations of the β-*catenin* gene in induced colonic adenocarcinomas and compared them with those found in colonic malignancies induced by AOM and DSS (32). Immunohistochemical expression of β-catenin, inducible nitric oxide synthase (iNOS) and cyclooxygenase (COX)-2 were also evaluated in colonic neoplasms.

Materials and methods

Animals, chemicals and diets

Male Crj: CD-1 (ICR) mice (Charles River Japan, Tokyo, Japan) aged 5 weeks were used. They were maintained at Kanazawa Medical University Animal Facility according to the Institutional Animal Care Guidelines. All animals were housed in plastic cages (4 or 5 mice/cage) with free access to drinking water and a pelleted basal diet, CRF-1 (Oriental Yeast, Tokyo, Japan), under controlled conditions of humidity (50 ± 10%), light (12/12 h light/dark cycle) and temperature (23 ± 2°C). After 7 days quarantine, they were randomized by body weight into experimental and control groups. PhIP and MeIQx were purchased from Wako Pure Chemical (Osaka, Japan). DSS (molecular weight 40 000) was obtained from ICN Biochemicals (Aurora, OH).

Experimental procedure

A total of 38 male ICR mice were divided into six experimental and control groups. Groups 1 (nine mice) and 2 (10 mice) were given a single i.g. intubation of PhIP (200 mg/kg body wt) and MeIQx (200 mg/kg body wt), respectively. Starting 1 week after the intubation, animals in groups 1 and 2 were given 2% (w/v) DSS in the drinking water for 7 days, and then followed without any further treatment for 14 weeks. Groups 3 (five mice) and 4 (five mice) were given PhIP and MeIQx alone, respectively. Group 5 (five mice) was given 2% DSS alone. Group 6 (five mice) was untreated. All animals were killed at week 16 by ether overdose. The large bowels were flushed with saline, excised, the length measured (from ileocecal junction to the anal verge), cut open longitudinally along the main axis and then washed with saline. Macroscopic inspection of the large bowels was carefully carried out and they were cut and fixed in 10% buffered formalin for at least 24 h. Histological examination was performed on paraffin-embedded sections after hematoxylin and eosin (H&E) staining. Some tumors were frozen at −80°C. On H&E-stained sections, histological alterations, such as mucosal ulceration, dysplasia and colonic neoplasms, were examined. Colonic neoplasms were diagnosed according to the description by Ward (33). Histopathological examination was also carried out on other organs.

Immunohistochemistry

Using the protocol of our previous study (32), immunohistochemistry for β-catenin, COX-2 and iNOS was performed on 3-μm-thick paraffin-embedded sections from the colons of mice in groups 1 and 2, utilizing the labeled streptavidin–biotin method using a LSAB KIT (DAKO, Glostrup, Denmark) with microwave accentuation. The paraffin-embedded sections were heated for 30 min at 65°C, deparaffinized in xylene and re-hydrated through graded ethanols at room temperature. A 0.05 M Tris–HCl buffer (pH 7.6) was used to prepare solutions and for washes between various steps. Incubations were performed in a humidified chamber. Sections were treated for 40 min at room temperature with 2% BSA and incubated overnight at 4°C with primary antibodies, such as anti-β-catenin mouse monoclonal antibody (diluted 1:1000, Transduction Laboratories, Lexington, KY), anti-COX-2 mouse monoclonal antibody (diluted 1:200, Transduction Laboratories), and anti-iNOS mouse monoclonal antibody (cat. no. N32020-150, diluted 1:250, Transduction Laboratories). To reduce the non-specific staining of mouse tissue by the mouse antibodies, a Mouse On Mouse IgG blocking reagent (Vector Laboratories, Burlingame, CA) was applied for 1 h. Horseradish peroxidase activity was visualized by treatment with H_2O_2 and 3,3′-diaminobenzidine for 5 min. At the last step, the sections were weakly counterstained with Mayer's hematoxylin (Merck, Tokyo, Japan). For each case, negative controls were performed on serial sections. On the control sections, incubation with the primary antibodies was omitted. Intensity and localization of immunoreactivities against all primary antibodies used were examined on all sections using a microscope (Olympus BX41, Olympus Optical, Tokyo, Japan) and recorded.

DNA extraction

For analysis of β-catenin mutations, seven colonic adenocarcinomas (three paraffin-embedded and four frozen materials) from PhIP/DSS-treated mice and one paraffin-embedded adenocarcinoma from a mouse treated with MeIQx/DSS were used. Also, 14 adenocarcinomas embedded in paraffin from our previous experiment (32) were used for analysis of β-catenin mutations for comparison. DNA was extracted from frozen tissue using Wizard® Genomic DNA Purification Kit (Promega, Madison, WI) or from paraffin-embedded sections using DEXPAT™ (TaKaRa Shuzo, Shiga, Japan). Tumor tissues were scraped off from paraffin sections using needles to avoid contamination with their surrounding tissue.

PCR-single strand conformation polymorphism (SSCP) analysis

DNA from colonic adenocarcinomas was PCR-amplified with primers (5′-primer, GCTGACCTGATGGAGTTGGA; 3′-primer, GCTACTTGCTCTTGCGTGAA), which were designed to amplify exon 3 of the β-*catenin* gene containing the consensus sequence for GSK-3β phosphorylation (25). The length of the PCR product with these primers is 227 bp. The primers were synthesized with a 394 DNA/RNA synthesizer (Applied Biosystems, Foster City, CA) and purified with an OPC cartridge (Applied Biosystems). PCR for non-radioisotopic SSCP was performed in 50 μl of reaction mixture consisting of 0.5 μM of each primer, 1× PCR buffer (Perkin Elmer, Applied Biosystems Division, Foster City, CA), 200 μM each dNTP, 2.5 U AmpliTaq Gold™ (Perkin Elmer) and 0.5–5 μl of template DNA. The mixture was heated at 94°C for 9 min and subjected to 40 or 35 cycles of denaturation (94°C, 1 min), annealing (55°C, 2 min) and extension (72°C, 3 min) using a Perkin Elmer-Cetus thermal cycler. The PCR products were purified and concentrated to 20 μl using Microcon 100 (Amicon, Beverley, MA). Ten volumes of 95% formamide, 20 mM EDTA, 0.05% bromophenol blue, 0.05% xylene cyanol were added to 0.5 μl of purified PCR products, heated to 90°C for 3 min and applied to 10% polyacrylamide gels containing 5% glycerol. Electrophoresis was carried out at 300 V for 2 h at 20°C and the gels were soaked in 10% trichloroacetic acid and in 50% methanol for 10 min each. DNA bands were detected by silver staining using 2-D Silver Staining Solution II (Daiichi Chemical DNA, Tokyo, Japan).

Restriction fragment length polymorphism (RFLP) assay for PCR products of β-catenin

To detect β-*catenin* mutations at codons 32, 33 and 34, PCR products were treated with a restriction enzyme *Hin*fI and electrophoresed on 5% agarose gels. Recognition sequences of *Hin*fI are GANTC. The PCR product of 227 bp is digested by *Hin*fI to 82, 7 and 138 bp in the case of the wild-type, to 89 and

138 bp with mutations at the first or second bases of codons 32 or 33 and to 82 and 145 bp with mutations at the second or third bases of codons 34 or 35.

Direct DNA sequencing

With 1 μl of the purified PCR products and 5'DyeAmidite-667-labeled 5' or 3' PCR primers (synthesized by Pharmacia Biotech, Tokyo, Japan), cycle sequencing reactions were carried out using a Thermo Sequenase™ fluorescent labeled primer cycle sequencing kit (Amersham) and the sequences were determined with an ALF express™ DNA sequencer (Pharmacia Biotech).

Statistical analysis

All measurements were compared by Student's *t*-test, Welch's *t*-test, χ^2 test or Fisher's exact probability test for paired samples.

Results

General observation

During the study, bloody stools were found during and soon after DSS exposure (days 12–21) in a few mice that received 2% DSS in the drinking water and their body weight gains were slightly decreased (data not shown). However, thereafter no such clinical symptoms were observed. The body and liver weights, and the lengths of the large bowel of mice in all groups were measured at the end of the study (week 16) and are listed in Table I. The mean body weight of group 1 (PhIP→2% DSS) was significantly larger than that of group 3 (PhIP alone, $P < 0.02$) or 6 (untreated, $P < 0.05$). The mean length of the large bowel of mice in group 1 was significantly lower than that of mice in group 3 ($P < 0.01$). The mean length of the large bowel in the mice of group 2 (MeIQx→2% DSS) was significantly smaller than that of mice in group 4 (MeIQx alone, $P < 0.005$). These shortenings were caused by DSS-induced inflammation in the colonic mucosa. Those values in groups 3 ($P < 0.02$) and 4 ($P < 0.05$) were significantly greater than that of group 6.

Pathological findings

Macroscopically, nodular, polypoid or flat-type colonic tumors were observed in the middle and distal colon of all mice in groups 1 (Figure 1a) and 2 (Figure 1b). Their histopathology was well or moderately differentiated tubular adenocarcinoma (Figures 2a, 3a, 4 and 5a) or tubular adenoma (Figures 2b and 3b). A few tumors were diagnosed as adenocarcinoma in adenoma (Figure 4). There were no tumors in any organs other than the large bowel in these two groups. As shown in Table II, the incidence of adenocarcinoma and tubular adenoma in group 1 was 56% with a multiplicity of 0.78 ± 0.97 and 33% with 0.44 ± 0.73 multiplicity, respectively. Two mice in group 2 had colonic neoplasms: two small tubular adenomas (20% incidence with 0.20 ± 0.42 multiplicity) and one well-differentiated tubular adenocarcinoma (10% incidence with 0.10 ± 0.32 multiplicity) in the distal colon (Table II). In the mice of groups 3–6, no neoplasms developed in any organs including the large bowel. Besides colonic neoplasms, all mice of groups 1 and 9 (90%) of 10 mice of group 2 had colonic dysplasia (Figures 2c and 3c). Their multiplicities were 3.11 ± 1.45 in group 1 and 2.30 ± 1.62 in group 2. As indicated in Table III, colonic dysplasia also developed in the mice of groups 3 (40% incidence with a multiplicity of 0.60 ± 0.80) and 4 (40% incidence with a multiplicity of 0.60 ± 0.80). There were no dysplastic lesions in the mice of groups 5 and 6. In addition, colonic mucosal ulceration was found in the distal colon of mice in groups 1, 2 and 5 (Table III).

Table I. Body weight and length of large bowel at the end of the experiment

Group no.	Treatment (no. of mice examined)	Body weight (g)	Length of large bowel (cm)
1	PhIP → 2% DSS (9)	46.5 ± 4.0[a–c]	13.2 ± 0.9[d]
2	MeIQx → 2% DSS (10)	46.6 ± 4.0	13.2 ± 0.5[e]
3	PhIP (5)	40.7 ± 2.8	14.7 ± 0.7[f]
4	MeIQx (5)	43.9 ± 2.1	14.9 ± 1.1[g]
5	2% DSS (4)	40.1 ± 3.8	13.5 ± 0.5
6	None (5)	41.1 ± 3.4	13.1 ± 0.9

[a]Mean ± SD.
[b]Significantly different from group 3 ($P < 0.02$).
[c]Significantly different from group 6 ($P < 0.05$).
[d]Significantly different from group 3 ($P < 0.01$).
[e]Significantly different from group 4 ($P < 0.005$).
[f]Significantly different from group 6 ($P < 0.02$).
[g]Significantly different from group 6 ($P < 0.05$).

Immunohistochemical findings

The immunoreactivities against β-catenin, COX-2 and iNOS were found in all colonic lesions, including neoplasms (four adenomas and seven adenocarcinomas in group 1; and two adenomas and one adenocarcinoma in group 2) and dysplastic lesions (28 in group 1; and 23 in group 2). The immunoreactivity showed dark brown reaction products with a slight variation in the intensity and distribution (Figures 5b–d and 6b–d). Strong β-catenin expression was seen in the nucleus and cytoplasm of adenocarcinoma cells (Figures 5b and 6b). Although the intensity was relatively weaker than carcinoma cells, adenoma cells showed positivity for β-catenin in their cytoplasm and cell membrane. β-Catenin immunoreactivity was also found in the cell membrane and cytoplasm of dysplastic cells. Non-lesional cryptal cells showed weak positivity of β-catenin in their cell membrane. In addition, positive reaction against the β-catenin antibody was found in the vascular endothelium, infiltrated inflammatory cells and ganglion cells in myenteric (Auerbach's) plexus. Strong COX-2 immunoreactivity was also found in adenocarcinoma (Figures 5c and 6c) and adenoma cells in their cytoplasm. Dysplastic cells showed weak positivity for COX-2, when compared with neoplastic cells. Non-lesional cryptal cells at lower part of crypts were weakly positive for COX-2, while a strongly positive reaction of COX-2 was seen in the endothelium of small blood vessels and inflammatory cells infiltrated in the lamina propria. Smooth muscle cells and fibroblasts in the wall of the large bowel showed a weak reaction of COX-2. iNOS-immunohistochemistry showed strong immunoreactivity in the cytoplasm of adenocarcinoma (Figures 5d and 6d) and adenoma cells: the intensity was greater in carcinoma cells when compared with adenoma cells. Also, dysplastic cells were positive for iNOS in their cytoplasm, but the intensity was weaker than adenoma cells. The faint positive reaction was found in the cytoplasm of non-lesional cryptal cells. Immunohistochemical iNOS expression was strong in the endothelial cells of small blood vessels and inflammatory cells in the lamina propria. COX-2- and iNOS-stained inflammatory cells were also frequently observed in areas of mucosal ulceration in groups 1, 2 and 5.

Mutation in β-catenin gene

In the current experiment, mutations of exon 3 of the β-*catenin* gene were investigated by PCR–SSCP and RFLP analyses

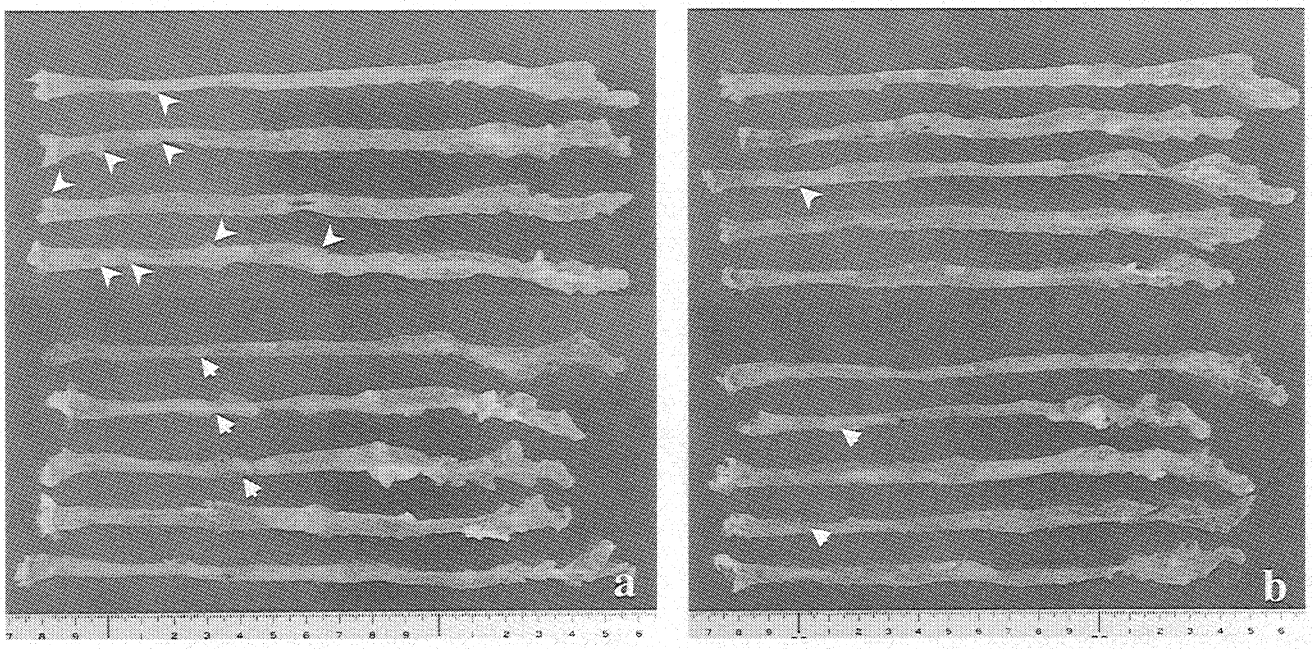


Fig. 1. Macroscopic view of large bowels. (**a**) Mice treated with PhIP/DSS (group 1) and (**b**) those given MeIQx/DSS (group 2). Arrows indicate colonic tumors.

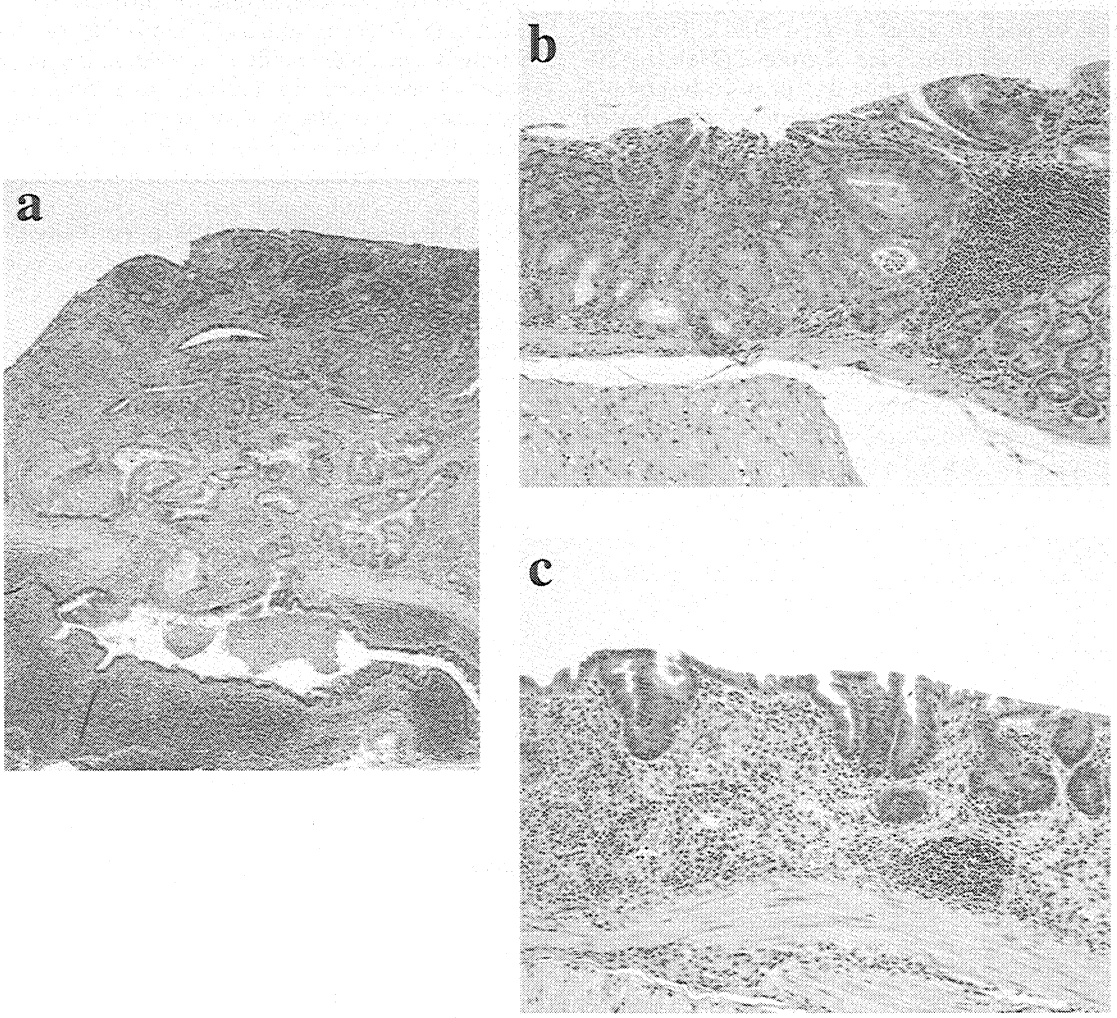


Fig. 2. Histopathology of colonic lesions developed in mice treated with PhIP/DSS. (**a**) A tubular adenocarcinoma invaded into the submucosa; (**b**) a tubular adenoma; and (**c**) dysplasia with mucosal ulceration. H&E stain, original magnification, (a) ×20, (b) ×50, (c) ×50.

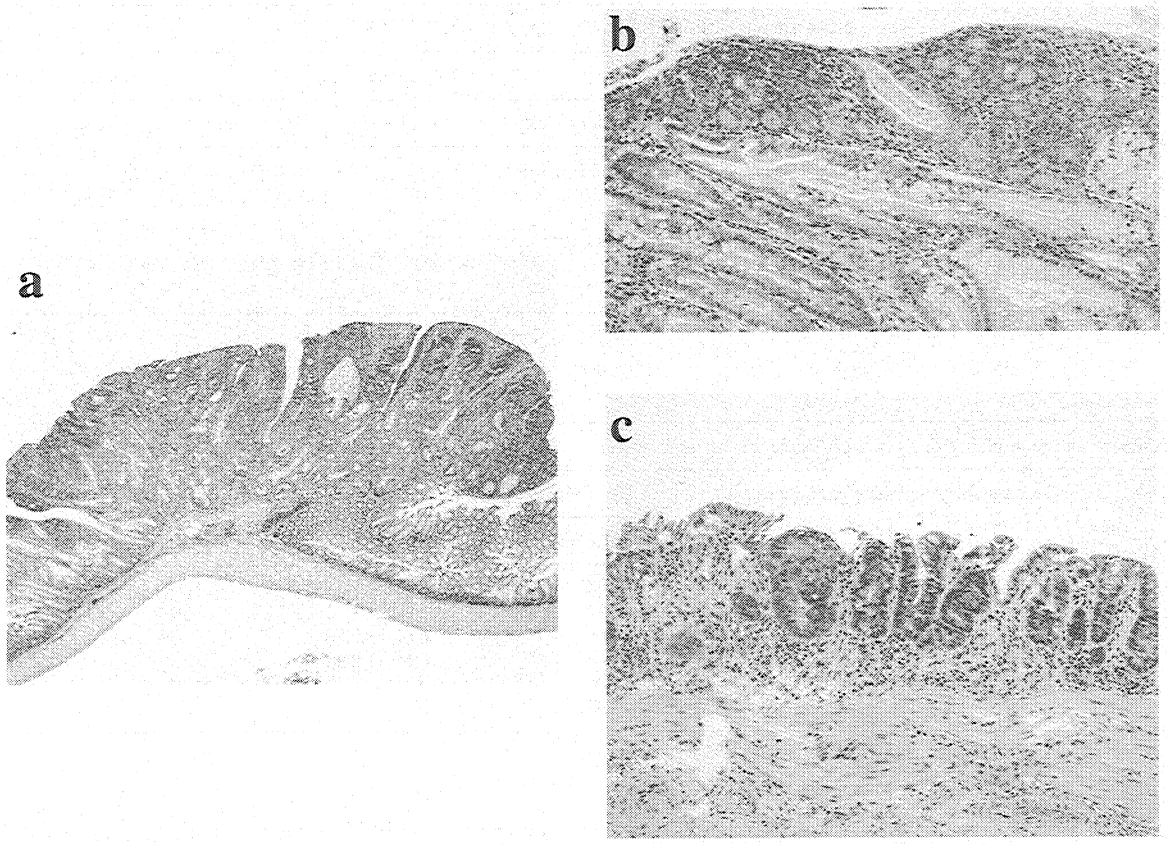


Fig. 3. Histopathology of colonic lesions developed in mice treated with MeIQx/DSS. (**a**) A polypoid tubular adenocarcinoma; (**b**) tubular adenomas; and (**c**) dysplasia with mucosal ulceration. H&E stain, original magnification, (a) ×10, (b) ×50, (c) ×50.



Fig. 4. Histopathology of an adenocarcinoma in adenoma developed in the large bowel of a mouse treated with PhIP/DSS. H&E stain, original magnification, ×50.

(Figures 7 and 8). Among the PhIP/DSS-treated mice, β-*catenin* genes of all of the seven colonic adenocarcinomas (100%) have mutations restricted to codons 32 and 34 (Table IV). In codon 32, the mutations found were GAT (Asp) to AAT (Asn) (PhIP/DSS-2, 3, 4, 5), to CAT (His) (PhIP/DSS-1) and TAT (Tyr) (PhIP/DSS-6) and in codon 34 GGA (Gly) to GTA (Val) (PhIP/DSS-7). However, mutation in the β-*catenin* gene was not detected in the MeIQx/DSS-induced colonic adenocarcinoma (Figures 7 and 8; Table IV), although only one sample was investigated. In these analyses, positive controls with mutations in codons 32 and 34 showed band shifts (Figures 7 and 8).

With respect to AOM/DSS-induced mouse colonic adenocarcinomas (32), β-*catenin* mutations in codons 32 through to 34 were detected in 11 (79%) out of 14 (Figures 7 and 8; Table V). These mutations included GAT (Asp) to AAT (Asn) (AOM/DSS-6, 11, 13), to GGT (Gly) (AOM/DSS-3) at codon 32, TCT (Ser) to TTT (Phe) at codon 33 (AOM/DSS-4, 8, 10), and GGA (Gly) to GAA (Glu) (AOM/DSS-7, 9, 12, 14) at codon 34 (Table V; Figure 8). Except for a mutation at the second base of codon 32 (AOM/DSS-3), all were G:C to A:T transitions (Figure 9).

Discussion

The results of the present work indicate that a single i.g. intubation of PhIP (200 mg/kg body wt) followed by 1-week exposure of 2% DSS in drinking water could produce colonic adenocarcinomas with 56% incidence and 0.78 ± 0.97 multiplicity in male ICR mice within 16 weeks. Also, a single gavage with MeIQx (200 mg/kg body wt) followed by 2% DSS in the drinking water induced colonic epithelial malignancy, although their incidence (10%) and multiplicity (0.10 ± 0.32) was low. Colonic adenocarcinomas induced by this treatment schedule were immunohistochemically positive for β-catenin, COX-2 and iNOS. Moreover, all examined adenocarcinomas in mice treated with PhIP/DSS and MeIQx/DSS had β-catenin mutations.

Table II. Incidence and multiplicity of colonic neoplasms induced by PhIP or MeIQx followed by DSS

Group no.	Treatment (no. of mice examined)	Total		Adenoma		Adenocarcinoma	
		Incidence	Multiplicity	Incidence	Multiplicity	Incidence	Multiplicity
1	PhIP→2% DSS (9)	78%	1.22 ± 1.20[a]	33%	0.44 ± 0.73	56%	0.78 ± 0.97
2	MeIQx→2% DSS (10)	30%	0.30 ± 0.48	20%	0.20 ± 0.42	10%	0.10 ± 0.32
3	PhIP (5)	0	0	0	0	0	0
4	MeIQx (5)	0	0	0	0	0	0
5	2% DSS (4)	0	0	0	0	0	0
6	None (5)	0	0	0	0	0	0

[a]Mean ± SD.

Table III. Incidence and multiplicity of dysplastic lesions in the large bowel

Group no.	Treatment (no. of mice examined)	Dysplastic lesions		Mucosal ulceration	
		Incidence	Multiplicity	Incidence	Multiplicity
1	PhIP→2% DSS (9)	100%	3.11 ± 1.45	100%	1.78 ± 0.92
2	MeIQx→2% DSS (10)	90%	2.30 ± 1.62	50%	0.80 ± 1.17
3	PhIP (5)	40%	0.60 ± 0.80	0%	0
4	MeIQx (5)	40%	0.60 ± 0.80	0%	0
5	2% DSS (4)	0%	0	100%	1.58 ± 0.87
6	None (5)	0%	0	0%	0

Several researchers have made great efforts to establish an efficient experimental animal model for colon carcinogenesis induced by PhIP or MeIQx (34,35). Nakagama's group developed efficient animal models for PhIP-induced colon carcinogenesis, where rats were given cycle treatments with dietary PhIP (300 or 400 p.p.m.) and a high-fat diet or PhIP in the diet followed by a high-fat diet (36,37). Tsukamoto *et al.* (35) also reported that i.g. administration of PhIP (three times a week for 7 weeks at a dose of 100 mg/kg body wt) could efficiently induce large intestinal tumors within 50 weeks in male F344 rats. Indeed, ACF and colonic neoplasms could develop in rats using such protocols, but their incidence and multiplicity were low and the experimental period was long. As for intestinal carcinogenicity of PhIP in mice, dietary PhIP (300 p.p.m.) in a high-fat diet for 40 weeks and followed by a high-fat diet without PhIP for 30 or 45 weeks induced small intestinal and cecal tumors (adenomas and adenocarcinomas) (17). There were no reports on MeIQx-induced colonic epithelial malignancies, although dietary feeding with MeIQx could produce ACF in mice (20). In the current study we could develop large bowel neoplasms within 16 weeks by an experimental protocol of a single and low-dose i.g. administration of PhIP or MeIQx (200 mg/kg body wt) followed by 1-week exposure of 2% DSS in the drinking water. The findings also indicated a powerful tumor-promoting ability of DSS, as found in our previous experiment using AOM as a carcinogen (32). Thus, our model can be applied to investigate colonic carcinogenesis induced by environmental carcinogens (HCAs, etc.) and/or modulators (promoters and chemopreventors) (32,34) and to genetic analysis of the susceptibility to colon tumorigenesis (38).

There have been no studies on the mutation of β-*catenin* in mouse colonic tumors induced by HCAs, although β-*catenin* mutations at codons 32 and 34 are the most common in PhIP-induced colonic neoplasms in rats (35–37). Our results on β-catenin mutations are in accordance with these findings (35–37). To our knowledge, the mutation of β-catenin, GAT→CAT or TAT, at codon 32 was not reported. To identify whether these mutations came from DSS or were characteristics of the mice, more detailed analysis should be carried out. All mutations are involved in guanine, consistent with a report that PhIP preferentially forms DNA adducts at guanines (39). In the present study, we could not find a β-*catenin* gene mutation in a mouse colonic adenocarcinoma produced by MeIQx/DSS, but we will analyze the mutation in our on-going experiments where more colonic tumors will develop in mice treated with MeIQx and DSS. In AOM/DSS-induced colon tumors (32), mutations of the β-*catenin* gene were present in codons 32 through to 34. The location was slightly different from a report documenting that β-catenin mutations in mouse colon tumors induced by AOM were found in codons 33, 37 and 41, encoding serine and threonine that are direct targets for phosphorylation by GSK-3β (26). Codon 34 also encodes neighboring serine and threonine residues (26). Mutations of codons 33 and 34 were detected in both the present investigation and another report (26). However, mutation of codon 32 was not found in the other report (26). Therefore, it may be speculated that mutations of codons 33 and 34 might be caused by AOM exposure and that of codon 32 by DSS administration, as Koesters *et al.* (40) reported that the different mutational spectra observed in *Ctnnb1* directly relates to the particular carcinogenic treatment. We did not identify the mutations of codons 37 and 41 in the present study. This might be explained by the different experimental protocol between the present study and the previous report on β-catenin mutations in mouse colon cancer, where mice were treated with AOM at a dose of 10 mg/kg body wt, once a week for 6 weeks and the

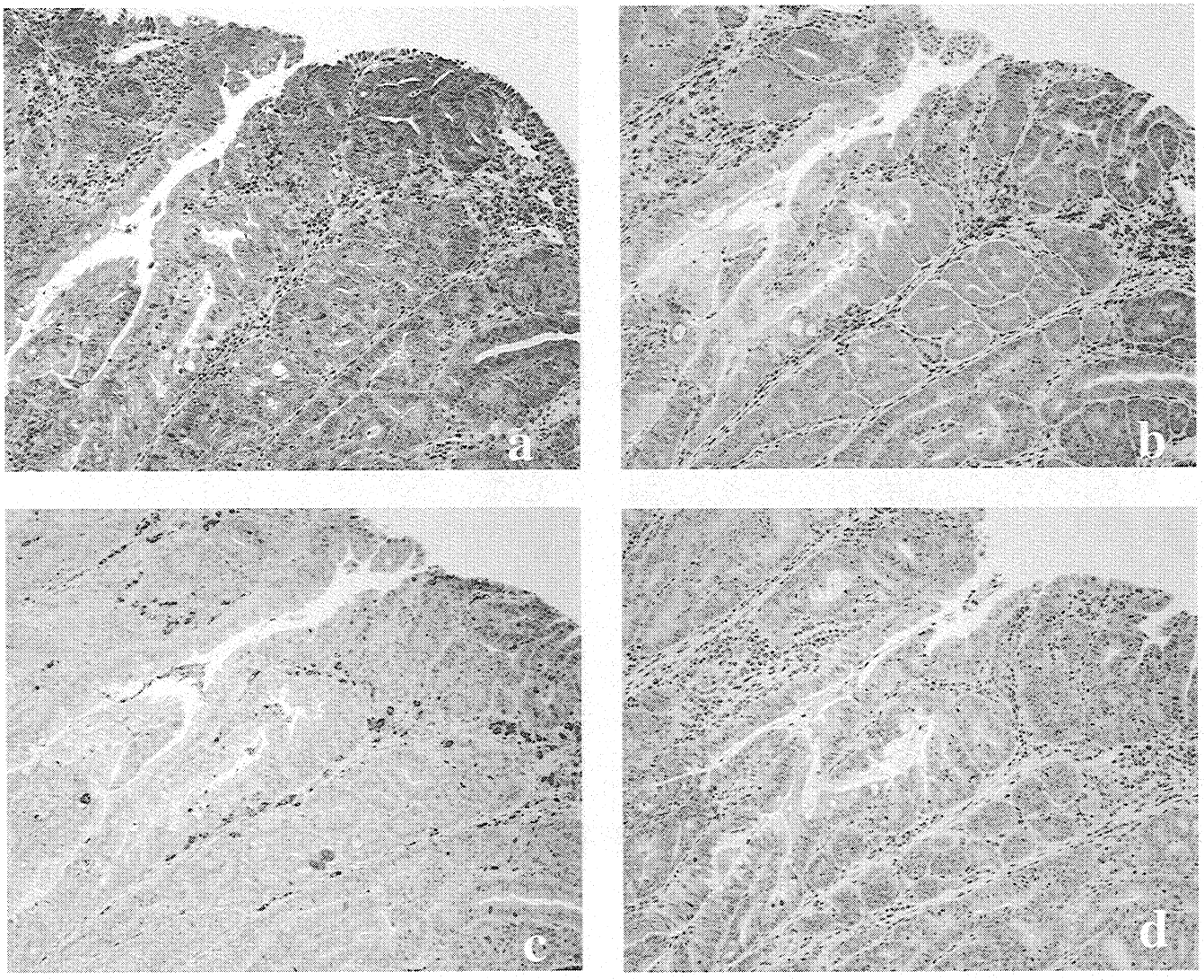


Fig. 5. Histopathology and immunohistochemistry of β-catenin, COX-2, and iNOS in a colonic adenocarcinoma developed in a mouse given PhIP/DSS. (**a**) H&E staining; (**b**) β-catenin immunohistochemistry; (**c**) COX-2 immunohistochemistry; and (**d**) iNOS immunohistochemistry. Original magnification, (a–d) ×50.

experiment was terminated at week 30 (26). The second G of the CTGGA sequence was commonly mutated to A in codons 32 and 34 of the rat β-*catenin* gene and this site is considered to be a mutational hot-spot with AOM (25,41). In this study, 10 of 11 mutations being G:C→A:T transitions at codons 32, 33 and 34, the mutation of the second G of the CTGGA might be particularly important in colon carcinogenesis. We reported recently the increased expression of COX-2 and iNOS in mouse colon adenocarcinoma in an AOM/DSS mouse colon carcinogenesis model (32). The reaction products of iNOS and COX-2, nitric oxide and prostaglandin E_2 respectively, could contribute to colon tumorigenesis. Also, there is evidence of an involvement of the Wnt–APC–β-catenin/Tcf pathway in COX-2 expression (42–44). Although the relationship between its pathway and iNOS expression is still unclear, β-catenin was accumulated in the cytoplasm and nucleus in the colonic tumors induced by AOM/DSS (32) and those developed in this study. Therefore, mutation of β-catenin may play important roles in mouse and rat colon carcinogenesis. Furthermore, mutation of β-catenin is an early event of colorectal carcinogenesis (35,41); analysis of this at an early stage of colon carcinogenesis should be done in this model. Since *c-myc* and *cyclinD1* were identified as targets of the β-catenin/APC pathway (45,46), this gene expression might also influence colon carcinogenesis in the present model.

In the present study, all colonic neoplasms induced by PhIP or MeIQx followed by DSS were immunohistochemically positive for iNOS and COX-2. The iNOS and COX-2 were reported to be over-expressed in colon tumors or ACF that develop in rats after the administration of the colon-specific carcinogen, AOM (41,47,48). iNOS may regulate COX-2 production of pro-inflammatory prostaglandins, which are known to play a key role in colon tumor development (49). The results in the current study indicate a powerful tumor-promoting ability of DSS, since the doses of PhIP and MeIQx used were too small to induce colonic neoplasms. It is probable that peroxynitrite acts as an oxidant for the heme of COX-2 and activates the enzyme (50,51). Our recent study using an AOM/DSS model (52) has suggested the possibility. Also, nitric oxide

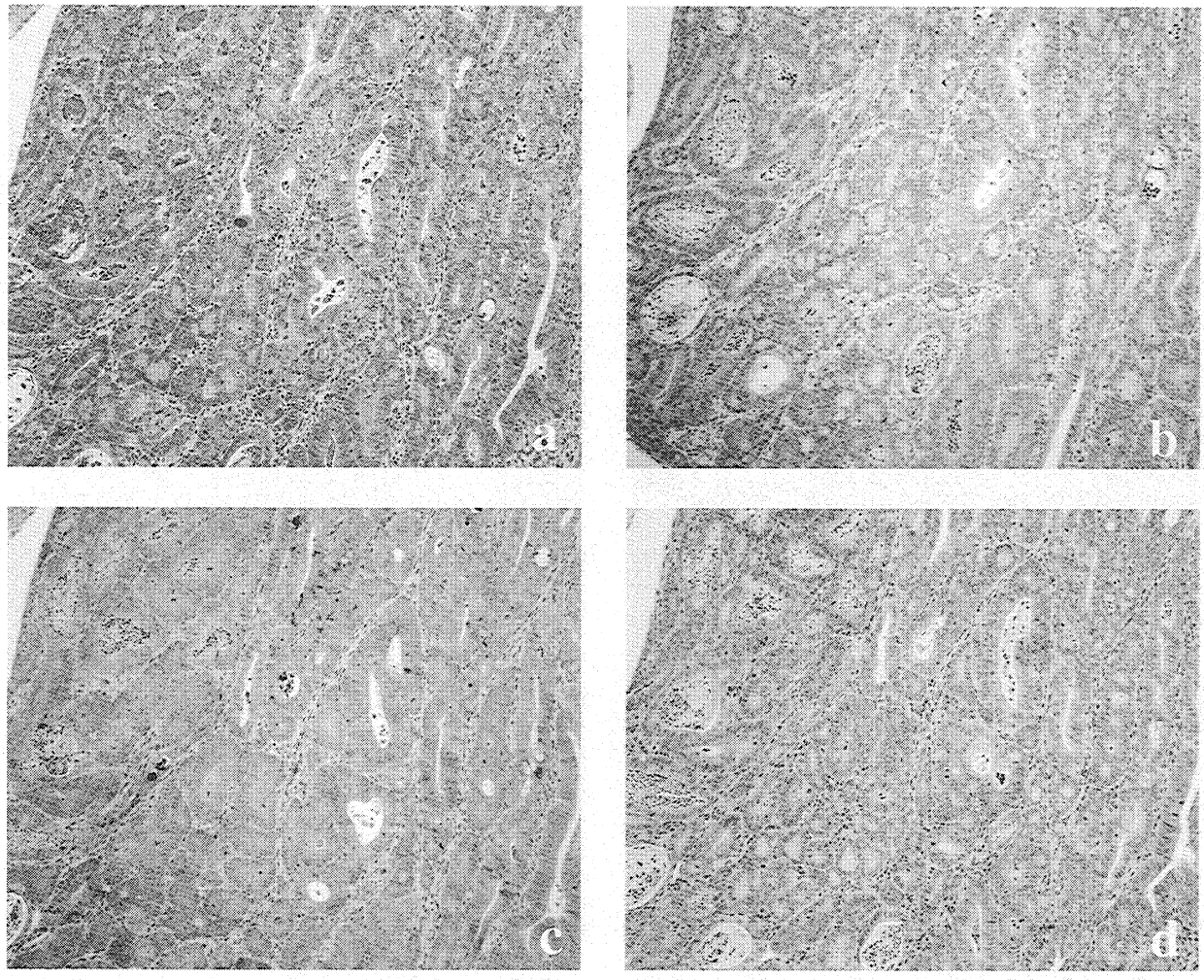


Fig. 6. Histopathology and immunohistochemistry of β-catenin, COX-2, and iNOS in a colonic adenocarcinoma developed in a mouse treated with MeIQx/DSS. (**a**) H&E staining; (**b**) β-catenin immunohistochemistry; (**c**) COX-2 immunohistochemistry; and (**d**) iNOS immunohistochemistry. Original magnification, (a–d) ×50.

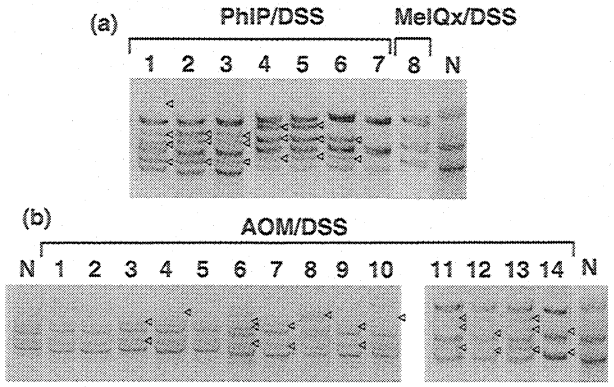


Fig. 7. PCR–SSCP analysis of the β-*catenin* gene in mouse colon adenocarcinomas. (**a**) PhIP/DSS-induced mouse colon adenocarcinomas (lanes 1–7); and MeIQx/DSS-induced mouse colon adenocarcinomas (lane 8). (**b**) AOM/DSS-induced mouse colon adenocarcinomas (lanes 1–14). Lanes N, normal colon mucosa samples. Tumor-specific bands are indicated by arrow heads.

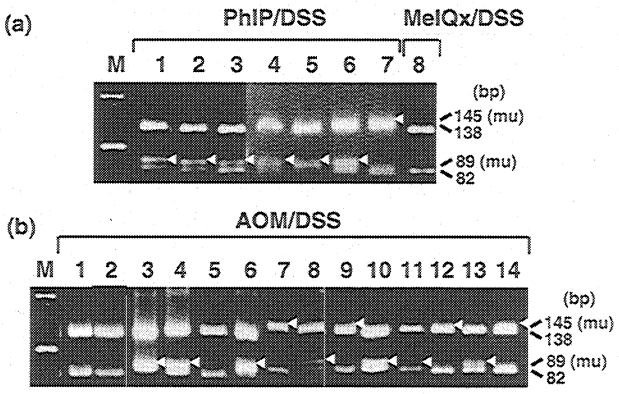


Fig. 8. RFLP analysis of the β-*catenin* gene in mouse colon adenocarcinomas. (**a**) PhIP/DSS (lanes 1–7) and MeIQx/DSS (lane 8) induced mouse colonic adenocarcinomas. (**b**) AOM/DSS-induced mouse colon adenocarcinomas (lanes 1–14). Lane M, DNA size markers (X174/*Hae*III digest). Tumor-specific bands are indicated by arrow heads.

and its metabolites may affect tumor formation and/or progression. As found in ulcerative colitis-related colon carcinogenesis in humans, iNOS expression and nitrotyrosine accumulation in inflamed colonic mucosa caused by DSS treatment may be involved in the colonic tumor development in the current study (32,53).

In conclusion, the results in the current study indicate that a single i.g. administration of a low dose of the

Table IV. Mutations in exon 3 of the β-*catenin* gene in PhIP/DSS or MeIQx/DSS-induced mouse colonic adenocarcinomas

Sample		β-Catenin status	Amino acid substitution
PhIP/DSS-1 (paraffin-embedded)	Codon 32	GAT→CAT	Asp→His
PhIP/DSS-2 (paraffin-embedded)	Codon 32	GAT→AAT	Asp→Asn
PhIP/DSS-3 (paraffin-embedded)	Codon 32	GAT→AAT	Asp→Asn
PhIP/DSS-4 (frozen tissue)	Codon 32	GAT→AAT	Asp→Asn
PhIP/DSS-5 (frozen tissue)	Codon 32	GAT→AAT	Asp→Asn
PhIP/DSS-6 (frozen tissue)	Codon 32	GAT→TAT	Asp→Tyr
PhIP/DSS-7 (frozen tissue)	Codon 34	GGA→GTA	Gly→Val
MeIQx/DSS-1 (paraffin-embedded)		Wild-type	

Table V. Mutations in exon 3 of the β-*catenin* gene in AOM/DSS-induced mouse colonic adenocarcinomas

Sample		β-Catenin status	Amino acid substitution
AOM/DSS-1 (paraffin-embedded)		Wild-type	-
AOM/DSS-2 (paraffin-embedded)		Wild-type	-
AOM/DSS-3 (paraffin-embedded)	Codon 32	GAT→GGT	Asp→Gly
AOM/DSS-4 (paraffin-embedded)	Codon 33	TCT→TTT	Ser→Phe
AOM/DSS-5 (paraffin-embedded)		Wild-type	
AOM/DSS-6 (paraffin-embedded)	Codon 32	GAT→AAT	Asp→Asn
AOM/DSS-7 (paraffin-embedded)	Codon 34	GGA→GAA	Gly→Glu
AOM/DSS-8 (paraffin-embedded)	Codon 33	TCT→TTT	Ser→Phe
AOM/DSS-9 (paraffin-embedded)	Codon 34	GGA→GAA	Gly→Glu
AOM/DSS-10 (paraffin-embedded)	Codon 33	TCT→TTT	Ser→Phe
AOM/DSS-11 (paraffin-embedded)	Codon 32	GAT→AAT	Asp→Asn
AOM/DSS-12 (paraffin-embedded)	Codon 34	GGA→GAA	Gly→Glu
AOM/DSS-13 (paraffin-embedded)	Codon 32	GAT→AAT	Asp→Asn
AOM/DSS-14 (paraffin-embedded)	Codon 34	GGA→GAA	Gly→Glu

genotoxic food-derived carcinogens, especially PhIP, followed by DSS resulted in a high incidence of colonic epithelial malignancies with β-catenin mutations within 16 weeks. Also, our findings suggest the importance of inflammation caused by DSS exposure in mouse colon carcinogenesis under this experimental condition. The experimental protocol described here could be applied to investigate colonic carcinogenesis induced by environmental carcinogens and/or modulators and to genetic analysis of the susceptibility to colon tumorigenesis. Such collaborating studies with other laboratories are on-going in order to fight against colon cancer development.

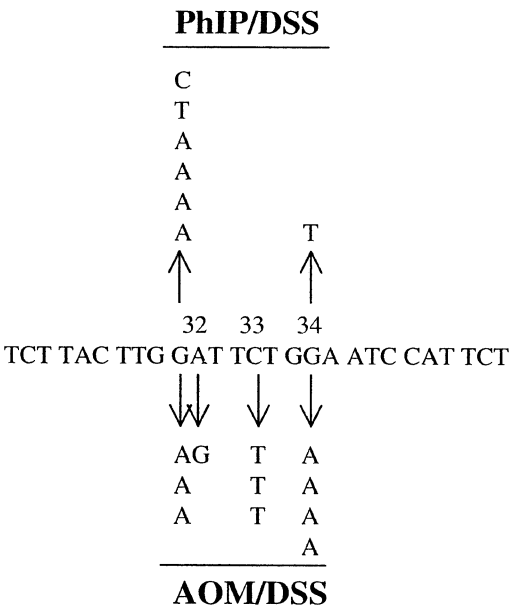


Fig. 9. Sequence of β-*catenin* exon 3 with the codon numbers and β-*catenin* mutations found in PhIP/DSS-, MeIQx/DSS- and AOM/DSS-induced mouse colonic tumors.

Acknowledgements

We express our thanks to the staff of the Research Animal Facility. We also thank Mrs Sotoe Yamamoto for her secretarial assistance. This study was supported in part by the Grant-in-Aid for Cancer Research from the Ministry of Health, Labour and Welfare of Japan; the Grant-in-Aid for the 3rd Term for a Comprehensive 10-year Strategy for Cancer Control from the Ministry of Health, Labour and Welfare of Japan; the Grants-in-Aid for Scientific Research (nos 152052 and 15592007) from the Ministry of Education, Culture, Sports, Science and Technology of Japan; and the grants (H2004-6 and C2004-4) from Kanazawa Medical University.

References

1. Sugimura,T. (2000) Nutrition and dietary carcinogens. *Carcinogenesis*, **21**, 387–395.
2. Kotake,K., Honjo,S., Sugihara,K., Kato,T., Kodaira,S., Takahashi,T., Yasutomi,M., Muto,T. and Koyama,Y. (2003) Changes in colorectal cancer during a 20-year period: an extended report from the multi-institutional registry of large bowel cancer, Japan. *Dis. Colon Rectum*, **46** (10 suppl.), 532–543.
3. Tamakoshi,K., Tokudome,S., Kuriki,K., Takekuma,K. and Toyoshima,H. (2001) Epidemiology and primary prevention of colorectal cancer (in Japanese). *Jpn. J. Cancer Chemother.*, **28**, 146–150.
4. Nagao,M. (1999) A new approach to risk estimation of food-borne carcinogens–heterocyclic amines-based on molecular information. *Mutat. Res.*, **431**, 3–12.
5. Sugimura,T. (1997) Overview of carcinogenic heterocyclic amines. *Mutat. Res.*, **376**, 211–219.
6. Ohgaki,H. (2000) 7.1 Rodents. In Nagao,M. and Sugimura,T. (eds), *Food Borne Carcinogens: Heterocyclic Amines*. John Wiley & Sons, Ltd, New York, NY, pp. 198–228.
7. Weisburger,J.H. (2002) Comments on the history and importance of aromatic and heterocyclic amines in public health. *Mutat. Res.*, **506/507**, 9–20.
8. Wakabayashi,K., Nagao,M., Esumi,H. and Sugimura,T. (1992) Food-derived mutagens and carcinogens. *Cancer Res.*, **52** (suppl.), 2092s–2098s.
9. Gerhardsson de Verdier,M., Hagman,U., Peters,R.K., Steineck,G. and Overvik,E. (1991) Meat, cooking methods and colorectal cancer: a case-referent study in Stockholm. *Int. J. Cancer*, **49**, 520–525.
10. Sinha,R. and Rothman,N. (1997) Exposure assessment of heterocyclic amines (HCAs) in epidemiologic studies. *Mutat. Res.*, **376**, 195–202.
11. Sinha,R. and Norat,T. (2002) *Meat Cooking and Cancer Risk, Volume 156*. IARC Scientific Publications, IARC, Lyon, pp. 181–186.

12. Wakabayashi,K., Ushiyama,H., Takahashi,M., Nukaya,H., Kim,S.B., Hirose,M., Ochiai,M., Sugimura,T. and Nagao, M. (1993) Exposure to heterocyclic amines. *Environ. Health Perspect.*, **99**, 129–134.
13. Bird,R.P. (1987) Observation and quantification of aberrant crypts in the murine colon treated with a colon carcinogen: preliminary findings. *Cancer Lett.*, **37**, 147–151.
14. Ochiai,M., Nakagama,H., Watanabe,M., Ishiguro,Y., Sugimura,T. and Nagao,M. (1996) Efficient method for rapid induction of aberrant crypt foci in rats with 2-amino-1-methyl-6-phenylimidazo[4,5-*b*]pyridine. *Jpn. J. Cancer Res.*, **87**, 1029–1033.
15. Kristiansen,E. (1996) The role of aberrant crypt foci induced by the two heterocyclic amines 2-amino-3-methyl-imidazo[4,5-*f*]quinoline (IQ) and 2-amino-1-methyl-6-phenyl-imidazo[4,5-*b*]pyridine (PhIP) in the development of colon cancer in mice. *Cancer Lett.*, **110**, 187–192.
16. Ito,N., Hasegawa,R., Sano,M., Tamano,S., Esumi,H., Takayama,S. and Sugimura,T. (1991) A new colon and mammary carcinogen in cooked food, 2-amino-1-methyl-6-phenylimidazo[4,5-*b*]pyridine (PhIP). *Carcinogenesis*, **12**, 1503–1506.
17. Ochiai,M., Imai,H., Sugimura,T., Nagao,M. and Nakagama,H. (2002) Induction of intestinal tumors and lymphomas in C57BL/6N mice by a food-borne carcinogen, 2-amino-1-methyl-6-phenylimidazo[4,5-*b*] pyridine. *Jpn. J. Cancer Res.*, **63**, 478–483.
18. Fujita,H., Nagano,K., Ochiai,M., Ushijima,T., Sugimura,T., Nagao,M. and Mastushima,T. (1999) Difference in target organs in carcinogenicity of a heterocyclic amine, 2-amino-3,4-dimethylimidazo[4,5-*f*]quinoline, in different strains of mice. *Jpn. J. Cancer Res.*, **90**, 1203–1206.
19. Tanakamaru,Z., Mori,I., Nishikawa,A., Furukawa,F., Takahashi,M. and Mori,H. (2001) Essential similarities between spontaneous and MeIQx-promoted aberrant crypt foci in the F344 rat colon. *Cancer Lett.*, **172**, 143–149.
20. Okonogi,H., Ushijima,T., Shimizu,H., Sugimura,T. and Nagao,M. (1997) Induction of aberrant crypt foci in C57BL/6N mice by 2-amino-9H-pyrido[2,3-*b*]indole (AαC) and 2-amino-3,8-dimethylimidazo[4,5-*f*] quinoxaline (MeIQx). *Cancer Lett.*, **111**, 105–109.
21. Miller,J.R. and Moon,R.T. (1996) Signal transduction through β-catenin and specification of cell fate during embryogenesis. *Genes Dev.*, **10**, 2527–2539.
22. Kishida,S., Yamamoto,H., Ikeda,S., Kishida,M., Sakamoto,I., Koyama,S. and Kikuchi,A. (1998) Axin, a negative regulator of the wnt signaling pathway, directly interacts with adenomatous polyposis coli and regulates the stabilization of β-catenin. *J. Biol. Chem.*, **273**, 10823–10826.
23. Dashwood,R.H., Suzui,M., Nakagama,H., Sugimura,T. and Nagao,M. (1998) High frequency of β-catenin (ctnnb1) mutations in the colon tumors induced by two heterocyclic amines in the F344 rat. *Cancer Res.*, **58**, 1127–1129.
24. Suzui,M., Ushijima,T., Dashwood,R.H., Yoshimi,N., Sugimura,T., Mori,H. and Nagao,M. (1999) Frequent mutations of the rat β-catenin gene in colon cancers induced by methylazoxymethanol acetate plus 1-hydroxyanthraquinone. *Mol Carcinogen.*, **24**, 232–237.
25. Takahashi,M., Fukuda,K., Sugimura,T. and Wakabayashi,K. (1998) β-Catenin is frequently mutated and demonstrates altered cellular location in azoxymethane-induced rat colon tumors. *Cancer Res.*, **58**, 42–46.
26. Takahashi,M., Nakatsugi,S., Sugimura,T. and Wakabayashi,K. (2000) Frequent mutations of the β-*catenin* gene in mouse colon tumors induced by azoxymethane. *Carcinogenesis*, **21**, 1117–1120.
27. Morin,P.J., Sparks,A.B., Korinek,V., Barker,N., Clevers,H., Vogelstein,B. and Kinzler,K.W. (1997) Activation of β-catenin-Tcf signaling in colon cancer by mutations in β-catenin or APC. *Science*, **275**, 1787–1790.
28. Miyoshi,Y., Nagase,H., Ando,H., Horii,A., Ichii,S., Nakatsuru,S., Aoki,T., Miki,Y., Mori,T. and Nakamura,Y. (1992) Somatic mutations of the *APC* gene in colorectal tumors: mutation cluster region in the *APC* gene. *Hum. Mol. Genet.*, **1**, 229–233.
29. Powell,S.M., Zilz,N., Beazer-Barclay,Y., Bryan,T.M., Hamilton,S.R., Thibodeau,S.N., Vogelstein,B. and Kinzler,K.W. (1992) APC mutations occur early during colorectal tumorigenesis. *Nature*, **359**, 235–237.
30. Sparks,A.B., Morin,P.J., Vogelstein,B. and Kinzler,K.W. (1998) Mutational analysis of the APC/β-catenin/Tcf pathway in colorectal cancer. *Cancer Res.*, **58**, 1130–1134.
31. Iwamoto,M., Ahnen,D.J., Franklin,W.A. and Maltzman,T.H. (2000) Expression of β-catenin and full-length APC protein in normal and neoplastic colonic tissues. *Carcinogenesis*, **21**, 1935–1940.
32. Tanaka,T., Kohno,H., Suzuki,R., Yamada,Y., Sugie,S. and Mori,H. (2003) A novel inflammation-related mouse colon carcinogenesis model induced by azoxymethane and dextran sodium sulfate. *Cancer Sci.*, **94**, 965–973.
33. Ward,J.M. (1974) Morphogenesis of chemically induced neoplasms of the colon and small intestine in rats. *Lab. Invest.*, **30**, 505–513.
34. Nakagama,H., Ochiai,M., Ubagai,T., Tajima,R., Fujiwara,K., Sugimura,T. and Nagao,M. (2002) A rat colon cancer model induced by 2-amino-1-methyl-6-phenylimidazo[4,5-*b*]pyridine, PhIP. *Mutat. Res.*, **506–507**, 137–144.
35. Tsukamoto,T., Tanaka,H., Fukami,H., Inoue,M., Takahashi,M., Wakabayashi,K. and Tatematsu,M. (2000) More frequent β-catenin gene mutations in adenomas than in aberrant crypt foci or adenocarcinomas in the large intestines of 2-amino-1-methyl-6-phenylimidazo[4,5-*b*]pyridine (PhIP)-treated rats. *Jpn. J. Cancer Res.*, **91**, 792–796.
36. Ubagai,T., Ochiai,M., Kawamori,T., Imai,H., Sugimura,T., Nagao,M. and Nakagama,H. (2002) Efficient induction of rat large intestinal tumors with a new spectrum of mutations by intermittent administration of 2-amino-1-methyl-6-phenylimidazo[4,5-*b*]pyridine in combination with a high fat diet. *Carcinogenesis*, **23**, 197–200.
37. Ochiai,M., Ushigome,M., Fujiwara,K., Ubagai,T., Kawamori,T., Sugimura,T., Nagao,M. and Nakagama,H. (2003) Characterization of dysplastic aberrant crypt foci in the rat colon induced by 2-amino-1-methyl-6-phenylimidazo[4,5-*b*]pyridine. *Am. J. Pathol.*, **163**, 1607–1614.
38. Nakagama,H., Souda,K., Ochiai,M., Ishiguro,Y., Sugimura,T. and Nagao,M. (1999) Genetic analysis of the susceptibility in rats to aberrant crypt foci formation by 2-amino-1-methyl-6-phenylimidazo [4,5-*b*]pyridine, PhIP. *Cancer Lett.*, **143**, 205–209.
39. Nagaoka,H., Wakabayashi,K., Kim,S.B., Kim,I.S., Tanaka,Y., Ochiai,M., Tada,A., Nukaya,H., Sugimura,T. and Nagao,M. (1992) Adduct formation at C-8 of guanine on *in vitro* reaction of the ultimate form of 2-amino-1-methyl-6-phenylimidazo[4,5-*b*]pyridine with 2′-deoxyguanosine and its phosphate esters. *Jpn. J. Cancer Res.*, **83**, 1025–1029.
40. Koesters,R., Hans,M., Benner,A., Prosst,R., Boehm,J., Gahlen,J. and Doeberitz,M.K. (2001) Predominant mutation of codon 41 of the β-catenin proto-oncogene in rat colon tumors induced by 1,2-dimethylhydrazine using a complete carcinogenic protocol. *Carcinogenesis*, **22**, 1885–1890.
41. Takahashi,M., Mutoh,M., Kawamori,T., Sugimura,T. and Wakabayashi,K. (2000) Altered expression of β-catenin, inducible nitric oxide synthase and cyclooxygenase-2 in azoxymethane-induced rat colon carcinogenesis. *Carcinogenesis*, **21**, 1319–1327.
42. Prescott,S.M. and White,R.L. (1996) Self-promotion? Intimate connections between APC and prostaglandin H synthase-2. *Cell*, **87**, 783–786.
43. Howe,L.R., Subbaramaiah,K., Chung,W.J., Dannenberg,A.J. and Brown,A.M. (1999) Transcriptional activation of *cyclooxygenase-2* in Wnt-1-transformed mouse mammary epithelial cells. *Cancer Res.*, **59**, 1572–1577.
44. Mei,J.M., Hord,N.G., Winterstein,D.F., Donald,S.P. and Phang,J.M. (1999) Differential expression of prostaglandin endoperoxide H synthase-2 and formation of activated β-catenin-LEF-1 transcription complex in mouse colonic epithelial cells contrasting in *Apc*. *Carcinogenesis*, **20**, 737–740.
45. Tetsu,O. and McCormick,F. (1999) β-Catenin regulates expression of cyclin D1 in colon carcinoma cells. *Nature*, **398**, 422–426.
46. He,T.C., Sparks,A.B., Rago,C., Hermeking,H., Zawel,L., da Costa,L.T., Morin,P.J., Vogelstein,B. and Kinzler,K.W. (1998) Identification of c-MYC as a target of the APC pathway. *Science*, **281**, 1509–1512.
47. Tanaka,T., Kohno,H., Shimada,R., Kagami,S., Yamaguchi,F., Kataoka,S., Ariga,T., Murakami,A., Koshimizu,K. and Ohigashi,H. (2000) Prevention of colonic aberrant crypt foci by dietary feeding of garcinol in male F344 rats. *Carcinogenesis*, **21**, 1183–1189.
48. Rao,C.V., Indranie,C., Simi,B., Manning,P.T., Connor,J.R. and Reddy,B.S. (2002) Chemopreventive properties of a selective inducible nitric oxide synthase inhibitor in colon carcinogenesis, administered alone or in combination with celecoxib, a selective cyclooxygenase-2 inhibitor. *Cancer Res.*, **62**, 165–170.
49. Lala,P.K. and Chakraborty,C. (2001) Role of nitric oxide in carcinogenesis and tumour progression. *Lancet Oncol.*, **2**, 149–156.
50. Seril,D.N., Liao,J., Ho,K.L., Yang,C.S. and Yang,G.Y. (2002) Inhibition of chronic ulcerative colitis-associated colorectal adenocarcinoma development in a murine model by *N*-acetylcysteine. *Carcinogenesis*, **23**, 993–1001.
51. Mabley,J.G., Liaudet,L., Pacher,P., Southan,G.J., Salzman,A.L. and Szabo,C. (2002) Part II: beneficial effects of the peroxynitrite decomposition catalyst FP15 in murine models of arthritis and colitis. *Mol. Med.*, **8**, 581–590.
52. Suzuki,R., Kohno,H., Sugie,S. and Tanaka,T. (2004) Sequential observations on the occurrence of preneoplastic and neoplastic lesions in the mouse colon treated with azoxymethane and dextran sodium sulfate. *Cancer Sci.*, **95**, 721–727.
53. Ohshima,H. and Bartsch,H. (1994) Chronic infections and inflammatory processes as cancer risk factors: possible role of nitric oxide in carcinogenesis. *Mutat Res.*, **305**, 253–264.

Received July 21, 2004; revised September 15, 2004; accepted September 17, 2004

Sequential observations on the occurrence of preneoplastic and neoplastic lesions in mouse colon treated with azoxymethane and dextran sodium sulfate

Rikako Suzuki,[1,2] Hiroyuki Kohno,[2] Shigeyuki Sugie[2] and Takuji Tanaka[2,3]

[1]Research Fellow of the Japan Society for the Promotion of Science, 6 Ichiban-cho, Chiyoda-ku, Tokyo 102-8471; and [2]Department of Oncologic Pathology, Kanazawa Medical University, 1-1 Daigaku, Uchinada, Ishikawa 920-0293

(Received June 24, 2004/Revised July 26, 2004/Accepted August 2, 2004)

Previously, we proposed a novel mouse model for colitis-related colon carcinogenesis using azoxymethane (AOM) and dextran sodium sulfate (DSS) (*Cancer Sci* 2003; 94: 965–73). In the current study, sequential analysis of pathological alterations during carcinogenesis in our model was conducted to establish the influence of inflammation caused by DSS on colon carcinogenesis in this model. Male ICR mice were given a single intraperitoneal injection of AOM (10 mg/kg body weight) and given 2% (w/v) DSS in the drinking water for 7 days, starting 1 week after the AOM injection. They were sequentially sacrificed at weeks 2, 3, 4, 5, 6, 9, 12, and 14 for histopathological and immunohistochemical examinations. Colonic adenomas were found in 2 (40% incidence and 0.40±0.49 multiplicity) of 5 mice at week 3 and colon carcinomas developed in 2 (40% incidence and 2.00±3.52 multiplicity) of 5 mice at week 4. Their incidence gradually increased with time and reached 100% (6.20±2.48 multiplicity) at week 6. At week 14, the multiplicity of adenocarcinoma was 9.75±2.49 (100% incidence). In addition, colonic dysplasia was noted at all time-points. The scores of colonic inflammation and nitrotyrosine immunohistochemistry were extremely high at early time-points and were well correlated. Our results suggest that combined treatment of mice with AOM and DSS generates neoplasms in the colonic mucosa via dysplastic lesions induced by nitrosative stress. (Cancer Sci 2004; 95: 721–727)

In the developed countries, colorectal cancer (CRC) is one of the commonest non-smoking related causes of cancer deaths. Remarkable differences in the incidence worldwide have led to the hypothesis that this variation could be explained largely by environmental influences.[1)]

The occurrence of inflammatory bowel disease (IBD), including ulcerative colitis (UC) and Crohn's disease (CD), is affected by several factors, including race and geography.[2,3)] Life style, particularly intake of high amount of animal fat, is involved in the occurrence of IBD.[4)] Over recent decades the incidence of IBD has been rising throughout the world, including Japan, as it has been in the last 50 years in Europe and North America.[5)] This increase may be caused by increased intake of animal fat.[6)] CRC is one of the most serious complications of IBD, especially UC and CD. The risk of CRC becomes greater with increasing extent and duration of the disease. A recent meta-analysis has estimated the incidence rate at 7 per 1000 person-years duration and 12 per 1000 persons per year duration in the second and third decades of UC, respectively.[7)] The risk for CRC development in CD patients is also high.[8)] The highest risk of CRC in CD patients was reported to be 26.6 (standardized incidence ratio), although the estimate applied only to patients younger than 21 years of age.[9)] Gillen *et al.*[10)] compared the CRC risk in patients with UC and CD and found an 18-fold increase in the risk of developing CRC in extensive CD and a 19-fold increase in risk in extensive UC when compared with the general population.

The pathogenesis of IBD-related CRC is still unclear, although there have been various attempts to investigate the pathogenesis using animal models. In earlier animal models for investigating the pathogenesis of UC, carageenan was used,[11)] but dextran sodium sulfate (DSS) has been the most widely used chemical to induce colitis.[12)] Also, this DSS animal model is available for examining IBD-related CRC. Intestinal tumors in rats fed 5% DSS in the diet developed between 134 and 215 days.[13)] Colorectal carcinomas developed in rats fed DSS for as long as 6 months.[14)] Recently, Cooper *et al.*[15)] reported a relationship between the severity of DSS-induced inflammation and colorectal carcinogenesis which is similar to that of human UC-associated dysplasia and cancer regarding histopathology. However, these studies basically need a long experimental period or repeated administration of DSS.[14–16)] In addition, our previous study demonstrated that treatment with the non-genotoxic carcinogen DSS enhances the development of putative precursor lesions (aberrant crypt foci) for colonic adenocarcinoma in rats.[17)]

In the first report of our experimental studies of inflammation-related carcinogenesis in mouse colon, we proposed a novel mouse model, using azoxymethane (AOM) and DSS.[18)] In our model, exposure to a single dose of AOM followed by 1-week treatment with 2% DSS could induce a number of colonic epithelial malignancies within 20 weeks. Moreover, the first colonic adenocarcinoma was found as early as 12 weeks.[18)] However, time-course analysis of pathological alterations was not performed. Therefore, in the present study, we investigated the time-course of alterations of colonic morphology in male ICR mice treated with AOM followed by DSS, in order to understand the effects of DSS-induced inflammation on colon carcinogenesis in this model. Since inducible nitric oxide synthase (iNOS) is expressed in inflamed colonic mucosa and is associated with the production of peroxynitrite and nitration of cellular protein in the colon in human IBD[19,20)] and chemically induced colitis of rodents,[21)] we also immunohistochemically assessed the expression of nitrotyrosine, which is a specific marker of nitrosative stress,[22)] in the colon.

Materials and Methods

Animals, chemicals, and diets. In this study, 5-week-old male

[3]To whom correspondence should be addressed.
E-mail: takutt@kanazawa-med.ac.jp

Abbreviations: AOM, azoxymethane; DSS, dextran sodium sulfate; CRC, colorectal cancer; IBD, inflammatory bowel disease; UC, ulcerative colitis; CD, Crohn's disease; iNOS, inducible nitric oxide synthase; i.p., intraperitoneal; NO, nitric oxide; COX, cyclooxygenase.

Crj:CD-1 (ICR) mice (Charles River Japan, Inc., Tokyo) were used. They were acclimated for 1 week with tap water and a pelleted basal diet, CRF-1 (Oriental Yeast Co., Ltd., Tokyo) *ad libitum*, before the start of the experimentation. Mice were then randomized by body weight into 8 groups. They were maintained at Kanazawa Medical University Animal Facility according to the Institutional Animal Care Guidelines, and were housed under controlled conditions of humidity (50±10%), light (12/12 h light/dark cycle), and temperature (23±2°C). A colonic carcinogen AOM was purchased from Sigma Chemical Co. (St. Louis, MO). DSS with a molecular weight of 40,000 was purchased from ICN Biochemicals, Inc. (Aurora, OH).

Experimental procedure. All mice received a single intraperitoneal (i.p.) injection of AOM at a dose level of 10 mg/kg body weight. Starting 1 week after the AOM injection, animals were exposed to 2% DSS in the drinking water for 7 days. They were then sacrificed by ether overdose at weeks 2, 3, 4, 5, 6, 9, 12, and 14 (Fig. 1). At autopsy, their large bowel was flushed with saline, and excised. The large bowel (from the ileocecal junction to the anal verge) was measured, cut open longitudinally along the main axis, and then washed with saline. After macroscopic inspection, it was cut, and fixed in 10% buffered formalin for at least 24 h. Paraffin-embedded sections were made by routine procedures.

Histopathological analysis. The histopathological alterations in the colon were examined on hematoxylin and eosin-stained sections. Colitis with or without ulceration was scored on hematoxylin and eosin-stained sections, according to the following morphological criteria described by Cooper *et al.*[23]: grade 0, normal colonic mucosa (Fig. 2a); grade 1, shortening and loss of the basal one-third of the actual crypts with mild inflammation and edema in the mucosa (Fig. 2b): grade 2, loss of the basal two-thirds of the crypts with moderate inflammation in the mucosa (Fig. 2c); grade 3, loss of the entire crypts with severe inflammation in the mucosa, but with retention of the surface epithelium (Fig. 2d); and grade 4, loss of the entire crypts and surface epithelium with severe inflammation in the mucosa, muscularis propria, and submucosa (Fig. 2e). High- or low-grade dysplasia of colonic mucosa (Fig. 3) was diagnosed according to the criteria described by Riddell *et al.*[24] and Pascal.[25] Colonic neoplasms were diagnosed according to the description by Ward.[26]

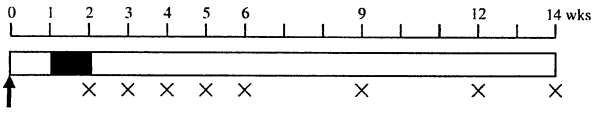


Fig. 1. Experimental protocol. □, basal diet and tap water; ■, 2% DSS; ↑, AOM, 10 mg/kg b.w., i.p.; ×, sacrifice.

Immunohistochemistry of nitrotyrosine. Immunohistochemistry of nitrotyrosine was used to evaluate tyrosine nitration, a marker of nitrosative damage in the colon. Paraffin embedded sections (4 μm) of the distal colon (1 cm from the anus) were deparaffinized, treated with 0.3% hydrogen peroxide for 15 min to block endogenous peroxidase activity, and then rinsed briefly in PBS. Non-specific binding was blocked by incubating the slides with a blocking solution (0.1 *M* PBS containing 0.1% Triton X-100 and 2% normal goat serum) for 2 h. Sections were incubated overnight with a primary rabbit polyclonal anti-nitrotyrosine (diluted 1:500, Upstate Biotechnology, Lake Placid, NY) or with control solution. Control sections included buffer alone or non-specific purified rabbit secondary antibody and the avidin-biotin-peroxidase complex (Vectastain Elite ABC kit, Vector Laboratories, Burlingame, CA). Reaction products were developed by immersing the sections in 3,3′-di-

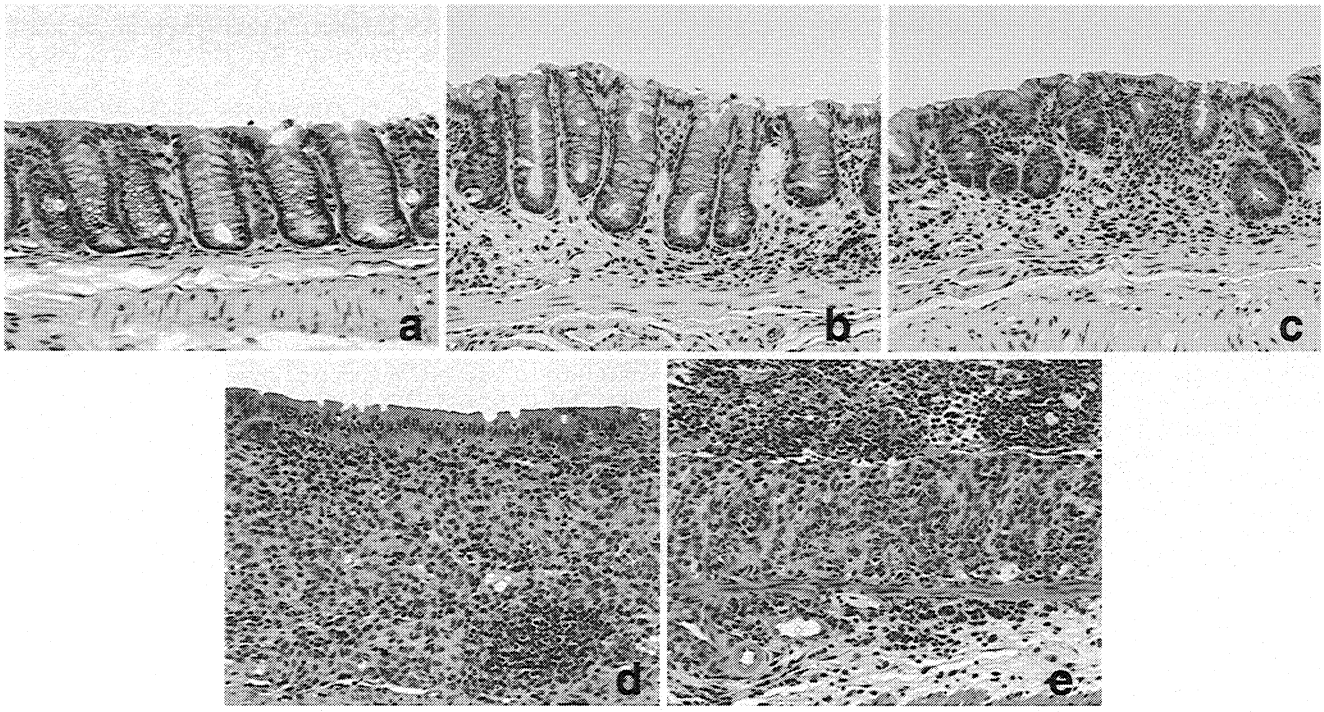


Fig. 2. Histology and various grades of colitis: (a) normal colonic mucosa (grade 0); (b) shortening of the basal one-third of the crypts with slight inflammation and edema in the lamina propria (grade 1); (c) loss of the basal two-thirds of the crypts with moderate inflammation in the lamina propria (grade 2); (d) loss of the entire crypts with severe inflammation in the lamina propria, but with retention of the surface epithelium (grade 3); and (e) loss of the entire crypts and surface epithelium with severe inflammation in the mucosa, muscularis propria, and submucosa. The exudates containing cell debris, inflammatory cells, fibrin, and mucus covers the damaged mucosa (grade 4). Hematoxylin and eosin stain. Original magnifications, ×20.

aminobenzidine 4HCl solution (Sigma Chemical Co.) containing 0.1% hydrogen peroxide. To quantitate the degree of nitrotyrosine stainability, a grading system (grades 0–4) was used: grade 0, no immunoreactivity; grades 1–3, increasing degrees of intermediate immunoreactivity; and grade 4, extensive immunoreactivity.[21]

Statistical analysis. All measurements were compared by the use of Student's *t* test or Welch's *t* test for paired samples.

Results

General observations. A few mice had bloody stools at week 2, but no such clinical symptoms were observed thereafter. At week 8, anal prolapse due to tumor development in the distal colon was noted in a few mice. Mean body and liver weights and mean lengths of large bowel at different time-points are shown in Table 1. No remarkable changes of mean body and liver weights were observed after week 4 or 5. No significant changes in the lengths of large bowel were noted after week 4. At week 14, the mean body weight, liver weight, and length of colon of untreated mice was 41.0±3.4 g, 2.78±0.26 g, and 13.1±0.9 cm, respectively (data was not shown in Table 1). The mean liver weight (2.27±0.37) of mice given 2% DSS at week 14 was significantly lower than that of untreated mice ($P<0.05$).

Colitis and colonic dysplasia. Colitis in the current study was present with or without colonic dysplasia in the middle or distal colon (Fig. 4a). As shown in Fig. 5a, the inflammation score was the highest (3.80±0.45) at week 2, and then gradually decreased during the study. The scores at weeks 2, 3 (3.40±0.55), 4 (3.20±0.45), 5 (3.20±0.84), and 6 (2.80±0.84) were much greater than that at week 14 (1.50±0.58). Mucosal ulceration was found at week 2, soon after the cessation of DSS exposure (Ul-I, 100% incidence with a multiplicity of 8.20±1.94; and Ul-II, 80% incidence with a multiplicity of 1.80±2.14). After this time-point, the incidence of mucosal ulceration was decreased with time, accompanied with regeneration, and there was a 25% incidence of Ul-I (0.25±0.43 multiplicity) at week 14. Ul-II ulcer was not found in the colon after week 6. Colonic dysplasia was also present at week 2 (Table 2). During the ex-

Table 1. Body and liver weights and lengths of colon

Wks	No. of mice examined	Body wt (g)	Liver wt (g)	Length of large bowel (cm)
2	5	23.8±2.2	1.41±0.13	6.7±0.4
3	5	28.6±2.2	2.10±0.80	8.7±1.2
4	5	36.4±3.0	2.50±0.40	10.7±1.1
5	5	39.8±2.2	3.10±0.70	11.2±0.6
6	5	39.6±1.9	2.78±0.40	11.2±0.6
9	5	40.3±1.9	2.65±0.30	11.6±0.6
12	5	40.1±1.6	2.98±0.10	11.1±0.4
14	4	39.7±1.0	2.27±0.37	11.8±1.0

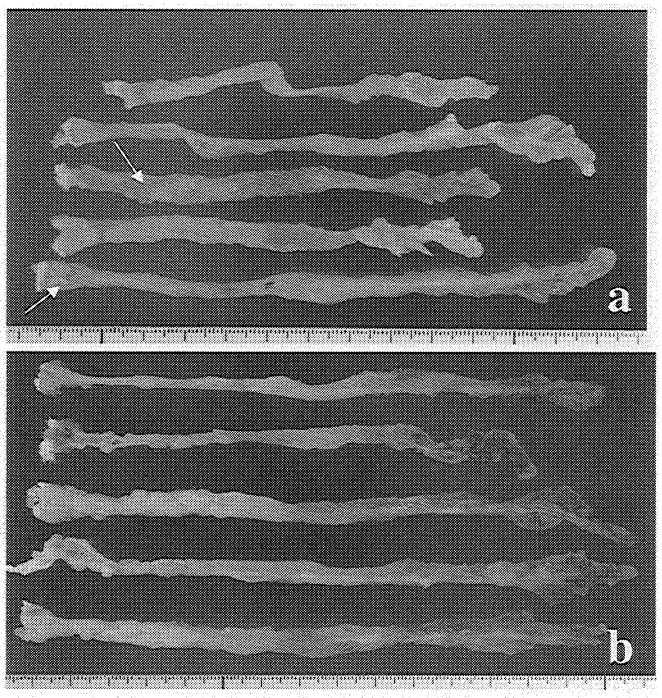


Fig. 4. Macroscopic view of the colon of mice treated with 2% DSS. (a) A small nodular tumor (arrow) is seen in the distal colon of 2 mice at week 3. (b) Nodular, polypoid, or caterpillar-like tumors are found in the distal and/or middle colon of all mice at week 12.

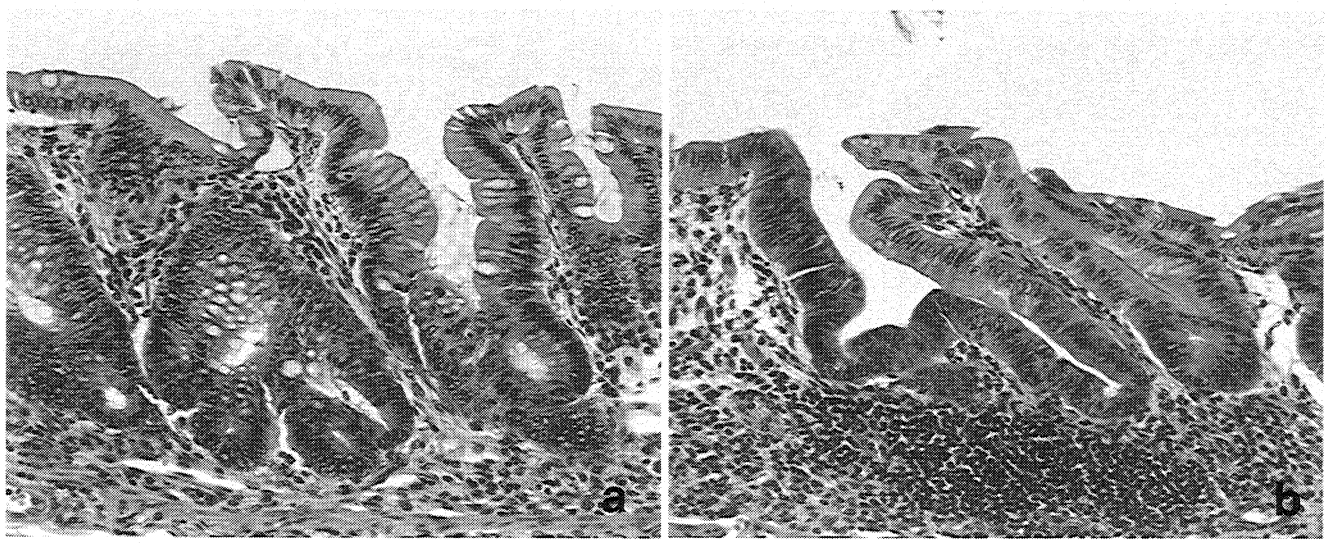


Fig. 3. Histopathology of colonic dysplasia. (a) Low-grade dysplasia, mild dysplastic changes with decreased goblet cells extend to the surface epithelium; and (b) high-grade dysplasia, a greater degree of cytologic atypia is evident. The nuclei are enlarged and have irregular contours. There is also a loss of normal polarity. Hematoxylin and eosin stain. Original magnifications, ×20.

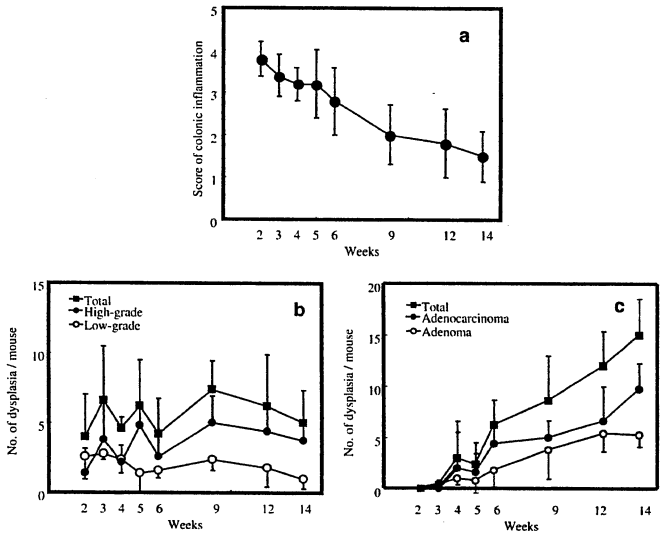


Fig. 5. (a) Colonic inflammation score at each time-point, (b) multiplicity of colonic dysplasia at each time-point, (c) multiplicity of colonic neoplasms at each time-point.

periment, the incidence of high-grade dysplasia gradually increased with time: 40% at week 2 and 100% at weeks 4–14. The multiplicity of high-grade dysplasia was 1.40±1.74/mouse at week 2 and thereafter the value slightly increased (Fig. 5b). However, the multiplicity of low-grade dysplasia decreased with time.

Incidence and multiplicity of large bowel neoplasms. Macroscopically, flat, nodular, polypoid, or caterpillar-like colonic tumors (Fig. 4b) were found in the middle and distal colon of mice. Table 3 summarizes the incidence of large bowel neoplasms at each time-point. Fig. 5c illustrates the multiplicity of colonic neoplasms at each time-point. At week 2, no colonic neoplasms developed. At week 3, colonic tubular adenoma (Fig. 6a) developed in 2 of 5 mice (40% incidence with a multiplicity of 0.40±0.49). As for colonic adenocarcinoma (Fig. 6b), the incidence and multiplicity were 40% and 2.00±3.52 at week 4, and 60% and 1.60±1.85 at week 5. Thereafter, the incidence of colonic adenocarcinoma was 100% and the multiplicity was increased. As shown in Table 4, all adenocarcinomas were

Table 2. Incidence of dysplasia in the colon

Wks	No. of mice examined	Incidence of dysplasia (%)		
		Total	Low-grade	High-grade
2	5	80	80	40
3	5	100	100	80
4	5	100	100	100
5	5	100	80	100
6	5	100	100	100
9	5	100	100	100
12	5	100	80	100
14	4	100	75	100

Table 3. Incidence of colonic neoplasms

Wks	No. of mice examined	Incidence of colonic neoplasms (%)		
		Total	Adenoma	Adenocarcinoma
2	5	0	0	0
3	5	40	40	0
4	5	80	80	40
5	5	80	40	60
6	5	100	80	100
9	5	100	100	100
12	5	100	100	100
14	4	100	100	100

located in colonic mucosa, at weeks 4 and 5, but the number of adenocarcinomas infiltrating into submucosa and muscularis propria was increased after week 6.

Nitrotyrosine immunohistochemistry. Immunoreactivity of nitrotyrosine was noted in the cryptal cells with or without disruption, infiltrated mononuclear inflammatory cells, and endothelial cells of the small vessels in the mucosa and submucosa. Stainability was strong in the infiltrated mononuclear inflammatory cells (Fig. 7, a and b). Adenocarcinoma cells also showed weakly or moderately positive immunoreactivity of nitrotyrosine (Fig. 7b). As shown in Fig. 8, scoring of the immunoreactivity revealed that the highest score of nitrotyrosine was at week 2 (7.32±1.35) and the scores at weeks 2, 3 (5.22±0.40), and 4 (5.40±1.32) were much higher than that at week 14 (2.75±0.25).

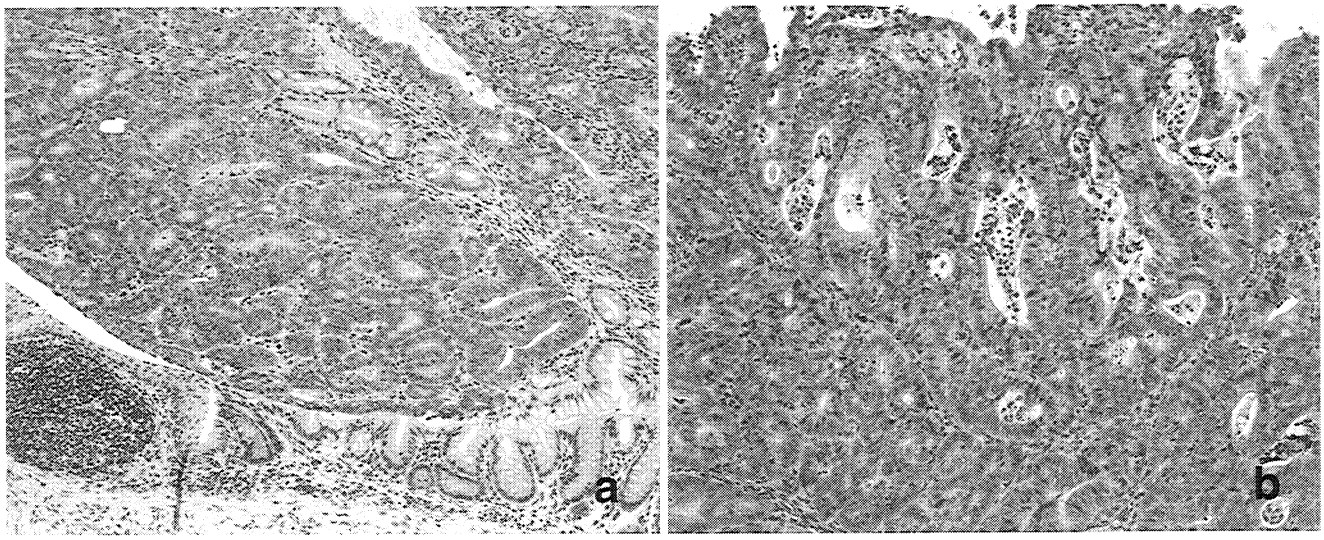


Fig. 6. Histopathology of (a) tubular adenoma and (b) adenocarcinoma. Hematoxylin and eosin stain. Original magnifications, (a) ×10 and (b) ×20.

Table 4. Invasiveness of colonic adenocarcinomas

Wks	Total no. of colonic adenocarcinoma (no. of mice with adenocarcinoma)	Depth of invasion			
		Mucosa	Submucosa	Muscularis propria	Serosa
2	0 (0/5)	0	0	0	0
3	0 (0/5)	0	0	0	0
4	10 (2/5)	10 (100%)	0	0	0
5	8 (3/5)	8 (100%)	0	0	0
6	22 (5/5)	21 (95%)	1 (5%)	0	0
9	25 (5/5)	23 (92%)	2 (8%)	0	0
12	33 (5/5)	27 (82%)	5 (15%)	1 (3%)	0
14	39 (4/4)	32 (82%)	6 (15%)	1 (3%)	0

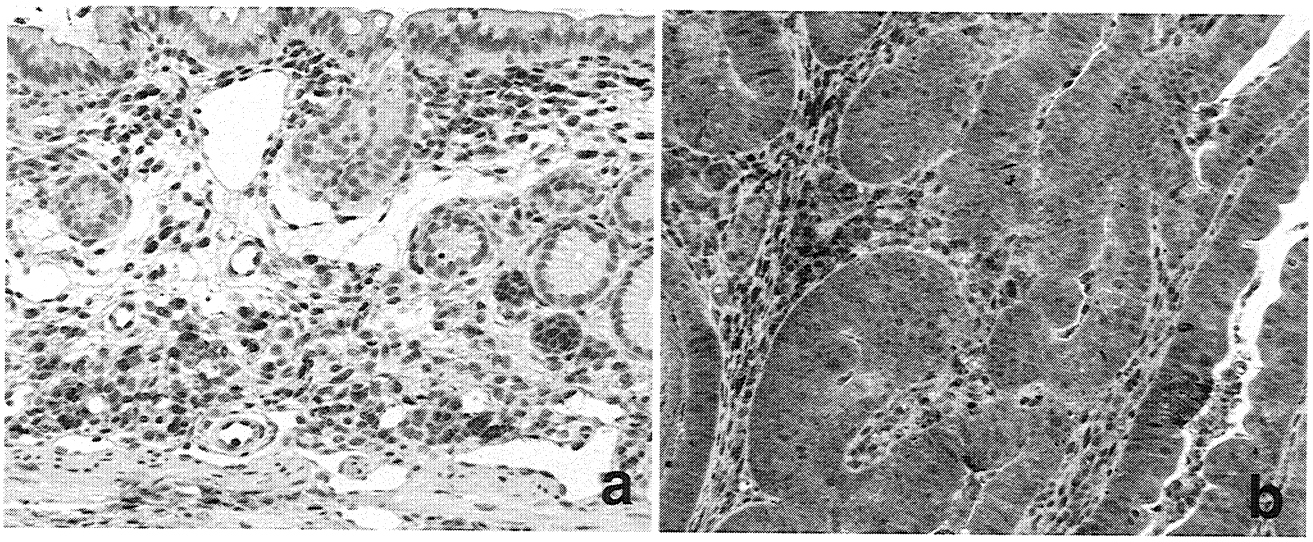


Fig. 7. Immunohistochemistry of nitrotyrosine. (a) Strongly positive immunoreactivity of nitrotyrosine in inflammatory cells (mostly macrophages) infiltrated in the lamina propria and (b) moderate immunoreactivity of nitrotyrosine in adenocarcinoma cells with surrounding macrophages showing strong immunoreactivity of nitrotyrosine. Original magnifications, ×20.

Discussion

In the current study, treatment with a single dose of genotoxic colonic carcinogen AOM (10 mg/kg body weight, i.p. injection) followed by 1-week oral exposure to a non-genotoxic carcinogen DSS (2% in drinking water) could induce colonic adenoma within 3 weeks after the start of the experiment. Colonic adenocarcinoma also developed as early as 4 weeks. These findings support our earlier work[18] demonstrating a powerful tumor-promoting activity of DSS, which has colitis-inducing ability in the mouse colon.

In the current study, DSS induced colitis in the middle and distal parts of the colon, as reported by others.[23,27] Besides these inflammatory changes, low- or high-grade dysplasia was present at all time-points and colonic neoplasms were observed even at week 3 or 4 in the current study. Severe colitis with ulceration soon after the end of 2% DSS exposure in this study might be caused by a direct cytotoxic effect of DSS.[28] Kitajima *et al.* demonstrated the presence of macrophages phagocyting DSS in the middle and distal colon of mice the day after the oral administration of 5% DSS,[29] suggesting that DSS could be absorbed in the colonic mucosa and act as a tumor-promoter in the colon initiated with a low dose of AOM.

Inflammatory damage in UC is associated with increased production of nitric oxide (NO) through the iNOS pathway.[30] In accordance with this report, a good biomarker for "nitrating species," nitrotyrosine,[31] showed a high immunohistochemical reaction score for 2 weeks (from week 2 to week 4), beginning soon after the cessation of DSS exposure, in this study. Also, changes of inflammation score with or without ulceration paralleled the nitrotyrosine-immunohistochemical score during the study. High scores of these parameters were noted at the earlier time-points, and then both scores decreased with time: the scores for nitrotyrosine positivity and inflammation reached a

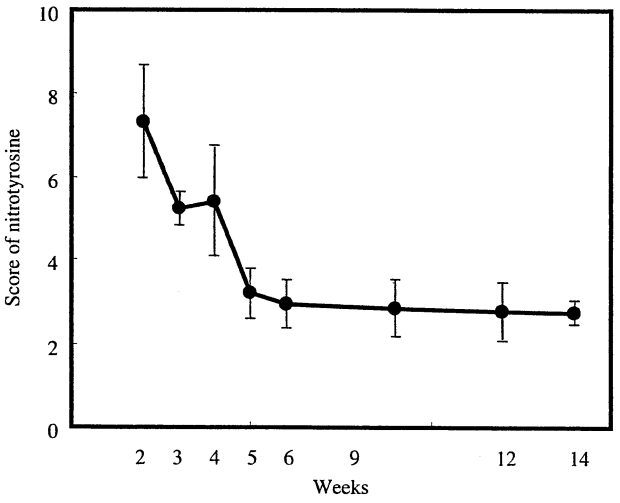


Fig. 8. Score of nitrotyrosine immunoreactivity at each time-point.

plateau after week 5 and week 9, respectively. iNOS is reported to be over-expressed in colonic tumors of humans.[32] In our previous investigation[18] with this model, immunohistochemical expression of iNOS and cyclooxygenase (COX)-2 was found in colonic adenocarcinomas. In this study, colonic adenocarcinoma was noted as early as at 4 weeks, when nitrotyrosine immunoreactivity was still high. This supports our previous report showing a powerful tumor-promoting effect of DSS in this model.[18] Although we did not investigate the immunohistochemical expression of COX-2 or iNOS in this study, we observed the positive reaction of both enzymes in colonic neoplasms as well as their surrounding inflammatory cells in this model.[18] We consider that these enzymes are involved in colitis-related colon carcinogenesis.[18] In fact, increased expression of iNOS and COX-2 was reported in colonic epithelial malignancy and pre-malignancy induced by chemical carcinogen,[33,34] and also in human colonic neoplasms.[32,35] Moreover, increases in the amounts of their reaction products, NO and prostaglandin E_2, might contribute to the development of colonic neoplasms, since specific inhibitors of both enzymes can inhibit colon carcinogenesis in this model (manuscript in preparation).

Oxidative stress accompanied with inflammation contributes to neoplastic transformation.[36] IBD is considered one of the major "oxyradical overload" diseases, whereby chronic inflammation results in a cancer-prone phenotype.[37] Oxidative stress with its associated cellular damage is thought to play a key role in the pathogenesis of the colitis itself,[38] as well as in rat colon carcinogenesis.[39] Indeed, measures of oxidative stress, including 8-oxoguanine and 4-hydroxy-2-nonenal-modified proteins, were increased in colonic mucosa of IBD patients[40–42] and inflamed colonic tissue of rodents treated with DSS.[43,44] An ongoing study in our laboratory will clarify the contribution of oxidative stress to colon carcinogenesis in our model.

In conclusion, the results in the current study demonstrated that a single dose of AOM followed by 2% DSS produced colonic adenocarcinoma within 4 weeks and resulted in 100% incidence at week 6. Our findings might suggest that genotoxic damage caused by AOM and subsequent severe inflammation induced by DSS result in a high incidence of colonic epithelial malignancy.

We are indebted to Ms. S. Yamamoto for her excellent technical assistance and staff of the Research Animal Facility of Kanazawa Medical University for care of the animals. This study was supported in part by a Grant-in-Aid for the 3rd Term Comprehensive 10-Year Strategy for Cancer Control from the Ministry of Health, Labour and Welfare, Japan; by a Grant-in-Aid (nos. 15592007 and 15·2052) from the Ministry of Education, Culture, Sports, Science and Technology, Japan: and by grants (H2004-6 and C2004-4) from Kanazawa Medical University.

1. Potter JD. Risk factors for colon neoplasia—epidemiology and biology. *Eur J Cancer* 1995; **31**:1033–8.
2. Grossman A, Fireman Z, Lilos P, Novis B, Rozen P, Gilat T. Epidemiology of ulcerative colitis in the Jewish population of central Israel 1970–1980. *Hepatogastroenterology* 1989; **36**: 193–7.
3. Sonnenberg A, McCarty DJ, Jacobsen SJ. Geographic variation of inflammatory bowel disease within the United States. *Gastroenterology* 1991; **100**: 143–9.
4. Reif S, Klein I, Lubin F, Farbstein M, Hallak A, Gilat T. Pre-illness dietary factors in inflammatory bowel disease. *Gut* 1997; **40**: 754–60.
5. Rampton DS, Phil D. New treatments for inflammatory bowel disease. *World J Gastroenterol* 1998; **4**: 369–76.
6. Fujimoto K. IBD and feeding behavior. *Pathol Clin Med* 2002; **20**: 1226–30 (in Japanese).
7. Eaden JA, Abrams KR, Mayberry JF. The risk of colorectal cancer in ulcerative colitis: a meta-analysis. *Gut* 2001; **48**: 526–35.
8. van Hogezand RA, Eichhorn RF, Choudry A, Veenendaal RA, Lamers CB. Malignancies in inflammatory bowel disease: fact or fiction? *Scand J Gastroenterol Suppl* 2002; **236**: 48–53.
9. Weedon DD, Shorter RG, Ilstrup DM, Huizenga KA, Taylor WF. Crohn's disease and cancer. *N Engl J Med* 1973; **289**: 1099–103.
10. Gillen CD, Walmsley RS, Prior P, Adndrews HA, Allan RN. Ulcerative colitis and Crohn's disease: a comparison of the colorectal cancer risk in extensive colitis. *Gut* 1994; **35**: 1590–2.
11. Marcus R, Watt J. Colonic ulceration in young rats fed degraded carrageenan. *Lancet* 1971; **ii**: 765–6.
12. Seril DN, Liao J, Yang GY, Yang CS. Oxidative stress and ulcerative colitis-associated carcinogenesis: studies in humans and animal models. *Carcinogenesis* 2003; **24**: 353–62.
13. Hirono I, Kuhara K, Hosaka S, Tomizawa S, Golberg L. Induction of intestinal tumors in rats by dextran sulfate sodium. *J Natl Cancer Inst* 1981; **66**: 579–83.
14. Tamaru T, Kobayashi H, Kishimoto S, Kajiyama G, Shimamoto F, Brown WR. Histochemical study of colonic cancer in experimental colitis of rats. *Dig Dis Sci* 1993; **38**: 529–37.
15. Cooper HS, Murthy S, Kido K, Yoshitake H, Flanigan A. Dysplasia and cancer in the dextran sulfate sodium mouse colitis model. Relevance to colitis-associated neoplasia in the human: a study of histopathology, β-catenin and p53 expression and the role of inflammation. *Carcinogenesis* 2000; **21**: 757–68.
16. Yamada M, Ohkusa T, Okayasu I. Occurrence of dysplasia and adenocarcinoma after experimental chronic ulcerative colitis in hamsters induced by dextran sulphate sodium. *Gut* 1992; **33**: 1521–7.
17. Tanaka T, Kohno H, Yoshitani S, Takashima S, Okumura A, Murakami A, Hosokawa M. Ligands for peroxisome proliferator-activated receptors α and γ inhibit chemically induced colitis and formation of aberrant crypt foci in rats. *Cancer Res* 2001; **61**: 2424–8.
18. Tanaka T, Kohno H, Suzuki R, Yamada Y, Sugie S, Mori H. A novel inflammation-related mouse colon carcinogenesis model induced by azoxymethane and dextran sodium sulfate. *Cancer Sci* 2003; **94**: 965–73.
19. Singer II, Kawka DW, Scott S, Weidner JR, Mumford RA, Riehl TE, Stenson WF. Expression of inducible nitric oxide synthase and nitrotyrosine in colonic epithelium in inflammatory bowel disease. *Gastroenterology* 1996; **111**: 871–85.
20. Kimura H, Hokari R, Miura S, Shigematsu T, Hirokawa M, Akiba Y, Kurose I, Higuchi H, Fujimori H, Tsuzuki Y, Serizawa H, Ishii H. Increased expression of an inducible isoform of nitric oxide synthase and the formation of peroxynitrite in colonic mucosa of patients with active ulcerative colitis. *Gut* 1998; **42**: 180–7.
21. Zingarelli B, Szabo C, Salzman AL. Reduced oxidative and nitrosative damage in murine experimental colitis in the absence of inducible nitric oxide synthase. *Gut* 1999; **45**: 199–209.
22. Beckman JS. Oxidative damage and tyrosine nitration from peroxynitrite. *Chem Res Toxicol* 1996; **9**: 836–44.
23. Cooper HS, Murthy SN, Shah RS, Sedergran DJ. Clinicopathologic study of dextran sulfate sodium experimental murine colitis. *Lab Invest* 1993; **69**: 238–49.
24. Riddell RH, Goldman H, Ransohoff DF, Appelman HD, Fenoglio CM, Haggitt RC, Ahren C, Correa P, Hamilton SR, Morson BC. Dysplasia in inflammatory bowel disease: standardized classification with provisional clinical applications. *Hum Pathol* 1983; **14**: 931–68.
25. Pascal RR. Dysplasia and early carcinoma in inflammatory bowel disease and colorectal adenomas. *Hum Pathol* 1994; **25**: 1160–71.
26. Ward JM. Morphogenesis of chemically induced neoplasms of the colon and small intestine in rats. *Lab Invest* 1974; **30**: 505–13.
27. Okayasu I, Hatakeyama S, Yamada M, Ohkusa T, Inagaki Y, Nakaya R. A novel method in the induction of reliable experimental acute and chronic ulcerative colitis in mice. *Gastroenterology* 1990; **98**: 694–702.
28. Ni J, Chen SF, Hollander D. Effects of dextran sulphate sodium on intestinal epithelial cells and intestinal lymphocytes. *Gut* 1996; **39**: 234–41.
29. Kitajima S, Takuma S, Morimoto M. Tissue distribution of dextran sulfate sodium (DSS) in the acute phase of murine DSS-induced colitis. *J Vet Med Sci* 1999; **61**: 67–70.
30. Kankuri E, Hamalainen M, Hukkanen M, Salmenpera P, Kivilaakso E, Vapaatalo H, Moilanen E. Suppression of pro-inflammatory cytokine release by selective inhibition of inducible nitric oxide synthase in mucosal explants from patients with ulcerative colitis. *Scand J Gastroenterol* 2003; **38**: 186–92.
31. Halliwell B. What nitrates tyrosine? Is nitrotyrosine specific as a biomarker of peroxynitrite formation *in vivo*? *FEBS Lett* 1997; **411**: 157–60.
32. Ambs S, Merriam WG, Bennett WP, Felley-Bosco E, Ogunfusika MO, Oser SM, Klein S, Shields PG, Billiar TR, Harris CC. Frequent nitric oxide synthase-2 expression in human colon adenomas: implication for tumor angiogenesis and colon cancer progression. *Cancer Res* 1998; **58**: 334–41.
33. Takahashi M, Mutoh M, Kawamori T, Sugimura T, Wakabayashi K. Altered expression of β-catenin, inducible nitric oxide synthase and cyclooxygenase-

2 in azoxymethane-induced rat colon carcinogenesis. *Carcinogenesis* 2000; **21**: 1319–27.
34. Yamada Y, Yoshimi N, Hirose Y, Matsunaga K, Katayama M, Sakata K, Shimizu M, Kuno T, Mori H. Sequential analysis of morphological and biological properties of β-catenin-accumulated crypts, provable premalignant lesions independent of aberrant crypt foci in rat colon carcinogenesis. *Cancer Res* 2001; **61**: 1874–8.
35. Eberhart CE, Coffey RJ, Radhika A, Giardiello FM, Ferrenbach S, DuBois RN. Up-regulation of cyclooxygenase 2 gene expression in human colorectal adenomas and adenocarcinomas. *Gastroenterology* 1994; **107**: 1183–8.
36. Klaunig JE, Kamendulis LM. The role of oxidative stress in carcinogenesis. *Annu Rev Pharmacol Toxicol* 2004; **44**: 239–67.
37. Hussain SP, Hofseth LJ, Harris CC. Radical causes of cancer. *Nat Rev Cancer* 2003; **3**: 276–85.
38. Itzkowitz SH, Yio X. Inflammation and cancer IV. Colorectal cancer in inflammatory bowel disease: the role of inflammation. *Am J Physiol Gastrointest Liver Physiol* 2004; **287**: G7–17.
39. Tanaka T, Kawabata K, Kakumoto M, Hara A, Murakami A, Kuki W, Takahashi Y, Yonei H, Maeda M, Ota T, Odashima S, Yamane T, Koshimizu K, Ohigashi H. Citrus auraptene exerts dose-dependent chemopreventive activity in rat large bowel tumorigenesis: the inhibition correlates with suppression of cell proliferation and lipid peroxidation and with induction of phase II drug-metabolizing enzymes. *Cancer Res* 1998; **58**: 2550–6.
40. Lih-Brody L, Powell SR, Collier KP, Reddy GM, Cerchia R, Kahn E, Weissman GS, Katz S, Floyd RA, McKinley MJ, Fisher SE, Mullin GE. Increased oxidative stress and decreased antioxidant defenses in mucosa of inflammatory bowel disease. *Dig Dis Sci* 1996; **41**: 2078–86.
41. Bartsch H, Nair J. Potential role of lipid peroxidation derived DNA damage in human colon carcinogenesis: studies on exocyclic base adducts as stable oxidative stress markers. *Cancer Detect Prev* 2002; **26**: 308–12.
42. D'Inca R, Cardin R, Benazzato L, Angriman I, Martines D, Sturniolo GC. Oxidative DNA damage in the mucosa of ulcerative colitis increases with disease duration and dysplasia. *Inflamm Bowel Dis* 2004; **10**: 23–7.
43. Tardieu D, Jaeg JP, Cadet J, Embvani E, Corpet DE, Petit C. Dextran sulfate enhances the level of an oxidative DNA damage biomarker, 8-oxo-7,8-dihydro-2′-deoxyguanosine, in rat colonic mucosa. *Cancer Lett* 1998; **134**: 1–5.
44. Araki Y, Andoh A, Fujiyama Y. The free radical scavenger edaravone suppresses experimental dextran sulfate sodium-induced colitis in rats. *Int J Mol Med* 2003; **12**: 125–9.

Research Signpost
37/661 (2), Fort P.O., Trivandrum-695 023, Kerala, India



Carcinogenesis and Modification of Carcinogenesis, 2005: 177-185 ISBN: 81-308-0059-4
Editors: Takuji Tanaka and Hiroyuki Tsuda

12

Suppressing effects of yeast, magnesium (Mg), zinc (Zn), Mg-enriched yeast and Zn-enriched yeast on azoxymethane-induced aberrant crypt foci in rats

Shigeyuki Sugie[1], Toshiya Kuno[2], Kunihiro Kawabata[2], Shouji Shimada[3] and Hideki Mori[2]
[1]Department of Oncologic Pathology, Kanazawa Medical University, 1-1 Daigaku, Uchinada, Ishikawa 920-0293, Japan; [2]Department of Tumor Pathology, Gifu University School of Medicine, 1-1 Yanagido, Gifu 501-1194 Japan; [3]Oriental Yeast Co. Ltd., Tokyo, Japan

Abstract

The modifying effect of dietary administration of yeast, magnesium (Mg), zinc (Zn), Mg-enriched yeast (Mg-yeast) and Zn-enriched yeast (Zn-yeast) on azoxymethane (AOM)-induced colonic aberrant crypt foci (ACF) were investigated in male F344 rats. To induce ACF, 6-week old rats were given subcutaneous

Correspondence/Reprint request: Dr. Shigeyuki Sugie, Department of Oncologic Pathology, Kanazawa Medical University, 1-1 Daigaku, Uchinada, Ishikawa 920-0293, Japan. E-mail: sugie@kanazawa-med.ac.jp

injections of AOM (15 mg/kg body weight) once a week for 3 weeks. One week before the AOM treatment they were started on diet containing 10 or 5% yeast, 720 ppm $Mg(OH)_2$, 2500 ppm $Zn(CH_3COO)_2$, 10% Mg-yeast and 5% Zn-yeast for 5 weeks. All animals were sacrificed and measured ACF in the colon, microscopically, at 5 weeks after the start of experiment AOM exposure produced 128 ± 28 ACF/rat at the end of the study (week 5). Dietary administration of 10 % yeast, 720 ppm $Mg(OH)_2$, 2500 ppm $Zn(CH_3COO)_2$, 10% Mg-yeast and 5% Zn-yeast caused significant reduction in the frequency of ACF: 98 ± 20 ACF/rat, 72 ± 10 ACF/rat, 78 ± 18 ACF/rat, 70 ± 6 ACF/rat, 73 ± 26 ACF/rat, respectively. Average number of ACF /cm^2 colon mucosa was also decreased in those groups compared with AOM alone group. 5% yeast diet did not reduced ACF, significantly. These data suggest that constituents of yeast, Mg, Zn, Mg-yeast and Zn-yeast are possible dietary preventatives for human colon cancers.

Introduction

Dietary factors play an important role in prevention of human diseases, including cancers (1,2). Experimental and epidemiological evidence suggests that increased dietary fiber is associated with a decreased risk of colon cancer, which is the third most malignant neoplasm in the world (3) and the second leading cause of cancer deaths in the USA. In Japan, the progressive introduction of Western dietary habits, especially an increasing fat intake and decreasing carbohydrate and dietary fiber intake, has increased colon cancer incidence (4). Recent research has also focused on the presence of minor constituents or non-nutrients, which possess antimutagenic and anticarcinogenic properties, in diets (5). Essential elements are candidates of chemopreventive agents (6, 7). Such compounds are candidates for chemopreventive agents against cancer development in humans. We have previously reported inhibitory effects of natural non-nutritive compounds on the development of aberrant crypt foci (ACF) (8-10), which are precursor lesions for colon carcinoma (11-13).

Several trace elements have been reported to exert chemopreventive effects in several target organs of rodent carcinogenesis models (14). For example, selenium has been reported the chemopreventive effect in some organs (15,16). We also reported the chemopreventive effect of organic selenium in colon, breast and liver carcinogenesis (17,18). The suppressing effects of Mg and Ca reported in tumorigenesis by heavy metals (19,20,21).

Epidemiological studies have been reported some data to relate Mg concentrations in water, food and air to cancer mortality (22-26) and it has been reported that Mg is relate to a low cancer mortality of people living at high altitudes (27,28,29). From such reports, Mg was thought to be one of the

candidates of chemopreventive agent. We examined the effect of magnesium hydroxide ($Mg(OH)_2$) in rat intestinal carcinogenesis and found that $Mg(OH)_2$ was reduced the incidence of colon cancer and cell proliferation (30). $Mg(OH)_2$ is one of the inorganic magnesium compounds and used as the antacid and relaxant for human beings.

Epidemiologic studies suggest that zinc (Zn) deficiency may be associated with increased risk of cancer, especially esophageal cancer (31). In animal study, Zn deficiency has been reported to enhance colon carcinogenesis, mammary tumorigenesis, and esophageal carcinogenesis (32-34). Fong et al. reported that Zn replenishment reduces esophageal cell proliferation and N-nitrosomethylbenzylamine (NMBA)-induced esophageal tumor incidence in Zn-deficient rats. However, few studies have been conducted with Zn supplementation in animals and humans.

The effects of yeast in carcinogenesis have not been known. Some investigators have reported Se supplemented yeast reduced carcinogenesis. However, they have not given the diet with yeast to the rat and the effects of yeast have not been discussed.

Recently, Oriental Yeast Co. Ltd. developed Mg- and Zn-enriched yeast (Mg-yeast and Zn-yeast). In this study, we studied the effects of Yeast, Zn, Mg, Mg-yeast and Zn-yeast in 4-AOM-induced colon ACF. In this study, we examine the effects of dietary administration of baker's yeast, Mg, Zn, Mg-yeast and Zn-yeast in AOM-induced colon ACF formation.

Materials and methods

Animals and diet

A total of 77 male F344 rats, 4 weeks old (Shizuoka Laboratory Animal Center, Shizuoka, Japan) were used. All animals were housed in wire cages (three or four rats per cage) with free access to drinking water and basal diet (MF; Oriental Yeast Co. Ltd., Tokyo, Japan), under controlled conditions of humidity (50 ± 10%), lighting (12 h light/dark cycle) and temperature (23 ± 2°C). They were quarantined for 7 days and randomized into experimental and control groups. AOM was obtained from Sigma Chemical Co. (St. Louis, MO). Pellet MF diet was used as the basal diet throughout the study. All of experimental diets were produced and provided by Oriental Yeast Co. Ltd. Five or 10 % yeast, 5% Zn-yeast, 2500 ppm $Zn(CH_3COO)_2$, 720 ppm $Mg(OH)_2$ and 10 % Mg-yeast were mixed in the basal diet MF and made in pellet. These experimental diets were stored in a cold room (<4°C) until use. Mg concentration in the Mg-yeast were made to be equivalent to that in 720 ppm $Mg(OH)_2$ diet. Zn concentration in the Zn-yeast were made to be equivalent to that in 2500 ppm $Zn(CH_3COO)_2$ diet.

Experimental procedure

Seventy-seven rats were divided into 14 groups as shown in Figure 1. Groups 1-7 received three weekly subcutaneous (s.c.) injections of AOM at a dose of 15 mg/kg body wt. Rats in group 1 were fed the basal diet alone and those in groups 2-7 were given the diets containing 5 or 10 % yeast, 5% Zn-yeast, 2500 ppm. $Zn(CH_3COO)_2$, 720 ppm $Mg(OH)_2$ and 10 % Mg-yeast, respectively, for 5 weeks, starting 1 week before the first dosing with AOM. Groups 8-13 were given the experimental diets alone. Group 14 was an untreated control. At week 5, all animals were killed and the colons were fixed in 10% buffered formalin and stained with a 0.2% methylene blue solution for analysis of ACF.

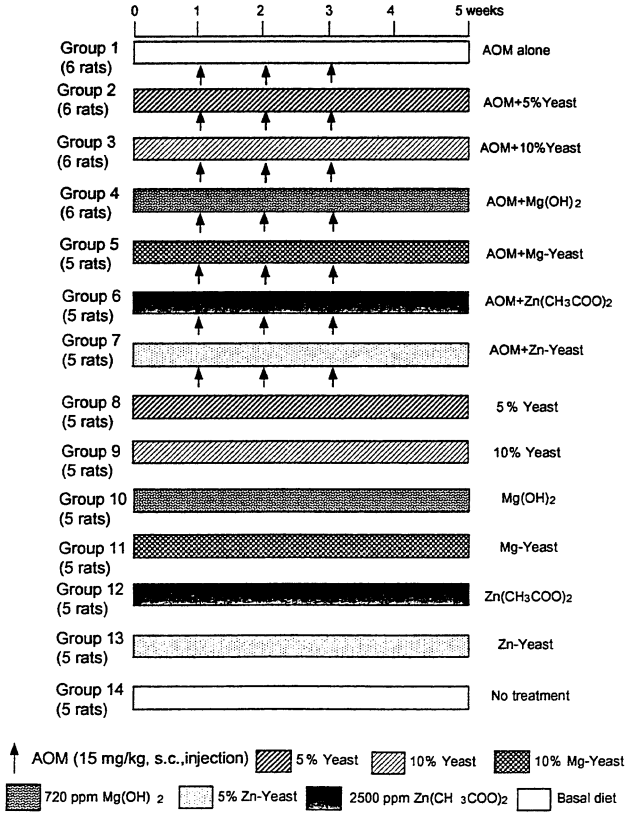


Figure 1. Experimental protocol.

Determination of ACF

At autopsy, the colons were flushed with saline, excised, cut open longitudinally along the main axis and then washed with saline. The colons were cut into three sections (~4 cm each) starting from the anus, placed between filter papers to reduce mucosal folding and fixed in 10% buffered formalin for at least 24 h. Fixed colon sections were dipped in a 0.2% solution of methylene blue in distilled water for 30 s, then briefly washed with distilled water. Using a light microscope at a magnification of x40, ACF were distinguished by their increased size, their more prominent epithelial cells and their increased pericryptal space compared with surrounding normal crypts. The number of ACF observed per colon, the number of aberrant crypts observed in each focus and the location of each focus were recorded.

Statistical methods

Fisher's exact probability test, Student's unpaired *t*-test or Welch's *t*-test was used for statistical analyses. A value of $P < 0.05$ was considered significant.

Results

Among AOM treated groups, 10% yeast, Mg, Mg-yeast diet reduced the body and liver weights compared to AOM alone group (Table 1). However, significant differences could not be found in body weight and liver weight gains among groups that did not treated with AOM. There are no significant differences in relative liver weight among groups. There was no clear evidence

Table 1. Body, Liver, and Relative Liver Weights of Rats.

Group no.	Treatment	No. of rats examined	Body weight (g)	Liver weight (g)	Relative liver weight (g/100 g body weight)
1	AOM alone	6	196±8.60[a]	9.0±0.89	4.58±0.38
2	AOM + 5% Yeast	6	191±12.6	9.0±0.89	4.73±0.43
3	AOM + 10% Yeast	6	174±8.62**b**	7.8±0.75**c**	4.51±0.34
4	AOM + 720 ppm Mg	6	177±2.73**d**	7.9± 0.80**c**	4.48±0.43
5	AOM + 10% Mg-Yeast	6	186±8.85**c**	7.8±0.42**c**	4.25±0.28
6	AOM + 2500 ppm Zn	6	183±9.25	8.5±1.38	4.44±0.25
7	AOM + 5% Zn- Yeast	6	191±9.0	9.2±1.92	4.25±0.54
8	5% Yeast	5	216±6.32	8.5±0.71	3.91±0.84
9	10% Yeast	5	218±10.5	8.6±0.89	3.90±0.41
10	720 ppm Mg	5	220±2.19	8.4±0.89	4.08±0.32
11	10% Mg-Yeast	5	206±13.0	8.4±1.71	4.11±0.49
12	2500 ppm Zn	5	209±6.72	8.2±0.84	3.93±0.46
13	5% Zn- Yeast	5	210±5.59	8.1±1.14	3.86±0.56
14	Vehicle control	5	214±7.48	8.2±0.45	3.83±0.14

[a]Mean ±SD.

b-d: Significantly different from group 1 by Student's *t*-test (b: P<0.005, c: P<0.05, d: P<0.001).

for toxicity in animals exposed to yeast, Mg, Zn, Mg-yeast and Zn-yeast diet. Histologically, there were no toxic changes in liver, kidney, lung and heart of the rats in all groups.

As shown in Table 2, colonic ACF were recognized only in rats treated with AOM (groups 1-7). The total number of ACF/colon and number of ACF/cm^2 colon of groups given 5% yeast, Mg, Zn, Mg-yeast and Zn-yeast diet were significantly smaller than of group 1. The total number of ACF/colon and number of ACF/cm^2 colon of groups given 10% yeast diet were smaller than of group 1, although statistical difference could not be found.

Table 2. AOM-induced ACF Formation in Male F344 Rats.

Group no.	Treatment	No. of rats examined	Total no. / colon	No. of ACF/cm^2
1	AOM alone	6	128±28	14.0±3.3
2	AOM + 5% Yeast	6	98±12[b]	10.0±0.73[b]
3	AOM + 10% Yeast	6	111±20	12.9±1.6
4	AOM + 720 ppm Mg	6	72 ±10[c]	7.52±1.3[c]
5	AOM + 10% Mg-Yeast	6	70 ±6[c,d]	7.21±1.1[f,g]
6	AOM + 2500 ppm Zn	6	78 ±18[c]	8.20 ±2.0[c]
7	AOM + 5% Zn-Yeast	6	73±26[e]	7.57 ±2.6[c,h]
8	5% Yeast	5	0	0
9	10% Yeast	5	0	0
10	720 ppm Mg	5	0	0
11	10% Mg-Yeast	5	0	0
12	2500 ppm Zn	5	0	0
13	5% Zn-Yeast	5	0	0
14	Vehicle control	5	0	0

[a]Mean ±SD.
b,c,d Significantly different from group 1 (b:P<0.05, c:P<0.005, f:P<0.0001, e: P<0.001).
f, g: Significantly different from group 3 by Student's *t*-test (d:P<0.001, g:P<0.0001).
h: Significantly different from group 2 by Student's *t*-test (P<0.005).

Discussion

In this study, yeast, Mg, Zn, Mg-yeast and Zn-yeast diets reduced AOM-induced colonic ACF formation. Lower concentration of yeast diet was more effective than higher concentration. ACF in groups fed Mg-yeast and Zn-yeast diet were significantly lower than that in groups fed yeast and slightly lower than that in group fed Mg and Zn diet in each. However, synergistic effect and additive effect could not be found.

Suppressing effects of $Mg(OH)_2$ were already examined in rat methylazoxymethanol (MAM) acetate- or 1,2-dimethylhydrazine (DMH)-induced colon carcinogenesis. Modifying effects of $Mg(OH)_2$ on cell proliferation of colon mucosa were also analyzed (30). $Mg(OH)_2$ suppressed 5-bromo-2'-deoxyuridine (BrdU)-labeling indices in rat colon mucosa. Dietary $Mg(OH)_2$ also suppressed the MAM acetate-induced expression of *c-myc*

proto-oncogene, and reduced the increased proliferating cell nuclear antigen (PCNA)-labeling indices by MAM acetate in rat colon mucosa. BrdU-labeling indices increased by cholic acid was also reduced by $Mg(OH)_2$ as did calcium lactate. Such an inhibitory effect on the DNA synthesis of the epithelial cells by $Mg(OH)_2$ may be related to the suppressive action of the essential trace element on the carcinogen-induced colon carcinogenesis.

Epidemiologic studies suggest that Zn deficiency may be associated with increased risk of cancer (31). However, few studies have been conducted with Zn supplementation in animals and humans. Zn deficiency has been reported to enhance DMH-induced colon carcinogenesis, N-methyl-N-nitrosourea (NMU)-induced mammary tumorigenesis and N-nitrosomethylbenzylamine (NMBA)-induced esophageal carcinogenesis. The mechanism of suppressive effect of Zn in carcinogenesis is not clear (32-34). In animal study, upper aerodigestive tract squamous cell carcinomas induced by 4-nitroquinoline 1-oxide were increased in rats fed Zn deficiency diet compared with Zn sufficient rats, and cyclooxygenase (COX)-2 is often over-expressed in these cancers (32). Fong et al. reported that Zn-deficient diet induces the cell proliferation and Zn replenishment reduces esophageal cell proliferation (34). These finding indicate that Zn concerned with the regulation of cell proliferation. Zn deficiency has been also reported to induce DNA damage. Dietary Zn deficiency is associated with an increased formation of O^6-methylguanine in the esophageal DNA of Zn-deficient animals treated with methylbenzyl-nitrosamine (31). Dietary deficiencies in Zn can contribute to single- and double-strand DNA breaks and oxidative modifications to DNA that increase risk for cancer development (36).

Some studies about the effect of dietary Zn administration has been reported and mentioned the mechanisms. Zn replenishment of NMBA-treated Zn-deficient rats rapidly induces apoptosis in esophageal epithelial cells and thereby substantially reduces the development of esophageal cancer (37). Zn replenishment reduced COX-2 overexpression in rat tongue tumor (38). Zn supplementation is associated with decreased oxidative stress and improved immune function, which may be among the possible mechanisms for its cancer preventive activity (39). However, few studies have been conducted with Zn supplementation in animals and humans.

In this experiment, we also found that yeast suppressed AOM-induced ACF. The mechanism of suppressive effect of yeast in carcinogenesis is not clear. Some components of yeast have been reported to activate the immune response (40).

Se-enriched yeast has been used as the supplementation and studied in animal experiment and human (41,42). Epidemiological data have supported the chemopreventive effects of Se (41). Se is mainly contained as organo-selenium, selenomethionine, in yeast (42). Mg and Zn are also contained as

organic form in yeast. Mg and Zn are less toxic than Se. From these results, Mg and Zn are supposed to be effective against carcinogenesis regardless organic or inorganic form.

Thus, in the present study inhibitory effects of yeast, Mg, Zn, Mg-yeast and Zn-yeast on AOM-induced colon preneoplastic lesion, ACF. Although the exact mechanisms of the chemopreventive effects and constituents of yeast, Mg, Zn, Mg-yeast and Zn-yeast need to be determined, the evidence described here warrants further research on the modifying effects of the constituents of yeast, Mg, Zn, Mg-yeast and Zn-yeast on colon carcinogenesis.

Acknowledgments

This work was supported in part by a Grant-in-Aid from the Ministry of Agriculture, Forestry and Fisheries of Japan, and a Grant (C2004-4) for Promoted Research from Kanazawa Medical University.

References

1. Doll, R., and Peto, R. 1981, J. Natl Cancer Inst., 66, 1191.
2. Rogers, A.E., Zeisel, S., and Groopman, J. 1993, Carcinogenesis, 14, 2205.
3. Shike, M., Winawer, S.J., Greenwald, P.H., Bloch, A., Hill, M.J., and Swaroop, S.V. 1990, Bull. World Health Organ., 68, 377.
4. Weisburger, J.H. 1991, Am. J. Clin. Nutr., 53, 226s.
5. Wattenberg, L.W. 1993, Food and Cancer Prevention: Chemical and Biological Aspects, K.W. Waldron, I.T. Johnson, and G.R. Fenwick (Eds.) The Royal Society of Chemistry, Cambridge, UK, 12.
6. Kasprzak, K.S., Waalkes, M.P. 1986, Adv. Exp. Med. Biol., 1986, 206, 497.
7. Schreier, P. 2005, Dev. Ophthalmol., 38, 1.
8. Tanaka, T., and Mori, H. 1996, J. Toxicol. Pathol., 9, 139.
9. Tanaka, T., Kawabata, K., Makita, H., Kakumoto, M., Satoh, K., Hara, A., and Mori, H. 1997, Carcinogenesis, 18, 2155.
10. Tanaka, T., Kawabata, K., Honjo, S., Kohno, H., Murakami, M., Shimada, R., Matsunaga, K., Yamada, Y., and Shimizu, M. 1999, Oncol. Rep., 6, 1333.
11. Bird, R.P. 1995, Cancer Lett., 93, 55.
12. Pretlow, T.P., Barrow, B.J., Ashton, W.S., O'Riordan, M.A., Pretlow, T.G., Jurcisek, J.A., and Stellato, T.A. 1991, Cancer Res., 51, 1564.
13. Pretlow, T.P., O'Riordan, M.A., Somich, G.A., Amini, S.B., and Pretlow, T.G. 1992, Carcinogenesis, 13, 1509.
14. Jacob, M.M., and Griffin, A.C. 1981, Inhibition of Tumors Induction and Development, M.S. Zedeck, and M. Lipkin (Eds.), Plenum Press, New York, 169.
15. Greiffin, A.C. 1979, Adv. Cancer Res., 29, 419.
16. Buell, D.N. 1983, Semin. Oncol., 10, 311.
17. Tanaka, T., Reddy, B.S., and El-Bayoumy, K. 1985, Jpn. J. Cancer Res. (Gann), 76, 462.
18. Sugie, S., Reddy B.S., El-Bayoumy, K. and Tanaka, T. 1989, Jpn. J. Cancer Res., 80, 952.

19. Poirier, L.A., Kasprzak, K.S., Hoover, K.L. and Wenk, M.L. 1983, Cancer Res., 43, 4575.
20. Poirier, L.A., Theiss, J.C., Arnold, L.J. and Shimkin, M.B. 1984, Cancer Res., 44, 1520.
21. Kasprzak, K.S., Ward, J.M., Poirier, L.A., Reichardt, D.A., Denn, A.C., III, and Reynolds, C.W. 1987, Carcinogenesis, 8, 1005.
22. Armstrong, R.W. 1972, Ann. N.Y. Acad. Sci., 199, 239.
23. Schrauzer, G.N. 1976, Med. Hypotheses, 2, 39.
24. Schroeder, H.A., Nason, A.P., and Tipton, I.H. 1969, J. Chronic Dis., 21, 815.
25. Comstock, G.W. 1979, Am. J. Epidemiol., 110, 375.
26. Sauer, H.I., Parke, D.W., and Neill, M.L. 1970, Trace Substances in Environmental Health, D.D. Hemphill (Ed.), University of Missouri, Columbia, 318.
27. Burton, A.C. 1975, Eur. J. Cancer, 11, 365.
28. Burton, A.C., and Cornhill J.F. 1977, J. Toxicol. Envirn. Health, 3, 465.
29. Henrotte, J.G., Constans, H., Constans, J., Bisseliches, F., and Coudert, J. 1972, Arch. Internatl. Physiol. Biochem., 80, 941.
30. Sugie, S., Tanaka, T., Morishita, Y., Wang, A., Yoshimi, N., and Mori, H. 1997, Food Facters for Cancer Prevention, H. Ohigashi, T. Osawa, J. Terao, S. Watanabe, and T. Yoshikawa (Eds.), Springer-Verlag, Tokyo, 396.
31. Barch, DH. 1989, J. Am. Coll. Nutr., 8, 99.
32. Carter, J.W., Lancaster, H., Hardman, W.E., Cameron, I.L. 1997, Nutr. Cancer, 27, 217.
33. Lee, S., Simpson, M., Nimmo, M., and Xu, Z. 2004, Carcinogenesis, 25, 1879.
34. Fong, L.Y., and Magee, P.N. 1999, Cancer Lett., 143, 63.
35. Fong, L.Y., Farber, J.L., and Magee, P.N. 1998, Carcinogenesis, 19, 1591.
36. Ho, E. 2004, J, Nutr, Biochem., 15, 572.
37. Fong, L.Y., Nguyen, V.T., and Farber, J.L. 2001, J. Natl. Cancer Inst., 93, 1525.
38. Fong, L.Y., Zhang, L., Jiang, Y., and Farber, J.L. 2005, J. Natl. Cancer Inst., 97, 40.
39. Prasad, A.S., and Kucuk, O. 2002, Cancer Metastasis Rev., 21, 291.
40. Zimmerman, J.W., Lindermuth, J., Fish, P.A., Palace, G.P., Stevenson, T.T., and DeMong, D.E. 1998, J. Biol. Chem., 273, 22014.
41. Combs, G.F. Jr., Clark, L.C., and Turnbull, B.W. 2001, Biofactors., 14, 153.
42. McIntosh, G.H., Scherer, B., and Royle, P.J. 2004, Asia Pac. J. Clin. Nutr., 13(Suppl), S93.

Research Signpost
37/661 (2), Fort P.O., Trivandrum-695 023, Kerala, India



Carcinogenesis and Modification of Carcinogenesis, 2005: 187-198 ISBN: 81-308-0059-4
Editors: Takuji Tanaka and Hiroyuki Tsuda

13

A polyisoprenylated benzophenone garcinol inhibits azoxymethane-induced rat colon carcinogenesis

Rikako Suzuki[1,2], Hiroyuki Kohno[1], Shigeyuki Sugie[1], Fumio Yamaguchi[3] Shigehiro Kataoka[3], Toshiaki Ariga[3] and Takuji Tanaka[1]
[1]Department of Oncologic Pathology, Kanazawa Medical University, 1-1 Daigaku Uchinada, Ishikawa 920-0293, Japan; [2]Research Fellow of the Japan Society for the Promotion of Science; [3]Research and Development Division, Kikkoman Corporation, 399 Noda, Noda City, Chiba 278-0037, Japan

Abstract

A polyisoprenylated benzophenone garcinol present in Guttiferae (Garcinia indica, Garcinia huillkensis and Garcinia cambogia) in diet effectively inhibits the development of putative precursor lesions of colonic adenocarcinoma in rats initiated with azoxymethane (AOM). In the present study, we investigated the possible inhibitory effect of dietary administration of garcinol on the development of colonic neoplasms in a

Correspondence/Reprint request: Dr. Rikako Suzuki, Department of Oncologic Pathology, Kanazawa Medical University, 1-1 Daigaku, Uchinada, Ishikawa 920-0293, Japan. E-mail: rikako@kanazawa-med.ac.jp

long-term animal colon carcinogenesis model with AOM. Male F344 rats were divided into 5 groups: group 1 was given two weekly subcutaneous injections of AOM (20 mg/kg body weight); groups 2 and 3 received diets containing 50 ppm and 250 ppm garcinol for 34 weeks, respectively, starting one week after the last dosing of AOM; group 4 was given 250 ppm garcinol alone throughout the experiment; and group 5 served as an untreated control. At the termination of the study (Week 36), the incidence of colonic adenocarcinoma was 80% in the AOM alone group. Dietary administration of 50 ppm (45%, P=0.0241) and 250 ppm (50%, P=0.0479) garcinol after AOM initiations caused reduction in the incidence of colonic adenocarcinoma. The multiplicity of colorectal adenocarcinoma (number of tumors/rat) was also lowered by feeding of garcinol containing diets. The treatment with garcinol decreased polyamine content in the non-tumorous mucosa. Garcinol feeding decreased the prostaglandin E_2 level, reduced the proliferating cell nuclear antigen-labeling index, and increased the number of apoptotic cells in the colonic adenocarcinomas. Our results suggest that dietary garcinol has inhibitory effect on AOM-induced rat colon carcinogenesis. Although the exact mechanisms involved in the modulation effects of garcinol are not fully known, suppression of cell proliferating activity and induction of apoptotic index in colon adenocarcinoma could be contributed to the modulation effect of garcinol.

Introduction

Among the several types of cancer, colon cancer is one of the leading causes of cancer deaths in Western countries and is recently increased in Asia due to the changes in dietary factors including meat consumption, as well as other lifestyle factors into Asian society [1, 2]. In Japan, mortality rates from colorectal cancer in 2000 are 16.32/100,000 in men and 9.74/100,000 in women [3]. Although the advances in early detection and basic or clinical trials of promising new therapies, morbidity and mortality of cancer is one of the important public health issues in the world [4]. Cancer prevention studies including its mechanisms have a substantial need for reducing the spread of the increase in the morbidity or mortality of cancer.

Chemoprevention is a focus of attention and a rapidly expanding field. It is defined as the use of natural, synthetic, or biologic chemical agents to reverse, suppress, or prevent carcinogenic progression to invasive cancer [5]. Numerous reports concerning chemopreventive agents have been published [6-8]. Dietary factors play an important role in prevention of various human diseases, including cancer. Several studies have demonstrated the relationship between the generous consumption of vegetables and the reduction in the risk of colon cancer [9-11]. For instance, the intake of 400-600 g/day of fruits and vegetables is associated with reduced incidence of common types of cancer [12]. In addition, minor

constituents or non-nutrients are known to modify the development of tumors [13, 14]. Phytochemicals, the bioactive non-nutrient plant compounds, found in fruits, vegetables, grains, and other plant foods have been linked to reductions in the risk of major chronic diseases including cancer [15].

A polyisoprenylated benzophenone garcinol (Figure 1), also called camboginol [16], is present in Guttiferae (*Garcinia indica*, *Garcinia huillkensis* and *Garcinia cambogia*). *Garcinia* is a rich source of secondary metabolites including xanthones, flavanoids, benzophenones, lactones, and phenolic acids [17]. In India, the dried rind of *Garcinia indica* ("Kokum") containing a yellow pigment of garcinol (2-3%, w/w) is used as a garnish for curry and in some of the folklore medicine [18-20]. Garcinol has attracted considerable interest because of its health promoting properties, including antibiotic activities [21, 22], antioxidant properties [23], antiulcer activities [24], and induction of apoptosis [25-27]. To our knowledge, its preventive activity against tongue carcinogenesis is only a report showing cancer prevention activity of garcinol [28]. In our earlier study, dietary garcinol inhibited colonic aberrant crypt foci (ACF) formation [29]. Since ACF is precursor lesions of colonic adenocarcinoma [30], garcinol might be regarded as useful candidate for colon cancer chemopreventive agent.

In the current study, we conducted the experiment investigating the modifying effect of garcinol on azoxymethane (AOM)-induced rat colon carcinogenesis using a long-term bioassay. Also, biomarkers such as proliferating cell nuclear antigen (PCNA)-labeling index and apoptotic index were measured in colonic neoplasms, since certain chemopreventive agents exerts their inhibitory action via reduction of the PCNA index [31, 32], and induction of apoptosis [33]. Polyamine levels in the colonic mucosa were also determined, since polyamine is intimately involved in growth related process

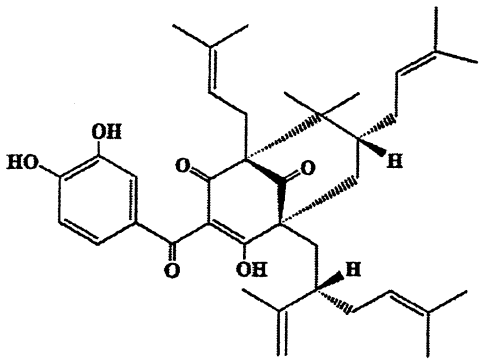


Figure 1. Chemical structure of garcinol.

including colon tumorigenesis [34] and its metabolism is a target for cancer chemoprevention [35]. Also, effect of dietary garcinol on prostaglandin (PG) E_2 levels in colonic adenocarcinoma and colonic mucosa were assayed.

Materials & methods

Animals, chemicals, and diets

Four-weeks-old male F344 rats were obtained from Charles River Japan, Inc. (Yokohama, Japan). The rats were maintained in the Kanazawa Medical University Animal Facility according to the Institutional Animal Care Guidelines. All animals were housed in plastic cages (3 or 4 rats/cage) with free access to drinking water and a basal diet, CE-2 (CLEA Inc., Tokyo, Japan), under controlled conditions of relative humidity (50±10%), lighting (12-h light/dark cycle) and temperature (23±2°C). AOM was purchased from Sigma Chemical Co. (St. Louis, MO, USA). Garcinol (>98% purity) purified from *G. indica* dried fruit rind ('Kokum', purchased from Indo World Trading Co., New Delhi, India) was provided from Kikkoman Corporation (Noda City, Japan). Experimental diets were prepared by mixing with garcinol into the basal diet (CE-2) at dose of 50 or 250 ppm.

Experimental procedure

The experimental procedure is shown in Figure 2. Male F344 rats, 5 weeks of age were divided into five groups. At 5 weeks of age, the rats in groups 1 through 3, designated for carcinogen treatment, were subcutaneously injected with AOM (20 mg/kg body weight) once a week for 2 weeks. Group 1 was fed the basal diet throughout the experiment. Groups 2 and 3 were fed the diets containing garcinol at 50 and 250 ppm, respectively, for 34 weeks, starting 1 week after the last dosing of AOM. Groups 4 and 5 were fed the diet 250 ppm garcinol alone and basal diet (CE-2) alone, respectively for 36 weeks. All rats

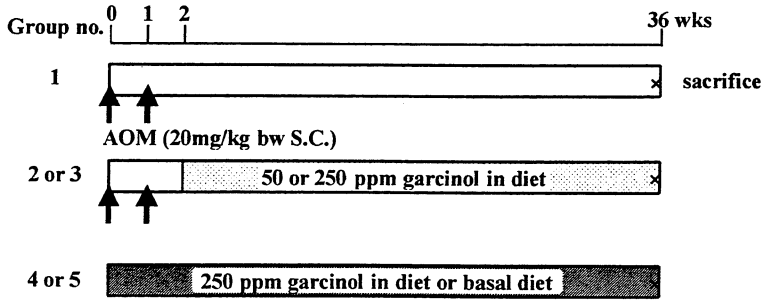


Figure 2. Experimental protocol.

were provided with the experimental diets and tap water *ad libitum*, and weighed weekly. The food intake was also recorded weekly. At the termination of the study (week 36), all rats were sacrificed using an overdose of ether. At autopsy, all organs, especially the intestine, were carefully examined grossly, and then all abnormal lesions were examined histologically. Their colons were fixed in 10% buffered formalin and processed for histopathological examination by routine methods. Intestinal neoplasms were diagnosed according to the criteria described by Pozharisski [36]. The weighed liver and kidney were also submitted to histological examination for checking the toxicity of garcinol.

Polyamine level

Scraped colonic mucosa without tumors was stored at -70 °C until measured. Proteins were extracted from the mucosa, and then tissue polyamine levels in the extraction were determined by the method described by Koide *et al.* [37].

Measurement of PGE_2 level

For PGE_2 determination, the scraped colonic mucosa of randomly selected 5 rats or colonic adenocarcinoma from each group was homogenized in a 400 μL of PBS on ice. After centrifugation at 10,000 × g for 5 min, the supernatants obtained were diluted at the ratio of 1:9, and measured for the PGE_2 concentration using a commercial experimental kit (Cayman, Ann Arbor, MI, USA) according to the protocol of the manufacturer. Protein concentrations for tissue samples were determined using the Bradford method [38].

Measurement of PCNA and apoptotic indices in the colonic neoplasms

All colonic tumors were used for counting PCNA-labeling and apoptotic indices. Tumor tissues fixed in 10% buffered formalin for 2 days were embedded in paraffin. Serial cross-sections of 3 μm were cut, and mounted onto gelatin-coated glass slides. PCNA and apoptotic cells were determined by immunohistochemistry. A mouse monoclonal primary antibody against PCNA (1:50 dilution; PC10, DAKO Japan, Kyoto, Japan) and a rabbit polyclonal primary antibody against single stranded DNA (ssDNA, 1:300 dilution; DAKO Japan, Kyoto, Japan) were applied to the sections according to the manufacturer's protocol (DAKO LSAB 2 kit/HRP, DAKO Japan, Kyoto, Japan). All incubation steps were carried out for 15 min at 37°C. Negative controls were prepared by omitting the primary antibodies. As secondary antibody, goat polyclonal anti-rabbit/mouse immunoglobulin labeled with biotin (DAKO Japan, Kyoto, Japan) was used. The labeled streptavidin-biotin

immunoperoxidase technique was applied for immunohistochemistry. All nuclei which densely immunoreacted with PCNA or ssDNA antibody were regarded as PCNA or ssDNA positive. The PCNA and apoptotic indices were determined by counting the number of positive cells among at least 200 cells in the tumor, and were indicated as percentages.

Statistical evaluation

Where applicable, data were analyzed using Bonferroni correction or Fisher's exact probability test with $P<0.05$ as the criterion of significance.

Results

General observation

Throughout the experiment, clinical signs of toxicity, low survival, and poor condition were not observed in all rats. These were confirmed by histological examinations in liver, kidney, heart and lungs of the rats. Body and liver weights had no significant difference among the groups (Figure 3). Food intake also did not significantly differ among the groups (data not shown). These results suggest that feeding of 50 or 250 ppm garcinol containing diets were well tolerated and supported normal growth for rats without any adverse effects.

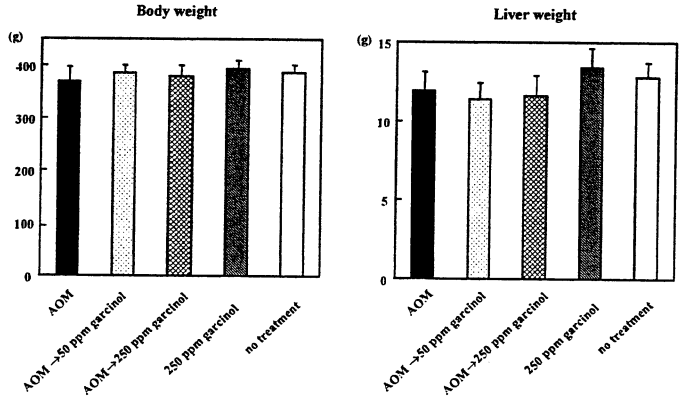


Figure 3. Body and liver weights at the end of the study.

Incidence and multiplicity of the intestinal neoplasms

As shown in Figure 4, the incidence and multiplicity of colonic adenocarcinoma were 80% and 1.50±1.12/rat in the AOM alone group (group 1). Feeding of 50 ppm (group 2) or 250 ppm (group 3) of garcinol reduced the

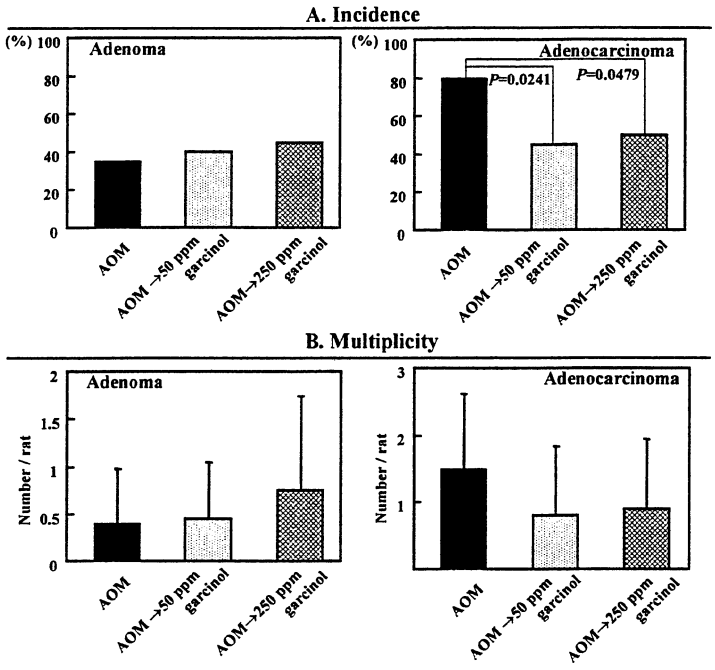


Figure 4. Incidence and multiplicity of large bowel tumors.

frequency of this malignancy: 45% (P=0.0241) by 50 ppm garcinol and 50% (P=0.0479) by 250 ppm garcinol. The multiplicities in the groups 2 and 3 were also lower when compared to group 1: 0.80±1.03/rat and 0.90±1.04/rat, respectively. However the differences were insignificant. In groups 4 (250 ppm garcinol alone) and 5 (no treatment), tumors were not found in any organs of animals. The differences of incidences and multiplicities of colonic adenoma among groups 1-3 were not statistically significant.

Polyamine content and PGE_2 level

The data on assays of polyamine content and PGE_2 level in the colonic mucosa determined at the end of the study are summarized in Figure 5. Total polyamine content of colonic mucosa without tumors in group 1 (16.9±1.6 nmol/mg protein, P<0.001) was significantly greater than that of group 5 (10.9±1.1 nmol/mg protein). The value of group 3 (12.3±1.9 nmol/mg protein, P<0.01) was significantly smaller than group 1. Similarly, PGE_2 content in non-lesional colonic mucosa in group 1 (91.6±16.5 pg/mg protein, P<0.01) was

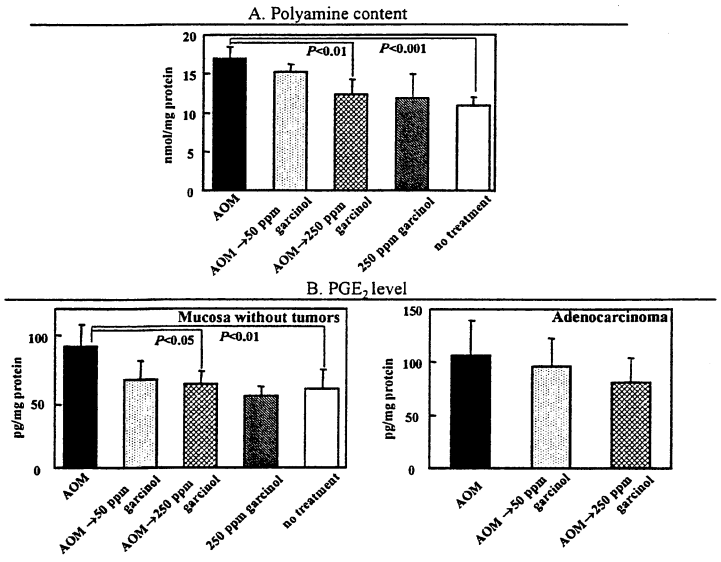


Figure 5. Colonic polyamine levels and PGE_2 contents of rats.

significantly greater than group 5 (59.6±14.2 pg/mg protein), and feeding 250 ppm garcinol (group 3, 63.2±9.7 pg/mg protein, $P<0.05$) significantly lowered the value when compared to group 1. No significant differences of PGE_2 content in colonic adenocarcinomas were noted among the groups 1-3.

PCNA and apoptotic indices in the colonic neoplasms

As shown in Figure 6A, the PCNA-positive indices of adenocarcinomas developed in group 2 (35±7%, $P<0.001$) and group 3 (32±6%, $P<0.001$) were statistically smaller than in group 1 (49±7%). Figure 6B indicates the apoptotic index in the colonic neoplasms. Apoptotic indices of adenocarcinomas in group 2 (4.65±0.49%, $P<0.01$) and group 3 (5.36±0.95%, $P<0.001$) were significantly larger than in group 1 (3.62±0.44%). As for adenomas, PCNA-positive indices in group 2 (27±3%, $P<0.01$) was statistically smaller than in group 1 (34±5%). However, the differences of apoptotic indices did not show the statistical difference among adenomas in groups 1-3.

Discussion

The results described here indicate that dietary feeding of garcinol suppresses the occurrence of colonic adenocarcinoma induced by AOM. In

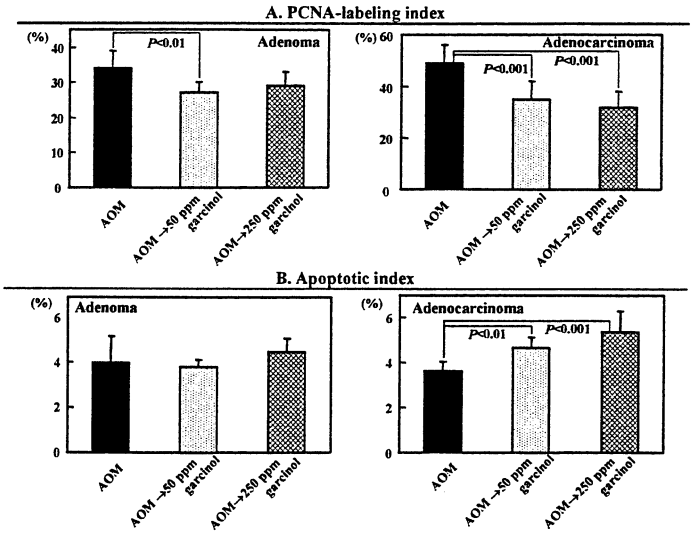


Figure 6. PCNA-labeling, and apoptotic indices in the large bowel tumors in rats.

contrast, the incidence and multiplicity of colonic adenoma in rats that received garcinol were higher than AOM alone group. These results suggested that garcinol modulates the malignant transformation from colonic adenoma to adenocarcinoma. In our tongue carcinogenesis study, animals received the diets containing 100 or 500 ppm garcinol were significantly reduced the incidence and multiplicity of squamous cell carcinoma without any adverse effect [28]. In the current study, administration of garcinol at both doses (50 and 250 ppm) exerted effective inhibitory action in rat colon carcinogenesis. The results may indicate the presence of optimal dose of garcinol, that is over 50 ppm, could suppress chemically induced carcinogenesis.

Cell proliferation is known to play an important role in carcinogenesis [39]. Natural product possessing suppression effect on cell proliferation activity could be candidate chemopreventive agent. Previously, we confirmed the suppressing effect of garcinol on cell proliferation activity in tongue squamous epithelium [28], colonic ACF, and colonic crypt cells of rats [29]. Recently, inhibitory effect of garcinol on the growth of human hepatocellular carcinoma cell, HepG2 was reported [40]. Our results of the expression of cell proliferation biomarkers such as PCNA-labeling index and polyamine level were in accordance with these reports [28, 29, 40]. Thus, it is likely that the prevention of AOM-induced colonic adenocarcinoma by dietary garcinol is due in part to the alteration of cell proliferating activity in the colonic neoplasms.

Apoptosis seems to be a reliable biomarker for the evaluation of potential agents for cancer prevention [41]. Induction of apoptosis is one of the major contributing factors for anti-tumorigenic properties of several natural compounds [8]. In this study, dietary exposure of garcinol at both doses significantly increased the apoptotic index in the colonic adenocarcinoma. Recently reports describing apoptosis induction by garcinol in HeLa cell [26] and HL60 cell [25, 27] also support our findings. We speculate that the induction of apoptosis may be one of the mechanisms for the chemopreventive action of garcinol.

The high level of PGE_2 is often the case with AOM-induced colonic tumors [42]. Colonic mucosa without tumors of rat that received AOM alone contained high amount of PGE_2 when compared with the no treatment group. PGE_2 content of colonic adenocarcinoma in group 1 was much higher than colonic mucosa without tumors in the same group. When rats were fed the diet containing garcinol after AOM exposure, PGE_2 level decreased in colonic mucosa without tumors and colonic adenocarcinoma. Thus, the reduction of PGE_2 also may contribute to the chemopreventive activity of garcinol. This reduction may led to the lowered cell proliferation and induction of apoptosis [43]. PGE_2 is produced from arachidonic acid by cyclooxygenase (COX) enzymes. In our recent work, dietary administration of garcinol decreased COX-2 immunoreactivity in the tongue neoplasms [28]. Furthermore, suppressing effects of garcinol on lipopolysaccharide- and interferon-γ-induced COX-2 expression were determined in mouse macrophage RAW 264.7 cells [29]. The reduction of PGE_2 level in colonic mucosa or adenocarcinoma might attribute to the decreasing of COX-2 expression by garcinol, although we did not assay COX-2 expression in the current study.

In a short-term assay of rat colonic ACF, garcinol feeding significantly elevated glutathione *S*-transferase and quinone reductase activity in the liver [29], which have a central role in the detoxification and excretion of activated metabolites of activated products. In addition, free radical damage which induces oxidative stress can cause DNA mutation and cell damage [44]. Ultimately these damages implicated in the etiology and progression of many diseases, including cancer [44]. Garcinol inhibited 12-*O*-tetradecanoylphorbol-13-acetate induced superoxide anion generation in human promyelocytic HL-60 cells [29]. The antioxidant activity and potent free radical scavenging activities of garcinol were reported [23, 24]. Especially, its scavenging activity against the most dangerous reactive oxygen species hydroxyl radical was stronger than that of DL-α-tocopherol [24].

In conclusion, our investigation described here demonstrates for the first time that dietary administration with garcinol suppresses the development of colonic adenocarcinomas induced by AOM. The modulation of colon tumorigenesis by garcinol might be caused through a number of mechanisms

including the alteration of cell proliferation activity, apoptosis activity, and the reduction of PGE_2 content in colon.

Acknowledgements

This work was supported in part by the Grant-in-Aid for Cancer Research, for the Third-Term Comprehensive 10-Year Strategy for Cancer Control from the Ministry of Health, Labour and Welfare of Japan; the Grants-in-Aid (nos. 15592007 and 15·2052) for Scientific Research from the Ministry of Education, Culture, Sports, Science and Technology of Japan; the grant (C2004-4) for the Collaborative Research from Kanazawa Medical University; and the grant (H2004-6) for the Project Research from the High-Technology Center of Kanazawa Medical University.

References

1. Jemal, A., Tiwari, R.C., Murray, T., Ghafoor, A., Samuels, A., Ward, E., Feuer, E.J., Thun, M.J., American Cancer Society. 2004, CA Cancer J. Clin., 54, 8.
2. Kono, S. 2004, Eur. J. Cancer Prev., 13, 127.
3. Bosetti, C., Malvezzi, M., Chatenoud, L., Negri, E., Levi, F., La Vecchia, C. 2005, Int. J. Cancer, 113, 339.
4. Bailar, J.C.3rd., Gornik, H.L. 1997, N. Engl. J. Med., 336, 1569.
5. Sporn, M.B. 1976, Cancer Res., 36, 2699.
6. Greenwald, P., Kelloff, G., Burch-Whitman, C., Kramer, B.S. 1995, CA Cancer J. Clin., 45, 31.
7. Greenwald, P. 2002, BMJ, 324, 714.
8. Tsuda, H., Ohshima, Y., Nomoto, H., Fujita, K., Matsuda, E., Iigo, M., Takasuka, N., Moore, M.A. 2004, Drug Metab. Pharmacokinet., 19, 245.
9. Steinmetz, K.A., Potter, J.D. 1991, Cancer Causes Control, 2, 325.
10. Block, G., Patterson, B., Subar, A. 1992, Nutr. Cancer, 18, 1.
11. Potter, J.D., Steinmetz, K. 1996, IARC Sci. Publ., 139, 61.
12. American Institute for Cancer Research and World Cancer Research Fund., Food, nutrition, and the prevention of cancer:a global perspective, American Institute for Cancer Research, Washington, DC, 1997.
13. Wattenberg, L.W., Hanley, A.B., Barany, G., Sparnins, V.L., Lam, L.K., Fenwick, G.R. 1985, Princess Takamatsu Symp., 16., 193.
14. Tanaka, T., Kohno, H., Mori, H. 2001, Asian Pac. J. Cancer Prev., 2, 165.
15. Ames, B.N., Gold, L.S. 1991, Mutat. Res., 250, 3.
16. Rama Rao, A.V., Venkatswamy, G., Pendse, A.D. 1980, Tetrahedron Lett., 21, 1975.
17. Gustafson, K.R., Blunt, J.W., Munro, M.H.G., Fuller, R.W., McKee, T.C., Cardellina, J.H.I., McMahon, J.B., Cragg, G.M., Boyd, M.R. 1992, Tetrahedron, 48, 10093.
18. Krishnamurthy, N., Lewis, Y.S., Ravindranath, B 1981, Tetrahedron Lett., 22, 793.
19. Krishnamurthy, N., Ravindranath, B. 1982, Tetrahedron Lett., 23, 2233.
20. Krishnamurthy, N., Ravindranath, B, Sampathu, S.R.D. 1987, Indian patent 160753.

21. Bakana, P., Claeys, M., Totte, J., Pieters, L.A., Van Hoof, L., Tamba-Vemba., Van den Berghe, D.A., Vlietinck, A.J. 1987, J. Ethnopharmacol., 21, 75.
22. Iinuma, M., Tosa, H., Tanaka, T., Kanamaru, S., Asai, F., Kobayashi, Y., Miyauchi, K., Shimano, R. 1996, Biol. Pharm. Bull., 19, 311.
23. Yamaguchi, F., Ariga, T., Yoshimura, Y., Nakazawa, H. 2000, J. Agric. Food Chem., 48, 180.
24. Yamaguchi, F., Saito, M., Ariga, T., Yoshimura, Y., Nakazawa, H. 2000, J. Agric. Food Chem., 48, 2320.
25. Pan, M.H., Chang, W.L., Lin-Shiau, S.Y., Ho, C.T., Lin, J.K. 2001, J. Agric. Food Chem., 49, 1464.
26. Balasubramanyam, K., Altaf, M., Varier, R.A., Swaminathan, V., Ravindran, A., Sadhale, P.P., Kundu, T.K. 2004, J. Biol. Chem., 279, 33716.
27. Matsumoto, K., Akao, Y., Kobayashi, E., Ito, T., Ohguchi, K., Tanaka, T., Iinuma, M., Nozawa, Y. 2003, Biol. Pharm. Bull., 26, 569.
28. Yoshida, K., Tanaka, T., Hirose, Y., Yamaguchi, F., Kohno, H., Toida, M., Hara, A., Sugie, S., Shibata, T., Mori, H. 2005, Cancer Lett., 221, 29.
29. Tanaka, T., Kohno, H., Shimada, R., Kagami, S., Yamaguchi, F., Kataoka, S., Ariga, T., Murakami, A., Koshimizu, K., Ohigashi, H. 2000, Carcinogenesis, 21, 1183.
30. Pereira, M.A., Barnes, L.H., Rassman, V.L., Kelloff, G.V., Steele, V.E. 1994, Carcinogenesis, 15, 1049.
31. Kohno, H., Tanaka, T., Kawabata, K., Hirose, Y., Sugie, S., Tsuda, H., Mori, H. 2002, Int. J. Cancer., 101, 461.
32. Suzuki, R., Kohno, H., Sugie, S., Sasaki, K., Yoshimura, T., Wada, K., Tanaka, T. 2004, Cancer Lett., 210, 159.
33. Pereira, M.A. 1999, Adv. Exp. Med. Biol., 470, 55.
34. Takami, H., Romsdahl, M.M., Nishioka, K. 1979, Lancet, 2, 912.
35. Seiler, N., Atanassov, C.L., Raul, F. 1998, Int. J. Oncol., 13, 993.
36. Pozharisski, K.M., Tumors of the intestines. In Turusov,V.S. and Mohr,V. (eds) Pathology of Tumors in Laboratory Animals, Vol. 1, IARC Scientific Publications, Lyon, 1990.
37. Koide, T., Sakai, S., Kawada, Y., Hara, A., Sawada, H. 1990, Hinyokika Kiyo., 36, 1103.
38. Bradford, M.M. 1976, Anal. Biochem., 72, 248.
39. Cohen, S.M., Ellwein, L.B. 1990, Science, 249, 1007.
40. Ohnishi, H., Asamoto, M., Tujimura, K., Hokaiwado, N., Takahashi, S., Ogawa, K., Kuribayashi, M., Ogiso, T., Okuyama, H., Shirai, T. 2004, Cancer Sci., 95, 936.
41. Samaha, H.S., Kelloff, G.J., Steele, V., Rao, C.V., Reddy, B.S. 1997, Cancer Res., 57, 1301.
42. Rao, C.V., Rivenson, A., Simi, B., Zang, E., Kelloff, G., Steele, V., Reddy, B.S. 1995, Cancer Res., 55, 1464.
43. Wendum, D., Masliah, J., Trugnan, G., Flejou, J.F. 2004, Virchows Arch., 445, 327.
44. Loft, S., Poulsen, H.E. 1996, J. Mol. Med., 74, 297.

Research Signpost
37/661 (2), Fort P.O., Trivandrum-695 023, Kerala, India



Carcinogenesis and Modification of Carcinogenesis, 2005: 213-227 ISBN: 81-308-0059-4
Editors: Takuji Tanaka and Hiroyuki Tsuda

15

The modifying effects of hesperidin glycoside on chemically-induced tongue and colon carcinogenesis in F344 rats

Takuji Tanaka[1], Hiroyuki Kohno[1], Rikako Suzuki[1,2], Shigeyuki Sugie[1] and Takashi Kometani[3]
[1]Department of Oncologic Pathology, Kanazawa Medical University, 1-1 Daigaku, Uchinada, Ishikawa 920-0293, Japan; [2]Research Fellow of the Japan Society for the Promotion of Science; [3]Biochemical Research Laboratory Ezaki Glico, Co. Ltd., 4-6-5 Utajima, Nishiyodogawa-ku, Osaka 555-8502, Japan

Abstract

A flavonoid hesperidin is reported to inhibit chemically induced mouse and rat carcinogenesis in several organs, such as stomach, tongue, colon, and urinary bladder. We recently synthesized hesperidin glycoside (Hsp-Gn) by cyclodextrin glucanotransferase from hesperidin to improve its solubility. In the current study, we conducted two experiments to investigate the

Correspondence/Reprint request: Dr. Takuji Tanaka, Departments of Oncologic Pathology, Kanazawa Medical University, 1-1 Daigaku, Uchinada, Ishikawa 920-0293, Japan. E-mail: takutt@kanazawa-med.ac.jp

modifying effects of Hsp-Gn on 4-nitroquinoline 1-oxide (4-NQO)-induced tongue tumorigenesis (Exp. 1) and azoxymethane (AOM)-induced colon carcinogenesis (Exp. 2) using male F344 rats. Animals in each experiment were divided into 5 groups: group 1 was given 4-NQO (20 ppm) or AOM (20 mg/kg body weight) alone; groups 2 and 3 were given the carcinogen, and then animals were given the drinking water containing Hsp-Gn (0.1% for group 2 and 1% for group 3); groups 4 was given Hsp-Gn (1%) alone throughout the experiment; and group 5 served as an untreated control. At week 39 of Exp. 1, the incidences of tongue tumors were 100% in group 1 (4-NQO alone group), 60% (P=0.0068) in group 2 (4-NQO→0.1% Hsp-Gn), and 80% in group 3 (4-NQO→1% Hsp-Gn). At week 38 of Exp. 2, the incidences of colonic tumors were 86% in group 1 (AOM alone group), 65% in group 2 (AOM→0.1% Hsp-Gn), and 58% (P=0.0443) in group 3 (AOM→1% Hsp-Gn). Administration of Hsp-Gn in drinking water also decreased the cell proliferation biomarker expression in tongue tissue. In addition, Hsp-Gn exposure elevated the activities of phase II enzymes (glutathione S-transferase and quinone reductase) in both experiments. These results suggest that Hsp-Gn could modify chemically induced tongue and colon carcinogenesis in rats.

Introduction

A flavonoid hesperidin (3'-5,7-trihydroxy-4'-methoxyflavanone 7-rhamnoglucoside) is present in certain vegetables and fruits [1, 2]. Especially, hesperidin is common constituent of citrus fruits and contained in orange juice ranges from 200 to 590 mg/l [3]. It is isolated in large amounts from the discard rinds of the ordinary orange *Citrus aurantium* L.

It is known that hesperidin possesses as certain biological activities including antioxidant property [4], anti-inflammation effect [5], suppression of cell proliferation [6-8], and inhibition of inducible isoforms of cyclooxygenase (COX)-2 and inducible nitric oxide synthase (iNOS) [9]. Our previous studies have shown that hesperidin exerts cancer chemopreventive activity in rat oesophageal [10], oral [11], and colon [6] carcinogenesis and mouse urinary-bladder carcinogenesis [7]. However, the use of hesperidin for chemoprevention study is limited because of the low solubility in aqueous solution. Kometani *et al.* have recently reported that the solubility of hesperidin was greatly improved by transglycosylation, hesperidin mono- and diglucoside each having solubility about 300 times greater than that of hesperidin [12, 13]. Also hesperidin glycoside (Hsp-Gn, Figure 1) can stabilize the color of pigments by absorbing ultraviolet light [14] and prevent the formation of hesperidin crystal which causes turbidity in canned mandarin orange syrup or cloud in clarified mandarin orange juice, in aqueous solutions [15], application of Hsp-Gn is expected for industrial use. As for the biological

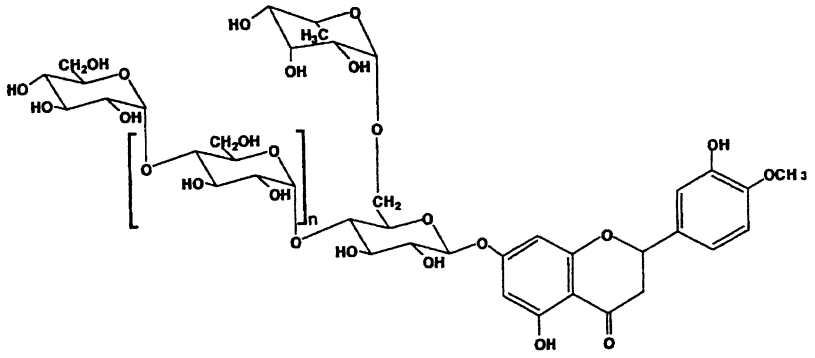


Figure 1. Chemical structure of hesperidin glycoside.

activity of Hsp-Gn, there is no report to our knowledge. However, cancer preventive effect could be expected because of the chemopreventive efficacy of hesperidin in several organs [6, 7, 10, 11].

The oral cancer is relatively uncommon in the developed world, but is common in the developing world [16]. In Japan, although the frequency of oral cancer is not high, the trend in incidence of this cancer is increasing year by year [17]. Tobacco [16, 18, 19], smokeless tobacco [20, 21], and alcohol are considered a contributing agent in development oral cancer [16]. Colon cancer is one of the commonest non-smoking related causes of cancer deaths in the developed countries. In Japan, the incidence and mortality of the colon cancer are increasing [22]. It is partly caused by the progressive introduction of Western dietary habits, especially increased fat intake and reduced dietary fiber intake [23]. Despite the advances in early detection and basic or clinical trials of promising new therapies for both tongue and colorectal cancers, the five year survival has not significantly altered [24, 25]. In this context, primary prevention including chemoprevention against such epithelial malignancies is very important.

In the present study, two experiments were conducted to investigate the modifying effects of Hsp-Gn on 4-nitroquinoline 1-oxide (4-NQO)-induced tongue carcinogenesis (Exp. 1) and azoxymethane (AOM)-initiated colon carcinogenesis (Exp. 2) using male F344 rats. We also examined the influence of Hsp-Gn on cell proliferation activity (ornithine decarboxylase (ODC) activity, polyamine content, and proliferating cell nuclear antigen (PCNA)-labeling index) and detoxification activity (glutathione *S*-transferase (GST) and quinone reductase (QR)) in the target organs, since the agents which can modulate these activities are possible to be chemopreventive agents [26].

Animals, diets, carcinogen, and statistics processing

Male F344 rats (Charles River Japan, Inc., Yokohama, Japan), 5 weeks old, were used for each experiment. All animals were housed in wire cages (3 or 4 rats/cage) under controlled conditions of humidity (50±10%), light (12-h light/dark cycle) and temperature (23±2°C). As a basal diet for modifying effect of Hsp-Gn on tongue and colon tumorigenesis, MF diet (Oriental Yeast Co., Ltd., Tokyo, Japan) and CE-2 (CLEA Japan, Tokyo, Japan) were used, respectively. A tongue carcinogen, 4-NQO, was obtained from Tokyo Kasei Kogyo Co., Ltd. (Tokyo, Japan). AOM, a colon carcinogen, was purchased from Sigma Chemical Co. (St Louis, MO, USA). Hesperidin (hesperetin-7-rhamnbglucoside) was obtained from Sigma Chemical Co. (St.Louis, MO, USA). Hsp-Gn was synthesized using cyclodextrin glucanotransferase (CGTase) [12]. The reaction mixture, which contained 0.25% hesperidin as an acceptor, 5% soluble starch as a donor and 2units/ml of CGTase from an alkalophilic *Bacillus* species, was incubated at 40 ◦C and pH 9.5 for 16h. The composition of the prepared sample for the experiments was 6.0% hesperidin, 7.5% hesperidin monoglucoside, 5.0% hesperidin diglucoside, 3.5% hesperidin triglucoside, 4.0% hesperidin tetraglucoside, 2.0% hesperidin pentaglucoside, and 3.0% hesperidin oligomer (more than hexaglucoside). Drinking water containing Hsp-Gn (0.1 or 1%) and 4-NQO (20 ppm) were prepared on a weekly basis and they were stored in a cold room (<4◦C) until used. Basal diet and experimental drinking water were freely available during the study.

For statistical analysis, the data were analyzed using the Fisher's exact probability test or one-way ANOVA with Bonferroni correction, taking $P<0.05$ as the level of significance.

The modifying effect of Hsp-Gn on tongue carcinogenesis (Exp. 1)

To evaluate the effect of Hsp-Gn on tongue carcinogenesis, a total of 62 male F344 rats were divided into five groups (Figure 2). Rats of groups 1 through 3 received 20 ppm 4-NQO in drinking water for 9 weeks to induce tongue neoplasms. Groups 2 and 3 were given the drinking water that contained 0.1% or 1% Hsp-Gn for 29 weeks, starting 1 week after cessation of 4-NQO exposure. Group 4 was given the drinking water containing 1% Hsp-Gn throughout the experiment. Group 5 served as an untreated control. At the termination of the study (39 weeks), all organs including tongue were carefully inspected for the presence of pathological lesions. The tongue of all rats was longitudinally cut into halves for histopathological and immunohistochemical examinations. For histological examination, tissues and gross lesions were fixed in 10% buffered formalin, embedded paraffin blocks, and stained with

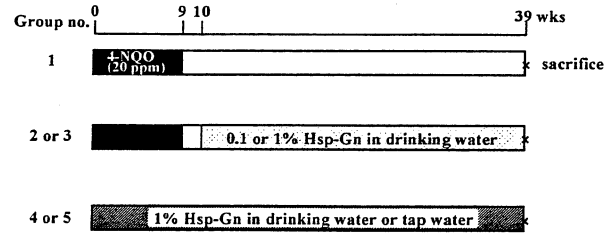


Figure 2. Experimental protocol for the modifying effect of Hsp-Gn on tongue tumorigenesis.

hematoxylin and eosin. Tongue lesions (hyperplasia, dysplasia, and neoplasms) were diagnosed according to the criteria described by Kramer *et al.* [27].

During the study, no clinical signs of toxicity were present in any groups. Tongue squamous cell tumors (papilloma and carcinoma) and dysplasia developed in the posterior tongue (dorsal region) of rats treated with 4-NQO (groups 1-3). No preneoplastic and neoplastic lesions in any organs, including tongue, were present in groups 4 and 5. The mean body weight and liver weight were insignificant among the groups (data not shown).

The incidence and multiplicity of tongue neoplasms are given in Figure 3. The incidence of total tongue tumors found in rats received 0.1% Hsp-Gn after 4-NQO exposure (group 2, 60%, P=0.0068) was significantly lower than the 4-NQO alone group (group 1, 100%). The incidences of tongue papilloma were 50% in group 1, 7% in group 2, and 20 % in group 3 (4-NQO→1% Hsp-Gn).

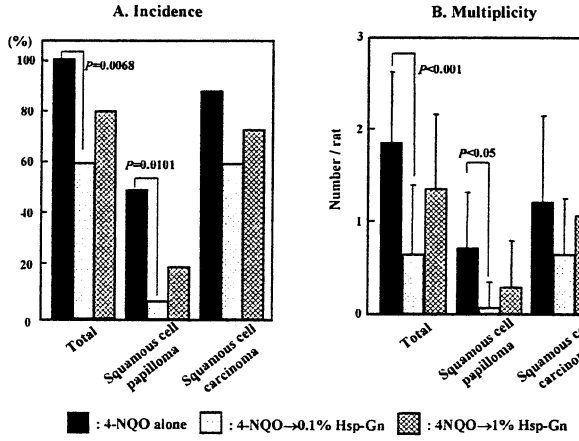


Figure 3. Incidence and multiplicity of tongue tumors.

Statistical analysis revealed a significant reduction in the incidence of tongue papilloma in rats of group 2 (P=0.0101), when compared with that in group 1. Also, significant reduction in the multiplicity of total tumors (0.71±0.61, P<0.001) and squamous cell papilloma (0.07±0.27, P<0.05) were found in group 2. Although the incidence and multiplicity of squamous cell carcinoma developed in rats of groups 2 and 3 were reduced, the differences were insignificant. Besides these neoplasms, a number of severe dysplasia, which is considered to be preneoplastic lesions for tongue cancer, were also present in the tongue of rats in groups 1-3 (Figure 4). The incidence of tongue severe dysplasia in groups 2 (47%, P=0.0193) and 3 (53%, P=0.0437) were significantly smaller than that in group 1 (88%).

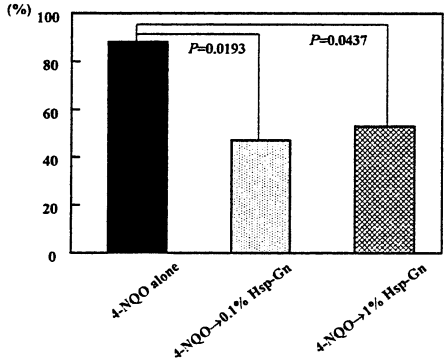


Figure 4. Incidence of tongue severe dysplasia.

For determination of ODC activity and polyamine level in the tongue, we followed the method by Calhoun *et al.* [28] and Koide *et al.* [29], respectively. PCNA-positive index was determined as described previously [30]. The expression of cell proliferation biomarkers of tongue epithelium are presented in Figure 5. Cell proliferation activity was suppressed by Hsp-Gn exposure in drinking water without significant difference. The PCNA-labeling index in group 1 (22±3%, P<0.05) was significantly greater than that in group 5 (14±4%). To assess whether Hsp-Gn can modify GST and QR activities in tongue, mucosal scrapings of the tongue were processed to obtain the cytosolic fraction [31]. Enzymes activities were determined by previously method [30]. Figure 6 summarizes GST and QR activities in the tongue tissue. Administration of Hsp-Gn after 4-NQO exposure (groups 2 and 3) slightly increased the tongue GST activitvity, when compared with that of group 1. The QR activities of groups 2 and 3 were decreased when compared with group 1 although statistical differences were not found.

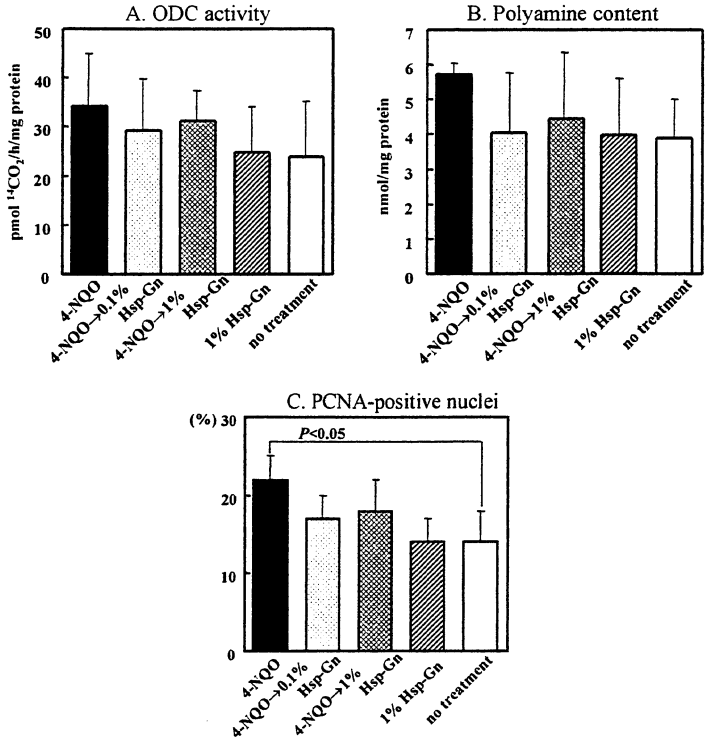
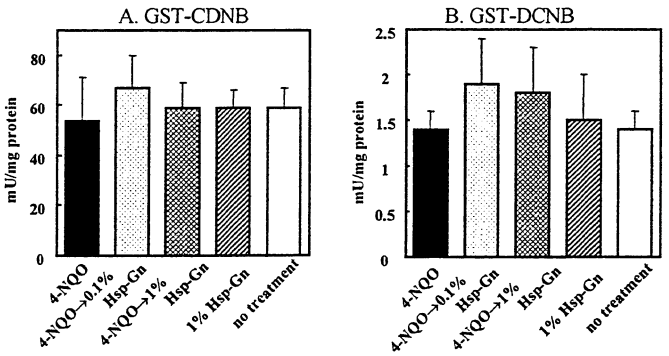


Figure 5. Ornithine decarboxylase (ODC) activity, polyamine content, and proliferating cell nuclear antigen (PCNA)-labeling index in the tongue.

Figure 6.



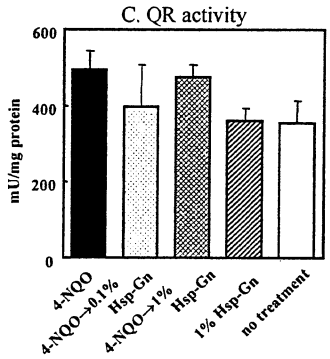


Figure 6. Glutathione *S*-transferase (GST) and quinone reductase (QR) activity in the tongue.

The modifying effect of Hsp-Gn on colon carcinogenesis (Exp. 2)

In the first, we investigated the inhibitory effect of Hsp-Gn on rat colonic aberrant crypt foci (ACF), which are putative precursor lesions for colon cancer in rodents [32] and human [33]. Short-term bioassay of ACF was frequently used for screening compound with possible colonic cancer chemopreventive ability. Subsequently, a long-term bioassay was performed to confirm and evaluate the preventive effects of Hsp-Gn on AOM-induced colon carcinogenesis.

In a pilot study for ACF bioassay, rats were divided into 5 groups as shown in Figure 7A. Groups 1-3 were initiated with AOM by two weekly subcutaneous injections at a dose of 20 mg/kg body weight. Rats of groups 2 and 3 were given drinking water containing Hsp-Gn at 0.1 or 1% throughout the experiment. Group 4 was given drinking water containing 1% Hsp-Gn alone during the experiment. Group 5 served as an untreated control. At Week 4, rats were killed to count colonic ACF. At autopsy, the colons were flushed with saline, excised, cut open longitudinally along the main axis and then washed again with saline. The colons were cut into three sections (~4 cm each) starting from the anus, placed between filter papers to reduce mucosal folding and fixed in 10% buffered formalin for at least 24 h. Fixed colonic sections were dipped in a 0.2% solution of methylene blue in distilled water for 30 s and briefly rinsed with distilled water. Using a light microscope at a magnification of ×40, ACF were distinguished from surrounding normal crypts by their large size, more prominent epithelial cells and increased pericryptal space. At the end of the study (Week 4), there was a significant difference in

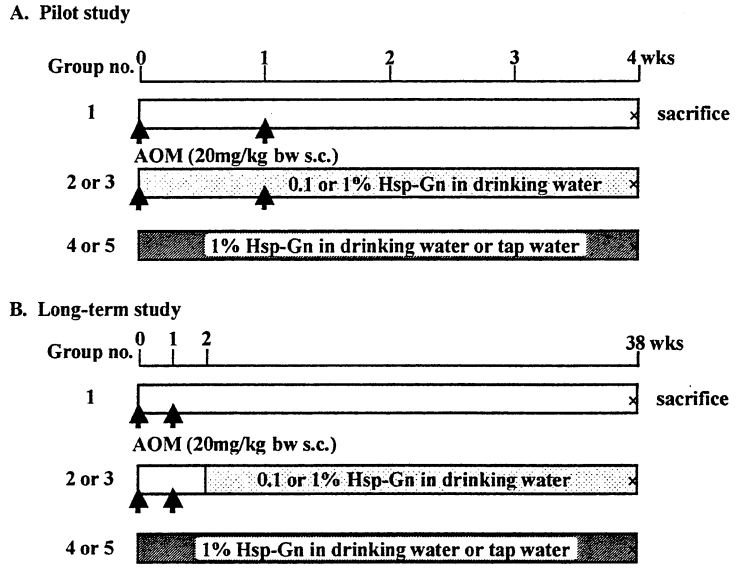


Figure 7. Experimental protocol for the modifying effect of Hsp-Gn on colon tumorigenesis.

mean body weights between groups 4 (171±7 g, $P<0.001$) and 5 (208±9 g). The mean liver weights were not significantly different among the groups. The mean daily intakes of drinking water in any groups had no significant differences. During the study, no clinical signs of toxicity were observed in any groups. Histologically, there were no toxic changes in the liver, kidneys, lung and heart of the rats in any groups. As indicated in Table 1, the total number of ACF/colon, the total number of aberrant crypts /colon, the number of aberrant crypts/focus, and the number of ACF consisting of more than 4 crypts in rats received both doses of Hsp-Gn were significantly lower ($P<0.001$) than that in the AOM alone group (group 1). According to the method by Habig *et al.* [34], we assayed the GST activity of large intestine (Figure 8). The GST activity (mu/mg protein) in rats exposed 1% Hsp-Gn after AOM injection (111±21, $P<0.05$) was significant increased when compared with group 1 (79±10).

For the long-term study (Figure 7B) to confirm the results from an ACF bioassay, rats were randomly divided into 5 groups. Groups 1-3 were initiated with AOM by two weekly subcutaneous injections at a dose of 20 mg/kg body weight. Rats of groups 2 and 3 were given drinking water containing 0.1 and 1% Hsp-Gn, respectively for 36 weeks, starting 1 week after the last dosing of AOM. Group 4 was given drinking water containing 1% Hsp-Gn for 38 weeks.

Table 1. Effect of Hsp-Gn on AOM-induced ACF Formation in Male F344 Rats.

Group no.	Treatment (no. of rats examined)	Incidence (%)	Total no. of ACF*/colon	Total no. of ACs**/colon	No. of ACs/focus	No. of ACF consisted of 4 or more ACs
1	AOM alone (8)	8/8 (100%)	115±23[a]	297±64	2.60±0.15	27±5
2	AOM→0.1% Hsp-Gn (7)	7/7 (100%)	55±21[b]	119±41[b]	2.18±0.11[b]	5±2[b]
3	AOM→1% Hsp-Gn (7)	7/7 (100%)	44±13[b]	100±35[b]	2.24±0.17[b]	6±3[b]
4	1% Hsp-Gn (4)	0/4 (0%)	0	0	0	0
5	No treatment (4)	0/4 (0%)	0	0	0	0

*ACF, aberrant crypt foci; **ACs, aberrant crypts.

[a]Mean ±SD.

[b]Significantly different from group 1 ($P<0.001$).

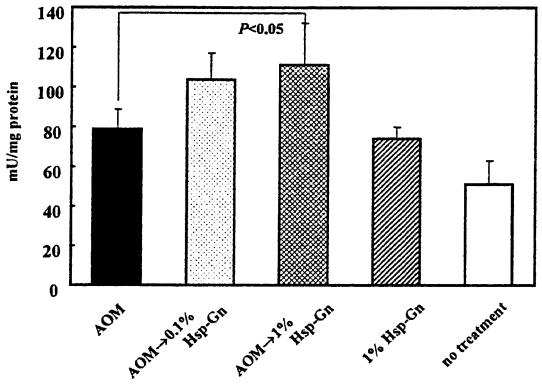


Figure 8. Effect of Hsp-Gn on glutathione *S*-transferase (GST) activity in the large intestine in rats.

Group 5 served as an untreated control. All animals were sacrificed at Week 38 by an ether overdose to assess the incidences of large bowel tumors, kidney mesenchymal tumors and altered liver cell foci. At autopsy, the intestine was excised, opened longitudinally, flushed clean with saline and examined for the presence of tumors. Colons, kidney and liver were fixed in 10% buffered formalin and then processed for histopathological examination by conventional methods. Neoplasms in the intestine were diagnosed according to the criteria described by Pozharisski [35].

As in the case of the pilot study (ACF bioassay), the daily drinking intake among the groups also did not differ in the long-term bioassay. In addition,

drinking administration of the test compound did not cause any clinical signs of toxicity, low survival or poor clinical condition. At the end of the study, the body weight of rats received 0.1% Hsp-Gn after AOM exposure (group 2, 362±17 g, $P<0.05$) was significantly heavier than AOM alone group (group 1, 345±18 g, Figure 9A). The liver weights of group 1 (12.4±1.1 g, $P<0.001$) and Hsp-Gn alone group (group 4, 12.4±0.8 g, $P<0.001$) were statistically higher than that of no treatment group (group 5, 10.0±1.0 g, Figure 9B). Macroscopically, most intestinal tumors developed in the large intestine (mainly the middle and distal colon) and some in the small intestine of rats in groups 1-3. They were sessile or pedunculated tumors histologically diagnosed as tubular adenomas, tubular adenocarcinomas or mucinous carcinomas, with a higher incidence of tubular adenocarcinoma. Animals of groups 4 and 5 did not have neoplasms in any organs, including the intestines. The incidence and multiplicity of large bowel neoplasms are shown in Figure 10. The incidence of colonic adenoma in groups 2 (35%, 7 of 20 rats, $P=0.0155$) and 3 (32%, 6 of 19 rats, $P=0.0288$) were statistically higher than group 1 (5%, 1 of 22 rats). The incidences of total colonic tumor and adenocarcinoma in group 3 (total tumor, 58%, 11 of 19 rats, $P=0.0443$; and adenocarcinoma, 47%, 9 of 19 rats, $P=0.0228$) were significantly lower than those of group 1 (total tumor, 86%, 19 of 22 rats; and adenocarcinoma, 82%, 18 of 22 rats). As for the multiplicity, the value of adenoma in group 2 (0.45±0.69, $P<0.05$) was statistically higher than that of group 1 (0.05±0.21).

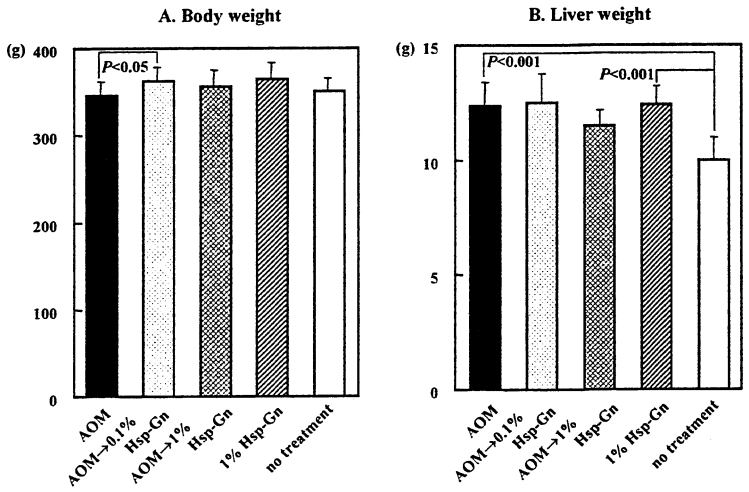


Figure 9. Body and Liver weights at the end of the long-term study.

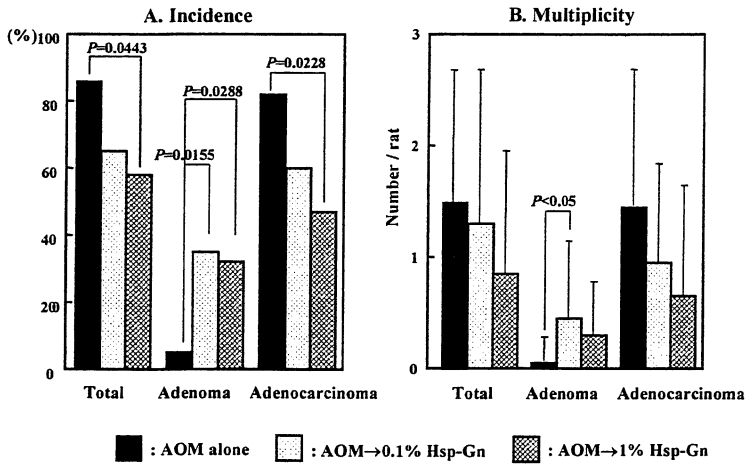


Figure 10. Incidence and multiplicity of colon tumors.

Discussion

We described here cancer chemopreventive ability of Hsp-Gn in experimental rat carcinogenesis models of tongue and colon when Hsp-Gn was administrated to rats after the carcinogen exposure. Hsp-Gn used in the present study contained 24% glycosides, 6 % hesperidin, and 70% cyclodextrin. Cyclodextrins are cyclic oligomers of glucose that can form water-soluble inclusion complexes with small molecules and portions of large compounds, and used in a variety of food because of its lack of toxicity [36]. As far as we know, cyclodextrin has no carcinogenic action. Inhibitory effects of Hsp-Gn on tongue and colon tumors development in the current study may come from its glycosides.

Oral cavity is the only route for ingesting food, and thus the most important factor in defining the oral uptake of food should be its absorbability across the intestinal epithelium. Previously we confirmed that Hsp-Gn permeate across Caco-2 cell monolayers, which is extensively used as a good model for intestinal epithelial cells [37]. Also we found that glycosylated hesperidin could be absorbed in intestinal tract of mice (unpublished data).

In the present study, the degree of inhibition activity in carcinogenesis depended on the dose of Hsp-Gn. In tongue tumorigenesis, a low dose (0.1%) of Hsp-Gn exerted more effective suppression activity than a high dose (1%). Lower dose of this material (<0.1%) might show stronger preventive efficacy against tongue tumor development. In contrast, the frequency of colon tumors was decreased in rats given a high dose of Hsp-Gn. These results suggested that Hsp-Gn has a different optimal dose for each cancer type.

Pathologically, carcinogenesis has multi-step processes that neoplastic changes evolve over a period of time due to the accumulation of somatic mutations in a single cell, resulting in phenotypic progression from normal to hyperplastic to dysplastic, and finally, to fully malignant phenotypes [38, 39]. Hsp-Gn effectively reduced the frequencies of dysplasia and squamous cell papilloma, but not carcinoma in the tongue. On the other hand, occurrence of ACF and colonic adenocarcinoma was efficiently suppressed by administration of Hsp-Gn. These results suggested that Hsp-Gn might prevent different process of carcinogenesis in different type of cancer.

Although the exact mechanisms involved in the suppressing effects of 4-NQO-induced tongue carcinogenesis and AOM-induced colon tumorigenesis by administration of Hsp-Gn is not fully known, several mechanisms could be considered. Phase II enzymes such as GST and QR have a central role in the detoxification of activated metabolites of procarcinogens produced by phase I reactions. Thus, phase II detoxifying enzyme inducers might have possibility of chemopreventive agents against cancer development [40]. In the current study, administration of Hsp-Gn elevated GST activity in both tongue and large intestine, however influence on QR activity was slight. These results suggested that the increase in GST activity has stronger relationship with the inhibitory effect of Hsp-Gn on tumor development.

Cell proliferation has long been suspected to play a significant role in the initiation step as well as the promotion/progression of carcinogenesis [41]. In the current examination, ODC activity, polyamine content, and PCNA-labeling index in the tongue were reduced by administration of Hsp-Gn after 4-NQO exposure. Thus, the inhibitory effect of Hsp-Gn might be, in part, due to the modification of cell proliferation activity. Decreasing effect of hesperidin on cell proliferation was reported in chemically induced carcinogenesis in urinary-bladder [7], colon [6], oesophageal [10], and oral cavity [11]. Hsp-Gn might be expected to have the biological activity similar to that of hesperidin. Recently we found that hesperidin attenuates lipopolysaccharide-induced over-expression of COX-2 and iNOS protein in mouse macrophage cells [9]. Chemically-induced rat tongue carcinogenesis was reduced by inhibition of iNOS and/or COX-2 expression [42]. The expression of enzymes such as iNOS and COX-2 were also reported to be elevated in colonic cancer of human [43, 44] and rodents [45, 46]. Although we did not determine the expression of these enzymes in the current study, Hsp-Gn might reduce the expression of these enzymes in the target organs.

In summary, the results described here may suggest that Hsp-Gn could reduce the chemically-induced tongue and colonic tumorigenesis. The modulatory effects of Hsp-Gn might be partly caused through multiple mechanisms including the alteration of cell proliferation activity and detoxification enzyme activity in the target organs. Although further

investigations including mechanistic studies and chemopreventive investigations in other organs are warranted to fully evaluate the efficacy of this material as a cancer chemopreventive agent, we hope the practical use of Hsp-Gn in clinical trials in the near future.

Acknowledgements

This work was supported in part by the Grant-in-Aid for Cancer Research, for the Third-Term Comprehensive 10-Year Strategy for Cancer Control from the Ministry of Health, Labour and Welfare of Japan; the Grants-in-Aid (nos. 15592007 and 15·2052) for Scientific Research from the Ministry of Education, Culture, Sports, Science and Technology of Japan; the grant (C2004-4) for the Collaborative Research from Kanazawa Medical University; and the grant (H2004-6) for the Project Research from the High-Technology Center of Kanazawa Medical University.

References

1. Justesen, U., Knuthsen, P., Leth, T. 1998, J. Chromatogr., A 799, 101.
2. Nielsen, S.E., Freese, R., Klemola, P., Mutanen, M. 2002, Cancer Epidemiol. Biomarkers Prev., 11, 459.
3. Tomas-Barberan, F.A., Clifford, M.N. 2000, J. Sci. Fd. Agric., 80, 1073.
4. Tirkey, N., Pilkhwal, S., Kuhad, A., Chopra, K. 2005, BMC Pharmacol., 5, (in press).
5. Guardia, T., Rotelli, A.E., Juarez, A.O., Pelzer, L.E. 2001, Farmaco., 56, 683.
6. Tanaka, T., Makita, H., Kawabata, K., Mori, H., Kakumoto, M., Satoh, K., Hara, A., Sumida, T., Tanaka, T., Ogawa, H. 1997, Carcinogenesis, 18, 957.
7. Yang, M., Tanaka, T., Hirose, Y., Deguchi, T., Mori, H., Kawada, Y. 1997, Int. J. Cancer, 73, 719.
8. Zhang, M., Zhang, J.P., Ji, H.T., Wang, J.S., Qian, D.H. 2000, Acta. Pharmacol. Sin., 21, 253.
9. Sakata, K., Hirose, Y., Qiao, Z., Tanaka, T., Mori, H. 2003, Cancer Lett., 199, 139.
10. Tanaka, T., Makita, H., Kawabata, K., Mori, H., Kakumoto, M., Satoh, K., Hara, A., Sumida, T., Fukutani, K., Tanaka, T., Ogawa, H. 1997, Carcinogenesis, 18, 761.
11. Tanaka, T., Makita, H., Ohnishi, M., Mori, H., Satoh, K., Hara, A., Sumida, T., Fukutani, K., Tanaka, T., Ogawa, H. 1997, Cancer Res., 57, 246.
12. Kometani, T., Terada, Y., Nishimura, T., Takii, H., Okada, S. 1994, Biosci. Biotechol. Biochem., 58, 1990.
13. Kometani, T., Nishimura, T., Nakae, T., Takii, H., Okada, S. 1996, Biosci. Biotechnol. Biochem., 60, 645.
14. Nishimura, T., Kometani, T., Okada, S., Kobayashi, Y., Fukumoto, S. 1998, Nippon Shokuhin Kagaku Kaishi, 45, 186.
15. Terada, Y., Kometani, T., Nishimura, T., Takii, H., Okada, S. 1995, Food. Sci. Technol. Int., 1, 29.
16. Das, B.R., Nagpal, J.K. 2002, Med. Sci. Monit., 8, 258.
17. Ioka, A., Tsukuma, H., Ajiki, W., Oshima, A. 2005, Jpn. J. Clin. Oncol., 35, 45.
18. Petersen, P.E. 2003, Oral Health Prev. Dent., 1, 309.

19. Taybos, G. 2003, Am. J. Med. Sci., 326, 189.
20. Rai, R., Kulkarni, V., Saranath, D. 2004, Oral Oncol., 40, 1033.
21. Johnson, G.K., Squier, C.A. 1993, Pediatr. Dent., 15, 169.
22. Bosetti, C., Malvezzi, M., Chatenoud, L., Negri, E., Levi, F., La Vecchia, C. 2005, Int. J. Cancer, 113, 339.
23. Williams, G.M., Williams, C.L., Weisburger, J.H. 1999, Toxicol. Sci., 52, 72.
24. Silverman, S.J. 2001, J. Am. Dent. Assoc., 132, 7S.
25. Chung-Fayem, G.A., Kerr, D.J. 2000, B.M.J., 321, 1397.
26. Tsuda, H., Ohshima, Y., Nomoto, H., Fujita, K., Matsuda, E., Iigo, M., Takasuka, N., Moore, M.A. 2004, Drug Metab. Pharmacokinet., 19, 245.
27. Kramer, I.R., Lucas, R.B., Pindborg, J.J., Sobin, L.H. 1978, Oral Surg. Oral Med. Oral Pathol., 46, 518.
28. Calhoun, K.H., Stanley, D., Stiernberg, C.M., Ahmed, A.E. 1989, Arch. Otolaryngol. Head Neck Surg., 115, 484.
29. Koide, T., Sakai, S., Kawada, Y., Hara, A., Sawada, H. 1990, Hinyokika Kiyo., 36, 1103.
30. Tanaka, T., Kawabata, K., Kohno, H., Honjo, S., Murakami, M., Ota, T., Tsuda, H. 2000, Jpn. J. Cancer Res., 91, 25.
31. Tanaka, T., Makita, H., Kawabata, K., Mori, H., El-Bayoumy, K. 1997, Cancer Res., 57, 3644.
32. Bird, R.P. 1995, Cancer Lett., 93, 55.
33. Pretlow, T.P., Barrow, B.J., Ashton, W.S., O'Riordan, M.A., Pretlow, T.G., Jurcisek, J.A., Stellato, T.A. 1991, Cancer Res., 51, 1564.
34. Habig, W.H., Pabst, M.J., Jakoby, W.B. 1974, J. Biol. Chem., 249, 7130.
35. Pozharisski, K.M., Tumors of the intestines. In Turusov,V.S. and Mohr,V. (eds) Pathology of Tumors in Laboratory Animals, Vol. 1, IARC Scientific Publications, Lyon, 1990.
36. Eastburn, S.D., Tao, B.Y. 1994, Biotechnol. Adv., 12, 325.
37. Kim, M., Kometani, T., Okada, S., Shimuzu, M. 1999, Biosci. Biotechnol. Biochem., 63, 2183.
38. Califano, J., Leong, P.L., Koch, W.M., Eisenberger, C.F., Sidransky, D., Westra, W.H. 1999, Clin. Cancer Res., 5, 1862.
39. Potter, J.D. 1999, J. Natl. Cancer Inst., 91, 916.
40. Wilkinson, J.t., Clapper, M.L. 1997, Proc. Soc. Exp. Biol. Med., 216, 192.
41. Cohen, S.M., Ellwein, L.B. 1990, Science., 249, 1007.
42. Yoshida, K., Tanaka, T., Kohno, H., Sakata, K., Kawamori, T., Mori, H., Wakabayashi, K. 2003, Histol. Histopathol., 18, 39.
43. Ambs, S., Merriam, W.G., Bennett, W.P., Felley-Bosco, E., Ogunfusika, M.O., Oser, S.M., Klein, S., Shields, P.G., Billiar, T.R., Harris, C.C. 1998, Cancer Res., 58, 334.
44. Eberhart, C.E., Coffey, R.J., Radhika, A., Giardiello, F.M., Ferrenbach, S., DuBois, R.N. 1994, Gastroenterology, 107, 1183.
45. Takahashi, M., Fukuda, K., Ohata, T., Sugimura, T., Wakabayashi, K. 1997, Cancer Res., 57, 1233.
46. Takahashi, M., Mutoh, M., Kawamori, T., Sugimura, T., Wakabayashi, K. 2000, Carcinogenesis, 21, 1319.

Int. J. Cancer: **118,** 25–34 (2006)
© 2005 Wiley-Liss, Inc.

Dextran sodium sulfate strongly promotes colorectal carcinogenesis in $Apc^{Min/+}$ mice: Inflammatory stimuli by dextran sodium sulfate results in development of multiple colonic neoplasms

Takuji Tanaka[1*], Hiroyuki Kohno[1], Rikako Suzuki[1], Kazuya Hata[2], Shigeyuki Sugie[1], Naoko Niho[3], Katsuhisa Sakano[3], Mami Takahashi[3] and Keiji Wakabayashi[3]

[1]*Department of Oncologic Pathology, Kanazawa Medical University, Uchinada, Ishikawa, Japan*
[2]*BMR Laboratories, Sunplanet Co., Ltd., Kamiishidu, Gifu Japan*
[3]*Cancer Prevention Basic Research Project, National Cancer Center Research Institute, Chuo-ku, Tokyo, Japan*

The mouse model for familial adenomatous polyposis, $Apc^{Min/+}$ mouse, contains a truncating mutation in the *Apc* gene and spontaneously develops numerous adenomas in the small intestine but few in the large bowel. Our study investigated whether dextran sodium sulfate (DSS) treatment promotes the development of colonic neoplasms in $Apc^{Min/+}$ mice. $Apc^{Min/+}$ and $Apc^{+/+}$ mice of both sexes were exposed to 2% dextran sodium sulfate in drinking water for 7 days, followed by no further treatment for 4 weeks. Immunohistochemistry for cyclooxygenase-2, inducible nitric oxide synthase, β-catenin, p53, and nitrotyrosine, and mutations of β-*catenin* and K-*ras* and loss of wild-type allele of the *Apc* gene in the colonic lesions were examined. Sequential observation of female $Apc^{Min/+}$ mice that received DSS was also performed up to week 5. At week 5, numerous colonic neoplasms developed in male and female $Apc^{Min/+}$ mice but did not develop in $Apc^{+/+}$ mice. Adenocarcinomas developed in $Apc^{Min/+}$ mice that received DSS showed loss of heterozygosity of *Apc* and no mutations in the β-*catenin* and K-*ras* genes. The treatment also significantly increased the number of small intestinal polyps. Sequential observation revealed increase in the incidences of colonic neoplasms and dysplastic crypts in female $Apc^{Min/+}$ mice given DSS. DSS treatment increased inflammation scores, associated with high intensity staining of β-catenin, cyclooxygenase-2, inducible nitric oxide synthase and nitrotyrosine. Interestingly, strong nuclear staining of p53 was specifically observed in colonic lesions of $Apc^{Min/+}$ mice treated with DSS. Our results suggest a strong promotion effect of DSS in the intestinal carcinogenesis of $Apc^{Min/+}$ mice. The findings also suggest that strong oxidative/nitrosative stress caused by DSS-induced inflammation may contribute to the colonic neoplasms development.
© *2005 Wiley-Liss, Inc.*

Key words: $Apc^{Min/+}$; mice; dextran sodium sulfate; colon carcinogenesis; p53; nitrotyrosine

Carcinogenesis and inflammation are pathological consequences of injury and repair at the cellular and molecular levels[1,2] and are influenced by several life style factors, including dietary factors.[3] Recent studies suggest inflammation in enhancing the risk of various types of cancer[2] including colon cancer.[4] In fact, individuals suffering with inflammatory bowel disease (IBD) are at high risk of developing colon cancer.[5,6] We recently proposed a novel mouse colon carcinogenesis model and demonstrated the powerful tumor-promoting effects of dextran sodium sulfate (DSS), which can induce colonic mucosal inflammation, resembling the histopathology of one of the IBD ulcerative colitis (UC),[7] on colon carcinogenesis initiated with azoxymethane (AOM),[8–10] 1,2-dimetylhydrazine (DMH)[11] or heterocyclic amines (HCAs)[12] in mice. Thus, inflammation/inflammatory stimuli induced by a short-term (for a week) treatment with 2% DSS in drinking water after initiation with a low-dose of carcinogens is effective for rapid induction of colon neoplasms possessing β-catenin gene mutations in mice.[11,12] Similarly, Cooper *et al.*[13] found that inflammation plays an important role in the dysplasia-cancer sequence in the colon. They also reported the development of colon cancer in 60-day-old $Apc^{Min/+}$ mice that received 4% DSS alone.[14] In addition, Barbour *et al.*[15] suggested that a relationship between chronic inflammation and small intestinal tumorigenesis in $Apc^{Min/+}$ mice.

Cyclooxygenase (COX)-2 and inducible nitric oxide synthase (iNOS) play an important role in colon tumor growth and progression. COX catalyzes the committed step in the conversion of arachidonic acid to protumorigenic eicosanoids, such as prostaglandin E_2, which are involved in the maintenance of tumor integrity.[16] COX-2 is frequently undetectable in normal tissues but is induced by cytokines, growth factors, reactive oxygen species and tumor promoters.[17] Gene expression of COX-2 is upregulated in 80–85% of human colonic adenocarcinomas,[18] in colonic tumors induced by AOM in rodents[19] and in 80–85% of $Apc^{Min/+}$ mouse adenomas.[20] Nitric oxide (NO) is endogenously produced by a family of enzymes. NO is reported to cause mutagenesis[21] and DNA deamination,[22] and is implicated in the inflammatory responses and in the production of vascular endothelial growth factor.[23] Several studies also report that iNOS is up-regulated in human cancers, including colon cancer[24,25] and in AOM-induced colon tumors in rodents.[26] In addition, one study reported that iNOS inhibitors suppress the development of AOM-induced aberrant crypt foci in rats.[27] Although the role of iNOS plus NO and related radical species in intestinal polyposis is still controversial,[28,29] NO/iNOS may be involved in intestinal tumorigenesis.[30–33] The interaction between iNOS and p53 as a crucial pathway in inflammatory-mediated carcinogenesis is also suggested.[34] An increased cancer risk occurs in the tissues undergoing chronic inflammation.[35] Thus, NO is a candidate free radical, and the *p53* tumor suppressor gene is a candidate molecular target.[36]

Familial adenomatous polyposis (FAP) is an inherited form of human colon cancer characterized by the development of 100–1,000 adenomas in the large intestine.[37] If not removed, these benign epithelial neoplasms inevitably progress to carcinomas.[37] FAP can be caused by germline mutations in the adenomatous polyposis coli (*APC*) tumor suppressor gene.[38] Min mice were a germline mutation in the *Apc* gene and develop multiple polyps in the intestine.[39] *Apc*-deficient mice including Min mice are considered to be good models of FAP and have been used for investigating the influence of environmental factors, such as dietary factors, carcinogens, chemopreventive agents and other xenobiotics.[40] However, unfortunately, unlike human FAP, most of the neo-

Abbreviations: AOM, azoxymethane; APC, adenomatous polyposis coli; COX, cyclooxygenase; DMH, 1,2-dimethylhydrazine; DSS, dextran sodium sulfate; FAP, familial adenomatous polyposis; H&E, hematoxylin and eosin; HCAs, heterocyclic amines; IBD, inflammatory bowel disease; iNOS, inducible nitric oxide synthase; LOH, loss of heterozygosity; NO, nitric oxide; UC, ulcerative colitis.

Grant sponsor: Ministry of Health, Labour and Welfare of Japan; Grant sponsor: Ministry of Education, Culture, Sports, Science and Technology of Japan; Grant number: 15592007; Grant sponsor: Kanazawa Medical University; Grant number: C2004-4; Grant sponsor: High-Technology Center of Kanazawa Medical University; Grant number: H2004-6.
***Correspondence to:** Fax: +81-76-826-6926.
E-mail: takutt@kanazawa-med.ac.jp
Received 9 February 2005; Accepted after revision 26 April 2005
DOI 10.1002/ijc.21282
Published online 27 July 2005 in Wiley InterScience (www.interscience.wiley.com).

Publication of the International Union Against Cancer
global cancer control

plasms occur predominantly in the small intestine of these genetically altered mice. Yamada *et al.*[41] recently reported that a number of adenomatous lesions together with a few tumors are present in the colon of old $Apc^{Min/+}$ mice. The finding suggests the presence of precursor cryptal lesions for colonic epithelial malignancies and the possibility of progression of the lesions to epithelial neoplasms under appropriate experimental conditions. Mutations of several genes, including *Apc*, β-*catenin*, K-*ras*, *DCC*, *p53* and alterations proteins' expression, such as COX-2, β-catenin, iNOS and Wnt/Apc/β-catenin signaling, play important roles in both chemically induced colon carcinogenesis and human cancer development.[33] Thus, colon carcinogenesis is characterized by a succession of molecular changes involving basic cellular process such as cell proliferation, cell signaling and DNA integrity, but it is poorly understood what sifts the balance between them, causing a cryptal cell to lose its normal phenotype. Such knowledge could be crucial for the first step in fighting colon cancer development.

In our study, we investigated whether acute inflammation induced by DSS enhances small and large intestinal carcinogenesis in $Apc^{Min/+}$ mice. Mutational analysis of β-*catenin* and K-*ras* genes and immunohistochemical analysis of Apc, β-catenin, COX-2, iNOS and p53 expression were also performed in the colonic neoplasms. The immunohistochemistry of nitrotyrosine, a good marker for oxidative stress caused by inflammation,[42] was performed on the colonic mucosa of mice given DSS. In addition, sequential pathological alteration of the large intestines of female $Apc^{Min/+}$ mice exposed to DSS was investigated to test our hypothesis that inflammation induced by DSS promotes the growth of the early colonic cryptal lesions, dysplastic aberrant crypt foci[43] or adenomatous lesions[41] and the treatment resulted in the high frequency of colonic neoplasms in the short-term (5 weeks).

Material and methods

Animals, chemicals and diets

Male and female C57BL/6J $Apc^{Min/+}$ and $Apc^{+/+}$ mice aged 3 weeks were obtained from The Jackson Laboratory (Bar Harbor, ME). Mice were genotyped to identify carriers of the *Min* allele of *Apc* with a PCR assay as described.[44] They were housed in plastic cages (4 or 5 mice/cage) under controlled conditions of humidity (50 ± 10%), light (12/12 hr light/dark cycle) and temperature (23 ± 2°C). Drinking water and a pelleted basal diet, CE-2 (CLEA Japan, Inc., Tokyo, Japan) were available *ad libitum*. They were quarantined for 7 days after arrival and then randomized by body weights into experimental and control groups. DSS with a molecular weight of 40,000 was purchased from ICN Biochemicals, Inc. (Aurora, OH).

Experimental procedure

Forty-seven $Apc^{Min/+}$ mice (16 males and 31 females) and 50 $Apc^{+/+}$ mice (29 males and 21 females) were used. Animals of the experimental groups were given 2% (w/v) DSS in drinking water for 1 week, starting 4 weeks of age. The control group (9 male and 10 female $Apc^{Min/+}$ mice, and 17 male and 11 female $Apc^{+/+}$ mice) were given the tap water without DSS throughout the experiment. Among them, 14 female $Apc^{Min/+}$ mice exposed to 2% DSS were sequentially sacrificed at weeks 2 (4 mice), 3 (5 mice) and 4 (5 mice) to monitor the pathological alterations in the large intestine. All the remaining animals were sacrificed at week 5. At sacrifice, all organs were removed, and the small and large intestines were cut open along their longitudinal axis, and fixed flat in 10% buffered formalin for 24 hr at room temperature after macroscopic inspection. Longitudinal sections of the large intestine were made, and then processes for histopathological examination were performed by routine procedures. Small intestine was divided into 3 equal segments (proximal, middle and distal parts), the number and distribution were determined under a dissecting microscope Nikon SMZ1000 (Nikon Co., Tokyo, Japan). After counting, cross sections of the small intestine were made at 2 mm intervals and processed for histopathological evaluation of the polyps by routine procedures. Histological examination was performed on hematoxylin and eosin (H&E)-stained sections. On H&E-stained sections, histological alterations, such as mucosal dysplasia and colonic tumors, were examined. Colonic mucosal dysplasia was diagnosed according to the criteria described by Paulsen *et al.*[43] Colonic tumors were diagnosed according to the description by Ward.[45]

Scoring of inflammation in the intestinal mucosa

Mucosal inflammation with or without ulceration in the entire intestine was analyzed on H&E-stained sections. Small and large intestinal inflammation with or without mucosal ulceration was graded according to the following morphological criteria described by Cooper *et al.*:[46] grade 0, normal appearance; grade 1, shortening and loss of the basal 1/3 of the actual crypts with mild inflammation in the mucosa; grade 2, loss of the basal 2/3 of the crypts with moderate inflammation in the mucosa; grade 3, loss of the entire crypts with severe inflammation in the mucosa and submucosa, but with retainment of the surface epithelium and grade 4, presence of mucosal ulcer with severe inflammation (neutrophil, lymphocyte and plasma cell infiltration) in the mucosa, submucosa, muscularis propria and/or subserosa. The scoring was made on the entire colon with or without proliferative lesions and expressed as a mean average score/mouse.

Immunohistochemistry

Immunohistochemical analyses for β-catenin, COX-2, iNOS, p53 and nitrotyrosine were carried out with 4 μm-thick paraffin-embedded sections as previously described[8,9,47] or a report by Mollersen *et al.*[48] As the primary antibodies, anti-β-catenin mouse monoclonal antibody (diluted 1:1,000, Transduction Laboratories, Lexington, KY), anti-COX-2 mouse monoclonal antibody (diluted 1:200, Transduction Laboratories), anti-iNOS mouse monoclonal antibody (diluted 1:250, Transduction Laboratories), anti-p53 rabbit polyclonal antibodies (CM5, diluted 1:100, Novocastra Laboratories, Ltd., Newcastle, UK) and rabbit polyclonal anti-nitrotyrosine (diluted 1:500, Upstate Biotechnology, Lake Placid, NY) were used. To reduce the nonspecific staining of mouse tissue by the mouse antibodies, a Mouse On Mouse IgG blocking reagent (Vector Laboratories, Inc., Burlingame, CA) was applied. For p53 and nitrotyrosine immunohistochemistry, normal rabbit serum was used to block background staining. Nonspecific binding was blocked by incubating the slides with a blocking solution (0.1 M PBS containing 0.1% triton X-100 and 2% normal goat serum) for nitrotyrosine. Staining was performed using a LSAB KIT or DAKO EnVision kit (DAKO, Glostrup, Denmark) or Vectastain Elite ABC Kit (Vector Laboratories, Burlingame, CA). At the last step, the sections were counterstained with hematoxylin. As a negative control, omission of the primary antibody was used. To quantitate the degree of nitrotyrosine stainability, the grading system (Grade 0–4) was used according to the following criteria described by Zingarelli *et al.*[49]: Grade 0, no immunoreactivity; Grades 1–3, increasing degrees of intermediate immunoreactivity and Grade 4, extensive immunoreactivity.

Apc allelic loss analysis

Seventeen tissues (14 colonic adenocarcinomas and 3 colonic mucosa) from male $Apc^{Min/+}$ mice that received 2% DSS, and 5 tissues (2 colonic adenocarcinomas and 3 colonic mucosa) from male $Apc^{Min/+}$ mice that received tap water without DSS were selected at random for *Apc* allelic loss analysis. They were digested overnight at 50°C in 20 μl of lysis buffer containing 500 μg/ml proteinase K, 10 mmol/liter Tris-HCl (pH 8.0), 50 mmol/liter KCl, 0.45% NP40 and 0.45% Tween 20. The proteinase K was heat inactivated (10 min at 95°C). The tubes were centrifuged for 5 min, and the supernatant was transferred to new tubes. Loss of heterozygosity (LOH) of the *Apc* gene was checked using PCR with mismatched primers, as described previously.[50]

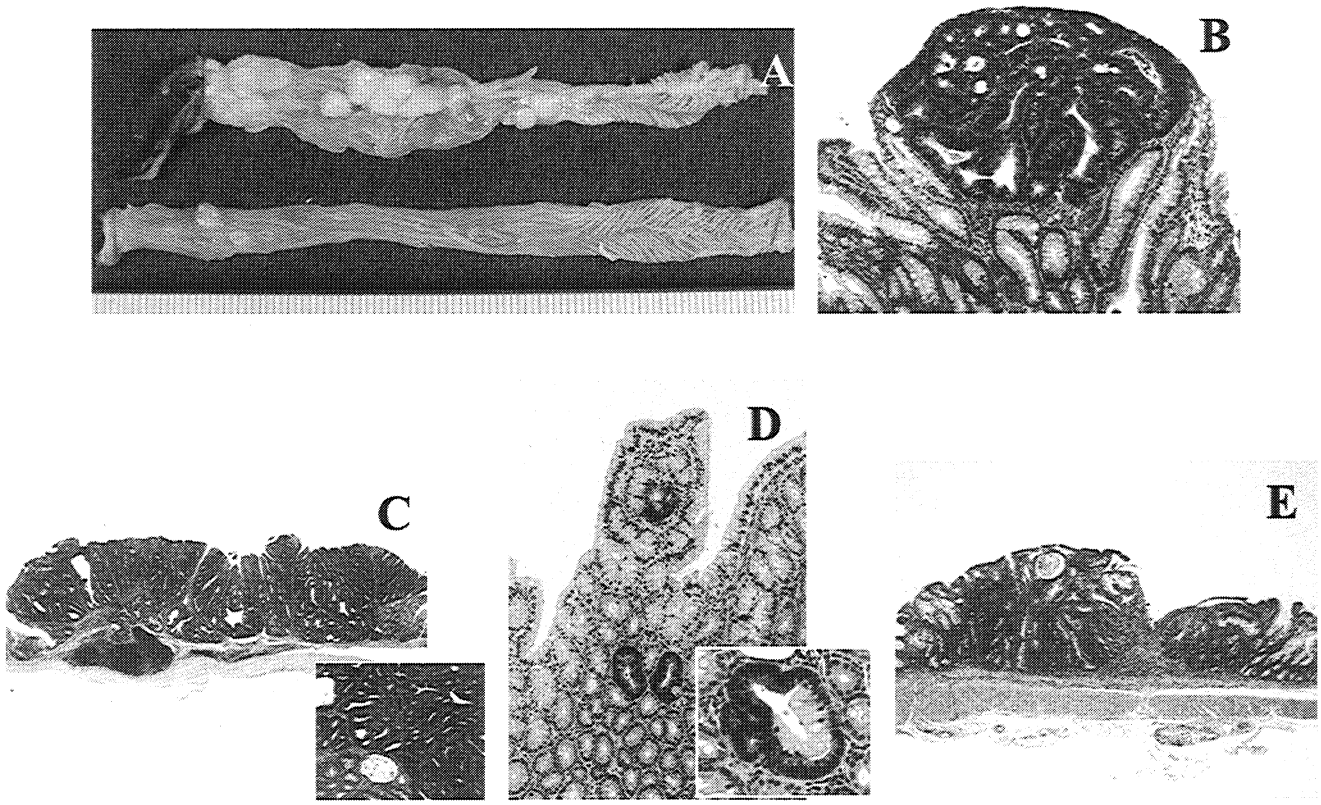


FIGURE 1 – Macroscopic view of the large bowel (*a*) and histopathology of the colonic lesions (*b–e*) of male $Apc^{Min/+}$ mice treated with 2% DSS. (*a*) Male $Apc^{Min/+}$ mice given 2% DSS had multiple colonic tumors (upper), while male $Apc^{Min/+}$ mice given tap had a few colonic tumors (lower); (*b*) A polypoid tumor is diagnosed as tubular adenoma compressing surrounding crypts; (*c*) A nodular tumor is diagnosed as well-differentiated tubular adenocarcinoma (insert: cancer cells with tubular pattern); (*d*) Three dysplastic crypts with hyperchromatic nuclei (insert: a dysplastic crypt with bud formation) are noted in the colonic mucosa; and (*e*) Colonic mucosal ulcer with regenerative hyperplasia is seen in the colonic mucosa. H&E stain, original magnification: (*b*), (*d*), ×100; (*c*), ×10; (*e*) ×20; (*c*, insert), ×100; and (*d*, insert), ×200.

Briefly, the amplification of the Apc^{Min} allele resulted in a 155 bp PCR product with 1 *Hind*III site, whereas the 155 bp product from the Apc^{+} allele contained 2 *Hind*III sites. *Hind*III digestion of PCR-amplified DNA from $Apc^{Min/+}$ heterozygous tissue resulted in a 123 bp product from the Apc^{+} allele and a 144 bp product from the Apc^{Min} allele. Therefore, PCR products from tissue with LOH displayed only 1 band (144 bp) from the Apc^{Min} allele. Samples were assayed at least twice, independently.

DNA sequencing and mutation analysis of β-catenin and K-Ras genes

A total of 17 tissues (14 colonic adenocarcinomas and 3 colonic mucosa) from male $Apc^{Min/+}$ mice that received 2% DSS were subjected to analysis of β-*catenin* and K-*ras*. Also, a total of 5 tissues (2 colonic adenocarcinomas and 3 colonic mucosa) from male $Apc^{Min/+}$ mice that received tap water without DSS were subjected to analysis of these genes. PCR was performed in β-*catenin* and K-*ras* genes and the statuses were determined by direct sequencing. Exon 3 of the β-*catenin* gene (McatF, 5′-TCTCCTTGG CTGGCCTTTCTA-3′; McatR, 5′-GTCACACAGCCCTGTCAAGA-3′) and exon 1 of the k-*ras* gene (MrasF, 5′-GCCTGCTGAAAATGACTGAG-3′; MrasR, 5′-CTTTACAAGCGCACGCAGAC-3′) were amplified by PCR. Primers were included in the following PCR reaction mixture, which contained in a total volume of 20 μl: 20 μM of each primer, 200 μM of each deoxynucleotide triphosphate, 1 unit of *Taq* polymerase in 1 × PCR buffer (Promega, Madison, WI) and template DNA. The mixture was heated at 94°C for 5 min and subjected to 30 cycles of denaturation (94°C, 45 sec), annealing (57°C, 45 sec) and extension (72°C, 1 min) using a GeneAmp PCR System 9700 (Applied Biosystems, Foster City, CA). The products were sequenced directly after gel-purification in both directions using a BigDye Terminator Cycle Sequencing kit (Applied Biosystems) according to the manufacturer's recommendations. Reactions were analyzed on an ABI Prism 3100 DNA Sequencer (Applied Biosystems).

Statistical analysis

Statistical significance of differences was evaluated by one-way ANOVA with Bonferroni correction or Fisher's exact probability test. Values were considered significantly different when $p < 0.05$.

Results

Pathological findings

$Apc^{Min/+}$ mice, but not $Apc^{+/+}$ mice, of both sexes exposed to 2 % DSS had bloody stools during DSS exposure. Other animals were healthy during the study. At week 5, macroscopically, a number of nodular, polypoid or caterpillar-like colonic tumors (Fig. 1*a*) were observed mainly in the middle and distal colon of male and female $Apc^{Min/+}$ mice treated with 2% DSS, but few in those treated with tap water. Microscopically, they were tubular adenoma (Fig. 1*b*) or well-/moderately-differentiated tubular adenocarcinoma (Fig. 1*c*). Similarly, dysplastic crypts (Fig. 1*d*) were frequently observed in all $Apc^{Min/+}$ mice of both sexes. Also, mucosal ulcer was noted in mice given 2% DSS in drinking water (Fig. 1*e*).

TABLE I – INCIDENCE AND MULTIPLICITY OF LARGE INTESTINAL TUMORS AND DYSPLASTIC CRYPTS AT WEEK 5

Genotype	Sex	Total: incidence (multiplicity[1])		Colonic tumors: incidence (multiplicity) AD[2]		ADC[2]		Dysplastic crypts	
		2% DSS	Tap water	2% DSS	Tap water	2% DSS	Tap water	2% DSS	Tap water
$Apc^{min/+}$	Male	7/7, 100%[3] (9.43±3.31[4])	3/9, 33% (0.44±0.73)	7/7, 100%[4] (3.86±2.19[4])	2/9, 22% (0.22±0.44)	7/7, 100%[4] (5.57±2.37[4])	2/9, 22% (0.22±0.44)	7/7, 100% (18.86±2.18[4])	9/9, 100% (6.56±1.67)
	Female	7/7, 100%[5] (8.29±5.02)[5]	3/10, 30% (0.50±0.97)	5/7, 71% (3.29±3.04[6])	2/10, 20% (0.30±0.67)	7/7,100% (5.00±2.16[5])	2/10, 20% (0.20±0.42)	7/7, 100% (13.29±3.45[6])	10/10, 100% (7.70±4.14)
$Apc^{+/+}$	Male	0/12, 0% (0)	0/17, 0% (0)	0/12, 0% (0)	0/17, 0% (0)	0/12, 0% (0)	0/17, 0% (0)	0/12, 0% (0)	0/17, 0% (0)
	Female	0/10, 0% (0)	0/11, 0% (0)	0/10, 0% (0)	0/11, 0% (0)	0/10, 0% (0)	0/11, 0% (0)	0/10, 0% (0)	0/11, 0% (0)

[1]No. of tumors/mouse, Mean ± SD.–[2]AD, adenoma; and ADC, adenocarcinoma.–[3]Significantly different from $Apc^{Min/+}$ males received tap water by one-way ANOVA with Fisher's exact probability test ($P < 0.05$).–[4]Significantly different from $Apc^{Min/+}$ males received tap water by Fisher's exact probability test or one-way ANOVA with Bonferroni correction ($P < 0.01$).–[5]Significantly different from $Apc^{Min/+}$ females received tap water by Fisher's exact probability test or one-way ANOVA with Bonferroni correction ($P < 0.01$).–[6]Significantly different from $Apc^{Min/+}$ females received tap water by one-way ANOVA with Bonferroni correction ($P < 0.05$).

The incidences and multiplicities of colonic neoplasms (adenomas and adenocarcinomas) and total colonic tumors are summarized in Table I. The incidences of total tumors and adenocarcinomas in $Apc^{Min/+}$ mice of both sexes given 2% DSS were significantly greater than those given tap water alone (total tumors: males, 100% *vs.* 33%, $p < 0.05$ and females, 100% vs. 30%, $p < 0.01$; adenocarcinoma: males, 100% *vs.* 22%, $p < 0.01$ and females, 100% *vs.* 20%, $p < 0.01$). Treatment with 2% DSS significantly increased the incidence of colonic adenomas in male $Apc^{Min/+}$ mice when compared to that of male $Apc^{Min/+}$ given tap water alone ($p < 0.01$). As for dysplastic foci (Table I), the frequencies in *ApcMin/+* mice of both sexes given 2% DSS were significantly greater than those given tap water alone ($p < 0.01$ for males and $p < 0.05$ for females).

Time-course observation of colonic tumors in female $Apc^{Min/+}$ mice revealed that the initial tumor (histologically tubular adenoma) developed at week 2 (Fig. 2*a*). The incidence of colonic adenomas reached 100% at week 3 and that of adenocarcinomas did at week 5, respectively (Fig. 2*a*), and their multiplicitis gradually increased up to week 5 (Fig. 2*b*). As for the frequency of dysplastic foci, there was no further increase in dysplastic crypts from week 4 to week 5 (Fig. 2*c*). The value at week 5 was significantly larger than that at week 2 ($p < 0.05$).

As summarized in Table II, a number of small intestinal polyps (histologically tubular adenoma) developed in all $Apc^{Min/+}$ mice with both sexes treated with or without 2% DSS, but not in $Apc^{+/+}$ mice with both sexes treated with or without 2% DSS. Their frequencies in $Apc^{Min/+}$ males and females given 2% DSS were significantly greater than in those given tap water alone ($p < 0.05$ for males and $p < 0.05$ for females). Considering the distribution of the polyps, significant increases in number were found at the distal region ($p < 0.01$ for males and $p < 0.01$ for females) in $Apc^{Min/+}$ mice of both sexes treated with 2% DSS when compared to those in $Apc^{Min/+}$ mice that received tap water. At the middle regions of small intestine the numbers of polyps were significantly decreased ($p < 0.05$ for males and $p < 0.01$ for females) in 2% DSS treated *ApcMin/+* mice of both sexes. Also, 2% DSS treatment increased the size (by 18%) of polyps in the small intestine. On the other hand, we could not find any polyps or tumors in the small intestine of wild type mice.

Score for inflammation in the iintestine

Table III summarizes data on colonic inflammation scores at week 5. The values in $Apc^{Min/+}$ and $Apc^{+/+}$ mice of both sexes treated with 2% DSS were significantly larger than those given tap water alone ($p < 0.01$). No significant differences on the degrees of colonic mucosal inflammation were noted between mice of 2 genotypes, $Apc^{Min/+}$ and $Apc^{+/+}$. Scoring of inflammation in the time-course study indicated that the value decreased after the cessation of 2% DSS (Fig. 2*d*). DSS exposure also produced small intestinal inflammation in both $Apc^{Min/+}$ and $Apc^{+/+}$ mice of both sexes: the inflammation scores in $Apc^{Min/+}$ mice were relatively greater than those in $Apc^{+/+}$ mice (data not shown). The scores of $Apc^{Min/+}$ mice that received 2% DSS were high in order of the distal (1.29±0.76 for males and 1.14±0.69 for females), middle (0.57±0.79 for males and 0.43±0.79 for females) and proximal (0.43±0.53 for males and 0.29±0.49 for females) parts.

Immunohistochemistry of β-catenin, COX-2, iNOS, p53 and nitrotyrosine

The immunoreactivities against β-catenin, COX-2, iNOS and nitrotyrosine were found in all colonic lesions including neoplasms and dysplastic crypts (Fig. 3) in the large intestine of $Apc^{Min/+}$ and $Apc^{+/+}$ mice of both sexes that received 2% DSS. Their intensity in the normal mucosa and the lesions induced in mice given tap water was relatively weaker than that in $Apc^{Min/+}$ mice treated with 2% DSS. p53 was positive in the nuclei of the colonic lesions developed in $Apc^{Min/+}$, while negative in those in $Apc^{+/+}$ mice. The immunoreactivity against 3 antibodies (β-catenin, COX-2 and iNOS) was also observed in the small intestinal polyps (tubular adenomas) in $Apc^{Min/+}$ mice of both sexes: the intensity in mice given tap water was lower than those treated with DSS.

β-Catenin staining in adenoma cells showed positive in their cell membrane and/or a few nuclei (Fig. 3*a*) in $Apc^{Min/+}$ mice treated with 2% DSS. Strong β-catenin expression was observed in the nucleus and cytoplasm of adenocarcinoma cells (Fig. 3*b*) in $Apc^{Min/+}$ mice given 2% DSS. The intensity of β-catenin staining in adenoma cells was relatively weak when compared to carcinoma cells. β-Catenin immunoreactivity was also observed in the cell membrane, cytoplasm, and a few nuclei of dysplastic cells (Fig. 3*c*). Nonlesional cryptal cells showed weak positivity of bgr;-catenin in their cell membrane. In addition, a positive reaction against β-catenin antibody was noted in the vascular endothelium, infiltrated inflammatory cells and ganglion cells in Auerbach's plexus.

Strong COX-2 immunoreactivity was present in adenoma (Fig. 3*d*) and adenocarcinoma cells (Fig. 3*e*) in their cytoplasm in $Apc^{Min/+}$ mice treated with 2% DSS. Dysplastic cells (Fig. 3*f*) showed relatively strong positivity for COX-2 when compared to neoplastic cells. Nonlesional cryptal cells at the lower part of crypts were weakly positive for COX-2, while strongly positive reaction of COX-2 was seen in the endothelium of small blood vessels and inflammatory cells infiltrated in the lamina propria. Smooth muscle cells and fibroblasts in inflamed large bowel showed weak reaction of COX-2.

iNOS-immunohistochemistry showed strong immunoreactivity in the cytoplasm of adenoma (Fig. 3*g*) and adenocarcinoma cells (Fig. 3*h*) in $Apc^{Min/+}$ mice given 2% DSS: the intensity was greater in carcinoma cells when compared to adenoma

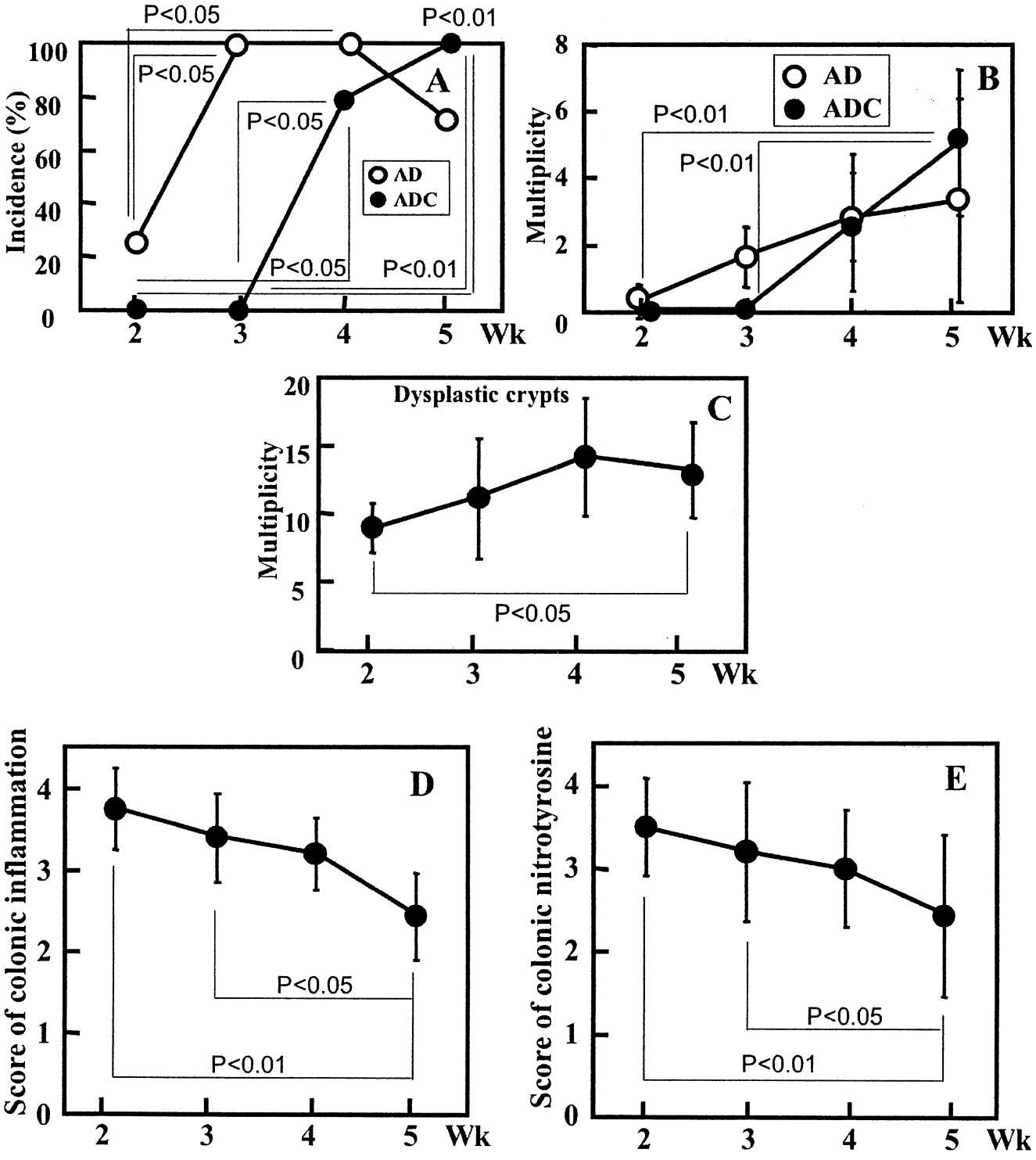


FIGURE 2 – Time-course observation of colonic lesions in female $Apc^{Min/+}$ mice treated with 2% DSS. The incidence (*a*) and multiplicity (*b*) of colonic neoplasms and the multiplicity (*c*) of colonic dysplastic crypt were gradually increased with time. Scores of colonic inflammation (*d*) and nitrotyrosine-positivity (*e*) gradually decreased after the cessation of DSS treatment with time. AD and ADC refer to adenoma and adenocarcinoma, respectively. Data represent mean±SD (n = 4 mice at week 2, 5 mice at week 3, 5 mice at week 4, and 8 mice at week 5). Statistical significance of differences was evaluated by Fisher's exact probability test (*a*) or one-way ANOVA with Bonferroni correction (*b–e*). Statistical significances of the squared correlation coefficients were found for the multiplicity of adenoma ($r = 0.9817$, $p < 0.05$), inflammation score ($r = -0.9618$, $p < 0.05$), and nitrotyrosine positive score ($r = -0.9764$, $p < 0.05$).

cells. Also, dysplastic cells (Fig. 3*i*) were positive for iNOS in their cytoplasm and the intensity was relatively greater than neoplastic cells. The faint positive reaction was found in the cytoplasm of nonlesional cryptal cells. Immunohistochemical iNOS expression was strong in the endothelial cells of small blood vessels and inflammatory cells in the lamina propria. COX-2- and iNOS-stained inflammatory cells were also frequently observed in the mucosa.

TABLE II – INCIDENCE AND MULTIPLICITY OF SMALL INTESTINAL POLYPS AT WEEK 5

Genotype	Sex	Incidence (multiplicity) of small intestinal polyps at							
		Proximal region		Middle region		Distal region		Total	
		2% DSS	Tap water	2% DSS	Tap water	2% DSS	Tap water	2% DSS	Tap water
$Apc^{Min/+}$	Male	7/7, 100% (9.4±2.4[1])	9/9, 100% (9.1±2.1)	7/7, 100% (11.6±2.6[2])	9/9, 100% (16.0±3.7)	7/7, 100% (42.9±10.4[3])	9/9, 100% (24.7±5.8)	7/7, 100% (64.3±13.3[2])	9/9, 100% (49.8±9.8)
	Female	7/7, 100% (7.2±2.4)	10/10, 100% (8.5±2.3)	7/7, 100% (8.7±2.3[4])	10/10, 100% (14.1±3.0)	7/7,100% (35.3±4.8[4])	10/10, 100% (20.0±5.1)	7/7, 100% (51.2±5.4[5])	10/10, 100% (42.6±9.3)
$Apc^{+/+}$	Male	0/12, 0% (0)	0/17, 0% (0)	0/12, 0% (0)	0/17, 0% (0)	0/12, 0% (0)	0/17, 0% (0)	0/12, 0% (0)	0/17, 0% (0)
	Female	0/10, 0% (0)	0/11, 0% (0)	0/10, 0% (0)	0/11, 0% (0)	0/10, 0% (0)	0/11, 0% (0)	0/10, 0% (0)	0/11, 0% (0)

[1]The number of polyps per mouse (Mean±SD).–[2]Significantly different from $Apc^{Min/+}$ males received tap water by one-way ANOVA with Bonferroni correction ($P < 0.05$).–[3]Significantly different from $Apc^{Min/+}$ males received tap water by one-way ANOVA with Bonferroni correction ($P < 0.01$).–[4]Significantly different from $Apc^{Min/+}$ females received tap water by one-way ANOVA with Bonferroni correction ($P < 0.01$).–[5]Significantly different from $Apc^{Min/+}$ females received tap water by one-way ANOVA with Bonferroni correction ($P < 0.05$).

TABLE III – SCORES OF INFLAMMATION AND NITROTYROSINE IMMUNOHISTOCHEMISTRY OF COLONIC MUCOSA AT WEEK 5

Genotype	Sex	Score of inflammation (number of mice examined)		Score of nitrotyrosine-immunohistochemistry (number of mice examined)	
		2% DSS	Tap water	2% DSS	Tap water
$Apc^{Min/+}$	Male	2.86±0.69[1,2] (7)	0.22±0.44 (9)	2.71±0.95[2] (7)	0.11±0.33 (9)
	Female	2.14±0.69[3] (7)	0.20±0.42 (10)	2.14±0.69[3] (7)	0.10±0.32 (10)
$Apc^{+/+}$	Male	2.33±0.65[4] (12)	0.24±0.44 (17)	2.25±1.06[4] (12)	0.12 ± 0.33 (17)
	Female	2.10±0.74[5] (10)	0.18±0.41 (11)	2.14±0.69[5] (10)	0.09±0.30 (11)

[1]Mean ± SD.–[2]Significantly different from $Apc^{Min/+}$ males received tap water by one-way ANOVA with Bonferroni correction ($P < 0.01$).–[3]Significantly different from $Apc^{Min/+}$ females received tap water by one-way ANOVA with Bonferroni correction ($P < 0.01$).–[4]Significantly different from $Apc^{+/+}$ males received tap water by one-way ANOVA with Bonferroni correction ($P < 0.01$).–[5]Significantly different from $Apc^{+/+}$ females received tap water by one-way ANOVA with Bonferroni correction ($P < 0.001$).

Immunoreactivity of nitrotyrosine was noted in the cryptal cells with or without disruption, infiltrated mononuclear inflammatory cells, and endothelial cells of the small vessels in the colonic mucosa and submucosa in $Apc^{Min/+}$ and $Apc^{+/+}$ mice that received 2% DSS. Among them, the stainability was strong in the infiltrated mononuclear inflammatory cells. Adenoma cells (Fig. 3*j*), adenocarcinoma cells (Fig. 3*k*) and dysplastic cryptal cells (Fig. 3*l*) also showed moderately positive immunoreactivity of nitrotyrosine in their cytoplasm. The intensity in the colonic lesions in $Apc^{Min/+}$mice given 2% DSS was strong when compared to that observed in $Apc^{+/+}$ mice given tap water alone. As summarized in Table III, scores of nitrotyrosine-immunoreactivity in the colonic mucosa of $Apc^{Min/+}$and $Apc^{+/+}$ mice of both sexes given 2% DSS were significantly greater than those given tap water alone ($p < 0.001$). The score in the time-course observation indicated that the value decreased after the cessation of 2% DSS (Fig. 2*e*), as was the value of inflammation (Fig. 2*d*).

P53 immunoreactivity was observed in the nuclei of neoplastic cells (adenoma and adenocarcinoma cells) with a variety of stainability, which developed in the colon of $Apc^{Min/+}$ mice treated with DSS (Fig. 3*m,n*) but not in those given tap water alone. Also, the nuclei of dysplastic crypts were positive for p53 antibody (Fig. 3*o*). Surrounding the mucosal ulcer, some nuclei of regenerative hyperplastic crypts in the colon were weakly positive for p53 antibody in the colon of $Apc^{Min/+}$ mice treated with DSS (date not shown). No stainability of p53 was observed in the small intestinal polyps (data not shown) in $Apc^{Min/+}$ mice treated with or without DSS.

Apc allelic loss in colonic neoplasms

One hundred percent (14 of 14) of adenocarcinomas and 0% (0 of 3) of histologically normal colonic mucosa from male $Apc^{Min/+}$ mice that received 2% DSS showed LOH of *Apc*. In male $Apc^{Min/+}$ mice that received tap water alone, 100% (2 of 2) of adenocarcinomas showed LOH of *Apc* and 0% (0 of 3) of histologically normal colonic mucosa was negative for LOH.

Mutation of β-catenin and K-Ras genes

β-*Catenin* and K-*ras* mutations were not detected in any of the colonic adenocarcinomas examined.

Discussion

In our study, we investigated the influences of the inflammation induced by 1-week exposure of 2% DSS in the drinking water on intestinal carcinogenesis in $Apc^{Min/+}$ mice and found that the treatment resulted in a much higher incidence and multiplicity of large intestinal neoplasms in $Apc^{Min/+}$ mice up to 5 weeks. Also, the treatment significantly increased the number of small intestinal polyps (tubular adenomas) at the distal regions. Thus, we developed an $Apc^{Min/+}$ mouse model with multiple colonic neoplasms, which develop within 4 weeks after 1-week exposure DSS, in addition to the increase in the number of small intestinal polyps. Regardless of the types of gene and gender, all mice treated with 2% DSS had intestinal mucosal inflammation with various degrees. However DSS treatment did not induce preneoplastic and neoplastic lesions in the large bowel wild-type ($Apc^{+/+}$) mice of either sex. This report describing rapid development of a number of colonic neoplasms in $Apc^{Min/+}$ mice within a short-term period (5 weeks) support an earlier work by Cooper *et al.*,[14] who found that treatment with 2 cycles of 4% DSS results in 40% incidence of colon cancer with a multiplicity of 0.67±0.27 in female Min mice at 42 days. Our findings suggest that the development of colonic dysplastic crypts and/or neoplasms in the short-term (up to 5 weeks) needs both the gene (*Apc*) mutation and subsequent inflammatory stimuli, but not either alone under the current exper-

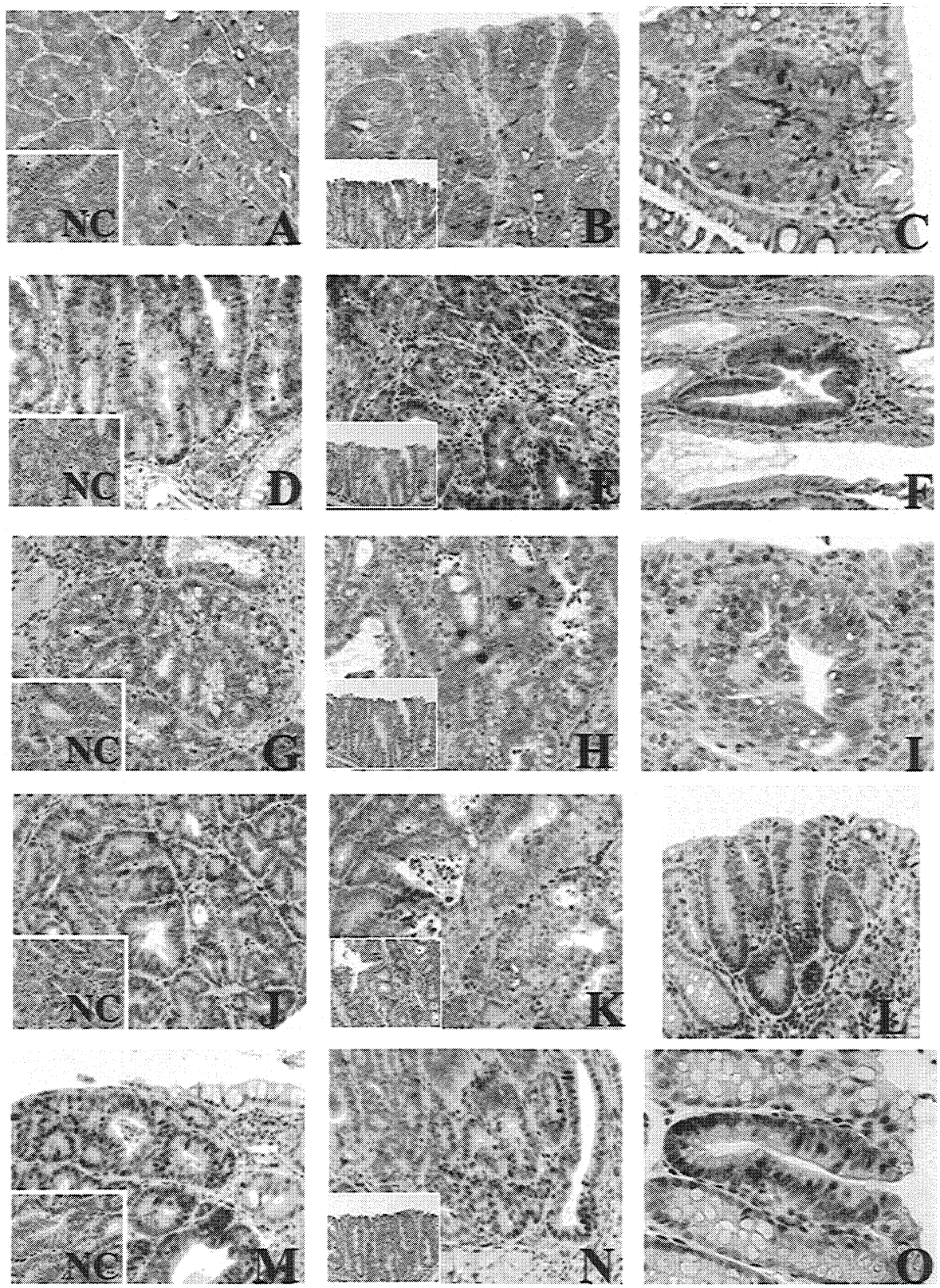


FIGURE 3 – Immunohistochemistry of the colonic lesions developed in male $Apc^{Min/+}$ mice treated with 2% DSS. (*a*)–(*c*), β-catenin immunohistochemistry; (*d*)–(*f*), COX-2 immunohistochemistry; (*g*)–(*i*), iNOS immunohistochemistry; (*j*)–(*l*), nitrotyrosine immunohistochemistry and (*m*)–(*o*), p53 immunohistochemistry. Adenomas (*a*, *d*, *g*, *i* and *m*), adenocarcinomas (*b*, *e*, *h*, *k* and *n*), and dysplastic crypts (*c*, *f*, *i*, *l* and *o*) show positive reaction with a variety of intensity against β-catenin, COX-2, iNOS, nitrotyrosine and p53 antibodies. Inserts of *a*, *d*, *g*, *j* and *m* are negative controls (NC) immunostained without antibodies show negative reactions. Inserts of *b*, *e*, *h*, *k* and *n* are immunohistochemistry of adenocarcinomas developed in $Apc^{Min/+}$ mice given tap water. Original magnification: (*a*), (*b*), (*d*), (*e*), (*g*), (*h*), (*j*), (*k*), (*l*), (*m*) and (*n*), ×100; (*c*), (*f*), (*i*) and (*o*), ×200; inserts, ×200.

imental condition. Our results also support the findings of our previous works,[8,9,12] suggesting the importance of inflammatory stimuli as a promotion event after the initiation events (genetic alterations) in colon carcinogenesis. There were no differences between males and females in the effects of DSS on large and small intestinal carcinogenesis of $Apc^{Min/+}$, and the histopathology of colonic lesions including neoplasms was similar in both sexes.

As for the development of small intestinal polyps, treatment with DSS significantly increased their number and size, especially at the distal portion of the small intestine. Macrophages engulfing DSS particles were observed in the large intestine and surrounding lymph nodes of mice 1 day after DSS exposure, and then found in the jejunum and ileum 7 days after DSS treatment.[51] In our study, mild mucosal inflammation was observed in the distal portion of the small intestine of mice given 2% DSS. Thus, DSS could also influence the formation of small intestinal polyp in $Apc^{Min/+}$ mice. The Min mouse has been regarded as a human FAP model in spite of the fact that the polyps (adenomas) develop in the small intestine. Although the biological pathways in human colon and Min intestine are assumed to be similar, our model described here could be applied for investigation of the genesis, pathophysiology and chemoprevention of human FAP and/or inflammation-related colon tumorigenesis.

In our study, sequential observation on the pathological alteration in the large intestines of female $Apc^{Min/+}$ mice after 1-week exposure to 2% DSS revealed that the frequencies of dysplastic crypts and colonic neoplasms (adenoma and adenocarcinoma) gradually increased over time (Fig. 2*a*,*b*), indicating that dysplastic crypts[43] or adenomatous lesions[41] are precursor lesions for colon carcinoma and DSS treatment could promote their growth. The findings support an earlier report by Cooper *et al.*,[14] but their incidence of colonic cancer was low: 22% in Min mice exposed to 1-cycle of DSS (administration 4% DSS for 4 days and H_2O for 17 days) and 40% in Min mice exposed to 2-cycle of DSS. The discrepancy existing in these 2 studies may be due to the differences in the treatment period and the dose and molecular weight of DSS. In the present study, the incidence of colonic adenocarcinoma was 80% at week 4 and 100% at week 5 (Fig. 2*a*). When compared to our previous study on the effects of DSS on chemically induced colon carcinogenesis,[9] where we observed 40% and 100% incidences of colonic epithelial malignancy at week 4 and week 6, respectively, in male ICR mice, it is likely that deletion of the *Apc* gene plays an important role in colitis-associated carcinogenesis, as suggested by Cooper *et al.*[14]

In our study, we investigated the immunohistochemical expression of β-catenin, COX-2, iNOS and p53, in the colonic lesions developed in *ApcMin/+* mice that received 2% DSS. The results on immunohistochemistry against these antibodies except for p53 expression in the lesions were similar to those observed in our previous studies, where the lesions were induced by AOM[8,9], HCAs[12] or DMH[11] followed by DSS in ICR mice, suggesting the similarity of histopathology and immunohistochemistry, and biological nature of the lesions observed in ICR mice given a colonic carcinogen and DSS and $Apc^{Min/+}$ mice treated with DSS. Increased immunohistochemical expression of COX-2 and iNOS in the colonic tumors of either $Apc^{Min/+}$ mice that received 2% DSS was confirmed by reverse transcription-polymerase chain reaction (data not shown). The findings of nitrotyrosine immunohistochemistry in the current study are also in accordance with those in our previous study[9] and suggest that oxidative/nitrosative stress strongly promotes the development of colonic neoplasms in $Apc^{Min/+}$ mice. iNOS has been shown to be the only isoform involved in stimulating tumor growth, probably through an increase in vascular endothelial growth factor production.[52] Moreover, NO regulates COX-2 expression.[53] Our results on the immunohistochemistry of iNOS and COX-2 indicate that the inflammatory response, the interaction between NO synthase and COX pathways may stand at the center of the pathophysiological basis of inflammation-related colon carcinogenesis in $Apc^{Min/+}$ mice treated with DSS, as are the cases of inflammatory diseases,[54] and chemically induced colon carcinogenesis.[33]

In the current study, we also screened for mutations of β-*catenin* and K-*ras* in colon tumors developed in male $Apc^{Min/+}$ mice. In contrast with previous reports,[12,33,55] we did not detect the mutations of these genes in any of the colonic adenocarcinomas examined. However, our results are not surprising. Suzui *et al.*[56] reported that adenocarcinomas developed in $Apc^{Min/+}$ mice treated with AOM did not have β-*catenin* gene mutations. In our study, cytoplasmic and/or nuclear accumulation of β-catenin protein was detected in the colonic neoplasms, but β-*catenin* gene mutations were not present. In the FAP patients, mutations of *APC* are common, but mutations of β-*catenin* were rare.[57,58] In addition, β-*catenin* germline mutations were not found in FAP patients with germline *APC* mutations.[57] Thus, concerning the β-*catenin* mutation, the colon tumors developed in the current animal model may imitate the colon carcinogenesis as in the FAP patients, that is, by a second hit in the *APC* gene such as loss of Apc^{+} allele or somatic mutations in the *Apc* gene. Immunohistochemical staining with an antibody for the C-terminal of *Apc* showed the loss of wild-type *Apc* in colonic tumors in $Apc^{Min/+}$ mice (data not shown). As for the mutation of K-*ras*, no mutations were found in the colonic adenocarcinomas examined in the current study. Our results on K-*ras* mutations are in accordance with IBD-related colon carcinogenesis[59] and suggest that activation of the K-*ras* gene is not essential for the development and growth of colonic neoplasms in our model.

p53 gene mutation occurs in the late stage of human colon carcinogenesis.[33,59] In our study, p53 immunohistochemistry revealed positive reaction in the nuclei of neoplastic cells in $Apc^{Min/+}$ mice treated with DSS, although we did not examine its mutation in our study. The accumulation of p53 shown in our study is interesting and may be important for colon cancer development in *Apc*-deficient mice, since an increased *p53* mutation load in the inflamed colon tissue from UC patients being a high-risk for colon cancer[60] and a potential mechanism link between NO and p53 in UC and sporadic colon cancer[61] were reported. In addition, COX-2, iNOS and p53 are suggested to be fundamental "play-makers" of the angiogenesis processes.[62]

Taken together, our results suggest that a novel $Apc^{Min/+}$ mouse model with DSS may provide new insight into the genesis and chemoprevention of colon cancer development in FAP patients. In our model, a single allele *Apc* gene followed by appropriate promotional stimuli is sufficient for the development and growth of colonic neoplasms in $Apc^{Min/+}$ mice, and COX-2, iNOS, p53, oxidative/nitrosative stress and interactions of these may play important roles in colon carcinogenesis in $Apc^{Min/+}$ mice given DSS. Our model can be applied for investigating the pathogenesis in carcinogenesis of IBD, since the Wnt/β-catenin signaling pathway may be involved in carcinogenesis of UC.[59,63] Our ongoing microarray analysis will provide new information of the mechanism(s) for the effects of DSS on large and small intestinal tumorigenesis in $Apc^{Min/+}$ mice.

Acknowledgements

Dr. R. Suzuki is a Research Fellow of the Japan Society for the Promotion of Science, 6 Ichiban-cho, Chiyoda-ku, Tokyo 102-8471, Japan.

References

1. Balkwill F, Mantovani A. Inflammation and cancer: back to Virchow? Lancet 2001;357:539–45.
2. Ohshima H, Tatemichi M, Sawa T. Chemical basis of inflammation-induced carcinogenesis. Arch Biochem Biophys 2003;417:3–11.
3. Szilagyi A. Altered colonic environment, a possible predisposition to colorectal cancer and colonic inflammatory bowel disease: rationale of dietary manipulation with emphasis on disaccharides. Can J Gastroenterol 1998;12:133–46.

4. Seril DN, Liao J, Yang GY, Yang CS. Oxidative stress and ulcerative colitis-associated carcinogenesis: studies in humans and animal models. Carcinogenesis 2003;24:353–62.
5. Munkholm P. Review article: the incidence and prevalence of colorectal cancer in inflammatory bowel disease. Aliment Pharmacol Ther 2003;18:1–5.
6. van der Woude CJ, Kleibeuker JH, Jansen PL, Moshage H. Chronic inflammation, apoptosis and (pre-)malignant lesions in the gastrointestinal tract. Apoptosis 2004;9:123–30.
7. Okayasu I, Hatakeyama S, Yamada M, Ohkusa T, Inagaki Y, Nakaya R. A novel method in the induction of reliable experimental acute and chronic ulcerative colitis in mice. Gastroenterology 1990;98:694–702.
8. Tanaka T, Kohno H, Suzuki R, Yamada Y, Sugie S, Mori H. A novel inflammation-related mouse colon carcinogenesis model induced by azoxymethane and dextran sodium sulfate. Cancer Sci. 2003;94:965–73.
9. Suzuki R, Kohno H, Sugie S, Tanaka T. Sequential observations on the occurrence of preneoplastic and neoplastic lesions in the mouse colon treated with azoxymethane and dextran sodium sulfate. Cancer Sci. 2004;95:721–7.
10. Suzuki R, Kohno H, Sugie S, Tanaka T. Dose-dependent promoting effect of dextran sodium sulfate on mouse colon carcinogenesis initiated with azoxymethane. Histol Histopathol 2005;20:483–92.
11. Kohno H, Suzuki R, Sugie S, Tanaka T. β-*Catenin* mutations in a mouse model of inflammation-related colon carcinogenesis induced by 1,2-dimethylhydrazine and dextran sodium sulfate. Cancer Sci 2005; 96:69–76.
12. Tanaka T, Suzuki R, Kohno H, Sugie S, Takahashi M, Wakabayashi K. Colonic adenocarcinomas rapidly induced by the combined treatment with 2-amino-1-methyl-6-phenylimidazo[4,5-*b*]pyridine and dextran sodium sulfate in male ICR mice possess bgr;-catenin gene mutations and increase immunorectivity for bgr;-catenin, cyclooxygenase-2, and inducible nitric oxide synthase. Carcinogenesis 2005;26: 229–38.
13. Cooper HS, Murthy S, Kido K, Yoshitake H, Flanigan A. Dysplasia and cancer in the dextran sulfate sodium mouse colitis model. Relevance to colitis associated neoplasia in the human: study of histopathology, beta-catenin and p53 expression and the role of inflammation. Carcinogenesis 2000;21:757–68.
14. Cooper HS, Everley L, Chang W-C, Pfeeiffer G, Lee B, Murthy S, Clapper ML. The role of mutant Apc in the development of dysplasia and cancer in the mouse model of dextran sulfate sodium–induced colitis. Gastroenterology 2001;121:1407–16.
15. Barbour KW, Davis T, White A, Baumann H, Berger FG. Haptoglobin, inflammation, and tumorigenesis in the MIN mouse. Redox Rep 2001;6:366–8.
16. Hansen-Petrik MB, McEntee MF, Jull B, Shi H, Zemel MB, Whelan J. Prostaglandin E2 protects intestinal tumors from nonsteroidal anti-inflammatory drug-induced regression in Apc$^{Min/-}$ mice. Cancer Res 2002;62:403–8.
17. Prescott SM, Fitzpatrick FA. Cyclooxygenase-2 and carcinogenesis. Biochim Biophys Acta 2000;1470:M69–78.
18. Eberhart CE, Coffey RJ, Radhika A, Giardiello FM, Ferrenbach S, DuBois RN. Up-regulation of cyclooxygenase 2 gene expression in human colorectal adenomas and adenocarcinomas. Gastroenterology 1994;107:1183–8.
19. DuBois RN, Radhika A, Reddy BS, Entingh AJ. Increased cyclooxygenase-2 levels in carcinogen-induced rat colonic tumors. Gastroenterology 1996;110:1295–62.
20. Hull MA, Booth JK, Tisbury A, Scott N, Bonifer C, Markham AF, Coletta PL. Cyclooxygenase 2 is up-regulated and localized to macrophages in the intestine of Min mice. Br J Cancer 1999;79:1399–405.
21. Arroyo PL, Hatch-Pigott V, Mower HF, Cooney RV. Mutagenicity of nitric oxide and its inhibition by antioxidants. Mutat Res 1992;281:193–202.
22. Wink DA, Kasprzak KS, Maragos CM, Elespuru RK, Misra M, Dunams TM, Cebula TA, Koch WH, Andrews AW, Allen JS. DNA deaminating ability and genotoxicity of nitric oxide and its progenitors. Science (Washington, DC) 1991;254:1001–3.
23. Xiong M, Elson G, Legarda D, Leibovich SJ. Production of vascular endothelial growth factor by murine macrophages: regulation by hypoxia, lactate, and the inducible nitric oxide synthase pathway. Am J Pathol 1998;153:587–98.
24. Kojima M, Morisaki T, Tsukahara Y, Uchiyama A, Matsunari Y, Mibu R, Tanaka M. Nitric oxide synthase expression and nitric oxide production in human colon carcinoma tissue. J Surg Oncol 1999;70:222–9.
25. Bing RJ, Miyataka M, Rich KA, Hanson N, Wang X, Slosser HD, Shi SR. Nitric oxide, prostanoids, cyclooxygenase, and angiogenesis in colon and breast cancer. Clin Cancer Res 2001;7:3385–92.
26. Takahashi M, Fukuda K, Ohata T, Sugimura T, Wakabayashi K. Increased expression of inducible and endothelial constitutive nitric oxide synthases in rat colon tumors induced by azoxymethane. Cancer Res 1997;57:1233–7.
27. Rao CV, Kawamori T, Hamid R, Reddy BS. Chemoprevention of colonic aberrant crypt foci by an inducible nitric oxide synthase-selective inhibitor. Carcinogenesis 1999;20:641–4.
28. Ahn B, Ohshima H. Suppression of intestinal polyposis in Apc$^{Min/+}$ mice by inhibiting nitric oxide production. Cancer Res. 2001;61: 8357–60.
29. Scott DJ, Hull MA, Cartwright EJ, Lam WK, Tisbury A, Poulsom R, Markham AF, Bonifer C, Coletta PL. Lack of inducible nitric oxide synthase promotes intestinal tumorigenesis in the Apc$^{Min/+}$ mouse. Gastroenterology 2001;121:889–99.
30. Mabley JG, Pacher P, Bai P, Wallace R, Goonesekera S, Virag L, Southan GJ, Szabo C. Suppression of intestinal polyposis in *Apc*$^{Min/+}$ mice by targeting the nitric oxide or poly(ADP-ribose) pathways. Mutat Res 2004;548:107–16.
31. Lala PK, Chakraborty C. Role of nitric oxide in carcinogenesis and tumour progression. Lancet Oncol 2001;2:149–56.
32. Hofseth LJ, Hussain SP, Wogan GN, Harris CC. Nitric oxide in cancer and chemoprevention. Free Radic Biol Med 2003;34: 955–68.
33. Takahashi M, Wakabayashi K. Gene mutations and altered gene expression in azoxymethane-induced colon carcinogenesis in rodents. Cancer Sci 2004;95:475–80.
34. Hussain SP, Hofseth LJ, Harris CC. Radical causes of cancer. Nat Rev Cancer 2003;3:276–85.
35. Ames BN, Gold LS, Willett WC. The causes and prevention of cancer. Proc Natl Acad Sci U S A 1995;92:5258–65.
36. Hussain SP, Hofseth LJ, Harris CC. Tumor suppressor genes: at the crossroads of molecular carcinogenesis, molecular epidemiology and human risk assessment. Lung Cancer 2001;34:S7–S15.
37. Kinzler KW, Vogelstein B. Lessons from hereditary colorectal cancer. Cell 1996;87:159–70.
38. Powell SM, Petersen GM, Krush AJ, Booker S, Jen J, Giardiello FM, Hamilton SR, Vogelstein B, Kinzler KW. Molecular diagnosis of familial adenomatous polyposis. N Engl J Med 1993; 329:1982–7.
39. Moser AR, Luongo C, Gould KA, McNeley MK, Shoemaker AR, Dove WF. ApcMin: a mouse model for intestinal and mammary tumorigenesis. Eur J Cancer 1995;31A:1061–4.
40. Paulsen JE. Modulation by dietary factors in murine FAP models. Toxicol Lett 2000;112–113:403–9.
41. Yamada Y, Hata K, Hirose Y, Hara A, Sugie S, Kuno T, Yoshimi N, Tanaka T, Mori H. Microadenomatous lesions involving loss of *Apc* heterozygosity in the colon of adult *Apc*$^{Min/+}$ mice. Cancer Res 2002; 62:6367–70.
42. Murata M, Kawanishi S. Oxidative DNA damage induced by nitrotyrosine, a biomarker of inflammation. Biochem Biophys Res Commun 2004;316:123–8.
43. Paulsen JE, Steffensen I-L, Loberg EM, Husoy T, Namork E, Alexander J. Qualitative and quantitative relationship between dysplastic aberrant crypt foci and tumorigenesis in the *Min*/+ mouse colon. Cancer Res 2001;61:5010–5.
44. Steffensen I-L, Paulsen JE, Eide TJ, Alexander J. 2-Amino-1-methyl-6- phenylimidazo[4,5-*b*]pyridine increases the numbers of tumors, cystic crypts and aberrant crypt foci in multiple intestinal neoplasia mice. Carcinogenesis (Lond.) 1997;18:1049–54.
45. Ward JM. Morphogenesis of chemically induced neoplasms of the colon and small intestine in rats. Lab Invest 1974;30:505–13.
46. Cooper HS, Murthy SN, Shah RS, Sedergran DJ. Clinicopathologic study of dextran sulfate sodium experimental murine colitis. Lab Invest 1993;69:238–49.
47. Kohno H, Suzuki R, Noguchi R, Hosokawa M, Miyashita K, Tanaka T. Dietary conjugated linolenic acid inhibits azoxymethane-induced colonic aberrant crypt foci in rats. Jpn J Cancer Res 2002;93:133–42.
48. Mollersen L, Paulsen JE, Olstorn HB, Knutsen HK, Alexander J. Dietary retinoic acid supplementation stimulates intestinal tumour formation and growth in multiple intestinal neoplasia (Min)/+ mice. Carcinogenesis 2004;25:149–53.
49. Zingarelli B, Szabo C, Salzman AL. Reduced oxidative and nitrosative damage in murine experimental colitis in the absence of inducible nitric oxide synthase. Gut 1999;45:199–209.
50. Luongo C, Moser AR, Gledhill S, Dove WF. Loss of *Apc*+ in intestinal adenomas from Min mice. Cancer Res 1994;54:5947–52.
51. Kitajima S, Takuma S, Morimoto M. Tissue distribution of dextran sulfate sodium (DSS) in the acute phase of murine DSS-induced colitis. J Vet Med Sci 1999;61:67–70.
52. Konopka TE, Barker JE, Bamford TL, Guida E, Anderson RL, Stewart AG. Nitric oxide synthase II gene disruption: implications for tumor growth and vascular endothelial growth factor production. Cancer Res 2001;61:3182–7.
53. Salvemini D, Misko TP, Masferrer JL, Seibert K, Currie MG, Needleman P. Nitric oxide activates cyclooxygenase enzymes. Proc Natl Acad Sci U S A 1993;90:7240–4.

54. Perez-Sala D, Lamas S. Regulation of cyclooxygenase-2 expression by nitric oxide in cells. Antioxid Redox Signal 2001;3: 231–48.
55. Takahashi M, Nakatsugi S, Sugimura T, Wakabayashi K. Frequent mutations of the β-*catenin* gene in mouse colon tumors induced by azoxymethane. Carcinogenesis 2000;21:1117–20.
56. Suzui M, Okuno M, Tanaka T, Nakagama H, Moriwaki H. Enhanced colon carcinogenesis induced by azoxymethane in min mice occurs via a mechanism independent of β-*catenin* mutation. Cancer Lett 2002;183:31–41.
57. Muller O, Nimmrich I, Finke U, Friedl W, Hoffmann I. A β-catenin mutation in a sporadic colorectal tumor of the RER phenotype and absence of β-catenin germline mutations in FAP patients. Genes Chromosomes Cancer 1998;22:37–41.
58. Miyoshi Y, Ando H, Nagase H, Nishisho I, Horii A, Miki Y, Mori T, Utsunomiya J, Baba S, Petersen G, Hamilton S, Kinzler K et al. Germ-line mutations of the *APC* gene in 53 familial adenomatous polyposis patients. Proc Natl Acad Sci. U S A. 1992;89:4452–6.
59. Itzkowitz SH, Yio X. Inflammation and cancer IV. Colorectal cancer in inflammatory bowel disease: the role of inflammation. Am J Physiol Gastrointest Liver Physiol 2004;287:G7–17.
60. Hussain SP, Amstad P, Raja K, Ambs S, Nagashima M, Bennett WP, Shields PG, Ham AJ, Swenberg JA, Marrogi AJ, Harris CC. Increased p53 mutation load in noncancerous colon tissue from ulcerative colitis: a cancer-prone chronic inflammatory disease. Cancer Res 2000; 50:3333–7.
61. Goodman JE, Hofseth LJ, Hussain SP, Harris CC. Nitric oxide and p53 in cancer-prone chronic inflammation and oxyradical overload disease. Environ Mol Mutagen 2004;44:3–9.
62. Chiarugi V, Magnelli L, Gallo O. Cox-2, iNOS and p53 as playmakers of tumor angiogenesis (review). Int J Mol Med 1998;2: 715–9.
63. Uthoff SM, Eichenberger MR, Lewis RK, Fox MP, Hamilton CJ, McAuliffe TL, Grimes HL, Galandiuk S. Identification of candidate genes in ulcerative colitis and Crohn's disease using cDNA array technology. Int J Oncol 2001;19:803–10.

平成１６年度

奨励研究成果報告書

1．研究課題名：　各種脂肪酸・抗酸化ビタミン摂取量、血清高感度 CRP と血圧との関連に関する大規模疫学研究（研究番号 S2004-1）

2．キーワード：1）脂肪酸（fatty acids）
2）抗酸化ビタミン（antioxidant vitamins）
3）高感度 CRP（C-reactive protein）
4）血圧（blood pressure）
5）疫学（epidemiology）

3．研究者氏名：　三浦克之・医学部・助教授・健康増進予防医学部門

4．研 究 目 的

高血圧は動脈硬化性循環器疾患の最大の危険因子の一つであり、その予防はわが国の国民的課題となっている。高血圧は、食塩、飲酒などの生活習慣が大きな原因とされてきたが、近年新たに様々な栄養素と血圧との関連が示唆されてきている。特に注目されるのは米国 DASH 研究が豊富な野菜・果物・魚摂取・低脂肪乳製品という食事パターン（DASH 食）による効果的な血圧低下を証明したことであり、そのメカニズムとして、少ない飽和脂肪酸、多い植物性（多価不飽和）脂肪酸、魚に多い n-3 系脂肪酸、抗酸化ビタミンなどが推察されているがいまだ明らかになっておらず、国際的に大きな課題となっている。一方、新たな動脈硬化危険因子として炎症反応指標である血清高感度 CRP が注目されているが、脂質・ビタミン類など酸化ストレス関連要因との関連や、血圧との関連については明らかになっていない。

本研究では大規模な成人集団において各種脂肪酸(飽和脂肪酸、一価不飽和脂肪酸、多価不飽和脂肪酸、n-3 系脂肪酸、n-6 系脂肪酸）および各種抗酸化ビタミン（ビタミン A, C, E, B 群）の摂取量を厳密に評価し、血清高感度 CRP および血圧値との関連を検討することを目的とする。

5．研 究 計 画

北陸地方の製造業事業所従業員の 20-60 歳の成人男女約 7000 人を対象として、食物摂取状況調査および血清高感度 CRP 測定、厳密に標準化された２回の血圧測定を行った。

食物摂取状況調査は 15 ページにわたる自記式調査であり、量頻度法を主にするものである。国立健康・栄養研究所佐々木敏氏の開発によるもので、佐々木氏との共同研究にて実施した。本調査法の妥当性・信頼性は、３日間食事記録法、24 時間蓄尿、血中指標等を用いて確認がされており、各種脂肪酸摂取量および各種抗酸化ビタミン摂取量についても精度の高い結果が得られる。調査票は 6527 人から回収され回収率は 89.3%であった。

血清高感度 CRP は 35-60 歳の従業員男女 3621 人においてラテックスネフェロメトリ

一法にて測定された（Behring Nephelometer Analyzer II, Behring)。血圧測定は標準化された自動血圧計を用い、7306 人の対象者において５分間の座位安静後２回厳密に測定された。

解析においては、各種脂肪酸・抗酸化ビタミンを始めとした各種摂取素摂取量と高感度 CRP、血圧との関連を、多変量解析を用いて年齢・肥満度・飲酒・喫煙等の交絡要因の影響を調整して明らかにした。血清高感度 CRP については 10mg/L 以上の人は除外し、対数変換値を用いて解析した。

６．研究成果

対象者の平均年齢は男女とも 47 歳、平均 BMI は男性 23.5kg/m^2、女性 22.7kg/m^2、血清高感度 CRP の幾何平均値は男性 0.43mg/L、女性 0.27mg/L であった。脂肪、飽和脂肪酸、一価不飽和脂肪酸、多価不飽和脂肪酸の摂取エネルギー比は男性が 20.8%kcal、5.1%kcal、7.2%kcal、5.4%kcal、女性が 27.0%kcal、6.8%kcal、9.2%kcal、6.8%kcal、そして n-6/n-3 比は男性が 2.7、女性が 2.9 で男性より女性で大きい値をとった($p<0.001$)。

収縮期血圧と各種栄養素摂取量（エネルギー調整値）との関連を、重回帰分析を用いて年齢、肥満度、飲酒、喫煙を調整し、男女別に検討した。男性においては総炭水化物摂取量と負の有意な関連を示した($p<0.01$)。しかし、各種の脂肪摂取量の指標及びビタミン類摂取量との関連は示さなかった。女性においては、総脂肪摂取、飽和脂肪摂取、一価不飽和脂肪摂取、多価不飽和脂肪摂取、および n-6 系脂肪酸摂取と有意な負の関連を示したが、n-3 系脂肪酸摂取との関連は示さなかった。各種脂肪酸の中では、オレイン酸摂取との負の関連が最も強かった($p<0.01$)。ビタミン類では、レチノール及びビタミン A との有意な負の関連を示した($p<0.001$)。

血清高感度 CRP は女性では年齢が高くなるにつれ統計学的に有意に高くなった($p<0.001$)。また BMI が大きくなるにつれ男女とも血清高感度 CRP は統計学的に有意に高くなった($p<0.001$)。

各種脂肪酸摂取を５分位に分けときの高感度 CRP の多変量調整幾何平均値はオレイン酸($p=0.007$)、リノール酸($P=0.018$)、パルミトレイン酸($p=0.025$)、α―リノレン酸($p=0.037$)、ステアリン酸($p=0.049$)で摂取エネルギー比が高いほど有意に低い傾向を認めた。長鎖 n-3 脂肪酸（EPA＋DHA）の摂取量に関して低摂取群、中程度摂取群、高摂取群の３群に分けて高感度 CRP と主な脂肪酸との関連を見たところ、長鎖 n-3 脂肪酸の中程度摂取群でのみオレイン酸 ($P=0.003$)、リノール酸 ($p=0.005$)、α―リノレン酸 ($p=0.009$)ともに統計学的に有意な負の関連を示した。

７．研究の考察・反省

血清高感度 CRP は近年新たな循環器疾患リスクファクターとして注目され、その科学的根拠が確立してきた。全身の動脈硬化の進行自体が低レベルの炎症を引き起こし、高感度 CRP 値は動脈硬化の進行度のマーカーであるとする考えもあるが、一方

で、酸化ストレスや代謝症候群が炎症を促進し動脈硬化の原因になるとする説もある。高感度 CRP は一般に加齢とともに上昇し、また肥満による上昇も多くの疫学研究で確認されており、今回の我々の検討においても同様の知見が得られた。しかし食事要因が血清高感度 CRP にどのように影響するかは未だ明らかになっていない。今回我々は大規模な日本人の集団における詳細な栄養調査から栄養摂取と高感度 CRP との関連を検討し、これまで高感度 CRP との関連が明らかになっていないオレイン酸、または炎症作用が報告されているアラキドン酸の前駆体であるリノール酸、そして抗炎症作用のあるエイコタペンタエン酸の前駆体であるα—リノレン酸の低摂取群より高摂取群で高感度 CRP が低い結果を得た。また日本人で摂取の多い長鎖 n-3 脂肪酸（EPA＋DHA）の中程度摂取群でのみ、高感度 CRP はオレイン酸、リノール酸、α—リノレン酸で統計学的に特に強い負の関連があったことは重要な点である。δ-5 desaturase とδ-6 desaturase によりα—リノレン酸は EPA に伸張し抗炎症作用のある PGE_3 に、リノール酸はアラキドン酸に伸張し炎症作用のある PGE_2 と LTE_4 を産生し、オレイン酸は EPA の疑似体のエイコサトリエン酸に伸張し抗炎症作用に働くとされている。これらの伸張は競合するので各々の脂肪酸の摂取比率により抗炎症、炎症作用が決まるとされているがメカニズム等は完全に解っていない。我々の結果は魚に多く含まれる EPA や DHA の日本人の平均的な摂取がオレイン酸、リノール酸、α—リノレン酸の抗炎症作用を有効に働かせることを示唆したものであり、循環器疾患予防のための脂肪摂取のあり方に新たな知見を提供するものである。

1．研究課題名：ウイルス感染症を伴う肥満者におけるアディポサイトカインの診断及び治療への応用
（研究番号 S2004-2）

2．キーワード：1）肥満（obesity）
2）ウイルス感染症（viral infection）
3）アディポサイトカイン（adipocytokine）

3．研究者氏名：高橋　孝・金沢医科大学・医学部・講師・総合内科学（総合診療科）

4．研究目的

現代病と言われている肥満は、糖代謝異常や内分泌異常を惹起し、易感染性や感染症の重篤化を招く場合が多いと言われている。これまでは、感染症との関わりを糖代謝及び内分泌の病的な状況という視点から説明されてきた。

しかし、脂肪組織が生体最大の内分泌臓器であるという概念から、肥満と感染症との直接的な関わりを検証する重要性があり、この点が本研究の意義である。これまでに、敗血症におけるレプチンの生体防御を示唆する報告はあるが、ウイルス感染症に対するレプチンの役割は検証されていない。SARS ウイルスを含む新興感染症が人類の生命を脅かす社会情勢においては、本研究が解明したい感染症に対する脂肪組織特異的な内分泌蛋白質の解析が急務であると考える。

そこで、本研究は、サイトカインの感染性疾患への関わりを脂肪組織特異的な生理活性物質（アディポサイトカイン）の視点から解析することによって、ウイルス感染症を伴う肥満者に対するアディポサイトカインの臨床診断（特に、予後予測因子の同定）、そして治療への応用を展開したい。そして、感染症を伴う肥満者に対するサイトカイン補充療法という治療方法の開発が期待できる。

5．研究計画

レプチン欠損肥満マウス（*ob* マウス）を用いて、encephalomyocarditis（EMC）ウイルスを接種させることによってウイルス性心筋炎という疾患モデルを作製する。

①　致死的なウイルス感染症（ウイルス性心筋炎）の発症下において、疾患マウスの生存率を評価する共に、アディポサイトカインの血中レベルの経時的変動を検討する。その結果から、本病態の予後を推測するマーカーを同定する。

②　感染症病巣（心臓局所）におけるアディポサイトカイン及びその mRNA の発現量と EMC ウイルスの力価定量との関連性を解析する。その結果に基づいて、局所でのウイルス力価と関連するアディポサイトカインを推定する。

③　上記の病態における予後改善に関与するアディポサイトカインを判定するために、外因性の同サイトカイン投与による生存観察や心筋障害を評価する。その結果から、予後の観点から見たアディポサイトカイン治療を想定する。

6．研究成果

①　*ob* マウスにおいて発症したウイルス性心筋炎において、野生型マウスでのウイルス性心筋炎と比較して、重篤な心筋壊死と共に、ウイルス接種後 10 日間という短期間において有意に低い生

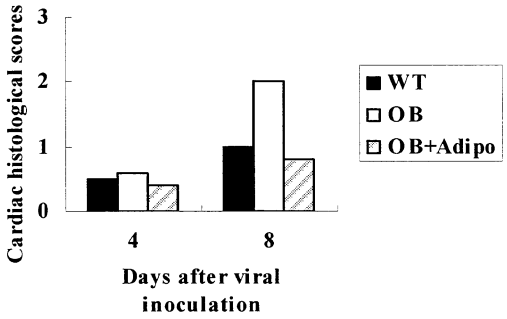
存率が観察された。*ob*マウスへのウイルス接種と共に、組換えマウスレプチン(300 μg/day 腹腔内投与)を補充した場合、生存率の改善が認められた。しかし、ウイルス感染後4日目と8日目に各群において測定した血中アディポネクチン値に有意な差は見られず、長寿因子である同サイトカインが肥満におけるウイルス感染症の予後マーカーであるというエビデンスは今回得られなかった。

② ウイルス接種後8日目に*ob*マウスより得られた心臓におけるアディポネクチンmRNA発現レベル(Real-time RT-PCR)及び蛋白質発現レベル(ELISA)は、野生型マウスと比較して、局所でのEMCウイルス高力価と共に有意な低値を示した。一方、同時期の*ob*マウスにおける心臓内TNF-α mRNA及び蛋白質発現レベルは、野生型と比べて、有意に増加した。免疫組織化学(IHC)を用いたアディポネクチン及びTNF-αの心筋細胞における発現に関しても、同様な結果が認められた。実際、心筋梗塞や拡張型心筋症といった臨床検体においても、障害心筋細胞自身におけるアディポネクチンとその受容体及びTNF-αの発現がIHCによって確認された。

アディポネクチンは、AMP活性化プロテインキナーゼやシクロオキシゲナーゼ-2(COX-2)を介してその作用を標的細胞において発現する。COX-2 ヘテロ欠損マウスがウイルス性心筋炎を発症した場合、野生型の心筋炎と比較して、局所のウイルス力価に有意差は認められないが、アディポネクチン発現低下とTNF-α発現亢進を伴って心筋細胞の障害が増悪する所見を見出した。

③ ①に提示したように、*ob*マウスにおけるウイルス性心筋炎は、重篤な心筋障害と低い生存率を示したが、組換えマウス全長アディポネクチン(30 μg/g/day 皮下投与)をウイルス接種と同時に連日補充することによって、心筋細胞におけるアディポネクチン受容体の発現増強と共に有意な心筋障害の抑制作用が認められた。そして、生存率の上昇という短期的な予後改善効果が確認された。

＜アディポネクチン補充療法と心筋障害抑制＞



WT:野生型マウス、OB:*ob*マウス、OB+Adipo:*ob*マウスにアディポネクチン補充

7．研究の考察・反省

① 肥満マウスにおける致死的なウイルス感染症のモデルは確立され、野生型マウスと比較して重篤な心筋障害と有意な生存率の減少が確認された。しかし、血中レベルでのアディポネクチンが予後因子となり得るという所見は認められず、今後、本病態の予後改善を推測する他の血中バイオマーカーを同定する必要がある。

② ウイルス力価と関連する局所発現のサイトカインとしてアディポネクチンやTNF-αが推定され、心筋細胞のアディポネクチン発現による自己防御機構の可能性が示唆された。今後は、心筋細胞あるいは脾臓細胞の培養系を確立して、アディポネクチンとウイルス複製抑制との直接的な関連性を確認したい。

③ ウイルス性心筋炎を伴う肥満マウスへのアディポネクチン補充療法による予後の改善が確認された。しかし、アディポネクチンの至適な投与量の設定には至っておらず、今後、同サイトカイン投与量の調整を検討したい。長期的な予後改善効果の確認も今後の課題である。

8．研究発表

Takahashi T, Yu F, Saegusa S, Sumino H, Nakahashi T, Iwai K, Morimoto S, Kurabayashi M, Kanda T. Impaired expression of cardiac adiponectin in leptin-deficient mice with viral myocarditis. *Int Heart J* 2006; 47: 107-123. (MLDB)

Takahashi T, Yu F, Zhu S, Moriya J, Sumino H, Morimoto S, Yamaguchi N, Kanda T. Beneficial effect of brewers' yeast extract on daily activity in a murine model of chronic fatigue syndrome. *Evid Based Complement Alternat Med* 2006; 3: 109-115. (MLDB)

Honda H, Iwahashi J, Kashiwagi T, Imamura Y, Hamada N, Anraku T, Ueda S, Kanda T, Takahashi T, Morimoto S. Outbreak of human metapneumovirus infection in elderly inpatients in Japan. *J Am Geriatr Soc* 2006; 54: 177-180. (MLDB)

Kanda T, Takahashi T, Sumino H, Nakahashi T, Iwai K, Morimoto S, Matsumoto M. Hypoadiponectinemia in bedridden female patients younger than 75. *J Am Geriatr Soc* 2005; 53: 2039-2041. (MLDB)

Takahashi T, Zhu S, Sumino H, Saegusa S, Nakahashi T, Iwai K, Morimoto S, Kanda T. Inhibition of cyclooxygenase-2 enhances myocardial damage in a mouse model of viral myocarditis. *Life Sci* 2005; 78: 195-204. (MLDB)

Takahashi T, Saegusa S, Sumino H, Nakahashi T, Iwai K, Morimoto S, Kanda T. Adiponectin replacement therapy attenuates myocardial damage in leptin-deficient mice with viral myocarditis. *J Int Med Res* 2005; 33: 207-214. (MLDB)

Takahashi T, Saegusa S, Sumino H, Nakahashi T, Iwai K, Morimoto S, Nojima T, Kanda T.

Adiponectin, T-cadherin and tumor necrosis factor-a in damaged cardiomyocytes from autopsied specimens. *J Int Med Res* 2005; 33: 236-244. (MLDB)

Kotajima N, Takahashi T, Ito H, Sumino H, Fukumura Y, Kurabayashi M, Murakami M, Kanda T. Clinical features associated with circulating concentration of soluble leptin receptor in patients with diabetes. *J Int Med Res* 2005; 33: 61-67. (MLDB)

Goto M, Takahashi T, Kanda T, Iwamoto A. Detection of *Toxoplasma gondii* by polymerase chain reaction in cerebrospinal fluid from human immunodeficiency virus-1-infected Japanese patients with focal neurological signs. *J Int Med Res* 2004; 32: 665-670. (MLDB)

Impaired Expression of Cardiac Adiponectin in Leptin-Deficient Mice With Viral Myocarditis

Takashi TAKAHASHI,[1] MD, Fei YU,[1] MD, Seiichiro SAEGUSA,[1] MD, Hiroyuki SUMINO,[3] MD, Takeshi NAKAHASHI,[2] MD, Kunimitsu IWAI,[2] MD, Shigeto MORIMOTO,[2] MD, Masahiko KURABAYASHI,[3] MD, *and* Tsugiyasu KANDA,[1] MD

SUMMARY

A mouse model of encephalomyocarditis (EMC) virus-induced myocarditis was used to investigate the expression of adiponectin in damaged cardiomyocytes. We intraperitoneally injected EMC virus into leptin-deficient *ob/ob* (OB) mice and wild-type (WT) mice. OB mice were divided into two subgroups consisting of mice with no intervention and mice receiving leptin replacement starting simultaneously with viral inoculation. We determined differences in heart weight, cardiac histological score, numbers of infiltrating and apoptotic cells in the myocardium, expression levels of adiponectin and TNF-α mRNA in the heart, adiponectin immunoreactivity in myocytes, adiponectin and TNF-α concentrations in the heart, and immunoreactivity of adiponectin receptors in myocytes between OB mice and WT mice. There was significantly decreased adiponectin mRNA expression, immunoreactivity, and protein level in the heart, and reduced immunoreactivity of adiponectin receptor 1 in myocytes from OB mice on days 4 and 8 after viral inoculation as compared with those in WT mice, together with increased cardiac weight, severe inflammatory myocardial damage, and increased levels of cardiac TNF-α mRNA and protein. Replacement of leptin in OB mice inhibited the development of severe myocarditis through augmentation of adiponectin mRNA, immunoreactivity, and protein level, increased adiponectin receptor 1 immunoreactivity in myocytes, and suppressed levels of TNF-α mRNA and protein. These results suggest that impaired expression of cardiac adiponectin may contribute to the progression of viral myocarditis through enhanced expression of TNF-α under a leptin-deficient condition. (Int Heart J 2006; 47: 107-123)

Key words: Adiponectin, Leptin deficiency, Viral myocarditis, Cardiomyocyte

HEART failure is generally considered to begin with myocyte damage caused by a variety of pathological conditions that include ischemia, toxins, and myocardial infection. The heart compensates by dilatation and cellular hypertrophy, and eventually decompensates, resulting in heart failure. A proinflammatory cytok-

From the Departments of [1] General Medicine and [2] Geriatric Medicine, Kanazawa Medical University, Ishikawa and [3] Department of Medicine and Biological Science, Gunma University Graduate School of Medicine, Gunma, Japan.

Address for correspondence: Tsugiyasu Kanda, MD, Department of General Medicine, Kanazawa Medical University, 1-1 Daigaku, Uchinada-machi, Kahoku-gun, Ishikawa 920-0293, Japan.

Received for publication January 24, 2005.

Revised and accepted May 9, 2005.

ine, tumor necrosis factor-α (TNF-α), has recently been postulated to be one of the pathogenetic factors responsible for the progression from compensated to decompensated heart failure. Mann and colleagues in 1996 demonstrated that the nonfailing human heart does not express, whereas the failing human heart expresses a significant amount of TNF-α.[1] Moreover, TNF-α immediately inhibits the contractility of isolated cardiac myocytes in a dose-dependent manner, and this negative inotropic action is completely reversible upon the removal of TNF-α.[2]

Identification of leptin is a good example of a contribution made by molecular biology to understanding the mechanisms initially hypothesized from classic physiological studies.[3] Several papers have focused on the association between leptin and cardiovascular disease, such as hypertension and cachexia, in chronic heart failure.[4-6] A reduced leptin concentration may diminish the degree of cardiac adaptation to heart failure.[7] It has also been shown that plasma leptin levels are inappropriately low in patients with cachectic chronic heart failure.[5] We have recently found that leptin deficiency enhances myocardial necrosis and lethality in a mouse model of viral myocarditis, suggesting a protective action of leptin against myocyte damage.[8] However, it is still unclear how severe inflammatory myocardial injury induced by viral infection develops under leptin deficiency.

Adiponectin, also known as 30-kDa adipocyte complement-related protein,[9] is a hormone secreted by adipocytes that acts as an antidiabetic and antiatherogenic cytokine.[10] The concentration of adiponectin in blood is diminished under conditions of obesity, insulin resistance, and type II diabetes.[9] Adiponectin administration is reported to have glucose-lowering effects and to improve insulin resistance in mice.[11] On the other hand, adiponectin-deficient mice develop insulin resistance and diabetes.[12] This effect of adiponectin appears to be mediated by elevation of fatty acid oxidation through activation of AMP-activated protein kinase[13] and peroxisome proliferator-activated receptor (PPAR)-α.[10] In clinical research, plasma adiponectin concentrations in subjects with both diabetes mellitus and coronary artery disease have been shown to be lower than in patients with coronary artery disease alone.[14] Individuals with very low plasma adiponectin levels may be at increased risk of developing both diabetes mellitus and coronary artery disease.

Comparison of the organization of the adiponectin gene with that of the obese gene, which encodes leptin, shows several striking similarities in humans.[15] These two genes, which are composed of three exons and have a long first intron, are expressed specifically in adipose tissue.[15] Adiponectin and leptin control fuel homeostasis, body weight, and insulin sensitivity. In another recent study, amelioration of insulin resistance, pancreatic β-cell degranulation, and diabetes after crossing leptin-deficient mice with globular domain adiponectin trans-

genic mice has been described, indicating that globular adiponectin and leptin may have overlapping functions.[10] Thus, adiponectin may also possess a function similar to the crucial role of leptin in the development of heart failure.

We hypothesized that cardiac expression of adiponectin could play a protective role against the progression of severe viral myocarditis under a leptin-deficient status. Therefore, we examined cardiac adaptation to heart failure through adiponectin expression in leptin-deficient mice with acute viral myocarditis, and the influence of leptin replacement therapy on adiponectin expression in the myocardium of leptin-deficient mice.

MATERIALS AND METHODS

Animals: Six-week-old female leptin-deficient *ob/ob* (OB) mice and C57BL wild-type (WT) mice were obtained from Jackson Laboratory (Bar Harbor, Maine, USA).

Virus: A myocarditic variant of encephalomyocarditis (EMC) virus was obtained from Y. Seto, PhD (Keio University, Tokyo, Japan). Virus preparations were stored at −80°C in Eagle's minimum essential medium supplemented with 0.1% fetal bovine serum until the time of use.

Infection protocol: Animals were intraperitoneally inoculated with 500 plaque-forming units of EMC virus suspended in 0.1 mL of saline.

Treatment protocol: WT ($n = 10$) and OB ($n = 40$) mice were injected with EMC virus. In addition, OB mice were randomly assigned to one of two groups. The first group ($n = 20$) received no interventional therapy. The second group ($n = 20$) of OB mice received a daily intraperitoneal injection of recombinant mouse leptin (300 μg per day, starting simultaneously with EMC virus inoculation, OB + Lep group).[8] Cardiac tissues were immediately extracted after sacrifice by cervical dislocation on days 4 and 8 after viral inoculation.

Histological examinations of hearts: Body weight was recorded before sacrifice. The heart was immediately weighed after sacrifice. Half of the cardiac tissue was fixed in 10% buffered formalin and stained with hematoxylin-eosin (H & E), while the other half was immediately frozen in liquid nitrogen and stored at −80°C for cytokine analyses. Two transverse sections of the ventricular myocardium were graded for the severity of necrosis and mononuclear cell infiltration by an experienced pathologist, who had no knowledge of the study design, according to the following scale: grade 1, lesions involving < 25% of the ventricular myocardium; grade 2, lesions involving 25 to 50% of the myocardium; grade 3, lesions involving 50 to 75% of the myocardium; and grade 4, lesions involving > 75% of the myocardium. We also performed staining of myosin to identify myocyte necrosis accurately. In addition, the pathologist randomly selected 5

high power fields (HPF) (× 400 magnification) from each transverse section of the myocardium, and counted the infiltrating cells. The number of apoptotic cells in 5 randomly selected HPF (× 400 magnification) per section in the transverse sections of myocardium was determined by *in situ* TUNEL as previously described.[16]

Detection of adiponectin mRNA in cardiomyocytes: *In situ* hybridization (ISH) using Digoxigenin (DIG) REMBRANDT for DNA ISH and a detection kit (Code HKD38003, Pan Path Co. Ltd., Amsterdam, Netherlands) was performed on serial sections of the heart from various mice on day 8 after viral inoculation as previously described.[17] The presence of adiponectin mRNA was also examined in cardiac tissue from a normal wild-type mouse with neither viral inoculation nor leptin administration. We used commercially synthesized DIG-labeled mouse adiponectin sense and antisense RNA probes (Hokkaido System Science Co. Ltd., Hokkaido, Japan). Each section was hybridized with the labeled probes at 37°C for 2 hours. This was followed by several washes in Tris-buffer and RNase A solutions. The sections were then incubated with alkaline phosphatase-conjugated rabbit anti-DIG Fab fragments (#D5105, DAKO Cytomation Co. Ltd., Kyoto, Japan). Signals were visualized with 4-nitro-blue-tetrazolium and 5-bromo-4-chloro-3-indolyl phosphate. The slides were blindly reviewed by the same pathologist, and the hybridization signal of adiponectin mRNA was determined for myocytes.

Comparative expression levels of adiponectin and TNF-α mRNA in cardiac tissues: RNA extraction was performed on half of each frozen cardiac tissue specimen as specified by the manufacturer (RNeasy Mini Kit, QIAGEN Inc., Tokyo). Total RNA concentration was determined by measuring the optical density at 260 nm. Aliquots of 20 μL of RNA from each tissue sample were used for the production of cDNA. Comparative expression levels of adiponectin mRNA in cardiac tissue from different groups were determined using quantitative real-time reverse transcriptase-polymerase chain reaction (RT-PCR) as described previously.[18] The expression levels of TNF-α mRNA were also examined by quantitative real-time RT-PCR. We used a commercially available kit for TNF-α and adiponectin RT-PCR (Mm00443258 mL and Mm00456425 mL, respectively, Applied Biosystems Inc., Foster City, CA, USA). The optimal number of cycles of RT-PCR was examined for the adiponectin mRNA level. The glyceraldehyde-3-phosphate dehydrogenase (GAPDH) gene was used as an endogenous internal standard, and was amplified with specific primers for the number of cycles. The gradient of the cycle numbers for adiponectin to GAPDH was determined. Adiponectin mRNA levels in the heart were calculated as comparative values, which were normalized to adiponectin mRNA in the heart from a normal wild-type mouse with neither viral inoculation nor leptin administration (assigned value

equal to 1).

Adiponectin immunoreactivity in cardiomyocytes: Immunohistochemical staining using the streptavidin biotin complex method (#K0675 and #E0353, DAKO Cytomation) was performed on serial transverse sections of ventricular myocardium from different mice on days 4 and 8 after viral inoculation. As a normal control, adiponectin immunoreactivity was determined in a heart from a normal wild-type mouse with neither viral inoculation nor leptin administration. We used the following commercially available primary antibody at a dilution of 1:50; rabbit polyclonal anti-mouse adiponectin antibody (#ACRP303-A, Alpha Diagnostic International Inc., San Antonio, TX, USA). Control slides were treated with normal diluted rabbit serum. The slides were blindly reviewed by the same pathologist, and were semiquantitatively graded according to the degree of immunoreactivity: 0 for absence of staining, 1+ for weak, 2+ for moderate, and 3+ for strong staining.[19] They were compared with the respective control slides to exclude nonspecific staining. Adiponectin immunoreactivity was assessed in 30 randomly selected myocytes corresponding to the surviving cells found in respective H&E- and myosin-stained slides.

Concentrations of adiponectin and TNF-α in heart: Adiponectin and TNF-α levels in the homogenate of each tissue were measured using the other half of frozen cardiac tissue samples. An enzyme-linked immunosorbent assay (ELISA), which used a polyclonal antibody specific for mouse TNF-α or adiponectin precoated onto a microtiter plate (ELISA kit for TNF-α: BioSource International Inc., Camarillo, CA, USA; ELISA kit for adiponectin: Otsuka Pharmaceutical Co., Ltd., Tokyo), was performed on tissue samples according to the manufacturers' instructions. As a normal control, cardiac levels of adiponectin and TNF-α were determined in the heart from a normal WT mouse without viral infection. For data processing, we allocated the minimum values detected by the ELISA assay to all samples with concentrations below the detection threshold. The ELISA kit used for TNF-α concentration showed that the limit of sensitivity and the intra- and interassay variations were 3.0 pg/mL, 6.5%, and 8.7%, respectively. The ELISA kit used for adiponectin levels demonstrated sensitivity, intra-assay variance, and cross-reactivity of 0.25 ng/mL, less than 10%, and no response for specimens from other animals including sheep, respectively.

Immunoreactivity of adiponectin receptors in cardiomyocytes: To examine the immunoreactivity of adiponectin receptors 1 and 2 (AdipoR1 and AdipoR2) in the heart, immunohistochemical staining by the streptavidin biotin complex method was performed on serial sections of myocardium on days 4 and 8, which had been used to determine the adiponectin immunoreactivity of myocytes. The immunoreactivity of AdipoR1 and AdipoR2 in vessels and macrophages was considered as a positive control. As a normal control, the immunoreactivity of

AdipoR1 or AdipoR2 was determined in the heart from a normal wild-type mouse with neither viral inoculation nor leptin administration. We used the following primary antibodies at a dilution of 1:50: rabbit polyclonal anti-mouse AdipoR1 or AdipoR2 antibodies (#ADIPOR11-A or ADIPOR21-A, Alpha Diagnostic International Inc.). Control slides were treated with normal diluted rabbit serum. The slides were blindly reviewed by the same pathologist, and were semiquantitatively graded according to the criteria for immunoreactivity as used for adiponectin immunoreactivity. They were compared with the respective control slides, and AdipoR1 or AdipoR2 immunoreactivity was evaluated in 30 myocytes corresponding to cells where adiponectin immunoreactivity was observed.

Statistical analyses: Data are expressed as the mean ± standard deviation. Analysis of variance (ANOVA) was used to evaluate the differences in body and cardiac weights, numbers of infiltrating and apoptotic cells in the myocardium, comparative expression level of adiponectin mRNA in cardiac tissue, and adiponectin concentration in the heart, as compared with those in the WT group. The Kruskal-Wallis test was used for nonparametric analysis to assess the differences in cardiac histological score and immunoreactivity of adiponectin or its receptors in myocytes. A value of $P < 0.05$ was considered to be statistically significant.

RESULTS

Mortality in different mice with viral myocarditis: The numbers of mice with viral myocarditis that died were 1, 9, and 2 in the WT, OB, and OB + Lep groups, respectively, during the period of the treatment protocol. The numbers of mice in different groups from which heart specimens were obtained on days 4 and 8 after viral inoculation were 5 and 4 in the WT group, 6 and 5 in the OB group, and 10 and 8 in the OB + Lep group, respectively.

Body weight and cardiac weight: Body weight on days 0, 4, and 8 after viral infection was significantly greater in the OB and OB + Lep groups than in the WT group ($P < 0.05$, Table). Heart weight in the OB group on day 8 after viral inocu-

Table. Body Weight and Cardiac Weight in Different Mice Groups After Viral Inoculation

	Body weight (g)			Cardiac weight (mg)	
	Day 0	Day 4	Day 8	Day 4	Day 8
WT	18.1 ± 1.2	18.3 ± 1.5	18.9 ± 1.7	97 ± 5	101 ± 8
OB	37.3 ± 2.5*	37.1 ± 2.9*	38.2 ± 3.1*	105 ± 7	118 ± 15*
OB + Lep	36.9 ± 2.8*	37.2 ± 3.5*	35.1 ± 4.1*	99 ± 8	103 ± 11

WT indicates wild-type mice; OB, ob/ob mice; and OB ± Lep, ob/ob mice receiving leptin. Data are expressed as means ± SD. * $P < 0.05$ compared with WT mice group.

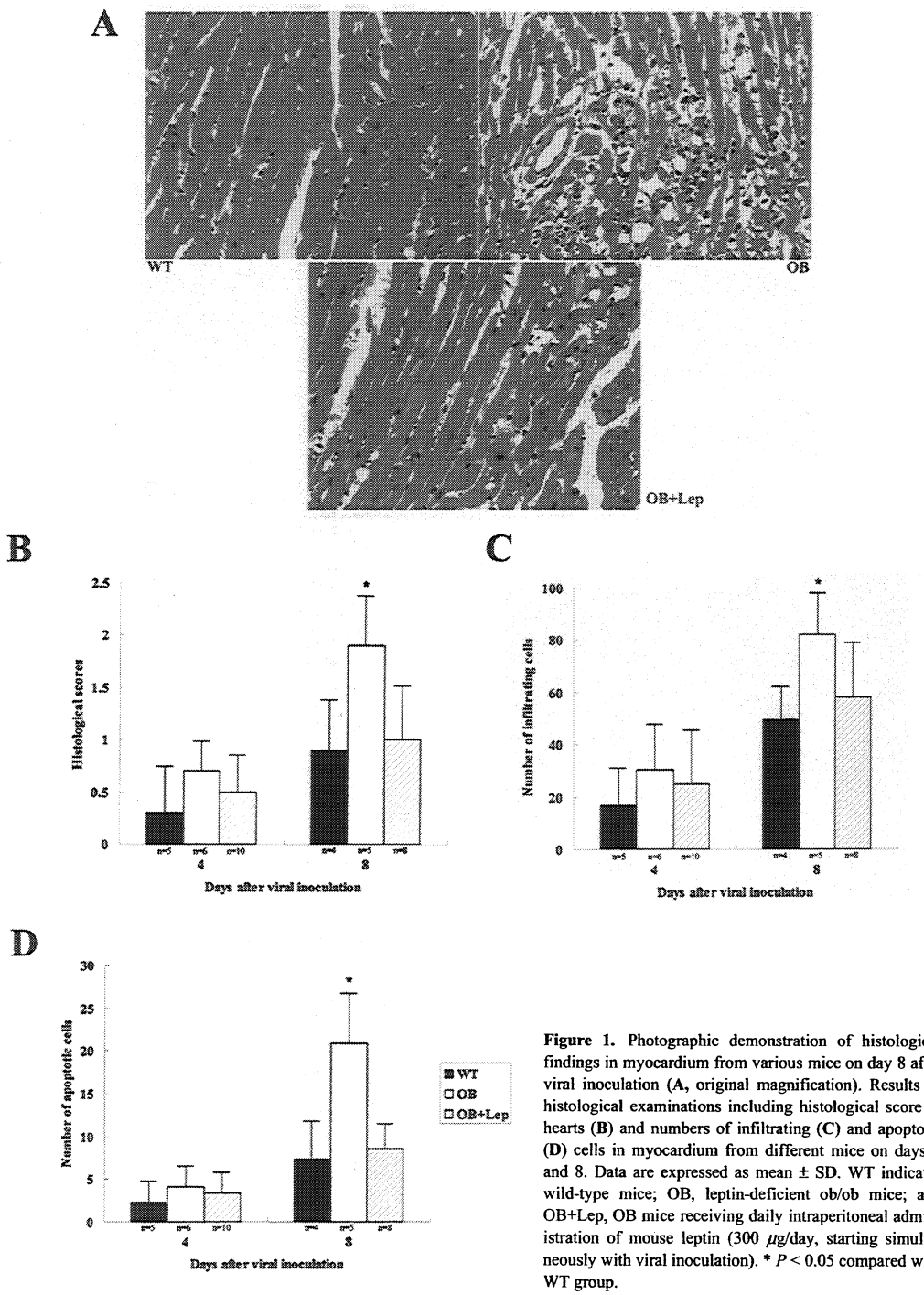


Figure 1. Photographic demonstration of histological findings in myocardium from various mice on day 8 after viral inoculation (**A**, original magnification). Results of histological examinations including histological score in hearts (**B**) and numbers of infiltrating (**C**) and apoptotic (**D**) cells in myocardium from different mice on days 4 and 8. Data are expressed as mean ± SD. WT indicates wild-type mice; OB, leptin-deficient ob/ob mice; and OB+Lep, OB mice receiving daily intraperitoneal administration of mouse leptin (300 μg/day, starting simultaneously with viral inoculation). * $P < 0.05$ compared with WT group.

lation was significantly increased as compared with that in the WT group ($P < 0.05$, Table). There was no significant difference in cardiac weight between the OB + Lep group and the WT group.

Histological findings in heart: Photographic demonstration of the histological findings in the myocardium from various mice on day 8 after virus infection is shown in Figure 1A. The histological score and numbers of infiltrating and apoptotic cells per field in hearts from different mice on days 4 and 8 are shown in Figures 1B, 1C, and 1D, respectively. The hearts from the OB group showed severe myocardial necrosis and mononuclear cell infiltration. The histological score for myocardial necrosis and cell infiltration on day 8 was significantly higher in the OB group than in the WT group ($P < 0.05$, Figure 1B). The number of infiltrating cells per field in the ventricular myocardium on day 8 in the OB group was significantly elevated as compared with that in the WT group ($P < 0.05$, Figure 1C). The number of apoptotic cells per field in the heart on day 8 was significantly higher in the OB group than in the WT group ($P < 0.05$, Figure 1D). There were no significant differences in histological score and numbers of infiltrating and apoptotic cells between the OB + Lep mice and WT mice.

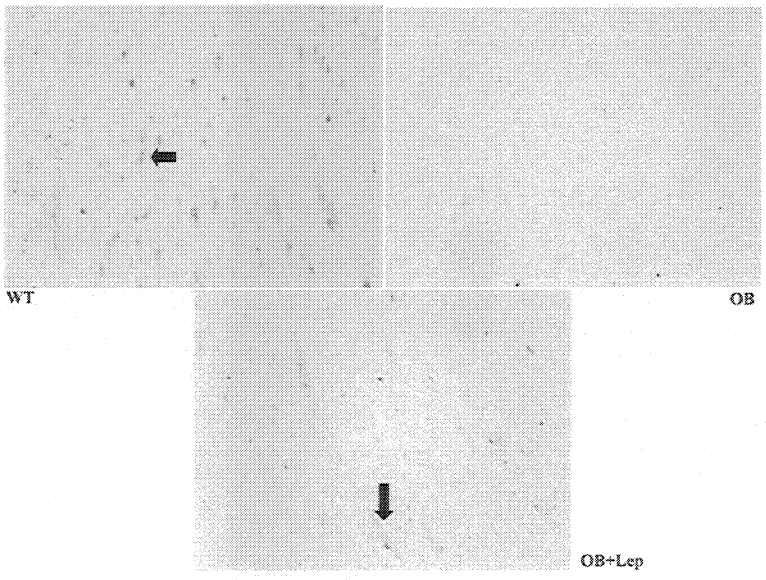


Figure 2. Detection of adiponectin mRNA (arrows) by *in situ* hybridization in myocardium from various mice on day 8 after viral infection. *In situ* hybridization using a digoxigenin-labeled adiponectin antisense riboprobe was performed on myocardial sections from different mice. WT indicates wild-type mice; OB, leptin-deficient ob/ob mice; and OB + Lep, OB mice receiving daily intraperitoneal administration of mouse leptin (300 μg/day, starting simultaneously with viral inoculation).

Detection of adiponectin mRNA in cardiomyocytes: To investigate the localization of adiponectin mRNA in the heart, ISH was performed on myocardial sections using an adiponectin antisense RNA probe. Adiponectin mRNA was not found in myocytes from a normal wild-type mouse. A moderate to strong signal for adiponectin mRNA was detected in myocytes from WT mice and OB + Lep mice on day 8 after viral infection (Figure 2). The adiponectin signal in the myocardium from OB mice at the same time was only very slight (Figure 2). There was no detectable adiponectin signal when ISH was performed on these sections using the sense probe.

Comparative expression levels of adiponectin and TNF-α mRNA in cardiac tissue: Comparative expression levels of adiponectin and TNF-α mRNA in the hearts from different mice on days 4 and 8 after virus infection are shown in Figures 3A and 3B, respectively. Adiponectin mRNA levels in the hearts on days 4 and 8 were significantly lower in OB mice than in WT mice ($P < 0.05$, Figure 3A). There was no difference in the cardiac levels of adiponectin mRNA between OB + Lep mice and WT mice. On the other hand, significantly elevated levels of TNF-α mRNA were observed on days 4 and 8 in the OB group compared with those in the WT group ($P < 0.05$, Figure 3B). There was no significant difference in TNF-α mRNA levels between the OB + Lep group and WT group.

Adiponectin immunoreactivity in cardiomyocytes: Adiponectin immunoreactivity was not observed in the myocardium from a normal wild-type mouse. Photo-

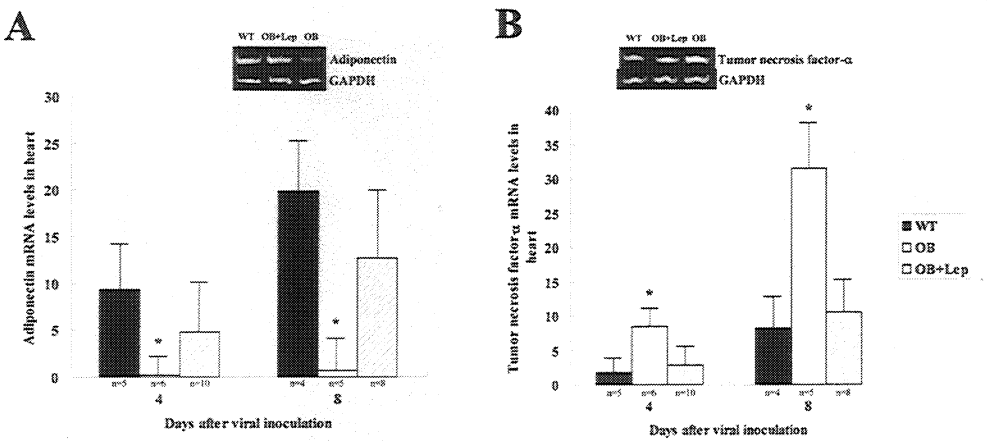


Figure 3. Comparative adiponectin (**A**) and tumor necrosis factor-α (**B**) mRNA levels using quantitative real-time reverse transcriptase-polymerase chain reaction with hearts from various mice on days 4 and 8 after viral infection, and demonstration of amplified cardiac adiponectin (**A**) and tumor necrosis factor-α (**B**) mRNA and corresponding glyceraldehyde-3-phosphate dehydrogenase gene on agarose gel, which were derived from various mice on day 8 after viral inoculation. Data are expressed as mean ± SD. WT indicates wild-type mice; OB, leptin-deficient ob/ob mice; and OB + Lep, OB mice receiving daily intraperitoneal administration of mouse leptin (300 μg/day, starting simultaneously with viral inoculation). * $P < 0.05$ compared with WT group.

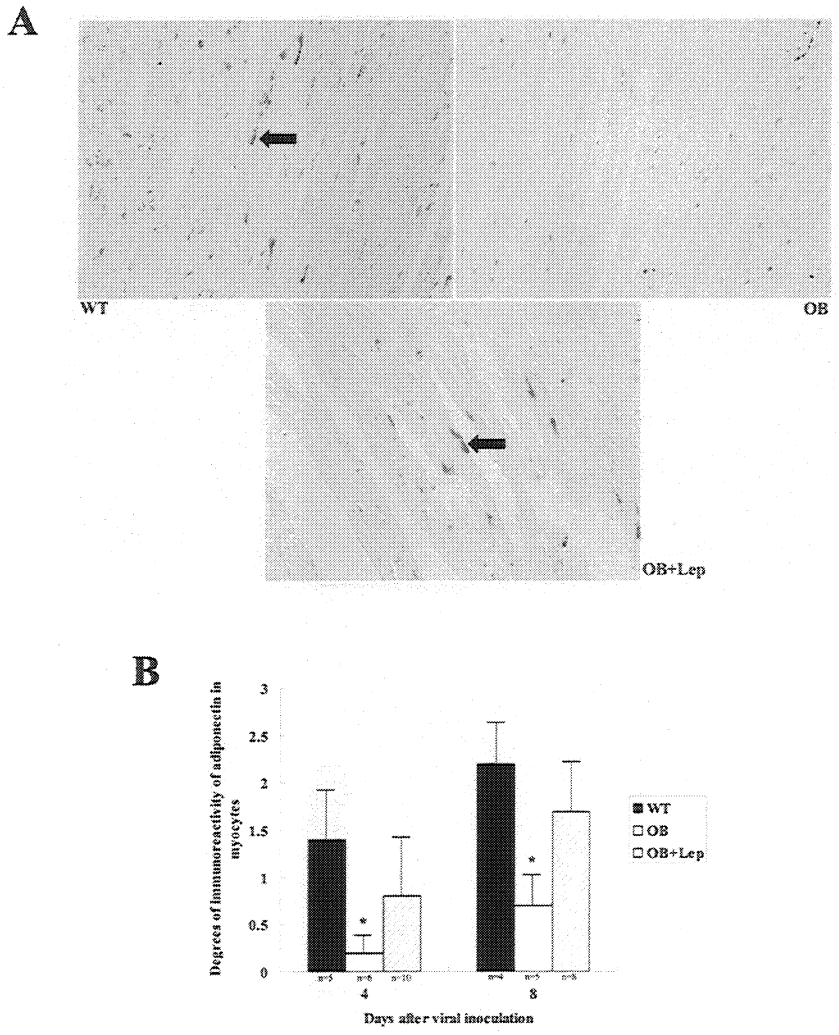


Figure 4. Adiponectin immunoreactivity in cardiomyocytes consisting of photographic demonstration of adiponectin immunoreactivity (arrows) in myocardium from different mice on day 8 after viral inoculation (**A**, original magnification) and adiponectin immunoreactivity in myocytes (**B**) from various mice on days 4 and 8. Data are expressed as mean ± SD. WT indicates wild-type mice; OB, leptin-deficient ob/ob mice; and OB + Lep, OB mice receiving daily intraperitoneal administration of mouse leptin (300 μg/day, starting simultaneously with viral inoculation). * $P < 0.05$ compared with WT group.

graphic demonstration of immunoreactivity of adiponectin in myocytes from different mice on day 8 after viral inoculation is shown in Figure 4A. Adiponectin immunoreactivity in myocytes from various mice on days 4 and 8 is shown in Figure 4B. We found significantly suppressed adiponectin immunoreactivity in myocytes from the OB group as compared with those from the WT group at the

same times ($P < 0.05$, Figure 4B). There was expression of adiponectin in myocardial cells from OB + Lep mice, which was similar to the findings of adiponectin immunoreactivity in myocytes from WT mice. The immunoreactive distribution of adiponectin protein in transverse ventricular sections largely overlapped with that of adiponectin mRNA observed using the ISH method.

Concentrations of adiponectin and TNF-α in heart: Specimens of heart from a normal wild-type mouse showed undetectable levels of each molecule. Adiponectin and TNF-α concentrations in the hearts from different mice on days 4 and 8 after viral infection are shown in Figures 5A and 5B, respectively. Cardiac concentrations of adiponectin on days 4 and 8 were significantly lower in the OB group than in the WT group ($P < 0.05$, Figure 5A). There was no difference in cardiac concentrations of adiponectin between the OB + Lep group and WT group. On the other hand, significantly increased concentrations of TNF-α were found on days 4 and 8 in OB mice compared with those in WT mice ($P < 0.05$, Figure 5B). There was no significant difference in TNF-α concentrations between OB + Lep mice and WT mice.

Immunoreactivity of adiponectin receptors in cardiomyocytes: AdipoR1 and AdipoR2 immunoreactivity was found in the arterial wall and macrophages obtained from a normal wild-type mouse, respectively. Photographic demonstration of immunoreactivity of adiponectin receptor 1 in myocardium from various mice on day 8 after viral inoculation is shown in Figure 6A. AdipoR1 and AdipoR2 immunoreactivity in myocardial cells from different mice on days 4 and 8 is shown in Figures 6B and 6C. We observed significantly lower AdipoR1 immunoreactivity in myocytes from OB mice at the same times (Figure 6B). The

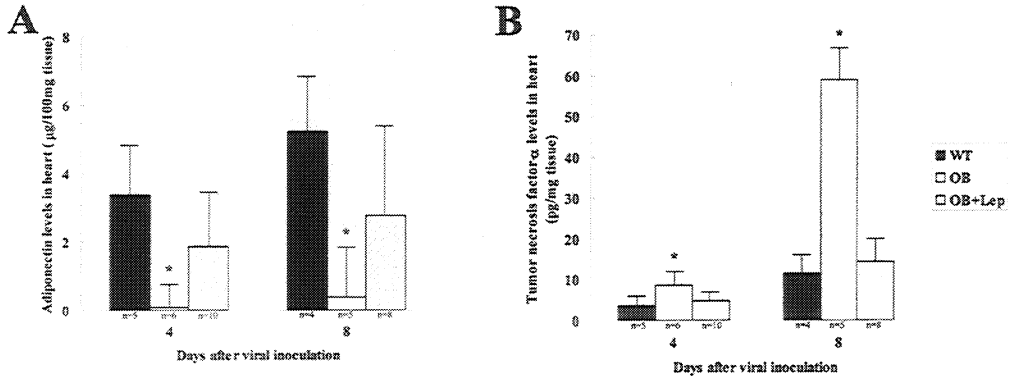


Figure 5. Concentrations of adiponectin (**A**) and tumor necrosis factor-α (**B**) in hearts from different mice on days 4 and 8 after viral inoculation. Data are expressed as mean ± SD. WT indicates wild-type mice; OB, leptin-deficient ob/ob mice; and OB + Lep, OB mice receiving daily intraperitoneal administration of mouse leptin (300 μg/day, starting simultaneously with viral inoculation). * $P < 0.05$ compared with WT group.

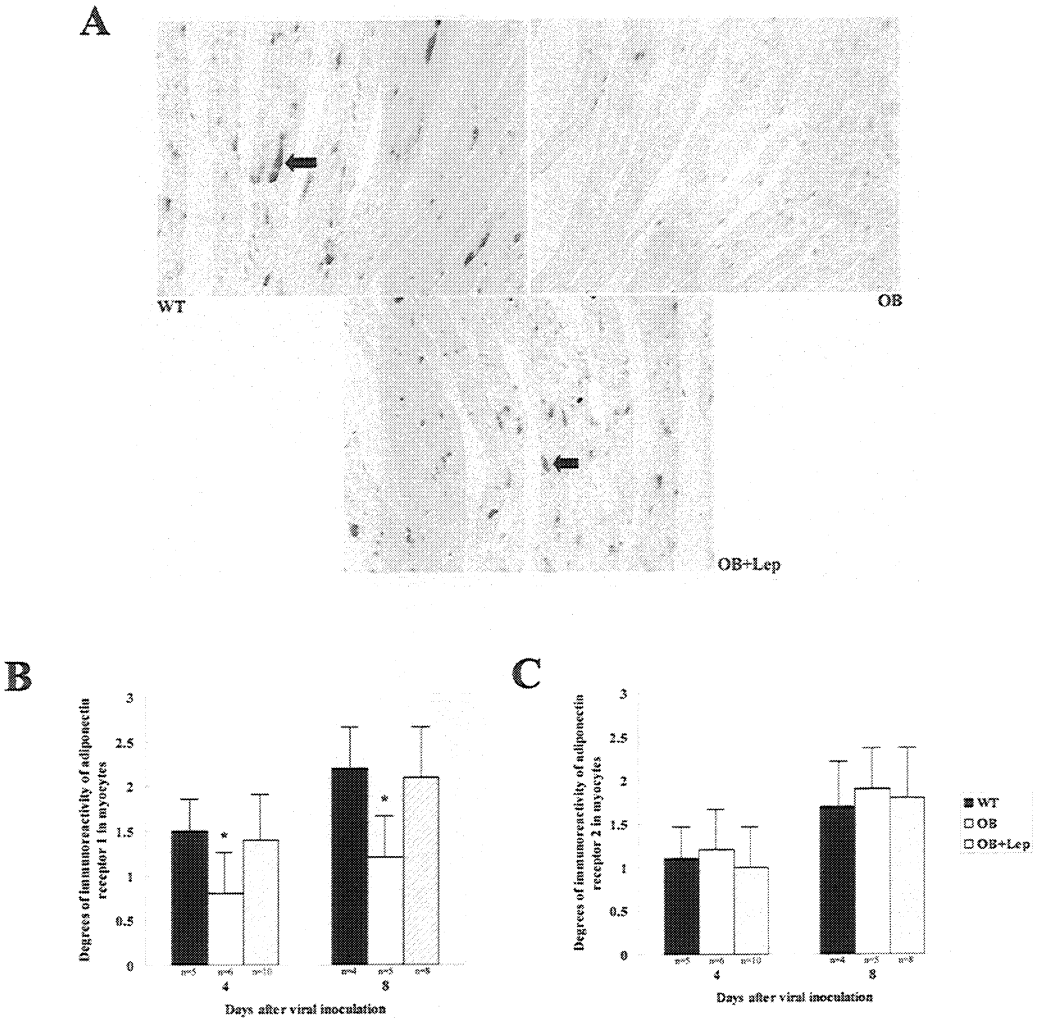


Figure 6. Adiponectin receptor immunoreactivity in cardiomyocytes consisting of photographic demonstration of adiponectin receptor 1 immunoreactivity (arrows) in myocardium from different mice on day 8 after viral inoculation (**A**, original magnification) and adiponectin receptor 1 (**B**) or 2 (**C**) immunoreactivity in myocytes from various mice on days 4 and 8. Data are expressed as mean ± SD. WT indicates wild-type mice; OB, leptin-deficient ob/ob mice; and OB + Lep, OB mice receiving daily intraperitoneal administration of mouse leptin (300 μg/day, starting simultaneously with viral inoculation). * $P < 0.05$ compared with WT group.

degree of AdipoR1 immunoreactivity in myocytes from OB + Lep mice was similar to that in myocytes from WT mice. There was no significant difference in AdipoR2 immunoreactivity in myocytes among all groups.

DISCUSSION

Cardiac expression of adiponectin was impaired in leptin-deficient mice with viral myocarditis. Adiponectin reactivity on immunostaining was recently reported to be observed at the periphery of surviving cardiomyocytes around lesions in the granulation stage in myocardial tissues obtained from 47 autopsied hearts with infarction.[20] In another immunohistochemical analysis, the boundary of mouse hepatocytes showed positive signals for adiponectin after 3-6 hours of carbon tetrachloride treatment, and their cytoplasm was intensely stained after 18 hours of treatment.[17] Adiponectin was suggested to be produced by the liver in mice, where it underwent tissue damage-induced transcriptional regulation.[17] Our data regarding adiponectin expression in surviving myocytes suggest that this adipocytokine may have important implications in the acute phase of viral myocarditis.

Adiponectin is reported to be involved in ending inflammatory responses through its inhibitory actions.[21] This cytokine increases mRNA expression of the anti-inflammatory molecule interleukin-10 (IL-10) at the transcriptional level, and promoted IL-10 protein secretion in an *in vitro* experiment in human monocyte-derived macrophages.[22] In addition, a reciprocal relationship between adiponectin and highly-sensitive C-reactive protein was shown in both human plasma and adipose tissue from subjects with coronary artery disease.[18] In our experiment, suppressed expression of cardiac adiponectin mRNA, immunoreactivity, and protein in OB mice was associated with the development of severe myocarditis, whereas increased expression of adiponectin in the hearts from WT mice and OB + Lep mice led to inhibition of the myocardial inflammatory process. Therefore, we speculate that local expression of adiponectin in the damaged heart may be a compensatory phenomenon against the severe inflammatory condition of viral myocarditis.

TNF-α mRNA was shown to be detectable in myocardium obtained from subjects with ischemic heart disease (IHD) and dilated cardiomyopathy (DCM) using Northern blot analysis, while there is no evidence for TNF-α gene expression in the nonfailing human heart.[1] Immunohistochemical examination also indicated that there was obvious TNF-α immunostaining of cardiomyocytes from patients with IHD and DCM, whereas TNF-α immunoreactivity was not detectable in the nonfailing heart.[1] Natriuretic peptides including atrial and B-type peptides are synthesized and secreted by the heart, and play a critical role in cardiovascular homeostasis.[23] Similarly to the previous demonstration, identification of adiponectin expression in the myocardium is also a good example of a contribution made by molecular biology to understanding the mechanisms for heart failure compensation.

Delporte and colleagues[24] have recently suggested a causal relationship exists between leptin and adiponectin in OB mice. The adiponectin content of visceral fat and adiponectin secretion by adipose tissue were blunted in OB mice. Leptin treatment of OB mice increased adiponectin mRNA, adiponectin content, and secretion from visceral fat by 50-80%. Leptin also directly stimulated adiponectin mRNA and secretion from adipocytes. Leptin replacement therapy was reported to restore adipose tissue adiponectin concentration and secretion, at least in part, via direct stimulation of adiponectin gene expression in OB mice. Therefore, we believe that leptin treatment might induce expression of cardiac adiponectin mRNA and content in OB mice with viral myocarditis through a similar mechanism.

We determined the expression levels of a proinflammatory cytokine, TNF-α mRNA, and protein in the heart from different mice on days 4 and 8 after viral inoculation as previously described.[8] Significantly increased levels of cardiac TNF-α mRNA and protein on both days were observed in OB mice compared with those in WT mice, together with severe myocarditis and reciprocal changes in adiponectin mRNA and protein. Administration of leptin to OB mice inhibited the progression of severe myocarditis through augmentation of adiponectin mRNA and protein levels and reduced levels of TNF-α mRNA and protein. Adiponectin-knockout mice revealed a high level of TNF-α mRNA in adipose tissue and a high plasma TNF-α concentration.[12] Adiponectin was also reported to inhibit TNF-α production in macrophages.[21] Therefore, adiponectin expression induced by leptin replacement seems to be able to protect against myocarditis through suppression of expression of TNF-α.

Cloning of cDNA encoding two adiponectin receptors (AdipoR1 and AdipoR2) has recently been demonstrated.[25] AdipoR1 is located at chromosome 1p36.13-q41, and AdipoR2 is located at chromosome 12p13.31. AdipoR1 and AdipoR2 are expressed ubiquitously in most organs, especially AdipoR1 in skeletal muscle and AdipoR2 in the liver.[25] Pancreatic β cells were also shown to express adiponectin receptors in a cell culture system.[26] These receptors include 7 transmembrane domains and activate signaling molecules such as PPAR-α, AMP-activated protein kinase, and mitogen-activated protein kinase.[25] Interestingly, we found AdipoR1 and AdipoR2 immunoreactivity as well as adiponectin immunoreactivity in myocardial cells in a mouse model of viral myocarditis. These results indicate that the surviving myocytes may possess an adiponectin-autocrine system, which leads to protection against the progression of myocardial inflammation.

Obesity reduces AdipoR1/R2 expression levels and decreases adiponectin sensitivity, which finally leads to insulin resistance. Improved adiponectin sensitivity should serve as a treatment target for obesity-related diseases.[27] Replace-

ment of leptin in OB mice inhibited the development of severe myocarditis through augmentation of AdipoR1, but not AdipoR2, immunoreactivity in myocytes. We found that adiponectin replacement therapy could attenuate myocardial damage in OB mice with viral myocarditis.[28] Adiponectin replacement also suppressed the development of severe myocarditis by enhancing myocyte AdipoR1, but not AdipoR2, immunoreactivity. Thus, there seems to be selectivity in the adiponectin receptor subtype in myocytes from OB mice. Similarly to our data, it has been demonstrated in another experiment that elevation of liver AdipoR1 expression and reduction in the AdipoR2 expression were observed in obese mice given a combination of leptin and a melanocortin receptor agonist, although there were no alterations in the AdipoR1 or AdipoR2 expression in the mice receiving the melanocortin receptor agonist alone.[29] In addition, changes in AdipoR1/R2 expression in skeletal muscle and adipose tissue have been reported in type 2 diabetic patients during PPAR-γ agonist therapy.[30] AdipoR1 expression was up-regulated in adipose tissue but down-regulated in muscle by rosiglitazone. On the other hand, AdipoR2 expression was not changed by rosiglitazone in either of the tissues. The increase in adipose tissue AdipoR1 expression with rosiglitazone was associated with increased postprandial triglyceride clearance and increased fasting fatty acid output. AdipoR1 is suggested to play a role in mediating adiponectin effects in specific tissues in relation to insulin sensitization and anti-inflammation. It is necessary to evaluate the effects of adiponectin using AdipoR1-knock out mice in the future.

Conclusion: We found reduced expression of adiponectin mRNA, immunoreactivity, and protein levels and decreased immunoreactivity of AdipoR1 in the heart from OB mice after viral infection, together with increased heart weight, severe myocardial inflammation, and elevated levels of cardiac TNF-α mRNA and protein. Administration of leptin to OB mice resulted in suppression of the development of severe myocarditis through augmentation of adiponectin mRNA, immunoreactivity, and protein levels, elevated AdipoR1 immunoreactivity in myocytes, and reduced levels of TNF-α mRNA and protein. Our observations suggest that impaired expression of adiponectin in the heart is associated with the development of viral myocarditis through enhancement of TNF-α expression under a leptin-deficient status.

ACKNOWLEDGMENTS

This study was supported in part by a Grant for Promoted Research from Kanazawa Medical University (S2004-2 and S2005-5), a Grant for Project Research from the High-Technology Center of Kanazawa Medical University (H2004-7), and the Science Research Promotion Fund of the Promotion and Mutual Aid Corporation for Private Schools of Japan.

REFERENCES

1. Torre-Amione G, Kapadia S, Lee J, *et al.* Tumor necrosis factor-alpha and tumor necrosis factor receptors in the failing human heart. Circulation 1996; 93: 704-11.
2. Yokoyama T, Vaca L, Rossen RD, Durante W, Hazarika P, Mann DL. Cellular basis for the negative inotropic effects of tumor necrosis factor-alpha in the adult mammalian heart. J Clin Invest 1993; 92: 2303-12.
3. Mantzoros CS. The role of leptin in human obesity and disease: a review of current evidence. Ann Intern Med 1999; 130: 671-80. (Review)
4. Miller KK, Parulekar MS, Schoenfeld E, *et al.* Decreased leptin levels in normal weight women with hypothalamic amenorrhea: the effects of body composition and nutritional intake. J Clin Endocrinol Metab 1998; 83: 2309-12.
5. Murdoch DR, Rooney E, Dargie HJ, Shapiro D, Morton JJ, McMurray JJ. Inappropriately low plasma leptin concentration in the cachexia associated with chronic heart failure. Heart 1999; 82: 352-6.
6. Wallace AM, McMahon AD, Packard CJ, *et al.* Plasma leptin and the risk of cardiovascular disease in the West of Scotland Coronary Prevention study (WOSCOPS). Circulation 2001; 104: 3052-6.
7. Makris TK, Stavroulakis GA, Krespi PG, *et al.* Elevated plasma immunoreactive leptin levels preexist in healthy offspring of patients with essential hypertension. Am Heart J 1999; 138: 922-5.
8. Kanda T, Takahashi T, Kudo S, Takeda T, Tsugawa H, Takekoshi N. Leptin deficiency enhances myocardial necrosis and lethality in a murine model of viral myocarditis. Life Sci 2004; 75: 1435-47.
9. Hu E, Liang P, Spiegelman BM. AdipoQ is a novel adipose-specific gene dysregulated in obesity. J Biol Chem 1996; 271: 10697-703.
10. Yamauchi T, Kamon J, Waki H, *et al.* Globular adiponectin protected ob/ob mice from diabetes and ApoE-deficient mice from atherosclerosis. J Biol Chem 2003; 278: 2461-8.
11. Berg AH, Combs TP, Du X, Brownlee M, Scherer PE. The adipocyte-secreted protein Acrp30 enhances hepatic insulin action. Nat Med 2001; 7: 947-53.
12. Maeda N, Shimomura I, Kishida K, *et al.* Diet-induced insulin resistance in mice lacking adiponectin/ACRP30. Nat Med 2002; 8: 731-7.
13. Yamauchi T, Kamon J, Minokoshi Y, *et al.* Adiponectin stimulates glucose utilization and fatty-acid oxidation by activating AMP-activated protein kinase. Nat Med 2002; 8: 1288-95.
14. Chan KC, Chou HH, Wu DJ, Wu YL, Huang CN. Diabetes mellitus has an additional effect on coronary artery disease. Jpn Heart J 2004; 45: 921-7.
15. Saito K, Tobe T, Minoshima S, *et al.* Organization of the gene for gelatin-binding protein (GBP28). Gene 1999; 229: 67-73.
16. Kanda T, Koike H, Arai M, *et al.* Increased severity of viral myocarditis in mice lacking lymphocyte maturation. Int J Cardiol 1999; 68: 13-22.
17. Yoda-Murakami M, Taniguchi M, Takahashi K, *et al.* Changes in expression of GBP28/adiponectin in carbon tetrachloride-administered mouse liver. Biochem Biophys Res Commun 2001; 285: 372-7.
18. Ouchi N, Kihara S, Funahashi T, *et al.* Reciprocal association of C-reactive protein with adiponectin in blood stream and adipose tissue. Circulation 2003; 107: 671-4.
19. Kanazawa K, Kawashima S, Mikami S, *et al.* Endothelial constitutive nitric oxide synthase protein and mRNA increased in rabbit atherosclerotic aorta despite impaired endothelium-dependent vascular relaxation. Am J Pathol 1996; 148: 1949-56.
20. Ishikawa Y, Akasaka Y, Ishii T, *et al.* Changes in the distribution pattern of gelatin-binding protein of 28 kDa (adiponectin) in myocardial remodelling after ischaemic injury. Histopathology 2003; 42: 43-52.
21. Yokota T, Oritani K, Takahashi I, *et al.* Adiponectin, a new member of the family of soluble defense collagens, negatively regulates the growth of myelomonocytic progenitors and the functions of macrophages. Blood 2000; 96: 1723-32.
22. Kumada M, Kihara S, Ouchi N, *et al.* Adiponectin specifically increased tissue inhibitor of metalloproteinase-1 through interleukin-10 expression in human macrophages. Circulation 2004; 109: 2046-9.
23. Grepin C, Dagnino L, Robitaille L, Haberstroh L, Antakly T, Nemer M. A hormone-encoding gene identifies a pathway for cardiac but not skeletal muscle gene transcription. Mol Cell Biol 1994; 14: 3115-29.

24. Delporte ML, El Mkadem SA, Quisquater M, Brichard SM. Leptin treatment markedly increased plasma adiponectin but barely decreased plasma resistin of ob/ob mice. Am J Physiol Endocrinol Metab 2004; 287: E446-53.
25. Yamauchi T, Kamon J, Ito Y, *et al.* Cloning of adiponectin receptors that mediate antidiabetic metabolic effects. Nature 2003; 423: 762-9.
26. Kharroubi I, Rasschaert J, Eizirik DL, Cnop M. Expression of adiponectin receptors in pancreatic β cells. Biochem Biophys Res Commun 2003; 312: 1118-22.
27. Kadowaki T, Yamauchi T. Adiponectin and adiponectin receptors. Endocr Rev 2005; 26: 439-51. (Review)
28. Takahashi T, Saegusa S, Sumino H, *et al.* Adiponectin replacement therapy attenuates myocardial damage in leptin-deficient mice with viral myocarditis. J Int Med Res 2005; 33: 207-14.
29. Bluher S, Ziotopoulou M, Bullen JW Jr, *et al.* Responsiveness to peripherally administered melanocortins in lean and obese mice. Diabetes 2004; 53: 82-90.
30. Tan GD, Debard C, Funahashi T, *et al.* Changes in adiponectin receptor expression in muscle and adipose tissue of type 2 diabetic patients during rosiglitazone therapy. Diabetologia 2005; 48: 1585-9.

Advance Access Publication 23 January 2006

eCAM 2006;3(1)109–115
doi:10.1093/ecam/nek012

Original Article

Beneficial Effect of Brewers' Yeast Extract on Daily Activity in a Murine Model of Chronic Fatigue Syndrome

Takashi Takahashi[1], Fei Yu[1], Shi-jie Zhu[1], Junji Moriya[1], Hiroyuki Sumino[4], Shigeto Morimoto[2], Nobuo Yamaguchi[3] and Tsugiyasu Kanda[1]

[1]Department of General Medicine, [2]Department of Geriatric Medicine and [3]Department of Serology, Kanazawa Medical University, Ishikawa, Japan and [4]Department of Medicine and Biological Science, Gunma University Graduate School of Medicine, Gunma, Japan

The aim of this study was to assess the effect of Brewers' yeast extract (BYE) on daily activity in a mouse model of chronic fatigue syndrome (CFS). CFS was induced by repeated injection of *Brucella abortus* (BA) antigen every 2 weeks. BYE was orally administered to mice in a dose of 2 g per kg per day for 2 weeks before injecting BA and for 4 weeks thereafter. We evaluated daily running activity in mice receiving BYE as compared with that in untreated mice. Weekly variation of body weight (BW) and survival in both groups was monitored during the observation period. Spleen weight (SW), SW/BW ratio, percent splenic follicular area and expression levels of interferon-γ (IFN-γ) and interleukin-10 (IL-10) mRNA in spleen were determined in both groups at the time of sacrifice. The daily activity during 2 weeks after the second BA injection was significantly higher in the treated group than in the control. There was no difference in BW between both groups through the experimental course. Two mice in the control died 2 and 7 days after the second injection, whereas no mice in the treated group died. Significantly decreased SW and SW/BW ratio were observed in the treated mice together with elevation of splenic follicular area. There were suppressed IFN-γ and IL-10 mRNA levels in spleens from the treated mice. Our results suggest that BYE might have a protective effect on the marked reduction in activity following repeated BA injection via normalization of host immune responses.

Keywords: Brewers' yeast extract – chronic fatigue syndrome – daily activity – spleen

Introduction

Fatigue is a common clinical feature in subjects with various immunologic disorders or infectious diseases (1). However, the pathophysiology of fatigue status is still unclear. Several cytokines produced during the immune response to infection are described to be mediators of some symptoms including fever, somnolence, lymphadenopathy and appetite loss (2). It is suggested that these cytokines also have a role in eliciting such fatigue condition (3).

Chronic fatigue syndrome (CFS) is an incapacitating illness defined by disabling chronic fatigue and characteristic accompanying signs (4). A reduction in daily activity >50% for at least 6 months is a major criterion for diagnosis of CFS (5). Hypotheses about the etiology of CFS propose the involvement of a specific bacterial or viral infection and immune dysfunction associated with the infection. Previous research described an immunologic model of CFS induced by intraperitoneal administration of bacterial antigen; however, the duration of fatigue condition evaluated by wheel running was shown to be short (6). Ottenweller *et al.* (7) have reported the establishment of a mouse model of CFS which could be induced by *Brucella abortus* (BA) administration. In this model, the mice were found to diminish their voluntary

For reprints and all correspondence: Prof. Tsugiyasu Kanda, Department of General Medicine, Kanazawa Medical University, 1-1 Daigaku, Uchinada-machi, Kahoku-gun, Ishikawa 920-0293, Japan. Tel: +81-76-286-2211 ext. 3841; Fax: +81-76-286-2702; E-mail: kandat@kanazawa-med.ac.jp

© The Author (2006). Published by Oxford University Press. All rights reserved.

The online version of this article has been published under an open access model. Users are entitled to use, reproduce, disseminate, or display the open access version of this article for non-commercial purposes provided that: the original authorship is properly and fully attributed; the Journal and Oxford University Press are attributed as the original place of publication with the correct citation details given; if an article is subsequently reproduced or disseminated not in its entirety but only in part or as a derivative work this must be clearly indicated. For commercial re-use, please contact journals.permissions@oxfordjournals.org

activity in the running wheel after intravenously injecting the fixed killed whole BA ring test antigen (7). The advantage of using this model is that the experiment uses voluntary exertion, and that the ability to run for longer periods characterizes recovery. Thus, the BA-induced mouse model is a good one for studying the biological underpinnings of chronic fatigue. We have recently demonstrated the effectiveness of Hochu-ekki-to (TJ-41), a Japanese herbal medicine for the daily running activity in the same model of CFS (8). BA administration was also known to induce changes in cytokine expression characterized by elevated interleukin-10 (IL-10) and interferon-γ (IFN-γ) in $CD4^+$ T cells in mice (9).

Beer is a complex alcoholic beverage made from malt, hops, water and Brewers' yeast. Scientific evidence has accumulated over the past 10 years pointing to the cancer preventive potential of selected hops-derived beer constituents, i.e. prenylflavonoids including xanthohumol and isoxanthohumol, and hop bitter acids (10). Generally, a strain of Brewers' yeast such as *Saccharomyces pastorianus* or *Saccharomyces cerevisiae* is applied as yeast for beer fermentation, and after brewing, a part of the yeast is recovered from the brewing instrument and used for additional yeast products including the Brewers' yeast extract (BYE) as well as the dried yeast. This extract has been widely used as a food ingredient and a seasoning. Although BYE includes many soluble components of vitamin B group, amino acids, peptides and mineral materials, nutritional or pharmacological aspects of BYE have yet to be fully understood. Since the vitamins and microelements are frequently utilized for the prevention and therapy for CFS, BYE is a candidate of the nutritional supplement for CFS.

Puri *et al.* (11) have reported eicosapentaenoic acid-rich essential fatty acid supplementation in CFS associated with symptom remission and structural brain changes. We describe the effect of BYE on daily running activity in a murine model of CFS. In addition, the differences in pathological modification and cytokine gene expression in spleen between BYE-treated mice and control are determined.

Materials and Methods

Living Conditions

Female BALB/c mice, 8 weeks of age, were obtained from Charles River (Kanagawa, Japan), and housed singly in cages (230 × 100 × 100 mm) including running wheels (230 mm in diameter), counters showing running wheel activity and water taps, which were obtained from Natsume Seisakusho Co., Ltd (Tokyo, Japan). These cages were maintained under a light–dark photoperiod (10 h versus 14 h) provided by fluorescent bulbs fitted in the cage floor. We fed all the mice ($n = 20$) every day during the course of the experiment. Environmental air temperature was maintained at 24–25°C. The daily running activity of mice was defined as the number of wheel complete turns per 24 h. The running activity was measured at 9 o'clock when the environmental lighting was turned on. Approval for this experiment was obtained from the animal experiment committee in Kanazawa Medical University.

Induction of CFS by BA

Fixed killed whole BA ring test antigen (BA strain 1119-3, lot no. 302) was obtained from the National Veterinary Services Laboratories in the United States Department of Agriculture. CFS was induced by two repeated injections of original BA antigen solution (0.2 ml per mouse) via the tail vein every 2 weeks (8). In the pilot experiment, we had already confirmed that the mice with a single administration of BA showed less running activity for 2–3 weeks after injection and recovery from the reduced activity thereafter (8). The criteria for establishing induction of CFS were statistically significant decreases of the running activity after first or second BA injection as compared with the baseline levels.

Treatment of Mice with Brewers' Yeast Extract

We obtained BYE (lot no. 909031) from Asahi Breweries, Ltd (Tokyo, Japan). The components in BYE are shown in Table 1. This agent was dissolved in distilled water and diluted with water to the appropriate concentration. The BYE solution was administered orally in a dose of 2 g per kg once daily through a feeding cannula inserted down the throat of the

Table 1. Components of brewing yeast extract used in the study

Components	Amount (per 100 g extract)
Vitamin B_1	13.11 mg
Vitamin B_2	5.10 mg
Vitamin B_6	4.73 mg
Pantothenate	4.48 mg
Zinc	6.76 mg
Glutathione	180 mg
Arginine	4.66 g
Lysine	5.36 g
Histidine	1.65 g
Phenylalanine	2.60 g
Tyrosine	0.83 g
Leucine	3.95 g
Isoleucine	3.06 g
Methionine	1.03 g
Valine	3.89 g
Alanine	4.55 g
Glycine	3.25 g
Proline	2.42 g
Glutamic acid	7.44 g
Serine	3.12 g
Threonine	3.07 g
Asparaginic acid	6.90 g
Tryptophan	0.87 g
Cystine	0.58 g

mice ($n = 10$) for 2 week before the induction of CFS and for 4 weeks thereafter. The dose of the BYE was determined on the basis of findings of another research applying the same BYE for the fatigue mice (12). Untreated mice ($n = 10$) were given saline during the same period. The mice in this experiment were randomly assigned to the BYE-treated or the control group.

Daily Running Activity, Body Weight and Survival in Mice

We started to examine the running activity during 2 weeks at baseline levels after 2 weeks of housing, since the activity was stabilized after 2–3 weeks of housing (7,8). Daily activity during 2 weeks after each injection of BA was evaluated in the mice receiving BYE as compared with that in the untreated mice. We measured body weight (BW) in both groups weekly from the start of treatment with the extract to the end of experiment. Survival in both groups was also monitored during the observation period.

Organ Weights and Pathological Examination in Spleen and Thymus

The mice in both groups were sacrificed by cervical dislocation 4 weeks after the first BA injection. Ratios of spleen weight (SW) (mg) to BW (g) (SW/BW), thymus weight (TW) (mg) to BW (TW/BW), heart weight (HW) (mg) to BW (HW/BW) and lung weight (LW) (mg) to BW (LW/BW) as well as the weights of the organs and the body were assessed between both groups at the time of sacrifice. One half of spleen and thymus was fixed in 10% buffered formalin and stained with hematoxylin–eosin; the other half was frozen and stored at −80°C until analysis of cytokine gene expression. We performed measurements of the splenic lymphoid follicular area and thymic medullary area to be expressed as a percentage of total splenic or thymic area in the long-axis sections (13). The splenic follicular area and thymic medullary area were examined in a normal female BALB/c mouse. Each tissue was evaluated blindly by an experienced pathologist who had no knowledge of the study design.

Expression Levels of INF-γ and IL-10 mRNA in Spleen

RNA extraction for each frozen splenic tissue was performed as described by the manufacturer (RNeasy Mini Kit, QIAGEN Inc., Tokyo, Japan). Procedure of DNase was performed during the RNA extraction to avoid DNA contaminations. The total RNA concentrations were determined by measuring the optical density at 260 and 280 nm. Aliquots of 20 μl RNA from each tissue were applied for production of cDNA. Comparative expression levels of IFN-γ (proinflammatory cytokine) and IL-10 (anti-inflammatory cytokine) mRNA in spleens from both groups were determined by using real-time quantitative RT–PCR as described previously (7,8). We applied TaqMan MGB Probe (Applied Biosystems Inc., CA, USA) for the RT–PCR. Commercially available kits for IFN-γ and IL-10 RT–PCR (Mm00801778_m1 and Mm00439616_m1, Applied Biosystems Inc.) were used. Each threshold cycle number up to 50 cycles (C_t value) within the RT–PCR was examined for the IFN-γ and IL-10 mRNA levels. Glyceraldehyde-3-phosphate dehydrogenase (GAPDH) gene was used as an endogenous internal standard, and was amplified with specific primers for the number of cycles. A negative control without template cDNA was always included. ΔC_t values referred to differences between the C_t values for each target gene and the GAPDH gene. After confirming that efficiencies of amplification of each molecule and GAPDH transcripts were approximately equal, amount of the IFN-γ or IL-10 transcript relative to the GAPDH transcript was determined using the comparative C_t method described in Perkin Elmer Applied Biosystems User Bulletin #2 (1997). Data are expressed as fold-increases relative to the baseline (value = 1) in spleen from a normal female BALB/c mouse.

Statistical Analyses

Data are expressed as mean values ± SD. Significant changes of the activity after first or second BA injection as compared with the baseline levels were evaluated by the paired Student's t-test. Data differences between the mice treated with the yeast extract and the control were analyzed by the unpaired Student's t-test. A P-value of <0.05 was considered to be statistically significant.

Results

Daily Running Activity, Body Weight and Survival in Mice

Daily running activity in both mouse groups before and after repeated BA injection is indicated in Fig. 1. Significant decreases of the activity after first or second BA injection as compared with the baseline levels were observed in the treatment and control groups, showing the induction of CFS. The baseline activity and the activity during 2 weeks after the first BA injection were not significantly different between both groups (Fig. 1). However, the activity during 2 weeks after the second BA injection was significantly higher in the group treated with BYE than in the control (8966 + 1647 versus 4821 + 1355, respectively, $P < 0.05$). There was no significant difference in BW between both the groups through the observation course, although a transient decline in BW was found in the control (Fig. 2). Two mice in the untreated group died 2 and 7 days after the second BA injection, whereas no mice in the group treated with BYE died.

Organ Weights and Pathological Examination in Spleen and Thymus

Ratios of each organ to BW as well as BW, SW, TW, HW and LW in both groups are shown in Table 2. Significant reduction in SW was found in the mice treated with BYE as compared with that in the control (329 ± 73 mg versus 517 ± 98 mg,

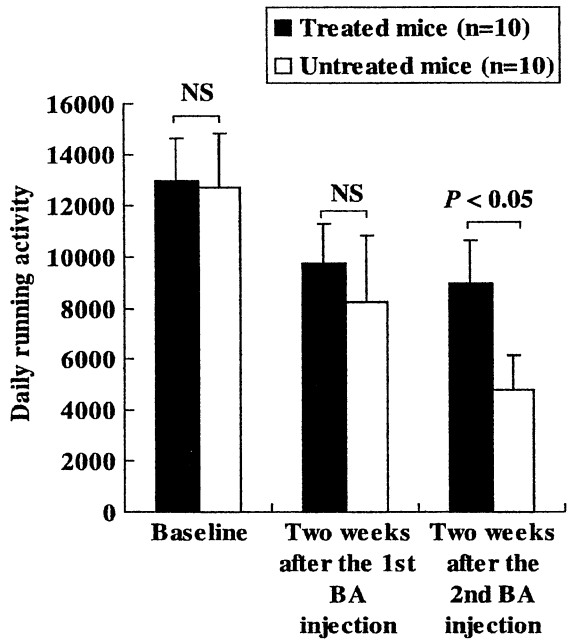


Figure 1. Effect of brewing yeast extract on daily running activity in a mouse model of chronic fatigue syndrome. Data are expressed as means ± SD. NS, not significant; BA, *Brucella abortus*. Daily running activity was defined as the number of wheel turns per 24 h. Asterisk represents two mice in the untreated group died 2 and 7 days after the second injection of BA, while no mice in the treated group died.

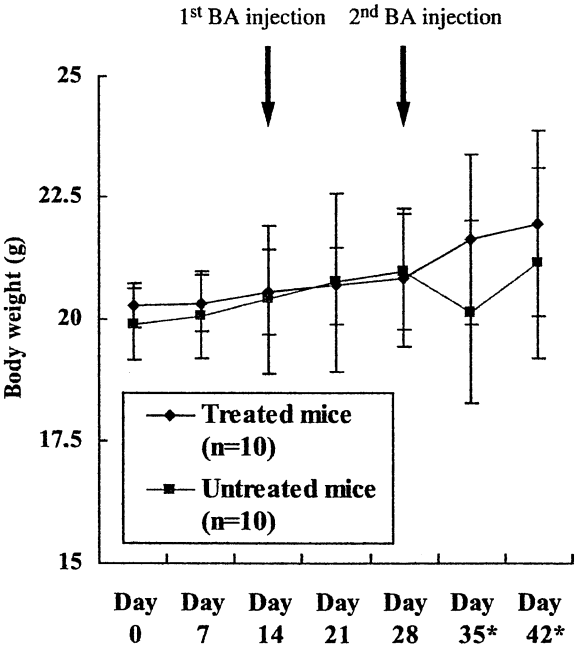


Figure 2. Weekly variation of body weight between different mice from the start of treatment with brewing yeast extract to the end of experiment. Data are expressed as means ± SD. NS, not significant; BA, *Brucella abortus*. Asterisk represents two mice in the untreated group died 2 and 7 days after the second injection of BA, while no mice in the treated group died.

Table 2. Effect of brewing yeast extract on body weight and weight of organs including spleen, thymus, heart and lungs at the time of sacrifice

	BW (g)	SW (mg)	TW (mg)	HW (mg)	LW (mg)
Treated mice	22.0 ± 1.9	329 ± 73*	44 ± 7	114 ± 15	158 ± 22
(n = 10)		(15.0 ± 3.4*)	(2.1 ± 0.2)	(5.2 ± 0.7)	(7.2 ± 1.0)
Untreated mice	21.2 ± 2.0	517 ± 98	42 ± 4	111 ± 10	152 ± 20
(n = 8)**		(24.5 ± 4.7)	(2.0 ± 0.2)	(5.1 ± 0.5)	(7.1 ± 0.9)

Data are expressed as means ± SD. BW, body weight; SW, spleen weight; TW, thymus weight; HW, heart weight; LW, lungs weight. Parentheses show ratio of each organ weight to body weight.
*P < 0.05 compared with spleen weight in the untreated mice.
**Two mice in the untreated group died 2 and 7 days after the second injection of BA.

respectively, $P < 0.05$), whereas there were no differences in the weights of other organs between both the groups (Table 2). SW/BW ratio was significantly lower in the group treated with BYE than in the untreated group at the time of sacrifice (15.0 ± 3.4 versus 24.5 ± 4.7, $P < 0.05$), while TW/BW, HW/BW and LW/BW ratios were not significantly different between both the groups (Table 2). The percent follicular area and medullary area were 31 and 28% in spleen and thymus of the normal female BALB/c mouse. Significantly, increase of splenic follicular area was observed in the treated mice as compared with that in the untreated group (24 ± 8% versus 14 ± 6%, respectively, $P < 0.05$). As shown in Fig. 3B, the lymphoid follicles were found to be impaired in spleens of the untreated mice. However, there was no difference in thymic medullary area between both the groups (Fig. 3A).

Expression Levels of IFN-γ and IL-10 mRNA in Spleen

Comparative expression levels of IFN-γ and IL-10 mRNA in spleen are shown in Fig. 4A and B. The IFN-γ and IL-10 mRNA levels in spleens of the mice treated with BYE were significantly lower than those in the control (7.67 ± 5.97 versus 13.87 ± 4.77 and 5.18 ± 1.36 versus 8.45 ± 1.94 in IFN-γ and IL-10 mRNA levels, respectively, $P < 0.05$).

Discussion

Vitamins and microelements such as high amounts of vitamins B, K and essential amino acids are very important for the prevention and treatment for individuals with fatigue. In a clinical study, a nutritional supplement 'Nagipol' made on the basis of Brewers' yeast in Russia was applied for the prevention and treatment of CFS patients (14). The results showed that this food was useful in CFS because of the clinical status improvement, positively influencing cognitive CNS functions and symptoms of emotional instability and normalizing blood biochemical parameters, suggesting recommendation of the food as preventive medical dietetic means for this pathology. We have also found the beneficial effect of BYE on daily running activity in a murine model of CFS. It might be worth

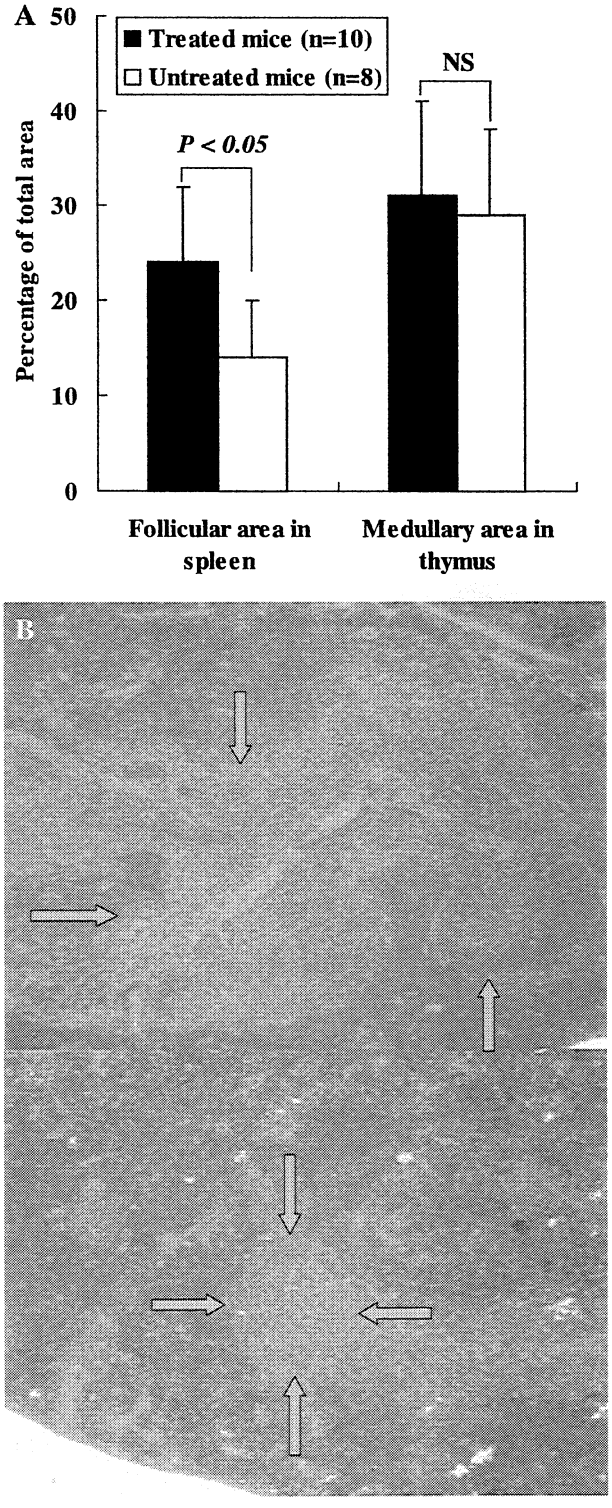


Figure 3. Percentages of splenic lymphoid follicular area and thymic medullary area between different mice (**A**) and pathological findings of the follicular area in spleen (**B**, upper image in the treated mice and lower image in the control). Data are expressed as means ± SD. NS, not significant; BA, *Brucella abortus*. Arrows show the follicular area in the spleen.

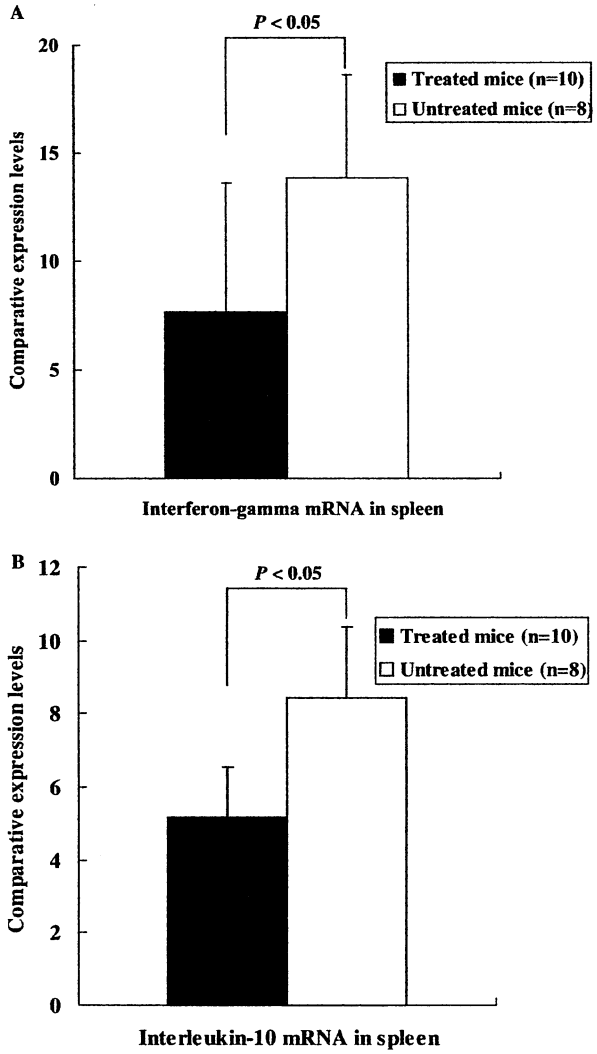


Figure 4. Comparative expression levels of interferon-γ (INF-γ) (**A**) and interleukin-10 (**B**) mRNA in spleen between different mice. Data are expressed as means ± SD. The INF-γ and interleukin-10 mRNA levels were calculated as comparative values, which were normalized to the cytokines' mRNA in the spleen from normal female BALB/c mouse (value = 1).

investigating the effectiveness of BYE on symptoms in the CFS or fatigue subjects with other various disorders in future clinical study.

Previous study reported clinical aspects of 21 individuals with chronic brucellosis (15). Seventeen patients suffered from chronic disease and had no history of any acute episode of brucellosis. The most common symptoms in the patient population were tiredness, fatigue, depression, arthralgia and muscular pains. Most of these subjects had already been receiving psychiatric treatment. Clinical examination was largely negative, but lymphadenopathy was found in nine cases. Based on these clinical manifestations, the fatigue induced by BA administration which was used in the present research might be applicable to a mouse model of CFS.

There are manuscripts regarding splenomegaly induced by brucellosis (16,17). Inhibition of *in vitro* lymphocyte proliferation by brucella-activated macrophages was also found during experimental murine brucellosis (18). Increase of SW and SW/BW ratio after the repeated BA injection was observed together with decrease of splenic follicular area in the present study, and there was significant improvement of SW, SW/BW ratio and splenic follicular area in the treated group, suggesting that the measurement of splenic enlargement and follicular area might be useful to monitor improvement of immune stimulation during treatment.

We found significant decreases of IFN-γ (proinflammatory cytokine) and IL-10 (anti-inflammatory cytokine) mRNA levels in the spleens of the mice treated with BYE as compared with those of the control. Svetic *et al.* (9) described that simultaneous elevation in Th1 cytokine, IFN-γ, and Th2 cytokine, IL-10, appeared in type 1 immune responses after the BA injection. Reduced expression of IL-2 and -4 as well as increased expression of IL-10 were found in another study using BA (7). Although it is uncertain whether IL-10 plays a role in suppressing severity of inflammatory response mediated by IFN-γ, BYE treatment could contribute to normalization of host immune responses in the CFS mouse model, suggesting that these cytokines' expression might be a biomarker in the treatment for CFS.

There are few investigations showing the effectiveness of alternative and complementary approaches including nutritional supplements for subjects with CFS. Cox *et al.* (19) reported that magnesium treatment might improve the well-being of the CFS patients because of low red blood cell magnesium in CFS. In a placebo-controlled study, there were no significant differences in symptoms between the group treated with red-cell membrane essential fatty acids and placebo in CFS (20). In addition, no significant difference was apparent between response to placebo and that to liver extract containing folic acid and cyanocobalamin (21). In our study, daily running activity during 2 weeks after the second BA injection was significantly higher in the group treated with BYE in a dose of 2 g per kg per day than in the control. Significantly lowered SW and SW/BW ratio was observed in the treated mice together with increase of splenic follicular area. There were decreased IFN-γ and IL-10 mRNA levels in spleens of the treated group. These data suggest that BYE treatment might possess a preventive effect on the marked reduction in running activity following the repeated BA injection via normalization of host immune responses, although the optimum dose and the appropriate time of initiating the treatment with BYE have not been established in this study. Further investigations are required to elucidate these ancesus. L-arginine increases nitric oxide (NO) release into circulation via endothelial NO synthase. NO suppresses the activation of the key gene of inflammation, nuclear factor kappa B (22), and might account for the beneficial effect of BYE. Therefore, we should consider administering L-arginine alone in a future study.

Acknowledgements

The authors thank Dr Masaaki Yasue (Fundamental Research Laboratory, Asahi Breweries, Ltd, Ibaraki, Japan) for his helpful suggestions. This study was supported in part by a grant for promoted research from Kanazawa Medical University (S2004-2 and S2005-5), a grant for project research from the High-Technology Center of Kanazawa Medical University (H2004-7) and a research grant from Grant-in-Aid for Scientific Research (C), the Ministry of Education, Science and Culture of Japan (No. 17590767).

References

1. Krupp LB, LaRocca NG, Muir-Nash J, Steinberg AD. The fatigue severity scale. Application to patients with multiple sclerosis and systemic lupus erythematosus. *Arch Neurol* 1989;46:1121–3.
2. Tracey KJ, Vlassara H, Cerami A. Cachectin/tumour necrosis factor. *Lancet* 1989;1:1122–6.
3. Chao CC, Strgar F, Tsang M, Peterson PK. Effects of swimming exercise on the pathogenesis of acute murine *Toxoplasma gondii* Me49 infection. *Clin Immunol Immunopathol* 1992;62:220–6.
4. Fukuda K, Straus SE, Hickie I, Sharpe MC, Dobbins JG, Komaroff A. The chronic fatigue syndrome: a comprehensive approach to its definition and study. International Chronic Fatigue Syndrome Study Group. *Ann Intern Med* 1994;121:953–9.
5. Holmes GP, Kaplan JE, Gantz NM, Komaroff AL, Schonberger LB, Straus SE, et al. Chronic fatigue syndrome: a working case definition. *Ann Intern Med* 1988;108:387–9.
6. Chao CC, DeLaHunt M, He S, Close K, Peterson PK. Immunologically mediated fatigue: A murine model. *Clin Immunol Immunopathol* 1992;64:161–5.
7. Ottenweller JE, Natelson BH, Gause WC, Carroll KK, Beldowicz D, Zhou XD, et al. Mouse running activity is lowered by *Brucella abortus* treatment: a potential model to study chronic fatigue. *Physiol Behav* 1998;63:795–801.
8. Wang XQ, Takahashi T, Zhu SJ, Moriya J, Saegusa S, Yamakawa J, et al. Effect of Hochu-ekki-to (TJ-41), a Japanese herbal medicine, on daily activity in a murine model of chronic fatigue syndrome. *Evid Based Complement Alternat Med* 2004;1:203–6.
9. Svetic A, Jian YC, Lu P, Finkelman FD, Gause WC. *Brucella abortus* induces a novel cytokine gene expression characterized by elevated IL-10 and IFN-γ in CD4+ T cells. *Int Immunol* 1993;5:877–83.
10. Gerhauser C. Beer constituents as potential cancer chemopreventive agents. *Eur J Cancer* 2005;41:1941–54.
11. Puri BK, Holmes J, Hamilton G. Eicosapentaenoic acid-rich essential fatty acid supplementation in chronic fatigue syndrome associated with symptom remission and structural brain changes. *Int J Clin Pract* 2004;58:297–9.
12. Nakagawasai O, Tadano T, Yasue M. Effect of brewers yeast extract on a physical fatigue-induced stress in mice. *Presentation abstracts of the 58th annual scientific meeting: the Japanese Society of Nutrition and Food Science* 2004,265.
13. Kanda T, McManus JEW, Nagai R, Imai S, Suzuki T, Yang DC, et al. Modification of viral myocarditis in mice by interleukin-6. *Circ Res* 1996;78:848–56.
14. Dotsenko VA, Mosiichuk LV, Paramonov AE. Biologically active food additives for correction of the chronic fatigue syndrome. *Vopr Pitan* 2004;73:17–21.
15. Sacks N, Van Rensburg AJ. Clinical aspects of chronic brucellosis. *S Afr Med J* 1976;50:725–8.
16. Oth D, Sabolovic D, Le Garrec Y. Genetic (h-2) dependence of the duration of splenomegaly induced by *Brucella abortus*. *Folia Biol (Praha)* 1974;20:20–5.
17. Demetropoulos KC, Lindenauer SM, Rapp R, Robins J. Target calcifications of the spleen in chronic brucellosis (Brucella suis). *J Can Assoc Radiol* 1974;25:161–3.

18. Riglar C, Cheers C. Macrophage activation during experimental murine brucellosis. II. Inhibition of in vitro lymphocyte proliferation by brucella-activated macrophages. *Cell Immunol* 1980;49:154–67.
19. Cox IM, Campbell MJ, Dowson D. Red blood cell magnesium and chronic fatigue syndrome. *Lancet* 1991;337:757–60.
20. Warren G, McKendrick M, Peet M. The role of essential fatty acids in chronic fatigue syndrome. A case-controlled study of red-cell membrane essential fatty acids (EFA) and a placebo-controlled treatment study with high dose of EFA. *Acta Neurol Scand* 1999; 99:112–6.
21. Kaslow JE, Rucker L, Onishi R. Liver extract-folic acid-cyanocobalamin vs placebo for chronic fatigue syndrome. *Arch Intern Med* 1989;149:2501–3.
22. Grumbach IM, Chen W, Mertens SA, Harrison DG. A negative feedback mechanism involving nitric oxide and nuclear factor kappa-B modulates endothelial nitric oxide synthase transcription. *J Mol Cell Cardiol* 2005;39:595–603.

Received September 10, 2005; accepted December 25, 2005

OUTBREAK OF HUMAN METAPNEUMOVIRUS INFECTION IN ELDERLY INPATIENTS IN JAPAN

To the Editor: Human metapneumovirus (hMPV), a newly discovered pneumovirus of the *Paramyxoviridae* family,

has been isolated from young children with acute respiratory tract illness (RTI) in the Netherlands.[1] Serological analyses have indicated that the prevalence of hMPV in the Dutch population is high, because virtually all children became seropositive before the age of 6,[1] indicating that hMPV is a common and ubiquitous human pathogen. Subjects aged 65 and older were reported to account for 45.9% of Canadian patients with community-acquired hMPV infection hospitalized for RTI.[2]

Between January 18 and 31, 2005, a cluster of eight inpatients (mean age 79; range 65–89; 6 male, 2 female) developed RTI in a 23-bed ward in a hospital for older people in Japan. The clinical features and outcomes of the subjects are shown in Table 1. All individuals were sharing the same day-care room on the ward. Two patients had bronchiolitis (Cases 1 and 7), five bronchitis (Cases 2–5 and 8), and one upper RTI (Case 6) based on the clinical symptoms and chest roentgenograms. Mean duration of exothermic reaction (>37.0°C) was 4 days (range 0–6). Wheezing and dyspnea were observed in only two subjects; coryza and productive cough were observed in all. White blood cell count (mean 4.1×10^9 cells/L, range 2.3–6.5×10^9), and C-reactive protein blood levels (25.7 mg/L, range 1.7–52.9) remained low. Treatment for RTI included aminophylline, oxygen supplementation, antibiotics, and acetaminophen. All subjects showed recovery from acute RTI, although two patients newly developed asthma and secondary pneumonia (*Klebsiella pneumoniae* identified in sputum).

hMPV fusion gene was detected using reverse-transcription polymerase chain reaction (RT-PCR)[3] in nasal swabs from all subjects at onset. The genotype of the amplified products from every specimen was identical to that of the prototype strain (designated NL/1/99, Gene Bank accession no. AY525843), which belongs to genetic lineage B1.[4] The results of other viral cultures, antigen tests (influenza virus A/B, adenovirus, and respiratory syncytial virus (RSV)), and RT-PCR (RSV, parainfluenza virus (types 1–4), coronavirus, and rhinovirus) were all negative. hMPV was not found in swabs from other inpatients without RTI (n = 6) in the same ward or the care workers (n = 4).

Immunoglobulin (Ig) G antibody to hMPV with indirect immunofluorescence assay[1,5,6] was already present in serum from eight hMPV-infected patients and 10 control individuals in the acute phase. The IgG titers in six hMPV-infected subjects except Cases 4 and 7 were more than four times as high in the convalescent phase, and the titers in one of the controls were more than four times as high as in the convalescent phase. Two months after recovery of the final patient, purified protein derivative (PPD) reaction was retrospectively investigated in the hMPV-infected subjects (n = 8), the controls (n = 8), and the care workers (n = 9). Seven individuals (87.5%) (all except Case 4) showed a negative reaction, whereas the controls and the workers showed negative rates of 37.5% and 22.2%, respectively.

The clinical symptoms induced by hMPV infection in children are similar to those caused by RSV infection, ranging from mild respiratory problems to severe cough, bronchiolitis, and pneumonia.[1] hMPV ribonucleic acid was detected in respiratory samples from hospitalized patients aged 65 and older with RTI, whereas RSV was not found in the same elderly group.[7] A cluster of eight hMPV-infected cases with RTI was found in a hospital for older people. Thus, hMPV rather than RSV should be considered as a causative pathogen in elderly subjects with RTI.

One study[8] has reported detection of hMPV antigens in nasal secretions obtained from 48 hospitalized children with RTIs using an immunofluorescent-antibody test (IFA). IFA is a rapid and useful test for the diagnosis of hMPV infections in children, although the sensitivity of IFA (73.3%) is lower than that of RT-PCR. It is important to establish rapid virus detection assays, including RT-PCR or antigen tests, especially for older people, as are currently applied for diagnosing infections with other viral pathogens, because older people with pneumonia who are infected with hMPV are at risk of death due to respiratory failure.[2]

In addition, a difference was found in the PPD reaction between the hMPV-infected patients and control subjects or care workers, although the reaction was checked retrospectively. This observation suggests that a negative PPD reaction, reflecting reduced cellular immunity, is a potential risk factor for hMPV infection, as well as tuberculosis and shingles, in older people. It is necessary to conduct a wide-ranging prospective study to better evaluate risk factors that may be associated with hMPV infection.

Haruhito Honda, MD
Jun Iwahashi, MD
Takahito Kashiwagi, MD
Yoshihiro Imamura, MD
Nobuyuki Hamada, MD
Department of Virology
Kurume University School of Medicine
Kurume, Fukuoka, Japan

Takehiko Anraku, MD
Seiichiro Ueda, MD
Ueda Hospital
Chikugo, Fukuoka, Japan

Tsugiyasu Kanda, MD
Takashi Takahashi, MD
Department of General Medicine
Shigeto Morimoto, MD
Department of Geriatric Medicine
Kanazawa Medical University, Kahoku, Ishikawa, Japan

ACKNOWLEDGMENTS

The authors thank Ms. Satoko Matsueda (Department of Immunology, Kurume University School of Medicine, Fukuoka, Japan) and Mr. Akio Hayashi and Mr. Ryouichi Onda (Mitsubishi Kagaku Bio-Clinical Laboratories, Tokyo, Japan) for their excellent technical assistance.

Financial Disclosure: Dr. Morimoto was supported by a grant-in-aid for scientific research from the Ministry of Health, Labour and Welfare of Japan. Dr. Kanda was supported by a grant for project research from the High-Technology Center of Kanazawa Medical University (H2004-7) and a grant-in-aid for scientific research (C) from the Ministry of Education, Culture, Sports, Science and Technology of Japan (C17590767). Dr. Takahashi was supported by a grant for promoted research from Kanazawa Medical University (S2004-2 and S2005-5). There is no conflict of interest regarding the present study.

Table 1. Clinical Features and Outcome for a Cluster of Eight Elderly Inpatients in Japan Infected with Human Metapneumovirus

No.	Age	Sex	Main Cause of Admission	Date of Onset (January 2005)	Highest Body Temperature (°C)	Exothermic Duration (>37.0°C) (Days)	Coryza	Sore Throat	Hoarseness	Cough	Sputum	Wheezing	Chest X-Ray	Dyspnea	Minimum Oxygen Saturation in Arterial Blood (%)	Cyanosis	White Blood Cell Count (× 10^9 cells/L)	C-Reactive Protein (mg/L)	Treatment	Outcome
1	84	F	Cyclothymic disorder	18	38.9	6	(+)	(+)	(−)	Productive	White viscous	(+)	Hyperinflation, patchy and linear shadows in left lower field	(+)	88	(+)	3	52.9	APAP, aminophylline, O_2 (1 L/min), CTRX	BA and secondary pneumonia (*Klebsiella pneumoniae*)
2	71	M	Senile depression	24	38.8	5	(+)	(+)	(+)	Productive	White viscous	(−)	Patchy and linear shadows in right hilar and lower fields	(−)	NT	(−)	5	41.2	APAP, CTRX	Recovered
3	65	M	MCLI	24	38.5	5	(+)	(+)	(−)	Productive	White or yellow viscous	(−)	No change	(−)	NT	(−)	2.3	39.4	APAP, CTRX	Recovered
4	74	M	Schizophrenia	24	38.1	4	(+)	(+)	(+)	Productive	White viscous	(−)	NT	(−)	NT	(−)	2.3	1.7	APAP, RXM	Recovered
5	81	F	MCLI	27	38.6	4	(+)	(+)	(+)	Productive	White viscous	(−)	NT	(−)	NT	(−)	3.3	9.1	APAP, RXM	Recovered
6	86	M	MCLI	27	38.5	4	(+)	(+)	(−)	Productive	(−)	(−)	No change	(−)	NT	(−)	5.3	45	APAP, RXM	Recovered
7	89	M	MCLI	31	37.8	4	(+)	(+)	(+)	Productive	White viscous	(+)	Hyperinflation	(+)	91	(−)	6.5	13.7	APAP, aminophylline, O_2 (1 L/min), CTRX	BA and secondary pneumonia (*K. pneumoniae*)
8	86	M	MCLI	31	36.8	0	(+)	(+)	(−)	Productive	White viscous	(−)	Linear shadows in bilateral lower fields	(−)	NT	(−)	5.4	3.1	APAP, RXM	Recovered

M = male; F = female; − = negative; + = positive; APAP = acetaminophen; O_2 = oxygen; CTRX = ceftriaxone; BA = bronchial asthma; NT = not tested; MCLI = multiple cerebral lacunar infarction; RXM = roxithromycin.

Author Contributions: Haruhito Honda, Takashi Takahashi, and Shigeto Morimoto contributed study concept and design. Jun Iwahashi, Takahito Kashiwagi, Takehiko Anraku, Seiichiro Ueda, Yoshihiro Imamura, and Nobuyuki Hamada performed acquisition of subjects and data. Haruhito Honda, Tsugiyasu Kanda, and Shigeto Morimoto analyzed and interpreted the data. Haruhito Honda, Takashi Takahashi, and Shigeto Morimoto prepared the manuscript.

Sponsor's Role: The sponsors had no role in this manuscript.

REFERENCES

1. van den Hoogen BG, de Jong JC, Groen J et al. A newly discovered human pneumovirus isolated from young children with respiratory tract disease. Nat Med 2001;7:719–724.
2. Boivin G, Abed Y, Pelletier G et al. Virological features and clinical manifestations associated with human metapneumovirus: A new paramyxovirus responsible for acute respiratory-tract infections in all age groups. J Infect Dis 2002;186:1330–1334.
3. Peret TC, Boivin G, Li Y et al. Characterization of human metapneumoviruses isolated from patients in North America. J Infect Dis 2002;185:1660–1663.
4. van den Hoogen BG, Herfst S, Sprong L et al. Antigenic and genetic variability of human metapneumoviruses. Emerg Infect Dis 2004;10:658–666.
5. Ebihara T, Endo R, Kikuta H et al. Human metapneumovirus infection in Japanese children. J Clin Microbiol 2004;421:126–132.
6. Ishiguro N, Ebihara T, Endo R et al. Immunofluorescence assay for detection of human metapneumovirus-specific antibodies by use of baculovirus-expressed fusion protein. Clin Diagn Lab Immunol 2005;12:202–205.
7. van den Hoogen BG, van Doornum GJJ, Fockens JC et al. Prevalence and clinical symptoms of human metapneumovirus infection in hospitalized patients. J Infect Dis 2003;188:1571–1577.
8. Ebihara T, Endo R, Ma X et al. Detection of human metapneumovirus antigens in nasopharyngeal secretions by an immunofluorescent-antibody test. J Clin Microbiol 2005;43:1138–1141.

HYPOADIPONECTINEMIA IN BEDRIDDEN FEMALE PATIENTS YOUNGER THAN 75

To the Editor: Older people have several hormonal alterations, but the effect on the endocrine function of adipose tissue in older bedridden patients has not been fully elucidated. Adiponectin is a newly discovered antiinflammatory protein, secreted exclusively by adipocytes, that plays a protective role against atherosclerosis.[1] Hypoadiponectinemia plays a crucial role in atherosclerosis in men, but there have been no studies of plasma adiponectin in bedridden women. The aim of the present study was to estimate plasma adiponectin concentration in bedridden elderly female patients in comparison with age-matched healthy volunteers.

Seventy-four bedridden female patients admitted to geriatric wards and nursing homes in Osaka, Japan, and age-matched volunteers were studied. Clinical diagnoses were defined using detailed physical examination and routine biochemical analyses of blood and urine, as well as clinical tools including computed tomography. Their mean bedridden period ± standard deviation was 49.4 ± 37.4 months. All plasma analyses were performed on samples from fasting subjects. Adiponectin was measured using high-sensitive radioimmunoassay (Linco Research, St. Louis, MO). Bedridden subjects and healthy volunteers were divided into two groups: younger than 75 and aged 75 and older. All statistical analyses were performed using the SPSS (SPSS Inc., Chicago, IL). The statistical differences in the variables were compared using the Mann-Whitney *U* test, and the association between any two parameters was assessed using Spearman correlation.

Table 1. Clinical Characteristics of 74 Bedridden Female Patients and 42 Healthy Age-Matched Volunteers

Characteristic	Healthy Female Volunteers		Bedridden Patients	
	Age 60–74 (n = 22)	Age 75–98 (n = 20)	Age 60–74 (n = 18)	Age 75–98 (n = 56)
Body mass index, mean ± SD	24.1 ± 2.3	23.8 ± 2.7	23.6 ± 2.6	24.9 ± 3.8
Systolic blood pressure, mmHg, mean ± SD	138 ± 22	140 ± 33	154 ± 19*	144 ± 20
Diastolic blood pressure, mmHg, mean ± SD	73 ± 10	77 ± 13	82 ± 14	84 ± 13
Plasma adiponectin, μg/mL, mean ± SD	15.9 ± 7.2	16.2 ± 7.7	11.8 ± 4.8*	14.3 ± 6.9
Serum albumin, g/dL, mean ± SD	4.2 ± 0.3	4.1 ± 0.3	3.6 ± 0.2*	3.5 ± 0.3*
Total cholesterol, mg/dL, mean ± SD	228 ± 24	211 ± 19	183 ± 15*	178 ± 16*
Cerebrovascular accident as cause of bedridden state, %	NA	NA	76	68

*$P < .05$ vs healthy age-matched volunteer.
SD = standard deviation; NA = not assessed.

The clinical characteristics of the subjects are shown in Table 1. Of 74 bedridden patients, the main cause of being bedridden was cerebrovascular accident (CVA, 70%); others were bone fracture, infection, and cardiovascular disease. There was no statistical difference in body mass index between the four groups. Bedridden women aged 60 to 74 were characterized by significantly lower plasma adiponectin (11.8 ± 4.8 μg/mL) concentration than healthy women of the same age (15.9 ± 7.2 μg/mL, $P < .01$). In the entire studied group, a weak, positive, but insignificant, correlation was found between plasma adiponectin concentration and age ($r = 0.18$, $P = .12$). There was no correlation between serum adiponectin and albumin or total cholesterol levels. Additionally, significant correlation was found between plasma adiponectin concentration and the length of time patients had been bedridden when analyzed separately ($r = 0.27$, $P = .04$).

The relationship between aging and plasma adiponectin concentration has recently been described in some manuscripts. Men aged 70 and older have significantly higher plasma adiponectin concentrations than younger men, whereas plasma adiponectin concentration in women does not change significantly with age.[2] The results of the current study in female patients aged 60 and older were consistent with these reports. Sex differences of adiponectin levels are also reported in older diabetic patients.[3]

The main cause of being bedridden was CVA in female patients in this study. The relationship between CVA and lower adiponectin level is controversial. A recent report reported that CVA was associated with hypoadiponectinemia with or without diabetes mellitus,[4] but in a Swedish study, adiponectin levels were not associated with CVA in men.[5] The current results concerning hypoadiponectinemia in younger bedridden female patients mainly caused by cerebrovascular disease would indicate a relationship between hypoadiponectinemia and occurrence of CVA. Hypoadiponectinemia may be due to the severity of cerebrovascular atherosclerosis in bedridden patients.

Precise mechanisms underlying recovery of adiponectin level in long-term bedridden patients are not known. First, being bedridden may affect the decrease in adiposity caused by multiple factors including immobilization, malnutrition, and disease, although several causes could be responsible, including aspiration pneumonia, urinary tract infection, and pressure ulcers. Indeed, the current results showed that albumin and total cholesterol levels in bedridden female patients were significantly lower than in healthy controls. Nutritional restriction due to controlled feeding increases the survival of mammalians by delaying the aging process.[6] Decrease in adiposity due to being bedridden longer may induce higher levels of circulating adiponectin in elderly female patients. A second possibility may be the effects of exercise in bedridden patients. Lack of skeletal muscle exercise is apt to induce adiposity by decreasing the release of cytokine interleukin-6, which stimulates lypolysis.[7] Third, that hypoadiponectinemia was observed mainly in those who had been bedridden for a shorter length of time may reflect greater endothelial dysfunction. A vascular study showed that severity of endothelial dysfunction was closely associated with plasma adiponectin levels in Japanese subjects according to the measurement of forearm blood flow.[8] Elevated adiponectin level would be related to longevity even in bedridden women. Longitudinal studies of serum adiponectin levels and prognosis of bedridden state should be conducted to elucidate the mechanism of lipid metabolism in bedridden patients to help with their future health care.[9]

Tsugiyasu Kanda, MD
Takashi Takahashi, MD
Department of General MedicineHiroyuki Sumino, MD
Second Department of Internal Medicine
Gunma University School of Medicine
Maebashi, Gunma, Japan

Takeshi Nakahashi, MD
Kunimitsu Iwai, MD
Shigeto Morimoto, MD
Masayuki Matsumoto, MD
Department of Geriatric Medicine
Kanazawa Medical University
Kahoku, Ishikawa, Japan

ACKNOWLEDGMENTS

Financial Disclosure: Dr. Kanda was supported by a grant for project research from the High-technology Center of Kanazawa Medical University (H2004-7) and a grant

ACKNOWLEDGMENTS

Financial Disclosure: Dr. Kanda was supported by a grant for project research from the High-technology Center of Kanazawa Medical University (H2004-7) and a grant from Grant-in-Aid for Scientific Research (C17590767). Dr. Takahashi was supported by a grant to promote research from Kanazawa Medical University (S2003-2 and S2004-2). There was no conflict of interest regarding the present study.

Author Contributions: Tsugiyasu Kanda and Takashi Takahashi: study concept and design. Takeshi Nakahashi, Kunimitsu Iwai, Shigeto Morimoto, and Masayuki Matsumoto: acquisition of subjects and/or data. Hiroyuki Sumino, Tsugiyasu Kanda, and Shigeto Morimoto: Analysis and interpretation of data. Tsugiyasu Kanda, and Takashi Takahashi: preparation of manuscript.

Sponsor's Role: There was no sponsorship regarding the present study.

REFERENCES

1. Scherer PE, Williams S, Fogliano W et al. A novel serum protein similar to C1q, produced exclusively in adipocytes. J Biol Chem 1995;270:26746–26749.
2. Adamczak M, Rzepka E, Chudek J et al. Ageing and plasma adiponectin concentration in apparently healthy males and females. Clin Endocrinol (Oxf) 2005;62:114–118.
3. Kanaya AM, Harris T, Goodpaster BH et al. Adipocytokines attenuate the association between visceral adiposity and diabetes in older adults. Diabetes Care 2004;27:1375–1380.
4. Chen MP, Tsai JC, Chung FM et al. Hypoadiponectinemia is associated with ischemic cerebrovascular disease. Arterioscler Thromb Vasc Biol 2005;25: 821–828.
5. Soderberg S, Stegmayr B, Stenlund H et al. Leptin, but not adiponectin, predicts stroke in males. J Intern Med 2004;256:128–136.
6. Pahlavani MA. Influence of caloric restriction on aging immune system. J Nutr Health Aging 2004;8:38–47.
7. Tomas E, Kelly M, Xiang X et al. Metabolic and hormonal interactions between muscle and adipose tissue. Proc Nutr Soc 2004;63:381–385.
8. Shimabukuro M, Higa N, Asahi T et al. Hypoadiponectinemia is closely linked to endothelial dysfunction in man. J Clin Endocrinol Metab 2003;88: 3236–3240.
9. Wu AW, Yasui Y, Alzola C et al. Predicting functional status outcomes in hospitalized patients aged 80 years and older. J Am Geriatr Soc 2000;48: S6–S15.

Available online at www.sciencedirect.com
SCIENCE DIRECT
Life Sciences
ELSEVIER
Life Sciences 78 (2005) 195 – 204
www.elsevier.com/locate/lifescie

Inhibition of cyclooxygenase-2 enhances myocardial damage in a mouse model of viral myocarditis

Takashi Takahashi [a], Shi-jie Zhu [a], Hiroyuki Sumino [b], Seiichiro Saegusa [a], Takeshi Nakahashi [c], Kunimitsu Iwai [c], Shigeto Morimoto [c], Tsugiyasu Kanda [a,*]

[a] *Department of General Medicine, Kanazawa Medical University, 1-1 Daigaku, Uchinada-machi, Kahoku-gun, Ishikawa 920-0293, Japan*
[b] *Second Department of Internal Medicine, Gunma University School of Medicine, Gunma 371-8511, Japan*
[c] *Department of Geriatric Medicine, Kanazawa Medical University, Ishikawa 920-0293, Japan*

Received 27 October 2004; accepted 18 April 2005

Abstract

To determine critical role of cyclooxygenase-2 (COX-2) for development of viral myocarditis, a mouse model of encephalomyocarditis virus-induced myocarditis was used. The virus was intraperitoneally given to COX-2 gene-deficient heterozygote mice (*COX-2*$^{+/-}$) and wild-type mice (WT). We examined differences in heart weights, cardiac histological scores, numbers of infiltrating or apoptotic cells in myocardium, cardiac expression levels of COX-2, tumor necrosis factor-α (TNF-α), and adiponectin mRNA, immunoreactivity of COX-2, TNF-α, and adiponectin in myocytes, cardiac concentrations of TNF-α and adiponectin, prostaglandin E_2 (PGE_2) levels in hearts, and viral titers in tissues between *COX-2*$^{+/-}$ and WT. We observed significantly decreased expression of COX-2 mRNA and reactivity in hearts from *COX-2*$^{+/-}$ on day 8 after viral inoculation as compared with that from WT, together with elevated cardiac weights and severe inflammatory myocardial damage in *COX-2*$^{+/-}$. Cardiac expression of TNF-α mRNA, reactivity, and protein on day 8 was significantly higher in *COX-2*$^{+/-}$ than in WT, together with reciprocal expression of adiponectin mRNA, reactivity, and protein in hearts. Significantly reduced cardiac PGE_2 levels on day 8 were found in *COX-2*$^{+/-}$ compared with those in WT. There was no difference in local viral titers between both groups on day 4. Infected WT treated with a selective COX-2 inhibitor, NS-398, also showed the augmented myocardial damage on day 8. These results suggest that inhibition of COX-2 may enhance myocardial damage through reciprocal cardiac expression of TNF-α and adiponectin in a mouse model of viral myocarditis.
© 2005 Elsevier Inc. All rights reserved.

Keywords: Cyclooxygenase-2; Myocardial damage; Viral myocarditis; Prostaglandin E_2; Tumor necrosis factor-α; Adiponectin

Introduction

Cyclooxygenase (COX) catalyzes oxidation of arachidonic acid, producing prostaglandin (PG) H_2, which is then isomerized to biologically active eicosanoids and thromboxanes. Two distinct COX isoforms are identified: COX-1 is present in most cells and is constitutively expressed, whereas COX-2 is both inducible and the major isoform of inflammatory cells (DeWitt et al., 1993). COX-1 gene is more than 22 kb, and is located on chromosome arm 9q32–q33.3 in humans (Kosaka et al., 1994). The COX-2 gene is encoded by a gene more than 8 kb in size located on the long arm of chromosome 1q25.2–q25.3 (Kosaka et al., 1994). This gene is very similar to the mouse and chicken COX-2 genes (Kosaka et al., 1994). Mice with disrupted COX-1 or COX-2 genes have been generated using gene-targeting strategies (Langenbach et al., 1995; Morham et al., 1995), and the characteristics of these mice have been reviewed (Langenbach et al., 1999).

While a role of COX-1 in inflammation is largely unknown, COX-2 is likely to play a role in the inflammatory process and has been implicated as a mediator of various inflammatory diseases. Reduction of PG production by inhibition of COX is thought to be main mechanism of action of most non-steroidal anti-inflammatory drugs. It has also been described that COX-2-deficient mice are resistant to endotoxin-induced inflammation and death (Ejima et al., 2003). On the other hand, COX-2 deficiency has been reported to fail in altering inflammatory responses in several standard models (Dinchuk et al., 1995).

* Corresponding author. Tel.: +81 76 286 2211x3841; fax: +81 76 286 2702.
E-mail address: kandat@kanazawa-med.ac.jp (T. Kanda).

0024-3205/$ - see front matter © 2005 Elsevier Inc. All rights reserved.
doi:10.1016/j.lfs.2005.04.060

Viral infection, i.e. infection of encephalomyocarditis (EMC) virus is shown to stimulate COX-2 expression and PGE_2 accumulation through activation of nuclear factor-kappa B (NF-κB) in macrophages (Steer et al., 2003), and inhibitors of COX-2 enzymatic activity attenuate viral replication (Chen et al., 2000; Zhu et al., 2002), suggesting that the expression of COX-2 and the increased production of PG may possess an important role in viral replication. COX-2 enzyme is also described to be protective against pulmonary fibrogenesis, indicating that COX-2 generation of PGE_2 is a critical factor in resolving inflammation (Bonner et al., 2002).

COX-2 is reported to be up-regulated in an animal model of cardiac failure (Adderley and Fitzgerald, 1999), and its induction and activation of NF-κB has been detected in cardiomyocytes of patients with congestive heart failure (Wong et al., 1998). Deletion of the COX-2 gene may result in myocardial fibrosis (Dinchuk et al., 1995). Several manuscripts suggest that COX-2 plays a crucial role in mediating cardioprotective effects of ischemic preconditioning, which is the most potent anti-ischemic intervention known to date in terms of endogenous protection of ischemic myocardium (Shinmura et al., 2000; Bolli et al., 2002), since PGE_1 of COX-2 metabolites exerts cardioprotective action such as reduction in infarct size (Simpson et al., 1988).

We hypothesized that endogenous cardiac expression of COX-2 could play a cardioprotective role in establishment of severe inflammatory conditions induced by EMC virus. Therefore, we determined degrees of myocardial damage in the COX-2-deficient mice with acute viral myocarditis based on the histopathological findings and cardiac expression of tumor necrosis factor-alpha (TNF-α) mRNA, immunoreactivity, and protein in comparison with those in the wild-type mice with myocarditis.

Materials and methods

Animals

B6;129S7-*Ptgs2*^{tm1Jed} (*COX-2*$^{+/-}$) mice and C57BL/6 wild-type (WT) mice (3–5 weeks old) were purchased from the Jackson Laboratory (Bar Harbor, Maine, USA) as described previously (Yokota et al., 2002). High mortality and unavailability precluded use of homozygous *COX-2*$^{-/-}$ animals in this experiment.

Virus

A myocarditic variant of EMC virus was obtained from Y. Seto, Ph.D. (Keio University, Tokyo, Japan). Virus preparations were stored at −80 °C in Eagle's minimum essential medium (MEM) supplemented with 0.1% fetal bovine serum until the time of use.

Infection protocol

Animals were intraperitoneally inoculated with 500 plaque-forming units of EMC virus suspended in 0.1 ml of saline.

Treatment protocol

We administered EMC virus to WT ($n=12$) and *COX-2*$^{+/-}$ ($n=12$) mice. A normal WT mouse without viral inoculation was also included. Cardiac tissues were immediately extracted after sacrifice by cervical dislocation in both groups on days 4 and 8 after the EMC virus inoculation.

Histological examinations of hearts

Hearts were immediately weighed after sacrifice. Body weights were also recorded before sacrifice. Ratios of heart weight to body weight were calculated in both groups. Halves of cardiac tissues were fixed in 10% buffered formalin and stained with hematoxylin–eosin (H&E), while the other halves were immediately frozen in liquid nitrogen and stored at −80 °C for the studies of COX-2, PGE_2, and cytokine. Two transverse sections of the ventricular myocardium were graded for the severity of necrosis and mononuclear cell infiltration by an experienced pathologist, who had no knowledge of our study design, according to the following scale: grade 1, lesions involving <25% of the ventricular myocardium; grade 2, lesions involving 25% to 50% of the myocardium; grade 3, lesions involving 50% to 75% of the myocardium; and grade 4, lesions involving >75% of the myocardium. We also performed the staining on myosin as well as the H&E staining to identify the myocyte necrosis accurately. In addition, the pathologist randomly selected five high power fields (HPF) (×400 magnification) from each transverse section of the myocardium, and counted the infiltrating cells. The number of apoptotic cells in the randomly selected 5 HPF (×400 magnification) per section in the transverse sections of the myocardium was determined with in situ TUNEL as previously described (Kanda et al., 1999).

Comparative expression levels of COX-2, TNF-α, and adiponectin mRNA in hearts

RNA extraction for each half of frozen cardiac tissues was performed as described by the manufacturer (RNeasy Mini Kit, QIAGEN Inc., Tokyo, Japan). Procedure of DNAase was performed during the RNA extraction to avoid DNA contaminations. The total RNA concentrations were determined by measuring the optical density at 260 and 280 nm. Aliquots of 20 μl RNA from the each tissue were applied for production of cDNA. Comparative expression levels of COX-2, TNF-α, and adiponectin mRNA in cardiac tissues from both groups were determined using a quantitative real-time reverse transcriptase–polymerase chain reaction (RT–PCR) as described previously (Takeda et al., 2004). We applied TaqMan MGB Probe (Applied Biosystems Inc., CA, USA) for the real-time PCR. Primers and probe for quantification of COX-2 transcript (synthesized by Hokkaido System Science Co. Ltd., Hokkaido, Japan) were designed using a primer design software Primer Express (Applied Biosystems Inc.). We used a commercially available kit for TNF-α and

adiponectin RT-PCR (Mm00443258 m1 and Mm00456425 m1, Applied Biosystems Inc.). Each threshold cycle number up to 50 cycles (C_t value) within the RT–PCR was examined for the COX-2, TNF-α, and adiponectin mRNA levels. Glyceraldehyde-3-phosphate dehydrogenase (GAPDH) gene was used as an endogenous internal standard, and was amplified with specific primers for the number of cycles. A negative control without template cDNA was always included. ΔC_t values referred to differences between the C_t values for the each target gene and the GAPDH gene. After confirming that efficiencies of amplification of the each molecule and GAPDH transcripts were approximately equal, amount of the COX-2, TNF-α, or adiponectin transcript relative to the GAPDH transcript was determined using the comparative C_t method described in Perkin Elmer Applied Biosystems User Bulletin #2 (1997). Data are expressed as fold-increases relative to the baseline values in heart from a normal WT mouse without viral inoculation.

Immunoreactivity of COX-2, TNF-α, and adiponectin in cardiomyocytes

Immunohistochemical staining by streptavidin biotin complex method (#K0675 and #E0466 or #E0353, DAKO Cytomation Co. Ltd., Kyoto, Japan) was performed for the sections of transverse ventricular myocardium obtained from both groups on days 4 and 8 after viral infection. As a normal control, the immunoreactivity of COX-2, TNF-α, and adiponectin was determined with heart from a normal WT mouse without viral inoculation. We used the following commercially available primary antibodies; goat polyclonal anti-mouse COX-2 antibody at dilution of 1:100 (#sc-1747, Santa Cruz Biotechnology Inc., CA, USA), goat polyclonal anti-mouse TNF-α antibody at dilution of 1:50 (#RC410, DAKO Cytomation Co. Ltd.), and rabbit polyclonal anti-mouse adiponectin antibody at dilution of 1:50 (#ACRP303-A, Alpha Diagnostic International Inc., TX, USA). Control slides were treated with normal diluted goat or rabbit serum. The slides were blindly reviewed by the same pathologist, and were semiquantitatively graded according to the positive degrees of immunoreactivity as 0 for absence of staining and 1+ for weak, 2+ for moderate, and 3+ for strong staining (Kanazawa et al., 1996). They were compared with the respective control slides to exclude nonspecific staining. The positive degrees of COX-2, TNF-α, and adiponectin reactivity were assessed for randomly selected 30 myocytes corresponding to the surviving cells found on the respective H&E and myosin-stained slides.

Cardiac levels of TNF-α and adiponectin

Partial remnants of frozen cardiac tissues were applied to measurement of TNF-α and adiponectin tissue levels with the homogenate of each tissue. Enzyme-linked immunosorbent assay (ELISA) method, which used a polyclonal antibody specific for mouse TNF-α or adiponectin pre-coated onto a microtiter plate (ELISA kit for TNF-α; BioSource International Inc., CA, USA) (ELISA kit for adiponectin; Otsuka Pharmaceutical Co., Ltd., Tokyo, Japan), was performed with cardiac samples according to the instructions of manufactures. As a normal control, cardiac levels of TNF-α and adiponectin were determined with heart from a normal WT mouse without viral infection. The ELISA kit applied for TNF-α concentrations showed that the limit of sensitivity and the within- and between-assay variations were 3.0 pg/ml, 6.5%, and 8.7%, respectively. The kit used for adiponectin levels demonstrated that the limit of sensitivity, the intra-assay variation, and the cross-reactivity were 0.25 ng/ml, less than 10%, and no responses for specimens from other animals including sheep, respectively.

Concentrations of PGE2 in hearts

Partial remnants of frozen cardiac samples from both groups on day 8 after viral infection were applied to measurement of PGE_2 tissue levels with the homogenate of each tissue as described previously (LaPointe et al., 2004). We also examined PGE_2 concentration with heart from a normal WT mouse without viral inoculation. Radioimmunoassay (RIA) method was performed using a commercially available kit with the tissue samples according to the instructions of manufactures (Prostaglandin E_2 [^{125}I] RIA Kit, Perkin Elmer Life Sciences Inc., MA, USA). This RIA kit used for plasma PGE_2 levels demonstrated that the sensitivity limit and the intra- and inter-assay variations were 0.5 pg/ml, 9.0–9.4%, and 6.7–11.6%, respectively.

Viral titers in hearts

EMC viral titers in hearts were determined in terms of the viral cytopathic effects, and were expressed as the tissue culture mean infectious dose ($TCID_{50}$). On day 4 after the inoculation ($n=6$ for each group), hearts were partially

Table 1
Body weight, cardiac weight, and ratio of cardiac weight to body weight in different mice groups after viral inoculation

	Body weight (g)			Cardiac weight (mg)		Ratio of cardiac weight to body weight	
	Day 0	Day 4	Day 8	Day 4	Day 8	Day 4	Day 8
WT	19.3±1.1	18.9±1.9	17.9±2.3	98±8	102±11	5.3±0.4	5.8±0.7
COX-2$^{+/-}$	19.5±1.6	19.0±2.2	16.2±2.5	102±10	116±13*	5.5±0.5	7.2±0.9*
NS-398	19.9±1.3	19.2±1.8	16.8±2.8	104±13	127±19*	5.6±0.7	7.5±1.1*

WT, wild-type mice; *COX-2*$^{+/-}$, mice with heterozygous deficiency of cyclooxygenase-2 gene; NS-398, wild-type mice treated with a selective inhibitor of cyclooxygenase-2, NS-398, at a dose of 3 mg/kg/day starting simultaneously with viral inoculation. Data are expressed as means±S.D.
* $P<0.05$ compared with WT mice group.

homogenized in 2 ml of MEM. After centrifugation, the supernatants were added into 96-well microtiter plates containing human amnion cells in MEM supplemented with 10% fetal calf serum as described previously (Kanda et al., 2000). The microtiter plates were observed daily for 5 days for the appearance of any cytopathic effects.

Reassessment study by a selective COX-2 inhibitor

In order to confirm the augmented myocardial damage, we orally administered WT mice ($n=12$) a selective COX-2 inhibitor, NS-398 (EMD Biosciences Inc., Darmstadt, Germany), at dosing of 3 mg/kg/day starting simultaneously with

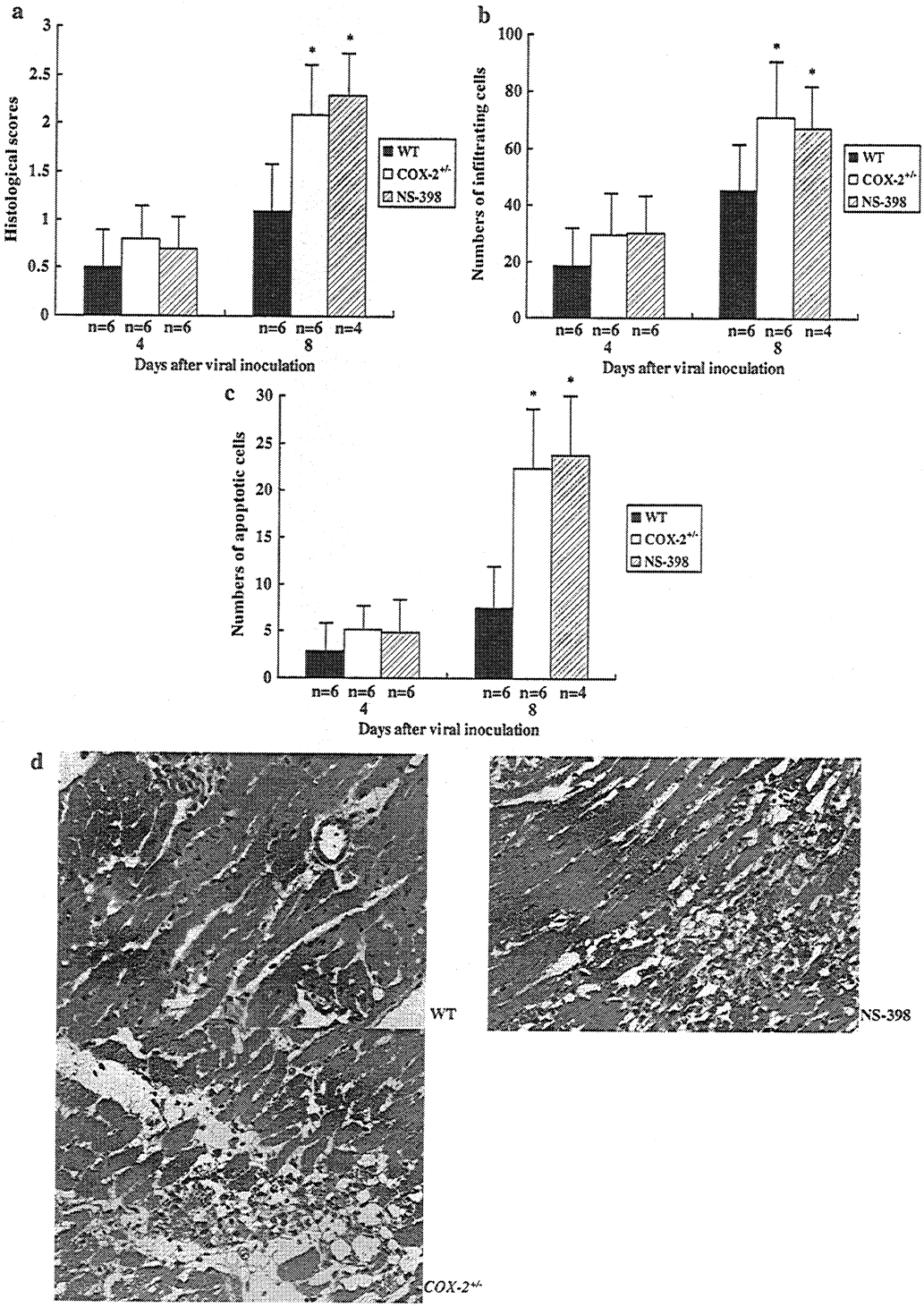


Fig. 1. Results of histological examination including histological scores in heart (a), numbers of infiltrating cells (b) or apoptotic cells (c) in myocardium from different mice on days 4 and 8 after viral inoculation, and photographic demonstration of myocardial damage in three groups on day 8 (d, original magnification). Data are expressed as mean ± S.D. WT, wild-type mice; *COX-2*$^{+/-}$, mice with heterozygous deficiency of cyclooxygenase-2 gene; NS-398, wild-type mice treated with a selective inhibitor of cyclooxygenase-2, NS-398, at a dose of 3 mg/kg/day starting simultaneously with viral inoculation. *$P<0.05$ compared with the WT group.

viral inoculation as described previously (LaPointe et al., 2004). Histological examinations (cardiac histological scores and numbers of infiltrating or apoptotic cells in myocardium), as well as body weights, heart weights, and ratios of heart weight to body weight, were assessed with hearts obtained on days 4 and 8 after viral infection. Data were compared with those in infected WT mice without intervention of the COX-2 inhibitor.

Statistical analysis

Data are expressed as mean±standard deviations. A two-tailed analysis of variance was applied to evaluate differences in body and cardiac weights, ratios of heart weight to body weight, cardiac histological scores, numbers of infiltrating or apoptotic cells in myocardium among three groups. An unpaired two-tailed Student's *t*-test was used to assess differences in comparative expression levels of COX-2, TNF-α, and adiponectin mRNA in hearts, immunoreactivity of COX-2, TNF-α, and adiponectin in myocytes, cardiac levels of TNF-α and adiponectin, PGE_2 concentrations in hearts, and local EMC viral titers between the *COX-2*$^{+/-}$ mice and the WT mice. A value of $P<0.05$ was considered to be statistically significant.

Results

Mortality in different mice with viral myocarditis

There were no dead mice with viral myocarditis in the WT group and the *COX-2*$^{+/-}$ group. Numbers of mice in each group from which specimens of hearts were obtained on days 4 and 8 after EMC viral inoculation, were 6 on each day in the WT mice and 6 on each day in the *COX-2*$^{+/-}$ mice, respectively.

Body weights, cardiac weights, and ratios of cardiac weight to body weight

Body weights, heart weights, and ratios of heart weight to body weight in different groups are shown in Table 1. Cardiac weights in the *COX-2*$^{+/-}$ group on day 8 after viral infection were significantly increased as compared with those in the WT group ($P<0.05$, Table 1). There was also significant difference in ratios of cardiac weight to body weight between the *COX-2*$^{+/-}$ mice and the WT mice on day 8 ($P<0.05$, Table 1).

Histological findings in hearts

Histological scores and numbers of infiltrating or apoptotic cells per field in the hearts obtained from different mice on days 4 and 8 after viral inoculation are shown in Fig. 1a, b, and c, respectively. The hearts from the *COX-2*$^{+/-}$ group showed severe myocardial necrosis and mononuclear cell infiltration (Fig. 1d). The histological scores based on myocardial necrosis and cell infiltration on day 8 were significantly higher in the *COX-2*$^{+/-}$ mice than in the WT mice ($P<0.05$, Fig. 1a). The number of infiltrating cells per field in the myocardium from the *COX-2*$^{+/-}$ group on day 8

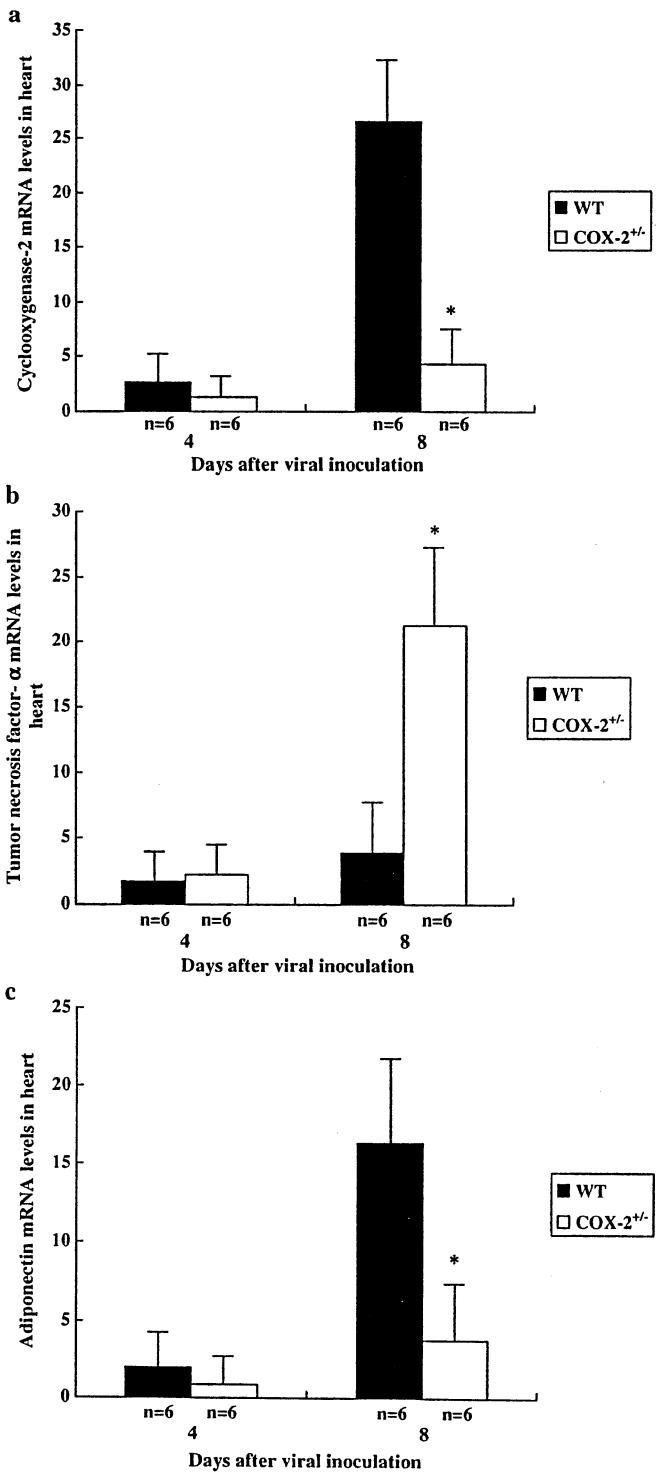


Fig. 2. Results of comparative expression levels of cyclooxygenase-2 (a), tumor necrosis factor-α (b), and adiponectin (c) mRNA using a quantitative real-time reverse transcriptase–polymerase chain reaction with hearts from different mice on days 4 and 8 after viral infection. Data are expressed as mean±S.D. WT, wild-type mice; *COX-2*$^{+/-}$, mice with heterozygous deficiency of cyclooxygenase-2 gene; COX-2, cyclooxygenase-2; TNF-α, tumor necrosis factor-α. *$P<0.05$ compared with the WT group.

was significantly elevated as compared with that in the WT group ($P<0.05$, Fig. 1b). The number of apoptotic cells per field in the hearts on day 8 was significantly higher in the *COX-2*$^{+/-}$ mice than in the WT mice ($P<0.05$, Fig. 1c). There were no significant differences in histological scores and numbers of infiltrating or apoptotic cells between the *COX-2*$^{+/-}$ group and the WT group on day 4.

Comparative expression levels of COX-2, TNF-α, and adiponectin mRNA in hearts

Tissue sample of heart from a normal WT mouse was assigned to each value of 1 for tissue expression levels of COX-2, TNF-α, and adiponectin mRNA, respectively. Cardiac levels of COX-2, TNF-α, and adiponectin mRNA from

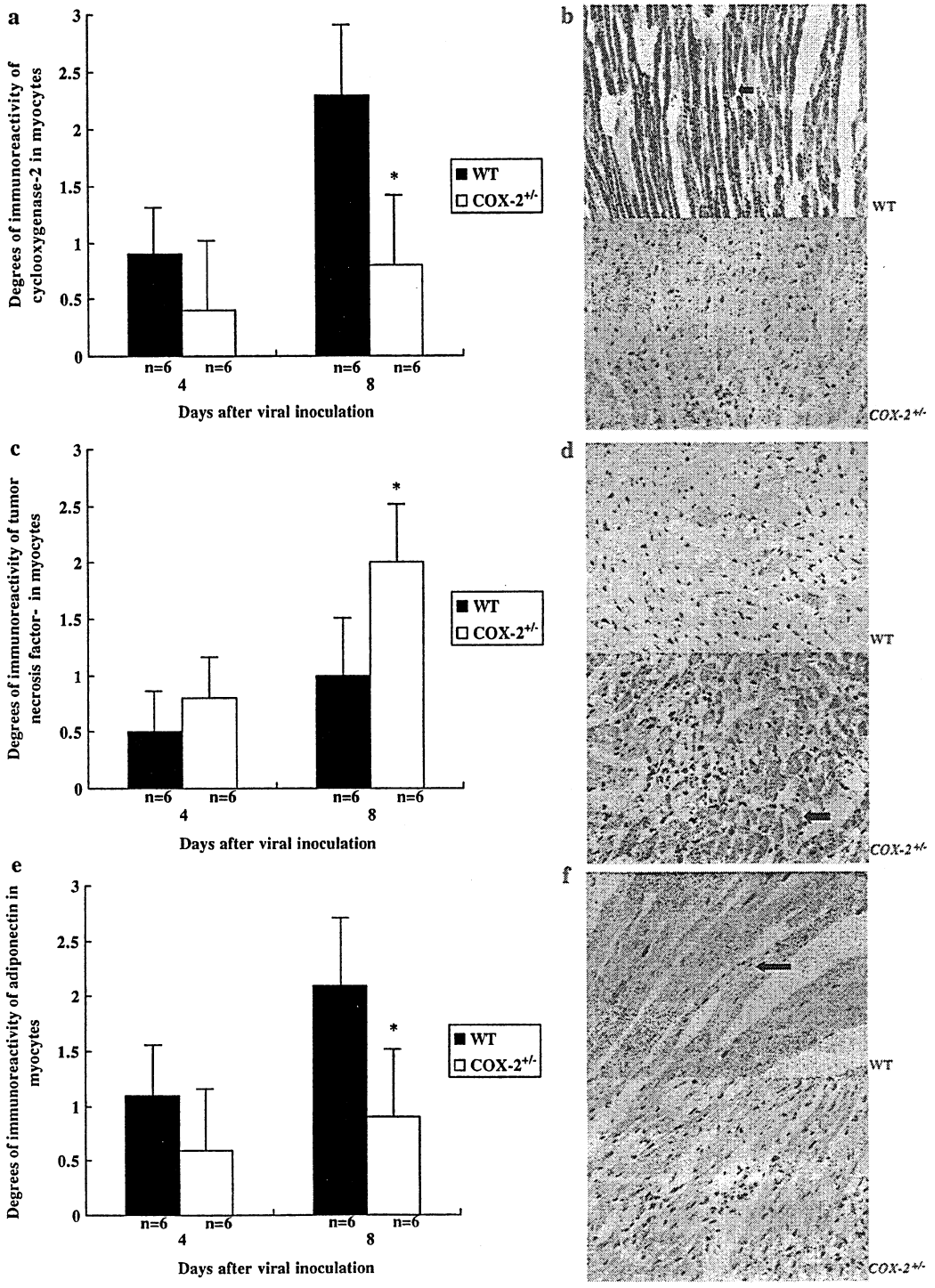


Fig. 3. Results of immunoreactivity degrees of targeted proteins including cyclooxygenase-2 (a), tumor necrosis factor-α (c), adiponectin (e) in myocytes from different mice on days 4 and 8 after viral inoculation, and photographic demonstration (arrows) of cyclooxygenase-2 (b, original magnification), tumor necrosis factor-α (d, original magnification), and adiponectin (f, original magnification) reactivity in myocardium from various mice on day 8. Data are expressed as mean±S.D. WT, wild-type mice; *COX-2*$^{+/-}$, mice with heterozygous deficiency of cyclooxygenase-2 gene. *$P<0.05$ compared with the WT group.

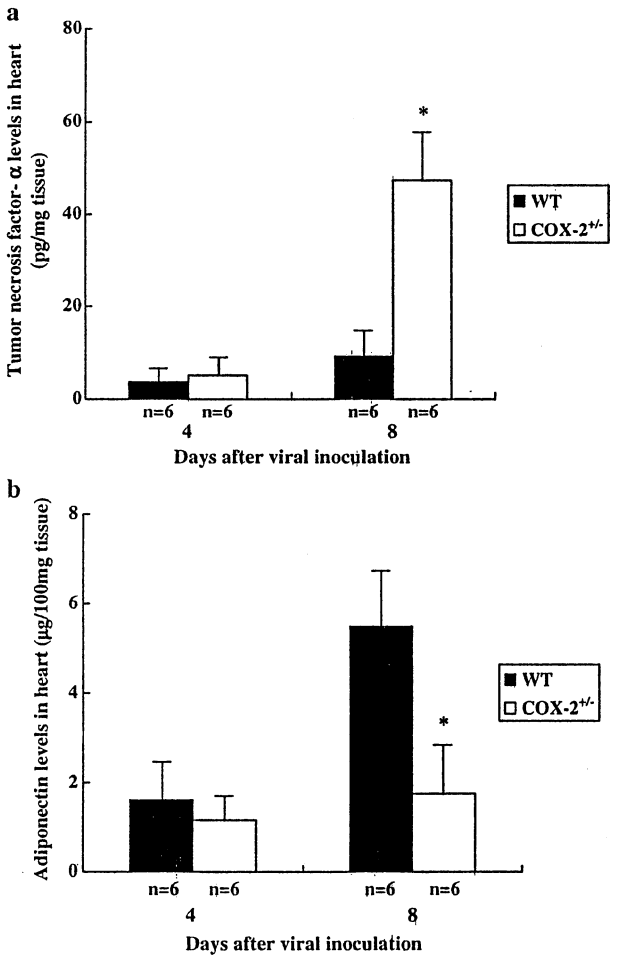


Fig. 4. Results of tumor necrosis factor-α (a) and adiponectin (b) levels in hearts from different mice on days 4 and 8 after viral inoculation. Data are expressed as mean±S.D. WT, wild-type mice; *COX-2*$^{+/-}$, mice with heterozygous deficiency of cyclooxygenase-2 gene. *$P<0.05$ compared with the WT group.

different mice on days 4 and 8 after viral infection are shown in Fig. 2a, b, and c, respectively. COX-2 mRNA levels in hearts on day 8 were significantly lower in the *COX-2*$^{+/-}$ group than in the WT group ($P<0.05$, Fig. 2a). On the other hand, we observed the significantly increased levels of TNF-α mRNA in cardiac tissues from the *COX-2*$^{+/-}$ mice at the same time as compared with those from the WT mice ($P<0.05$, Fig. 2b). Adiponectin mRNA levels in hearts on day 8 were significantly suppressed in the *COX-2*$^{+/-}$ group than in the WT group ($P<0.05$, Fig. 2c). There was no difference in cardiac levels of COX-2, TNF-α, and adiponectin mRNA between the WT mice and the *COX-2*$^{+/-}$ mice on day 4.

Immunoreactivity of COX-2, TNF-α, and adiponectin in cardiomyocytes

Immunoreactivity of COX-2, TNF-α, and adiponectin was not observed in heart from a normal WT mouse. The degrees of COX-2, TNF-α, and adiponectin reactivity in damaged myocytes from different mice on days 4 and 8 after viral inoculation are shown in Fig. 3a, c, and e, respectively. Photographic demonstration of immunoreactivity of COX-2, TNF-α, and adiponectin in cardiac tissues from various mice on day 8 is indicated in Fig. 3b, d, and f, respectively. We found the significantly suppressed reactivity of COX-2 in myocytes from the *COX-2*$^{+/-}$ group on day 8 as compared with that from the WT group ($P<0.05$, Fig. 3a and b). On the other hand, the degrees of TNF-α reactivity in myocytes at the same time were significantly higher in the *COX-2*$^{+/-}$ mice than in the WT mice ($P<0.05$, Fig. 3c and d). The degrees of adiponectin reactivity in myocytes on day 8 were significantly decreased in the *COX-2*$^{+/-}$ group than in the WT group ($P<0.05$, Fig. 3e and f). There were no differences in degrees of COX-2, TNF-α, and adiponectin reactivity between the WT mice and the *COX-2*$^{+/-}$ mice on day 4.

Cardiac levels of TNF-α and adiponectin

Specimen of heart from a normal WT mouse showed undetectable values for each targeted molecule. TNF-α and adiponectin levels in hearts from different mice on days 4 and 8 after viral infection are shown in Fig. 4a and b, respectively. Cardiac concentrations of TNF-α on day 8 were significantly higher in the *COX-2*$^{+/-}$ mice than in the WT mice ($P<0.05$, Fig. 4a). On the other hand, there were significantly reduced adiponectin levels in hearts from the *COX-2*$^{+/-}$ group at the same time as compared with those from the WT group ($P<0.05$, Fig. 4b). There were no differences in cardiac concentrations of TNF-α and adiponectin between the *COX-2*$^{+/-}$ mice and WT mice on day 4.

Concentrations of PGE2 in hearts

Tissue specimen of heart obtained from a normal WT mouse showed 0.96 pg/mg protein. Cardiac PGE_2 concentrations from different mice on day 8 after viral infection are shown in Fig. 5. The PGE_2 tissue levels on day 8 were significantly lower in the *COX-2*$^{+/-}$ mice than in the WT mice ($P<0.05$, Fig. 5).

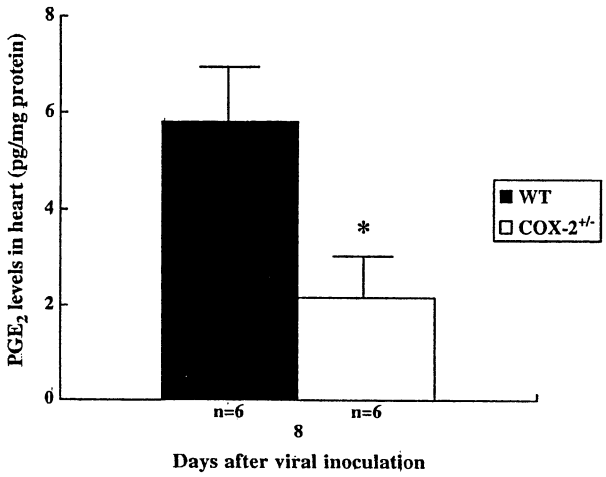


Fig. 5. Results of cardiac prostaglandin E_2 concentrations from different mice on day 8 after viral inoculation. Data are expressed as mean±S.D. WT, wild-type mice; *COX-2*$^{+/-}$, mice with heterozygous deficiency of cyclooxygenase-2 gene. *$P<0.05$ compared with the WT group.

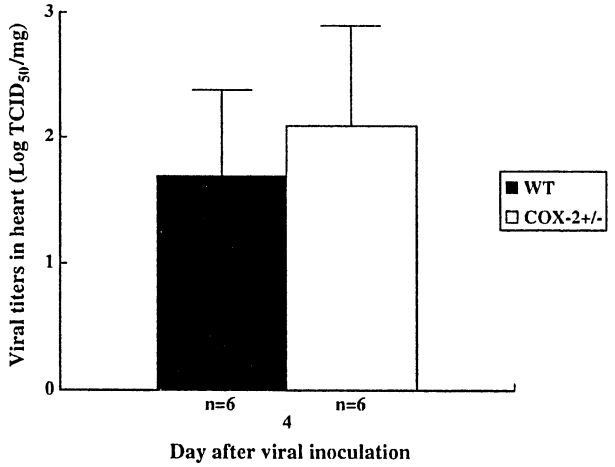


Fig. 6. Results of encephalomyocarditis viral titer in hearts from different mice on day 4 after viral infection. Data are expressed as mean±S.D. WT, wild-type mice; *COX-2*$^{+/-}$, mice with heterozygous deficiency of cyclooxygenase-2 gene; $TCID_{50}$, tissue culture mean infectious dose 50%.

Viral titers in hearts

EMC viral titers in hearts from various mice on day 4 after viral inoculation are indicated in Fig. 6. There was no difference in local viral titers between the *COX-2*$^{+/-}$ mice and the WT mice on day 4 after viral inoculation.

Reassessment study by a selective COX-2 inhibitor

We observed two dead WT mice treated with NS-398 on day 8 after viral infection. The numbers of mice from which hearts were extracted on days 4 and 8 were six and four, respectively. Cardiac weights and ratios of heart weight to body weight in the NS-398 group on day 8 were significantly increased compared to those in the WT group ($P<0.05$, Table 1). The histological scores and numbers of infiltrating or apoptotic cells in myocardium on day 8 were significantly higher in the WT mice treated with NS-398 than in the WT mice without intervention ($P<0.05$, Fig. 1a, b, and c). The augmented myocardial damage in the WT mice treated with NS-398 is shown in Fig. 1d. There were no differences in the histological scores and numbers of infiltrating or apoptotic cells between the NS-398 group and the WT group on day 4.

Discussion

The fold-increase of COX-2 mRNA expression in *COX-2*$^{+/-}$ mice compared to that in sham-infected animal was "one-seventh fold" less than the fold-increase in WT mice on day 8 after viral inoculation. Cardiac PGE_2 levels on day 8 were about one-third suppressed in the *COX-2*$^{+/-}$ group compared to those in the WT group. EMC virus infection has recently been reported to stimulate COX-2 expression in macrophages in in vitro experiment (Steer et al., 2003). Another study showed no expression of COX-2 mRNA in *COX-2*$^{-/-}$ primary embryonic fibroblasts and less expression of mRNA in *COX-2*$^{+/-}$ fibroblasts under stimulation (Dinchuk et al., 1995). Thus, decreased expression of COX-2 mRNA in hearts from *COX-2*$^{+/-}$ mice with viral infection seems to be due to the disruption of one COX-2 allele.

COX-2 products can exhibit both beneficial and deleterious effects on inflammatory process in the same organ such as the kidney (Wang et al., 2000). COX-2 expression is also described to protect against apoptosis in several types of cells, particularly in colon cancer cells (Kinoshita et al., 1999). Myocardial COX-2 expression is demonstrated in rat heart during cardiac transplant rejection (Yang et al., 2000), and COX activity induced by doxorubicin in rat neonatal cardiomyocytes is due to COX-2 gene expression (Hemler and Lands, 1976). It has recently been reported that COX-2 expression may provide some degrees of protective effects against the myocardial damage in the rat model of doxorubicin-induced cardiotoxicity (Dowd et al., 2001). On the other hand, COX-2 is indicated to play a deleterious role in heart after myocardial infarction caused by chronic occlusion of left anterior descending coronary artery (LaPointe et al., 2004). COX-2 inhibition partly reverses both the increase in cardiac collagen content and hypertrophy and the decrease in cardiac function in the mouse model of myocardial infarction. Similarly to the findings in the former manuscript, we observed impaired expression of cardiac COX-2 resulted in augmented myocardial injury in *COX-2*$^{+/-}$ mice with EMC virus-induced myocarditis as compared with that in WT mice. Since the inoculation of EMC virus promotes COX-2 expression and PGE_2 generation (Steer et al., 2003), the up-regulation of COX-2 expression is considered to play a crucial role for compensatory mechanism in the mouse model of heart failure induced by EMC virus infection.

TNF-α mRNA is shown to be detectable in myocardium obtained from subjects with ischemic heart disease (IHD) and dilated cardiomyopathy (DCM) using northern blot analysis, while there is no evidence for TNF-α gene expression in non-failing human hearts (Torre-Amione et al., 1996). Immunohistochemical examinations also indicated that there was obvious TNF-α immunostaining of cardiomyocytes in the myocardium from patients with IHD and DCM, whereas the TNF-α immunoreactivity was not detectable in the non-failing hearts (Torre-Amione et al., 1996). Natriuretic peptides including atrial and B-type peptides are synthesized in and secreted from hearts, and play a critical role in cardiovascular homeostasis (Grepin et al., 1994). Similarly to the previous demonstration, identification of TNF-α expression in hearts from mice with viral myocarditis in our study is also a good example of contribution made by molecular biology to understanding of mechanisms for heart failure compensation.

Prostaglandins acts on 2 classes of receptors consisting of surface transmembrane-spanning, G-protein-coupled receptors and peroxisome proliferator-activated receptors (PPARs), which are nuclear membrane receptors. Prostaglandins and their precursors are ligands for several PPARs including PPARα, PPARδ, and PPARγ (Bishop-Bailey and Hla, 1999). PPARγ activates transcription level of adiponectin with liver receptor homologue-1 by binding the promoter region of

adiponectin gene (Ouchi et al., 2004). Cardiac expression of adiponectin was impaired together with decreased PGE_2 concentrations in hearts from *COX-2*$^{+/-}$ mice with viral myocarditis. Reactivity of adiponectin for immunostaining has recently been reported to be observed at periphery of surviving cardiomyocytes around the lesions at granulative stage in myocardial tissues obtained from 47 autopsied hearts with infarction (Ishikawa et al., 2003). In another immunohistochemical analysis, boundary of mouse hepatocytes showed positive signals for adiponectin after 3–6 h of carbon tetrachloride treatment, and their cytoplasma was intensely stained after 18 h of the treatment (Yoda-Murakami et al., 2001). Adiponectin was considered to be produced by the liver in mice, where it underwent tissue damage-induced transcriptional regulation (Yoda-Murakami et al., 2001). Our data regarding adiponectin expression in damaged myocytes suggest that this adipocyte-specific cytokine might have important implications for acute phase of viral myocarditis.

Adiponectin is described to be involved in ending inflammatory responses through its inhibitory functions (Yokota et al., 2000). This cytokine increases mRNA expression of anti-inflammatory molecule, interleukin-10 (IL-10), at the transcriptional level, and elevates IL-10 protein secretion in in vitro experiment of human monocyte-derived macrophages (Kumada et al., 2004). In addition, reciprocal relationship between adiponectin and high-sensitive C-reactive protein is shown in both human plasma and adipose tissue from subjects with coronary artery disease (Ouchi et al., 2003). In our experiment, suppressed expression of cardiac adiponectin mRNA and immunoreactivity in *COX-2*$^{+/-}$ mice was associated with the development of severe myocarditis, whereas increased expression of adiponectin in hearts from WT mice resulted in the inhibition of cardiac inflammatory process. Therefore, we speculate that local expression of adiponectin in the damaged myocardium might be a compensatory phenomenon against the severe inflammatory conditions of viral myocarditis.

A COX-2 inhibitor, Dup-697, suppressed the biological action of adiponectin on differentiation of cloned stromal preadipocytes (Yokota et al., 2002). Adiponectin was described to inhibit TNF-α production in macrophages (Yokota et al., 2000). Adiponectin-knockout mice revealed high levels of TNF-α mRNA in adipose tissue and high plasma TNF-α concentrations (Maeda et al., 2002). Thus, impaired COX-2 functions seem to link to increased cardiac expression of TNF-α mRNA, immunoreactivity, and protein through the reduced expression of adiponectin mRNA, reactivity, and protein in our experiment.

In conclusion, decreased expression of COX-2 mRNA and immunoreactivity in myocardium from *COX-2*$^{+/-}$ mice after viral infection were observed together with increased heart weights, severe myocardial inflammation, and suppressed cardiac PGE_2 concentrations in *COX-2*$^{+/-}$ mice. There was also an enhanced expression of TNF-α mRNA, reactivity, and protein in hearts, while attenuated cardiac expression of adiponectin mRNA, reactivity, and protein was found in *COX-2*$^{+/-}$ mice with viral myocarditis. Moreover, infected WT mice treated with the selective COX-2 inhibitor showed the augmented myocardial damage on day 8. Our observations suggest that inhibition of COX-2 and subsequent reduced PGE_2 production in heart may contribute to enhanced myocardial injury through reciprocal cardiac expression of TNF-α and adiponectin in a mouse model of viral myocarditis.

Acknowledgment

This study was supported in part by Grant for Promoted Research from Kanazawa Medical University (S2003-2 and S2004-2), Grant for Project Research from High-Technology Center of Kanazawa Medical University (H2004-7), and the Science Research Promotion Fund of the Promotion and Mutual Aid Corporation for Private Schools of Japan.

References

Adderley, S.R., Fitzgerald, D.J., 1999. Oxidative damage of cardiomyocytes is limited by extracellular regulated kinases 1/2-mediated induction of cyclooxygenase-2. Journal of Biological Chemistry 274 (8), 5038–5046.

Bishop-Bailey, D., Hla, T., 1999. Endothelial cell apoptosis induced by the peroxisome proliferator-activated receptor (PPAR) ligand 15-deoxy-Delta12, 14-prostaglandin J2. Journal of Biological Chemistry 274 (24), 17042–17048.

Bolli, R., Shinmura, K., Tang, X.L., Kodani, E., Xuan, Y.T., Guo, Y., Dawn, B., 2002. Discovery of a new function of cyclooxygenase (COX)-2: COX-2 is a cardioprotective protein that alleviates ischemia/reperfusion injury and mediates the late phase of preconditioning. Cardiovascular Research 55 (3), 506–519.

Bonner, J.C., Rice, A.B., Ingram, J.L., Moomaw, C.R., Nyska, A., Bradbury, A., Sessoms, A.R., Chulada, P.C., Morgan, D.L., Zeldin, D.C., Langenbach, R., 2002. Susceptibility of cyclooxygenase-2-deficient mice to pulmonary fibrogenesis. American Journal of Pathology 161 (2), 459–470.

Chen, N., Warner, J.L., Reiss, C.S., 2000. NSAID treatment suppresses VSV propagation in mouse CNS. Virology 276 (1), 44–51.

DeWitt, D.L., Meade, E.A., Smith, W.L., 1993. PGH synthase isoenzyme selectivity: the potential for safer nonsteroidal antiinflammatory drugs. American Journal of Medicine 95 (2A), 40S–44S.

Dinchuk, J.E., Car, B.D., Focht, R.J., Johnston, J.J., Jaffee, B.D., Covington, M.B., Contel, N.R., Eng, V.M., Collins, R.J., Czerniak, P.M., Gorry, S.A., Trzaskos, J.M., 1995. Renal abnormalities and an altered inflammatory response in mice lacking cyclooxygenase II. Nature 378 (6555), 406–409.

Dowd, N.P., Scully, M., Adderley, S.R., Cunningham, A.J., Fitzgerald, D.J., 2001. Inhibition of cyclooxygenase-2 aggravates doxorubicin-mediated cardiac injury in vivo. Journal of Clinical Investigation 108 (4), 585–590.

Ejima, K., Layne, M.D., Carvajal, I.M., Kritek, P.A., Baron, R.M., Chen, Y-H., Vom Saal, J., Levy, B.D., Yet, S.F., Perrella, M.A., 2003. Cyclooxygenase-2-deficient mice are resistant to endotoxin-induced inflammation and death. FASEB Journal 17 (10), 1325–1327.

Grepin, C., Dagnino, L., Robitaille, L., Haberstroh, L., Antakly, T., Nemer, M., 1994. A hormone-encoding gene identifies a pathway for cardiac but not skeletal muscle gene transcription. Molecular and Cellular Biology 14 (5), 3115–3129.

Hemler, M., Lands, W.E., 1976. Purification of the cyclooxygenase that forms prostaglandins. Demonstration of two forms of iron in the holoenzyme. Journal of Biological Chemistry 251 (18), 5575–5579.

Ishikawa, Y., Akasaka, Y., Ishii, T., Yoda-Murakami, M., Choi-Miura, N.H., Tomita, M., Ito, K., Zhang, L., Akishima, Y., Ishihara, M., Muramatsu, M., Taniyama, M., 2003. Changes in the distribution pattern of gelatin-binding protein of 28 kDa (adiponectin) in myocardial remodelling after ischaemic injury. Histopathology 42 (1), 43–52.

Kanazawa, K., Kawashima, S., Mikami, S., Miwa, Y., Hirata, K., Suematsu, M., Hayashi, Y., Itoh, H., Yokoyama, M., 1996. Endothelial constitutive nitric oxide synthase protein and mRNA increased in rabbit atherosclerotic aorta

despite impaired endothelium-dependent vascular relaxation. American Journal of Pathology 148 (6), 1949–1956.

Kanda, T., Koike, H., Arai, M., Wilson, J.E., Carthy, C.M., Yang, D., McManus, B.M., Nagai, R., Kobayashi, I., 1999. Increased severity of viral myocarditis in mice lacking lymphocyte maturation. International Journal of Cardiology 68 (1), 13–22.

Kanda, T., Tanaka, T., Sekiguchi, K., Seta, Y., Kurimoto, M., Wilson,, McManus, J.E., Nagai, R., Yang, D., McManus, B.M., Kobayashi, I., 2000. Effect of interleukin-18 on viral myocarditis: enhancement of interferon-gamma and natural killer cell activity. Journal of Molecular and Cellular Cardiology 32 (12), 2163–2171.

Kinoshita, T., Takahashi, Y., Sakashita, T., Inoue, H., Tanabe, T., Yoshimoto, T., 1999. Growth stimulation and induction of epidermal growth factor receptor by overexpression of cyclooxygenases 1 and 2 in human colon carcinoma cells. Biochimica et Biophysica Acta 1438 (1), 120–130.

Kosaka, T., Miyata, A., Ihara, H., Hara, S., Sugimoto, T., Takeda, O., Takahashi, E., Tanabe, T., 1994. Characterization of the human gene (PTGS2) encoding prostaglandin-endoperoxide synthase 2. European Journal of Biochemistry 221 (3), 889–897.

Kumada, M., Kihara, S., Ouchi, N., Kobayashi, H., Okamoto, Y., Ohashi, K., Maeda, K., Nagaretani, H., Kishida, K., Maeda, N., Nagasawa, A., Funahashi, T., Matsuzawa, Y., 2004. Adiponectin specifically increased tissue inhibitor of metalloproteinase-1 through interleukin-10 expression in human macrophages. Circulation 109 (17), 2046–2049.

Langenbach, R., Morham, S.G., Tiano, H., Loftin, C., Ghanayem, B.I., Chulada, P.C., Mahler, J.F., Lee, C., Goulding, E.H., Kluckman, K.D., Kim, H.S., Smithies, O., 1995. Prostaglandin synthase 1 gene disruption in mice reduces arachidonic acid-induced inflammation and indomethacin-induced gastric ulceration. Cell 83 (3), 483–492.

Langenbach, R., Loftin, C., Lee, C., Tiano, H., 1999. Cyclooxygenase knockout mice: models for elucidating isoform specific functions. Biochemical Pharmacology 15 (8), 1237–1246.

LaPointe, M.C., Mendez, M., Leung, A., Tao, Z., Yang, X-P., 2004. Inhibition of cyclooxygenase-2 improves cardiac function after myocardial infarction in the mouse. American Journal of Physiology. Heart and Circulatory Physiology 286 (4), H1416–H1424.

Maeda, N., Shimomura, I., Kishida, K., Nishizawa, H., Matsuda, M., Nagaretani, H., Furuyama, N., Kondo, H., Takahashi, M., Arita, Y., Komuro, R., Ouchi, N., Kihara, S., Tochino, Y., Okutomi, K., Horie, M., Takeda, S., Aoyama, T., Funahashi, T., Matsuzawa, Y., 2002. Diet-induced insulin resistance in mice lacking adiponectin/ACRP30. Nature Medicine 8 (7), 731–737.

Morham, S.G., Langenbach, R., Loftin, C., Tiano, H., Vouloumanos, N., Jennette, J.C., Mahler, J.F., Kluckman, K.D., Ledford, A., Lee, C., Smithies, O., 1995. Prostaglandin synthase 2 gene disruption causes severe renal pathology in the mouse. Cell 83 (3), 473–482.

Ouchi, N., Kihara, S., Funahashi, T., Nakamura, T., Nishida, M., Kumada, M., Okamoto, Y., Ohashi, K., Nagaretani, H., Kishida, K., Nishizawa, H., Maeda, N., Kobayashi, H., Hiraoka, H., Matsuzawa, Y., 2003. Reciprocal association of C-reactive protein with adiponectin in blood stream and adipose tissue. Circulation 107 (5), 671–674.

Ouchi, N., Kobayashi, H., Kihara, S., Kumada, M., Sato, K., Inoue, T., Funahashi, T., Walsh, K., 2004. Adiponectin stimulates angiogenesis by promoting cross-talk between AMP-activated protein kinase and Akt signaling in endothelial cells. Journal of Biological Chemistry 279 (2), 1304–1309.

Shinmura, K., Tang, X.L., Wang, Y., Xuan, Y.T., Liu, S.Q., Takano, H., Bhatnagar, A., Bolli, R., 2000. Cyclooxygenase-2 mediates the cardioprotective effects of the late phase of ischemic preconditioning in conscious rabbits. Proceedings of the National Academy of Sciences of the United States of America 97 (18), 10197–10202.

Simpson, P.J., Mickelson, J., Fantone, J.C., Gallagher, K.P., Lucchesi, B.R., 1988. Reduction of experimental canine myocardial infarct size with prostaglandin E1: inhibition of neutrophil migration and activation. Journal of Pharmacology and Experimental Therapeutics 244 (2), 619–624.

Steer, S.A., Moran, J.M., Maggi, L.B., Buller, R.M.L., Perlman, H., Corbett, J.A., 2003. Regulation of cyclooxygenase-2 expression by macrophages in response to double-stranded RNA and viral infection. Journal of Immunology 170 (2), 1070–1076.

Takeda, K., Lin, J., Okubo, S., Akazawa-Kudoh, S., Kajinami, K., Kanemitsu, S., Tsugawa, H., Kanda, T., Matsui, S., Takekoshi, N., 2004. Transient glucose deprivation causes upregulation of heme oxygenase-1 and cyclooxygenase-2 expression in cardiac fibroblasts. Journal of Molecular and Cellular Cardiology 36 (6), 821–830.

Torre-Amione, G., Kapadia, S., Lee, J., Durand, J.B., Bies, R.D., Young, J.B., Mann, D.L., 1996. Tumor necrosis factor-alpha and tumor necrosis factor receptors in the failing human heart. Circulation 93 (4), 704–711.

Wang, J.L., Cheng, H.F., Shappell, S., Harris, R.C., 2000. A selective cyclooxygenase-2 inhibitor decreases proteinuria and retards progressive renal injury in rats. Kidney International 57 (6), 2334–2342.

Wong, S.C., Fukuchi, M., Melnyk, P., Rodger, I., Giaid, A., 1998. Induction of cyclooxygenase-2 and activation of nuclear factor-κB in myocardium of patients with congestive heart failure. Circulation 98 (2), 100–103.

Yang, X., Ma, N., Szabolcs, M.J., Zhong, J., Athan, E., Sciacca, R.R., Michler, R.E., Anderson, G.D., Wiese, J.F., Leahy, K.M., Gregory, S., Cannon, P.J., 2000. Upregulation of COX-2 during cardiac allograft rejection. Circulation 101 (2000), 430–438.

Yoda-Murakami, M., Taniguchi, M., Takahashi, K., Kawamata, S., Saito, K., Choi-Miura, N.H., Tomita, M., 2001. Changes in expression of GBP28/adiponectin in carbon tetrachloride-administered mouse liver. Biochemical and Biophysical Research Communications 285 (2), 372–377.

Yokota, T., Oritani, K., Takahashi, I., Ishikawa, J., Matsuyama, A., Ouchi, N., Kihara, S., Funahashi, T., Tenner, A.J., Tomiyama, Y., Matsuzawa, Y., 2000. Adiponectin, a new member of the family of soluble defense collagens, negatively regulates the growth of myelomonocytic progenitors and the functions of macrophages. Blood 96 (5), 1723–1732.

Yokota, T., Meka, C.S., Medina, K.L., Igarashi, H., Comp, P.C., Takahashi, M., Nishida, M., Oritani, K., Miyagawa, J., Funahashi, T., Tomiyama, Y., Matsuzawa, Y., Kincade, P.W., 2002. Paracrine regulation of fat cell formation in bone marrow cultures via adiponectin and prostaglandins. Journal of Clinical Investigation 109 (10), 1303–1310.

Zhu, H., Cong, J.P., Yu, D., Bresnahan, W.A., Shenk, T.E., 2002. Inhibition of cyclooxygenase-2 blocks human cytomegalovirus replication. Proceedings of the National Academy of Sciences of the United States of America 99 (6), 3932–3937.

1．研究課題名：RNA interference における二本鎖 RNA 依存性プロテインキナーゼ PKR の関与（研究番号 S2004-3）

2．キーワード：1）RNA 干渉（RNA interference, RNAi）
2）二本鎖 RNA（double-stranded RNA, dsRNA）
3）二本鎖 RNA 依存性プロテインキナーゼ（dsRNA-activated protein kinase, PKR）

3．研究者氏名：松井　理・医学部・助手・ゲノム医科学（生化学Ⅰ）

4．研 究 目 的

RNA interference（RNAi）は、short interfering RNA（siRNA）と呼ばれる 21～23 塩基対（base pair, bp）の短い二本鎖 RNA（dsRNA）がそれと同じ配列を持つ mRNA に作用しその分解を誘導するという原理に基づく遺伝子発現抑制機構である。RNAi は比較的簡単な操作で特定遺伝子の発現を抑制できるため癌の遺伝子治療など臨床への応用が期待されているが、その作用機構には未だ不明な点も多く安全性が疑問視されている。特に、細胞内には dsRNA の関与する重要な系が他にもいくつか知られており、これらへの影響が懸念されている。そこで本研究では、このような dsRNA 分子を活性化因子とする dsRNA 依存性プロテインキナーゼ（PKR）の機能に対して、siRNA のような短い dsRNA がどのような影響を及ぼすかを明らかにすることを目的に研究を行う。PKR はウイルス感染などの細胞ストレス下でのサイトカイン産生やアポトーシス誘導など重要な生理現象において中心的な役割を担っており、PKR と RNAi との関連を明らかにすることは生物学的・医学的に大いに意義があると思われる。

5．研 究 計 画

(1) PKR 組換え蛋白質と様々な鎖長の dsRNA を作製し、それらを用いて、dsRNA の PKR 活性化に及ぼす効果を in vitro の実験によって調べることにより、siRNA が PKR 活性化能を有するかを明らかにする。

(2) 培養細胞へ様々な鎖長の dsRNA を導入し、これらの細胞内 PKR 活性に与える影響を調べることにより、RNAi 経路の PKR 経路への影響を明らかにする。

6．研 究 成 果

(1) PKR 組換え蛋白質（His-PKR）の作製

dsRNA が PKR の活性にどのような影響を与えるのかを in vitro で解析するために、以下のようにして PKR 組換え蛋白質（His-PKR）の作製を行った。まず、ヒト PKR cDNA を pET15b にクローニングし、発現プラスミド（pET15b-PKR）を構築した。このプラスミドを導入した大腸菌内で組換え蛋白質遺伝子の発現を行い、His-PKR 蛋白質を生

産した。大腸菌細胞を破砕した後、Ni-NTA アガロースビーズ、phosphocellulose カラムクロマトグラフィーによって精製し、精製 His-PKR 標品を得た。

(2) 様々な鎖長の合成 dsRNA の作製

様々な長さの dsRNA の作製は以下の手順にて行った。まず pGEM-3Zf(+) (Promega) の SP6 プロモーターの下流に合成二本鎖 DNA をクローニングし、11～41 bp の dsRNA 領域を持つ hairpin RNA 合成プラスミドを構築した。次にこれらのプラスミドを鋳型として用い、SP6 RNA polymerase によって in vitro で hairpin RNA を合成した。この hairpin RNA の一本鎖領域を Mung Bean nuclease で消化し、ポリアクリルアミドゲル電気泳動によって分離した後、ゲル片から dsRNA を抽出・回収し、精製 dsRNA 標品を得た。

(3) PKR の活性化における dsRNA の鎖長の依存性

様々な鎖長の dsRNA について、His-PKR の自己リン酸化活性に対する dsRNA の依存性を調べた。その結果、31 bp 以上の dsRNA (31～41 bp) では明らかな His-PKR の自己リン酸化の促進が観察されたのに対し、それよりも小さな dsRNA (11～26 bp) では His-PKR の自己リン酸化は全く促進されなかった。また、上記の PKR の自己リン酸化を促進する dsRNA の場合でも、コントロールとして用いた長鎖 (数百～数千 bp) の合成 dsRNA、Poly(I)・Poly(C)の場合と比較すると、活性化の効果は非常にわずかであった。この結果から、二本鎖 RNA による PKR の活性化は二本鎖 RNA の鎖長に依存しており、21～23 bp 程度の鎖長である siRNA は PKR の活性化因子として機能しないことが予想された。

(4) dsRNA と PKR との相互作用および dsRNA による PKR の構造変化

(3) で明らかになった dsRNA の鎖長の違いによる PKR 活性化能の違いが、dsRNA と PKR との相互作用の違いに基づくものなのかどうかを明らかにするためゲルシフトアッセイを行った。その結果、PKR 活性化能を持つ 31 bp 以上の dsRNA だけでなく PKR 活性化能を持たない 11～26 bp の dsRNA についても dsRNA と PKR との間の相互作用が検出された。さらにゲルシフトアッセイの結果を詳しく調べると、31 bp 以上の dsRNA では移動速度の遅いシフトバンドが新たに観察された。この新たなシフトバンドは PKR 二量体を示していると考えられる。従ってこの結果から、PKR の活性化に対する dsRNA の鎖長依存性は、PKR への結合能の違いによるものではなく、おそらく活性化中間体である PKR 二量体形成能の違いによるものと推察された。

(5) 短鎖 dsRNA による PKR の阻害

(4) の結果より、11～26 bp の dsRNA は、PKR に結合するが活性化しないことが判明した。この結果は、これらの長さの dsRNA が長鎖の dsRNA と拮抗して PKR の活性化を阻害することを示唆する。そこで、11～41 bp の dsRNA 存在下で Poly(I)・Poly(C) による His-PKR の自己リン酸化活性への影響を調べたところ、16 bp 以下の dsRNA は阻害効果を示さなかったのに対し、それよりも長い dsRNA (21～41 bp) は予想通り PKR の自己リン酸化を阻害した。

(6) 細胞内で発現させたhairpin RNAの細胞内PKR活性への影響

(5) のin vitroの実験では、siRNAサイズ（21～23 bp）のdsRNAが過剰量存在する場合、PKR活性を阻害することが明らかになった。そこで次に、細胞内で生産されたsiRNAが細胞内PKRを阻害するかどうかを調べた。まず、動物細胞内でsiRNAサイズのdsRNAを発現させるため、pSilencer1.0-U6（Ambion）のU6プロモーターの下流に合成DNAをつなげ、21 bpのdsRNA領域を持つ短鎖hairpin RNA（shRNA-21）発現プラスミドを作製した。shRNA-21は細胞内でプロセッシングされ、siRNAサイズのdsRNAとなることが予想された。shRNA-21発現プラスミドをヒト培養細胞に導入した後、細胞内PKR活性をルシフェラーゼレポーター遺伝子の発現でモニターしたところ、ルシフェラーゼの発現量が著しく促進したことから、PKR活性の阻害が示唆された。また、shRNA-21発現プラスミドを導入した細胞の抽出液について、抗リン酸化PKR抗体を用いたウェスタンブロッティングを行ったところ、shRNA-21を発現させない場合に比べて自己リン酸化されたPKRが著しく減少していた。以上の結果から、細胞内で過剰発現されたsiRNAサイズのdsRNAはPKRを阻害することが明らかになった。

7．研究の考察・反省

本研究の結果から、細胞内で合成させたsiRNAはPKRを活性化しないだけでなく、PKR活性を著しく阻害することが明らかになった。この作用機構としてはおそらく、siRNAがPKR活性化能を持つdsRNAとPKRとの結合を競合的に阻害するからだと考えられる。PKRは前述のように抗ウイルス作用に関わる蛋白質である。したがって、RNAiを臨床に応用する場合、本研究の結果によると、siRNAによって引き起こされるPKR機能の低下により人体がウイルスの感染に対して無防備になることが懸念される。今後は、ウイルス防御などPKRの関与する細胞機能への影響などを解明するため、さらに詳細な解析を継続する。

8．研究発表

松井　理，伊達孝保．短鎖二本鎖による二本鎖RNA依存性プロテインキナーゼ（PKR）の阻害．金医大誌　2005；30：551-559.

金医大誌（J Kanazawa Med Univ）30：551－559, 2005

短鎖二本鎖RNAによる二本鎖RNA依存性プロテインキナーゼ (PKR) の阻害

松井　理，伊達孝保

要　約：RNA干渉 (RNAi) はshort-interfering RNA (siRNA) と呼ばれる21～23bpの二本鎖RNA (dsRNA) によって引き起こされる遺伝子発現抑制機構である。本研究では，siRNAのような短いdsRNAがdsRNA依存性プロテインキナーゼ (PKR) に及ぼす影響について調べた。His-PKR組換え蛋白質と様々な鎖長 (11～41bp) の短鎖dsRNAを作製し，これらを用いて解析を行ったところ，26bp以下のdsRNAではHis-PKRの自己リン酸化は見られず，31bp以上のdsRNAではわずかに自己リン酸化が認められた。しかし，ゲルシフトアッセイの結果，用いた全ての短鎖dsRNAとHis-PKRとの間の結合が検出され，さらに短鎖dsRNAによってHis-PKRの活性化が阻害されることが明らかになった。siRNAを模した短鎖dsRNA (DP-dsRNA) を作製し，siRNAのPKRに及ぼす影響について解析したところ，DP-dsRNAは鎖長がほぼ同じ21bpのdsRNAと同程度His-PKRを阻害した。さらに，細胞内でDP-dsRNAへと変換される短鎖ヘアピンRNA (shRNA) 発現プラスミドを培養細胞に導入したところ，shRNA発現により新規蛋白質合成が促進され，細胞内PKRの阻害が示唆された。以上の結果から，siRNAのような短鎖dsRNAによるPKRの阻害が示された。また，これらの短鎖dsRNAが他のdsRNAで制御される蛋白質に影響を及ぼす可能性が示唆された。

キーワード：RNA干渉 (RNAi)，二本鎖RNA (dsRNA)，二本鎖RNA依存性プロテインキナーゼ (PKR)

はじめに

RNA干渉 (RNA interference，RNAi) は，small-interfering RNA (siRNA) と呼ばれる21～23塩基対からなる短い二本鎖RNA (double-stranded RNA，dsRNA) の関与によって配列特異的にmRNAが分解され，その結果遺伝子発現が抑制される現象である(1,2)。ヒトを含めた哺乳動物のRNAiでは，micro RNA (miRNA) と呼ばれる一群の細胞内短鎖 (19～25塩基) 一本鎖RNAの一部がsiRNAの役割を担っていると考えられている(3)。miRNAの細胞内合成は，まず複数のmiRNA前駆体からなる一続きのpri-miRNAとして合成された後，核内でRNaseⅢファミリーに属するDroshaを含むマイクロプロセッサー複合体 (Drosha/DGCR8複合体) によってヘアピン構造をした個々の前駆体miRNA (pre-miRNA) に切り取られる(4-7)。pre-miRNAはexportin-5を介して細胞質に輸送され(8,9)，そこでRNaseⅢ様酵素のDicerによってsiRNAに相当する二重鎖型miRNA (miRNA duplex) にプロセッシングされる(10,11)。二重鎖型miRNAのうち，一方のRNA鎖のみが最終的に成熟型miRNAとしてRISC (RNA-initiated silencing complex) に組み込まれ，標的mRNA分子に対するガイドとして働く(12)。RNAiは，選択的なmRNAの分解を誘導し，遺伝子発現を抑制できることから，現在分子生物学研究において広く利用されているだけでなく，病原遺伝子の発現を特異的に抑制することが期待されることから，臨床的にも注目されている。しかし，ヒト細胞内にはdsRNAの働く系が他にもいくつか知られており，中でもよく知られているのはインターフェロン (IFN) によって誘導されるウイルス防御機構である(13)。RNAウイルスは自己のRNAゲノムを複製する際の中間体としてdsRNAを合成するが，前述のウイルス防御機構はこのdsRNA中間体に応答して機能する。この機構において，中心的な役割を果たしているものの1つとしてdsRNA依存性プロテインキナーゼ (PKR) がある。PKRは細胞内では通常非活性化型の状態で存在しているが，dsRNA存在下で活性化される。活性化されたPKRは，翻訳開始因子eIF2をリン酸化し，その結果通常の蛋白質合成が停止され，さらにその状態が持続されると，細胞はアポトーシスへと導かれる(14-17)。このようなPKRの働きにより，ウイルス感染細胞内でウイルスが増殖することが抑制されるだけでなく，周囲の細胞へとウイルスが伝播することが防がれている。ウイルスの中には宿主細胞のウイルス防御機構から逃れるために，PKRの機能を阻害する分子を産生するものがあり，それらPKR阻害分子の中にはRNAからなるものも存

金沢医科大学ゲノム医科学（生化学）
石川県河北郡内灘町大学1-1
平成18年3月10日受理

在する(18)。これらはtRNAのようなステム・ループ構造をしており，ステムすなわち短い二本鎖領域を介してPKRのdsRNA結合領域に結合し，他のdsRNAが結合するのを妨げる。このことから，siRNAのような短いdsRNAはPKRに作用することが大いに考えられる。そこで，本研究では，siRNAと同程度のサイズの短鎖dsRNA作製し用いることにより，これらのdsRNAがPKRの機能に与える影響について解析を行った。

実験方法

1．His-PKR発現プラスミドの構築

バクテリオファージλ(λファージ) DNAよりPCR法にてλファージプロテインホスファターゼ (λ-PPase) 遺伝子断片を増幅し，これを*Bam*H Iと*Bgl* IIで処理した後，pET15b (Novagen) のBamH I部位に導入した (このプラスミドをpET15b/λPPと命名した)。次に，ヒト子宮頚癌由来HeLa細胞よりRNAを抽出し，これを用いてRT-PCR法によりヒトPKRのcDNA断片を増幅した。これを*Nde* Iと*Bam*H Iで処理した後，前述のpET15b/λPPの*Nde* I-*Bam*H I部位に導入し，発現プラスミドを作製した(pET15b-PKR/λPPと命名した)。

2．短鎖ヘアピンRNA (shRNA) 合成用プラスミドの構築

試験管内でのshRNA合成の鋳型DNAとなるプラスミドを以下のようにして作製した。まず，pGEM-3Zf(+) (Promega) のSP6プロモーターの直後に部位特異的変異導入法により*Apa* I認識配列を導入した (このプラスミドをpGEM-Aと命名した)。次に，*Apa* I認識配列を含みshRNAのステム部分となる配列，ループ部分となる10塩基からなる配列 (5'-CTTCCTGTCA-3')，ステム部分の相補配列，shRNAの尾部となるチミン残基5個とそれに続く*Dra* I配列，そして最後に*Eco*R I配列の順の配列からなる合成DNAを作製し，pGEM-Aの*Apa* I-*Eco*R I部位に挿入しshRNA合成用プラスミドを作製した。ステム部分の配列は，pGEM-3Zf(+)のマルチクローニングサイトの配列 (人工的な配列) を利用した。合成されるshRNAのステム部分の塩基対 (bp) の長さの違いにより，pGEM-HP10 (11bp)，pGEM-HP15 (16bp)，pGEM-HP20 (21bp)，pGEM-HP25 (26bp)，pGEM-HP30 (31bp)，pGEM-HP35 (36bp)，pGEM-HP40 (41bp) の7種類を作製した。培養細胞内で21bpのステム長のshRNA (shRNA21) を発現させるために，pGEM-HP20の挿入DNA断片 (*Apa* I-*Eco*R I断片) をsiRNA発現ベクターpSilencer1.0-U6 (Ambion) の*Apa* I-*Eco*R I部位に導入することにより培養細胞用shRNA21発現プラスミドを作製した (pSilencer-HP20と命名した)。

3．His-PKRの大腸菌内での発現，および精製

His-PKRを大腸菌内で大量発現させるため，pET15b-PKR/λPPをBL21(DE3)pLysS株に導入した後，既報の条件で大腸菌の培養，および組換え蛋白質の発現を行った(19)。

大腸菌からのHis-PKRの精製は以下のように行った。大腸菌を抽出バッファー (20mM Tris-HCl (pH 7.5)，200mM NaCl，5mM 2-メルカプトエタノール，1mM $MnCl_2$，0.01%(w/v) Brij-35，1mM PMSF) に懸濁後，超音波処理によって細胞を破砕した。大腸菌破砕液を12,000rpm，4℃で30分間遠心分離した後，得られた上清を細胞抽出液とした。細胞抽出液に終濃度10mMになるように1Mイミダゾールを加えた後，Ni-NTAアガロースビーズ (QIAGEN) を加え，4℃で1時間混合した。懸濁液をプラスチックカラム (Bio-Rad) に移し，洗浄バッファー (20mM Tris-HCl (pH 7.5)，200mM NaCl，5mM 2-メルカプトエタノール，10mMイミダゾール) でビーズに結合しなかった蛋白質を洗浄，除去した後，溶出バッファー (20mM Tris-HCl (pH 7.5)，200mM NaCl，5mM 2-メルカプトエタノール，100mMイミダゾール) でNi-NTAアガロースビーズ結合蛋白質を回収した (Ni-NTA溶出画分)。次に，これをバッファーT200 (20mM Tris-HCl (pH 7.5)，200mM NaCl，5mM 2-メルカプトエタノール) で平衡化したP11リン酸セルロース (Whatman) カラムに移し，蛋白質を吸着させた。カラムをバッファーH300 (20mM HEPES-NaOH (pH 7.5)，300mM NaCl，5mM 2-メルカプトエタノール) で洗浄した後，バッファーH400 (20mM HEPES-NaOH (pH 7.5)，400mM NaCl，5mM 2-メルカプトエタノール) でHis-PKRを溶出，回収した (リン酸セルロース溶出画分)。透析バッファー (20mM HEPES-NaOH (pH 7.5)，50mM KCl，2mMジチオトレイトール，25%(v/v)グリセロール) に対して2回，4℃で一晩透析し，濃縮，および蛋白質濃度決定後，精製標品を−80℃で凍結保存した。

4．dsRNAの合成，および精製

shRNA合成用プラスミド (pGEM-HP10～40) を*Dra* Iで処理した後，SP6 RNAポリメラーゼ (TaKaRa) を用いて37℃，6時間の条件で試験管内RNA合成反応を行った。反応液中の鋳型DNAをDNase Iで37℃，8時間分解処理した後，フェノール・クロロホルム抽出，エタノール沈殿を行い，shRNAを回収した。次に，shRNAをMung Beanヌクレアーゼを用いて室温で8時間処理し，一本鎖部分の消化を行った。フェノール・クロロホルム抽出，エタノール沈殿で回収した後，アルカリホスファターゼ (TaKaRa) で脱リン酸化処理を行った。反応物をエタノール沈殿で濃縮した後，8～10%ポリアクリルアミドゲルを用いた電気泳動で分離した。泳動後のゲルからdsRNAを含む部分を切り出し，ゲル片を蒸留水中に移し，室温で一晩，dsRNAを抽出した。抽出液をエタノール沈殿によって回収した後，蒸留水に溶解した。濃度決定後，−20℃で凍結保存した。DP-dsRNAは，shRNA21をDicer組換え蛋白質 (STRATAGENE) で37℃，一晩処理した後，上記の方法に従って精製した。

5．His-PKRの自己リン酸化活性の測定

精製したHis-PKRの自己リン酸化活性測定を既報の手順に従い行った(19)。短鎖dsRNAのHis-PKRの自己リン酸化に与える効果は，以下のようにして調べた。まず，短鎖dsRNAをHis-PKRと混合し25℃で10分間置いた後，0.1 μg/ml Poly(I)・Poly(C) (SIGMA)，[γ^{32}P]ATPを加えて15分間反応を行った。反応後のサンプルは，上記の手順に従い，電気泳動，および可視化を行った。

6．ゲルシフトアッセイ (Electrophoretic mobility shift assay, EMSA)

合成dsRNAの5'末端を[γ^{32}P]ATPとT4ポリヌクレオチドキナーゼ (TaKaRa) を用いて標識した。標識したdsRNA (11 ng～41 ng) とHis-PKR (0.1 μg) を混合し室温に10分間置いた後，4%ポリアクリルアミドゲルで電気泳動 (室温，60V，1時間) を行った。泳動後ゲルを乾燥し，イメージングプレート (FUJI FILM) に一晩露光させた。イメージングプレートをSTORM 860イメージングシステム (GE HEALTH) でスキャンし可視化した。

7．ルシフェラーゼアッセイ

ヒト肝由来HepG2細胞を35mmのプレートに3×10^5個の密度でまき，10%のウシ胎児血清 (FCS) を含むダルベッコ変法イーグル培地 (DMEM) で37℃，20時間培養した。ホタルルシフェラーゼ発現プラスミド (pGL3 Control Vector (Promega)) 0.25 μg，ウミシイタケルシフェラーゼ発現プラスミド (phRL-TK Vector (Promega)) 0.25 μgに加えて，コントロールベクター (pcDNA 3.1(+)(Invitrogen))，shRNA21発現プラスミド (pSilencer-HP20)，野生型PKR発現プラスミド (pcDNA3.1-HAPKR)，変異型PKR発現プラスミド (pcDNA3.1-HAPKR (K296R)) のいずれか1.5 μg，合計2 μgのプラスミドDNAを，リポフェクトアミン2000試薬 (Invitrogen) を用いてHepG2細胞に導入した。トランスフェクション後45時間で細胞を集め，PBSで2回洗浄後，溶解バッファー (Passive Lysis Buffer (Promega)) に再懸濁し細胞を破砕した。細胞破砕液を遠心分離した後，上清 (細胞抽出液) の蛋白質濃度を決定し，それぞれ蛋白質量1 μgを含む細胞抽出液を用いてルシフェラーゼアッセイを行った。ルシフェラーゼアッセイはキット (Dual-Luciferase Reporter Assay System (Promega)) のプロトコールに従い行った。

結　　果

1．His-PKRの作製

我々は，以前にヒトPKRのN末端にグルタチオン-S-トランスフェラーゼ (GST) を融合させた組換え蛋白質 (GST-PKR) を作製し，報告した(19)。しかし，PKRのRNA結合ドメインはN末端付近に存在することから，N末端に巨大なGSTが融合したGST-PKRの場合，dsRNAとの結合性に何らかの影響があることが懸念された。そこで，新たに，GSTよりも小さく，6個の連続したHis残基 (His-tag) を含む20アミノ酸残基からなる配列をPKRのN末端に融合させた新たな組換え蛋白質 (His-PKR) を作製した。大腸菌で発現させたHis-PKRを破砕した細胞抽出液より，Ni-NTAアガロース，リン酸セルロースカラムクロマトグラフィーによってHis-PKRを精製した(図1A)。次に，精製したHis-PKRが活性を持つかどうかを調べたところ，長鎖 (数百～数千bp) のdsRNAであるPoly(I)・Poly(C)依存的に自己リン酸化する活性を持つことが明らかになった(図1B)。PKRはdsRNA濃度依存的に活性化されるが，dsRNAがある濃度を超えると逆に活性が阻害されることが知られている(20,21)。His-PKRの場合も，Poly(I)・Poly(C)濃度が1 μg/ml付近に活性のピークがあり，これまでに報告されているPKRの特徴を示した。

2．短鎖dsRNAの作製

dsRNAを得るために，試験管内で合成したshRNA (図2A，レーン2) をMung Beanヌクレアーゼ (MBN) で処理して一本鎖部分を消化することによりdsRNA (図2A，レーン3) を得た。このようにして作製した様々な鎖長 (11～41bp) のdsRNAをポリアクリルアミドゲル電気泳動で精製し，精製標品を得た (図2B)。

3．短鎖dsRNAによるHis-PKRの自己リン酸化

様々な鎖長のdsRNAを用いて，His-PKRの自己リン酸化活性のdsRNA依存性について調べた (図3)。その結果，31bp以上のdsRNAで0.1 μg/ml付近をピークにわずかに活性化が認められたのに対し，26bp以下のdsRNAではHis-PKRの活性化はまったく認められなかった。しかし，31～41bpのdsRNAで認められた

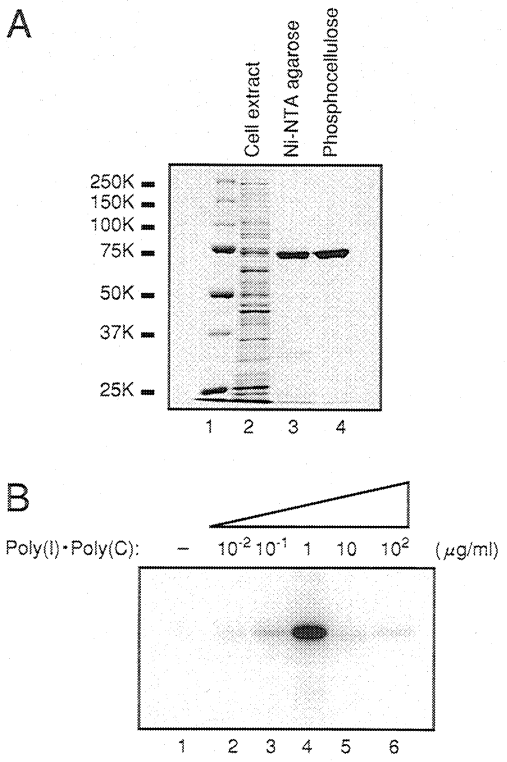


図1．His-PKRの作製。(A) His-PKRの精製。分子量マーカー (プレシジョンPlusブルースタンダード (BIO-RAD)) (レーン1)，細胞抽出液10 μg (レーン2)，Ni-NTA溶出画分2 μg (レーン3)，リン酸セルロース溶出画分2 μg (レーン4) を10%SDSポリアクリルアミドゲル電気泳動 (SDS-PAGE) で分離した後，泳動ゲルをコマジーブリリアントブルー (CBB) R-250で染色した。(B) His-PKRの自己リン酸化活性。緩衝液10 μl中でHis-PKR 0.1 μgを図中に示した濃度のPoly(I)・Poly(C)と混合した後，20 μM ATP (14.8 KBq [γ-^{32}P]ATPを含む) を加えて25℃で15分間反応させた。反応液を10%SDS-PAGEで分離した後，オートラジオグラフィーにより可視化した。

His-PKRの自己リン酸化活性は長鎖dsRNAであるPoly(I)・Poly(C)に比べて非常にわずかであった。このように，PKRの活性化にdsRNAの鎖長依存性があることが示された。

4．短鎖dsRNAとHis-PKRとの結合

図3の結果より，His-PKRの自己リン酸化活性がdsRNAの長さに依存することが明らかになった。そこで，これがHis-PKRへのdsRNAの結合の有無によるのかどうかを明らかにするために，標識したdsRNAをプローブに用いてゲルシフトアッセイ(EMSA) を行った (図4)。その結果，実験に用いた全ての長さ(11～41bp) のdsRNAについて，His-PKRとの間に結合が検出された。この結果から，26bp以下のdsRNAにおいてPKRの自己リン酸化が見られないのは，これらのdsRNAがPKRに結合しない

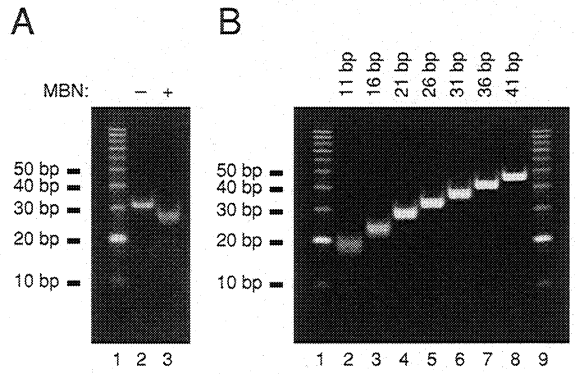


図2．dsRNAの作製。(A) shRNA21のMung Beanヌクレアーゼ(MBN) による消化。MBN処理前のshRNA21 (レーン2)，shRNA21をMBNで処理したもの (レーン3)，DNAサイズマーカー (10bp DNA Step Ladder (Promega)) (レーン1) を10% PAGEで分離した後，エチジウムブロミド (EtBr) で染色した。(B) 精製後のdsRNA。11～41 bpのdsRNA精製標品各0.2 μg (レーン2～8)，DNAサイズマーカー (レーン1，9) を10%PAGEで分離後，EtBrで染色した。

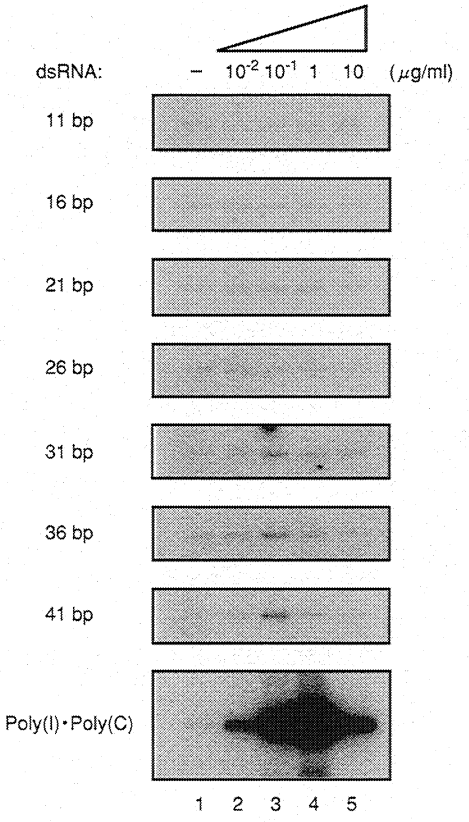


図3．短鎖dsRNA依存的His-PKR自己リン酸化。緩衝液10 μl中でHis-PKR 0.1 μgを図中に示した濃度のdsRNAと混合した後，20 μM ATP (14.8 KBq [γ-^{32}P]ATPを含む) を加えて25℃で15分間反応させた。反応液を10%SDS-PAGEで分離した後，オートラジオグラフィーにより可視化した。

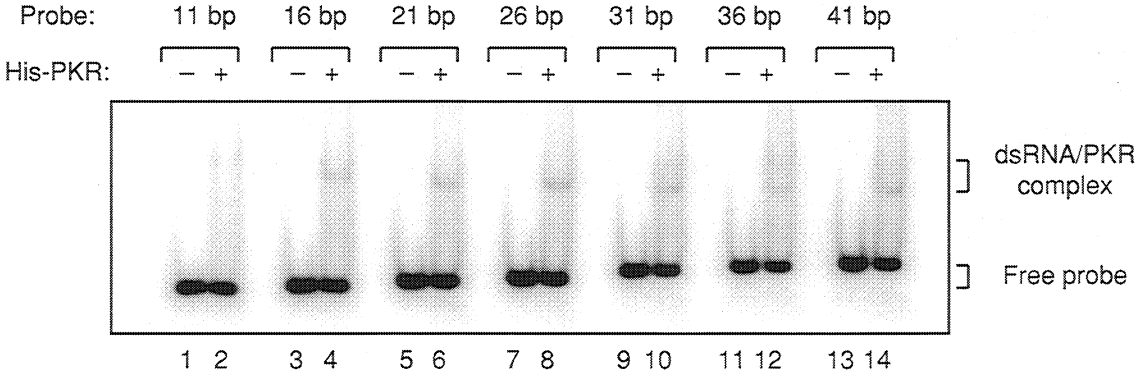


図4．短鎖dsRNAとHis-PKRとの相互作用。^{32}Pで標識したdsRNAプローブ (レーン1, 3, 5, 7, 9, 11, 13)，およびHis-PKR (0.1 μg) と標識したdsRNAプローブとの混合物 (レーン2, 4, 6, 8, 10, 12, 14) を，4% PAGE (室温，1時間) で分離した。泳動ゲルを乾燥後，オートラジオグラフィーにより可視化した。標識したdsRNAプローブはそれぞれ，11 ng (レーン1, 2)，16 ng (レーン3, 4)，21 ng (レーン5, 6)，26 ng (レーン7, 8)，31 ng (レーン9, 10)，36 ng (レーン11, 12)，41 ng (レーン13, 14) 使用した。

ためではないことが明らかになった。ここでさらにEMSAの結果を詳しく見たところ，26bp以下のdsRNAでは，dsRNAとHis-PKRからなる複合体を示すシフトバンドは1本であるのに対し(図4,レーン2,4,6,8)，31bp以上の場合はdsRNA/His-PKR複合体のシフトバンドは2本認められた(図4,レーン10,12,14)。従って，図3の結果と照らし合わせると，PKRを自己リン酸化しないdsRNA (26bp以下) は EMSAではバンド1本であるのに対し，PKRを自己リン酸化するdsRNA (31bp以上) はEMSAで2本バンドであることがわかる。後者で新たに出現する移動度の小さい方のバンドは，PKR量を増加させるとさらにバンドが太くなることから，His-PKR二分子を含む複合体であると考えられる(未発表データ)。PKRが自己リン酸化する際，二量体を形成することが必要である。従って，以上の結果は，PKRの二量体形成にはある長さ以上のdsRNAが必要であり，PKRを二量体化できるdsRNAがPKRを活性化，すなわち自己リン酸化できることを示唆している。

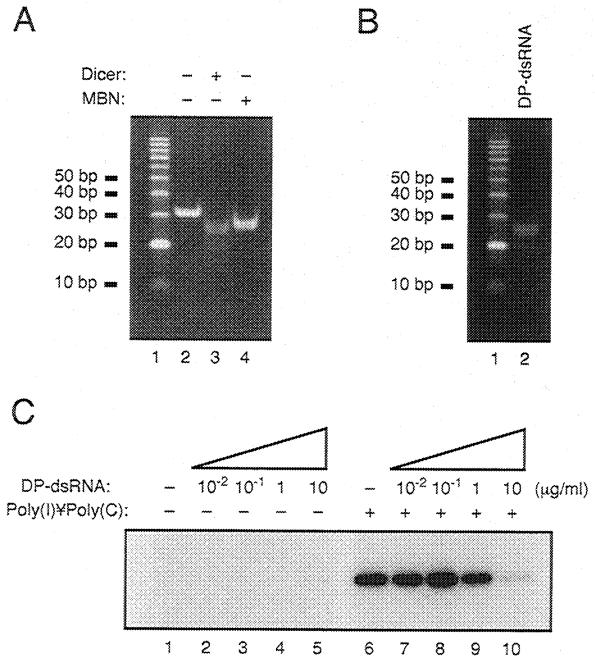


図6．DP-dsRNAの作製，およびHis-PKRの自己リン酸化活性に与える影響。(A) shRNA21のDicer組換え蛋白質による消化。ヌクレアーゼ処理前のshRNA21 (レーン2)，shRNA21をDicerで処理したもの (レーン3)，shRNA21をMBNで処理したもの (レーン4) を10% PAGEで分離した後，エチジウムブロミド (EtBr) で染色した。(B) 精製後のDP-dsRNA。DP-dsRNA精製物0.2μgを10%PAGEで分離後，EtBrで染色した。(C) Poly(I)・Poly(C)の非存在下，または存在下でのHis-PKRの自己リン酸化活性へのDP-dsRNAの効果。図3，図5で行った実験と同条件で，DP-dsRNA依存的His-PKRの自己リン酸化 (レーン1～5)，DP-dsRNAのPoly(I)・Poly(C)依存的His-PKR自己リン酸化への影響 (レーン6～10) を調べた。

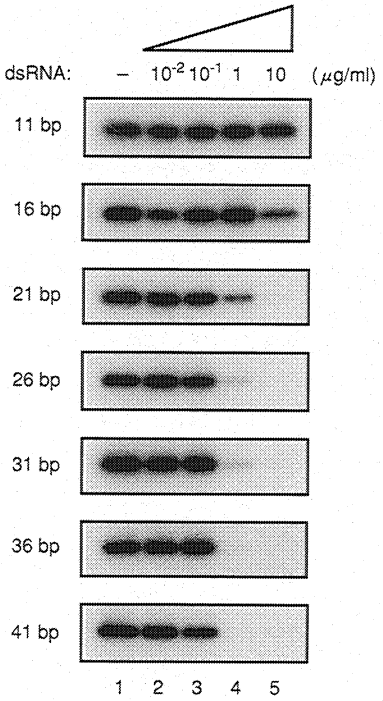


図5．短鎖dsRNAによるPoly(I)・Poly(C)依存的His-PKR自己リン酸化の阻害。緩衝液10μl中でHis-PKR 0.1μgを図中に示した濃度のdsRNAと混合した後，20μM ATP (14.8 KBq [γ-32P]ATPを含む)，および0.1μg/ml Poly(I)・Poly(C)を加えて25℃で15分間反応させた。反応液を10% SDS-PAGEで分離した後，オートラジオグラフィーにより可視化した。

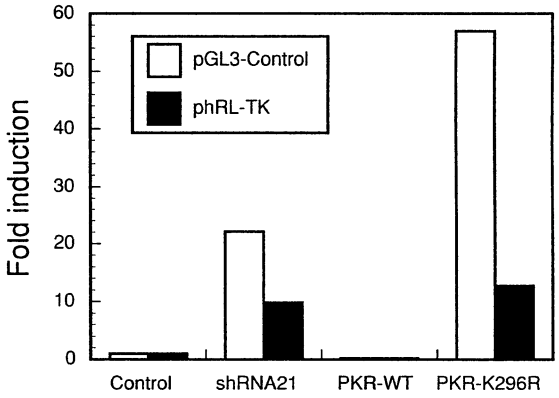


図7．shRNA21発現の細胞内新規蛋白質合成に与える影響。ホタルルシフェラーゼ発現プラスミド (pGL3-Control Vector)，ウミシイタケルシフェラーゼ発現プラスミド (phRL-TK Vector) 各0.25μgに加え，コントロールベクター (pcDNA3.1(+))，shRNA21発現プラスミド (pSilencer-HP20)，野生型PKR (PKR-WT) 発現プラスミド (pcDNA3.1-HAPKR)，変異型PKR (PKR-K296R) 発現プラスミド (pcDNA3.1-HAPKR(K296R)) のいずれか1.5μg，合計2μgのプラスミドDNAをHepG2細胞に共導入した。それぞれ1μgの蛋白質を含む細胞抽出液を用いてルシフェラーゼアッセイを行った。

5．短鎖dsRNAによるPKRの阻害

図3，図4の結果から，11～41bpのdsRNAはPKRに結合するもののPKRの活性化能はない，あるいは長鎖dsRNA (Poly(I)・Poly(C)) よりも著しく低いことが明らかになった。このことは，これらの短鎖dsRNAがPKR活性化能のある長鎖dsRNAと拮抗する可能性を示唆する。そこでこの仮説を検証するため，短鎖dsRNAがPoly(I)・Poly(C)によるPKRの自己リン酸化へ与える影響を調べた (図5)。その結果，21bp以上のdsRNAについて，Poly(I)・Poly(C)によるPKRの自己リン酸化活性に拮抗的に阻害することが明らかになった。11bpのdsRNAでは全く，16bpのdsRNAではほとんどPKRの自己リン酸化の阻害が見られなかった。また，21～41bpのdsRNAについて，鎖長が長くなるにつれてより低濃度でもPKR活性を阻害することができることも明らかになった。これらの結果は，実験に用いた鎖長の範囲内 (11～41bp) において，dsRNAの鎖長が短くなるほどPKRに対する親和性が低くなり，鎖長が長くなるほど親和性が高くなることに起因していると考えられる。

6．Dicerによってプロセッシングされたds RNA (DP-dsRNA) によるPKRの阻害

図5の結果より，siRNAと同程度のサイズである21bpのdsRNAがPKRの活性化を阻害することが明らかになった。さらにsiRNAがPKRの活性化を阻害するかどうかを解析するため，動物細胞内で産生されるsiRNA (または二重鎖型miRNA) と同じくshRNAからDicerによる消化によって生じるdsRNA (Dicer-produced dsRNA, DP-dsRNA) を作製し (図6A, B, レーン2)，PKRの自己リン酸化に対する影響を調べた (図6C)。その結果，DP-dsRNAは同サイズ (21bp) のdsRNAと同様にPKRの自己リン酸化能はなく (図6C, レーン1～5)，21bpのdsRNAと同程度のPKR自己リン酸化阻害活性を持つことが明らかになった (図6C, レーン6～10)。

7．細胞内で発現されたshRNAによるPKRの阻害

図6の結果では，試験管内で擬似的に作製したsiRNA (DP-dsRNA) がPKRの活性化を阻害しうることが明らかになった。そこで，実際に細胞内でsiRNAサイズのdsRNAがPKR活性を阻害するかどうかを明らかにするために，DP-dsRNAの作製に用いたshRNA21をHepG2細胞内で発現させ，PKR活性への影響を調べた。PKR活性が増強されると蛋白質合成が阻害され，逆にPKR活性が阻害されると蛋白質合成が促進されることから，PKR活性の増減をそれぞれ異なる発現プロモーターを持つ (SV40プロモーター，HSV-TKプロモーター) 2種類のルシフェラーゼ (ホタル，ウミシイタケ) レポーター遺伝子の発現量でモニターした (図7)。ルシフェラーゼアッセイの結果によると，野生型PKR (PKR-WT) 発現プラスミドを導入した場合，コントロールに比べてルシフェラーゼ活性はいずれも約22%に低下したのに対し，内在性PKRの活性を強く阻害する変異型PKR (PKR-K296R) 発現プラスミドを導入した場合，ホタルルシフェラーゼ活性は約57倍，ウミシイタケルシフェラーゼ活性は約13倍増加した。shRNA21発現プラスミドを導入した場合，ホタルルシフェラーゼ活性は約22倍，ウミシイタケルシフェラーゼ活性は約10倍増加した。ここで用いたshRNA21の配列は人工的な配列でヒトゲノム内に相同的な配列は存在しないため，shRNA21発現による蛋白質合成の促進は，細胞内の特定遺伝子の発現がRNAiによって抑制された結果ではないと思われる。また，shRNA21のループ配列は細胞質への移行活性を持つことから，細胞質内でDicerにより消化されDP-dsRNA (擬似siRNA) に変換されていると予想される。従って，以上の実験結果から，細胞内で過剰に産生されたsiRNAサイズのdsRNAによって，配列非特異的に細胞内PKRが阻害されることが示唆された。加えて，以上のルシフェラーゼアッセイの結果が再現性良く得られることも確認した。

考　　察

本研究では，まず，11～41bpの短鎖dsRNAを用いて，PKR活性に与える効果について調べた。ヒト腎臓由来293細胞から精製したPKRを用いた実験によると，34bpとそれよりも長いdsRNAはPKRを活性化し，それよりも短い23bpと15bpのdsRNAはPKRを活性化しないことが既に報告されている(22)。今回，我々は大腸菌発現系を用いてHis-PKR組換え蛋白質作製し，同様の実験を行ったところ，31bp以上のdsRNAによって活性化され，それよりも短いdsRNAでは活性化されなかった。従って，His-PKR組換え蛋白質とヒト培養細胞から精製されたPKRは，dsRNAに対して同様の鎖長依存性を示した。PKRのRNA結合ドメインの立体構造によると，PKR上でdsRNAが占めるのはおよそ16bp分の長さであると予想された(23)。しかし，PKRの活性化に最低限必要なのは，それの約2倍である30bp前後である。PKRは活性化の際に二量体を形成し，一方の分子が他方の分子をリン酸化することによって活性化されることから(24,25)，dsRNAの鎖長依存性から予想されるPKRの活性化のモデルとして，dsRNA一分子に二分子のPKRが結合することによって二量体が形成され，その結果自己リン酸化による活性化が起こることが推察される。実際に，図4のEMSAの結果を見ると，His-PKRを活性化しない26bp以下のdsRNAの場合，dsRNA一分子とPKR一分子が結合した複合体を示すバンド一本のみが観察されるのに対し，His-PKRを活性化できる31bp以上のdsRNAでは，dsRNA一分子にdsRNA一分子が結合した複合体以外にPKR二分子が結合したと思われる複合体の2本のバンドが観察された。

本研究では，siRNAサイズの短鎖dsRNAが，試験管内でも細胞内でもPKR活性を阻害することを明らかにしたが，本研究以外にもこれまでにsiRNAが細胞内PKR活性へ与える影響についていくつかのグループにより報告されている。Williamsらのグループは21bpのsiRNAを細胞にトランスフェクションすると，細胞内のリン酸化型PKRが増加し，IFN-βの発現が誘導されることを報告している(26)。PKRはIκBキナーゼ (IKK) の活性化にも関わっており，転写因子NF-κBの活性化によりIFN-βの発

現を誘導する(27-29)。従って，この報告では，siRNAによってPKRが活性化されたことを示している。一方，別のグループの報告によると，21bpのsiRNAおよびDicerの基質となる27bpのsiRNA前駆体を細胞にトランスフェクションした場合，PKRの活性化もサイトカインの産生も認められなかった(30)。どちらのグループも細胞外から化学合成したsiRNAを細胞にトランスフェクションしたという点で手法は同じであるであるにもかかわらず，異なった結果が得られたのはどうしてなのか。本研究では，これらのグループと異なり，RNA発現ベクターを用いて細胞内で合成したsiRNAによるPKRへの影響を調べたところ，前述の後者のグループと同様にPKRは活性化されず，逆にPKR活性を阻害するという結果を得た。また，我々のHis-PKRの実験では，siRNAサイズのdsRNAはPKRを直接活性化しないという結果であった (図3，図6C)。従って，Williamsらのグループが報告した結果は，siRNAによる直接的なPKRの活性化ではなく，おそらく別のメカニズムによるものと思われる。その1つの可能性として，Toll様受容体 (Toll-like receptor，TLR) を介したシグナル伝達によることが考えられる。TLRは自然免疫における外来物質の認識に関わっており，認識する物質の種類によってTLRのタイプは異なる。このうちのTLR3はウイルスRNA (dsRNA) を認識するとされており，細胞外dsRNAと結合することによりNF-κBの活性化およびサイトカイン産生を誘導することが報告されている(31)。また，TLR3からのシグナル伝達の下流でPKRが働いていることも明らかにされている(32)。以上のことから，siRNAでPKRが活性化されるのは，細胞外にあるTLR3にsiRNAが結合することによって起こると考えられ，本研究のように，細胞内でsiRNAを合成させるような場合には，TLR3を介したPKRの活性化は起こらないだろうと推察される。

本研究では，siRNA発現ベクターを用いて細胞内でsiRNAを合成させた場合，PKRの機能が阻害された。しかし，細胞内では通常，siRNAと同サイズの二重鎖型miRNAが存在しているにも関わらず，これによってPKRが阻害されているという報告はない。この理由として次のようなことが考えられる。図6の結果が示すように，siRNAによってPKRが阻害されるためには大過剰量のsiRNAが必要であり，生理条件下での二重鎖型miRNAの発現量は，おそらくPKRを阻害するほどに満たないことが考えられる。また，RNAiにおいて，細胞質内で前駆体からDicerでプロセッシングされたsiRNAがRISCへと運ばれる際，ショウジョウバエではR2D2，線虫ではRDE-4と呼ばれるdsRNA結合蛋白質が介在することが報告されている(33,34)。従って，ヒト細胞の場合も，通常，二重鎖型miRNAが細胞内で遊離した状態で存在していないと予想され，それ故PKRの阻害に至らないのだろうと考えられる。しかし，本研究のようにshRNA発現ベクターによって強制的に細胞内でsiRNAを発現させるような場合，内在性のmiRNAの場合と異なり，過剰に生産された短鎖dsRNAが遊離した状態で細胞内に蓄積され，その結果，PKRの阻害が引き起こされると考えられる。

PKRは，細胞の抗ウイルス作用において重要な働きをしており，PKRの機能が阻害された場合，ウイルス感染に対して細胞が脆弱になることが予想される。従って，RNAiを臨床に応用するような場合，本研究の結果から，shRNA発現ベクターを用いた場合，ウイルス感染に特に注意する必要があると思われる。また，細胞内には研究で調べたPKR以外にもdsRNAに関わる蛋白質が存在することから，RNAiを治療に応用するためには，安全性の観点から，siRNAが細胞にどのような影響を及ぼすのかを今後さらに詳細に解析していく必要があるように思われる。

稿を終えるにあたり，本研究の遂行に多大なご援助ご協力をいただきました金沢医科大学ゲノム医科学の皆様に厚くお礼を申し上げます。本研究は，平成15～16年度金沢医科大学奨励研究(S2003-3，S2004-3)，平成16～17年度文部科学省科学研究費補助金(16590643) の助成を受けた。

文　献

1. Fire A, Xu S, Montgomery MK et al: Potent and specific genetic interference by double-stranded RNA in *Caenorhabditis elegans*. Nature 1998; **391:** 806-11.
2. Elbashir SM, Lendeckel W, Tuschl T: RNA interference is mediated by 21- and 22-nucleotide RNAs. Genes Dev 2001; **15:** 188-200.
3. McManus MT, Sharp PA: Gene silencing in mammals by small interfering RNAs. Nat Rev Genet 2002; **3:** 737-47.
4. Lee Y, Ahn C, Han J et al: The nuclear RNase III Drosha initiates microRNA processing. Nature 2003; **425:** 415-9.
5. Denli AM, Tops BB, Plasterk RH et al: Processing of primary microRNAs by the Microprocessor complex. Nature 2004; **432:** 231-5.
6. Gregory RI, Yan KP, Amuthan G et al: The Microprocessor complex mediates the genesis of microRNAs. Nature 2004; **432:** 235-40.
7. Han J, Lee Y, Yeom KH et al: The Drosha-DGCR8 complex in primary microRNA processing. Genes Dev 2004; **18:** 3016-27.
8. Yi R, Qin Y, Macara IG et al: Exportin-5 mediates the nuclear export of pre-microRNAs and short hairpin RNAs. Genes Dev 2003; **17:** 3011-6.
9. Lund E, Guttinger S, Calado A et al: Nuclear export of microRNA precursors. Science 2004; **303:** 95-8.
10. Lee Y, Jeon K, Lee JT et al: MicroRNA maturation: stepwise processing and subcellular localization. EMBO J 2002; **21:** 4663-70.
11. Hutvagner G, Zamore PD: A microRNA in a multiple-turnover RNAi enzyme complex. Science 2002; **297:** 2056-60.
12. Schwarz DS, Hutvagner G, Du T et al: Asymmetry in the assembly of the RNAi enzyme complex. Cell 2003; **115:** 199-208.
13. Samuel CE: Antiviral actions of interferons. Clin Microbiol Rev 2001; **14:** 778-809
14. Clemens MJ, Elia A: The double-stranded RNA-dependent protein kinase PKR: structure and function. J Interferon Cytokine Res 1997; **17:** 503-24.
15. Jagus R, Joshi B, Barber GN: PKR, apoptosis and cancer. Int J Biochem Cell Biol 1999; **31:** 123-38.
16. Williams BR: PKR; a sentinel kinase for cellular stress. Oncogene 1999; **18:** 6112-20.
17. Gil J, Esteban M: Induction of apoptosis by the dsRNA-dependent protein kinase (PKR): mechanism of action. Apoptosis 2000; **5:** 107-14.
18. Gale M Jr, Katze MG: Molecular mechanisms of interferon resistance mediated by viral-directed inhibition of PKR, the interferon-induced protein kinase. Pharmacol Ther 1998; **78:** 29-46.
19. Matsui T, Tanihara K, Date T: Expression of unphosphorylated form of human double-stranded RNA-activated protein kinase in Escherichia coli. Biochem Biophys Res Commun 2001; **284:** 798-807.
20. Galabru J, Hovanessian A: Autophosphorylation of the protein kinase dependent on double-stranded RNA. J Biol Chem 1987; **262:** 15538-44.
21. Galabru J, Katze MG, Robert N et al: The binding of double-stranded RNA and adenovirus VAI RNA to the interferon-induced protein kinase. Eur J Biochem 1989; **178:** 581-9.

22. Manche L, Green SR, Schmedt C et al: Interactions between double-stranded RNA regulators and the protein kinase DAI. Mol Cell Biol 1992; **12:** 5238-48.
23. Nanduri S, Carpick BW, Yang Y et al: Structure of the double-stranded RNA-binding domain of the protein kinase PKR reveals the molecular basis of its dsRNA-mediated activation. EMBO J 1998; **17:** 5458-65.
24. Thomis DC, Samuel CE: Mechanism of interferon action: evidence for intermolecular autophosphorylation and autoactivation of the interferon-induced, RNA-dependent protein kinase PKR. J Virol 1993; **67:** 7695-700.
25. Thomis DC, Samuel CE: Mechanism of interferon action: characterization of the intermolecular autophosphorylation of PKR, the interferon-inducible, RNA-dependent protein kinase. J Virol 1995; **69:** 5195-826.
26. Sledz CA, Holko M, de Veer MJ et al: Activation of the interferon system by short-interfering RNAs. Nat Cell Biol 2003; **5:** 834-9.
27. Zamanian-Daryoush M, Mogensen TH, DiDonato JA et al: NF-κB activation by double-stranded-RNA-activated protein kinase (PKR) is mediated through NF-κB-inducing kinase and IκB kinase. Mol Cell Biol 2000; **20:** 1278-90.
28. Gil J, Alcami J, Esteban M: Activation of NF-κB by the dsRNA-dependent protein kinase, PKR involves the IκB kinase complex. Oncogene 2000; **19:** 1369-78.
29. Bonnet MC, Weil R, Dam E et al: PKR stimulates NF-κB irrespective of its kinase function by interacting with the IκB kinase complex. Mol Cell Biol 2000; **20:** 4532-42.
30. Kim DH, Behlke MA, Rose SD et al: Synthetic dsRNA Dicer substrates enhance RNAi potency and efficacy. Nat Biotechnol 2005; **23:** 222-6.
31. Alexopoulou L, Holt AC, Medzhitov R et al: Recognition of double-stranded RNA and activation of NF-κB by Toll-like receptor 3. Nature 2001; **413:** 732-8.
32. Jiang Z, Zamanian-Daryoush M, Nie H et al: Poly(I-C)-induced Toll-like receptor 3 (TLR3)-mediated activation of NFκB and MAP kinase is through an interleukin-1 receptor-associated kinase (IRAK)-independent pathway employing the signaling components TLR3-TRAF6-TAK1-TAB2-PKR. J Biol Chem 2003; **27:** 16713-9.
33. Liu Q, Rand TA, Kalidas S et al: R2D2, a bridge between the initiation and effector steps of the Drosophila RNAi pathway. Science 2003; **301:** 1921-5.
34. Tabara H, Yigit E, Siomi H et al: The dsRNA binding protein RDE-4 interacts with RDE-1, DCR-1, and a DExH-box helicase to direct RNAi in *C. elegans*. Cell 2002; **109:** 861-71.

Inhibition of double-stranded RNA-activated protein kinase (PKR) by short double-stranded RNA

Tadashi Matsui and Takayasu Date

Department of Biochemistry, Kanazawa Medical University, Uchinada, Ishikawa 920-0293, Japan.

RNA interference (RNAi) is a post-transcriptional gene silencing mediated by short-interfering RNA (siRNA). Since siRNA is a short double-stranded RNA (dsRNA), it may affect the other dsRNA-mediated systems in the cell. In this study, we investigated the effect of short dsRNAs such as siRNA on the function of dsRNA-activated protein kinase (PKR) which is one of the dsRNA-regulated proteins. To analyze it in vitro, we constructed recombinant His-PKR and various sizes (11 ~ 41 bp) of short dsRNAs. The 11 ~ 26 bp-dsRNAs, containing the same size of dsRNA as siRNA, did not induce autophosphorylation of His-PKR whereas it was slightly autophosphorylated in the presence of the 31 ~ 41 bp-dsRNAs. However, the interactions between His-PKR and all the short dsRNAs were detected in electrophoretic mobility shift assay (EMSA). In vitro kinase assay also exhibited that short dsRNAs inhibit autophosphorylation of His-PKR by blocking binding of PKR-activating dsRNA such as poly(I) · poly(C) to PKR. To analyze the effect of siRNA on PKR function further, we constructed the siRNA-mimicked short dsRNA, named DP-dsRNA. In high concentration of DP-dsRNA, autophosphorylation of His-PKR was also inhibited as well as the 21 bp-dsRNA. Moreover, we introduced the expression vector producing short hairpin RNA (shRNA) converted to DP-dsRNA in the cell to cultured cells and analyzed the effect of siRNA on PKR function in the cell. Luciferase assay showed that the production of shRNA enhances protein synthesis, suggesting PKR inhibition by siRNA. These results indicate that the short dsRNAs such as siRNA inhibit PKR function and suggest that these short dsRNAs may affect the functions of other dsRNA-regulating proteins in the cell.

Keywords: RNA interference (RNAi), double-stranded RNA (dsRNA), double-stranded RNA-activated protein kinase (PKR)

１．研究課題名：心筋梗塞の新しい治療法の開発―体性幹細胞を用いた再生医療
（研究番号 S2004-4）

２．キーワード：１)心筋梗塞　・心不全（myocardial infarction ・ heart failure）
２)再生（regeneration）
３)体性幹細胞・骨髄間葉系細胞（stem cell ・mesenchymal stem cell）
４)ＳＰ細胞（side population cell）
５)心筋細胞（cardiac myocyte）

３．研究者氏名：赤澤純代（久藤）・医学部・助手・循環制御学（循環器内科学）
（現　生活習慣病センター）

４．研 究 目 的

高齢化、食生活の欧米化によりわが国において種々の動脈硬化性疾患が増加している。その代表が心筋梗塞でその終末像は心不全である。心筋梗塞は３０～４０％が発症時に死亡、１０％が病院内で死亡する。また、死を逃れた半数も心不全や不整脈によりQOLが低下するため、早急に克服すべき極めて重要な疾患である。

心筋梗塞には高血圧、高脂血症、喫煙といった、発症を促進する危険因子があり、食事療法や薬物療法等により危険因子を予防することで、心筋梗塞の発症をある程度減少させることができるが限界がある。心筋梗塞は心臓を養っている冠動脈が閉塞し心筋細胞が、虚血となる結果、細胞がネクローシスやアポトーシスにより死ぬ病態で、その結果、筋肉としてのポンプ機能が喪失し心不全を呈する。これまで心筋梗塞の治療法としては、閉塞した部位を一刻も早く再開通させるといった血栓溶解療法や血管形成術しかなく、それによっても虚血に弱い心筋を救うことは困難であった。発症後6時間以上たった場合には治療のすべはなく、それ以上梗塞範囲が広がらないように心臓の負荷をとるような姑息的な手段しかなかった。つまり心筋細胞にはほとんど再生能がないことより、一担死んでしまった心筋の機能を回復させることは不可能であった。そこで本研究においては今までと全く異なる新しい治療法として、心筋の再生療法の可能性について検討する。

５．研 究 計 画

１）骨髄間葉系細胞の心筋細胞への分化

骨髄間葉系細胞は脂肪、骨、軟骨、骨格筋など種々の細胞に分化することが知られている。

マウスではin vitro 及びin vivo　において心筋細胞に分化することも示されている。心筋梗塞時にG-CSF を投与することにより、おそらく骨髄より幹細胞が抹消に動員される結果、梗塞部に心筋細胞が再生し、梗塞巣が縮小して心機能が改善すると報告された。本研究においては、骨髄間葉系細胞の中のどの分画が心筋細胞に分化する

のか、心筋の幹細胞とも呼べるような細胞にはどのような特徴があるのかについて解析する。具体的には抗体を用いない新しい幹細胞純化方法ＳＰ（side population）細胞を用いて行う。これは、幹細胞では膜透過性が高く生細胞の状態でDNAのAT塩基配列に取り込まれる色素Hoechst33342を排出する性質があるという特徴を利用してside population 分画をＦＡＣＳにて選別し、心臓へ注入したり、心筋細胞との共培養することにより心筋細胞への分化を検討する。ＳＰ細胞が心筋細胞との共培養により心筋細胞へ分化した場合、その機序について液性因子や接着因子の役割を中心に解析する。

２）組織幹細胞の心筋細胞への分化

骨格筋芽細胞は一種の組織幹細胞（体性幹細胞）として、骨格筋ばかりでなく血液細胞、脂肪細胞などの他の細胞にも分化する。そこで骨格筋芽細胞が心筋細胞になるか否かを検討する。また、心臓より組織幹細胞の単離を試みる。

６．研究成果

１）骨髄間葉系細胞の心筋細胞への分化

骨髄間葉系細胞を心筋細胞と共培養することにより、骨髄間葉系細胞は心筋細胞特異的な遺伝子および蛋白を発現した。異なる色素にて予めラベルしておくことにより、骨髄間葉系細胞の心筋細胞化は２種類の細胞の融合によることがわかった。興味深いことに、融合した細胞は心筋細胞の形質をもち、しかも分裂能を獲得した。骨髄間葉系細胞以外にも骨格筋由来の細胞、内皮細胞、内皮前駆細胞、心臓線維芽細胞が心筋細胞との共培養にて融合し、いずれも心筋細胞の形質を示した。骨格筋由来の細胞、内皮細胞をマウスの心臓に注入したところ、in vivoにおいても、心筋細胞と融合し、心筋細胞特異的蛋白を発現した。また心臓に凍結傷害をくわえたところ、心筋細胞は周囲の内皮細胞と融合した。

２）組織幹細胞の心筋細胞への分化

心臓より幹細胞を単離する目的で、FACSによりSP(side population)分画を採取した。SP分画細胞はヘキストdyeを排出する分子であるbcrpを発現していた。SP細胞はオキシトシンの処理により、急速に分裂増殖し、３－４週後には自律拍動する心筋細胞に分化した。また培養条件をかえることにより、心臓由来SP細胞は脂肪細胞や骨細胞に分化した。

７．研究の考察・反省

最近の知見では、体性幹細胞のうち骨髄細胞は急性心筋梗塞患者に対する移植治療が開始されている。しかし、主要な機序は血管新生とそれによる心筋保護効果が虚血性心疾患に有効であるようです。

ここ２－3年のうちに成体の心筋から心筋幹細胞として、c-kit陽性細胞、Sca-1陽性

細胞、islet-1陽性細胞、ＳＰ細胞が報告されてきている。これらの報告された心筋幹細胞の分化のメカニズムがさらに解明されることにより、心筋内幹細胞の効率のよい増殖分化誘導と骨髄の他、皮膚、骨格筋、脂肪などの多くの体性幹細胞の心筋への分化誘導が可能となると思われる。
また、工学的技術との連携で大量培養、心筋シート作成などさまざまな分野の発展が見られるが、その中でもきわめて心筋幹細胞の分化のメカニズムの解明という基礎的データが大切であろうと思われる。

末期重症心不全の治療には移植以外には再生療法などしかなく、究極的治療の開発には心筋再生と血管再生・血管新生ということが大切であり、今後もさらなるメカニズムの解明などの研究が必要と思われます。

私どもは途中でありましたが、益々の発展を期待しています。

1．研究課題名：レトロウイルス発現系を用いたタイラーウイルス増殖メカニズムにおけるL*蛋白の役割の解明（研究番号 S2004-5）

2．キーワード：1）タイラーウイルス（Theiler’s murine encephalomyelitis virus）
2）L*蛋白（L* protein）
3）マクロファージ（macrophage）
4）アポトーシス（apoptosis）

3．研究者氏名：紺谷靖英・医学部・助手・生体感染防御学（微生物学）
（現南九州大学）

4．研究目的

タイラーウイルスは、ピコルナウイルス科に属し、マウスに急性致死性の灰白脳脊髄炎を引起す急性亜群（GDVII 株）と、マウス脊髄に持続感染し脱髄を引起す慢性亜群（DA 株）とに分類される。この慢性亜群による脱髄は、ヒトの代表的な脱髄疾患である多発性硬化症の動物モデルとして用いられている。脱髄発症の機序については未だ不明であるが、ウイルスの主たるリザーバーはマクロファージであると考えられている。慢性亜群では、ポリ蛋白の開始コドンの 13 塩基下流にある別の読み枠の開始コドン AUG から分子量約 18kDa の L*と呼ばれる蛋白が合成される。一方、急性亜群では、この AUG が ACG となっており L*蛋白は合成されない。このように L*蛋白は DA 亜群でのみ合成されることから、持続感染および脱髄を規定している重要な因子の一つであると考えられている。これまで L*蛋白の機能解析は DA 株の L*蛋白の開始コドン AUG を ACG に点変異させた DAL*-1 ウイルスを用いた‘loss-of-function’の系で行われており、L*蛋白非産生 DAL*-1 ウイルスはマクロファージ内で増殖しないことが明らかになっている。また、マクロファージ樹立細胞株である P388D1 細胞を用いた解析から DAL*-1 は感染後、GDVII 株と同様に宿主細胞にアポトーシスを起こすが、野生型の DA 株はアポトーシスを起こさないことが報告されている。

本研究の目的は、マクロファージ内でのウイルス増殖に対する L*蛋白の役割をレトロウイルス発現系を用いて‘gain-of-function の系’から明らかにすることである。

5．研究計画

1) L*蛋白が宿主細胞側に及ぼす影響を調べるために、アポトーシスへの関与の可能性が報告されているマクロファージ樹立細胞株 P388D1 に、レトロウイルス発現系を用いて L*蛋白遺伝子を導入し、L*蛋白を発現させた細胞株 L*/P388D1 を樹立する。

2) 遺伝子導入した細胞における L*蛋白の発現は、抗 L*ポリクローナル抗体を用いた Western blotting にて確認する。

3) マクロファージ内でのL*蛋白の役割を明らかにするために、L*蛋白非産生ウイルスDAL*-1をL*蛋白発現細胞に感染させ、ミトコンドリア内脱水素酵素活性を利用したWST-8 assayにより細胞の生存率を検討する。

4) マクロファージ内でのアポトーシスに対するL*蛋白の関与を明らかにするために、アガロース電気泳動によるDNA fragmentation解析を行う。

5) さらに、L*蛋白のアポトーシス制御機構を明らかにするために、アポトーシスシグナリング分子であるカスパーゼ-3 活性の測定およびミトコンドリアからのチトクロームcの放出について検討する。

6．研究成果

1) 形質導入したマクロファージ細胞株 P388D1 を限界希釈し、L*蛋白発現細胞L*/P388D1を樹立した。

2) 抗L*ポリクローナル抗体を用いたWestern blottingにより、単離した細胞におけるL*蛋白の発現が確認された。

3) L*蛋白非産生ウイルスDAL*-1をL*/P388D1細胞に感染させ、感染後11時間後の細胞の生存率を測定した結果、L*/P388D1 はコントロール細胞と比較してその生存率が有意に高かった。

4) ウイルス感染によるDNA fragmentationを解析した結果、コントロール細胞では感染後10.5時間でDNA fragmentationが検出された。一方、L*蛋白発現細胞L*/P388D1は感染後12時間でもわずかに検出される程度であった。

5) L*蛋白非産生ウイルスDAL*-1感染後10.5時間でコントロールおよびL*/P388D1細胞を回収し、カスパーゼ-3活性を測定した結果、コントロール細胞はウイルス感染によりその活性は2.4倍に増加し、この活性はZ-VAD（カスパーゼインヒビター）により抑制された。一方、L*/P388D1はウイルス感染後、カスパーゼ-3の活性に変化は認められなかった。また、ミトコンドリアからのチトクロームcの放出は両細胞において検出されなかった。

7．研究の考察・反省

本研究において樹立したL*蛋白発現細胞L*/P388D1を用いてL*蛋白のアポトーシス制御への関与について検討した。L*蛋白を発現しないコントロール細胞へのL*蛋白非産生ウイルスDAL*-1の感染実験から、本ウイルスはカスパーゼ-3を介したシグナリングでアポトーシスを起こすことが明らかとなった。さらに、L*蛋白発現細胞L*/P388D1への同ウイルス感染実験から、L*蛋白はDAL*-1ウイルスによるカスパーゼ-3を介したアポトーシスシグナリングを抑制することが‘gain-of-functionの系’から証明された。さらに、ミトコンドリアからのチトクロームcの放出が認められなかったことから本ウイルスによるアポトーシスシグナリングはdeath receptorを介した

経路（extrinsic pathway）であることが示唆された。

ここで示したL*蛋白の抗アポトーシス作用は、マクロファージにおけるウイルスゲノム維持に有利に働き、タイラーウイルスDA株の持続感染に重要な役割を果たしていると考えられる。マクロファージ内において、ウイルスゲノムの維持にL*蛋白が関与していることは非常に興味深い現象であり、今後、さらにL*蛋白がdeath receptorを介したアポトーシスシグナリング中のどの分子の制御に関わっているのか詳細に検討する必要がある。

8.研究発表

Himeda T, Ohara Y, Asakura K, Kontani Y, Sawada M. A lentiviral expression system demonstrates that L* protein of Theiler's murine encephalomyelitis virus (TMEV) has an anti-apoptotic effect in a macrophage cell line. Microb Pathog 2005; 38: 201-207. (MLDB)

Available online at www.sciencedirect.com
SCIENCE DIRECT
ELSEVIER
Microbial Pathogenesis 38 (2005) 201–207
MICROBIAL PATHOGENESIS
www.elsevier.com/locate/micpath

A lentiviral expression system demonstrates that L* protein of Theiler's murine encephalomyelitis virus (TMEV) has an anti-apoptotic effect in a macrophage cell line

Toshiki Himeda[a], Yoshiro Ohara[a,*], Kunihiko Asakura[a], Yasuhide Kontani[a], Makoto Sawada[b]

[a]*Department of Microbiology, Kanazawa Medical University, 1-1 Uchinada, Ishikawa 920-0293, Japan*
[b]*Institute for Comprehensive Medical Science, Fujita Health University, Aichi 470-1192, Japan*

Received 30 July 2004; accepted 14 January 2005
Available online 22 April 2005

Abstract

DA subgroup strains of TMEV persist in the CNS of infected mice and induce demyelination. The mechanism(s) of virus persistence and demyelination remains unknown. DA subgroup strains synthesize a 17-kDa protein, called L*, from an initiation site out-of-frame with the polyprotein. The previous study using a mutant virus, DAL*-1 (in which the L* AUG is substituted by an ACG) showed that L* has an anti-apoptotic effect in a macrophage cell line, P388D1. Therefore, we established P388D1 cells that continuatively express L*, in order to confirm its role in TMEV-induced apoptosis. The anti-apoptotic activity of L* may be important in TMEV pathogenesis.
© 2005 Elsevier Ltd. All rights reserved.

Keywords: Theiler's murine encephalomyelitis virus; L* protein; Lentiviral vector; Macrophage cell line; Apoptosis

1. Introduction

Theiler's murine encephalomyelitis virus (TMEV) belongs to the genus *Cardiovirus* of the family *Picornaviridae* and is divided into two subgroups [16,20,22]. DA (or TO) subgroup strains induce a non-fatal polioencephalomyelitis in weanling mice followed by chronic demyelination with virus persistence in the spinal cord. In contrast, GDVII subgroup strains cause an acute fatal polioencephalomyelitis without virus persistence or demyelination. DA-induced demyelinating disease serves as an experimental model of the human demyelinating disease, multiple sclerosis (MS). However, the precise mechanisms of virus persistence and demyelination caused by DA subgroup strains are still unknown [16,20,22]. A 17-kDa protein (sometimes described as 18 kDa), called L*, is translated out of frame with the polyprotein from an alternative AUG, 13 nucleotides downstream from the authentic polyprotein AUG [9,16,22]. L* protein is only synthesized in DA subgroup strains since the L* AUG is present in DA subgroup strains, but not in GDVII subgroup strains [12,16, 22]. Therefore, L* protein is thought to be a key protein regulating DA persistence and demyelination. A 'loss-of-function' experiment using a mutant virus, DAL*-1, in which the L* AUG initiation codon is mutated to an ACG, demonstrated that L* protein plays an important role in DA persistence and demyelination [1,5]. In contrast, other investigators, using a different DA infectious clone, found that this same L* AUG to ACG mutation had only a weak influence on the persistence of DA strain [26]; however, these investigators did show that the full-length L* protein is required for DA persistence [27]. Therefore, the precise function of L* protein is still under dispute.

Apoptosis is an intrinsic cellular defense that is present in a number of viral infections [4]. There are reports regarding apoptosis induced by TMEV infection as well [20]. An anti-apoptotic activity of L* protein in macrophages, a major site of TMEV persistence [2,11,23], has been demonstrated by comparing DAL*-1 virus with wild type DA infection [5]. A challenge in research related to L* protein is that its sequence overlaps with that of the polyprotein, making it

* Corresponding author. Tel.: +81 76 218 8096; fax: +81 76 286 3961.
E-mail address: ohara@kanazawa-med.ac.jp (Y. Ohara).

0882-4010/$ - see front matter © 2005 Elsevier Ltd. All rights reserved.
doi:10.1016/j.micpath.2005.01.005

impossible to introduce the DA L* coding sequence into the parental GDVII strain without changing the polyprotein sequence. Therefore, the goal of the present study was to generate macrophage cells that constitutively express L* protein in order to confirm an anti-apoptotic activity of this protein.

2. Results

2.1. Establishment of L*-expressing P388D1 clones

A lentiviral expression system was used for achieving a stable and efficient gene transfer of the L* protein. The third subculture of P388D1 cells infected with the lentiviral vector containing the L* coding sequence was seeded at a density of 0.5 cells per well. Cell propagation was observed in 58 wells of L*-transduced cells. FACS analysis selected nine L*-expressing clones (L*/P388D1). Fig. 1 shows the histograms of L*/P388D1/19 clone, which gave the highest GFP expression. L*/P388D1/19 cells propagated more slowly than the original P388D1 cells.

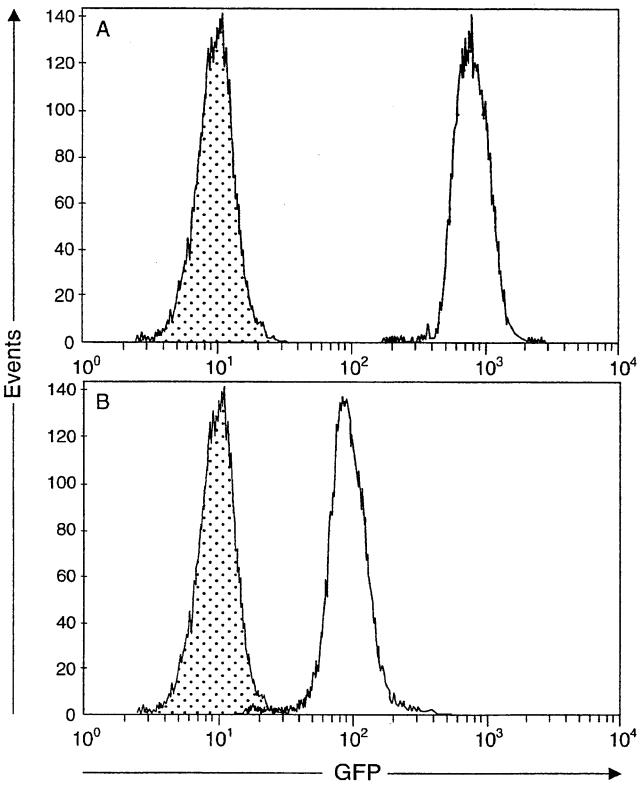


Fig. 1. Flow cytometric analysis of green fluorescent protein (GFP) fluorescence. P388D1 cells were infected and transduced with the lentiviral vector containing the L* protein sequence. The transduced cells were cloned by a limiting dilution. The figure shows the histograms of GFP fluorescence in a representative clone of the vector-transduced P388D1 cells (open area). The original P388D1 cells served as a control (closed area). (A) Control/P388D1/2 cells, which was transduced by an empty vector, as described in the text; (B) L*/P388D1/19 cells, which was transduced by the vector containing the L* sequence.

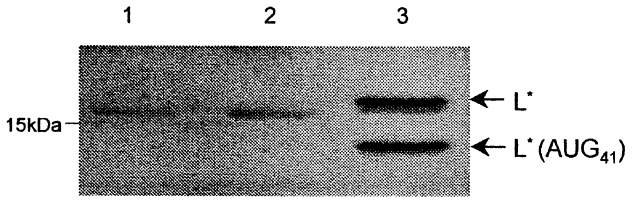


Fig. 2. Protein expression of the transgene (L* coding region) in L*/P388 D1/19 cells. The expression of the L* gene in L*/P388D1/19 cells was analyzed by Western blotting as described in the text. Lane 1, the original P388D1 cells; lane 2, control/P388D1/2 cells; lane 3, L*/P388D1/19 cells.

The property reverted to that of original P388D1 cells after several passages. Three empty vector-transduced clones (control/P388D1) were also obtained from the empty vector-transduced P388D1 cells and one of them, control/P388D1/2, served as a control, the growth of which was identical to that of the original P388D1 cells.

2.2. Confirmation of L* expression in L*/P388D1 cells

The expression of L* protein was further confirmed by Western blotting (WB). As shown in Fig. 2, αL* detected two specific bands in L*/P388D1/19 cells. The mobility of the upper band ranged between 18 and 17 kDa. That of the lower band ranged between 15 and 13 kDa. The expression of these bands was stable after forty passages of culture. The lower band may represent translation from an alternative translation initiation site in the L* coding region (see Section 3).

2.3. The effect of L* protein on survival of P388D1 cells

The role of L* protein in survival of P388D1 cells following TMEV infection was examined. We first examined the growth kinetics of DAL*-1 virus in those cells as previously described [19]. In L*/P388D1/19 cells, the titers of cell-free and cell-associated DAL*-1 virus reached a peak at 12 h p.i. (5.1×10^7 and 5.7×10^7 PFU/ml, respectively) and then gradually decreased (data no shown). We next examined the viability of cells following the infection of DAL*-1 virus by a WST-8 (2-(2-methoxy-4-nitrophenyl)-3-(4-nitrophenyl)-5-(24-disulfophenyl)-2H-tetrazolium, monosodium salt) assay. Fig. 3(A) shows the result. The cell viability of L*/P388D1/19 cells infected with DAL*-1 was 73%, whereas that of control/P388D1/2 was 64%. The difference was statistically significant (unpaired Student's t test, $p=0.032$). As a WST-8 assay indicates mitochondrial activity of cells, trypan blue dye exclusion test was performed to confirm the above data. At 12 h p.i., the cell viability of control/P388D1/2 infected with DAL*-1 was 78%, whereas the cell viability of L*/P388D1/19 infected with DAL*-1 was 87% (Fig. 3(B)). The difference was also statistically significant (unpaired Student's t test, $p=0.011$). The data suggest that L* protein

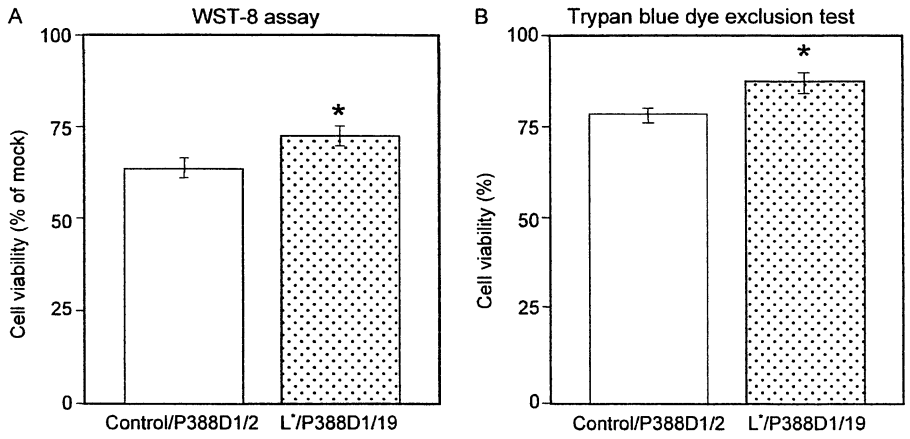


Fig. 3. Cell viability of L*/P388D1/19 cells following infection of DAL*-1 virus. (A) Cell survival was analyzed at 11 h post infection (p.i.) by WST-8 assay using a cell counting kit-8, as described in the text. Cell viability was calculated as % of absorbance of the supernatant of DAL*-1-infected control/P388D1/2 or L*/P388D1/19 cells to that of control/P388D1/2 or L*/P388D1/19 cells; (B) cell survival was also analyzed at 12 h p.i. by trypan blue dye exclusion test as described in the text. The percent viability was determined from the number of cells, which did not exclude the dye. All data were expressed as the mean ± standard deviation (SD) in three independent experiments. A statistical analysis was performed using unpaired Student's t test (*, $p<0.05$).

prevents P388D1 cells from the cell death caused by TMEV infection.

2.4. An anti-apoptotic effect of L* in L*/P388D1 cells

To further characterize the role of L* protein in the cell death mechanism(s) of P388D1 during TMEV infection, we next examined whether apoptosis is involved in this process. DNA laddering was observed in control/P388D1/2 cells infected with DAL*-1 virus at 10.5 h p.i., and was prominent at 12 h p.i. (Fig. 4). However, laddering was not observed in L*/P388D1/19 cells at 10.5 h p.i., and was only very weakly detected at 12 h p.i. (Fig. 4). The data suggest that DAL*-1 infection induces cell death through apoptosis, and that the induction of apoptosis in TMEV-infected P388D1 cells is suppressed by the presence of L* protein.

In order to investigate whether the apoptosis caused by TMEV infection is induced through a caspase pathway, we analyzed the activation of caspase-3 by using the CaspACE Assay System, Colorimetric (Promega, Madison, WI). In control/P388D1/2 cells, caspase-3 was activated at 10.5 h p.i. by DAL*-1 infection, and this activation was clearly inhibited by a caspase family inhibitor, Z-VAD-FMK (Fig. 5, left panel), suggesting that the apoptosis of P388D1 cells caused by DAL*-1 infection is induced through a caspase pathway. As shown in the right panel of Fig. 5, the activity of caspase-3 in L*/P388D1/19 cells infected with DAL*-1 was significantly suppressed compared with that in control/P388D1/2 cells (unpaired Student t test, $p=0.019$). The caspase-3 activity in L*/P388D1 cells following DAL*-1 infection was as low as that in Z-VAD-FMK-treated control/P388D1/2 or L*/P388D1/19 cells, suggesting that apoptosis is induced through caspase-3 activation, and that L* protein inhibits this pathway.

3. Discussion

In the present study, we have established a macrophage cell line which constitutively expresses L* protein. αL* detected two specific bands in L*-expressing P388D1 cells. The expression of L* was confirmed by WB using αL*, however, two bands of different mobilities were demonstrated—one band of the predicted 17.8 kDa and one of 13.2 kDa. It is reported that two forms of L* protein can be translated. A full-length L* can be expressed from the authentic initiation codon, and an N-terminally truncated L* can be translated from a downstream AUG initiation codon (AUG_{41}) [27]. We suspect that the 13.2 kDa band is related

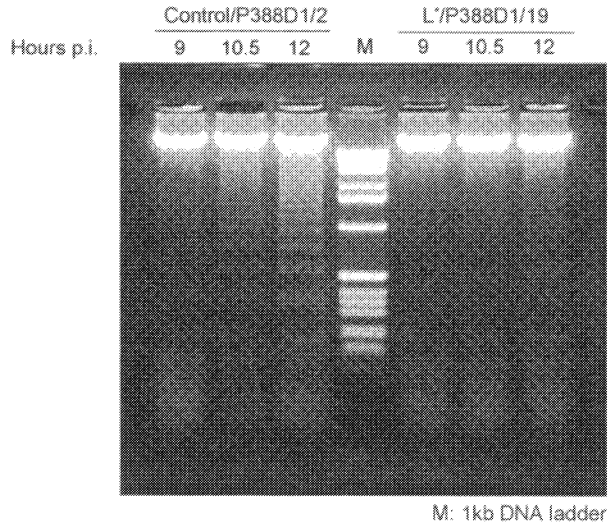


Fig. 4. DNA fragmentation analysis of control/P388D1/2 and L*/P388D1/19 cells following DAL*-1 infection. DNA was extracted from DAL*-1-infected control/P388D1/2 or L*/P388D1/19 cells and analyzed by agarose gel electrophoresis, as described in the text. The left and right three lanes represent control/P388D1/2 and L*/P388D1/19 cells, respectively. The number at the top of panel indicates hours p.i. M shows a 1 kb DNA ladder as a marker.

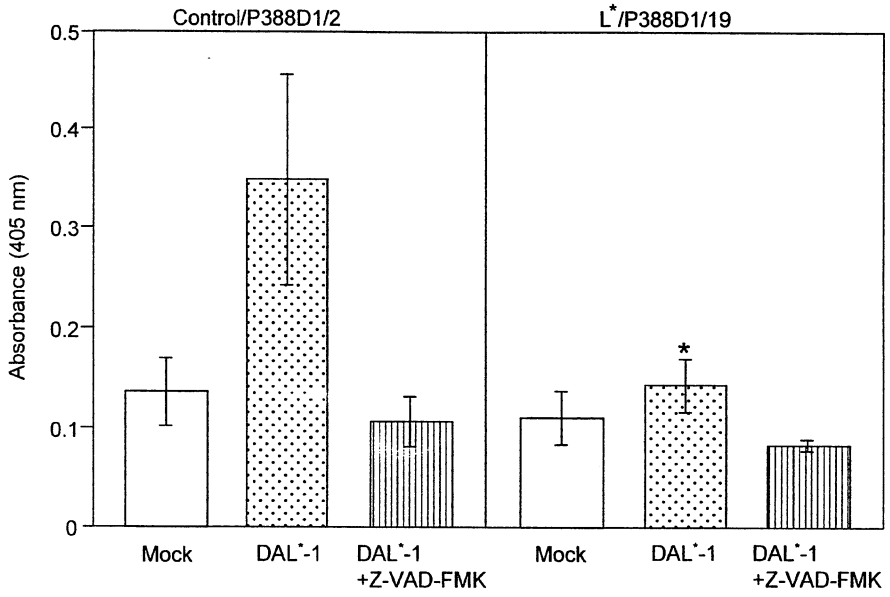


Fig. 5. The activity of caspase-3 in control/P388D1/2 and L*/P388D1/19 cells. The activity of caspase-3 in DAL*-1 virus-infected cells was analyzed by the CaspACE Assay System, as described in the text, at 10.5 h p.i. The absorbance of a mixture of the cell extract and DEVD-pNA substrate was measured at 405 nm. Treatment with Z-VAD-FMK was performed, as described in the text. Mock, mock-infected cells; DAL*-1, DAL*-1-infected cells; DAL*-1 + Z-VAD-FMK, cells treated with Z-VAD-FMK following DAL*-1 infection. Data were expressed as the mean ± SD in three independent experiments. A statistical analysis was performed using unpaired Student's t test (*, $p<0.05$).

to translation using the AUG_{41} in the L* coding region. The synthesized N-terminally truncated L* is not detected following DA infection presumably because an internal ribosomal entry site (IRES) may exert a presence of preferential or virtually exclusive L* synthesis from the first AUG.

By using L*-expressed P388D1 cells, we have demonstrated that L* protein has an anti-apoptotic effect in TMEV-infected P388D1 cells. We previously reported that apoptosis is induced by DA, GDVII, or DAL*-1 at 24 h p.i. in P388D1 cells [19]. Ghadge et al. also reported that DA-induced apoptosis increases from 12 h to 16 h p.i. in P388D1 [5]. The overall results with our present data indicate that L* protein suppresses TMEV-induced apoptosis at a certain period of time after the infection. The suppression activity of L* may not be so high as to absolutely inhibit the apoptosis.

The present study also demonstrated that apoptosis signaling through caspase-3 pathway is involved in the cell death caused by TMEV infection. Although data are not shown, we found no cytochrome c release in the cytoplasm of either L*/P388D1/19 or control/P388D1/2 cells following DAL*-1 infection. It is speculated that the major apoptotic pathway following DAL*-1 infection may be a death receptor-mediated pathway (extrinsic pathway), but not mitochondrion-mediated pathway (intrinsic pathway).

A number of investigators have studied apoptosis following TMEV infection in vitro or in vivo. Apoptosis of neurons is observed in mice in the acute stage following the infection of both a virulent (GDVII) and attenuated (DA) strains although the number of apoptotic neurons is much greater in GDVII infection [25]. Apoptosis of oligodendrocytes [25] or astrocytes [21] has also been reported. In addition, apoptosis of microglia [19] and T cells [20] has been studied. Among the cells potentially inducing apoptosis, monocyte/macrophage lineage cells are of great interest since macrophages are reported to be a major site of TMEV persistence in the chronic stage [2,11,23]. The inhibition of apoptosis in infected macrophages may foster maintenance of viral genome in those cells, initiating a cascade of immune responses, resulting in demyelination. DA subgroup strains may cause demyelination with virus persistence, but GDVII subgroup strains do not because DA synthesizes L* protein and is, therefore, able to inhibit apoptosis in infected macrophages, while GDVII does not synthesize L*.

Apoptosis has been observed following TMEV infection of BSC-1 cells, which are relatively non-permissive to infection, while infection of BHK-21 cells, a permissive cell line, had relatively little apoptosis [6]. These authors also found apoptosis in macrophage cell lines [7] and activated macrophages. They observed two independent mechanisms involved in apoptosis [8]: in an unactivated state, an intrinsic pathway which requires virus replication is utilized, while in an activated state, an extrinsic pathway with signaling through TNF-α-related apoptosis-inducing receptors is utilized. Although the state of activation of L*/P388D1/19 cells was not examined in detail in the present study, L* protein may inhibit an extrinsic pathway in P388D1 cells.

The present 'gain of function' experiment confirmed the anti-apoptotic activity of L* protein which has been

demonstrated by a 'loss of function' experiment by using DAL*-1 virus [5]. However, further studies are required to clarify the more detailed mechanism(s) of the inhibition of apoptosis by L* protein. This protein is also reported to remain in the cytoplasm without being incorporated into virions [18]. Therefore, the identification of proteins that interact with L* will be important, and a project using two-hybrid system is in progress. These studies will be helpful in clarifying the mechanism(s) of TMEV-induced demyelination, and may also increase our understanding of the pathogenesis of MS.

4. Materials and methods

4.1. Generation of a lentiviral vector containing L coding sequence*

The vector was constructed by using the transfer vector plasmid pCSII-EF-MCS-IRES-hrGFP, which was engineered by Drs Hiroyuki Miyoshi and Tomoyuki Yamaguchi, Laboratory of Genetics, The Salk Institute for Biological Studies. The plasmid has sequences of human elongation factor 1α subunit gene promoter (EF1α), a multiple cloning site (MCS), an IRES, and the coding region of a 'humanized, red-shifted' green fluorescent protein (hrGFP) in tandem. L* coding sequence was inserted into the MCS. Since the expression of both proteins are regulated by one promoter, L* protein and hrGFP are produced independently of each other. In order to generate vesicular stomatitis virus (VSV) G protein-pseudotyped lentiviral vector particles, the transfer vector plasmid pCSII-EF-(cDNA of L*)-IRES-hrGFP with the packaging plasmid pMDLg/pRRE, pRSV-Rev, and the VSV-G protein envelope plasmid pMD.G [15] were transfected into 293T cells, a human embryonic kidney epithelial cell line expressing the simian virus 40 (SV40) large T antigen. The cells were maintained in Eagle's minimum essential medium supplemented with 10% fetal calf serum, 2 mM L-glutamine, 5 μg/ml insulin, 0.2% glucose and 60 μg/ml kanamycin. After adding the calcium phosphate-DNA co-precipitates [13,14,24] containing the above four types of plasmids dropwise into subconfluent 293T cells, the cells were incubated in a 3% CO_2 atmosphere at 37 °C for 12–16 h. Subsequently, the medium was changed to the fresh complete growth medium supplemented with 10 μM forskolin and the cells were further incubated in a 10% CO_2 atmosphere at 37 °C. After 32–48 h, the supernatants were filtered through a 0.45 μm pore-size filter. High-titer virus stocks were prepared by centrifugation (43,600*g*, 3 h, 21 °C), the infectious titers of which were determined by counting the number of GFP-positive cells by fluorescence-activated cell sorting (FACS) analysis (FACSCalibur: BD Biosciences, San Jose, CA). One GFP staining cell was defined as one transducing unit (TU).

4.2. Establishment of L-expressing P388D1 clones*

P388D1 cells, a murine macrophage-like cell line [3,10], were maintained in an RPMI1640 medium supplemented with 10% fetal calf serum, 2 mM L-glutamine, and 60 μg/ml kanamycin. 2×10^5 P388D1 cells were infected with a lentiviral vector at a rate of 5 TU per one target cell and incubated in a 5% CO_2 atmosphere at 37 °C. The third subculture of the infected cells was seeded at a density of 0.5 cells per well onto 360 wells of HLA plates (Greiner bio-one, Tokyo, Japan) to establish an L*-expressing cell line by limiting dilution. The L*-expressing clones (L*/P388D1) were selected by FACS analysis using expression of GFP.

4.3. Detection of L expression by WB*

WB was performed as previously described [17]. Briefly, the cells were lysed in sample buffer (0.01 M Tris–Cl [pH 6.8], 1 mM EDTA, 2.5% SDS, 5% 2-mercaptoethanol, 10% glycerol, 0.01% bromophenol blue). The lysates were separated by sodium dodecyl sulfate polyacrylamide gel electrophoresis under reducing conditions on 15% polyacrylamide gels and transferred to nitrocellulose membranes by electroblotting. A polyclonal rabbit anti-L* antibody, designated αL*, was used as the first antibody. αL* is the serum from a rabbit immunized with an L* peptide corresponding to amino acid residues 70–88 [17,18]. Bound antibodies were detected with biotinylated secondary antibodies and horseradish peroxidase-conjugated streptavidin, using enhanced chemiluminescence reagents, ECL plus (Amersham Biosciences, Piscataway, NJ).

4.4. Determination of cell survival following the infection

Cell survival was analyzed by a WST-8 assay using a cell counting kit-8 (Dojindo, Kumamoto, Japan). 3×10^5 cells in a 12 well tissue culture plate were infected with DAL*-1 virus at a multiplicity of infection (MOI) of 10 PFU per cell. DAL*-1 virus is a mutant virus in which an AUG, the initiation codon of L* protein is mutated to ACG, and therefore, is not predicted to synthesize L* protein [1,9,16]. At 10 h post infection (p.i.), 0.1 volume of cell counting kit-8 (5 mM WST-8, 0.2 mM 1-Methoxy PMS, 150 mM NaCl) in maintenance medium was added and incubated for 1 h at 37 °C. The absorbance of supernatants was measured at 450 nm. The cell viability was expressed as % of the absorbance of the supernatant of DAL*-1-infected control/P388D1/2 or L*/P388D1/19 cells to that of mock-infected control/P388D1/2 or L*/P388D1/19 cells.

The cell survival was also analyzed by trypan blue dye exclusion test. 1×10^6 cells in a 6 well tissue culture plate were infected with DAL*-1 virus at an MOI of 10 PFU per cell. At 12 h p.i., the cells were harvested and resuspended in maintenance medium at a concentration of

$2–4 \times 10^6$ cells/ml. Then the cell suspension was mixed with the equal volume of 0.5% trypan blue solution. The percent viability was determined from the number of cells which did not exclude the dye.

4.5. Detection of apoptosis

DNA fragmentation was analyzed by agarose gel electrophoresis. 1×10^6 cells were infected with DAL*-1 virus at an MOI of 10 PFU per cell. At 9, 10.5, and 12 h p.i., cells were scraped and lysed in 400 μl of cell lysis buffer (10 mM Tris–Cl [pH 8.0], 100 mM EDTA, 0.5% SDS). The lysate was treated with RNase A (200 μg/ml) for 60 min at 37 °C, and then digested with proteinase K (400 μg/ml) for 2 h at 50 °C. The DNA was extracted with phenol–chloroform–isoamyl alcohol (25:24:1) and then purified by ethanol precipitation. Three microgram of DNA was subjected to electrophoresis in 1.5% agarose gel containing 0.5 μg/ml ethidium bromide in Tris–borate buffer.

4.6. Detection of caspase-3 activity

The activity of caspase-3 was analyzed by using the CaspACE Assay System, Colorimetric (Promega, Madison, WI). Briefly, 1×10^7 cells were infected with DAL*-1 virus at an MOI of 10 PFU per cell. At 10.5 h p.i., the cells were harvested by centrifugation at $450 \times g$ for 10 min at 4 °C and then washed by ice-cold phosphate-buffered saline without Ca^{2+} or Mg^{2+} (PBS). The cell pellets were resuspended in Cell Lysis Buffer at a concentration of 1×10^8 cells/ml. The cells were lysed by freezing and thawing, and then incubated on ice for 15 min. The supernatant fraction (cell extract) was collected by centrifugation at 15,000*g* for 20 min at 4 °C. The cell extract from 1×10^6 cells was mixed with caspase assay buffer, 2 μl of DMSO, 10 mM DTT, and 0.2 mM DEVD-pNA substrate, and then incubated at 37 °C for 4 h. The absorbance of the mixture was measured at 405 nm. The regulation of caspase-3 activity by a caspase family inhibitor, Z-VAD-FMK, was also examined as a control. Z-VAD-FMK was added into the maintenance media immediately after virus adsorption in a final concentration of 20 μM.

Acknowledgements

This work was supported by a Grant-in-Aid for Scientific Research from the Ministry of Education, Science, Sports and Culture, a Grant for Promoted Research from Kanazawa Medical University (S2004-5) and a Grant for Project Research from High-Technology Research Center of Kanazawa Medical University (H2004-7).

References

[1] Chen H-H, Kong W-P, Zhang L, Ward PL, Roos RP. A picornaviral protein synthesized out of frame with the polyprotein plays a key role in a virus-induced immune-mediated demyelinating disease. Nat Med 1995;1:927–31.

[2] Clatch RJ, Miller SD, Metzner R, Dal Canto MC, Lipton HL. Monocytes/macrophages isolated from the mouse central nervous system contain infectious Theiler's murine encephalomyelitis virus (TMEV). Virology 1990;176:244–54.

[3] Dawe CJ, Potter M. Morphologic and biologic progression of a lymphoid neoplasm of the mouse in vivo and in vitro. Am J Pathol 1957;33:603.

[4] Flint SJ, Enquist LW, Rachaniello VR, Skalka AM. In: Flint SJ, Enquist JW, Racaniello VR, Skalka AM, editors. Principles of virology. 2nd ed. Washington DC: ASM Press; 2004. p. 530–94.

[5] Ghadge GD, Ma L, Sato S, Kim J, Roos RP. A protein critical for a Theiler's virus-induced immune system-mediated demyelinating disease has a cell type-specific antiapoptotic effect and a key role in virus persistence. J Virol 1998;72:8605–12.

[6] Jelachich ML, Lipton HL. Theiler's murine encephalomyelitis virus kills restrictive but not permissive cells by apoptosis. J Virol 1996;70: 6856–61.

[7] Jelachich ML, Bramlage C, Lipton HL. Differentiation of M1 myeloid precursor cells into macrophages results in binging and infection by Theiler's murine encephalomyelitis virus and apoptosis. J Virol 1999; 73:3227–35.

[8] Jelachich ML, Lipton HL. Theiler's murine encephalomyelitis virus induces apoptosis in gamma interferon-activated M1 differentiated myelomonocytic cells through a mechanism involving tumor necrosis factor alpha (TNF-α) and TNF-α-related apoptosis-inducing ligand. J Virol 2001;75:5930–8.

[9] Kong W-P, Roos RP. Alternative translation initiation site in the DA strain of Theiler's murine encephalomyelitis virus. J Virol 1991;65: 3395–9.

[10] Koren HS, Handwerger BS, Wunderlich JR. Identification of macrophage-like characteristics in a cultured murine tumor line. J Immunol 1975;114:894–7.

[11] Lipton HL, Twaddle G, Jelachich ML. The predominant virus antigen burden is present in macrophages in Theiler's murine encephalomyelitis virus-induced demyelinating disease. J Virol 1995;69:2525–33.

[12] Michiels T, Jarousse N, Brachic M. Analysis of the leader and capsid coding regions of persistent and neurovirulent strains of Theiler's virus. Virology 1995;214:550–8.

[13] Miyoshi H, Takahashi M, Gage FH, Verma IM. Stable and efficient gene transfer into the retina using an HIV-based lentiviral vector. Proc Natl Acad Sci USA 1997;94:10319–23.

[14] Miyoshi H, Blömer U, Takahashi M, Gage FH, Verma IM. Development of a self-inactivating lentivirus vector. J Virol 1998; 72:8150–7.

[15] Naldini L, Blömer U, Gally P, Ory D, Mulligan R, Gage FH, et al. In vivo gene delivery and stable transduction of nondividing cells by a lentiviral vector. Science 1996;272:263–7.

[16] Obuchi M, Ohara Y. Theiler's murine encephalomyelitis virus and mechanisms of its persistence. Neuropathology 1998;18:13–8.

[17] Obuchi M, Yamamoto J, Uddin MN, Iizuka H, Ohara Y. L* protein of Theiler's murine encephalomyelitis virus is required for virus growth in a murine macrophage-like cell line. J Virol 2000;74:4898–901.

[18] Obuchi M, Odagiri T, Asakura K, Ohara Y. Association of L* protein of Theiler's murine encephalomyelitis virus with microtubules in infected cells. Virology 2001;289:95–102.

[19] Ohara Y, Himeda T, Asakura K, Sawada M. Distinct cell death mechanisms by Theiler's murine encephalomyelitis virus (TMEV) infection in microglia and macrophage. Neurosci Lett 2002;327: 41–4.

[20] Oleszak EL, Chang JR, Friedman H, Katsetos CD, Platsoucas CD. Theiler's virus infection: a model for multiple sclerosis. Clin Microbiol Rev 2004;17:174–207.

[21] Palma JP, Yauch RL, Lang S, Kim BS. Potential role of $CD4^+$ T cell-mediated apoptosis of activated astrocytes in Theiler's virus-induced demyelination. J Immunol 1999;162:6543–51.

[22] Roos RP. In: Semler BL, Wimmer E, editors. Molecular biology of picornaviruses. Washington DC: ASM Press; 2004. p. 427–35.

[23] Rossi CP, Delcroix M, Huitinga I, Mcallister A, van Rooijen N, Claassen E, Brahic M. Role of macrophages during Theiler's virus infection. J Virol 1997;71:3336–40.

[24] Sambrook J, Russell DW. In: Sambrook J, Russell DW, editors. Molecular cloning: a laboratory manual, 3rd ed, vol. 3. New York: Cold Spring Harbor Laboratory Press; 2001. p. 1619–20.

[25] Tsunoda I, Kurtz CIB, Fujinami RT. Apoptosis in acute and chronic central nervous system disease induced by Theiler's murine encephalomyelitis virus. Virology 1997;228:388–93.

[26] van Eyll O, Michiels T. Influence of the Theiler's virus L* protein on macrophage infection, viral persistence, and neurovirulence. J Virol 2000;74:9071–7.

[27] van Eyll O, Michiels T. Non-AUG-initiated internal translation of the L* protein of Theiler's virus and importance of this protein for viral persistence. J Virol 2002;76:10665–73.

1．研究課題名：日本人の白内障病型別有所見率・発症率と発症・進行予測および危険因子探索
(研究番号 S2004-6)

2．キーワード：1）白内障 (Cataract)
2）水晶体 (Crystalline lens)
3）疫学 (Epidemiology)
4）有所見率 (Prevalence)
5）WHO 白内障分類 (WHO cataract grading system)

3．研究者氏名：佐々木　洋・医学部・教授・感覚機能病態学 (眼科学)

4．研究目的

加齢白内障は現在の高齢化社会を象徴する代表的な眼疾患であり、わが国でもその患者数が着実に増加していることは厚生省労働省による患者調査でも明らかである。また治療としての白内障手術件数も年々増加の一途を辿り逼迫する医療経済の中で問題になっていることもよく知られている。先進国全般にかかわる現象であり、世界的にもこれへの対応を模索しているところであるが、国レベルでその検討が行われている地域は米国、オーストラリア、フランスなどまだ限られている。わが国でもこの立場からの白内障疫学研究が行われているが、申請者らの研究グループのみの研究にとどまっており、国際的な検討の場でも申請者らのこれまでの検討結果が議論のベースとなっている。本研究では本邦では初めてとなる無作為対象での日本人水晶体病型別の有所見率、手術施行例の頻度、5 年での発症率、進行率、壮年代初期を境に明らかに進行する水晶体透明度の低下に眼部紫外線被曝推定蓄積総量をはじめとする種々の危険因子がどの程度関与するのか等に視点を置いて検討することにある。既に申請者らはアイスランドで行った Reykjavik Eye Study で 5 年経過の 1,000 余名の無作為対象群から、今回意図した病型別発症率、進行率が明らかにすることができた。本研究の結果は世界最長寿国である日本での白内障の実態を明らかにし、欧米先進諸国での検討結果との差異を明確にし、同じ目的をもつ先進諸国の研究グループへも大きく貢献するはずである。

申請者らのグループはこれまで、能登地区、鹿児島県奄美地区、シンガポール、アイスランドで眼疫学調査を行ってきた。これらの調査では全て本研究代表者が細隙灯顕微鏡検査および白内障画像診断を行っており、全ての調査対象間での比較が可能である。本研究の特色は①、日本人にみられる白内障病型別の有所見率、進行率、発症率、手術受領率および白内障病型と視機能 (視力、コントラス感度) の関係を明らかにすることであり、得られた結果は今後の日本での眼科医療保険制度を再検討する際の基礎的データとなり得るはずである。②また、生活様式と白内障発症の関連については問診結果から検討するが、これと白内障発症前水晶体の散乱光強度を新たな指標として検討をする予定である。申請者らは散乱光強度と層間厚から水晶体の加齢変化の指標となり得る Lens Transparent Property (LTP) の有用性を報告している。これまでに散乱光強度を指標とした危険因子探索の検討はなく、この点も本研究の特色の 1 つである。③危険因子の中でも太陽紫外線被曝との関連についてはこれまでの調査でも検討を行ってきたが、マネキンモデルを用いた実験から申請者らが提唱する“推定眼部紫外線被曝蓄積量”と水晶体混濁との関連・

これに対する防御指針を本研究ではより具体的に提唱したい。国内はもとより海外でも眼部紫外線被曝量と白内障との関連についての研究は緒についたばかりであり、申請者らはこの領域では他の研究グループより一歩先んじた研究の蓄積があることより、本研究から白内障発症に至る眼部紫外線総被曝量の閾値が提唱できればと考えている。

5．研究計画

申請者らのグループが1998年から能登地域で行っている眼疫学調査Monzen Eye Studyの対象（無作為対象群；50歳以上の2,000名）について、すでに終了している1次調査の画像解析と5年目の縦断的調査を行う。1次調査では対象の60%以上について問診および水晶体撮影を含む眼科的検査を行った。本研究期間中に1次調査で収集したデータの解析と1次調査から5年を経過した症例を対象に2次調査を行う。2次調査では原則として1次調査で施行した全ての眼科的検査を行う。水晶体の解析は他のフィールド調査でも使用している前眼部解析装置での撮影画像を用いて行う。水晶体画像解析は1）水晶体散乱光強度、2）水晶体形状、3）3主病型（皮質、核、後嚢下混濁）の混濁程度の評価について行う予定である。生活視力の指標であるコントラスト感度と白内障病型の関連についての検討も行う。また、問診の結果について、全身疾患、眼疾患、内服薬、食生活、推定紫外線被爆量と水晶体混濁との関連を検討し、白内障発症および進行の予測、危険因子探索を行う。申請者らが提唱する“推定眼部紫外線被曝蓄積量”については、マネキンモデルでの実験から我々のグループが提唱した予測式を用い被爆量算出する。

6．研究成果

これまで石川県門前町の50歳以上の一般住民（無作為抽出）を対象に行った第1回の眼疫学調査の対象者1,105名中、本年度終了時点で632名について5年目の2次検診が終了した。5年での発症率は皮質混濁が 18.9% 、核混濁が3.0% 、後嚢下混濁が 2.0% で3病型とも加齢に伴い増加した。 進行率は皮質混濁 68.8% 、核混濁 24.8% 、後嚢下 25.6% であった。皮質混濁は若年者で進行率が高い傾向があった。5年での手術受療者は全体の8.2%で、混合型での受療率が高く、特に後嚢下混濁を合併する症例では受療率が高かった。研究者らがアイスランド一般住民を対象に行ったReykjavik Eye Studyの結果と比較し、日本人では皮質混濁が多くその進行も早いこと、核混濁はアイスランドに比べ発症率、進行率ともに低いことが明らかになった。また、皮質白内障の進行率は若年で早く、高齢者では遅いことも確認された。核および後嚢下白内障については年齢と進行との明らかな関連はなかった。本研究により日本人の白内障の特徴および自然経過が明らかになった。

前眼部解析装置と用い水晶体散乱光強度および皮質混濁面積の5年での変化についても検討した。散乱光強度は加齢に伴い上昇するが、年齢によりその上昇パターンが異なることが明になった。皮質深層では60歳代、70歳代に比べて50歳代でその増加率が高く、核部の散乱光強度は年齢との相関はなかった。また、核部散乱光強度の低い症例では皮質部散乱光強度の増加率が有意に高かった。本検討結果から散乱光強度測定は皮質および核混濁発症の予測に有用である可能性が示唆された。皮質混濁面積の増加量は初期混濁眼に比べ進行眼で多く、この結果から皮質混濁はある程度の混濁量に達すると急激に進行する可能性が示唆された。加齢白内障の皮質混濁には楔状混濁と輪状混濁の2病型があるが、混濁面積の増加速度は楔状混濁が有意に早いことも明ら

かになった。

副病型のなかのFiber foldsのコントラスト感度への影響を検討した。Fiber foldsは日本人に多く、皮質混濁を高率に合併するがCENがない場合はコントラストへの影響はほとんどないことが明らかになった。細隙灯顕微鏡検査において斜照法ではFiber foldsは皮質混濁と誤診されることもあり、本病型を正しく診断しコントラストを含めた視機能への影響が少ないことを啓蒙する必要がある。今後は他の主病型以外の混濁病型と3主病型の合併例での視機能についても検討し、日本人での白内障手術の適応基準を提唱したいと考えている。

7．研究の考察・反省

本研究から日本人における白内障3主病型および6副病型の有所見率と3主病型の5年での発症率、進行率が明らかになった。これまで本邦にはこのようなデータは全くなかったため、超高齢化社会で今後も増加が予想される白内障対策に有用な情報を提供できたと考えている。また、画像解析によりグローバルにもほとんど研究されていない白内障の自然経過についてもいくつかの有用なデータを出すことが出来た。眼部紫外線被曝量と白内障の関連いついては、Monzen Eye Study 対象者の問診情報に不備が多かったため今回の研究期間内に結果を出すことが出来なかった。今後、生活歴に関する再調査を行い改めて報告したい。幸いMonzen Eye Study対象者については今後も継続調査が可能であるため、10年での白内障自然経過に関して引き続き調査を継続していたいと考えている。

1．研究課題名：敗血症血管におけるαカテコラミン受容体刺激時の平滑筋収縮および内皮機能変化の検討（研究番号 S2004-7）

2．キーワード：1）内皮細胞由来弛緩因子
(EDRF; endothelium-derived relaxing factor)
2）内皮細胞由来過分極因子
(EDHF; endothelium- derived hyperpolarizing factor)
3）αアドレナリン受容体（alfa-adrenergic receptor)
4）βアドレナリン受容体（alfa-adrenergic receptor)
5）敗血症（sepsis)

3．研究者氏名：関　純彦・医学部・助教授・侵襲制御学（麻酔学）

4．研究目的

敗血症性ショックでは、カテコラミンα受容体刺激薬による血管収縮反応が減弱することが知られている。その機序として、平滑筋での誘導型一酸化窒素（NO）産生による血管拡張反応、活性酸素によるカテコラミンα受容体の不活化、平滑筋収縮機構自体の破綻などが考えられているが、敗血症の進行度や血管の部位によって機序が異なる可能性がある。

そこで本研究では、ラット腹膜炎敗血症モデルから大動脈および微小腸間膜動脈を摘出し、カテコラミンα受容体刺激薬フェニレフリンによる収縮反応を観察し、内皮機能との関係を検討する。

また、実際の臨床現場では、敗血症性ショック時には血管拡張作用を持つカテコラミンβ受容体刺激薬や鎮静薬プロポフォールがよく用いられる。そこで、フェニレフリン前収縮状態の血管で、これらの薬剤の血管拡張作用がどのように変化するのかも合わせて検討する。

5．研究計画

（1）腹膜炎敗血症ラットの作成

12時間絶食としたラットをセボフルラン麻酔下に開腹し、虫垂を取り出して結紮するとともに2カ所に穿孔を開け、閉腹する。対象群（シャム手術群）では、同様に開腹し虫垂を取り出すが、何も操作を加えないままに閉腹する。12時間、または24時間経過したラットを実験に用いる。

（2）大動脈実験

胸部大動脈を摘出し、長さ約 5 mm のリング状標本を作成する。一部は内腔を綿棒で擦って内皮を除去する。オルガン・バス内で張力トランスデューサーに接続し、フェニレフリン（10^{-8} -10^{-4} M）の累積投与による張力変化を記録する。内皮温存標

本において収縮反応減弱が観察された場合、NO 合成酵素阻害薬（L-NAME）、誘導型 NO 合成酵素阻害薬を前投与し、収縮反応減弱が改善するかどうかを検討する。また、β_1受容体刺激薬であるドブタミン（10^{-9} - 10^{-5} M）またはβ_2受容体刺激薬であるサルブタモール（10^{-9} - 10^{-5} M）を累積的に投与し、拡張反応を観察する。

（3）微小腸間膜動脈実験

直径 200μm 以下の腸間膜動脈を摘出し、長さ約 10 mm の標本を作成する。一部標本では、内皮を擦過して除去する。採取した血管標本の両端に微小ガラス・ピペットを挿入し、微小血管チャンバー内で、灌流圧・流量制御ポンプにて内圧を一定（60mmHg）に保つ。顕微鏡に装着した CCD カメラにて観察し、壁厚と内径の変化を測定・記録する。フェニレフリン累積投与による収縮反応の変化や、それに対する NO 合成酵素阻害薬（L-NAME）およびプロスタサイクリン産生阻害薬（シクロオキシゲナーゼ阻害薬、インドメタシン）の影響を観察する。また、この反応に麻酔薬プロポフォールがどのように影響するのかを検討する。

（4）免疫組織学的検討

誘導型一酸化窒素の発現と ONOO-の特異的なニトロ化合物であるニトロチロシンの発現を免疫組織学的に検討するため、腹膜炎ラットから摘出した胸部大動脈を用いて免疫染色を行い、染色陽性細胞率を比較検討する。また、マクロファージや顆粒球系細胞の内皮への接着を比較検討した。

6．研 究 成 果

（1）大動脈におけるフェニレフリン収縮の変化

対照群では、2回目、3回目のフェニレフリン累積投与においても1回目と同様の反応を示したが、24 時間後の敗血症モデルの内皮温存標本では、1回目の収縮反応に比較し、2回目、3回目の収縮が有意に抑制されるという現象が観察された。このフェニレフリン反復投与による収縮反応の減弱は、内皮除去標本では全く認めなかった。敗血症群におけるフェニレフリン反復投与時の収縮反応減弱は、L-NAME あるいはアミノグアニジンを前投与すると観察されなかった。

（2）大動脈におけるβ受容体刺激薬による拡張反応の変化

対照群では、内皮除去によりドブタミンによる拡張反応が大きく抑制されたが、サルブタモールによる拡張反応の抑制は軽度であった。12 時間後の敗血症群におけるドブタミンの拡張反応は、内皮の有無に係わらず、対照群と比較して差はなかった。内皮温存標本におけるサルブタモールの血管拡張反応は、対照群と比較して敗血症群で有意に抑制された。しかし、内皮除去標本では、対照群と差がなかった。

（3）微小腸間膜動脈におけるフェニレフリン収縮の変化

微小腸間膜動脈も大動脈同様フェニレフリンによって濃度依存性に収縮したが、高濃度では収縮弛緩を繰り返す律動運動を呈した。この律動運動は内皮除去で消失するが L-NAME およびインドメタシンを同時に前投与しても完全には消失せず、カルシ

ウム感受性カリウムチャネルの阻害薬（カリブドトキシン、アパミン）投与で消失する。このことから、律動にはEDHFが関与している可能性が強い。

敗血症モデルにおけるEDHF依存性律動の観察は今回の研究の目的のひとつであったが、微小細動脈は敗血症による平滑筋細胞自体の障害が大きく標本化が困難であるため、まだ観察できていない。

（4）微小腸間膜動脈におけるプロポフォールの影響

敗血症モデルにおける微小腸間膜動脈の標本化が困難であったため、対照群でのみフェニレフリン収縮に及ぼすプロポフォールの影響を観察した。その結果、臨床使用濃度（10^{-5} - 10^{-6} M）のプロポフォールはフェニレフリンによる収縮そのものには影響を与えないが、EDHF依存性律動運動を明らかに増強するという新たな知見を得た。

（5）摘出胸部大動脈標本における免疫組織学的検討

抗iNOS抗体、抗ニトロチロシン抗体を用いた免疫組織染色による陽性細胞率は、敗血症群では対照群と比較して有意に陽性細胞率の増加がみられた。このことから、敗血症では内皮でiNOS、ニトロチロシンが発現することが示唆された。抗マクロファージ抗体を用いた免疫組織染色による陽性細胞率は、敗血症群では内皮側において対照群と比較して陽性細胞数の増加がみられたが、統計学的には有意差はなかった。また、クロロアセテートエステラーゼ染色においても敗血症群では内皮側において対照群と比較して陽性細胞数の増加がみられたが、統計学的には有意差はなかった。このことから、血管収縮反応の減弱の機序に炎症細胞の接着・遊走は関与が少ないことが示唆された。

7．研究の考察・反省

前項目（1）の結果から、腹膜炎24時間後の敗血症では、まず内皮に誘導型NO合成酵素が誘導され、これによるNO産生がフェニレフリン収縮反応を減弱させると予想される。血管内皮には主にβ_1受容体が存在すると言われているが、（2）の結果から、内皮依存性拡張には内皮β_2受容体も弱いながら介在しており、腹膜炎12時間後ではまず内皮β_2受容体が障害を受けると推察される。今年度新たに検討を加えた（5）の結果から、収縮反応減弱にはNO産生誘導が関わっている可能性が示唆され、炎症細胞そのものの関与は弱いと考えられた。また、（4）の結果から微小腸間膜動脈においてプロポフォールはEDHF反応を増強させる可能性があることが示唆された。

8．研究発表

（3）（4）の結果についてAnesthesiology誌に投稿したが、採用されなかった。現在他誌への投稿を準備中である。（1）（2）（5）の結果についてはさらに病理学的・生化学的な検討を加えて投稿する予定である。

1．研究課題名：IL-2 投与が肺胞上皮細胞の分子生物学的機能特性に及ぼす影響に関する研究
（研究番号 S2004-8）

2．キーワード：1）癌免疫療法（cancer immunotherapy）
2）肺水腫（pulmonary edema）
3）肺胞上皮水分クリアランス（alveolar fluid clearance, AFC）

3．研究者氏名：杉田　真・医学部・講師・呼吸機能治療学（呼吸器外科）
（現 アストラゼネカ株式会社）

4．研究目的

【背景】遺伝子組み換え技術によって作成されたインターロイキン－２（IL－２）製剤を用いた免疫療法が、腎細胞癌、悪性黒色腫、血管肉腫等の悪性腫瘍と、その転移巣に対して、著明な抗腫瘍作用を有することが知られている。しかし、IL－２製剤投与では、25％程度の確率で重篤な肺水腫を発症させ、この副作用が大きな障壁となっている。これまでの基礎研究では、IL－２の全身投与は急性肺傷害を惹起し、これがこの肺水腫成立の原因である可能性が示唆されてきた。しかし、詳細なメカニズムに関してはいまだに不明である。一方、近年の研究により、肺胞上皮細胞の Na イオン輸送に依存する水分輸送能が、肺の水分バランス、さらには肺水腫からの回復に中心的な役割を担っていることが明確になってきている。また、肺胞上皮細胞の機能特性は各種サイトカインに影響を受け、肺胞上皮細胞には IL－２受容体が存在し、免疫担当細胞の制御を受ける可能性が示唆されている。

【研究目的】IL－２投与が肺胞上皮細胞の分子生物学的機能特性に及ぼす影響を詳細に検討し、より安全な免疫療法の確立を目指す事である。第一に、生理学的手法を用いて、IL－２投与が肺胞上皮細胞の水分輸送能に及ぼす影響を検討し、第二に、これら生理学的影響に関して、その詳細なメカニズムを分子生物学的に解明することである。そして、究極的には、より安全な癌免疫療法の確立を目指す事である。

5．研究計画

【実験項目 1】ラットを用い、100～20000 IU の組み換え IL-2 を気道内に投与し、肺胞水分クリアランスを用いて、肺胞上皮細胞の水分輸送能に及ぼす影響を解析する。肺胞水分クリアランスの測定は、肺循環の影響を除外するために、ラットを犠牲死させた直後に心肺を一塊として摘出し、体外（*ex vivo*）にて行う（以後の実験項目でも同様の方法を用いる）。

【実験項目 2】IL-2 投与によって亢進する肺胞水分クリアランスが、β受容体刺激に関与するか否かを明らかにする目的に、プロプラノロールを IL-2 と同時に投与して、肺胞水分クリアランスに対する影響を解析する。

【実験項目 3】IL-2 とβ受容体刺激薬であるテルブタリンを同時に投与して、肺胞水分クリアランスに対する影響を解析する。

【実験項目 4】肺胞水分クリアランスは、肺胞上皮細胞の Na チャンネルに部分的に依存する。よって、IL-2 投与が Na^+ channel に及ぼす影響を解析する目的にて、Na^+ channel 阻害薬のアミ

ロライドを同時に投与して肺胞水分クリアランスを測定する。

6．研究成果

【実験項目1】10000 IU以上のIL-2の気道内投与によって肺胞水分クリアランスが有意に亢進することが明らかになった。また、肺胞水分クリアランスの亢進するレベルは、β受容体刺激薬であるテルブタリン投与と同レベルであった。

【実験項目 2】β受容体刺激薬のテルブタリンは、プロプラノロールの同時投与によって、肺胞水分クリアランスに及ぼす影響は消失する。一方、プロプラノロールはIL-2の肺胞水分クリアランスに及ぼす影響に変化を及ぼさなかった。

【実験項目3】IL-2とβ受容体刺激薬であるテルブタリンを同時に投与しても、相乗的効果は示さなかった。

【実験項目 4】Na^+ channel の阻害薬であるアミロライドは、IL-2 によってもたらされる肺胞水分クリアランスの亢進を有意に低下させた。しかし、その低下は、テルブタリンに対する効果よりも有意に小さかった。

7．研究の考察・反省

これまでの臨床報告、研究報告によると、IL－２を血管内に投与した場合、肺水腫が惹起されることが明らかになっていた。しかし、その詳細なメカニズムに関しては不明であった。今回の研究では、IL－２を気道内に直接投与し、さらに、*ex vivo*にて肺胞水分クリアランスを測定することにより、IL－２が血管内皮細胞に及ぼす影響を除外し、肺胞上皮細胞の水分輸送機能に直接及ぼす影響に関して詳細に検討することが可能であった。その結果、IL－２は肺胞上皮細胞の水分輸送能を亢進させることが明らかになった。さらに、この亢進のメカニズムは、β受容体を介さないことが示唆された。

本研究の結果は、これまでの知見と矛盾するようだが、すでに発表されている研究では、IL－２の血管内投与の影響を検討したものであり、血管内皮細胞の障害が大きく関与していると推測できる。すなわち、IL－２の全身投与は、血管内皮細胞障害を惹起し、血管透過性が亢進する事に起因する過性亢進型肺水腫が、その病態の本体である可能性が高いと考えることが可能である。そして、本研究の結果は、この内皮細胞障害に対して、肺胞上皮細胞は水分輸送能を亢進させて肺水腫の病態に対して保護的な作用を有している可能性が高いことを示唆する。今後、血管内皮細胞に及ぼす影響に関する研究を本研究と並行して行うことにより、より詳細な IL－２投与による肺水腫発生のメカニズムの詳細が明らかになることと思う。

反省点

a) 本研究は、国内および国外の学会で発表済みである。ただし、論文の形式ではいまだに発表がない。現在、英文を作成中である。英文論文の完成が遅れており、大変に申し訳ないと思っている。

b) 予定していた実験の約70%のみが達成されており、いまだに30%程度が未達成である。今後、可及的にかつ慎重に残りの実験を遂行するように予定している。

1．研究課題名：異なる感覚情報の大脳新皮質における統合機序及びその生後発達に関する研究（研究番号 S2004-9）

2．キーワード：1）大脳皮質味覚野（gustatory insular cortex）
2）大脳皮質口腔体性感覚野（oral somatosensory cortex）
3）膜電位振動（voltage oscillation）
4）カフェイン（caffeine）
5）ラット（rat）

3．研究代表者名：吉村　弘・医学部・助教授・顎口腔機能病態学（口腔科学）

4．研 究 目 的

口腔領域における広義の味覚認知とは、純粋な基本味覚情報に、触覚、温度覚、浸透圧、刺激覚、などが加わった複合感覚として認識されるものと考えられる。この複合味覚認知や嗜好性は成長過程で一様ではなく、発達期前後で変化する。カフェインは嗜好性を有する苦味物質であるが、一方で強力な中枢神経作動薬としても知られており、脳における神経回路の機能を顕在化させるための有用な薬物である。我々の以前のカフェインを用いた研究により、情報伝達の場であるシナプスにおいてNMDA受容体-Ca^{2+}誘発性Ca^{2+}放出の機能連関が生後発達に伴って強化されることにより、大脳新皮質に振動性活動の発現することが明らかになった（Yoshimura, et.al, 2001、2002、2003）。そこで、本研究において、感覚認知と深くかかわっていると予想されている同期性膜電位振動現象を視点として、大脳皮質味覚野と口腔体性感覚野に焦点をあて、これら二つの大脳皮質間における機能的神経ネットワークの形成機序および生後発達にともなう機能獲得の様式について調べた。

5．研 究 計 画

＜平成15年度＞

内因性信号計測法を用いて、大脳皮質における味覚野を同定した。つぎに、電気生理学的計測と膜電位感受性色素を用いた光学的計測実験を相補的におこない、味覚、口腔体性感覚などの神経性入力がいかにして大脳皮質味覚野－口腔体性感覚野間の神経回路の発達・形成を促すのかについて、ラット脳スライスを用いて調べた。

＜平成16年度＞

味覚情報と視覚情報が融合する可能性のある脳梁膨大後野に注目し、この領域に存在する振動源の性質を調べた。さらに、異なる感覚情報が融合するために、膜電位振動現象がどのように関わっているのかを調べ、異なる感覚情報の統合機序や神経回路網発達の関係などを探った。

6．研究成果

我々は、温度、触、圧などの体性感覚情報と味覚などの化学感覚情報の異なる感覚情報が、口腔という閉じた環境の中で融合することに注目した。内因性信号計測法という新手法をもちいて、2種類の化学物質NaClとSucroseに関して、化学感覚情報の空間的符号化が大脳島皮質に存在することを明らかにした（NeuroReport 2004, Yoshimura et al)。

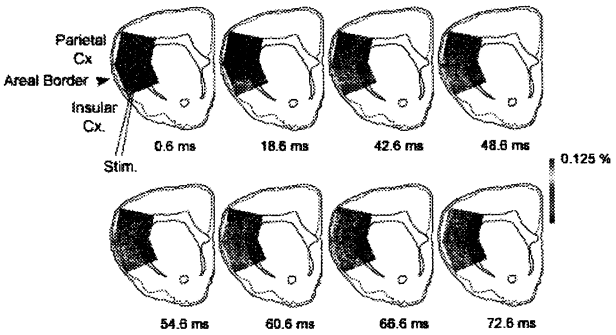
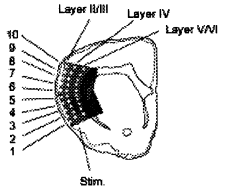


図 1　大脳皮質味覚野から大脳皮質口腔体性感覚野への信号伝播。
ニューロン膜電位の疑似カラー化をおこなった。赤色はニューロンの興奮を示している。信号強度は大脳皮質浅層で最も大きかった。味覚野を発した信号は、大脳皮質の浅層、中間層、深層をそれぞれ側方に伝播した。(Brain Research 2004, Yoshimura et al.)

脳における情報処理に重要な役割を演じているグルタミン酸受容体を、カフェインを用いて活性化させるという手法を用いて、味覚野-口腔体性感覚野間の情報伝播の動的な振る舞いを観察した。図1に示すように、味覚野からの信号が口腔体性感覚野へ伝播した。その後、口腔体性感覚野において振動性信号配信が出現した。味覚-口腔体性感覚野間の情報伝達は双方向性であり、また、振動現象は口腔体性感覚野で引き起こされることがわかった（図2)。ところが、幼弱期においては、味覚情報と口腔体性感覚情報を融合させるネットワークが形成されていなかった。この振動発生装置は生後発達に伴って獲得されることがわかった。



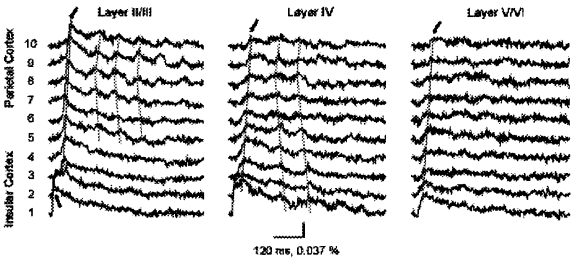


図 2　大脳皮質味覚野（島皮質)-口腔体性感覚野間の神経情報の往来
(Brain Research 2004, Yoshimura et al.)

次に、脳における情報処理活動の中心的役割を演じているNMDA受容体に注目し、細胞内カルシウム動態を調べたところ、幼弱期においては、NMDA受容体と細胞内カルシウム放出の機能連関が未発達で、成長に従ってこの機能連関が強化され、味覚-口腔体性感覚野間の双方向性情報伝達が形成されてくる、ということが示唆された。これらの結果より振動活動に依存する味覚-口腔体性感覚の情報連絡強化のメカニズムが示唆された（図3)。

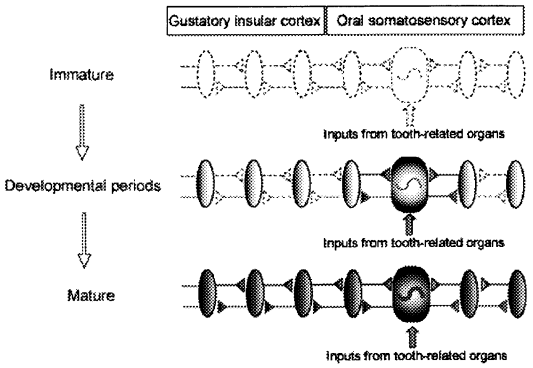


図3　振動活動依存性皮質情報伝播の強化機序
（上段）幼弱期；振動装置未発達。
（中段）発達期；振動装置が形成され、NMDA受容体依存性信号の配信。
（下段）成熟期；味覚野-口腔体性感覚野間の神経連絡の強化。

味覚情報と他の感覚情報が融合する可能性のある脳梁膨大後野にも振動装置が存在していることがわかった。脳梁膨大後野の振動装置が、中継装置として情報のやりとりを強化している可能性が示唆された（図 4）。

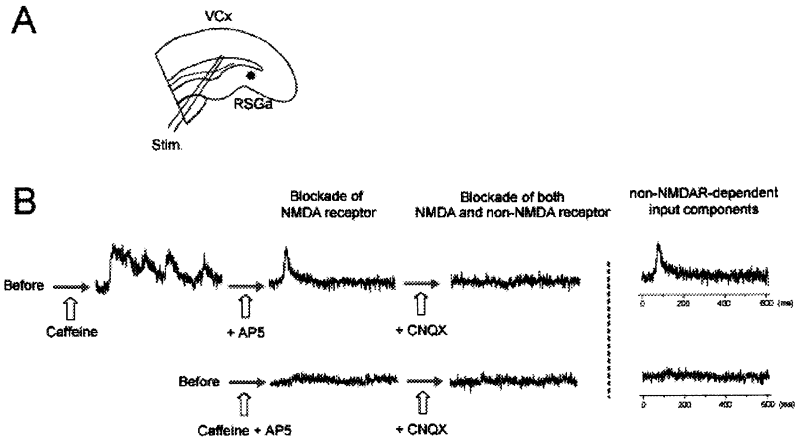


図4　脳梁膨大後野における振動装置の役割。（A）大脳皮質および脳梁膨大後野を含むスライス。刺激および記録の位置を図示した。(B) カフェイン存在下で脳梁膨大後野における膜電位振動を引き起こすと、non-NMDA受容体依存性の信号伝播が強化された。感覚情報をより遠方に伝播させるために、振動性活動が必要であった。（Brain Research 2005 Yoshimura et al.）

7．研究の考察・反省

「異なる情報を処理する大脳皮質間の連絡を強化するために、皮質振動中継装置が存在し、その振動装置は発達期に形成され、経験依存的にネットワークを形成する。」という概念は、今回の研究により始めて提唱された。従来の神経可塑性の概念をシナプスレベルから大脳皮質間ネットワークレベルに発展させることができた。

1．研究課題名：ヒト口唇小唾液腺由来の幹細胞の同定（研究番号S2004-10）

2．キーワード：1）唾液腺（salivary gland）
2）再生医療（regenerative medicine）
3）組織幹細胞（tissue stem cell）

3．研究者氏名：河南　崇典・医学部・助手・血液免疫制御学

4．研究目的

現在、国内におけるドライアイ、およびドライマウス(口腔乾燥症)の患者数は800万人以上と推定されている。これほど多数の患者数にもかかわらず、ドライアイ、ドライマウスは病気としての認識が低く、その治療の中心は対症療法にとどまっている。この原因として、シェーグレン症候群(以下SS)、頭頸部領域への放射線治療、種々の薬剤などによる唾液腺・涙腺の分泌低下があげられる。現在のところ、これらの対処として、人工唾液、人工涙液の使用や、残存する腺房細胞の分泌能を促進する薬剤が使用されている。しかし、腺組織の障害が軽度で分泌が低下した患者に対しては分泌を促進することも可能であるが、一度萎縮し、不可逆的な障害を受けた唾液腺、涙腺機能の回復は現在のところほとんど期待できず、失われた腺組織の再生、機能回復を目的とした根治的治療法が強く望まれている。近年、組織の再生において成体組織幹細胞に高い注目が寄せられている。動物の体を構成する多種多様な組織細胞の多くは恒常性の維持のために常に更新され続ける。このような個体の維持のため新たな細胞を供給する源となる細胞が組織幹細胞である。再生医療の材料として組織幹細胞は、自分自身の組織から単離できるので生命倫理問題が少なく、また移植による免疫拒絶を心配する必要がないといった利点がある。そこで本研究では、唾液線分泌障害に対する唾液腺組織幹細胞の細胞治療を目指し、ヒト唾液腺組織より組織幹細胞を分離・同定し、増幅する技術を確立し、唾液腺の再生医療を創始することを目的とした。

5．研究計画

個体中に極少数しか存在しない唾液腺幹細胞を純化するため、FACSと蛍光標識モノクローナル抗体を用いた精度の高い細胞分離法を確立し、その機能解析を行う。

A．ヒト口唇小唾液腺からの唾液腺培養細胞の初代培養

1)．生検時に得られたヒト口唇小唾液腺組織を細切し、角化細胞用無血清培地(Defined Keratinocyte SFM, Invitrogen) にインシュリン, EGF, FGF などからなるGrowth supplementを加えた無血清培地を用い、collagen type Ⅰコートしたプレートにて培養する。

2)．無血清培地を2, 3日ごと入れ替え、組織周囲から培養細胞が形成されてから7

ー14 日間培養し、継代を行う。(本研究においては、継代 3 回までの細胞を使用した。)

B．幼若な細胞にのみ発現する EGF-R を指標とした FACS による分取

ヒト培養唾液腺上皮細胞は、継代初期に EGF-R を発現するが、経時的にその発現を徐々に低下させ、継代後期に陰性化し、それに伴いα-amylase 1 の発現を増大させる機能分子の経時的な発現の変化を示す。これは培養細胞中の唾液腺幹細胞の分化の可能性を示唆するものである。培養唾液腺上皮細胞が継代初期の幼若な細胞にのみ EGF-R を発現することから EGF-R をマーカーとし、FACS によるソーティングを施行する。

C．side population(SP)法を用いたヒト唾液腺初代培養上皮細胞からの唾液腺組織幹細胞の分取

1）表面マーカーに依存しない、新しい幹細胞純化法として使用され始めた DNA 結合色素 Hoechst33342 を排出する能力を指標として分離する SP 法を施行し、幹細胞が高い割合で存在していると考えられる SP 細胞と non-SP 細胞 (main population (MP) 細胞)を採取し、RT-PCR をもちいて各種幹細胞マーカーの発現を解析する。幹細胞マーカーとしては次の分子について検討を行う。
collagen(線維芽細胞マーカー), amylase(腺房細胞マーカー), EGF-R(導管細胞マーカー), Bcrp1(SP 表現型の決定因子), c-Kit(血液, 膵臓, 肝臓の幹細胞マーカー), CD34(血液, 内胚葉前駆細胞, 筋幹細胞マーカー), nestin(外胚葉、神経、膵の前駆細胞マーカー), Oct4(内部細胞塊や ES 細胞など未分化な細胞に発現), Bcl-2(神経 sphere 細胞のマーカー), clusterin, PSCA(前立腺芽, 胃の幹細胞マーカー)

2）SP 細胞と MP 細胞で発現する遺伝子群を Real-time PCR にて定量的に比較解析し、ヒト唾液腺幹細胞を選択的に認識するマーカーの検索を行う。

D．ヒト唾液腺培養上皮細胞からの幹細胞の分離・同定

より純度の高い幹細胞分離を行うにはいくつかのマーカーを組み合わせる必要がある。そこで

1）EGF-Rをマーカーとし、分取した幼若な細胞群と、SP細胞の遺伝子発現を比較し、どちらの細胞群においても発現している、特異的なヒト唾液腺組織幹細胞のマーカーを検索する。

2）食物の消化・吸収・代謝という一連の「消化機能」は腸管・肝臓・膵臓・唾液腺など複数の臓器によって担われている。幹細胞システムの制御機構が「機能」の恒常性維持を目的としているならば、消化器官において、各臓器間共通の多能性幹細胞が存在するのではないかという仮説が考えられる。この考えに基づき、他の消化器官において同定された幹細胞マーカーのうち、c-Kit, c-Met (hepatocyte growth factor receptor)をさらなる分離マーカーとして使用する。これらのマーカーを組み合わせ、より純度の高い、ヒト唾液腺培養上皮細

胞からの組織幹細胞の分離・同定を行う。

6．研究成果

ヒト口唇小唾液腺培養細胞中の唾液腺組織幹細胞を同定するため、ひとつの方法として、唾液腺初代培養細胞の特異的な細胞表面抗原と機能分子の検索を行い、ヒト唾液腺培養細胞が、経時的に機能分子の発現を変化させること、また、継代初期の幼若な細胞には、他の幹細胞において発現が認められるPSCA、clusterinなどの幹細胞マーカーが発現していることを明らかにした。もうひとつのアプローチとして、細胞表面抗原に依存しない、幹細胞に共通した性質と考えられる色素排出機能を利用したSP法を施行し、組織幹細胞に富んだ分画を分取し、その細胞群に特異的に発現している遺伝子を検索した。その結果、ヒト唾液腺培養細胞には約0.5ー0.9%のSP細胞集団が存在し、この組織幹細胞に富んだ分画と考えられるSP細胞群においてもまた、特異的なPSCAの発現が確認された。PSCA発現をReal-time PCRにて定量したところ、non-SP分画細胞に比べ、SP分画細胞では約20倍高い発現を示した。この方法においても、前立腺の前駆／幹細胞マーカーと考えられるPSCAの特異的な発現が認められた事から、ヒト唾液腺培養上皮細胞はSP細胞群に組織前駆／幹細胞を含み、PSCAがそのマーカーとなる可能性が示唆された。

7．研究の考察・反省

継代初期の唾液腺培養細胞の表面マーカー検索と、表面マーカーに依存しない幹細胞に共通した性質を利用したSP法と、2つの異なった方法を用い、それぞれの細胞群における遺伝子発現解析を行った。その結果、両者に共通して発現するヒト唾液腺組織前駆／幹細胞マーカー候補分子としてPSCAを見いだした。PSCAは前立腺の発生・再生過程において、その発現動態が変化する分子として報告されている。前立腺の発生と分化に特異な発現を示すPSCAが唾液腺上皮細胞において発現する意味は何であろうか？前立腺は泌尿生殖洞の内胚葉由来の上皮組織から出芽と分枝を繰り返し形成される。唾液腺もまた頬上皮から上皮芽が形成され、口腔上皮の増殖と間葉との相互作用にて発生、分化、増殖、形態形成を経て成熟する。細胞の中で特定の物質を合成し、細胞体外へ放出する「腺細胞」の大部分は上皮に由来していることから、PSCAは、上皮細胞から腺構造が形成される過程をたどるよい指標となるかもしれない。今後、ヒト唾液腺上皮細胞中のPSCAの動態を明らかにする事で、特異的なヒト唾液腺組織幹細胞の同定および唾液腺の発生、再生過程について更なる知見が得られるものと考えている。本研究の成果は唾液腺の再生医療の端緒を開くばかりでなく、発生・分化制御の解析により、多臓器の再生医療への応用に繋がる可能性も含んでいる。

1．研究課題名：Chorea-acanthocytosis の発症機序に関する研究（研究番号 S2004-11）

2．キーワード：1）horea-acanthocytosis
2）常染色体優性遺伝（autosomal dominant heredity）
3）遺伝性舞踏病（hereditary chorea）
4）CADASIL

3．研究者氏名： 斉木臣二・医学部・助手・脳脊髄神経治療学（神経内科学）
（現 Department of Medical Genetics, Cambridge Institute for Medical Reserch, University of Cambridge）

4．研究目的

neuroacanthocytosis［chorea-acanthocytosis（以下 ChAc），McLeod 症候群（以下 MS）、abetalipoproteinemia、Huntington's disease-like 2 with acanthocytosis（以下 HDL2 associated with acanthocytosis）］は basal ganglial degeneration による extrapyramidal features 及び peripheral acanthocytosis を特徴とする疾患群とされ、わが国では最も ChAc の頻度が高い。ChAc の病態機序解明は、neuroacanthocytosis だけでなく、phenotype の類似する Huntington 病（以下 HD）などの多くの大脳基底核変性疾患の機序解明に繋がることが期待され、意義深いものと思われる。今回我々は ChAc 常染色体劣性遺伝家系において同定された responsible gene である CHAC（その後 VPS13A と改称された）の機能を、我々が世界で初めて見出した常染色体優性遺伝家系（以下 AD-ChAc）における変異の解析により明らかにする。また neuroacanthocytosis を含む遺伝性舞踏病は時に臨床的な鑑別診断が困難であるが、VPS13A 遺伝子産生タンパク chorein の機能を生検筋標本を用いて免疫組織学的手法にて解析し、他の遺伝性舞踏病との鑑別に用いることができるかを検討する。さらに ChAc mutation analysis を実行する中で、exon に mutation が集積する巨大な responsible gene の mutation screening を cDNA を用いて行う手法を確立したため、同様の神経変性疾患でも cDNA を基盤とした遺伝子解析を行い、診断的意義を確認する。

5．研究計画

1）AD-ChAc2 家系における遺伝子変異同定、他の neuroacanthocytosis 責任遺伝子との関連の検討
2）患者と他疾患の骨格筋組織における独自に合成した抗原ペプチドに対する 3 種類の抗体を用いた CHAC protein（chorein or VPS13A protein）発現の免疫組織学的検討（患者骨格筋、他疾患患者、正常コントロールとの比較及びミトコンドリア呼吸鎖異常の検討）

3）完全長 cDNA が 10kb を超える巨大な responsible gene の mutation analysis を他の神経変性疾患（CADASIL、responsible gene: Notch3）での検討

4）ChAc における不随意運動に対する $5\text{-}HT_{1A}$ agonist である tandospirone citrate（以下 TC）内服効果の評価

6．研究成果

1）A）AD-ChAc 2家系においてまったく新しい VPS13A 変異を同定し、AR-ChAc での責任遺伝子 CHAC の変異が AD-ChAc の原因にもなりうることを証明した。これらは先天性ミオトニア（Becker 型、Thomsen 型）と同様に、常染色体劣性遺伝でも常染色体優性遺伝でも同一の疾患が発症しうることを示し、mutant chorein が、dominant negative effect を獲得する可能性を示唆する。

B）我々の同定した AD-ChAc 2家系は、Walker らが報告した AD-ChAc とは genotype、phenotype とも異なることを報告した。

Walker RH, et al. Neurology 2003;61:1002-4

2）A）抗 chorein 抗体によるヒト骨格筋組織の染色が、ATP 染色、NADH-TR 染色と同様のパターンを呈することを見出し、ChAc 患者骨格筋では筋膜の chorein 発現が不十分であり、他の遺伝性舞踏病との鑑別が可能であることを証明した。また chorein 機能不全は筋線維内にも及んでいた。患者筋生検組織にミトコンドリア機能異常を見出すことはできなかった。

B）研究者及び共同研究者酒井宏一郎（現順天堂大学脳神経内科及び藤田保健衛生大学神経内科客員教授、東京臨海病院内科部長）は上記の業績が認められ、下記英文教科書の分担執筆を行った。

Saiki S and Sakai K. Neuroacanthocytosis. In: Jankovic J, Tolosa E, eds. Parkinson's disease and movement disorders. 5th ed. Philadelphia, PA: Lippincott Williams & Wilkins (in press)

C）研究者は上記の業績が認められ、下記国際シンポジウムの organizer を務めた。

Third International Neuroacanthocytosis Symposium: The Asian Perspective, Kyoto, Japan, October 28th 2006

3）ChAc 同様に成人期発症で、かつ responsible gene が約 10kb の CADASIL 家系を臨床的に同定し、患者皮膚から抽出した mRNA を用いて mutation search を行ったところ、全く新しい type の mutation を同定した。本疾患は既存の手法では genome DNA を用いた PCR-SSCP などの煩雑な手法による mutation analysis が必要であったが、迅速かつ簡便に、また electron microscopy による病理学的検討よりも信頼性の高い遺伝子診断を行うことができることを報告した。

4）患者母集団が小規模であったため、case control study または randomized controlled trial は困難であり、TC の治療効果の paper を英文にて publish することはできなかった。

7． 研究の考察・反省

1）mutation screening は今回実施した mRNA 検索に続き、genome DNA の検索を行う流れで、大半の mutation を証明できるが、数 exon を含む large deletion については直接的に genome DNA を用いた Southern blotting によって証明する必要があると考えられた。研究者は上記手法を Wellcome Trust Human Genetics Centre, Oxford University 及び Department of Neurology, University of Munich と共同で、継続的に施行していく予定である。

2）抗 chorein 抗体による骨格筋染色では、ChAc にのみ異常を認め、他の遺伝性舞踏病では異常を認めなかったことから診断的価値を有するものの、ChAc と HD などの他の遺伝性舞踏病との common pathway を明らかにすることはできなかった。Oxford University の AP Monaco らの group は同様の免疫組織学的検討を患者赤血球膜抽出蛋白にて行い、類似した診断的価値を報告している。

Dobson-Stone C, et al. Chorein detection for the diagnosis of chorea-acanthocytosis. Ann Neurol 2004;56:299-302.

3）抗 chorein 抗体による免疫染色では、筋膜が不連続で時に deposit を認めた。これは VPS13A の homology 検索からの trans-Golgi network 及び early endosome または lysosome 間の membranous trafficking に関与するという蛋白機能予想に矛盾しないと考えられた。現在 VPS13A の modified gene constructs 及び RNAi などの手法を用いて、培養細胞を用いて正常機能を検索している。HD, Parkinson's disease (PD)において、様々な角度からの membranous protein trafficking の機能異常が、misfolding protein の集積に関与するとの知見が出されているが、本疾患剖検脳でも、ubiquitin, alpha-synuclein 陽性の inclusion body などを検出することはできなかった。これは dominant-negative effect による gain-of-function function よりも、むしろ正常 chorein 機能低下による loss-of function effect を支持する所見と考えられた。研究者は現在、多面的な神経変性疾患と vacuolar protein sorting の関連を microarray 及び RNAi screening などの網羅的手法に加え、あらゆる動物モデルを用いて検索を進めている。

4）現在 levetiracetam の hereditary choreic diseases における choreic movement の効果を Department of Neurology, Mount Sinai Medical School, NY, USA 及び Dept of Neurology, University of Munich, Germany などとの多施設間共同研究にて行う予定である。

1．研究課題名：ミトコンドリア障害に関与する活性酸素生成酵素の研究（研究番号 S2004-12）

2．キーワード：1）ミトコンドリア（mitochondria）
2）パラコート（paraquat）
3）活性酸素（reactive oxygen）
4）フリーラジカル（free radical）
5）細胞障害（cytotoxicity）

3．研究者氏名：島田ひろき・医学部・講師・分子細胞形態科学（解剖学）

4．研究目的

パラコート(1,1'-dimethyl-4,4'-bipyridinium dichloride)は安価で即効性のある除草剤として世界中で使用されているが，人体への毒性は強く，多量の摂取は多臓器障害を引き起こし致死的なものとなる。現在，誤飲や自殺企図での事故を防ぐため，催吐剤や低毒性ジクワットを添加した製剤が使用されるようになってきたが，中毒患者に対する根本的な治療法はいまだ確立されていない。また，近年，Parkinson病のリスクファクターとしても注目されているが，その作用機構は解明されていない。

従来，パラコートの細胞毒性機構は小胞体薬物代謝系酵素によるものとされてきたが，我々はこの機構がミトコンドリア外膜に局在する新規酵素NADH-quinone oxidoreductase$_m$(NQO_m)によって引き起こされるというミトコンドリア障害説を電顕細胞化学的，生化学的に証明してきた。即ち，パラコートはNQO_mによってNADHを電子供与体として還元されてパラコートラジカルとなり，引き続き生成する各種活性酸素種がミトコンドリアを障害して細胞死へ至らしめるという説である。

本研究の目的はNQO_mの構成タンパク質成分を解析してその本態を明らかにすることである。

5．研究計画

＜全体計画＞

1）ラット肝よりミトコンドリアを単離し，抗体，阻害物質を用いてNQO_m活性に与える影響を形態学的，生化学的に調べ，反応機構を解析する。

2）ラット肝ミトコンドリアよりNQO_mを精製し，外膜局在性タンパク質の各種抗体によるウェスタンブロット等を行い，その構成タンパク質を同定する。

＜平成15年度＞

1）ラット肝より単離したミトコンドリアで，パラコート由来の活性酸素生成を測定し，各種薬剤，抗体を用いて酵素成分を解析する。

2）単離ミトコンドリアより調製した外膜から，界面活性剤処理およびクロマトグラフィーを行って酵素活性陽性成分を抽出・分画する。

＜平成16年度＞

3）酵素画分に対する各種薬剤，抗体の影響を解析する。また，免疫沈降を行って酵素成分を解析する。

4）酵素画分のZymographyにより酵素蛋白を特定し，ウェスタンブロット法により酵素成分を解析する。

6．研究成果

1）ラット肝臓より単離したミトコンドリアをガラス上に吸着させ，10 mMパラコート，2 mM NADHを基質として反応させた。生成した superoxide の不均化反応によって生ずる過酸化水素を，dichloro fluorescin-diacetate(DCFH)蛍光法によって検出すると，パラコートまたはNADH単独では，ブランクと比べて蛍光強度に差は見られなかったが，両者を同時に添加すると蛍光を発する数，強度とも増加した。この反応はアニオンチャンネルブロッカーである4,4'-diisothiocyanatostilbene -2,29-disulfic acid (DIDS)， voltage-dependent anion channel (VDAC)の結合物質であるN,N'-dicyclohexylcarbodiimide(DCCD)，および抗VDAC抗体によって抑制された。

2）ミトコンドリア外膜より 1% Triton X-100/1%デオキシコール酸および 0.06% SDS/0.1% NP-40の２段階処理で活性成分を抽出し，DEAE-陰イオン交換クロマトグラフィーにより酵素画分を調製した。

3）酵素画分にパラコートとNADHを基質として反応させたときに生ずるsuperoxideをnitroblue tetrazorium(NBT)還元法により測定したところ，単離ミトコンドリアでの実験と同様に，NADHとパラコートの同時添加により活性が現れ，DIDS，DCCDおよび抗VDAC抗体によって抑制された。また，抗VDAC抗体による免疫沈降を行い，画分中のVDACを減少させたところ，活性は抑制された。

4）酵素画分をnative-ポリアクリルアミド電気泳動(PAGE)し，NBT法によるzymographyを行ったところ，分子量500 kDaに活性が現れた。このバンドを切出してSDS-PAGEにかけたところ，複数の蛋白バンドが検出された。抗VDAC抗体でウェスタンブロットしたところ，抗体に反応する蛋白質が含まれていた。

7．研究の考察・反省

本研究より，NQO_mが１)NADHを電子供与体としてパラコートを還元してラジカルを生成すること，２）分子量500 kDaの外膜に結合した蛋白複合体であること，３）複合体の成分に外膜イオンチャネルのVDACが含まれていることが明らかとなった。

VDACはミトコンドリアの外膜に存在し，アデニンヌクレオチドトランスロケーター(ANT)，シクロフィリンDなどと複合体を形成して，膜電位の維持やアポトーシスに関連しているといわれている。最近になって，細胞膜型VDACに酸化還元酵素活性をもつという報告がなされているが，ミトコンドリアのVDACが酸化還元酵素として働いているという報告は今だなされていない。

現在（平成17年度），実際に細胞内でVDACがパラコート還元酵素としてその毒性に関わっているかを調べるため，HeLa細胞へのプラスミドVDAC遺伝子導入またはRNAi法によるVDAC遺伝子のノックダウンをおこなって解析している。その結果，高発現細胞ではパラコートによる活性酸素生成が増加して毒性が増すこと，逆にノックダウンすると活性酸素生成が低下して毒性が抑えられるというデータを得ている（投稿中）。また，NQO_mはフラノナフトキノン系物質の抗癌作用にも関わっており，パラコートと同様にVDACがその活性に関与していることが明らかとなっている（印刷中）。

NQO_m活性がVDAC単独によるものなのか，ANTやシクロフィリンDなど他の成分を必要とするのかは今後の課題であり，さらに解析を進める必要がある。また，パラコートとParkinson病との関連性においてNQO_mの関与があるかどうかを神経細胞等を用いて調べていく予定である。

8．研究発表

Simamura E, Hirai K-I, Shimada H et. al. Furanonaphthoquinones cause apoptosis of cancer cells by inducing the production of reactive oxygen species by the mitochondrial voltage-dependent anion channel. Cancer Biology and Therapy 2006(in press)(MLDB)

1．研究課題名：Gene33/mig-6による心肥大シグナルの制御（研究番号S2004-13）

2．キーワード：1）細胞内情報伝達（intracellular signal transduction）
2）心筋細胞（cardiac myocytes）
3）心肥大（cardiac hypertrophy）
4）上皮成長因子受容体（epidermal growth factor receptor）

3．研究者氏名：竹田健史・医学部・助手・循環制御学（循環器内科学）

4．研究目的

心筋梗塞や心筋炎などの心疾患では、限りある心筋細胞の一部がネクローシスやアポトーシスによって失われ、結果として残存する心筋細胞に過度の負荷がかかるようになる。この圧負荷、容量負荷などの刺激に対応して、心臓では収縮力を増すために個々の心筋細胞を肥大させ心機能を維持しようとする。しかし過剰な負荷によりこの適応反応が破綻し、心肥大から心拡大、心不全へと移行する。この心肥大過程には、様々な生理活性化ペプチド(アンジオテンシンIIやエンドセリン-1など)が関与することが知られているが、近年これらのシグナルが、最終的には上皮成長因子(EGF)受容体のトランスアクチベーションに集約されることが報告されており、心筋EGF受容体シグナル伝達系の阻害が心肥大抑制の新たなターゲットとして考えられている。

Gene33（human homologはMig6と呼ばれる)は、低酸素刺激や生理活性化ペプチド（アンジオテンシンIIや、EGF、インシュリンなど）の刺激で急速に誘導される前初期遺伝子の一つとして当初考えられていたが、近年EGF受容体の負の制御因子として作用し、この遺伝子の導入によりEGF受容体を過剰発現している癌細胞の増殖を抑制できることが報告された。しかしながら、心筋におけるGene33の発現や機能に関しては、これまでに全く報告されていない。最近我々は、ラットを用いた心筋虚血再灌流モデルにおいて、再灌流時に心臓で*gene33*遺伝子の発現が亢進していること見いだした。本研究の目的は、Gene33の心筋細胞内での機能を、特に心肥大シグナル伝達経路に注目して解析することである。

5．研究計画

Gene33は、Ack-1 homology domain(AH domain)を介してEGF受容体の活性化を阻害することが報告されている。そこで、心筋細胞内にこのAH domainを導入する事で、心肥大シグナルに重要な役割を果たすHB-EGFによるEGF受容体の活性化を抑制できるか否かを最初に検討する。さらに、*gene33*遺伝子を心筋細胞へ導入し、一過性発現による心肥大シグナルへの影響を解析する。また、Gene33を安定に発現する細胞株の樹立も試みる。最後に、この遺伝子発現の調節機構を明らかにするために、ラットゲノ

ム DNA から、上流プロモーター領域をクローニングし、レポーターアッセイによる転写調節領域の解析を行う。

6．研究成果

① 新生児ラット初代培養心筋細胞やラット心筋細胞株 H9c2 を用いた Real-time PCR による遺伝子発現解析や Western blot による蛋白発現解析により、Gene33 は酸化ストレスや心肥大を惹起するペプチド刺激に応答した発現誘導が起きることを明らかにした。

② Protein transduction domain (PTD)融合蛋白質として VP22 を利用した Gene33 の AH domain をバクテリアの発現系により大量発現し、この VP22-AH domain の蛋白精製に成功した。VP22-AH domain は、培地へ添加後 30 分以内に VP22 と同様の効率で、心筋細胞内への導入が観察された。導入された VP22-AH domain は、細胞質と核へ局在することが明らかになった。

③ 心筋細胞への HB-EGF 刺激により、EGF 受容体の活性化を介して速やかに下流の MAP Kinase ファミリーである ERK1/2 及び JNK1/2 の活性化と、さらに下流の転写因子 Elk1 や c-Jun の活性化が起きるが、VP22-AH domain の導入によるこれらの抑制効果は認められなかった。

④ プラスミドベクターを用いた *gene33* 遺伝子の一過性発現により、H9c2 細胞において Elk1 の活性化が見られた。さらに、心房性ナトリウム利尿ペプチド(ANP)遺伝子のプロモーター領域を組み込んだルシフェラーゼベクターを作製し、レポーターアッセイによる ANP 遺伝子の発現誘導活性を測定したところ、Gene33 を一過性に発現した心筋細胞において有意に ANP プロモーター活性の上昇が認められた。これらの結果は、心筋細胞において Gene33 は、心肥大シグナルに対して負の制御機構に働くのではなく、むしろ心肥大の進行に関与することを示唆した。

⑤ H9c2 細胞へのプラスミドベクターによる遺伝子導入効率は低く(30%以下)、さらに導入試薬による毒性が、微量なリン酸化蛋白の高感度アッセイに影響している可能性が考えられたため、安定形質発現細胞株の樹立を行った。*gene33* 遺伝子発現ベクターが保持する *neo* 耐性遺伝子を利用し、抗生物質 G418 の添加による薬剤スクリーニングを行い、最終的に発現レベルの異なる 4 つの Gene33 安定発現 H9c2 細胞株の樹立に成功した。現在、この樹立した細胞株を用いて心肥大シグナルへの関与について解析中である。

⑥ 酸化ストレスや HB-EGF 刺激による *gene33* 遺伝子発現の調節機構を解析するために、ラットゲノム DNA から、この遺伝子の転写開始点より上流約 5kbp の領域をクローニングすることに成功した。現在、レポーターアッセイによりこのプロモーター領域を解析中である。

7．研究の考察・反省

培養心筋細胞へのHB-EGF刺激によるEGF受容体活性化が、VP22-AH domain導入により阻害されなかった。さらに、*gene33*遺伝子導入による一過性発現においてもHB-EGFによる心肥大シグナル伝達を抑制しなかったが、予想に反して転写因子Elk1の活性化と、ANP遺伝子プロモーターを活性化した。これらの結果は、HB-EGFにより心筋細胞で急速に誘導されたGene33は、その肥大シグナルを促進する方向に制御している可能性が考えられる。

EGF受容体を高レベルで発現している一部のbreast cancer cell lineでは、Mig6 (Gene33) がEGF受容体シグナルに対する負の制御機構に働き、細胞増殖の抑制に働くことが報告されているが、一方でMDA-MB231のようにMig6が恒常的に高いレベルで発現しているbreast cancer cell lineも存在することが最近報告されている。さらにラットrenal mesangial cellでは、Gene33の過剰発現によりJNK1/2の特異的な活性化が認められるとの報告もあり、Gene33の機能が細胞種によりかなり異なることを示唆している。このことはGene33のアミノ酸配列の相同性解析からも、分子内にAH domainのみならず多様な調節因子と結合しうる複数の機能ドメインが存在することからも推測される。したがって、心筋以外の特定の細胞種によっては、本研究によって作製したVP22-AH domainによる細胞内導入により、EGF受容体のシグナル伝達系を阻害できる可能性が考えられる。

今回、心筋細胞への発現ベクター導入による一過性発現の効率の低さから、心筋細胞内でGene33と結合するターゲットの同定には至らなかった。しかし、Gene33を安定発現する心筋細胞株の樹立に成功したので、今後これらの細胞株を使用して心肥大シグナルの関与について再検討するとともに、ターゲット分子の同定を試みたい。

1．研究課題名：プロテインキナーゼ PKU-βの姉妹染色体の正確な分配に対する関与
（研究番号 S2004-14）

2．キーワード：1）PKU-β/TLK1
2）中心体（centrosome）
3）ミオシン II 型（Myosin II）

3．研究者氏名：橋本光正・医学部・助手・ゲノム医科学（生化学）

4．研 究 目 的

正常な細胞の維持と増殖のためには、細胞分裂において 2 本の姉妹染色分体が正確に分配される必要がある。この分配は、微小管およびそれに付随するモータータンパクが姉妹染色分体を細胞の両極に移動させることによってなされることが知られている。さらに近年の研究において、この分配にはコヒーシン、Anaphase Promoting Complex さらにミオシン II 型などが関与することが明らかにされた。しかしその詳細は未だ不明な点が多い。本学のゲノム医科学講座で発見されたセリン/スレオニンプロテインキナーゼである PKU-β/TLK1（Gene 202, 193-201）は従来細胞周期の S 期進行や DNA 修復に関与するタンパクであると考えられてきた。しかしこのタンパクはそればかりではなく、RNAi の手法を用いた PKU-β/TLK1 遺伝子ノックダウン実験によって、姉妹染色体分配の正確な分配にも関与することがわかった。

そこで本研究の目的は、PKU-β/TLK1 の細胞周期進行特に細胞分裂期における役割を明らかにすること。さらに PKU-β/TLK1 の制御下にあるタンパクおよび PKU-β/TLK1 を制御するタンパクを同定し、細胞分裂の詳細な機構解明に寄与することである。

5．研 究 計 画

PKU-β/TLK1 の機能解明について、以下のことを行った。

① PKU-β/TLK1 遺伝子ノックダウン細胞の樹立
② その時の表現形を明確にする。細胞周期、染色体モード、免疫染色によるα-チューブリン、β-チューブリン、中心体と染色体 DNA の時間的、空間的位置関係
③ PKU-β/TLK1 遺伝子ノックダウン細胞に対する、X 線、紫外線、クロスリンク剤などの DNA 損傷をもたらす処理に対する感受性
④ PKU-β/TLK1 遺伝子ノックダウン細胞を用いて、細胞分裂に関連するタンパク、特に染色体分配サイクルに関連するタンパクの量、リン酸化活性を調べ、正常細胞と比較する。このことによって、PKU-β/TLK1 とその関連タンパクの相互関係を検討する。
⑤ 中心体の両極への移動に直接関与すると考えられているのは、アクチン、ミオシン II などの細胞骨格に関するタンパク質であるが、現時点でこれらのタンパク質が細胞周期進行に直接プログラムされたものとは考えにくい。そこでこれらを活性化するタンパク質が、PKU-β/TLK1 それ自身あるいは、PKU-β/TLK1 と相互作用を持つものの中にあるかどうかを調べ、PKU-β/TLK1 を中心とした中心体

移動の開始とその経路、および姉妹染色分体の正確な分配機構を明らかにする。

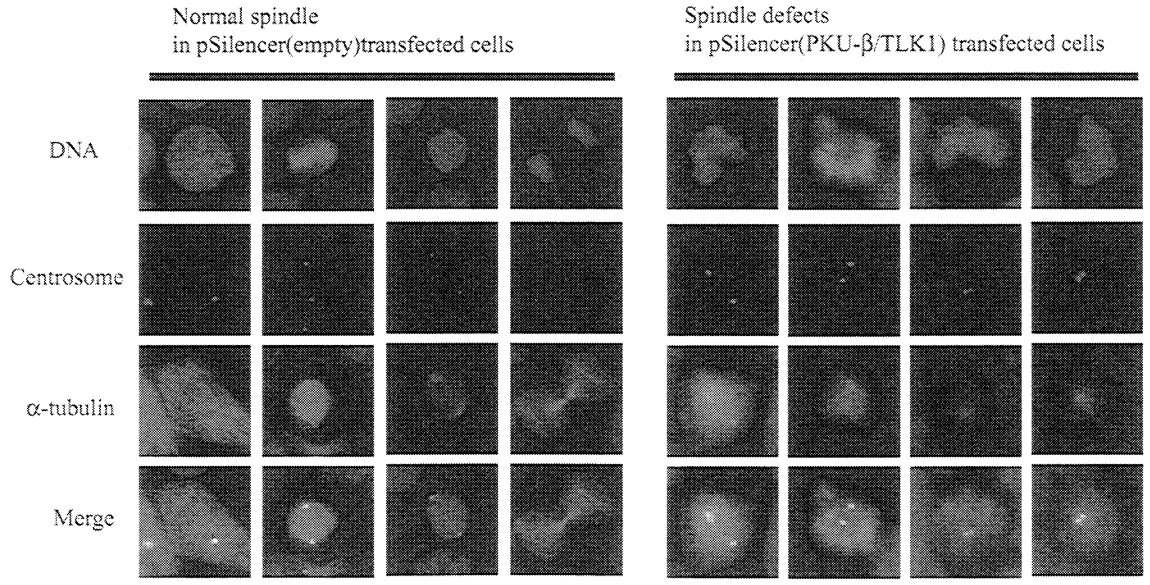
6．研究成果

研究計画①についての成果

siRNA を用いた PKU-β/TLK1 遺伝子欠損細胞作成の方法を確立した。PKU-β/TLK1 遺伝子に特異的な塩基配列で他の遺伝子配列に干渉しない 21bp を選び siRNA を合成した。これを細胞にトランスフェクションすることによって達成した。本方法は、ヒト培養細胞の HeLa、MCF7、HepG2 について有効であった。また同配列の siRNA を発現するプラスミド pSilencer (PKU-β/TLK1)を構築し、これを用いることによって同様の結果を得た。

研究計画②についての成果

HeLa、MCF7、HepG2 の PKU-β/TLK1 遺伝子欠損細胞ではいずれも、(1) 細胞周期 M 期前期において、中心体の両極移動が抑制されること（下図)、(2) その結果として姉妹染色体分配が正確に完了されないこと、(3) 倍数性異常の細胞が高頻度に出現すること、(4) 染色体モードの異常、などが観察された。



研究計画③についての成果

PKU-β/TLK1 遺伝子欠損細胞では、X 線、紫外線、クロスリンク剤などの DNA 損傷をもたらす処理に対して高い感受性を示すことがわかった。

研究計画④についての成果

HeLa 細胞において、ダブルチミジン法で細胞周期の G1 期同調した後、

siRNA(PKU-β/TLK1)をトランスフェクトすると、その後24時間でG2期からM期への進行が著しく遅延していることがわかった。この原因として、G2期からM期への進行をプロモートするタンパクCdk1の活性が低下してことを見出した。また細胞周期チェックポイント機構を支配するタンパクChk1とChk2のタンパク量を低下していることを見出した。さらに、これを培養し続けると、異数性の細胞が頻度高く現れることがわかった。これらの発見は上記のDNA損傷をもたらす処理によるPKU-β/TLK1遺伝子欠損細胞の高感受性を説明するものと考えられる。

研究計画⑤についての成果

MCF7細胞において、siRNA(PKU-β/TLK1)をトランスフェクトすると、中心体移動を制御するタンパク質MyosinⅡのリン酸化が抑制されることを見出した。

7．研究の考察・反省

以上の結果より、PKU-β/TLK1がG2期からM期への移行の段階で、DNA損傷による中心体移動の停止（**中心体チェックポイント**）と、細胞周期G2/M期の停止（**G2/M期チェックポイント**）の両方のシグナル伝達に関与するタンパク質であると考えている。

即ち、放射線などによってDNAに二本鎖切断が生じると、ATMが活性化される。活性化されたATMは、直接もしくは、ATMにより活性化されるChk1を経由して、PKU-β/TLK1の活性を抑制する。PKU-β/TLK1の活性が抑制されると、MyosinⅡのリン酸化活性が抑制されることになり、中心体の両極移動が起こらないという**中心体チェックポイント**が起動する。またChk1がCdc25Cを介してサイクリンB/Cdc2の活性を抑制する経路とは別に、PKU-β/TLK1の活性抑制が、サイクリンB/Cdc2の活性を抑制する。もしくはPKU-β/TLK1が、Cdc25Cを抑制して、その下流のサイクリンB/Cdc2の活性を抑制する可能性もある。これら少なくとも二つの経路で、**G2/M期チェックポイント**が起動することになる。以上よりPKU-β/TLK1は、二つのチェックポイントを通じてG2期からM期への細胞周期進行を監視する重要なタンパク質であると考えている。

本研究の反省点は、原著論文としての投稿が、遅れていることである。現在、鋭意、準備中であり、完成しだい速やかに投稿する予定である。

１．研究課題名：骨粗鬆症への応用を目的としたコラーゲントリペプチドの生理活性作用の解析（研究番号 S2004-15）

２．キーワード：１）コラーゲントリペプチド（collagen tripeptide）
２）Ｉ型コラーゲン（type Ｉ collagen）
３）骨芽細胞（osteoblast）

３．研究代表者名：鶴岡直樹・医学部・助手・ゲノム医科学（生化学）

４．研 究 成 果

本研究では骨芽細胞におけるコラーゲン合成の促進を目的とし、コラーゲンの酵素消化産物であるトリペプチド（コラーゲントリペプチド、CTP）を培養骨芽細胞に与え、その効果と作用機構の解析を行った。

国内における骨粗鬆症患者は既に膨大な数に達し、予備軍を含めると 2,000 万人に達すると推定されている。同疾患は骨折リスクを高め、骨折後の生活に大幅な制約を強いることから、今後さらに高齢者が増加するなかで QOL の維持、医療・介護費用の面で深刻な問題となっている。骨粗鬆症の主な治療法は骨量低下の抑制であるが、すでに骨量が低下した高齢者の場合は顕著な回復効果が得られていない。骨形成能の低下は老齢化によって骨基質タンパク質の約 90%を占めるⅠ型コラーゲン合成が大きく減少することに依存しており、その回復には骨芽細胞におけるコラーゲン合成の促進が必須であると考えられる。

CTP には培養線維芽細胞のコラーゲン合成を促進することが既に明らかとなっており、骨芽細胞においても同様の効果を示す可能性がある。また、豚皮などの家畜の未利用資源を原料とし工業的な生産系が確立されているため、安定かつ安価に供給しうる食品素材である。CTP が骨芽細胞に対してもコラーゲン産生の促進効果を示し、その作用機構が解明されれば、今後同疾患の治療にかかると推定される膨大な医療･介護費用の削減につながると考えられる。

５．研 究 計 画

本研究では培養骨芽細胞を使用した *in vitro* の系において、CTP の生理作用の解析を行うものとした。以下に平成 16 年度分の実施項目を記した。

1) ヒト骨芽細胞（hFOB1.19 株）の増殖・分化を制御し、アッセイに最適な培養系を構築する。

2) CTP が培養骨芽細胞のコラーゲン合成に与える影響について、コラーゲン遺伝子・タンパク質の発現量を解析して評価する。

3) CTP が骨芽細胞の増殖・分化・石灰化など種々の表現形に与える影響についての

解析する。

4)蛍光標識した CTP を用いて、培養系における CTP の局在性を明らかにする。

6．研 究 成 果

1) 培養系（アッセイ系）の最適化

骨芽細胞には数段階の分化過程があり各段階でその表現形が異なる。コラーゲンなど骨基質の発現量も変化することから、アッセイ系を構築するにあたっては増殖と分化の制御を可能にしたヒト骨芽細胞（hFOB1.19、 ATCC）を用いた。同細胞は温度感受性の SV40 large T antigen 遺伝子が導入されており、低温（34°C）で増殖が促進されるが、高温環境下（39°C）では増殖が抑制され分化が進行する。アッセイは、低温で培養した後、高温で骨基質産生が活発となる基質形成期まで分化を誘導して行うものとした。また、 *in vivo* により近い環境下で解析することを目的として培養系に種々の支持体を添加した結果、骨中における無機質の主成分であるハイドロキシアパタイト存在下でコラーゲン合成が誘導され、効率的に評価する系を構築することができた（図 1A)。

2) CTP が骨芽細胞のコラーゲン合成に与える影響

hFOB1.19 が発現した I 型コラーゲンα_1鎖遺伝子（*col Ia1*）の mRNA を Real Time PCR 法で測定した結果、培養系に CTP を添加することによって発現量が 1.3 倍程度まで増加した。ハイドロキシアパタイトビーズ存在下ではこの CTP の効果が増幅され、最大 2.4 倍程度に転写が促進された(図 1A)。

骨芽細胞の合成する I 型コラーゲンは細胞外で両末端のプロセッシングを受け、生じた末端のペプチドは遊離する。この遊離したペプチド（C 末端側、CICP）を ELISA にて定量化し、I 型コラーゲンの分泌量を評価した。その結果、細胞内で合成され分泌されるコラーゲン量が CTP の添加によって増加することがわかった（図 1B)。以上のことから、CTP には転写レベルでコラーゲン合成を促進させる効果があり、これに応じてタンパク質レベルでもコラーゲン量が増加することが明らかとなった。

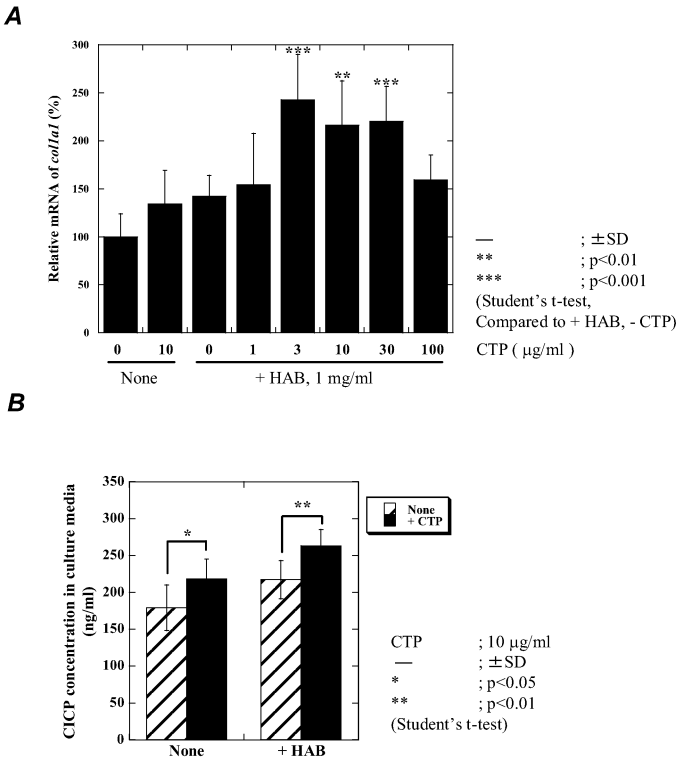


図 1 骨芽細胞における CTP のコラーゲン合成促進効果
CTP による *col Ia1* mRNA の発現量の変化(A)と培養液中の CICP の変化（B)。

3) hFOB1.19 の表現形に与える影響

CTP が hFOB1.19 に与える影響について種々検討を行ったところ、増殖や分化などに顕著な変化は見られなかった。一方、細胞外マトリックスの石灰化について解析したところ、CTP の添加によって細胞周辺に沈着したカルシウムが増加する傾向が見られ(図 2)、I 型コラーゲンの増加にともなって石灰化も促進されることがわかった。

4) 培養系における CTP の局在性

CTP 作用機構の解析にあたり、CTP が細胞内に取り込まれるのか、あるいは特異的な細胞表面受容体によって認識されているのかを明らかにすることが必要であると考えられた。そこで CTP の主成分である Gly-Pro-Hyp を蛍光標識して培養系に添加し、その局在性を共焦点レーザー顕微鏡で解析した。その結果、細胞内部に蛍光シグナルが検出され（図 3）、hFOB1.19 には細胞表面に CTP を取り込む機構が存在する可能性があると考えられた。

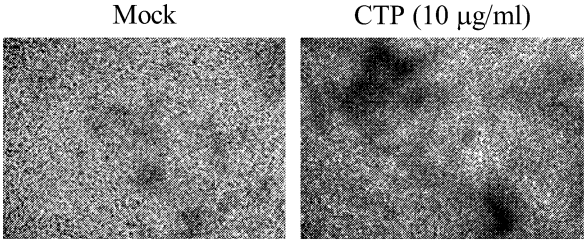


図 2 培養骨芽細胞系の石灰化

アリザリンレッドでカルシウムを染色した（黒色)。

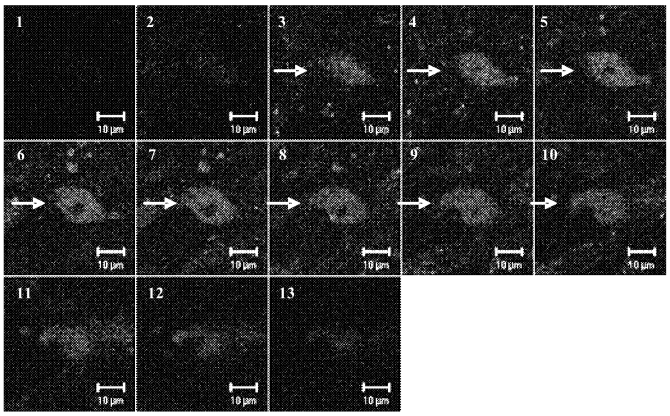


図 3 蛍光標識した CTP の局在性

Gly-Pro-Hyp-Lys-Tetramethyl Rhodamine を培養系に添加して共焦点レーザー顕微鏡システムで固定化した細胞を下端から上端まで 0.5 μm 間隔で解析した。断面化した細胞内部に蛍光シグナルが検出された（→)。

7．研究の考察・反省：

本研究により、CTP が培養骨芽細胞における I 型コラーゲンの発現を促進させることが明らかとなった。コラーゲンの発現を誘導するものとしては TGF-βスーパーファミリーや IGF1 などのサイトカインが既に報告されているが、CTP のように細胞の増殖や分化に顕著な影響を与えることなくコラーゲン産生を促進させるものはない。CTP はサイトカインと比較して非常に安価で安定して供給できることも含め、骨治療に非常に有用であると考えられる。

CTP はコラーゲンの発現を転写レベルで促進し、蛍光標識したトリペプチドによる実験では CTP が細胞内に取り込まれていることも示唆された。今後は CTP シグナルの伝達因子や、コラーゲン遺伝子の発現を直接制御する転写因子について解析し、その作用機構の解明を目指す。CTP のような短鎖ペプチドによって活性化されるシグナル伝達経路はこれまでに報告はなく、同解析を効率的に進めるためには DNA アレイシステムなどによる遺伝子発現の網羅的な解析が必要であると考えられる。

1．研究課題名：ヒト型モノクローナル抗体によるEBウイルス関連蛋白を標的とした
特異的治療法の開発（研究番号 S2004-16）

2．キーワード：1）ファージ・ディスプレイ（phage display）
2）EBウイルス（EB virus）
3）ヒト型モノクローナル抗体（Human monoclonal antibody）
4）悪性リンパ腫（Malignant lymphoma）
5）発現クローニング（Expression cloning）

3．研究代表者：正木康史・医学部・講師・血液免疫制御学（血液免疫内科学）

4．研究目的

バクテリオ・ファージ表面に抗体 Fab 分子を発現する Combinatorial antibody library system が開発され、ヒト型のモノクローナル抗体の作成が可能となり、モノクローナル抗体の応用範囲が従来の診断研究主体から治療応用主体へと大きく変遷しつつある。今回は、悪性リンパ腫における抗Epstein Barr ウイルス（EBV）抗体による標的療法の開発に重点を起き研究を行う。まずEBウイルス関連蛋白に高い親和性を有するヒト型の抗EBV抗体をクローニングする事を第一目標とした。更に、ヒト型の抗EBV抗体がEBV関連悪性リンパ腫細胞にも結合することを確認した上で、まずはそれを用いた免疫染色などによる診断的利用法の確立、次いで、その抗体に抗癌剤を結合させ腫瘍特異的な標的療法を開発する事を最終目標とした。

5．研究計画

EBVに対する抗体を高力価で有する患者由来のFabライブラリーを構築し、このファージ・ライブラリーを、ELISAプレート上にEBV関連蛋白（精製VCA抗原、精製EA抗原、EBV非精製抗原）やRajiおよびDaudi細胞の細胞遊離成分を固相化したもの、またはRajiおよびDaudi細胞の細胞浮遊液に対してライブラリーのファージ溶液を反応させる。非特異的ファージを洗い除いた後、特異的に結合しているファージのみを酸で溶出し、これを大腸菌XL-1 blueに感染させ増幅する。ここから再びファージを抽出し、この手法を3ー5ラウンド繰り返す（ファージ・パンニング）。すると、EBV 蛋白に対する特異的な抗体クローンが増幅されてくる。最終ラウンド後に大腸菌よりDNAを抽出しGeneIIIと呼ばれる遺伝子部分を制限酵素NheI-SpeIで切り出した後にセルフ・ライゲーションし可溶性型の Fab 溶液を作成する。20ー30 クローンのスクリーニングをELISA法や免疫染色法もしくはFACSにて行う。

陽性クローンが得られたらそこからDNAを抽出し軽鎖・重鎖それぞれの塩基配列を決定する。EBウイルスに対する抗体クローンが得られたら、まずそのエピトープをRajiまたはDaudi細胞の細胞遊離成分に対するウエスタン・ブロット法もしくは免疫沈降法にて検索する。また、実際のEBV陽性悪性リンパ腫組織に対しての親和性を免疫染色やFACSにて検討する。親和性が確認されたら、ラジオアイソトープ標識したFabを、EBV関連リンパ腫組織を移植したSCIDマウスに投与し、組織に到達しうるかどうかを判定する。

また、上記のように非精製蛋白を抗原にした発現クローニングを行うため、新たな腫瘍細胞

また、上記のように非精製蛋白を抗原にした発現クローニングを行うため、新たな腫瘍細胞蛋白に対するヒト型抗体およびその対応抗原が、とれてくる可能性もあり、その場合はそれらの精製同定、エピトープマッピングも行う。

6．研究成果

各種EBV関連蛋白やEBV陽性細胞株に対してPanningを行ったが、強く反応するFabが得られたのはEBV VCAに対するものだけであった。塩基配列にて、４個のFabクローンが決定された。ELISA, Inhibition ELISA, Western blot, 免疫蛍光法、免疫組織染色にて得られたFabクローンの感度、特異性を検討した。その結果、得られたFabのうち特に２つのクローン（aVCA-1, aVCA-21）はVCAにのみ特異的に濃度依存的に結合した。免疫蛍光法、免疫組織染色でEBV陽性細胞および組織に特異的な染色性を示した。

7．研究の考察・反省

今回得られたFabはEBVのVCAに対するものであり、VCAは細胞内蛋白であり細胞表面には表出してこない事から、当初目的としていたモノクローナル抗体を用いた標的療法としては使えない。しかしながら、EBV陽性細胞および組織に特異的な染色性を有した事から診断目的のツールとしては使える可能性があり、今後も検討していく。

更に、EBVのMAのような細胞表面に表出する蛋白を標的として、同ライブラリーからのPannningを行い、治療目的に使いうるモノクローナルFabをクローニングする事を検討中である。

8．研究発表

まだ、当研究結果による論文はアクセプトされていません。
現在論文はほぼ完成し、J. Immunologyに投稿準備中です。

1．研究課題名：迷走神経によるグルカゴン様ペプチド１受容機構の分子生物学的検討
（研究番号 S2004-17）

2．キーワード：１）インクレチン（incretin）
２）グルカゴン様ペプチド１（glucagon-like peptide-1; GLP-1）
３）迷走神経（vagus）
４）節神経節（nodose ganglion）
５）神経化学受容（neural chemoreception）

3．研究者氏名：中川　淳・医学部・助教授・内分泌代謝制御学（内分泌内科学）

4．研究目的

我々は従来より，ある種の膵・消化管ホルモンは，門脈血中に放出→肝を通過→全身循環を経た後に標的器官に作用するのみならず，門脈領域に存在するホルモン感受性迷走神経求心路を介した神経性反射により作用発現し得る可能性を提唱してきた。取り分けグルコース濃度依存性インスリン分泌促進作用（インクレチン作用）や食欲抑制作用により糖尿病治療への応用が期待されているグルカゴン様ペプチド１（GLP-1）に関しては早くから着目してきている。即ち，ラットを用いた電気生理学的実験より迷走神経肝臓枝によるGLP-1 受容機構の存在を見出し，さらに迷走神経求心線維１次ニューロンの存在する節神経節（NG）においてGLP-1 受容体遺伝子が発現していることを確認している。しかし，このNG でのGLP-1 感受性ニューロンがどのような神経伝達物質により中枢（延髄孤束核）へ投射しているか等，不明な点は極めて多く，本機構の分子生物学的解明は現在端緒に付いたばかりである。本研究では主として，GLP-1 感受性NG ニューロンでの中枢への神経伝達物質を同定することを目的とする。

5．研究計画

迷走神経GLP-1 受容機構に関与するニューロンがどのような神経伝達物質により延髄孤束核へ情報を伝達しているのかを同定するため，ラットNG でGLP-1 受容体遺伝子と神経伝達物質遺伝子の共発現の有無を２重染色 in situ hybridazation により検出する。GLP-1 は食欲抑制作用を示すことが知られているので，NG から孤束核への神経伝達物質も食欲抑制性である可能性が高い。従って，まず食欲抑制性神経伝達物質のNG での遺伝子発現をRT-PCR によりスクリーニングする。引き続き，これにより得られた知見に基づき，組織学的検索を行う。

・試料cDNA…　自由摂食下のWistar 系ラットより麻酔下にNG を摘出する。RT-PCR 用には，市販キットを用い総RNA を抽出，cDNA を合成する。In situ hybridization 用には，OCT-compound に包埋，新鮮凍結切片を作製する。

・RT-PCR … RT-PCR を用いて NG に発現する食欲抑制性神経伝達物質遺伝子の発現を検出する。目的とする神経伝達物質遺伝子として calcitonin gene-related peptide (CGRP), cocaine- and amphetamine-regulated transcript (CART), gastrin-releasing peptide (GRP), neurotensin/neuromedin N (NT/NMN), proopiomelanocortin (POMC) につき検索を行う。

・In situ hybridization … GLP-1 受容体 mRNA および神経伝達物質 mRNA に対する digoxigenin 標識および fluorescein 標識 cRNA プローブは, 5'端に T7 または SP6 プロモーター配列を付加したプライマーによる RT-PCR 産物を鋳型として, T7- または SP6-RNA polymerase を用いて作製する。これら標識プローブを用い, ラット NG 新鮮凍結切片に対して２重染色 in situ hybridization を行う。

６．研究成果

RT-PCR 法により, ラット NG において, CGRP およびそのアイソフォームである calcitonin-related polypeptide-β (Calcb), CART, NT/NMN 遺伝子の明瞭な発現が確認された。一方, GRP の発現はかなり弱く, POMC の発現はないか極めて僅かであった。

次いで, 以上の RT-PCR の成績に基づき, ラット NG ニューロンにおけるこれら神経伝達物質遺伝子と GLP-1 受容体遺伝子の共発現の組織学的証明を試みた。しかしながら現在のところ, CGRP, CART, GRP 遺伝子に関しては, GLP-1 受容体遺伝子と同一ニューロンにおける明らかな共発現を認める成績は得られていない。

迷走神経によるホルモン感受機構は, GLP-1 以外にも幾つかの膵・消化管ホルモンについても存在することが報告されているが, 申請者の属するグループはソマトスタチン (SS) もその一つであることを以前より報告している。SS 受容体には SSTR1ー5 の遺伝子の異なる５つのアイソフォームが存在するが, 迷走神経による SS 受容機構につき, いずれの受容体アイソフォームが関与するかは従来明らかではなかった。本研究課題からの派生的研究として, ラット NG に発現する SS 受容体が主として SSTR2A であることを半定量的 RT-PCR により見出し, さらに Northern blot 法および免疫組織化学を用いて確認した。

一方, GLP-1 と同様にグルカゴン遺伝子より転写・翻訳されプロセシングにより作られるグルカゴン様ペプチド２ (GLP-2) に関しては, 迷走神経による感受機構が存在するかどうかは従来明らかではなかった。これにつき今回, 以前より本研究者らと共同研究を行っている金沢大学保健管理センター中林　肇教授らが電気生理学的実験により否定的な成績を得たが, 本研究課題からの派生的研究として NG では GLP-2 受容体遺伝子は発現していないことを証明した。

７．研究の考察・反省

本研究により, ラット NG において種々の食欲抑制性神経伝達物質の遺伝子が発現してい

ることがRT-PCRを用いて確認された。このうちNT/NMN, GRP, POMC遺伝子発現の有無に関しては，本研究者の知る限り従来報告がなく，本研究により初めて明らかにされたものと思われる。また，派生的実験ではあるが，NGに発現するSS受容体がSSTR2Aであること，GLP-2受容体の発現は認められないことも，今回の一連の研究によって初めて明らかにされた。これらの新知見は，エネルギー代謝と食欲調節に関して迷走神経求心路がどのように関与しているかを理解するための基礎的理解に貢献するものと考えられる。

一方，上記成績に基づき行われたGLP-1受容体遺伝子との神経伝達物質の共発現に関する組織学的検討に関しては，今回の実施期間中に確定的な結果を得ることはできなかった。その理由として，以下のような理由が挙げられる；

・標識cRNAプローブ … 以前の実験では標識cRNAプローブ合成のための鋳型用に，PCR産物からTAクローニングによるプラズミド作製を共同研究者に依頼していた。しかし，本研究では同時に複数種のプローブ合成が必要となり，共同研究者の負担が多大となるため，T7またはSP6プロモーター配列を付加したプライマーによるRT-PCR産物を鋳型とする方法を選択した。本法は成書にも極く簡単に紹介されているが，実際に行ってみるとPCR産物の収量はプライマー間で一定せず，安定したcRNA合成を行うのにかなりの予備実験と方法上の改良を加える必要があった。

・In situ hybridization検出感度 … NGにおけるGLP-1受容体遺伝子の発現量は極めて僅かであり，事実，以前の研究でも^{32}Pを用いたNorthern blot法やアルカリフォスファターゼ発色によるin situ hybridizationでは３ー４日にも及ぶラジオグラフィや発色過程を必要とした。従って，本実験における２重染色に際して種々の検出法を試みたが，S/N比に関して必ずしも満足いくものではなかった。また，最近は多くの受容体蛋白や神経伝達物質に対する抗体が市販で入手可能となったため，困難なin situ hybridizationによる検出から市販抗体を用いた免疫染色への変更も試みたが，実験結果からは抗体の特異性に関する疑問が払拭しきれず，結局それに費やした時間が無駄となった。

但し現時点においては，標識cRNAプローブもほぼ安定して合成できるようになっており，in situ hybridizationの感度について，最も高感度な検出法とされるTSA法による検討を予定している。迷走神経によるGLP-1受容機構の理解には，本機構に関与する神経伝達物質の同定は避けては通れないと考えている。この神経伝達物質を明らかにすることで，各種病態時における本機構の偏倚を検証することが可能となり，ひいては糖尿病や肥満症の病態解明やGLP-1経路を介する新たな治療戦略の開発に結びつくことを期待している。

８．研究発表

・NGにおけるSS受容体アイソフォームに関しては投稿準備中

・NGでGLP-2受容体遺伝子発現が認められないことは他研究者により投稿準備中

1．　研究課題名　：　傍腫瘍性神経症候群に関連する神経抗原の in vivo における機能の解析
（研究番号 S2004-18）

2．　キーワード：1）傍腫瘍性神経症候群（paraneoplastic syndrome）
2）pcd-17
3）immunization with whole recombinant yeast
4）leucin-zipper

3．　研究者氏名　：　斉木三鈴　・　医学部　・　助手　・脳脊髄神経治療学（神経内科学）
（現　Centre for Brain Repair,　University of Cambridge）

4．研究目的

傍腫瘍性神経症候群の中でも小脳 Purkinje 細胞の細胞質に対する抗体が関与する小脳変性症（以下 PCD）の発症機序は、腫瘍と Purkinje 細胞の共通抗原に対する細胞性免疫が関与している可能性が示唆されている。しかしその詳細な機構については多くの点で不明である。我々は、これまでに組み換え体蛋白を adjuvant と共に能動免疫したり、その感作リンパ球の受動免疫を試みたり、抗原をコードする cDNA を真核細胞発現ベクターに組み換えた DNA 免疫の手法により in vivo での解析を行ってきた。

酵母細胞は、細胞膜に adjuvant 様の特性を有しており、酵母細胞を in vivo に投与することによって、酵母に発現する蛋白を抗原として認識する CD4 および CD8 双方の細胞性免疫を誘導できることが証明されている。この酵母を用いて組み換え体技術により蛋白を発現させた recombinant yeast を in vivo に投与する whole recombinant yeast 免疫の手法が開発され、臨床においても HIV や HBV に対するワクチンとしての応用が進められている。本研究では、PCD の発症機序を明らかにする目的で、PCD 関連抗原である pcd-17 蛋白を発現させた recombinant yeast を作製し、whole recombinant yeast 免疫の方法を用いて、in vivo マウスにおける細胞性免疫の誘導について検討した。

同時に、pcd-17 蛋白には leucine が繰り返し出現する特徴的な leucine zipper モチーフが存在し、他の蛋白との相互作用を介して神経細胞に重要な役割を果たしていると考えられる。我々は以前に PCD 患者にみられる抗神経細胞抗体の全てが、この leucine zipper を特異的に認識していることを報告した。これは抗原のアミノ酸構造の中でも、この leucine zipper に対する免疫応答が本疾患の病態に重要である可能性を示唆しており、本研究でも leucin zipper の関与についても検討した。

5．研究計画

1) mouse pcd-17 cDNA を pGAD424 ベクターに組み換え、表記の酵母細胞に形質転換して、recombinant yeast を作製し、約2×10^8の recombinant yeast を6－8週令の雌マウスへ1回ないしは2回皮下接種し感作した。細胞の抗原に対する免疫応答は、最終感作から7－9日後にリンパ節細胞を調整の上抗原存在下に3日間培養し、16時間の^{3}H-TdR の取り込みで測定した。

2) IFN-γ産生については、3日間抗原刺激後の培養上清を ELISA 測定した。

3) 抗体産生については、ABC 法による免疫組織化学と Western blotting により検討した。

6．研究成果

pcd－17 中の異なる部位に存在する複数のペプチドを、完全 Freund's adjuvant と共に 3 つの strain マウス（SJL/J、C57Bl/6、Balb/c）に免疫し、得られたリンパ球細胞の感作ペプチドに対する増殖反応を調べたところ、SJL マウスにおいて leucine zipper 部位に相当するペプチド(LZP)に対して有意な増殖反応が観察され、PCD 関連神経抗原の epitope 部位において SJL/J マウスは responder であることが確認された。

pcd17 を発現する recombinant yeast をマウスの皮下に感作後取り出したリンパ節細胞を用いて、抗原の LZP に対する反応性を検討した。前述の adjuvant と共にペプチドで感作した場合と同様に、recombinant yeast 単独で感作した SJL/J マウスのリンパ球は LZP に対して有意な増殖反応を認めた。B6 マウスでも反応を惹起し得たが、Balb/c マウスにおいては有意な増殖反応は認めなかった。

最も反応の見られた SJL マウスを用いて、recombinant yeast により感作されたリンパ球細胞と様々なペプチドとの免疫応答を調べた結果、LZP と LZP の C 末端を含む PCD1 に弱い反応を認めたが、それ以外のペプチドとの反応はみられなかった。さらに、Leucine zipper 領域における抗原部位を検討した結果、N 末端を含み C 末端を含まないペプチドでは反応が見られないのに対し、C 末端を含むペプチドでは有意な増殖反応が見られた。以上から、感作されたリンパ球は、leucin zipper 領域の中でも C 末端側のアミノ酸残基を中心に認識していることが考えられた。

ラット小脳組織を用いた免疫組織化学では、recombinant yeast で感作したマウスの血清に小脳 Purkinje 細胞と反応する抗神経細胞抗体が存在することが示された。また、マウス小脳ホモジュネートと recombinant 蛋白を抗原とした Western blotting 解析でも同様に、recombinant yeast により誘導された抗神経細胞抗体を確認した。

7．　研究の考察・反省

PCDにおいては、神経抗原に反応してCD8 T 細胞がinterferon gammaを産生することが示唆されており、recombinant yeastで感作されたリンパ球をLZPで抗原刺激したところ、control yeast感作群と比較して有意なinterferon gamma産生がみられた。さらに、CD8T細胞をpositive selectionし、MMC処理したリンパ節細胞の存在下に様々な抗原刺激をしinterferon gammaの産生をみた結果、control yeastで感作されたCD8T細胞はいずれの刺激でも産生は認めなかったが、pcd-17 yeastで感作されたCD8T細胞ではPCD-1ペプチド刺激で産生が見られず、LZP刺激で産生が観察された。これはwhole recombinant yeastで免疫感作したSJL/Jマウスにおいて、LZPを抗原認識するCD8陽性細胞が誘導されることを示していると考えられた。

以上から我々は、PCD関連神経抗原のエピトープであるleucine zipper構造に対してSJL/JがresponderであることをPCD神経抗原の組み換え体酵母をマウスに感作することによって神経抗原のleucine zipper構造に対して細胞性免疫応答を惹起し得ることを示した。さらに、SJL/Jにおける神経抗原のleucine zipper部位に対する免疫応答に際して、leucine zipper構造のC末端側のアミノ酸残基の認識を必要とした。さらにLZPを抗原として認識し、interferon-gammaを産生するCD8陽性T細胞の誘導を得ることを明らかにした。

今回私たちが開発した、遺伝子組み換え体酵母によるSJL/Jマウスに対する免疫誘導の手法は、PCDの神経抗原に対する細胞性免疫反応を解析する上で有用な手段となり得ると考えられた。

２００４　平成１６年度金沢医科大学共同研究成果報告書
奨励研究成果報告書

平成１８年１２月発行
編　集　研究推進評価委員会
発行所　金沢医科大学出版局
石川県河北郡内灘町大学１丁目１番地

禁無断転載